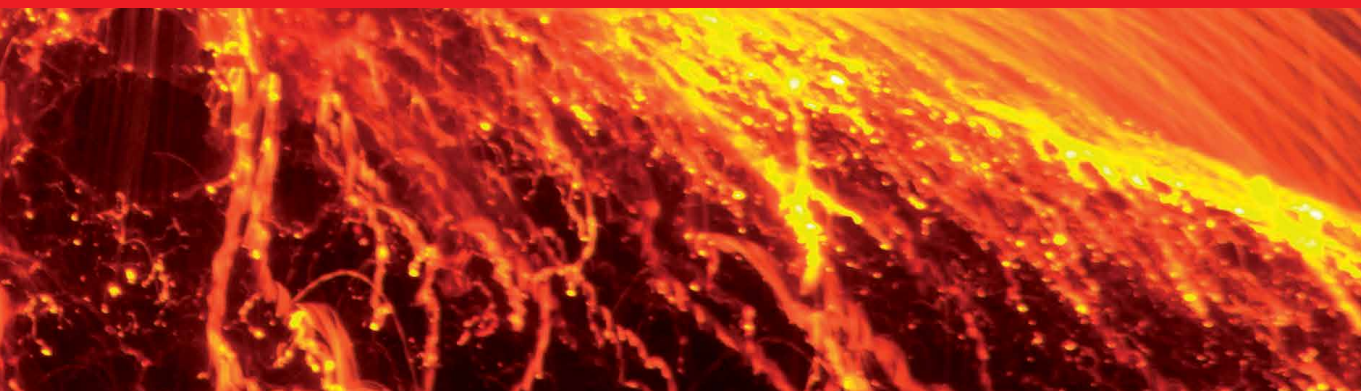




IntechOpen

Updates in Volcanology
Transdisciplinary Nature of Volcano Science

Edited by Károly Németh



Updates in Volcanology – Transdisciplinary Nature of Volcano Science

Edited by Károly Németh

Published in London, United Kingdom



IntechOpen





Supporting open minds since 2005



Updates in Volcanology – Transdisciplinary Nature of Volcano Science

<http://dx.doi.org/10.5772/intechopen.87815>

Edited by Károly Németh

Contributors

Gabriel Ureta, Felipe Aguilera, Károly Németh, Matias Vilches, Mauricio Aguilera, Ivana Torres, Alexander Scheinost, Rodrigo González, José Pablo Sepúlveda, Alan Bischoff, Andrew Nicol, Sverre Planke, Simon Holford, Nazim Imamverdiyev, Anar Valiyev, Sara Mountaj, Toufik Remmal, Samira Makhoukhi, Mhiyaoui Hassan, Fouad El Kamel, Boxin Li, Julie Palmer, Alan Palmer, Jing Wu, Jiaqi Liu, Jonathan Procter, Hugo Murcia, Philippe Robidoux, Julie Roberge, César Adams Urbina Oviedo, Polona Kralj, Ines Galindo, Carmen Romero, Nieves Sánchez, Juana Vegas, Esther Martín-González, Roberto Carniel, Silvina Guzman, Payson Sheets, Pedro Hernández, Javier Dóniz-Páez, Nemesio Pérez, William Hernández, Antonio Márquez, Ghislain Zangmo Tefogoum, David Guimolaire Nkouathio, Armand Kagou Dongmo, Merlin Gountié Dedzo, Tamas Sagi, Szabolcs Harangi, Theodoros Ntaflos, Vic Semeniuk, Margaret Brocx, Tom J. Casadevall, Dan Tormey

© The Editor(s) and the Author(s) 2021

The rights of the editor(s) and the author(s) have been asserted in accordance with the Copyright, Designs and Patents Act 1988. All rights to the book as a whole are reserved by INTECHOPEN LIMITED. The book as a whole (compilation) cannot be reproduced, distributed or used for commercial or non-commercial purposes without INTECHOPEN LIMITED's written permission. Enquiries concerning the use of the book should be directed to INTECHOPEN LIMITED rights and permissions department (permissions@intechopen.com).

Violations are liable to prosecution under the governing Copyright Law.



Individual chapters of this publication are distributed under the terms of the Creative Commons Attribution 3.0 Unported License which permits commercial use, distribution and reproduction of the individual chapters, provided the original author(s) and source publication are appropriately acknowledged. If so indicated, certain images may not be included under the Creative Commons license. In such cases users will need to obtain permission from the license holder to reproduce the material. More details and guidelines concerning content reuse and adaptation can be found at <http://www.intechopen.com/copyright-policy.html>.

Notice

Statements and opinions expressed in the chapters are these of the individual contributors and not necessarily those of the editors or publisher. No responsibility is accepted for the accuracy of information contained in the published chapters. The publisher assumes no responsibility for any damage or injury to persons or property arising out of the use of any materials, instructions, methods or ideas contained in the book.

First published in London, United Kingdom, 2021 by IntechOpen

IntechOpen is the global imprint of INTECHOPEN LIMITED, registered in England and Wales, registration number: 11086078, 5 Princes Gate Court, London, SW7 2QJ, United Kingdom
Printed in Croatia

British Library Cataloguing-in-Publication Data

A catalogue record for this book is available from the British Library

Additional hard and PDF copies can be obtained from orders@intechopen.com

Updates in Volcanology – Transdisciplinary Nature of Volcano Science

Edited by Károly Németh

p. cm.

Print ISBN 978-1-83881-214-0

Online ISBN 978-1-83881-856-2

eBook (PDF) ISBN 978-1-83881-857-9

We are IntechOpen, the world's leading publisher of Open Access books Built by scientists, for scientists

5,300+

Open access books available

130,000+

International authors and editors

155M+

Downloads

156

Countries delivered to

Our authors are among the
Top 1%

most cited scientists

12.2%

Contributors from top 500 universities



WEB OF SCIENCE™

Selection of our books indexed in the Book Citation Index
in Web of Science™ Core Collection (BKCI)

Interested in publishing with us?
Contact book.department@intechopen.com

Numbers displayed above are based on latest data collected.
For more information visit www.intechopen.com



Meet the editor



Károly Németh is a professor in Geology at Massey University, New Zealand. He obtained a Ph.D. in Geology from the University of Otago, New Zealand, in 2001, and a Ph.D. in Environmental Sciences from the University of Sopron, West Hungary, in 2003. His expertise includes sedimentology, volcanology and geoheritage. He was a member of the Executive Committee of the International Association of Volcanology and Chemistry of the Earth Interior (IAVCEI) from 2011 to 2015 for which he led commissions on volcanogenic sediments, monogenetic volcanism, and volcanic geoheritage. He was/is an editorial board member for *Bulletin of Volcanology*, *Journal of Volcanology and Geothermal Research*, *Open Geosciences*, *Water, Geosciences*, and *Geoconservation Research*. He has managed special issues of journals including *Geoheritage*, *JVGR*, *Bulletin of Volcanology*, *Central European Journal of Geosciences*, *Sedimentary Geology*, and *Geoheritage and Sustainability*.

Contents

Preface	XV
Section 1 Introduction	1
Chapter 1 Introductory Chapter: Updates in Volcanology - Transdisciplinary Nature of Volcano Science <i>by Károly Németh</i>	3
Section 2 Source and Magmatic Plumbing Systems	19
Chapter 2 Modeling of Olivine and Clinopyroxene Fractionation in Intracontinental Alkaline Basalts: A Case Study from the Carpathian-Pannonian Region <i>by Tamás Sági, Szabolcs Harangi and Theodoros Ntaflou</i>	21
Chapter 3 Late Cenozoic Collisional Volcanism in the Central Part of the Lesser Caucasus (Azerbaijan) <i>by Nazim Imamverdiyev and Anar Valiyev</i>	43
Chapter 4 Seismic Geomorphology, Architecture and Stratigraphy of Volcanoes Buried in Sedimentary Basins <i>by Alan Bischoff, Sverre Planke, Simon Holford and Andrew Nicol</i>	71
Chapter 5 Machine Learning in Volcanology: A Review <i>by Roberto Carniel and Silvina Raquel Guzmán</i>	105
Section 3 Monogenetic Volcanism	131
Chapter 6 Effusive Monogenetic Volcanism <i>by Hugo Murcia and Károly Németh</i>	133

Chapter 7	149
Study of Monogenic Volcanism in a Karstic System: Case of the Maar of Lechmine n'Aït el Haj (Middle Atlas, Morocco) <i>by Sara Mountaj, Hassan Mhiyaoui, Toufik Remmal, Samira Makhoukhi and Fouad El Kamel</i>	
Chapter 8	173
Syn-Eruptive Lateral Collapse of Monogenetic Volcanoes: The Case of Mazo Volcano from the Timanfaya Eruption (Lanzarote, Canary Islands) <i>by Carmen Romero, Inés Galindo, Nieves Sánchez, Esther Martín-González and Juana Vegas</i>	
Chapter 9	195
Spatial Visualization of Geochemical Data: Application to the Chichinautzin Volcanic Field, Mexico <i>by Philippe Robidoux, Julie Roberge and César Adams</i>	
Chapter 10	217
Basic Volcanic Elements of the Arxan-Chaihe Volcanic Field, Inner Mongolia, NE China <i>by Boxin Li, Károly Németh, Julie Palmer, Alan Palmer, Jing Wu, Jonathan Procter and Jiaqi Liu</i>	
Chapter 11	249
An Overview of the Mafic and Felsic Monogenetic Neogene to Quaternary Volcanism in the Central Andes, Northern Chile (18-28°Lat.S) <i>by Gabriel Ureta, Károly Németh, Felipe Aguilera, Matias Vilches, Mauricio Aguilera, Ivana Torres, José Pablo Sepúlveda, Alexander Scheinost and Rodrigo González</i>	
Section 4	277
Complex and Polygenetic Volcanism	
Chapter 12	279
The Caldera of Mount Bambouto: Volcanological Characterization and Classification <i>by Ghislain Zangmo Tefogoum, David Guimolaire Nkouathio, Armand Kagou Dongmo and Merlin Gountié Dedzo</i>	
Chapter 13	301
Submarine Stratovolcano Peperite Syn-Formational Alteration - A Case Study of the Oligocene Smrekovec Volcanic Complex, Slovenia <i>by Polona Kralj</i>	
Section 5	327
Volcanic Geoheritage and Geotourism	
Chapter 14	329
Volcanoes: Identifying and Evaluating Their Significant Geoheritage Features from the Large to Small Scale <i>by Margaret Brocx, Vic Semeniuk, Tom J. Casadevall and Dan Tormey</i>	

Chapter 15	347
A Globally Significant Potential Megascale Geopark: The Eastern Australian Mantle Hotspot Interacting with a North-Migrating Heterogeneous Continental Plate Creating a Variety of Volcano Types, Magmas, Xenoliths, and Xenocrysts <i>by Vic Semeniuk and Margaret Brocx</i>	
Chapter 16	363
From a Bulldozer Cut to a World Heritage Site <i>by Payson Sheets</i>	
Chapter 17	377
TFgeotourism: A Project to Quantify, Highlight, and Promote the Volcanic Geoheritage and Geotourism in Tenerife (Canary Islands, Spain) <i>by Javier Dóniz-Páez, Pedro A. Hernández, Nemesio M. Pérez, William Hernández and Antonio Márquez</i>	

Preface

Updates in Volcanology - Transdisciplinary Nature of Volcano Science is a new addition to the successful Updates in Volcanology book series that includes three other volumes: *A Comprehensive Approach to the Volcanological Problems*, *New Advances in Understanding Volcanic Systems*, and *From Volcano Modelling to Volcano Geology*. These previous books discuss the evolution of volcano science in the last 10 years, providing unstructured snapshots of research outputs of a diverse array of subject areas. The evolution of book titles and their contents reflect the changes of research focus within volcanology.

Chapters from the previous three volumes in the series garnered many downloads and citations, including Web of Science citations (**Table 1**). While books are not measured and observed in the same way as scientific journals, it is evident that the published book chapters have a global impact, and their impact is growing.

The main subjects of the previously published books indicate a general trend within volcano science toward more volcanic system-based research in which various disciplines are utilized to understand volcanism in general. The current volume is no exception. It provides interesting transdisciplinary aspects of volcano science.

The book *Updates in Volcanology - Transdisciplinary Nature of Volcano Science* is divided into five sections: 1) "Introduction"; 2) "Source and Magmatic Plumbing Systems"; 3) "Monogenetic Volcanism"; 4) "Complex and Polygenetic Volcanism"; and 5) "Volcanic Geoheritage and Geotourism." The seventeen chapters represent cover also a broad array of geographical array of works from Australia, Azerbaijan, Canary Islands (Spain), Chile, China, Colombia, Hungary, Mexico, Morocco, New Zealand, and Salvador. The chapters are a good mixture of technical papers and broad overviews of novel ideas. Overall, the book reflects well the current trends in volcanology, and we hope readers will find the information contained herein useful. It will provide useful information to the readers.

Book Title	Year	Total Downloads	CrossRef Citations	Web of Science Citations	Dimension Citations	Top Chapters and their Citation numbers
<i>From Volcano Modelling to Volcano Geology</i>	2016	19,405	16	34	48	15
<i>New Advances in Understanding Volcanic Systems</i>	2013	18,786	75	94	144	115
<i>A Comprehensive Approach to the Volcanological Problems</i>	2012	20,763	24	49	57	23

Table 1.
A summary of the bibliometric data of the Updates in Volcanology book series.

I would like to acknowledge IntechOpen for the opportunity to collate this valuable book. I am also thankful for the time provided to me to complete this volume by the School of Agriculture and Environment, Massey University, New Zealand.

Károly Németh
School of Agriculture and Environment,
Massey University,
Palmerston North, New Zealand

Section 1

Introduction

Introductory Chapter: Updates in Volcanology - Transdisciplinary Nature of Volcano Science

Károly Németh

1. Introduction

Transdisciplinary approach of science appeared in recent years, partially as a result of the urgent need to deal with global and planetary changes [1–12]. Transdisciplinary science is to answer and solve environmental science questions and problems became the foundation of sustainable development, nature conservation and various environmental science education including geoeducation [13–17]. Transdisciplinary approach within volcanology was always a key element of volcano science as volcanology addresses key questions over volcanic hazards, risk and resilience naturally moving along the interface of social science, humanities, natural science and non-academic (e.g. indigenous) knowledge [18–25]. Especially in recent years more and more researches were conducted on subjects to help to understand the interface between western science and traditional knowledge [26–30]. Such works explored various aspects of volcanism that affected the human societies greatly both as processes that produce natural resources for development and in other hand continuous fear that need to be dealt with to prevent societies from their destructive powers [28, 31–34]. The transdisciplinary aspects of volcanology is reflected well in the new volcano model and volcano geology approach to understand volcanic systems and placing them in a geosystem perspective [35] (**Figure 1**). In many volcano research aimed in recent years to develop some sort of volcano model that explain the volcanic processes, their resulting eruptive products, and the way such models can help to develop a better strategy for resilience against volcanic hazard within a general natural hazard framework [40–43].

2. From volcano geology to volcano model development

The various volcano models distinguish between type of volcanoes commonly categorized monogenetic versus polygenetic volcanoes (and volcanism) as a reflection of the total eruptive volume, the total duration of volcanic activity, the strength of the link to the magma generation source and the stability and longevity of a volcanic conduit [44, 45]. In these models obviously the end-member types of volcanoes define short, small, simple (versus long-lasting, large and complex). Recent decade of research in addition, provided ample evidences that the scale of observation (hence the detail of information could be mined from volcanic systems) is important, and provides evidences to support that in real world end member type of monogenetic volcanoes are rare, and most of them shows some sort of complexity in a near continuous spectrum [20, 46–52]. This is more apparent when the magma that form those volcanic geofoms are more evolved [53, 54]. In recent years attention



Figure 1.

Complex volcanic landscape in northern Chile is a fine example to demonstrate the volcano geology approach to interpret the present day geoforms. The landscape is ruled by the basaltic-andesite to dacite lava dome-dominated Ollagüe (5868 m asl) stratovolcano, which stands 1686 meters above the surrounding Salar de Carcote desert floor. The volcano has an active hydrothermal system in its top (note the white cloud in the right edge of the summit), while the volcano itself had its last eruption about 65 ka [36, 37]. In the side of the volcanic edifice satellite domes formed such as the El Ingenio lava dome in the NW (left in the image) side of the cone [38]. In the foreground a typical hummocky surface of volcanic debris avalanche that generated by a sector collapse can be seen that formed in the late-Pleistocene. The image was taken from a small scoria cone La Poruña, that is part of a monogenetic volcanic field nearby and formed after the sector collapse of the stratovolcano [39]. This complex geological setting of this volcanic system highlights the importance to study volcanoes from volcano geology perspective.

also turned toward effusive style of volcanism that is not obviously can fit into any of these categories. The current eruption of Iceland's Reykjanes Peninsula that started on the 19th March 2021 8.45 PM (Local Time) provided an exceptional occasion to observe how a volcano starts its life (**Figure 2A and B**). Commonly, the first moments of a volcano's growth are missed by direct observation and later on the initial eruptive products become covered by subsequent eruptive products, missing key elements of the early, very critical phase of the eruption [55]. The new eruption in Iceland, that gradually builds the new volcano Geldingadalir operating along an approximately 800-meter long fissure and at least 6 distinct vent zones (**Figure 2A and B**). The opportunity to observe the vent localization process commonly based on a combination of direct observation and study of older volcanic successions [56, 57] is valuable to understand fissure-fed eruptions. Such geological observations and records can provide a dynamic view on fissure-fed eruptions in basaltic systems and help to interpret the resulting eruptive products (**Figure 2C and D**). In this respect, the interlink between observation-based volcanology can be linked to various geoeducation works that provide good, evidence-based information to understand the volcanic geoheritage [58]. In the case of the growth of the Geldingadalir volcano, it provides insight on the formation of steep spatter cones documented from the geological records elsewhere, for instance during the 1256 Al Madinah eruption in Saudi Arabia [59].

Numerous research works have been completed with a prospect to provide volcanic hazard maps [60–65] as well as some sort of tools to communicate to communities volcanic hazards [66], co-design, co-product programs and products to help developing a more resilient community that can live with the volcanoes and their hazards [28, 67–78]. In recent years, there is also a strong movement visible

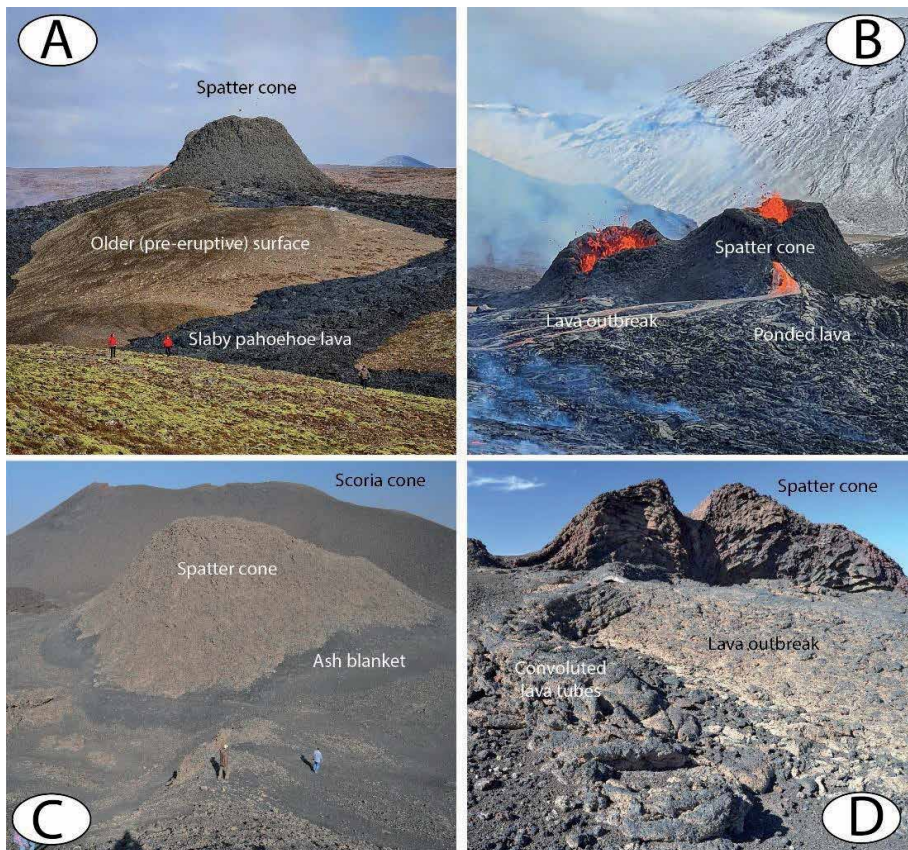


Figure 2. Lessons from the current volcanic eruption of the Geldingadalir volcano in Iceland can be used to better understand the first moments and processes of a volcano growth in basaltic systems (A, B). Flow localization formed vents that emitted lava and spatter creating steep spatter cones (A) through mild explosive event (B). To see this process in real can help to interpret similar volcanic successions elsewhere such as those formed during the 1256 Al Madinah eruption in Saudi Arabia (C) or during the Pleistocene and Holocene in the Harrat Khaybar, also in Saudi Arabia (D). The solidified inner structure of a spatter cone shows well the steep pile of spatters accumulated around the vent (D) similar how such process take place right now in Iceland (B). Photos of A and B are from the photo collection of Viktória Komjáti.

to conduct research jointly with other experts in archaeology for instance to better understand the impact of volcanism on early civilizations [79–93].

3. Volcanic geoheritage

Moreover in the last decades a boom of research is visible where volcanic geoheritage used and utilized as a main opportunity to develop geoeeducation programs accompanied with effective geoconservation programs (commonly formed as a result of citizen science, and co-design) to build a more resilience society against volcanic hazard [94–104]. Even new terms appeared such as social volcanology or paleo-social volcanology steamed from social geology to express the newly and rapidly evolving discipline formed recently [72, 105]. Most of this works based on a more precise and process-oriented understanding of volcanic systems such as monogenetic volcanoes. The dynamic progression on volcanic geoheritage, geodiversity and geotourism research made a new aspect of volcano science where interface between natural sciences, humanities and social sciences meet and put into practical sense making volcanology a more relevant science to human society and our natural environment

[103, 106]. In addition, an increased recognition of traditional knowledge and cultural aspects of volcanoes explored and made mainstream research outputs [107–111].

4. New advances in volcanology as a transdisciplinary science

Looking into detail of the recent evolution of volcano science we analyzed the accessible, mainstream literature data stored in the Thomson Reuters, Web of Sciences Core Database. Volcanology has two premier publication avenue such as Bulletin of Volcanology (Springer) [BV] that is also the official journal of the International Association of Volcanology and Chemistry of the Earth’s Interior. In addition, Journal of Volcanology and Geothermal Research (Elsevier) (JVGR) also considered as a main medium for scientific communication within volcanology. We were curious to see what research trend can be deduced from the published researches in the last 2 years (2019 to 2021, 20 April 2021) within these two premier Journals. We used search operators to identify keywords (including Author keywords and Web of Science generated keyword set). We understand that these keywords commonly reflecting general “umbrella subjects” and not obviously the main subject of the specific published papers, but we still think they are representative and informative to identify trends. For this, we created word clouds by using the WordArt online tool [<https://wordart.com/>] to visualize main keywords (larger words in more central position reflects more common appearance of such keywords). For the Bulletin of Volcanology 184 paper was identified. From these 184 papers keywords were extracted, while common non-informative words deleted as well as too generic words such as *volcanism, volcano, volcanic, eruption, magma, lava pyroclastic and based*. In addition, manually all the location keywords were deducted and inserted to a separate file to see the common locations research focused in the past 2 years. Following this method, the **Flow, Ash, Dome Size, Current** words stand out reflecting the research output intensity around tephra and various geophysical flow research (**Figure 3A**). The rest of the keywords show a fairly even distribution across the entire spectrum of subjects. Applying the similar techniques to the JVGR, on the basis of 557 papers published in the same period of time showed keywords as most common to be **System, Flow, Evolution, Model, Isotope, Hydrothermal, Fluid** (**Figure 3B**). To look at the common locations current volcanology research associated with published within BV showed **Bogoslof, Kilauea,**

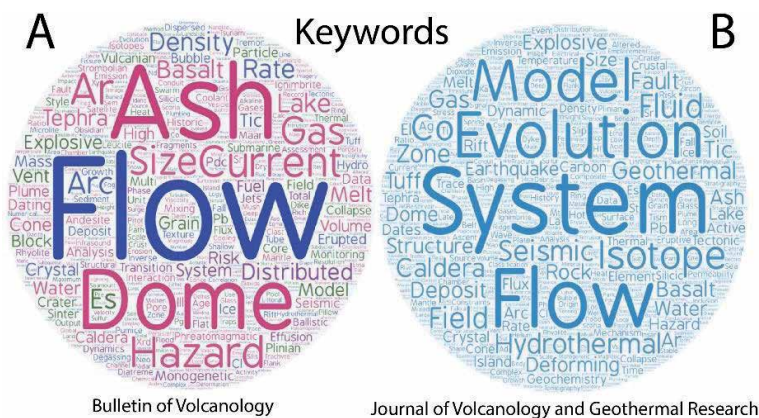


Figure 3. Keywords identified on Web of Science Core Database papers published since 2019 in the two major volcanology scientific magazines, Bulletin of Volcanology (A) and Journal of Volcanology and Geothermal Research (B).

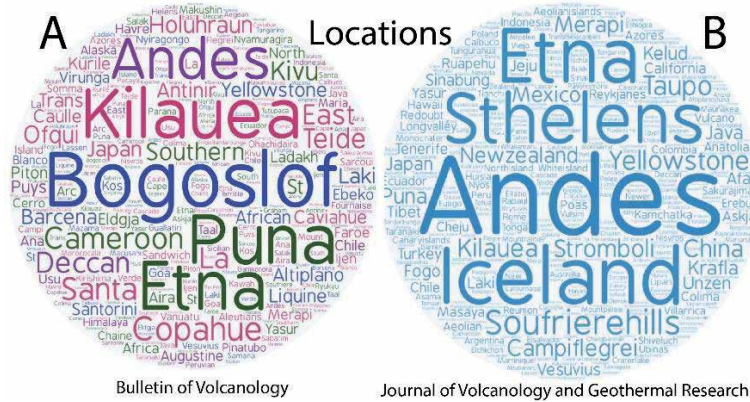


Figure 4. Location keywords identified on Web of Science Core Database in the papers published since 2019 in the two major volcanology scientific magazines, *Bulletin of Volcanology* (A) and *Journal of Volcanology and Geothermal Research* (B).

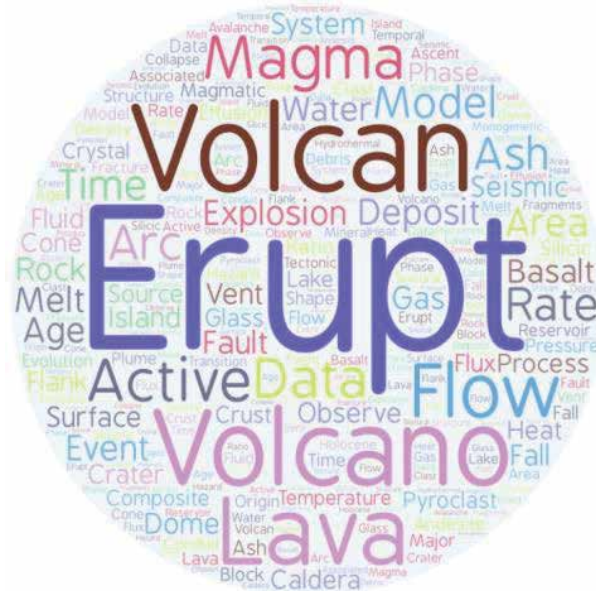


Figure 5. Word map derived from the title and abstracts of the last 12 months papers published in BV and JVGR based on Web of Science core database.

Puna, Andes and Etna as top for BV (**Figure 4A**), while **Andes, StHelens, Etna, and Iceland** having the most common location keywords for JVGR (**Figure 4B**).

The following method was applied for a narrower time frame (**last 12 months**) but looking at the **title, keywords and abstract** of the published papers in the two major volcanology magazines (**Figure 5**). From the 101 published papers the **Erupt, Volcan, Volcano, Lava, Magma** words were the most commonly used while in the “second” abundance more process-related words such as **Flow, Deposit, Data, Model, Explosion, System, Observe** etc. appeared.

As volcanic geoheritage became an important aspect of volcano science recently we checked the main keywords associated with researches identified under volcanic geoheritage topic search term from the Web of Sciences Core Databases. A total of

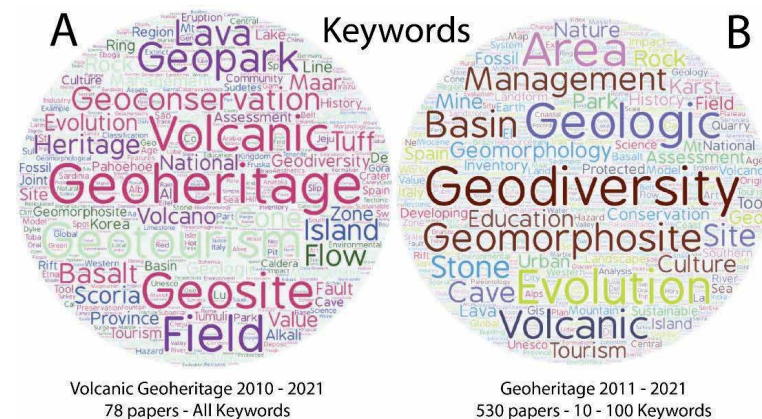


Figure 6. Word map of keywords identified from the Web of Science Core Database. (A) Keywords from the 78 published papers returned from topic search for volcanic geoheritage. (B) Keywords identified from 530 papers returned from topic search for geoheritage. Please note that non-generic keywords were excluded from this map that were too general to see the details of research outputs hence keyword resulted 10 to 100 scores were plotted on the diagram.

79 paper has been identified in the time period between 2010 and 2021, suggesting the very recent formulation of this term (**Figure 6A**). To see this results in a perspective we made a keyword search for Geoheritage that resulted a total of 530 published papers between 2011 and 2021 (only 10 years!!). By removing the most non-generic terms such as **Heritage, Geotour, Geoheritage, Geoconservation, Geosite and Geopark**, focusing on those keywords that were identified between 10 and 100 occasions we can see that **Volcanic** is a common keyword within geoheritage studies (**Figure 6B**). This suggests that volcano science gradually build a strong corner within geoheritage, geoconservation and geoeducation. For curiosity we made a survey to check the published papers by searching **Volcanic AND Transdisciplinary** that resulted 8 published papers between 2015 and 2021 indicating the recent identification of this technical terms.

In summary we can say that volcano science is a very colorful and fast evolving science. Its transdisciplinary nature is getting more and more recognized and applied for a very diverse array of research areas and practical approaches to community engagement. This book offers another snapshot to this process.

Conflict of interest

The author declares no conflict of interest.

Author details


Károly Németh^{1,2}

1 School of Agriculture and Environment, Massey University, Palmerston North, New Zealand

2 Institute of Earth Physics and Space Science, Sopron, Hungary

*Address all correspondence to: k.nemeth@massey.ac.nz

IntechOpen

© 2021 The Author(s). Licensee IntechOpen. This chapter is distributed under the terms of the Creative Commons Attribution License (<http://creativecommons.org/licenses/by/3.0>), which permits unrestricted use, distribution, and reproduction in any medium, provided the original work is properly cited. 

References

- [1] Acuna V, Roldan F, Tironi M, Juzam L. The Geo-Social Model: A Transdisciplinary Approach to Flow-Type Landslide Analysis and Prevention. *Sustainability*. 2021;13(5).
- [2] Bernardes FF. Landscape Ecology According to Geography: A Proposal of Tools for the Analysis and Management of the Environment. In: Luc M, Somorowska U, Szmanda JB, editors. *Landscape Analysis and Planning: Geographical Perspectives*. Springer Geography 2015. p. 175-185.
- [3] Carmen E, Watt A, Carvalho L, Dick J, Fazey I, Garcia-Blanco G, et al. Knowledge needs for the operationalisation of the concept of ecosystem services. *Ecosystem Services*. 2018;29:441-451.
- [4] Costanza R, Kubiszewski I. The authorship structure of “ecosystem services” as a transdisciplinary field of scholarship. *Ecosystem Services*. 2012;1(1):16-25.
- [5] de Long C, Cappy S, Finckh M, Funk D. A transdisciplinary analysis of water problems in the mountainous karst areas of Morocco. *Engineering Geology*. 2008;99(3-4):228-238.
- [6] Dendoncker N, Turkelboom F, Boeraeve F, Boerema A, Broekx S, Fontaine C, et al. Integrating Ecosystem Services values for sustainability? Evidence from the Belgium Ecosystem Services community of practice. *Ecosystem Services*. 2018;31:68-76.
- [7] Guimaraes MH, Balle-Beganton J, Bailly D, Newton A, Boski T, Dentinho T. Transdisciplinary conceptual modeling of a social-ecological system-A case study application in Terceira Island, Azores. *Ecosystem Services*. 2013;3:E22-E31.
- [8] Jacobs S, Dendoncker N, Martin-Lopez B, Barton DN, Gomez-Baggethun E, Boeraeve F, et al. A new valuation school: Integrating diverse values of nature in resource and land use decisions. *Ecosystem Services*. 2016;22:213-220.
- [9] Jax K, Furman E, Saarikoski H, Barton DN, Delbaere B, Dick J, et al. Handling a messy world: Lessons learned when trying to make the ecosystem services concept operational. *Ecosystem Services*. 2018;29:415-427.
- [10] Lamare S, Blanchard G. Structuring transdisciplinary research for environment and sustainable development at the University of La Rochelle. *Actualite Chimique*. 2008(325):26-29.
- [11] Luederitz C, Brink E, Gralla F, Hermelingmeier V, Meyer M, Niven L, et al. A review of urban ecosystem services: six key challenges for future research. *Ecosystem Services*. 2015;14:98-112.
- [12] Mauser W, Klepper G, Rice M, Schmalzbauer BS, Hackmann H, Leemans R, et al. Transdisciplinary global change research: the co-creation of knowledge for sustainability. *Current Opinion in Environmental Sustainability*. 2013;5(3):420-431.
- [13] Pop IG, Vaduva S, Talpos MF. Energetic Sustainability and the Environment: A Transdisciplinary, Economic-Ecological Approach. *Sustainability*. 2017;9(6).
- [14] Ranger S, Kenter JO, Bryce R, Cumming G, Dapling T, Lawes E, et al. Forming shared values in conservation management: An interpretive-deliberative-democratic approach to including community voices. *Ecosystem Services*. 2016;21:344-357.
- [15] Rincon-Ruiz A, Arias-Arevalo P, Hernandez JMN, Cotler H, Caso MA,

Meli P, et al. Applying integrated valuation of ecosystem services in Latin America: Insights from 21 case studies. *Ecosystem Services*. 2019;36.

[16] Ryfield F, Cabana D, Brannigan J, Crowe T. Conceptualizing 'sense of place' in cultural ecosystem services: A framework for interdisciplinary research. *Ecosystem Services*. 2019;36.

[17] Spangenberg JH, Gorg C, Settele J. Stakeholder involvement in ESS research and governance: Between conceptual ambition and practical experiences - risks, challenges and tested tools. *Ecosystem Services*. 2015;16:201-211.

[18] Pardo N, Pulgarin B, Betancourt V, Lucchi F, Jeronimo Valencia L. Facing geological mapping at low-latitude volcanoes: The Dona Juana Volcanic Complex study-case, SW-Colombia. *Journal of Volcanology and Geothermal Research*. 2019;385:46-67.

[19] Martí J, Groppelli G, Brum da Silveira A. Volcanic stratigraphy: A review. *Journal of Volcanology and Geothermal Research*. 2018;357:68-91.

[20] Tchamabé BC, Kereszturi G, Németh K, Carrasco-Núñez G. How polygenetic are monogenetic volcanoes: Case studies of some complex maar-diatreme volcanoes. In: Németh K, editor. *Updates in Volcanology – From Volcano Modelling to Volcano Geology Rijeka, Croatia: inTech Open; 2016*.

[21] Burchardt S, Galland O. Studying volcanic plumbing systems; multi-disciplinary approaches to a multi-faceted problem. In: Németh K, editor. *Updates in Volcanology – From Volcano Modelling to Volcano Geology Rijeka, Croatia: inTech Open; 2016*.

[22] Di Traglia F, Pistolesi M, Rosi M, Bonadonna C, Fusillo R, Roverato M. Growth and erosion: The volcanic geology and morphological evolution of

La Fossa (Island of Vulcano, Southern Italy) in the last 1000 years. *Geomorphology*. 2013;194:94-107.

[23] Németh K, Palmer J. Geological mapping of volcanic terrains: Discussion on concepts, facies models, scales, and resolutions from New Zealand perspective. *Journal of Volcanology and Geothermal Research*. 2019;385:27-45.

[24] Lucchi F. On the use of unconformities in volcanic stratigraphy and mapping: Insights from the Aeolian Islands (southern Italy). *Journal of Volcanology and Geothermal Research*. 2019;385:3-26.

[25] Bischoff A, Nicol A, Barrier A, Wang H. Paleogeography and volcanic morphology reconstruction of a buried monogenetic volcanic field (part 2). *Bulletin of Volcanology*. 2019;81(9).

[26] Pardo N, Espinosa ML, Gonzalez-Arango C, Cabrera MA, Salazar S, Archila S, et al. Working resilience in the Dona Juana Volcano-Paramo, Northern Andes (Colombia): A transdisciplinary view. *Natural Hazards*. 2021.

[27] Petterson MG. Interconnected geoscience for international development. *Episodes*. 2019;42(3):225-233.

[28] Cronin SJ, Gaylord DR, Charley D, Alloway BV, Wallez S, Esau JW. Participatory methods of incorporating scientific with traditional knowledge for volcanic hazard management on Ambae Island, Vanuatu. *Bulletin of Volcanology*. 2004;66(7):652-668.

[29] Nunn PD. Fished up or thrown down: The geography of Pacific Island origin myths. *Annals Of The Association Of American Geographers*. 2003;93(2):350-364.

[30] Nunn PD, Lancini L, Franks L, Compatangelo-Soussignan R,

- McCallum A. Maar Stories: How Oral Traditions Aid Understanding of Maar Volcanism and Associated Phenomena during Preliterate Times. *Annals of the American Association of Geographers*. 2019;109(5):1618-1631.
- [31] Petterson MG, Cronin SJ, Taylor PW, Tolia D, Papabatu A, Toba T, et al. The eruptive history and volcanic hazards of Savo, Solomon Islands. *Bulletin of Volcanology*. 2003;65(2-3):165-181.
- [32] Cronin SJ, Ferland MA, Terry JP. Nabukelevu volcano (Mt. Washington), Kadavu - a source of hitherto unknown volcanic hazard in Fiji. *Journal Of Volcanology And Geothermal Research*. 2004;131(3-4):371-396.
- [33] Cronin SJ, Neall VE. Impacts of volcanism on pre-European inhabitants of Taveuni, Fiji. *Bulletin of Volcanology*. 2000;62(3):199-213.
- [34] Németh K, Cronin SJ. Volcanic structures and oral traditions of volcanism of Western Samoa (SW Pacific) and their implications for hazard education. *Journal of Volcanology and Geothermal Research*. 2009;186(3-4):223-237.
- [35] de Vries BvW, Byrne P, Delcamp A, Einarson P, Gogus O, Guilbaud M-N, et al. A global framework for the Earth: putting geological sciences in context. *Global and Planetary Change*. 2018;171:293-321.
- [36] Tibaldi A, Bistacchi A, Pasquarè FA, Vezzoli L. Extensional tectonics and volcano lateral collapses: insights from Ollagüe volcano (Chile-Bolivia) and analogue modelling. *Terra Nova*. 2006;18(4):282-289.
- [37] Feeley TC, Davidson JP, Armendia A. The volcanic and magmatic evolution of volcan Ollague, a high-K, late Quaternary stratovolcano in the Andean Central Volcanic Zone. *Journal of Volcanology and Geothermal Research*. 1993;54(3-4):221-245.
- [38] Escudero G, Németh K, Torres I, Ureta G, Józsa S, Sági T. Morfometría y petrología del domo de lava El Ingenio, Antofagasta, Chile. 1st ALVO Congress. Antofagasta, Chile 2020.
- [39] Wörner G, Hammerschmidt K, Henjes-Kunst F, Lezaun J, Wilke H. Geochronology (Ar-40/Ar-39, K-Ar and He-exposure ages) of Cenozoic magmatic rocks from Northern Chile (18-22 degrees S): implications for magmatism and tectonic evolution of the central Andes. *Revista Geologica De Chile*. 2000;27(2):205-240.
- [40] Bebbington MS, Stirling MW, Cronin S, Wang T, Jolly G. National-level long-term eruption forecasts by expert elicitation. *Bulletin of Volcanology*. 2018;80(6).
- [41] Stirling M, Bebbington M, Brenna M, Cronin S, Christophersen A, Deline N, et al. Conceptual Development of a National Volcanic Hazard Model for New Zealand. *Frontiers in Earth Science*. 2017;5.
- [42] Stirling M, McVerry G, Gerstenberger M, Litchfield N, Van Dissen R, Berryman K, et al. National Seismic Hazard Model for New Zealand: 2010 Update. *Bulletin of the Seismological Society of America*. 2012;102(4):1514-1542.
- [43] Bebbington MS. Spatio-volumetric hazard estimation in the Auckland volcanic field. *Bulletin of Volcanology*. 2015;77(5).
- [44] Smith IEM, Németh K. Source to surface model of monogenetic volcanism: a critical review In: Németh K, Carrasco-Nuñez G, Aranda-Gomez JJ, Smith IEM, editors. *Monogenetic Volcanism*. Geological Society of London Special Publications. Geological Society of London, Special

Publications. Bath, UK: The Geological Society Publishing House; 2017. p. 1-28.

[45] Németh K, Kereszturi G. Monogenetic volcanism: personal views and discussion. *International Journal of Earth Sciences*. 2015;104(8):2131-2146.

[46] Jankovics MÉ, Harangi S, Németh K, Kiss B, Ntaflos T. A complex magmatic system beneath the Kissomlyó monogenetic volcano (western Pannonian Basin): Evidence from mineral textures, zoning and chemistry. *Journal of Volcanology and Geothermal Research*. 2015;301:38-55.

[47] Báez W, Carrasco-Nunez G, Giordano G, Viramonte J, Chiodi A. The polycyclic scoria cones of the Antofagasta de la Sierra basin, Southern Puna Plateau, Argentina. In: Németh K, Carrasco-Nuñez G, Aranda-Gomez JJ, Smith IEM, editors. *Monogenetic Volcanism*. Geological Society of London Special Publications. 446. Bath, UK: The Geological Society Publishing House; 2017.

[48] Fulop A, Kurszlauskis S. Monogenetic versus polygenetic kimberlite volcanism: In-depth examination of the Tango Extension Super Structure, Attawapiskat kimberlite field, Ontario. In: Németh K, Carrasco-Nuñez G, Aranda-Gomez JJ, Smith IEM, editors. *Monogenetic Volcanism*. Geological Society of London Special Publications. 446. Bath, UK: The Geological Society Publishing House; 2017.

[49] Hencz M, Karátson D, Németh K, Biró T. A Badacsony freatomagmás piroklasztitösszlete: következtetések a monogenetikus bazaltvulkáni működés folyamataira és formáira = The phreatomagmatic pyroclastic sequence of the Badacsony Hill: implications for the processes and landforms of monogenetic basaltic volcanism. *Földtani közlöny*. 2017;147(3):297-310.

[50] Murcia H, Borrero C, Németh K. Overview and plumbing system implications of monogenetic volcanism in the northernmost Andes' volcanic province. *Journal of Volcanology and Geothermal Research*. 2019;383:77-87.

[51] Brenna M, Németh K, Cronin SJ, Sohn YK, Smith IEM, Wijbrans J. Co-located monogenetic eruptions ~200 kyr apart driven by tapping vertically separated mantle source regions, Chagwido, Jeju Island, Republic of Korea. *Bulletin of Volcanology*. 2015;77(5).

[52] Sohn YK, Cronin SJ, Brenna M, Smith IEM, Németh K, White JDL, et al. Ilchulbong tuff cone, Jeju Island, Korea, revisited: A compound monogenetic volcano involving multiple magma pulses, shifting vents, and discrete eruptive phases. *Geological Society of America Bulletin*. 2012;124(3-4): 259-274.

[53] Kósik S, Németh K, Lexa J, Procter JN. Understanding the evolution of a small-volume silicic fissure eruption: Puketerata Volcanic Complex, Taupo Volcanic Zone, New Zealand. *Journal of Volcanology and Geothermal Research*. 2018.

[54] de Silva S, Lindsay JM. Chapter 15 - Primary volcanic landforms. In: Sigurdsson H, editor. *The Encyclopedia of Volcanoes (Second Edition)*. Amsterdam: Academic Press; 2015. p. 273-297.

[55] Murcia H, Németh K, El-Masry NN, Lindsay JM, Moufti MRH, Wameyo P, et al. The Al-Du'aythah volcanic cones, Al-Madinah City: implications for volcanic hazards in northern Harrat Rahat, Kingdom of Saudi Arabia. *Bulletin of Volcanology*. 2015;77(6).

[56] Jones TJ, Llewellyn EW, Houghton BF, Brown RJ, Vye-Brown C. Proximal lava drainage controls on

- basaltic fissure eruption dynamics. *Bulletin of Volcanology*. 2017;79(11).
- [57] Brown RJ, Kavanagh J, Sparks RSJ, Tait M, Field M. Mechanically disrupted and chemically weakened zones in segmented dike systems cause vent localization: Evidence from kimberlite volcanic systems. *Geology*. 2007;35(9): 815-818.
- [58] Moufti MR, Németh K. The intra-continental Al Madinah Volcanic Field, Western Saudi Arabia: a proposal to establish harrat Al Madinah as the first volcanic geopark in the Kingdom of Saudi Arabia. *Geoheritage*. 2013;5(3):185-206.
- [59] Moufti MR, Németh K, Murcia H, Lindsay JM, El-Masry N. Geosite of a steep lava spatter cone of the 1256 AD, Al Madinah eruption, Kingdom of Saudi Arabia. *Central European Journal of Geosciences*. 2013;5(2):189-195.
- [60] Neri M, Le Cozannet G, Thierry P, Bignami C, Ruch J. A method for multi-hazard mapping in poorly known volcanic areas: an example from Kanlaon (Philippines). *Natural Hazards and Earth System Sciences*. 2013;13(8):1929-1943.
- [61] Procter JN, Cronin SJ, Platz T, Patra A, Dalbey K, Sheridan M, et al. Mapping block-and-ash flow hazards based on Titan 2D simulations: a case study from Mt. Taranaki, NZ. *Natural Hazards*. 2010;53(3):483-501.
- [62] Sieron K, Siebe C. Revised stratigraphy and eruption rates of Ceboruco stratovolcano and surrounding monogenetic vents (Nayarit, Mexico) from historical documents and new radiocarbon dates. *Journal of Volcanology and Geothermal Research*. 2008;176(2):241-264.
- [63] Macias JL, Capra L, Arce JL, Espindola JM, Garcia-Palomo A, Sheridan MF. Hazard map of El Chichon volcano, Chiapas, Mexico: Constraints posed by eruptive history and computer simulations. *Journal of Volcanology and Geothermal Research*. 2008;175(4):444-458.
- [64] Damiani ML, Groppelli G, Norini G, Bertino E, Gigliuto A, Nucita A. A lava flow simulation model for the development of volcanic hazard maps for Mount Etna (Italy). *Computers & Geosciences*. 2006;32(4):512-526.
- [65] Jimenez D, Becerril L, Bartolini S, Escobar D, Marti J. Making a qualitative volcanic-hazards map by combining simulated scenarios: An example for San Miguel Volcano (El Salvador). *Journal of Volcanology and Geothermal Research*. 2020;395.
- [66] Pareschi MT, Cavarra L, Favalli M, Giannini F, Meriggi A. GIS and volcanic risk management. *Natural Hazards*. 2000;21(2-3):361-379.
- [67] Leonard GS, Stewart C, Wilson TM, Procter JN, Scott BJ, Keys HJ, et al. Integrating multidisciplinary science, modelling and impact data into evolving, syn-event volcanic hazard mapping and communication: A case study from the 2012 Tongariro eruption crisis, New Zealand. *Journal of Volcanology and Geothermal Research*. 2014;286:208-232.
- [68] Andreastuti S, Paripurno E, Gunawan H, Budianto A, Syahbana D, Pallister J. Character of community response to volcanic crises at Sinabung and Kelud volcanoes. *Journal of Volcanology and Geothermal Research*. 2019;382:298-310.
- [69] Ricci T, Barberi F, Davis MS, Isaia R, Nave R. Volcanic risk perception in the Campi Flegrei area. *Journal of Volcanology and Geothermal Research*. 2013;254:118-130.
- [70] Rolandi G. Volcanic hazard at Vesuvius: An analysis for the revision of

the current emergency plan. *Journal of Volcanology and Geothermal Research*. 2010; 189(3-4):347-362.

[71] Johannesdottir G, Gisladdottir G. People living under threat of volcanic hazard in southern Iceland: vulnerability and risk perception. *Natural Hazards and Earth System Sciences*. 2010;10(2):407-420.

[72] Donovan K. Doing social volcanology: exploring volcanic culture in Indonesia. *Area*. 2010;42(1):117-126.

[73] Limon-Hernandez C, Macias JL. Volcanic hazards and risk perception at the "Zoque" community of Chapultenango: El Chichon volcano, Chiapas, Mexico. *Geofisica Internacional*. 2009;48(1):113-132.

[74] Todesco M, Neri A, Demaria C, Marmo C, Macedonio G. E VIVO: Virtual eruptions at Vesuvius; A multimedia tool to illustrate numerical modeling to a general public. *Journal Of Volcanology And Geothermal Research*. 2006;155(3-4):323-328.

[75] Gregg CE, Houghton BF, Paton D, Swanson DA, Johnston DM. Community preparedness for lava flows from Mauna Loa and Hualalai volcanoes, Kona, Hawai'i. *Bulletin Of Volcanology*. 2004;66(6):531-540.

[76] Dominey-Howes D, Minos-Minopoulos D. Perceptions of hazard and risk on Santorini. *Journal Of Volcanology And Geothermal Research*. 2004;137(4):285-310.

[77] Cronin SJ, Petterson MG, Taylor PW, Biliki R. Maximising multi-stakeholder participation in government and community volcanic hazard management programs; A case study from Savo, Solomon Islands. *Natural Hazards*. 2004;33(1):105-136.

[78] Paton D, Millar M, Johnston D. Community resilience to volcanic

hazard consequences. *Natural Hazards*. 2001;24(2):157-169.

[79] Cole L. Volcanic hazards and disasters in human antiquity. *American Journal Of Archaeology*. 2003;107(4):668-670.

[80] Siebe C, Rodriguez-Lara V, Schaaf P, Abrams M. Radiocarbon ages of Holocene Pelado, Guespalapa, and Chichinautzin scoria cones, south of Mexico City: implications for archaeology and future hazards. *Bulletin Of Volcanology*. 2004;66(3):203-225.

[81] Siebe C, Macías JL. Volcanic hazards in the Mexico City metropolitan area from eruptions at Popocatepetl, Nevado de Toluca, and Jocotitlán stratovolcanoes and monogenetic scoria cones in the Sierra Chichinautzin Volcanic Field. In: Siebe C, Macías JL, Aguirre-Díaz GJ, editors. *Neogene-Quaternary Continental Margin Volcanism: A perspective from México*. Special Paper of the Geological Society of America: 402. Boulder, Colorado: Geological Society of America; 2006. p. 253-329.

[82] De Benedetti AA, Funicello R, Giordano G, Diano G, Caprilli E, Paterne M. Volcanology, history and myths of the Lake Albano maar (Colli Albani volcano, Italy). *Journal of Volcanology and Geothermal Research*. 2008;176(3):387-406.

[83] Rossi MJ, Kesseli R, Liuha P, Meneses JS, Bustamante J. A preliminary archaeological and environmental study of pre-Columbian burial towers at Huachacalla, Bolivian Altiplano. *Geoarchaeology-an International Journal*. 2002;17(7):633-648.

[84] Riede F, Barnes GL, Elson MD, Oetelaar GA, Holmberg KG, Sheets P. Prospects and pitfalls in integrating volcanology and archaeology: A review. *Journal of Volcanology and Geothermal Research*. 2020;401.

- [85] Karátson D, Telbisz T, Gertisser R, Strasser T, Nomikou P, Druitt T, et al. Constraining the landscape of Late Bronze Age Santorini prior to the Minoan eruption: Insights from volcanological, geomorphological and archaeological findings. *Journal of Volcanology and Geothermal Research*. 2020;401.
- [86] Groucutt HS. Volcanism and human prehistory in Arabia. *Journal of Volcanology and Geothermal Research*. 2020;402.
- [87] Athanassas CD, Modis K, Aliccek MC, Theodorakopoulou K. Contouring the Cataclysm: A Geographical Analysis of the Effects of the Minoan Eruption of the Santorini Volcano. *Environmental Archaeology*. 2018;23(2):160-176.
- [88] Chevrel MO, Siebe C, Guilbaud M-N, Salinas S. The AD 1250 El Metate shield volcano (Michoacan): Mexico's most voluminous Holocene eruption and its significance for archaeology and hazards. *Holocene*. 2016;26(3):471-488.
- [89] Riede F. Towards a science of past disasters. *Natural Hazards*. 2014;71(1):335-362.
- [90] Williams M. The similar to 73 ka Toba super-eruption and its impact: History of a debate. *Quaternary International*. 2012;258:19-29.
- [91] Alvarado GE, Soto GJ. Volcanoes in the pre-Columbian life, legend, and archaeology of Costa Rica (Central America). *Journal of Volcanology and Geothermal Research*. 2008;176(3):356-362.
- [92] Siebe C. Age and archaeological implications of Xitle volcano, southwestern Basin of Mexico-City. *Journal of Volcanology and Geothermal Research*. 2000;104(1-4):45-64.
- [93] Lowe DJ, Newnham RM, McFadgen BG, Higham TFG. Tephra and New Zealand archaeology. *Journal Of Archaeological Science*. 2000;27(10):859-870.
- [94] Quesada-Roman A, Zangmo GT, Perez-Umana D. Geomorphosite Comparative Analysis in Costa Rica and Cameroon Volcanoes. *Geoheritage*. 2020;12(4).
- [95] Dóniz-Páez J, Beltrán-Yanes E, Becerra-Ramírez R, Pérez NM, Hernández PA, Hernández W. Diversity of volcanic geoheritage in the Canary Islands, Spain. *Geosciences*. 2020;10:390.
- [96] Kil Y, Ahn KS, Woo KS, Lee KC, Jwa Y-J, Jung W, et al. Geoheritage Values of the Quaternary Hantangang River Volcanic Field in the Central Korean Peninsula. *Geoheritage*. 2019;11(3):765-782.
- [97] Fepuleai A, Németh K. Volcanic Geoheritage of Landslides and Rockfalls on a Tropical Ocean Island (Western Samoa, SW Pacific). *Geoheritage*. 2019;11(2):577-596.
- [98] Zacek V, Hradecky P, Kycl P, Sevcik J, Novotny R, Baron I. The Somoto Grand Canyon (Nicaragua)-a Volcanic Geoheritage Site One Decade After Discovery: from Field Geological Mapping to the Promotion of a Geopark. *Geoheritage*. 2017;9(3):299-309.
- [99] Szepesi J, Harangi S, Ésik Z, Novak TJ, Lukács R, Soos I. Volcanic Geoheritage and Geotourism Perspectives in Hungary: a Case of an UNESCO World Heritage Site, Tokaj Wine Region Historic Cultural Landscape, Hungary. *Geoheritage*. 2017;9(3):329-349.
- [100] Sheth H, Samant H, Patel V, D'Souza J. The Volcanic Geoheritage of the Elephanta Caves, Deccan Traps, Western India. *Geoheritage*. 2017;9(3):359-372.

- [101] Rapprich V, Lisec M, Fiferna P, Závada P. Application of Modern Technologies in Popularization of the Czech Volcanic Geoheritage. *Geoheritage*. 2017;this volume.
- [102] Németh K, Wu J, Sun C, Liu J. Update on the Volcanic Geoheritage Values of the Pliocene to Quaternary Arxan–Chaihe Volcanic Field, Inner Mongolia, China. *Geoheritage*. 2017;9(3):279-297.
- [103] Németh K, Casadevall T, Moufti MR, Marti J. Volcanic Geoheritage. *Geoheritage*. 2017;9(3):251-254.
- [104] Migon P, Pijet-Migon E. Overlooked geomorphological component of volcanic geoheritage-diversity and perspectives for tourism industry, Pogrze Kaczawskie Region, SW Poland. *Geoheritage*. 2016;8(4):333-350.
- [105] Riede F. Doing palaeo-social volcanology: Developing a framework for systematically investigating the impacts of past volcanic eruptions on human societies using archaeological datasets. *Quaternary International*. 2019;499:266-277.
- [106] Casadevall TJ, Tormey D, Roberts J. World Heritage Volcanoes: Classification, gap analysis, and recommendations for future listings. Gland, Switzerland: IUCN; 2019. 68 p.
- [107] Fepuleai A, Weber E, Németh K, Muliaina T, Iese V. Eruption Styles of Samoan Volcanoes Represented in Tattooing, Language and Cultural Activities of the Indigenous People. *Geoheritage*. 2017;9(3):395-411.
- [108] Lewis ID. Linking geoheritage sites: Geotourism and a prospective Geotrail in the Flinders Ranges World Heritage Nomination area, South Australia. *Australian Journal of Earth Sciences*. 2020;67(8):1195-1210.
- [109] Gravis I, Németh K, Twemlow C, Németh B. The Case for Community-Led Geoheritage and Geoconservation Ventures in Māngere, South Auckland, and Central Otago, New Zealand. *Geoheritage*. 2020;12(1).
- [110] Procter J, Németh K. Recognising indigenous peoples values and knowledge systems in Geoheritage: Case studies from New Zealand and the South Pacific. European Geosciences Union General Assembly 2017. Vienna, Austria: European Geosciences Union; 2017.
- [111] Turner S. Geoheritage and Geoparks: One (Australian) Woman's Point of View. *Geoheritage*. 2013;5(4):249-264.

Section 2

Source and Magmatic
Plumbing Systems

Modeling of Olivine and Clinopyroxene Fractionation in Intracontinental Alkaline Basalts: A Case Study from the Carpathian-Pannonian Region

Tamás Sági, Szabolcs Harangi and Theodoros Ntaflou

Abstract

Besides mantle peridotites primary basaltic melts are the best tool to investigate upper mantle petrology and geochemistry. However, de facto primitive melts are hard to found, as basaltic melts usually go through a fractionation process during their ascent towards the surface. Most primary melt calculators are based on the major or trace element compositions of olivine-phyric ocean island basalts and peridotites and are less accurate if clinopyroxene fractionation occurred. In this chapter a new fractionation modeling method of alkaline basalts will be introduced, which has been published earlier only in Hungarian. Olivine \pm clinopyroxene fractionation of four basaltic volcanoes have been modeled from different Miocene-Quaternary volcanic fields from the Carpathian-Pannonian Region (Stiavnica (Selmec) VF, Novohrad-Gemer (Nógrád-Gömör) VF, Perşani Mts. (Persányi Mts.) VF and from the Lucaret-Sanovița (Lukácskő-Sziklás) volcano.

Keywords: olivine, clinopyroxene, fractionation, intracontinental, monogenetic, alkaline basalt

1. Introduction

Intracontinental monogenetic alkaline basaltic volcanic fields consist of various types of small-scale volcanoes (e.g. scoria cones, tuff rings, maars, diatremes and related lava flows) [1]. However, the size of the volcanic edifices is usually smaller than 1 km³ and they are short-lived volcanoes, the total magma output rate of a monogenetic volcanic field can be compared with a polygenetic volcano [1]. The lifespan of the volcanic field can last for several millions of years (e.g. [2, 3]). Based on the geochemical and petrographic characteristics of the individual volcanoes, monogenetic basaltic volcanic fields could be very diverse both spatially and temporally (e.g. [4]). This diversity depends on several factors. Basaltic melt could be generated in the asthenosphere or in the lithosphere. Partial melting of the asthenosphere could be caused by a mantle plume (e.g. [5–7]), or mantle flows related to active rifting, collision or lithospheric delamination (e.g. [8–10]). Melt generation in the lithospheric mantle is often related to metasomatized peridotites

and pyroxenites which are rich in volatiles and alkalis (e.g. [3, 11–13]). Primitive alkaline basalts are excellent tools to study the petrological and geochemical heterogeneity and thermal characteristics of the upper mantle and the type of melt generation (e.g. [5, 14–17]), however a seemingly primitive basaltic magma could have undergone fractionation [18]. Only with fairly accurate knowledge on the primary melt composition it is possible to reveal the whole story and characterize the source region of the basalts (e.g. [14, 19, 20]).

To find primary melt compositions we have to study their ascent history and characterize the melt evolution from the source to the surface. Most common methods are based on the main and trace elements composition of the bulk rock (e.g. [14, 18–21]), and these methods are often less accurate if clinopyroxene fractionation occurred or if the source rock contained pyroxenite. To avoid the “pyroxene problem” a new olivine +/- clinopyroxene fractionation method has been developed by [22] and first published by [23] in Hungarian. Here we will show the method accuracy and some fractionation calculation results of alkaline basalts from [22, 23].

2. Concept of olivine and clinopyroxene fractionation modeling

Primitive magma compositions derived from less fractionated alkaline basalts are key tools to characterize the source region of upper mantle melts (i.e. petrology and geochemistry, depth and degree of melting, potential temperature of the upper mantle) (e.g. [7, 14, 17, 19, 24, 25]).

Most well-known primitive melt calculations are based on olivine addition or subtraction from bulk rock compositions of alkaline basalts from OIBs and LIPs [14, 19, 20, 24]. These methods could be misleading if the source rock of the basalt wasn't purely peridotitic and especially if not only olivine but clinopyroxene fractionation occurred [14]. Olivine addition to rocks that were generated from eclogitic/pyroxenitic mantle or went through clinopyroxene fractionation can produce unrealistically primitive melt compositions with too high MgO content, Mg# and mantle potential temperature [14].

Even primitive, high Mg# intracontinental alkaline basaltic rocks could be derivative melts after olivine and deep-seated clinopyroxene fractionation [18]. To develop a more realistic fractionation modeling method instead of pure olivine addition/subtraction the degree of clinopyroxene fractionation should be taken into account. During fractional crystallization both melt and newly-formed crystals' composition will change continuously. If this process can be modeled, an estimate for the degree of crystallization and for the main elements composition of the parental melt can be given.

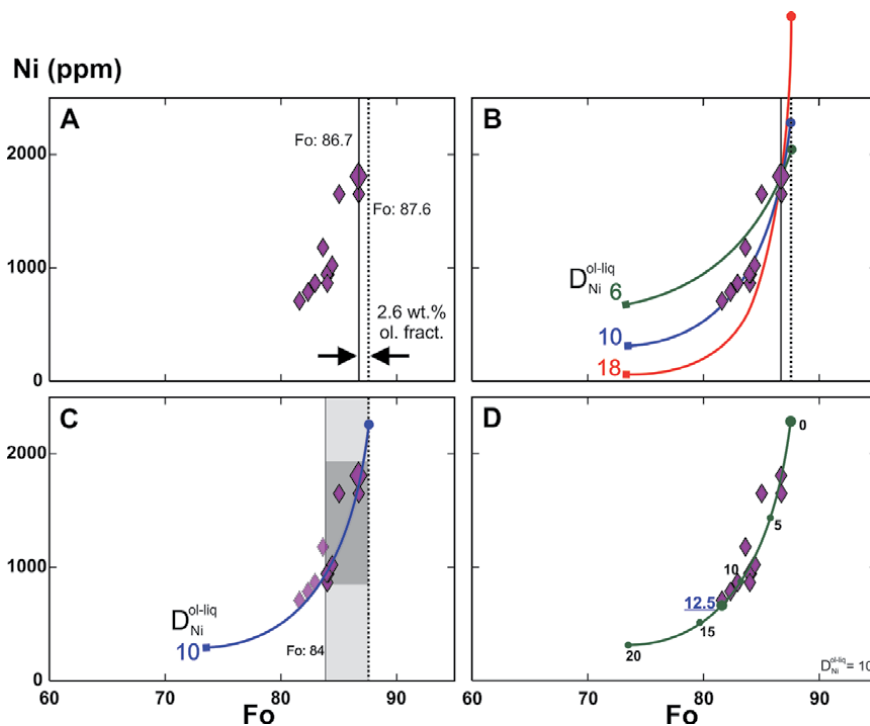
To find the degree of olivine \pm clinopyroxene fractionation quantitative estimations were performed.

With increasing degree of fractional crystallization of an alkaline basaltic melt the Fo and Ni content of olivine crystals will decrease. As it is a minor/trace element, the concentration of Ni in olivine depends on the D_{Ni}^{ol-liq} . In accordance with results of [26] it was suggested by [27] that on the Fo-Ni plot of olivines from an alkaline basalt the olivine-only fractionation would appear as a curve of exponentially decreasing Ni-content with decreasing Fo-content, while co-crystallization of olivine and clinopyroxene draws a linear (diagonal or nearly horizontal) trend on the same plot. The slope of the exponential curve is determined by the D_{Ni}^{ol-liq} , while the slope of the linear section depends on the $D_{Ni}^{(ol+cpX)-liq}$. It has been shown on olivine and clinopyroxene phyric rock samples that the primitive

(Fo and Ni-rich) population of olivine crystals will cluster dominantly around the upper part of the predicted exponential curve on the Fo-Ni plot and with decreasing Ni and Fo content at some point – when the clinopyroxene also begins to crystallize – the curve will change to diagonal [27]. Accordingly if other significant process that can modify the Fo-Ni pattern of olivines than crystallization of olivine and clinopyroxene can be ruled out, the degree of fractional crystallization of the two mineral phases can be estimated based on the composition of the olivine crystals and the bulk rock. The Fo-Ni pattern of fresh, unaltered olivine crystals depends on the Mg# and/or the Ni-content of the basaltic melt. Significant change in Mg# of alkaline basaltic melts – besides olivine ± clinopyroxene fractionation – could be caused by fractionation of amphibole or by incorporation of Mg/Fe rich minerals (olivine, clinopyroxene, amphibole and magnetite). The Ni-content of olivines during fractional crystallization could be changed by precipitation of minerals with $D_{Ni}^{min-liq}$ higher than 1. This value is the highest for magnetite (up to 30) and olivine (up to 25), and almost a magnitude lower for clinopyroxene (1–3) and amphibole (0.6–3) [28–31]. To avoid any processes than olivine and clinopyroxene fractionation during magma ascent the following filters have been used during sample selection. 1: only fresh, unaltered olivine and olivine-clinopyroxene phyric basalts without amphibole content were investigated. 2: samples contain only minor magnetite content (<1%) with very low Ni concentration (200–700 ppm). 3: there is no sign of olivine or clinopyroxene incorporation (mega- or antecrysts with significantly different petrographic or geochemical characteristics).

2.1 The steps of the modeling

1. Creating a corrected major elements composition for each rock sample from LOI-free raw data: redistributing the $Fe_2O_3^{tot}$ content into FeO and Fe_2O_3 assuming a Fe^{3+}/Fe^{2+} ratio of 0.15; recalculating Ni and Cr concentrations from ppm into NiO and Cr_2O_3 wt. % values. The Fe^{3+}/Fe^{2+} will be reflected in the Mg# of the rock ($Mg\#_{rock} = Mg / (Mg + Fe^{2+}) \times 100$, where Mg and Fe^{2+} are cation fractions. A different Fe^{3+}/Fe^{2+} ratio (and Mg#) of the rock would modify later calculations (e.g. the amount of olivine that is calculated in the 2nd step) as they will lead to another equilibrium olivine composition. Therefore highly oxidized samples cannot be used as they have significantly higher Fe^{3+} content and lower $Mg\#_{rock}$. If the exact ratio of Fe^{3+}/Fe^{2+} is known, it must be used instead of 0.15.
2. Calculating the Fo content of a hypothetical olivine (Fo*) being in equilibrium with the bulk rock composition, using the equation of Fo (mol%) = $100 - (X / (1 + X) * 100)$, where $X = ([100 * K_{D_{Fe-Mg}}^{ol-liq}] - [Mg\#_{rock}]) / Mg\#_{rock}$ and $K_{D_{Fe-Mg}}^{ol-liq} = 0.3$. If the difference between the calculated equilibrium Fo value (= Fo*) and the Fo content of the most primitive (richest in Ni and probably in Fo) olivine ($Fo_{ol^{Ni,max}}$) exceeds 0.1 mol%: the bulk rock composition has to be modified by olivine addition or subtraction in portions of 0.1 wt. % to reach equilibrium as follows (**Figure 1A**).
 - a. If $Fo^* < Fo_{ol^{Ni,max}}$: the composition of an olivine crystal (being in equilibrium with the instantaneous melt) has to be added to the bulk rock composition in steps of 0.1 wt. %. For this, real analyzed olivine compositions from the same rock can be used.
 - b. If $Fo^* > Fo_{ol^{Ni,max}}$: the composition of the most primitive olivine ($ol^{Ni,max}$) has to be subtracted from the bulk rock composition in steps of 0.1 wt. %.


Figure 1.

An example of olivine fractionation modeling (BRE basanite olivine Fo-Ni plots). A) the most primitive olivine phenocryst is not in equilibrium with the bulk rock composition. The difference between the most Ni-rich olivine (large symbol, $Fo_{86.7}$) and a hypothetical olivine being in equilibrium with the bulk rock ($Fo_{87.6}$) can be explained by 2.6 wt. % olivine fractionation. B) Calculation of olivine fractionation curves with different values of D_{Ni}^{ol-liq} . Starting point for calculation is the most Ni-rich olivine (large symbol, 1807 ppm Ni, $Fo_{86.7}$), from where the fractionation curve should be modeled by olivine addition (until reaching equilibrium with the bulk rock at $Fo_{87.6}$ olivine) and by olivine subtraction (until reaching 20 wt. % olivine fractionation, lower end of the curves). The Ni-content of the hypothetical, most primitive olivine ($Fo_{87.6}$) varies between 2061 and 2828 ppm, depending on the applied D_{Ni}^{ol-liq} value. C) Based on the composition of the most primitive olivine phenocrysts (olivine population over the 75th percentile by Fo-content or over Fo_{84} , marked by gray background) the best fitting olivine fractionation curve should be selected to assign the D_{Ni}^{ol-liq} of the rock. In this example the olivine fractionation curve related to $D_{Ni}^{ol-liq} = 10$ was selected. D) As the total olivine phenocryst population fits well to the selected fractionation curve, only olivine fractionation can be assumed. Green dots and numbers (wt. %) along the curve represent increasing olivine fractionation. The degree of olivine fractionation is 12.5 wt. %, it is marked by the most evolved crystal ($Fo_{81.6}$, Ni = 707 ppm). For a detailed description of fractionation modeling see the appendix of [23].

The amount of subtracted or added olivine (in wt. %) could represent the difference between the melt composition represented by the bulk rock and by the equilibrium melt related to the most primitive olivine in the sample. We call this ‘initial olivine fractionation’.

3. Calculating hypothetical (pure) olivine fractionation curves for $D_{Ni}^{ol-liq} = 5 - 20$ [29] on the Fo-Ni plot. The higher the D_{Ni}^{ol-liq} , the smoother the fractionation curve (**Figure 1B**).

- a. Modeling the decrease of MgO and Fo content in the melt and in equilibrium olivines simultaneously due to fractionation. Starting melts composition (Step 1.) has to be in equilibrium with the most Ni-rich olivine. Fractionation can be modeled by subtracting olivine in portions of 0.1 wt. % from the melt until 20 wt. % of total fractionation. During

calculation composition of analyzed olivine crystals (being nearly in equilibrium with the instantaneous melt) should be applied.

- b. Whereas the decrease of Fo content in olivines during fractionation has been calculated with a constant $K_{D_{Fe-Mg}^{ol-liq}}$ (0.3), the decrease of Ni concentration in the fractionated olivine crystals and in the equilibrium melt have to be modeled for each D_{Ni}^{ol-liq} value between 5 and 20, assuming Rayleigh fractionation. Ni content of the most Ni-rich, analyzed olivine crystal is taken as starting data.

4. Determination of the D_{Ni}^{ol-liq} of the investigated basalts.

Based on [27] in the case of pure olivine fractionation the most primitive olivine crystals should cluster along the upper, steep part of an exponential curve on the Fo-Ni plot. The most Mg-rich analyzed olivine crystals (over the 75th percentile by Fo-content and or over Fo₈₄) are compared to the calculated Fo-Ni curves (Step 2.) with the least squares method, and the best-fitting one will be accepted for the D_{Ni}^{ol-liq} of the investigated basalt (**Figure 1C**).

5. Estimation of the degree of the pure olivine fractionation.

The hypothetical, pure olivine fractionation trajectory should be compared with the total olivine Fo-Ni dataset of the sample, whether they are fitting well, or at some point the initially exponential trend of analyzed olivine crystals changes to a more straight, diagonal one.

- a. If they are fitting well, only olivine fractionation happened. The olivine crystal with lowest Fo-Ni content will draw the degree of fractionation, which can be easily read from the modeled Fo-Ni curve (**Figure 1D**). In this case the modeling has been ended here. Jump to Step 7.
- b. If the trend of the analyzed olivine crystals can be divided into an exponential and a linear section, the first part represents the initial pure olivine fractionation and the linear part the later olivine-clinopyroxene co-crystallization. The degree of pure olivine fractionation is determined by the intersection of the modeled olivine Fo-Ni curve and the linear section of the olivine dataset (**Figure 2**).

6. Modeling of the olivine+clinopyroxene co-crystallization (**Figure 2B**). The applied value of D_{Ni}^{ol-liq} has been selected in Step 3, while for $D_{Ni}^{cpx-liq}$ a constant value of 2.8 should be used [31].

- a. Calculating the composition of the equilibrium melt ('intermediate melt') for the olivine that represents the end of the initial pure olivine fractionation (Step 4a.) like equilibrium melt calculations in Step 1.
- b. Modeling the evolution of the "intermediate melt" by fractionation of olivine and clinopyroxene together. The decrease of olivines Ni concentration along the diagonal Fo-Ni trend has to be modeled by Rayleigh fractionation presuming different olivine/clinopyroxene ratios. As a thought experiment, the decrease of Ni concentration in olivines could be modeled by a given quantity of olivine (X wt. %) or

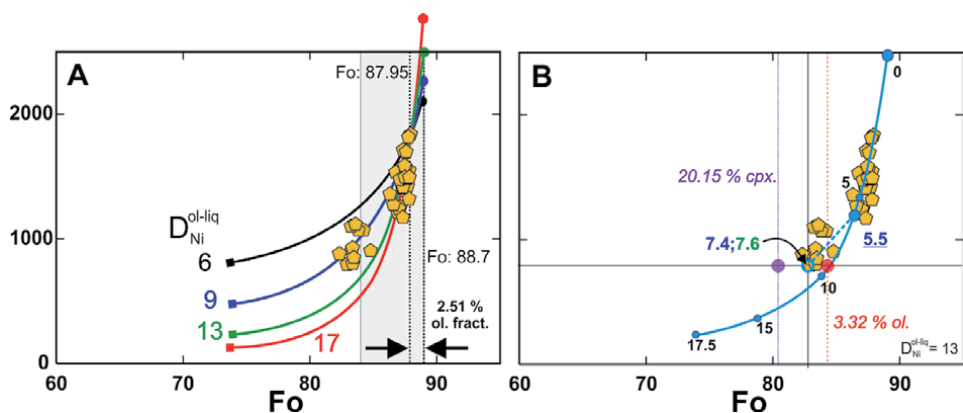


Figure 2.

An example of olivine and clinopyroxene fractionation modeling (SOR basanite olivine Fo-Ni plots). A) the most primitive olivine phenocryst ($Fo_{87.95}$) is not in equilibrium with the bulk rock composition. Olivine fractionation curves were modeled as in Figure 1. The most primitive olivine phenocrysts (marked by gray background) suggest a D_{Ni}^{ol-liq} value of 13, however the geochemical diversity of the total olivine population cannot be explained by pure olivine fractionation, as olivine crystals ($<Fo_{83.6}$) do not fit the curve. B) Based on the modeled Fo-Ni curve of $D_{Ni}^{ol-liq} = 13$ an initial olivine fractionation of 5.5 wt. % can be assumed. The composition of the more evolved olivine crystals ($<Fo_{83.6}$) suggest that besides olivine the fractionation of clinopyroxene has also begun [27]. The co-crystallization of the two minerals (i.e. the effect of clinopyroxene crystallization on olivine composition) can be modeled by the olivine population between the least primitive olivine crystal that fits to the calculated fractionation curve ($Fo_{86.3}$, $Ni = 1186$ ppm) and the most evolved crystal ($Fo_{83.4}$, $Ni = 801$ ppm). The decrease of Ni concentration (400 ppm) and Fo content (2.9 Mol%) in this olivine population have to be explained. If only olivine or clinopyroxene crystallization had occurred, the 400 ppm drop in Ni-concentration could be explained by 3.32 wt. % olivine or by 20.15 wt. % clinopyroxene fractionation (with a $D_{Ni}^{ol-liq} = 13$ and $D_{Ni}^{cpx-liq} = 2.8$ [31]). If this had happened, at the end of the fractionation, the Fo concentration of olivine crystals would have been $Fo_{84.3}$ (red dashed line and circle) or $Fo_{80.4}$ (purple dashed line and circle), respectively. None of them match the composition of the most evolved olivine crystal ($Fo_{83.4}$), therefore a co-crystallization of olivine and clinopyroxene must be assumed. The fractionation of the basaltic melt being in equilibrium with the $Fo_{86.3}$ olivine has been modeled with several different olivine/clinopyroxene ratio and amount. Fractionation of 2 wt. % olivine and 8 wt. % clinopyroxene would create a basaltic melt that would be in equilibrium with the most evolved analyzed olivine crystal ($Fo_{83.4}$). Because fractionation of 5.5 wt. % olivine had already taken place before this, the total degree of fractionation would be 7.39 wt. % olivine and 8.56 wt. % clinopyroxene (Initial olivine fractionation: 5.5 wt. % Olivine and clinopyroxene co-crystallization: $0.945 \times 2 = 1.89$ wt.% olivine and $0.945 \times 8 = 7.56$ wt.% clinopyroxene. Altogether 7.39 wt. % olivine and 7.56 wt. % clinopyroxene fractionation.). For a detailed description of fractionation modeling see the appendix of [23].

clinopyroxene (Y wt. %) fractionation only, however it must be a co-crystallization of the two minerals. Therefore, the decrease of Ni by fractional crystallization has to be calculated for each ol/cpx ratio from X wt. % olivine + 0 wt. % clinopyroxene to 0 wt. % olivine + Y wt. % olivine, changing the amount of each mineral by steps of 0.1 wt. %.

- c. Estimating the compositional change of the intermediate melt for all ratios of ol/cpx by subtracting these minerals from it. Subtraction of minerals is the same as in Step 1a. The calculated melt compositions are considered “final melts”.
- d. Estimating the Fo-content of equilibrium olivine for each final melt composition and compare them to the analyzed olivine crystals.
- e. That olivine/clinopyroxene fractionation ratio and amount will be accepted, for which the related final melts equilibrium olivine will have the same Fo-content as the lower end of the diagonal Fo-Ni trend of analyzed olivines.

7. The total degree of olivine and clinopyroxene fractionation will be the sum of the volumes calculated in “Step 4b” and “Step 5e”.
8. To find the major element composition of the parental melt (**Table 3**) the summerized amount of olivine or olivine+clinopyroxene have to be added to the bulk rock composition (**Tables 1** and **2**).
9. Optional check: it is possible to calculate parental melt composition by another method based only on olivine addition, like the method of PRIMELT2 [14] or Fractionate-PT [19]. If significant amount (>10 wt. %) fractionation of clinopyroxene has been calculated by the presented method, the mentioned programs should calculate a more Mg-rich parental melt (**Figure 3** and **Table 3**).

2.2 Remarks on limitations of the presented fractionation estimation method

1. Alkaline basalts that are derivative melts of fertile mantle peridotites will have an MgO content of 8–13 wt. % and equilibrium olivines with a Fo content of 86–89 mol% [17]. It is common that even the most primitive olivine phenocrysts of an alkaline basalt seemingly suitable for modeling (olivine +/- clinopyroxene phenocrysts, no signs of amphibole or early pyroxene crystallization or incorporation of mafic minerals) have quite low Fo and/or Ni-content (e.g. [34]). In this case a proper fractionation modeling is not possible, only a rough estimation can be performed based on a comparison with similar olivine datasets containing more Fo-rich olivines. An exact limit for proper calculations cannot be specified, only suggestions for it. Based on the empirical observations of [23] the fractionation modeling is more reliable if the olivine crystals over the 75th percentile by Fo-content draw a steep, semi

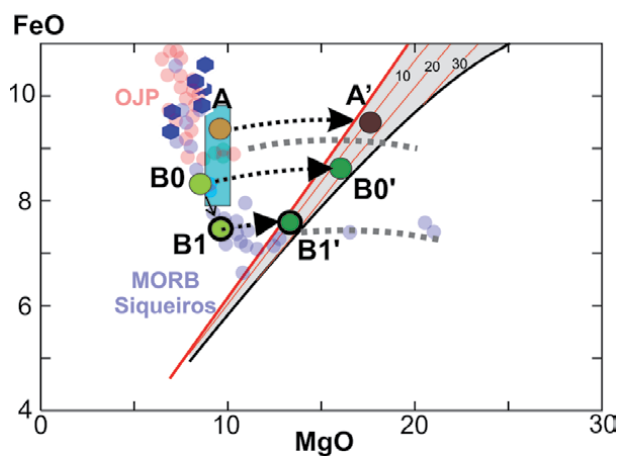
Sample		BRE	RAC2	SAN	SOR
GPS	N	48.403	46.032	45.811	48.226
	E	18.635	25.418	21.718	19.913
SiO ₂		44,71	46,87	49,30	44,86
TiO ₂		2,46	1,55	2,21	2,29
Al ₂ O ₃		13,18	15,8	14,80	15,81
Fe ₂ O ₃ Total		11,6	9,57	10,79	8,86
MnO		0,17	0,16	0,15	0,14
MgO		10,91	9,68	8,50	9,44
CaO		10,08	9,85	8,59	10,49
Na ₂ O		4,04	3,79	3,42	3,35
K ₂ O		1,72	1,63	1,64	2,25
P ₂ O ₅		0,77	0,39	0,60	0,6
LOI		0	0,2	0,80	1,4
Ni		219	216	170	153
Cr		342	431	247	212

Table 1. Composition of the basaltic samples applied for modeling. Oxides and LOI are given in wt. %, Ni and Cr in ppm. GPS: Coordinates of sample locations.

Sample	Olivine				Clinopyroxene	
	BRE	RAC2	SAN	SOR	SAN	SOR
olivine addition	12,4	10,35	16,53	7,39		
cpx addition					5,41	7,56
SiO ₂	40,09	40,57	39,31	39,93	48,70	47,73
TiO ₂	0,00		0,00	0,05	1,86	2,03
Al ₂ O ₃	0,01	0,04	0,03	0,16	4,69	7,34
Fe ₂ O ₃					3,19	3,21
FeO	11,74	11,27	16,73	15,25	4,27	3,65
MnO	0,24	0,19	0,24	0,26	0,13	0,14
MgO	46,76	47,88	43,22	44,31	14,00	13,52
CaO	0,27	0,20	0,24	0,31	22,40	22,07
Na ₂ O					0,40	0,59
NiO	0,24	0,29	0,18	0,14		0,03
Cr ₂ O ₃	0,04	0,09	0,05	0,01	0,03	0,03

Table 2.

The amount and average composition of olivine and clinopyroxene added to the bulk rock composition (m/m %) during parental melt calculations. Olivine and pyroxene addition are based on fractionation modeling (Figure 8).


Figure 3.

Estimation of primary melts' composition - the clinopyroxene problem. Figure modified after [32]. OJP – Ontong-Java plateau basalts, MORB – Siqueiros fracture zone basalts [32], dark blue hexagons represent the compositional diversity of the monogenetic volcano of Kissomlyó (West-Hungary) [33], while the pale blue rectangle the total diversity of a volcanic field (Novohrad-Gemer/Nógrád-Gömör VF, northern Hungary and southern Slovakia) [10]. FeO and MgO are in wt. %, gray area: Primary melts' composition after accumulated fractional melting of depleted mantle peridotite. Thick red line represents the solidus, thin red lines represent the degree of melting (%). Basaltic rocks to the left of the solidus are derivatives of primary melts, while rocks to the right are richer in MgO because of accumulation of MgO-rich minerals (typically olivine). If a basaltic magma was formed only by olivine fractionation/accumulation, the primary melts composition can be estimated from the bulk rock composition using olivine addition or subtraction (gray dotted curves) [24, 32]. The pale brown circle (A) represents a basaltic rock that was formed by olivine fractionation, therefore its primary melt composition (dark brown circle, A') can be calculated by olivine addition. The pale green circle (Bo) represents a basaltic rock that was formed by olivine and clinopyroxene fractionation. Its composition can be modified by adding the amount of fractionated clinopyroxene – to reach B1 (the pale green circle with a black rim). Adding olivine to the B1 melt its primary melt composition (B1', dark green circle with black rim) can be calculated. If the clinopyroxene fractionation had been ignored, the primary melts estimation by olivine addition would have been misleading (Bo'). The too high MgO- and FeO-content of Bo' melt would make all further estimations (e.g. temperature of the primary melt, degree of melting) inaccurate.

Calculation based on	PRIMELT2 software				Fractionation modeling presented in this article			
	BRE	RAC2	SAN	SOR	BRE	RAC2	SAN	SOR
SiO ₂	44,68	47,07	47,83	45,75	44,13	46,21	48,06	44,71
TiO ₂	2,17	1,46	1,78	2,21	2,15	1,39	1,77	2,1
Al ₂ O ₃	11,57	14,88	11,86	15,22	11,53	14,17	12,63	14,01
Fe ₂ O ₃	1,08	0,73	0,88	0,69	1,21	1,02	1,09	1,14
FeO	9,47	8,18	9,12	7,60	9,52	8,1	9,14	7,38
MnO	0,17	0,16	0,15	0,14	0,18	0,18	0,16	0,15
MgO	16,17	12,65	16,80	12,20	15,39	13,47	14,18	12,23
CaO	8,87	9,29	6,91	10,11	8,85	8,85	7,69	10,61
Na ₂ O	3,54	3,57	2,73	3,22	3,54	3,4	2,63	2,89
K ₂ O	1,51	1,53	1,31	2,16	1,51	1,46	1,53	1,91
P ₂ O ₅	0,68	0,37	0,48	0,58	0,67	0,35	0,38	0,51
NiO	0,07	0,05	0,12	0,04	0,05	0,04	0	0,03
Cr ₂ O ₃	0,05	0,06	0,03	0,03	0,05	0,06	0	0,03
Mg#	75,27	73,39	76,65	74,00	74,24	74,77	73,44	74,54
Olivin add. by Primelt2	14,20	7,10	23,40	6,60				

Table 3.

Primitive melt compositions calculated by the PRIMELT2 software [14] and by addition of olivine and clinopyroxene to the bulk rock based on fractionation modeling presented in this paper. Regardless of the applied method, the Mg# of the primitive melts will be quite similar in the case of olivine phyric rocks (BRE, RAC2). On the contrary, the Mg# of the primitive melts can depend on the applied method, if there were a significant amount of clinopyroxene in the sample (SAN). This means, that only by olivine addition – as the PRIMELT2 and similar softwares [14, 19, 20, 24] work – the Mg# of the primary melt will be over calculated.

vertical trend on the Fo-Ni plot and they have 89–82 mol% Fo and 2500–1200 ppm Ni content.

2. The deep-seated clinopyroxene fractionation [25] will not affect the composition of later crystallized olivines, while the presented method can reveal clinopyroxene crystallization only if it occurred together with olivine fractionation. Therefore, it cannot indicate the precipitation of clinopyroxene onto the wall rocks at great depth. To identify any modification of primary melts by reaction with mantle minerals is also beyond the limits of the presented method.

3. Since there are several variable parameters during fractionation modeling (the D_{Ni}^{ol-liq} value, the applied Fe^{3+}/Fe^{2+} ratio for the bulk rock, the amount and ratio of olivine and clinopyroxene, the composition of the intermediate melt), the calculation is a little bit cumbersome.

3. Case studies from the Carpathian-Pannonian region

3.1 Geological setting

From a volcanological and geodynamical point of view – based on its Neogene-Quaternary volcanism – the Carpathian-Pannonian Region (**Figure 4**) is a related to the broader Mediterranean area in terms of geodynamic setting [37].

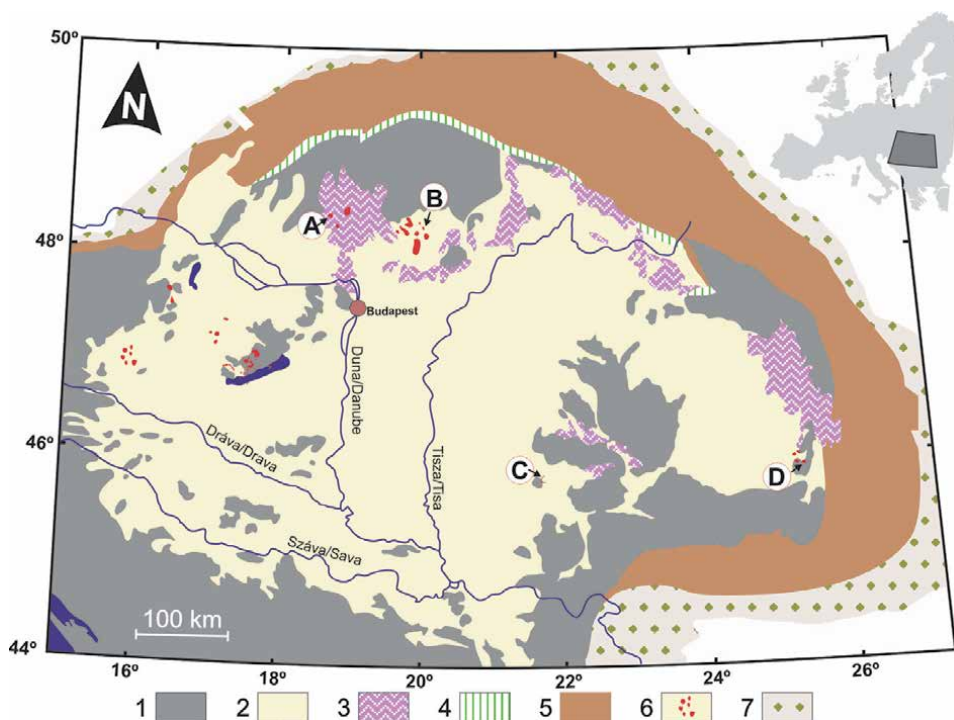


Figure 4. Map of the Carpathian-Pannonian region after [35, 36]. 1: Pre-Cenozoic basement, 2: Neogene-Quaternary sediments, 3: Neogene calc-alkaline volcanic rocks on the surface, 4: Pieniny Klippen Belt, 5: Alp-Carpathian Flysch Belt, 6: Neogene-Quaternary alkaline basaltic volcanic fields on the surface, 7: Alp-Carpathian Molasse Belt. Sample locations. A: Putikov Vřšok, B: Šurice (Sóreg), C: Lucaret-Sanovița (Lukácskő-Sziklás), D: Racoș (Alsórákos). The map insert on the upper right corner shows the position of the Carpathian-Pannonian region within Europe.

The post-Paleogene volcanic formations of the region can be divided by age and geochemical features into four groups [38]: 1) Miocene Si-rich-; 2) Miocene-Quaternary K- and high-K-; 3) Miocene-Quaternary calc-alkaline- and 4) late Miocene-Quaternary alkaline type. The latter group is represented by several alkaline basaltic monogenetic volcanic fields, some of which are deeply buried by late Miocene sediments [10, 39–41]. The most intense period of alkaline basaltic volcanism took place between 5 and 3 Ma ago. At that time numerous volcanoes formed, for example, in the Bakony-Balaton Highland Volcanic Field (e.g. [42]), in the Nógrád-Gömör/Novohrad-Gemer Volcanic Field (e.g. [40]) and in the Styrian Basin Volcanic Field (e.g. [35]). The alkaline rocks show a wide range in composition from the primitive, olivine-phyric basanites towards the more differentiated, clinopyroxene-rich phonotephrites (e.g. [10, 43, 44]). Based on their trace element content they show similarities both with the Neogene-Quaternary alkaline rocks of western and central Europe (e.g. [45, 46]) and with alkaline basaltic rocks of the Mediterranean area (e.g. [47, 48]). The driving force of the alkaline basaltic melt generation is still subject of debate as the Neogene-Quaternary basaltic volcanism of the region dominantly postdates the rifting of the Pannonian Basin and took place in the thermal inversion phase of the basin, in a compressional geodynamic regime [10, 37, 49]. There are two dominant theories for basalt generation in the area, both associate it with regional mantle flows, the differences are in the driving forces. 1) In the outer parts of the Pannonian Basin melting could have been associated with mantle upwelling related to the so-called thin-spot event, a dominantly vertical asthenospheric flow from under the deep roots of the surrounding mountain chains

or to lithospheric delamination while the sporadic volcanism in the central parts of the basin could have been related to strike-slip tectonics [10, 22, 37]. 2) The other theory comes from [50], who suggested that basaltic melt generation was caused by rather a regional, mostly horizontal mantle flow related to the north-eastward push of the Adria microplate.

3.2 Analytical methods

Whole-rock compositions were analyzed at Acme Labs (Vancouver, Canada). Major and minor elements were analyzed by ICP-ES, trace elements by ICP-MS. Petrographic descriptions were done with a Nikon YS2-T polarizing microscope using NIS-Elements Br software and an AMRAY 1830 I/T6 scanning electron microscope at the Department of Petrology and Geochemistry, Eötvös Loránd University (Budapest, Hungary). The polished and carbon-coated thin sections were analyzed with a CAMECA SX100 EMPA, equipped with one energy-dispersive and four wavelength-dispersive spectrometers at the Department of Lithospheric Research, University of Vienna (Austria). An accelerating potential of 15 kV and a beam current of 20 nA were used with at least 20 s counting time on peak position and 1 μm beam diameter. PAP correction procedure was applied on raw data. Analyses were done against natural and synthetic mineral standards: olivine (Mg), corundum (Al), quartz (Si), apatite (P), wollastonite (Ca), rutile (Ti), Mg-chromite (Cr), spessartine (Mn), almandine (Fe), Ni-oxide (Ni).

3.3 The investigated alkaline basalts

3.3.1 Samples

BRE: a massive basanitic lava rock sample (**Figures 5 and 6**) from the Putikov Vřšok volcano, Štiavnica (Selmec) Volcanic Field. The small scoria cone and related lava flow is the youngest alkaline basaltic volcano in the Carpathian-Pannonian Region with its age of 102 ± 11 ka [51]. Sample data were taken from [22, 23].

RAC2: a trachybasaltic vesicular scoria clast (**Figures 5 and 6**) from the Racoş (Rákos) scoria cone, Perşani (Persányi) Mts. Volcanic Field. Its age is 1221 ± 11 ka [52, 53]. Sample data were taken from [22, 53].

SAN: a massive trachybasaltic lava rock sample (**Figures 5 and 6**) from the Lucaret-Sanoviţa (Lukácskő-Sziklás) volcano, Banat Volcanic Field. Its age is between 2.5–2.6 Ma [54]. Sample data were taken from [23].

SOR: a massive basanite (**Figures 5 and 6**) from a dyke cutting the maar diatreme rocks at Šurice (Sőreg), Novohrad-Gemer/Nógrád-Gömör VF. Its age is 4 ± 0.29 Ma [54]. Sample data were taken from [22].

3.3.2 Petrography

BRE: an olivine phyric massive basanite sample with porphyritic-intergranular texture (**Figure 5**). Clinopyroxene phenocrysts are very rare (olivine/clinopyroxene ratio is 19/1, total phenocryst content: 6%). Olivine phenocrysts are normal zoned, dominantly hypidiomorphic-idiomorphic with an average size of 650–700 μm , they contain idiomorphic magnetite and Cr-spinel inclusions dominantly in the crystal rims. Largest grains are often resorbed and iddingsitized along crystal rims and cleavage tracks. Hypidiomorphic-idiomorphic pale brown clinopyroxene microphenocrysts are dominantly normal-, rarely sector zoned crystals with a maximal size of 400–500 μm . They often contain idiomorphic magnetite inclusions.

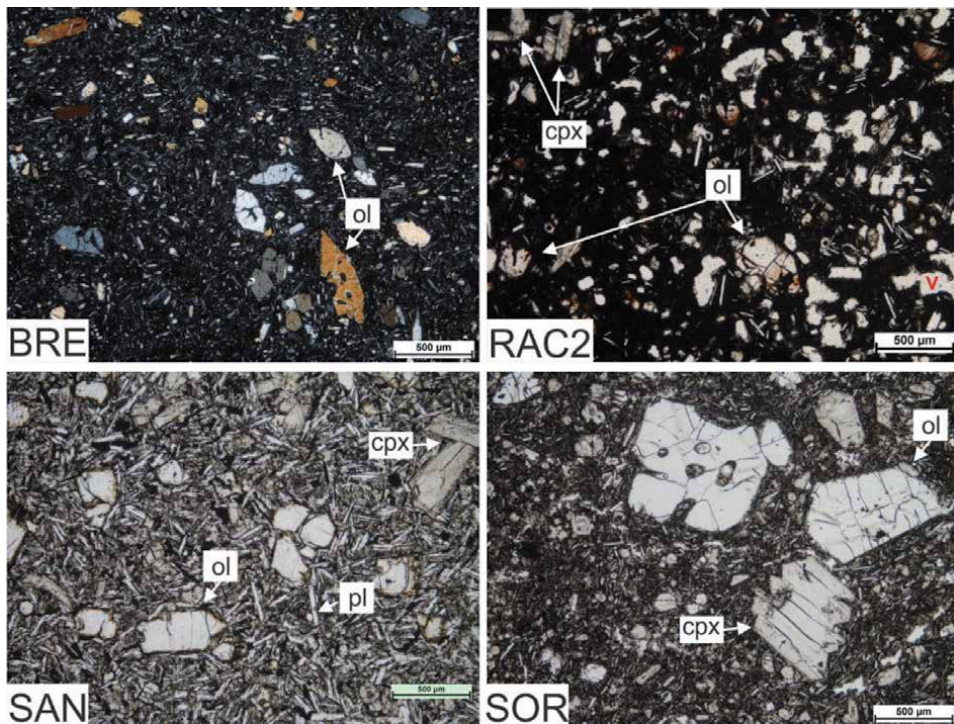


Figure 5. Photomicrographs of the investigated samples. BRE: Olivine phyric intergranular basanite (xpl), RAC2: Olivine phyric, intersertal and moderately vesicular trachybasalt (xpl), SAN: Olivine and clinopyroxene phyric, intergranular trachybasalt (ppl), SOR: Olivine and clinopyroxene phyric, intersertal basanite (ppl). Abbreviations: Ol – Olivine, cpx – Clinopyroxene, pl. – Plagioclase, v - vesicle.

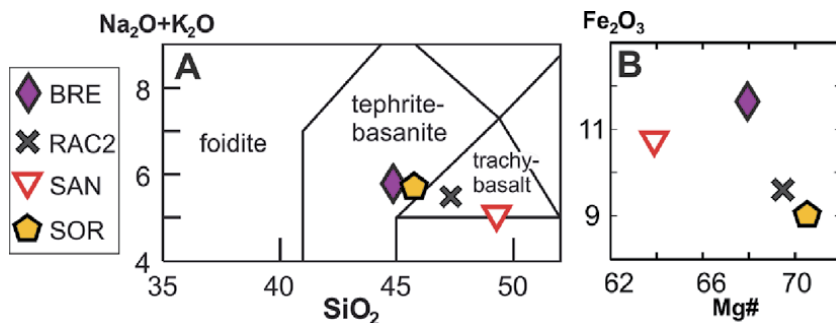


Figure 6. A: Nomenclature of the investigated alkaline basalts (s.l.). B: They have a high or moderate Mg# (BRE: 67.9, RAC2: 69.46, SOR: 70.54, SAN: 63.9). $Mg\# = Mg/(Mg + Fe^{2+}) \times 100$. By calculations of Mg# a Fe_2O_3/FeO ratio of 0.15 has been applied.

The groundmass contains plagioclase, clinopyroxene, olivine, nepheline and accessory magnetite and ilmenite.

RAC2: an olivine phyric trachybasaltic scoria clast with vesicular, porphyritic-intersertal texture (Figure 5). Clinopyroxene microphenocrysts are very rare (olivine/clinopyroxene ratio is 19/1, total phenocryst content: < 5%). Olivine phenocrysts are normal zoned, dominantly hypidiomorphic-idiomorphic, sometimes skeletal; with an average size of 500 µm, largest crystals reach 1250 µm. They are often strongly iddingsitized. Most oxidized grains contain few µm thick iron-oxide needles. Idiomorphic inclusions of Cr-spinel are common

in crystal rims. Hypidiomorphic-idiomorphic pale brown clinopyroxene microphenocrysts often form glomerocrysts. They are dominantly sector-, rarely normal zoned crystals with an average size of 300–350 μm . The groundmass contains plagioclase, clinopyroxene, olivine, glass, nepheline and accessory magnetite and ilmenite.

SAN: an olivine and clinopyroxene phyric trachybasaltic lava rock sample with porphyritic-intergranular texture (**Figure 5**). Clinopyroxene phenocrysts are quite common (olivine/clinopyroxene ratio is 4/1, total phenocryst content: 20%). Olivine phenocrysts are normal zoned, dominantly hypidiomorphic-idiomorphic, often resorbed; with an average size of 500 μm , largest crystals reach 1200 μm . They are often iddingsitized along crystal rims and cleavage tracks. Idiomorphic inclusions of Cr-spinel are common in crystal rims. Hypidiomorphic-idiomorphic pale brown clinopyroxene phenocrysts are sector zoned crystals with an average size of 300–400 μm , largest grains reach 1000 μm . They contain magnetite inclusions and they often form glomerocrysts. The groundmass contains plagioclase, clinopyroxene, olivine and accessory magnetite and ilmenite.

SOR: an olivine and clinopyroxene phyric basanitic dyke sample with slightly vesicular, porphyritic-intergranular/insertal texture (**Figure 5**). Clinopyroxene phenocrysts are common (olivine/clinopyroxene ratio is 5/5, total phenocryst content: 8%). Olivine phenocrysts are normal zoned, dominantly hypidiomorphic-idiomorphic, often resorbed; with an average size of 650 μm , largest crystals reach 3000 μm . Idiomorphic inclusions of Cr-spinel and magnetite are common in crystal rims. Idiomorphic-hypidiomorphic pale brown clinopyroxene phenocrysts are sector-, normal- or oscillatory zoned minerals with an average size of 470 μm , largest grains reach 2000 μm . They contain magnetite inclusions. Some clinopyroxene phenocrysts have an olive-green core. Few grains of completely opacitized amphibole megacrysts can be observed. The groundmass contains plagioclase, clinopyroxene, olivine, glass, nepheline and accessory magnetite.

3.3.3 Geochemistry

Geochemical data (**Tables 1 and 2, Figures 6 and 7**) were taken from [22, 23, 53, 55].

4. Results of olivine and clinopyroxene fractionation modeling

From two samples (BRE and RAC2) olivine crystals are fitting well to the modeled pure olivine fractionation curves that were calculated with $D_{Ni}^{ol-liq} = 10$. Based on this the calculated degree of olivine fractionation is 12.5 wt. % and 10.35 wt. %, respectively (**Figure 8A and B**). Adding this amount of olivine to the bulk rock composition the parental melt would have an Mg# of 74.24 and 74.77.

In the case of SAN and SOR only the most primitive, Mg-rich olivine crystals follow the modeled exponential olivine fractionation curve on the Fo-Ni plot and the more evolved ones draw a diagonal trend (**Figure 8C and D**). A D_{Ni}^{ol-liq} value of 12 and 13 were applied for SAN and SOR, respectively. The calculated degree of olivine fractionation is 9.5 wt. % for SAN and 5.5 wt. % for SOR during the initial, pure olivine crystallization period. Based on the olivine crystals that are falling onto the diagonal trend it is obvious that the evolution of both melts switched at some point from pure olivine fractionation to co-crystallization of olivine and clinopyroxene. The calculated degree of fractionation for olivine and clinopyroxene

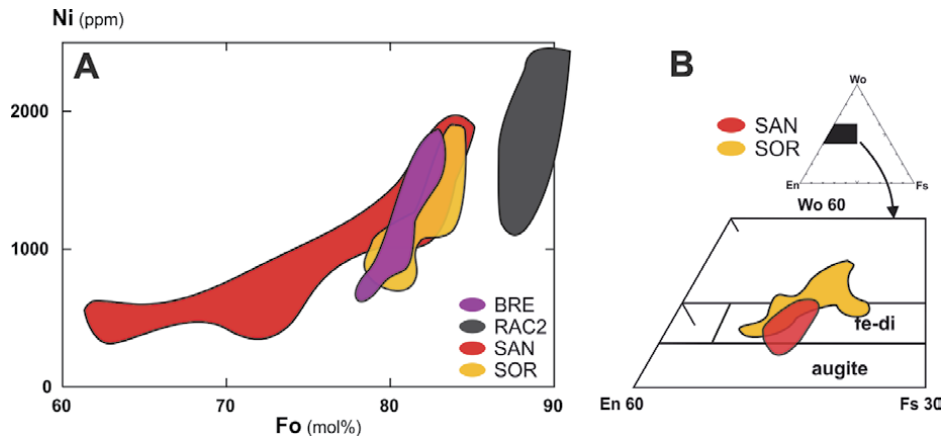


Figure 7. A) the majority of the olivine crystals fall into the range of Fo_{80–87}, the cores of the normal zoned crystals are Mg rich (Fo_{75–90}). Their Ni-concentration correlates positively with the Fo content, Mg-rich crystal cores could reach a Ni content of 2500 ppm, while in crystal rims only 100–700 ppm of Ni can be analyzed. B) the clinopyroxene phenocrysts of the SAN trachybasalt and SOR basanite are dominantly ferroan-diopsides, rarely augites. They are dominantly sector zoned with a primitive core and a more evolved rim, MgO-content varies between 9.2 and 15.9 wt. %. CaO varies between 21.1–23.2 wt. %, higher values can be measured in crystal rims. Especially in the SOR basanite clinopyroxenes are extremely rich in Ca, several crystals exceed Wo₅₀.

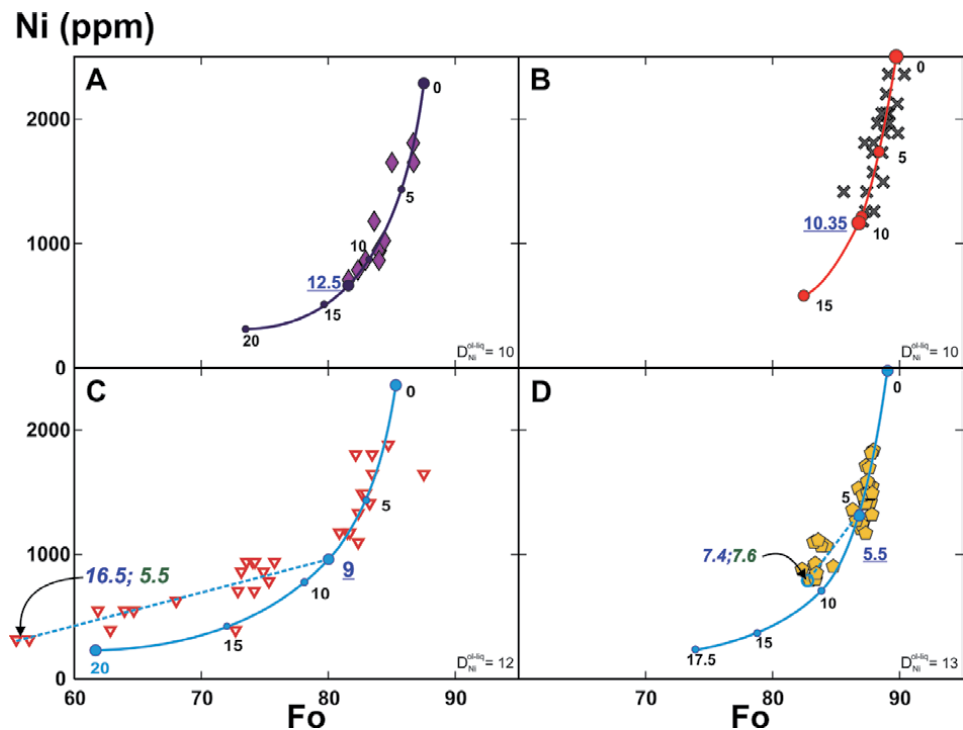


Figure 8. Results of olivine and clinopyroxene fractionation. The composition of olivine crystals suggest only olivine fractionation in the case of the BRE basanite (A) and the RAC2 trachybasalt (B), while a significant degree of clinopyroxene fractionation played role in the formation of the SAN trachybasalt (C) and SOR basanite (D). Calculated olivine fractionation curves are based on the indicated D_{Ni}^{ol-liq} values, black numbers indicate increasing degree of olivine fractionation along the curves. Blue, underlined numbers show the degree of pure olivine fractionation, blue and green italic numbers indicate total degree of olivine and clinopyroxene fractionation (wt. %), respectively. The most primitive olivine crystal in the RAC trachybasalt (B) is in equilibrium with the bulk rock composition and it is the starting point of the olivine fractionation curve. In the other samples the starting point is a hypothetical olivine which is in equilibrium with the bulk rock composition.

during this phase are 7 and 5.5 wt. % for SAN and 1.89 and 7.56 wt. % for SOR. The total degree of olivine and clinopyroxene fractionation is 16.5 and 5.5 wt. % for SAN and 7.39 and 7.56 wt. % for SOR. Adding this amount of the two mineral phases to the bulk rock composition the parental melt would have an Mg# of 73.44 and 74.54, respectively (**Table 3**).

5. Conclusions

The results of fractionation modeling are consistent with the petrographic observations, i.e. for the olivine phyric basalts (BRE, RAC2) only olivine fractionation have been calculated, while for those which have a considerable amount of phenocrystic clinopyroxene a significant clinopyroxene fractionation have been revealed by the model. The olivine/pyroxene ratio in the rock samples is 4/1 for SAN and 5/5 for SOR, this is fairly the same as the results of modeling (5.5/16.5 for SAN and 7.4/7.6 for SOR).

The calculated parental melts composition may resemble a mafic melt from a fertile peridotite. Parental melts composition and Mg# have been calculated with the Primelt2 software [14] too. For the olivine phyric rocks it gave a similar Mg# (BRE – 75.13, RAC2–73.27).

In the case of the SAN trachybasalt the Mg# calculated by the Primelt2 software is obviously too high (Mg# = 76.31), which is consistent with the high degree of clinopyroxene fractionation that was indicated by the fractionation modeling. This coincides with the fact that the Primelt2 program does not count on the possibility of clinopyroxene fractionation during primary melt calculations except that it gives a warning about the possible pyroxene fractionation.

The SOR basanite is little bit more interesting as the fractionation modeling have resulted the same amount of olivine and clinopyroxene fractionation, and the Mg# of the parental melts based on the modeling is somewhat higher compared to the result given by the Primelt2 [14]. In this case two important facts have to be considered. First, the modeled mineral fractionation fits very well to the petrographic observations in all case. It suggests that the pyroxene fractionation predicted by the modeling should also be realistic in the case of SOR basanite. Secondly, the Primelt2 program gives us warnings, if the calculation may be inaccurate because of pyroxenite source rocks or because of clinopyroxene fractionation. In the case of SOR basanite a pyroxene fractionation warning was given by the software, although the suggested olivine addition to reach primary melt (6.6 wt. %) is almost the same as it was given by fractionation modeling (7.39 wt. %).

The uncertainty, whether the result of the fractionation modeling or the Primelt2 is the more realistic may have arisen from two factors. Neither olivine, nor clinopyroxene is a dominant phase and probably this amount (<10 wt. %) of pyroxene is close to the limit what can be detected by the difference in primary melts' Mg#.

Despite its limitations, the presented olivine and clinopyroxene fractionation modeling based on olivine and bulk rock compositional data draw attention that it is not only olivine fractionated basalts that could be useful for primary melt calculations.

It is more important, that all possible tools have to be applied from petrographic observations to quite simple or more complicated geochemical modeling methods. We hope that the modeling presented in this chapter will inspire the reader to develop further ideas and methods to give a more realistic and better description of the fractionation process of alkaline basaltic melts.

Acknowledgements

First of all Tamás Sági would like to express his special thanks to M. Éva Jankovics, Zoltán Taracsák, Balázs Kiss and Csaba Szabó for the thought-provoking discussions about fractionation of alkaline basalts. The manuscript has been improved by the constructive comments and suggestions of Marco Brenna.

Author details

Tamás Sági^{1*}, Szabolcs Harangi¹ and Theodoros Ntaflos²

1 Department of Petrology and Geochemistry, Budapest, Hungary and MTA-ELTE Volcanology Research Group, Eötvös Loránd University, Budapest, Hungary

2 Department of Lithospheric Research, University of Vienna, Vienna, Austria

*Address all correspondence to: sagi.tamas@ttk.elte.hu

IntechOpen

© 2021 The Author(s). Licensee IntechOpen. This chapter is distributed under the terms of the Creative Commons Attribution License (<http://creativecommons.org/licenses/by/3.0>), which permits unrestricted use, distribution, and reproduction in any medium, provided the original work is properly cited. 

References

- [1] Németh K. Monogenetic volcanic fields: Origin, sedimentary record, and relationship with polygenetic volcanism. In: Canón-Tapia E, Szakács A, editors. *What Is a Volcano?* GSA; 2010. p. 43–66. DOI: 10.1130/2010.2470(04)
- [2] Connor CB, Conway FM. Basaltic Volcanic Fields. In: Sigurdsson H, editor. *Encyclopedia of Volcanoes*. 1st ed. San Diego: Academic Press; 2000. p. 331–343. ISBN: 9780080547985
- [3] Valentine GA, Perry FV. Tectonically controlled, time-predictable basaltic volcanism from a lithospheric mantle source (central Basin and Range Province, USA). *EPSL*. 2000; 261:201–216. DOI: 10.1016/j.epsl.2007.06.029
- [4] Valentine GA, Connor BC. Basaltic Volcanic Fields. In: Sigurdsson H, editor. *The Encyclopedia of Volcanoes*. 2nd ed. London: Academic Press; p. 423–439. DOI: <https://doi.org/10.1016/B978-0-12-385938-9.00023-7>
- [5] Sobolev AV, Krivolutsкая NA, Kuzmin DV. Petrology of the Parental Melts and Mantle Sources of Siberian Trap Magmatism. *Petrology*. 2009; 17/3:253–286. DOI: 10.1134/S0869591109030047
- [6] Gazel E, Hoernle K, Carr MJ, Herzberg C, Saginor I, Bogaard VDP, Hauff F, Feigenson M, Swisher C. Plume–subduction interaction in southern Central America: Mantle upwelling and slab melting. *Lithos*. 2011; 121/1–4:117–134. DOI: 10.1016/j.lithos.2010.10.008
- [7] Niu Y, O’Hara M. Origin of ocean island basalts: a new perspective from petrology, geochemistry, and mineral physics considerations. *JGR: Solid Earth*. 2003; 108:2209–2228. DOI: <http://dx.doi.org/10.1029/2002JB002048>
- [8] Kelemen PB, Holbrook WS. Origin of thick, high-velocity igneous crust along the U.S. East Coast Margin. *JGR: Atmospheres*. 1995; 100/B7:10077–10094. DOI: 10.1029/95JB00924
- [9] Wang K, Plank T, Walker JD, Smith EI. A mantle melting profile across the Basin and Range, SW USA. *JGR: Solid Earth*. 2002; 107/B1:ECV 5–1–ECV 5–21. DOI: 10.1029/2001JB000209
- [10] Harangi Sz, Jankovics MÉ, Sági T, Kiss B, Lukács R, Soós I. Origin and geodynamic relationships of the late Miocene to quaternary alkaline basalt volcanism in the Pannonian basin, eastern-central Europe. *IJES*. 2015; 104: 2007–2032. DOI: <https://doi.org/10.1007/s00531-014-1105-7>
- [11] Fitton JG, James D, Leeman WP. Basic magmatism associated with late Cenozoic extension in the western United States: compositional variations in space and time. *JGR: Atmospheres*. 1991; 96:13693–13711. DOI: 10.1029/91JB00372
- [12] Pilet S, Baker MB, Stolper M. Metasomatized Lithosphere and the Origin of Alkaline Lavas. *Science*. 2008; 320 (5878):916–919. DOI: <https://doi.org/10.1126/science.1156563>
- [13] Mayer B, Jung S, Romer R, Pfänder JA, Klügel A, Pack A, Gröner E. Amphibole in alkaline basalts from intraplate settings: implications for the petrogenesis of alkaline lavas from the metasomatised lithospheric mantle. *Contrib Mineral Petrol*. 2014; 167:989. DOI: 10.1007/s00410-014-0989-3
- [14] Herzberg C, Asimow PD. Petrology of some oceanic island basalts: PRIMELT2.XLS software for primary magma calculation. *G3*. 2008; Q09001. DOI: <http://doi.org/10.1029/2008GC002057>
- [15] Niu Y. The origin of alkaline lavas. *Science*. 2008; 320:883–884. DOI: 10.1126/science.1158378

- [16] Pilet S, Ulmer P, Villiger S. Liquid line of descent of a basanitic liquid at 1.5 Gpa: constraint on the formation of metasomatic veins. *Contrib Mineral Petrol.* 2009; 159:621–643. DOI: 10.1007/s00410-009-0445-y
- [17] Herzberg C. Identification of source lithology in the Hawaiian and Canary Islands: implications for origins. *Journal of Petrology.* 2011; 52:113–146. DOI: <https://doi.org/10.1093/petrology/egq075>
- [18] Smith IEM, Blake S, Wilson CJN, Houghton BF. Deep-seated fractionation during the rise of a small-volume basalt magma batch: Crater Hill, Auckland, New Zealand. *Contrib Mineral Petrol.* 2008; 155/4:511–527. DOI: <https://doi.org/10.1007/s00410-007-0255-z>
- [19] Lee C-TA, Luffi P, Plank T, Dalton H, Leeman WP. Constraints on the depths and temperatures of basaltic magma generation on Earth and other terrestrial planets. *EPSL.* 2009; 279:20–33. DOI: <https://doi.org/10.1016/j.epsl.2008.12.020>
- [20] Kimura J-I, Kawabata H. Ocean Basalt Simulator version 1 (OBS1): Trace element mass balance in adiabatic melting of apyroxenite-bearing peridotite. — *G3.* 2015; 16:267–300. DOI: <http://doi.org/10.1002/2014GC005606>
- [21] Putirka KD, Perfit M, Ryerson FJ, Jackson MG. Ambient and excess mantle temperatures, olivine thermometry, and active vs. passive upwelling. *Chemical Geology.* 2007; 241/3–4:177–206. DOI: <https://doi.org/10.1016/j.chemgeo.2007.01.014>
- [22] Sági T. A Persányi-hegység, a Selmecsi- és a Nógrád-Gömöri vulkáni terület alkáli bazaltjainak petrogenézise (Petrogenesis of the alkaline basalts of the Perşani Mts., Štiavnica and Novohrad-Gemer Volcanic Fields) [PhD thesis]. Budapest, Eötvös Loránd University; 2018. DOI: 10.15476/ELTE.2018.125
- [23] Sági T, Jankovics MÉ, Kiss B, Ntaflós T, Harangi Sz. Új módszer alkáli bazaltos magmák olivin- és klinopiroxén-frakcionációjának modellezésére (A new method for the olivine- and clinopyroxene fractionation modelling of alkaline basaltic magmas). *Földtani Közlöny.* 2018; 148/3:273–292. DOI: 10.23928/foldt.kozl.2018.148.3.273
- [24] Herzberg C, Asimow PD. PRIMELT3 MEGA.XLSM software for primary magma calculation: peridotite primary magma MgO contents from the liquidus to the solidus. *G3.* 2015; 16:563–578. DOI: 10.1002/2014GC005631
- [25] Putirka KD. Mantle potential temperatures at Hawaii, Iceland, and the mid-ocean ridge system, as inferred from olivine phenocrysts: Evidence for thermally driven mantle plumes. *G3.* 2005; 6:Q05L08. DOI: 10.1029/2005GC000915
- [26] Sato H. Nickel Content of Basaltic Magmas - Identification of Primary Magmas and a Measure of Degree of Olivine Fractionation. *Lithos.* 1977; 10/2: 113–120. DOI: [https://doi.org/10.1016/0024-4937\(77\)90037-8](https://doi.org/10.1016/0024-4937(77)90037-8)
- [27] Kawabata H, Hanyu T, Chang Q, Kimura JI, Nichols ARL, Tatsumi Y. The Petrology and Geochemistry of St. Helena Alkali Basalts: Evaluation of the Oceanic Crust-recycling Model for HIMU OIB. *Journal of Petrology.* 2011; 52/4:791–838. DOI: <https://doi.org/10.1093/petrology/egr003>
- [28] Villemant B, Jaffrezic H, Joron JL, Treuil M. Distribution Coefficients of Major and Trace-Elements – Fractional Crystallization in the Alkali Basalt Series of Chaîne-Des-Puys (Massif Central, France). *Geochimica et Cosmochimica Acta.* 1981; 45/11:1997–2016. DOI: [https://doi.org/10.1016/0016-7037\(81\)90055-7](https://doi.org/10.1016/0016-7037(81)90055-7)

- [29] Hart SR, Davis KE. Nickel Partitioning between Olivine and Silicate Melt. *EPSL*. 1978; 40/2:203–219. DOI: [https://doi.org/10.1016/0012-821X\(78\)90091-2](https://doi.org/10.1016/0012-821X(78)90091-2)
- [30] Lemarchand F, Villemant B, Calas G. Trace-Element Distribution Coefficients in Alkaline Series. *Geochimica et Cosmochimica Acta*. 1987; 51/5:1071–1081. DOI: [https://doi.org/10.1016/0016-7037\(87\)90201-8](https://doi.org/10.1016/0016-7037(87)90201-8)
- [31] Laubier M, Grove TL, Langmuir CH. Trace element mineral/melt partitioning for basaltic and basaltic andesitic melts: An experimental and laser ICP-MS study with application to the oxidation state of mantle source regions. *EPSL*. 2014; 392: 265–278. DOI: <https://doi.org/10.1016/j.epsl.2014.01.053>
- [32] Herzberg C, Asimow PD, Arndt, NT, Niu Y, Leshner CM, Fitton JG, Cheadle MJ, Saunders AD. Temperatures in ambient mantle and plumes: constraints from basalts, picrites and komatiites. *G3*. 2007; 8: Q02006. DOI: <http://doi.org/10.1029/2006GC001390>
- [33] Jankovics MÉ, Harangi Sz, Németh K, Kiss B, Ntaflos T. A complex magmatic system beneath the Kissomlyó monogenetic volcano (western Pannonian Basin): evidence from mineral textures, zoning and chemistry. *JVGR*. 2015; 301:38–55. DOI: <https://doi.org/10.1016/j.jvolgeores.2015.04.010>
- [34] Embey-Isztin A, Dobosi G. Composition of olivines in the young alkali basalts and their peridotite xenoliths from the Pannonian Basin. *Annales Musei Historico-naturalis Hungarici*. 2007; 99:5–22. ISSN: 0521–4726
- [35] Ali S, Ntaflos T, Upton BGJ. Petrogenesis and mantle source characteristics of Quaternary alkaline mafic lavas in the western Carpathian–Pannonian Region, Styria, Austria. *Chemical Geology*. 2013; 337–338:99–113. DOI: <http://doi.org/10.1016/j.chemgeo.2012.12.001>
- [36] Kováč M, Márton E, Oszczytko N, Vojtko R, Hók J, Králipková S, Plašienka, D, Klučiar T., Hudáčková N, Oszczytko–Clowes M. Neogene palaeogeography and basin evolution of the Western Carpathians, Northern Pannonian domain and adjoining areas. *Global and Planetary Change*. 2017; 155: 133–154. DOI: <https://doi.org/10.1016/j.gloplacha.2017.07.004>
- [37] Harangi Sz, Lenkey L. Genesis of the Neogene to Quaternary volcanism in the Carpathian–Pannonian region: Role of subduction, extension, and mantle plume. In: Beccaluva L, Bianchini G, Wilson M. editors. *Cenozoic Volcanism in the Mediterranean Area*. Boulder: GSA; 2007. p. 67–92. ISBN: 9780813724188
- [38] Harangi Sz. Neogene to Quaternary volcanism of the Carpathian–Pannonian Region — a review. *Acta Geologica Hungarica*. 2001; 44/2–3:223–258. ISSN: 02365278
- [39] Balázs E, Nusszer A. Magyarország medenceterületeinek kunsági (pannóniai s. str.) emeletbeli vulkanizmusa. (Lower Pannonian Volcanism of the basin areas of Hungary). *A Magyar Állami Földtani Intézet Évkönyve (Yearbook of the Hungarian Geological Institute)*. 1987; 69:95–113.
- [40] Konečný V, Balogh K; Orlický O, Vass D, Lexa J. Timing of the Neogene–Quaternary Alkaline Basalt Volcanism in Central and Southern Slovakia (Western Carpathians). *Geologica Carpathica Special Issue (Proceedings of XVII. Congress of Carpathian–Balkan Geological Association, Bratislava, September 1–4, 2002)*. 2002; 50/3.

- [41] Seghedi I, Popa RG, Panaiotu CG, Szakács A, Pécskay Z. Short-lived eruptive episodes during the construction of a Na-alkalic basaltic field (Perșani Mountains, SE Transylvania, Romania). *Bull Volcanol.* 2016; 78:69. DOI: <https://doi.org/10.1007/s00445-016-1063-y>
- [42] Martin U, Németh K. Mio/Pliocene Phreatomagmatic Volcanism in the Western Pannonian Basin. *Geologica Hungarica*, series *Geologica*. 2004; 26:1–192 p.
- [43] Embey-Isztin A, Downes H, James DE, Upton BGJ, Dobosi G, Ingram GA, Harmon RS, Scharbert HG. The Petrogenesis of Pliocene Alkaline Volcanic-Rocks from the Pannonian Basin, Eastern Central-Europe. *Journal of Petrology*. 1993; 34/2:317–343. DOI: <https://doi.org/10.1093/petrology/34.2.317>
- [44] Dobosi G, Downes H, Matthey D, Embey-Iszti A. Oxygen isotope ratios of phenocrysts from alkali basalts of the Pannonian Basin: evidence for an O-isotopically homogeneous upper mantle beneath a subduction-influenced area. *Lithos*. 1998; 42:213–223. DOI: [https://doi.org/10.1016/S0024-4937\(97\)00043-1](https://doi.org/10.1016/S0024-4937(97)00043-1)
- [45] Embey-Isztin A, Dobosi G. Mantle source characteristics for Miocene–Pleistocene alkali basalts, Carpathian–Pannonian Region: a review of trace elements and isotopic composition. *Acta Vulcanologica*. 1995; 7/2:155–166.
- [46] Lustrino M, Wislon M. The circum-Mediterranean anorogenic Cenozoic igneous province. *Earth Science Reviews*. 2007; 81:1–65. DOI: [10.1016/j.earscirev.2006.09.002](https://doi.org/10.1016/j.earscirev.2006.09.002)
- [47] Harangi Sz, Downes H, Seghedi I. Tertiary-Quaternary subduction processes and related magmatism in the Alpine-Mediterranean region. In: Gee DG, Stephenson RA, editors. *European Lithosphere Dynamics*. London: Mem Geol Soc Lond; 2006. p. 167–190. DOI: [10.1144/GSL.MEM.2006.032.01.10](https://doi.org/10.1144/GSL.MEM.2006.032.01.10)
- [48] Beccaluva L, Bianchini G, Natali C, Siena F. Geodynamic control on orogenic and anorogenic magmatic phases in Sardinia and Southern Spain: inferences for the Cenozoic evolution of the western Mediterranean. *Lithos*. 2011; 123:218–224. DOI: [10.1016/j.lithos.2011.01.007](https://doi.org/10.1016/j.lithos.2011.01.007)
- [49] Horváth F, Musitz B, Balázs A, Végh A, Uhrin A, Nádor A, Koroknai B, Pap N, Tóth T, Wórum G. Evolution of the Pannonian basin and its geothermal resources. *Geothermics*. 2015; 53:328–352. DOI: [10.1016/j.geothermics.2014.07.009](https://doi.org/10.1016/j.geothermics.2014.07.009)
- [50] Kovács I, Falus Gy, Suart G, Hidas K, Szabó Cs, Flower MFJ, Hegedűs E, Posgay K, Zilahi-Sebess L. Seismic anisotropy and deformation patterns in upper mantle xenoliths from the central Carpathian–Pannonian region: Asthenospheric flow as a driving force for Cenozoic extension and extrusion? *Tectonophysics*. 2012; 514: 168–179. DOI: <https://doi.org/10.1016/j.tecto.2011.10.022>
- [51] Šimon L, Maglay J. Dating of sediments underlying the Putikov vršok volcano lava flow by the OSL method. *Mineralia Slovaca*. 2005; 37: 7–40.
- [52] Panaiotu CG, Jicha BR, Singer BS, Tugui A, Seghedi I, Panaiotu AG, Necula C. ⁴⁰Ar/³⁹Ar chronology and paleomagnetism of Quaternary basaltic lavas from the Perșani Mountains (East Carpathians). *Physics of the Earth and Planetary Interiors*. 2013; 221:1–24. DOI: [10.1016/j.pepi.2013.06.007](https://doi.org/10.1016/j.pepi.2013.06.007)
- [53] Harangi Sz, Sági T, Seghedi I, Ntaflos T. A combined whole-rock and mineral-scale investigation to reveal the origin of the basaltic magmas of the Perșani monogenetic volcanic field, Romania, eastern–central Europe.

Lithos. 2013; 180–181:43–57. DOI:
<https://doi.org/10.1016/j.lithos.2013.08.025>

[54] Balogh K. A K/Ar és $40\text{Ar}/39\text{Ar}$ geokronológia fejlesztése és alkalmazása, I. rész (Development and geochronological application of the K/Ar and $40\text{Ar}/39\text{Ar}$ method, part I.) [DsC thesis]. Debrecen: Hungarian Academy of Sciences, 2006. 229 p.

[55] Tschegg C, Ntaflos T, Kiraly F, Harangi Sz. High temperature corrosion of olivine phenocrysts in Pliocene basalts from Banat, Romania. *Austrian Journal of Earth Sciences*. 2013; 103: 101–110.

Late Cenozoic Collisional Volcanism in the Central Part of the Lesser Caucasus (Azerbaijan)

Nazim Imamverdiyev and Anar Valiyev

Abstract

The chapter is devoted to petrogeochemical features of late Cenozoic collision volcanism of the Lesser Caucasus. It was determined that at the early and middle stages of crystallization of the rocks of the andesite-dacite-rhyolite association, amphibole fractionation played an important role in the formation of subsequent differentials. On the basis of computer modeling, it was found that when mixing andesite and rhyolite (taken as a contaminant) magma, it is possible to obtain a rock of dacitic composition. Under conditions of high water pressure, as a result of fractionation of olivine and pyroxene from primary high magnesian magma, high-alumina basalts are formed, which can be considered as the parent magma. Geochemical features of moderately alkaline olivine basalts indicate that the source of magma is metasomatized, phlogopite-garnet-rutile containing lithospheric mantle. The evolution of moderately alkaline olivine basalts occurs due to changes in the composition of the main rock-forming and accessory minerals. Medium rock formations are formed by the assimilation of poorly differentiated primary magma by an acidic melt. The calculations have shown that proportion of melting rhyolitic melt separated from andesite substrate is close to 15%. After removal of the remaining melt, restite is entirely consistent with the composition of the lower earth crust.

Keywords: late Cenozoic collision volcanism, Lesser Caucasus, geochemical, petrological features, AFC – modeling

1. Introduction

One of the pressing problems of collision zones of the study is to elucidate the evolution of magmatism occurring within them. Display magmatic associations, their petrochemical characteristics reflect the specificity of their manifestations, as well as the development of magmatism from magma generation to the evolution of magmatic melt in the Earth's crust. Materials on the distribution of rare and rare earth elements in different rock types, as well as other of their geochemical and petrological characteristics allow using the well-known models [1–8] to analyze some aspects of the processes of birth, evolution, and crystallization of deep magmatic melts.

In this sense, the study of the geochemical characteristics of mantle and crystal sources of magmatism that have come out in a collision like the continent – the continent is quite topical. Therefore, the study late collision volcanism of the Lesser Caucasus is a theoretical and practical interest.

Such, more than 10 geodynamic models have been proposed on the genesis of Cenozoic collision volcanism including the Eastern Anatolian-Caucasian zone. The most popular models are: (1) lateral upper mantle flow of plume material from the East African rifts [3, 6]; (2) break-off of a subduction slab at the early collision (inversion) stage and, as a result, formation of an asthenospheric uplift under the growing collision orogen directly below the Moho boundary [2, 4–6, 9–10]; (3) collision magmatism with a leading role of oxidation of deep fluids [1]; (4) Paleogene collision-riftogenic volcanoplutonic magmatism, which occurred from lateral compression of the lithosphere and uplift of a less compacted mantle substrate [11]; (5) relationship of late collision volcanism with longitudinal and latitudinal extension structures, which formed in the suture-collision zone during activation of an area along the junction zone [12]; and (6) collision-riftogenic origin of late collision volcanism with mantle metasomatism playing a leading role [13].

Some of these models do not contradict each other and, as noted by Koronovskii and Demina [1], differ in the heat sources necessary for melting and mechanisms by which sources of late collision volcanism melt. On the basis of seismic tomographic, geological-petrochemical, and geophysical data, we have developed a geodynamic model that relates the geodynamic processes and magmatism at the late collision stage of the evolution of the Lesser Caucasus. We also used seismic and seismic tomographic data for the Lesser Caucasus and adjacent collision regions (Eastern Anatolia, northwestern Iran). Having developed the model and analyzed previous models, we tried to assess the role of lithospheric mantle and asthenosphere in the Late Cenozoic collision volcanism of the Lesser Caucasus.

Late Cenozoic geodynamics of the Alpine-Himalayan belt is defined sector of the Mediterranean collision of Eurasian and the Afro-Arabian megaplate [1]. According to modern concepts, folded structures of the Caucasus emerged as a result of their

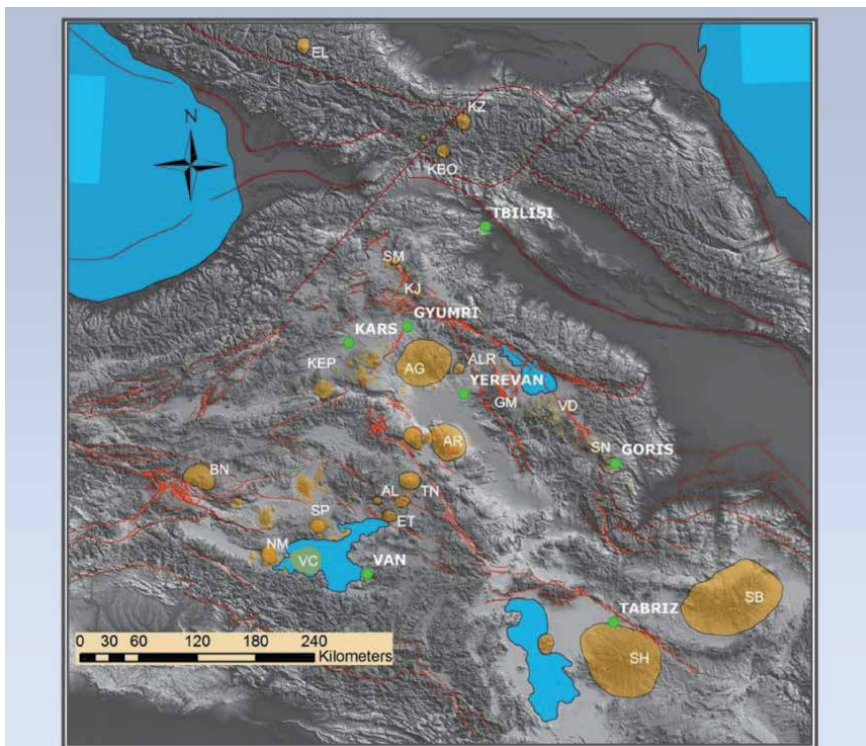


Figure 1. The distribution of Neogene-Quaternary volcanoes in Eastern Anatolia, the Caucasus, North-West Iran.

convergence. According to Koronovsky and Demina [1] in the Caucasian segment of the Alpine-Himalayan orogen Late Cenozoic volcanism manifested itself in an atmosphere of NS compression in the region, led to an accelerated movement towards the north of the Arabian plate due to disclosure in the Late Miocene (about 11–10 million years ago) the Red Sea [1]. This collision stage is divided into the stage of mild collisions (late Middle Eocene – Middle Miocene) and the stage of hard collisions (with the Late Miocene to present). This fragmentation of rigid crust was accompanied by volcanism; mark the sites of local stretching of the lithosphere.

Within the Lesser Caucasus Late Cenozoic volcanism covers part of the Transcaucasian transverse uplift (Akhalkalaki volcanic region, Kechut, Aragats volcano-structural sub-zones) and the eastern volcanic zone (Gegham, Vardenis, Syunik, Kaphan – in Armenia, Karabakh, Kelbajar, Nakhchivan in Azerbaijan) (**Figure 1**).

Since the Middle Miocene, in these zones formed a high volcanic terrain, located on 2–3 km above sea level. Their association corresponds to the Caucasian age of folding, when the intense collision of the Arabian and Eurasian plates. Due to volcanic activity, there were formed many relatively large volcano-tectonic structures, such as Aragats, Ishygly, and others, erupting volcanoes of the central, central-type fracture (**Figure 1**).

Products of the Late Cenozoic volcanism in the Azerbaijan distributions upper river Terter and Akera are characterized by lava flows and pyroclastics varied composition.

2. The late Cenozoic volcanism of the Lesser Caucasus

2.1 Neogene volcanism

Neogene volcanism in the Lesser Caucasus is mainly manifested itself, starting from the upper Sarmatian, Meotis-Ponte to the Upper Pliocene. However, Rustamov in the south-western part of Lesser Caucasus to carry a Molasse basin (Nakhchivan, Karadag) trachyandesite-teschenite and analcite alkaline basalt-trachyandesite, with the absolute age of 14–15 million years, volcanic fissure and concludes that the Neogene stage of volcanism in the region did not begin in the upper Sarmatians and in the Middle Miocene (based on determining the age of rocks with the K-Ar method, and by the stratigraphic position of the studied rocks) [11].

In the central part of the Lesser Caucasus upper-volcanogenic complex with a capacity of 200 m in the literature described as Agdzhagyz suite and submitted dacite, rhyolite, pyroclastic rhyodacites and their derivatives – dacite and rhyolite tuffs. The layers of fine-sedimentary rocks – carbonaceous shales, lignites are present between the volcanic rocks.

Volcanic complex with a thickness of 1150 m Meotis-Pont age first isolated as Basarkechar suite [14] and submitted dacite-trachydasite, andesite and trachyandesite, and latites (**Figure 2**). This complex with the angular and azimuthally unconformity lies at Agdzhagyz suite and places, Eocene and Cretaceous sediments. They overlap with an angular unconformity Upper Pliocene and Quaternary volcanic rocks in the volcanic highlands (**Figure 2**).

These volcanic complexes are distinguished in the differentiated andesite-dacite-rhyolite association [13]. Based on geological data, the age of association is defined as the Late Miocene-Low Pliocene. Volcanics of close age are also known in other regions of the Lesser Caucasus. For example, an Early Pliocene andesite-dacite association is developed within the Miskhan-Zangezour and Yerevan-Ordubad zones. Similar rocks are found within the Gegham and Vardenis highlands in Armenia.

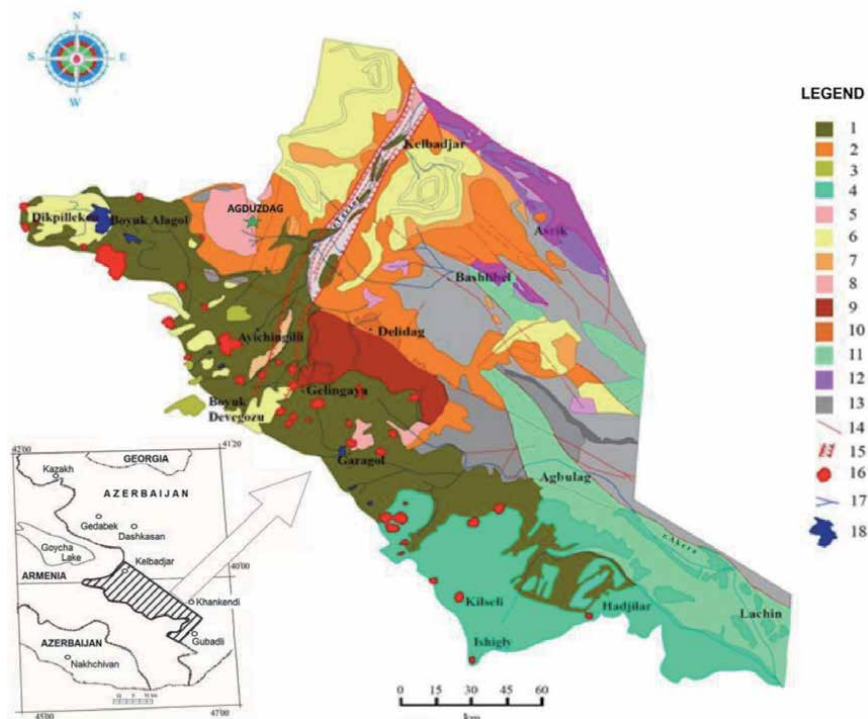


Figure 2. Geological map of Late Cenozoic volcanic associations in the central part of the Lesser Caucasus (Azerbaijan), scale 1:100,000. Compiled by Imamverdiyev [13]. Volcanic association: Quaternary: 1 – trachybasalts, basaltic trachyandesites, and trachyandesites; 2 – tuffs, volcanic ashes, tuff breccias; 3 – rhyolites, perlite, and obsidian; Upper Pliocene-Low Quaternary: 4 – trachybasalts, basaltic trachyandesites, and trachyandesites; Upper Miocene-Low Pliocene: 5 – dacites, rhyodacites, rhyolites; 6 – andesites, trachyandesites, quartz latites, dacites, trachydacites (Basarkechar formation) 7 – dacites, trachydacites, rhyodacites and rhyolites (Ajagz formation); 8 – diorites, granodiorites, syenites; Upper Oligocene-Low Miocene: 9 – granodiorites, granites, monsonites, quartz syenites; Eocene: 10 – andesites, trachyandesites and their tuffs; 11 – granodiorites, monsonites, quartz diorites; Base rocks (Cretaceous): 12 – ophiolites; 13 – flysch; limestone’s, sandstone’s, tuffs; 14 – faults; 15 – Terter deep fault; 16 – largest centers of volcano eruption; 17 – rivers; 18 – lakes.

2.2 Late Pliocene-quaternary acidic volcanic associations

Late Pliocene-quaternary acidic volcanic associations as independent volcanism are widely developed within the Caucasian segment of the Mediterranean belt. Within Azerbaijan, they are confined Kelbajar and Karabakh uplands and form a dome-shaped volcanoes, and a number of small extrusive domes (Kechaldag, Devegezy) with their lava flows composed of rhyolite, rhyodacites their subalkaline varieties, as well as obsidian and perlite (Figure 2).

The age of acidic volcanic rocks of the Lesser Caucasus in the studied region based on their stratigraphic position was considered late Pliocene-Akchagyl-Absheron [15]. This is confirmed by the absolute age. Thus, according to [16] age of rhyolite volcanic rocks Devegezy identified 0.61 million years, Kechaldagh 0.7 million years. Based on these data, the age of acidic volcanic rocks can be considered Quaternary.

Upper Pliocene-Quaternary volcanic associations with a more basic and medium composition, cover the entire Lesser Caucasus, form vast volcanic plateaus and large volcanoes and occupies about 5000 km² of surface area. These volcanic associations in the eastern area of Armenia and Azerbaijan within the differentiated form a continuous trachybasalt-basaltic trachyandesite-trachyandesite-trachyte

series and cover Geghama, Vardenis and Syunik, Karabakh, Kelbajar highlands. In Armenia Kaphan zone has recently been formed basanite-tephrite-picro-bazaltic series.

3. Research methods

This chapter used data from the Neogene-Quaternary volcanism of the Azerbaijan part of Lesser Caucasus based on the authors. Chemical analysis of rocks was determined by the Institute of Geology of Azerbaijan Academy of Sciences X-ray fluorescence method. Rare and rare-earth elements are in Geological and Geochemical Bronitsk expeditions in Russia. Microprobe analysis of mineral composition written in Institute of Geology of Ore Deposits, Petrography, Mineralogy, and Geochemistry, Russian Academy of Sciences, Moscow and Russian Geological Research Institute (VSEGEI), St. Petersburg. Measuring the isotopic composition of He performed in Geochemistry Institute of Academy of Sciences Russia, also used the data Sr and Nd [17, 18] performed on the material of Armenia and Georgia.

4. Petrography characteristics of the Late Cenozoic volcanic rocks

The rocks of the *andesite-dacite-rhyolite associations* form thin flows and subvolcanic body in the form of dikes, extrusions and other recent distributed along the Tartar, Lachin-Bashlybel, Istibulag-Agyatak deep faults (**Figure 2**). Texture of porphyritic rocks, with high (25–30%) content of phenocrysts. In andesites, trachyandesites, latites phenocrysts are plagioclase, feldspar, clinopyroxene, and amphibole. In the more acidic varieties (dacites, rhyodacites, rhyolites their varieties), the proportion of dark-colored minerals decreases, leucocratic minerals also increased to 10%, there is quartz, biotite. The bulk of these rocks have hyalopilitic, glass texture (**Figure 3**).

The compositions of plagioclase in the rocks have An_{30-40} and are paragenesis with amphibole, biotite, clinopyroxene, and feldspar. Plagioclases second generation are relatively acid composition (An_{20-30}), crystallized on its own effusive stage. Feldspar in the rocks present in quartz latites, trachyandesites. The composition ranges from $Or_{55.3}Ab_{26.3}An_{0.3}$ to $Or_{73.4}Ab_{44.0}An_{3.4}$ (**Table 1**). They belong to an intermediate structural-optical type and are monoclinic, but not homogeneous and presented albite and orthoclase phases. Composition of clinopyroxene varies from medium to acid rocks and the proportion of the component increases Fs: $Wo_{37.1-41.4}En_{43.9-40.0}Fs_{19-19.6}$ (for andesites), $Wo_{40.0-44.4}En_{45.4-44.8}Fs_{15.2-11.2}$ (for quartz latites), and $Wo_{41.7-42.7}En_{36.3-34.6}Fs_{22-22.7}$ (for dacites) (**Table 1**) [13, 19]. The compositions of amphiboles in the classification of B.E. Like [20] are responsible chermakit-, pargasit- and magnesian hornblendes.

Analyses of rock-forming minerals were carried out at the analytical laboratories of the Institute of Geology of Ore Deposits, Petrography, Mineralogy, and Geochemistry, Russian Academy of Sciences, Moscow State University; Moscow and Russian Geological Research Institute (VSEGEI), St. Petersburg on a Camebax microprobe. Magnetite was analyzed by conventional chemical techniques at Vernadsky Institute of Geochemistry and Analytical Chemistry, Russian Academy of Sciences. Analysts A.I. Tsepin, V.K. Garanin, and V.S. Pavshukov.

The rocks of the *rhyolite association* of petrographic composition and structural and textural features are divided into crystallized – rhyolites, trachyrhyolites, rhyodacites and glass – obsidians and perlites. Phenocrysts crystallized rocks are

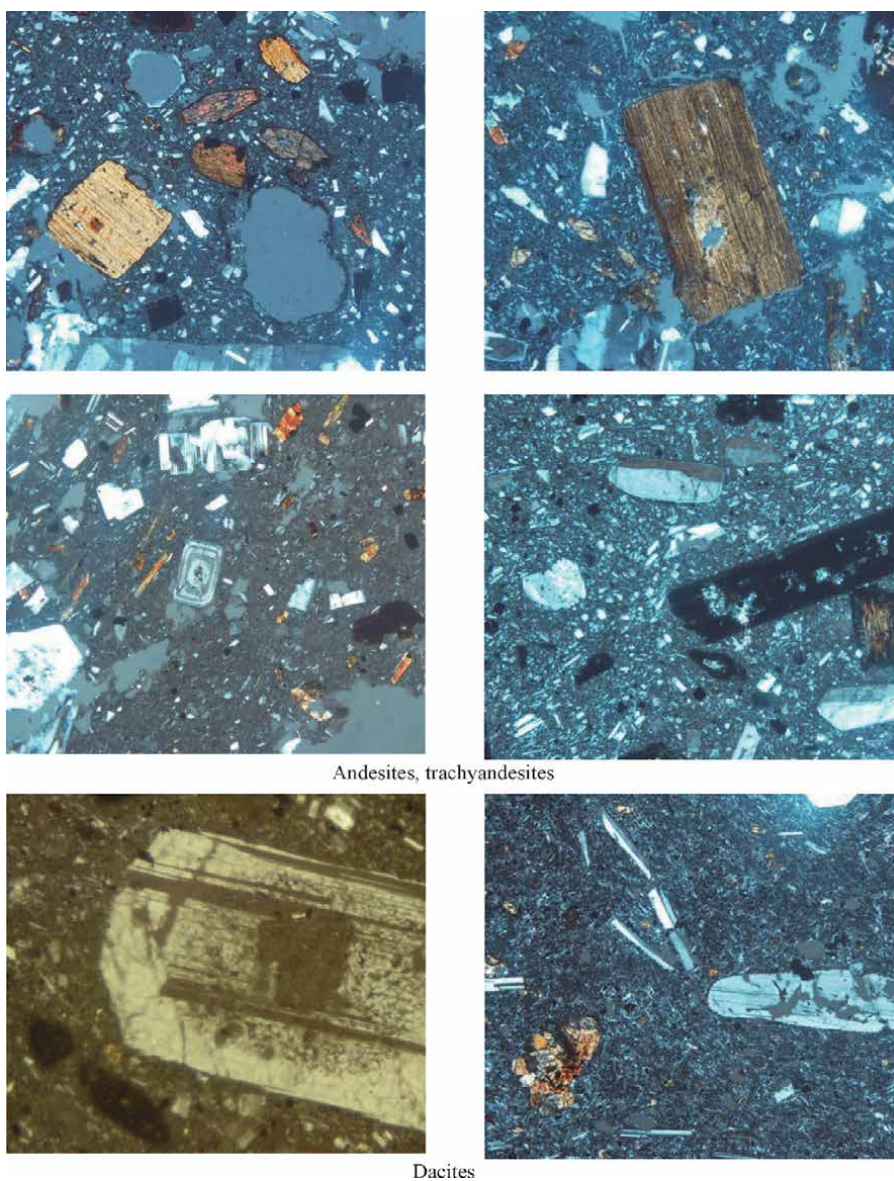


Figure 3. Photomicrographs of the thin sections of rocks of the andesite-dacite-rhyolite association. Plagioclase and hornblende phenocrysts in andesites and trachyandesites, $\times 80$, with an analyzer; zoned-plagioclase and quartz phenocrysts in dacites, $\times 80$, with an analyzer.

plagioclase (An_{30-40}), quartz, less feldspar, biotite and hornblende. Number of phenocrysts is 5–10%.

The rocks of the *trachybasalt-trachyandesites associations* form a continuous series of differentiated trachybasalts to trachyandesites, sometimes comes to trachytes. Moderately alkaline olivine basalts are the most mafic rocks of the studied association. They are porphyritic and aphyric and contain phenocrysts of olivine, clinopyroxene, plagioclase, and amphibole. In places, sanidine megacrysts occur. The rock matrix is of pilotaxitic, hyalopilitic, and microlitic textures (**Figure 4**).

Clinopyroxene rock associations more calcium and composition correspond to augite and salite. Plagioclases have relatively basic composition (An_{63-75}) (**Table 1**). Olivine in the mafic rocks is more magnesian (Fo_{83-87}) and corresponds to

Component	1	2	3	4	5	6	7	8	9	10
SiO ₂	53.51	50.60	52.28	49.54	48.93	39.57	42.97	42.17	39.32	40.71
TiO ₂	0.54	0.27	0.64	0.69	1.52	0.08	2.94	3.00	2.91	4.09
Al ₂ O ₃	3.92	2.34	5.00	4.10	6.98	—	11.56	10.79	13.55	13.87
FeO*	8.46	12.12	7.63	7.53	7.96	14.94	12.08	14.29	12.77	11.51
MnO	0.22	0.25	0.13	0.18	0.13	0.28	0.14	0.25	0.16	0.10
MgO	14.63	12.81	15.09	15.46	13.72	44.86	13.11	13.06	12.91	14.44
CaO	18.50	20.43	18.65	19.94	19.97	0.22	9.94	10.68	12.06	11.70
Na ₂ O	0.52	0.47	0.56	0.64	0.53	—	2.48	2.76	2.88	2.63
K ₂ O	—	—	—	0.04	0.04	—	0.92	0.92	1.42	1.49
Total	100.27	99.65	100.0	98.11	99.58	99.95	96.14	97.92	97.99	100.54
Component	11	12	13	14	15	16				
SiO ₂	58.47	64.59	62.87	57.06	52.52	51.39				
Al ₂ O ₃	25.23	19.48	24.02	26.82	28.94	30.62				
FeO*	0.42	0.09	0.22	0.36	0.43	0.75				
CaO	7.16	0.17	5.55	8.68	13.17	12.99				
Na ₂ O	7.61	4.12	6.96	6.14	4.39	3.79				
K ₂ O	0.63	11.22	1.02	0.87	0.12	0.23				
Total	99.52	99.66	100.63	99.93	99.52	99.77				
Component	17	18	19	20	21	22				
TiO ₂	1.10	4.14	5.49	6.10	5.41	11.10				
Al ₂ O ₃	0.60	2.71	3.04	4.55	4.23	5.10				
Fe ₂ O ₃	—	65.89	53.62	53.08	60.33	43.22				
FeO	91.0	14.02	28.39	19.60	15.68	17.76				
MgO	4.0	2.95	1.99	5.97	7.69	4.06				
Total	96.70	89.71	82.53	89.30	93.34	81.24				

Note: Rocks: Andesite-dacite-rhyolite association: 11, 17 – rhyodacite; 1, 7, 12, 18 – dacite; 2, 8, 13, 19 – andesite; trachybasalt-trachyandesites association: 3, 9, 14, 20 – basaltic trachyandesite; 4, 10, 15, 21 – trachybasalt; 5, 6, 16, 22 – alkaline olivine basalt.

Table 1. Chemical composition (wt %) of (1–5) clinopyroxene, (6) olivine, (7–10) amphibole, (11–16) plagioclase, and (17–22) magnetite from the late Cenozoic volcanic rocks [13, 19].

forsterite-chrysolite (**Table 1**). Olivine in trachyandesites and basaltic trachyandesites is more ferruginous (Fo_{61-70}).

The rocks occur as idiomorphic porphyritic crystals of apatite precipitates; the number of which reaches 0.5–1.25%, and fluoro-apatite. Often present as inclusions in phenocrysts of clinopyroxene and hornblende, indicating that the earlier crystallization.

In the rocks of andesite-dacite-rhyolite and trachybasalt-trachyandesites associations there are two types of inclusions: 1-inclusion, representing cumulates parent rocks, (pyroxenites, gabbro, hornblendites, etc.), 2-crustal inclusion - xenoliths of country rocks, trapped melts of crustal rocks (gabbro-amphibolites, quartz-diorite, quartz-feldspar rocks, etc.). Typical mantle inclusions in rocks associations are absent. Along with the rocks in the rocks of these associations are marked megacrysts sanidine, clinopyroxene, amphibole, phlogopite.

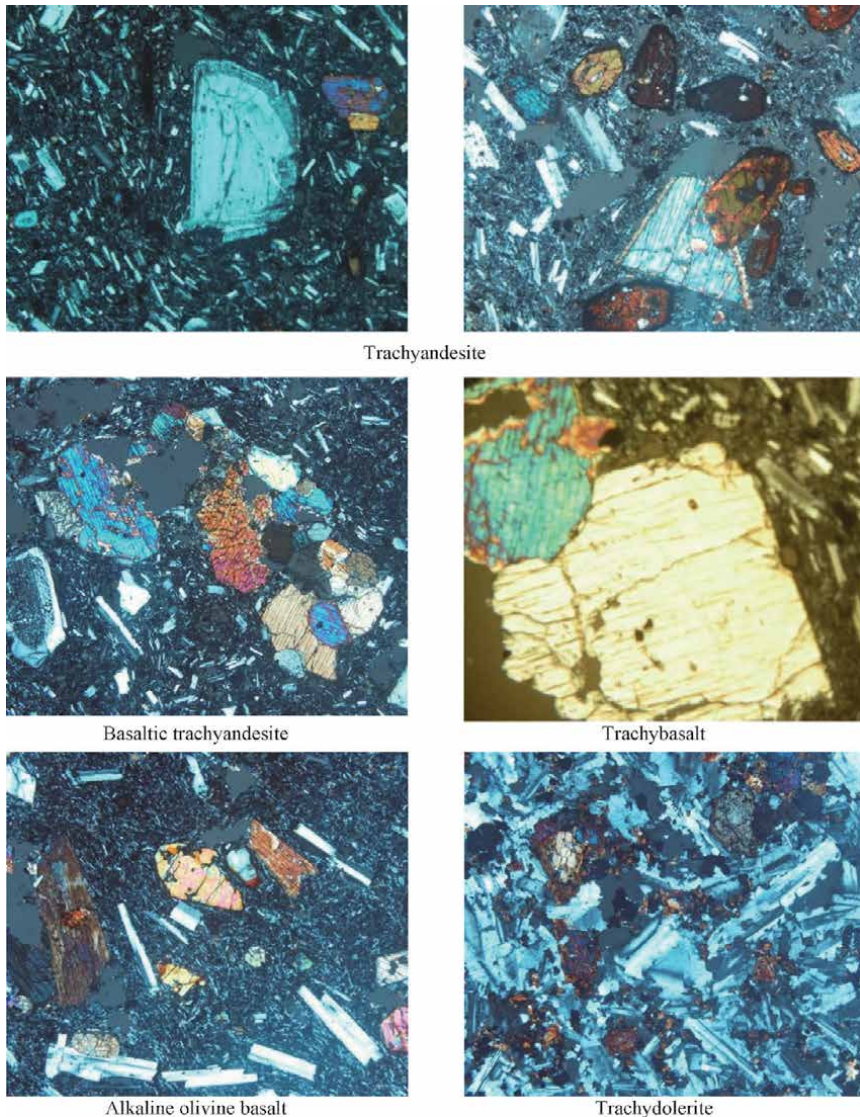


Figure 4. Photomicrographs of the thin sections of rocks of the trachybasalt-trachyandesite association. Trachyandesite (one can see a glomeroporphyritic cluster of clinopyroxenes and opacitized hornblende, plagioclase, and clinopyroxene phenocrysts), $\times 80$, with an analyzer; moderately alkaline olivine basalt with olivine, clinopyroxene, and plagioclase phenocrysts, $\times 80$, with an analyzer; crushed olivine in trachybasalt, $\times 80$, with an analyzer; trachydolerite, $\times 80$, with an analyzer.

5. Petrochemical features of the Late Cenozoic volcanic rocks

5.1 Andesite-dacite-rhyolite association

The association rocks form a continuous series from andesites to rhyolites by SiO_2 contents ($\text{SiO}_2 > 60\%$) (**Table 2**), and the ratio $(\text{Na}_2\text{O} + \text{K}_2\text{O})\text{-SiO}_2$ [21] are the rocks of normal alkalinity (**Figure 5**) (some rocks – mid alkaline) in the diagram $\text{K}_2\text{O-SiO}_2$ [22] most of the samples falls within the high K calc-alkaline series, the diagram $\text{FeO}^*/\text{MgO-SiO}_2$ composition points are located in the field calc-alkaline series.

	1	2	3	4	5	6	7	8	9	10	11	12	13	14	15	16
Elements	40	8	15	100	190	194	106	74	96	12/13	6/174	OA 409	MA 19	105	129	132
SiO ₂	61.09	62.1	62.32	62.99	63.75	63.89	64.81	65.99	68.19	73.99	75.51	76.75	77.01	51.23	48.35	48.88
TiO ₂	0.59	0.49	0.58	0.6	0.81	0.75	0.6	0.52	0.27	0.01	0.01	0.08	0.09	1.39	1.2	1.57
Al ₂ O ₃	15.7	15.41	16.9	16.6	14.81	17.15	17.03	16.41	15.77	13.48	13.79	12.85	12.67	16.49	15.77	15.86
Fe ₂ O ₃	3.47	2.5	3.91	3.28	3.91	4.94	3.38	3.59	1.69	1.2	0.55	n.d.	n.d.	7.74	6.38	5.61
FeO	1.29	0.94	1.01	1.29	2.46	0.43	0.73	0.28	0.43	1.78	0.71	0.66	0.71	0.86	2.16	2.73
MnO	0.06	0.06	0.04	0.09	0.1	0.09	0.03	0.09	0.04	0.01	0.01	0.08	0.06	0.13	0.15	0.14
MgO	1.85	1.77	1.95	1.9	3.18	1.86	1.43	1.31	0.05	0.14	0.36	0.11	0.05	6.04	6.74	6.29
CaO	4.85	5.34	4.24	4.32	6.13	5.25	3.97	3.19	1.32	0.53	1.9	0.44	0.47	8.33	9.8	9.09
Na ₂ O	4.19	3.93	4.07	4.08	3.37	3.3	4.27	4.05	4.57	3.27	2.92	4.44	4.06	4.22	3.61	4
K ₂ O	3.54	2.73	2.95	3.08	2.37	1.87	3.47	2.55	4.14	4.87	3.96	4.59	4.86	1.42	1.96	1.92
P ₂ O ₅	0.41	0.38	0.28	0.3	0.28	0.35	0.33	0.23	0.06	0.01	0.01	n.d.	0.01	0.65	1.03	1.18
LOI	0.81	1.96	0.54	0.46	0.13	0.83	0.47	0.96	0.27	0.38	0.54	n.d.	n.d.	0.7	1.5	0.93
Total	98.63	99.31	99.08	98.1	98.3	99.21	100.72	98.15	99.23	99.67	100.27	100	99.99	99.2	98.65	98.1
Rb	83	66	63	74	42	51	86	72	97	160	180	209	174	23	34	32
Li	20	14	19	19	19	8	12	14	13	67	70	n.d.	n.d.	9	9	9
Sr	1105	935	935	850	520	860	935	833	420	450	100	10	16	1190	1700	1700
Ba	1250	640	650	690	400	850	690	760	830	100	100	10	26	748	780	1060
Cr	120	180	180	180	n.d.	n.d.	180	100	n.d.	30	n.d.	3.13	2.75	346	412	270
V	170	40	60	60	150	110	40	100	40	n.d.	20	n.d.	n.d.	170	170	210
Ni	24	22	30	31	69	25	32	25	15	20	3	n.d.	n.d.	115	113	110
Co	20	30	35	16	34	24	3	15	9	5	3	0.1	0.2	31	29	50

	1	2	3	4	5	6	7	8	9	10	11	12	13	14	15	16
Zr	178	150	160	150	130	160	170	150	240	100	80	83	86	n.d.	230	240
Nb	12	10	11	10	8	11	14	14	17	15	10	37	34	n.d.	20	18
Ta	0.84	0.82	0.72	0.94	0.46	0.77	1.4	1.1	1.2	n.d.	n.d.	3.11	2.71	0.85	0.92	0.92
Hf	4.8	4	3.6	3.3	3.8	4.3	4.7	4.2	6	n.d.	n.d.	3.87	3.51	4.7	4.6	5.2
Th	11	11	9.3	10	n.d.	10	18	16	5.2	25	31	37.3	34.5	3.2	2.6	2.6
U	2.7	4.7	5.7	4.4	4	4	5.4	3.3	14	9.3	12	12.1	10.2	4	4	4
La	45	37	43	36	23	47	47	38	47	33.5	36	23.5	30.7	40	65	63
Ce	88	73	77	76	57	91	87	74	78	60	59	41.4	53	81	130	130
Sm	4.2	3.6	3.9	4.2	7.5	5.1	3.6	4.4	5	3	2.8	2.42	2.51	5.3	9.5	9.8
Eu	1.2	1	1.2	1	1.6	1.6	1.1	0.95	0.79	0.2	0.65	0.1	0.16	1.7	2.5	2.5
Tb	0.67	0.43	0.56	0.58	1.1	0.9	0.44	0.42	0.57	0.6	0.68	0.15	0.13	0.88	1.5	1.3
Yb	1.2	1.3	1.4	1.5	3.6	1.8	1.3	1.3	1.4	2.3	2.3	1.3	1.32	2.4	2.7	2.4
Lu	0.19	0.18	0.2	0.2	0.69	0.23	0.17	0.17	0.18	0.32	0.42	0.24	0.22	0.42	0.39	0.33
Y	36	16	11	10	11	16	n.d.	11	29	10	10	11	11	31	30	34
17	18	19	20	21	22	23	24	25	26	27	28	29	30	31	32	33
Elements	134	21	57	208	53	87	109	120	167	174	13	25	33	143	160	185
SiO ₂	48.05	51.84	49.42	52.97	53.32	53.05	54.92	55.67	54.31	54.01	57.66	58.52	59.85	57.08	59.28	57.85
TiO ₂	1.45	1.36	1.44	1.3	0.97	1.14	1.14	1.08	1.18	1.5	0.79	0.82	0.8	1.24	1.24	0.75
Al ₂ O ₃	15.53	16.64	16.27	16.46	17.39	17.46	16.38	17.13	16.82	17.49	16.41	16.23	16.57	17.25	16.55	17.7
Fe ₂ O ₃	3.55	6.11	7.16	7.04	6.11	5.66	4.54	6.59	5.02	5.79	4.09	4.8	4.88	4.62	4.95	n.d.
FeO	4.46	1.01	0.72	0.3	0.57	1.65	2.59	0.43	2.17	2.46	1.87	0.87	0.5	3.09	1.3	1.88
MnO	0.13	0.11	0.12	0.12	0.1	0.13	0.1	0.12	0.12	0.12	0.05	0.09	0.11	0.1	0.13	0.05

17	18	19	20	21	22	23	24	25	26	27	28	29	30	31	32	33
6.81	4.42	5.27	3.65	3.81	4.12	3.76	4.66	3.84	3.37	3.18	3.23	2.67	2.29	2.79	2.77	1.1
MgO																
9.19	8.58	9.1	7	7.17	6.71	6.88	6.24	6.66	6.8	6.25	6.24	5.61	6.09	5.82	6.12	2.2
CaO																
4.18	4.14	3.22	4.39	5.03	4.27	0.7	4.22	4.78	4.53	3.85	4	4.38	4.53	4.65	4.53	5.5
Na ₂ O																
1.73	2.92	2.48	3.16	2.8	2.77	2.17	2.6	2.96	3.25	3.01	2.8	3.11	2.87	3.46	2.89	4
K ₂ O																
1.13	1.31	1.04	0.93	0.82	0.83	0.94	0.58	0.75	0.94	0.57	0.68	0.79	0.68	0.76	0.44	0.35
P ₂ O ₅																
1.79	0.61	1.9	1.1	0.14	0.35	0.85	0.41	0.19	0.44	0.64	0.4	0.35	0.27	0.2	1.15	0.01
LOI																
98	99.05	98.14	98.42	98.23	98.14	98.47	99.07	98.8	100.7	98.32	98.68	99.72	100.12	101.1	100	100.19
Total																
34	60	31	60	37	36	42	54	70	43	55	49	66	40	56	48	70
Rb																
9	14	9	13	12	12	13	14	14	13	10	12	16	14	17	15	20
Li																
1700	2635	2550	1900	1615	1615	1445	1020	1275	1785	1360	1275	1615	1647	1360	790	1356
Sr																
990	1300	1170	1170	1140	1000	1080	680	1100	1770	830	1060	900	900	1016	930	1100
Ba																
450	170	220	n.d.	157	200	224	280	n.d.	n.d.	160	188	100	n.d.	n.d.	n.d.	140
Cr																
260	140	200	150	200	200	150	170	240	150	80	130	100	140	140	110	70
V																
100	43	64	45	46	48	34	65	40	39	50	54	50	33	29	31	13.5
Ni																
24	26	50	45	19	50	22	45	55	35	45	16	20	40	19	13	11
Co																
250	200	220	250	180	210	250	190	250	250	190	180	220	207	200	160	303
Zr																
20	28	27	23	10	21	18	19	23	22	18	13	18	21	23	15	33
Nb																
0.96	1.2	1.7	1.5	0.8	0.99	n.d.	1	1.4	1.3	0.81	0.87	1	0.98	1.4	0.88	1.43
Ta																
5.1	4.5	4.6	5.2	4.2	4.7	n.d.	4.4	4.8	5	4.8	4.5	5.3	4.7	4.7	4.3	6.6
Hf																
4.9	5.2	7.4	8.1	6.1	5.3	n.d.	5.6	6.4	6.5	6.3	6.5	8.8	5.6	9.5	9.7	3.2
Th																
4	4	4	3	4	4	n.d.	4	3	4	3.6	6.3	4	4	4	4	12.2
U																
62	76	77	77	59	66	69	52	96	80	60	60	70	59	67	48	72
La																

	17	18	19	20	21	22	23	24	25	26	27	28	29	30	31	32	33
Ce	120	150	160	160	120	130	130	98	120	160	120	120	120	120	140	88	115
Sm	9.1	10	11	9.5	6.3	7.4	7.4	5.9	7.4	9.8	5.7	5.3	5.8	7.2	8.6	5.7	6
Eu	2.4	2.5	2.8	2.5	1.6	1.8	2	1.7	2.2	2.7	1.6	1.7	1.7	2	2	1.4	1.5
Tb	1.1	1	1.3	1.3	1	1.4	1.1	0.9	1.1	0.95	1.1	0.94	0.85	1.8	1.2	0.59	1.12
Yb	2.2	1.8	1.9	2.3	1.8	2.1	2	2	2.2	2	1.8	1.9	2	2.2	2.1	1.3	2.1
Lu	0.31	0.22	0.34	0.34	0.25	0.28	0.22	0.39	0.31	0.27	0.31	0.3	0.26	0.25	0.24	0.24	0.25
Y	29	16	23	23	20	24	21	19	27	25	14	15	19	16	19	15	10

1-9 – andesite-dacite-rhyolite; 10-14 – rhyolitic association; 15-33 – trachybasalt-trachyandesite associations.

Table 2. Major (wt %) and trace-element (ppm) composition of a representative rocks of the Late Cenozoic associations in the Lesser Caucasus (Azerbaijan).

The rocks of this association are characterized by different contents of major elements. In volcanic rocks with increasing SiO_2 content decreases TiO_2 , Al_2O_3 , Fe_2O_3 , MgO , CaO , and P_2O_5 , due to fractionation of titanomagnetite, clinopyroxene, plagioclase, and possibly apatite. Weak rates increased content of K_2O . Na_2O is distributed evenly, but also an increase in the number of its slower rate. The reason for this pattern may be a potassium feldspar in the more acidic varieties of rocks.

5.2 Rhyolitic association

Rocks associations, in contrast to the previous rock associations, are characterized by ultra-structure and high alkalinity. There is approximately equal ratio of Na_2O and K_2O and low contents of CaO , MgO , and FeO (**Table 2**). In the normative composition of the rocks are calculated high content of silic components of quartz, feldspar, and corundum.

5.3 Trachybasalt-trachyandesite association

For silica rock associations form a continuous series from basalts to andesites (**Table 2**) and belong to the mildly alkaline series (**Figure 5**). In the diagram K_2O - SiO_2 composition points fall in the region high-K calc-alkaline and shoshonite series. In rock associations in the range of “trachybasalt-basaltic trachyandesite” with increasing silica content of TiO_2 , MgO , Fe_2O_3 , CaO , and P_2O_5 is reduced to a large extent, the contents of the same Al_2O_3 , Na_2O decreases the slow pace. In the transition to trachyandesites content of these elements varies in a narrow range. The maximum content of MgO is observed in trachybasalts and alkaline olivine basalts and varies from 3.97 to 6.81% (**Table 2**), and the coefficient of Mg^{\neq} (M) from 56 to 71. In subsequent decrease differentiates the content of MgO and “M.”

In the normative part of some mildly alkali olivine basalts and trachybasalts calculated normative nepheline and olivine, and in more acidic differentiates calculated hypersthene and quartz. Normative and mineral composition reflects the

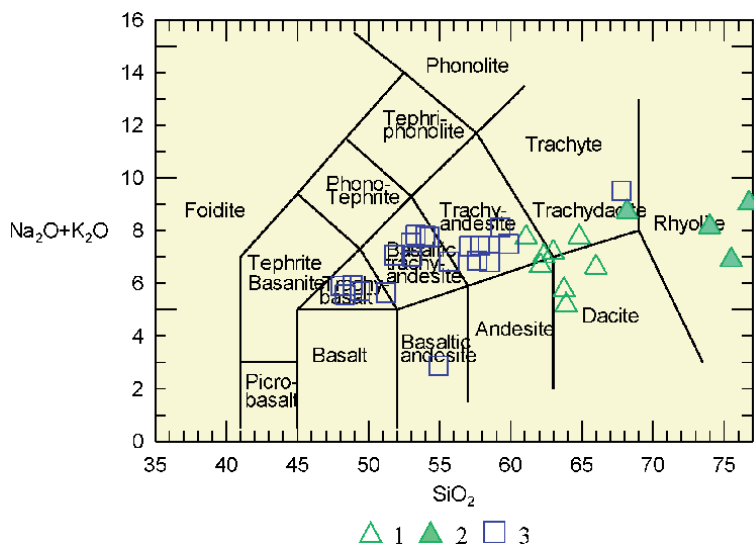


Figure 5. Total alkali vs. $-\text{SiO}_2$ (TAS) classification diagrams [21] of Late Cenozoic volcanic associations of the Lesser Caucasus. In. 1 – andesite-dacite-rhyolite; 2 – rhyolitic association; 3 – trachybasalt-trachyandesite associations.

characteristic feature of the association: transition nepheline-normative, olivine containing mildly alkaline rocks to hypersthene-normative, and sometimes quartz-bearing alkaline rocks.

6. Geochemical features of the Late Cenozoic volcanic rocks

The concentrations of rare and rare earth elements are in rocks of andesite-dacite-rhyolite association as a whole regularly changing. Thus, the concentration of lithophile elements increases from andesite to rhyolites (Rb from 44 to 128 ppm, Th 6 to 24 ppm) (Table 2). From the coherent elements in increasing the acidity of rocks in general, the content of V, Cr, Co, and Ni decreases. These elements are the same Sr form of silica negative dependence. Positive, but more vague correlation with silica form the content of Y and highly charged elements (HFSE – Nb, Zr, Hf). The above features show the leading role of crystallization differentiation in the association of rocks. As shown Dilek et al. [2] comparison of impurity elements rocks andesite-dacite-rhyolite association and the primitive mantle [23] shows the reduced content of Nb and Ta and elevated levels of lung large ionic lithophile elements (Rb, Ba, Th, La, Ce, and Sr) (LILE). Thus, in relation to the primitive mantle, there is a maximum Rb, Ba, Th, La, Ce, Sr, and negative Ta-Nb anomalies (Figure 6).

It is conceivable that this feature brings these rocks with subduction volcanic associations. From the same type of rocks of andesite-dacite-rhyolite association rocks rhyolite associations differ depleted femic components, a lower content of iron group elements, highly charged elements, and enrichment of ore elements in the earth crust, as well as lithophile elements (Pb, Th, U). The distribution of trace elements normalized to primitive mantle for the rhyolite showed that, like the rock of the previous association, rhyolite is enriched in LILE and depleted in highly charged elements. However, the nature of the schedule of rhyolites differs from the schedule of rocks of the previous association and is similar to the composition of the rocks of the earth's crust, which indicates a different genesis of the rocks of this association. In the rocks, trachybasalt-trachyandesite association occurs in about the same pattern as in the rocks of andesite-dacite-rhyolite association, but more clearly. Rocks of this association are inherent to the high content of Rb, Ba, La, Sr, as well as high values of La/Yb, La/Sm relations. Compared with the composition of

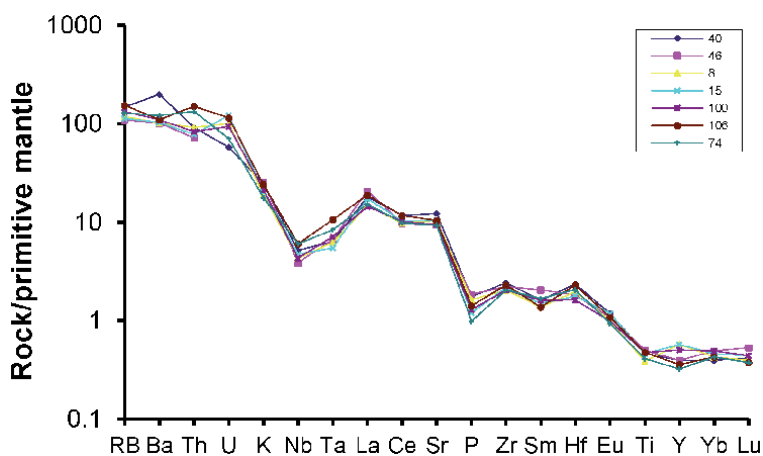


Figure 6. Normalized to the primitive mantle [23] spider diagrams for the andesite-dacite-rhyolite association.

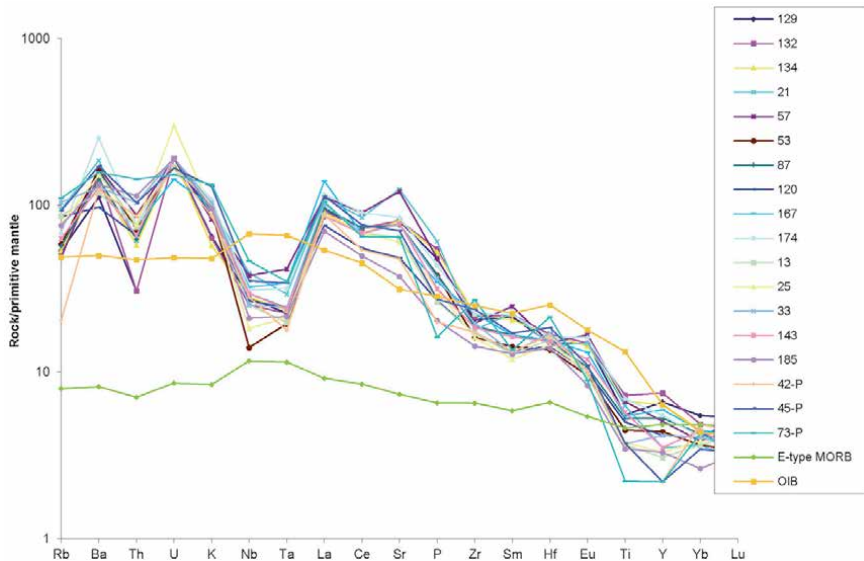


Figure 7.
Normalized to the primitive mantle [23] spider diagrams for the trachybasalt-trachyandesite association.

primitive mantle [23], alkaline basalts are enriched in most LILE and some highly charged elements: Rb, Ba, Th, La, Ce, Sr, Zr (**Figure 7**).

Geochemical data for this association show that the diversity of species association is due mainly to fractional crystallization. This is evidenced by: (1) with increasing SiO₂ content decreases compatible elements (Cr, Ni) and increasing concentrations of incompatible elements (Rb, Th, U) due to fractionation of olivine and clinopyroxene, and (2) revealed clear positive correlation connection LREE with phosphorus, calcium and fluoride, due to the concentration of light rare earth elements in apatite (the distribution coefficients of REE for apatite is 10–100). These data indicate that fractional crystallization is particularly important for trachybasalts and basaltic trachyandesites. In the process of differentiation of the content of trace elements naturally varies depending on the composition of the melt, its temperature, as well as the composition and crystal-chemical properties of rock-forming minerals. Content and types of spectra of these elements of the rock trachybasalt-trachyandesite associations of the Lesser Caucasus are close to the rocks of oceanic islands and the rift zones formed from the enriched mantle source. Similarity of plots, the distribution of elements on the primitive mantle may indicate comagmatic members of the association.

7. Isotopic composition of the Late Cenozoic volcanic rocks

For the Neogene-Quaternary rocks of the Lesser Caucasus, we have obtained for the seven samples of volcanic rocks and their nodules isotopic compositions of He (**Table 2**). The highest ratio of ³He/⁴He (³He/⁴He = 0.93 × 10⁻⁵) is characteristic for alkali olivine basalts, which brings them to the mantle derivatives. Approximately, the same value is obtained for amphibole megacrysts from trachyandesite approaching the isotope ratios of primary helium mantle reservoirs (1–5 × 10⁻⁵) [24] and to the gases carbon sources, the most active areas associated with manifestations of modern volcanism of the Lesser Caucasus (³He/⁴He = 10⁻⁵) [24]. A fractional difference between the rocks of trachybasalt-trachyandesite association, their nodules, as well as andesite of andesite-dacite-rhyolite association has lower

No samples	Rocks and minerals	$^3\text{He}/^4\text{He}\cdot 10^{-6}$	$^4\text{He}\cdot 10^{-6}$
132	Alkaline olivine basalte	9.29 (± 1.46)	0.604 (± 0.006)
21	Trachybasalte	1.76 (± 0.27)	2.70 (± 0.03)
13	Trachyandesite	1.05 (± 0.18)	1.54 (± 0.02)
15	Andesite	0.924 (± 0.162)	2.36 (± 0.02)
Nodules			
25-b	Pyroxsenites	3.33 (± 0.49)	3.43 (± 0.03)
13-m	Megacryste amphybole	9.39 (± 1.42)	2.90 (± 0.03)

Table 3.
Isotopic composition He in Late Cenozoic rocks of the Lesser Caucasus.

values of helium isotopes (**Table 3**). These data indicate that differentiate the first association, incorporation, and andesite second association crystallized in the earth crust.

Unfortunately, Sr and Nd isotope data for Late Cenozoic volcanics in the Azerbaijani part of the Lesser Caucasus are absent. There is anecdotal evidence about the Armenian and Georgian part of the Lesser Caucasus. Chernyshev and his co-workers [17, 18] determined the absolute age of alkali basalts Javakheti Plateau; they proposed a new version of the geochronological scale of the Neogene-Quaternary magmatism of the Caucasus. Dan precisens absolute age of rhyolite volcanism for different volcanic highlands of the Lesser Caucasus [16]. Data above authors argue that the dominant role in the petrogenesis of lavas played by processes of fractional crystallization and contamination of the parent melts geochemically distinct from them, crustal matter [17]. A sour rhyolite volcanism developed in the context of tectonic and thermal activity of mantle lesions and relationship with the processes of local anatexis in the lower crust zones of metamorphism [16]. Our petrology and geochemistry data confirm these findings.

8. Discussion of results

This section discusses the nature of the mantle substrate region under study as well as the origin of each of volcanic associations.

8.1 Mantle sources of the Late Cenozoic rocks

These isotopic compositions of Sr and Nd for late Cenozoic volcanic rocks of the Lesser Caucasus show that the primary melts to produce a mantle sources. Acid rock has mostly crustal origin. There have been offset mantle and crustal magmas. In general, this assumption is acceptable for the Azerbaijan part of the region.

A common feature for most of the Neogene-Quaternary volcanic rocks of the Lesser Caucasus is a relative enrichment in light REE and large lithophile elements (Rb, Ba), and weak depletion for heavy rare earth elements, as well as Nb, Ta, Hf [1–3, 7–8, 13, 18, 25–33]. These geochemical data confirm the presence of restite of garnet in the magmatic source for the andesite-dacite-rhyolite and trachybasalt-trachyandesite associations. In addition, we believe in the petrogenesis of Late Cenozoic collision basaltoids important role played mantle substance metasomatically processed by previous subduction processes, as evidenced by the relatively high oxidized rocks associations.

Figure 8 $(Ce/Yb)_{MN} - Yb_{MN}$ shows the calculated line of equilibrium partial melting of garnet peridotite with different contents of garnet. Calculated trends melting portions of garnet peridotite, containing 2.5, and 4% garnet, borrowed from [34]. As seen from **Figure 8**, composition points of rocks of andesite-dacite-rhyolite associations are in the range of values with a relatively high degree of melting (3–10%) mantle source containing 4% garnet. Lineups alkali basaltoids trachybasalt-trachyandesite association on this chart are in the range of values with a low degree of melting (1–2.5%) garnet peridotite and, apparently, mantle source was more metasomatized [13]. It can be assumed that a lower degree of melting of the mantle of the substrate led to the association of basaltic melt at high alkalinity and a significant enrichment of the melt K, P, F, Ba, LREE due priority to the melting of phlogopite, apatite, amphibole, which are the main carriers of these elements.

At present, the association of these volcanic rocks is often associated with the association of subduction “windows” (slab-window) and sees the result of decompression melting of asthenospheric diapir. These volcanics differ from typical subduction magma and have geochemical characteristics of OIB sources. They are described for the active continental margin of North America, Philippines, Kamchatka, East Sikhote-Alin [35, 36]. For collision volcanics, this idea is developed [3–10, 25–26, 30–33, 37]. Such rocks are called adakites. They are characterized by high ratio LREE/HREE and are formed by melting of garnet containing material (eclogite) oceanic plate.

Note that we also do not deny the delamination subduction lithospheric slab in the association of Late Cenozoic volcanic rocks of the Lesser Caucasus [2, 7–8, 30–31]. This is evidenced Seismic and some of petrology and geochemistry data. Part of Late Cenozoic andesite and dacite of the Lesser Caucasus can be considered derivatives adakites melts. They $(La/Yb)_n$ vary from 17.5 to 26.4, the concentration of Y from 6 to 13 ppm, Yb from 1.2 to 1.8 ppm. Figure Sr/Y-Y majority of species fall into the field adakites [38] (**Figure 9**).

Thus, it is found that the rocks of the Neogene andesite-dacite-rhyolite and Upper Pliocene-Quaternary trachybasalt-trachyandesite association smelt garnet sources at a

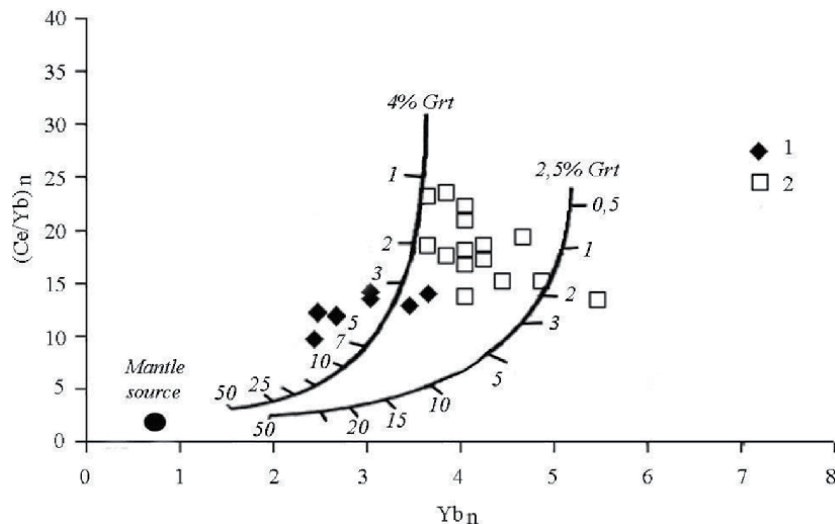


Figure 8. Normalized to primitive mantle [23] the ratio of $Ce/Yb - Yb$ in the Late Cenozoic basalts and andesites of the Lesser Caucasus. Calculated trends melting portions of garnet peridotite, containing 2.5 and 4% garnet [38]. The numbers along the curves – the percentage of melting. Legend: 1 – andesite-dacite-rhyolite association, 2 – trachybasalt-trachyandesite association.

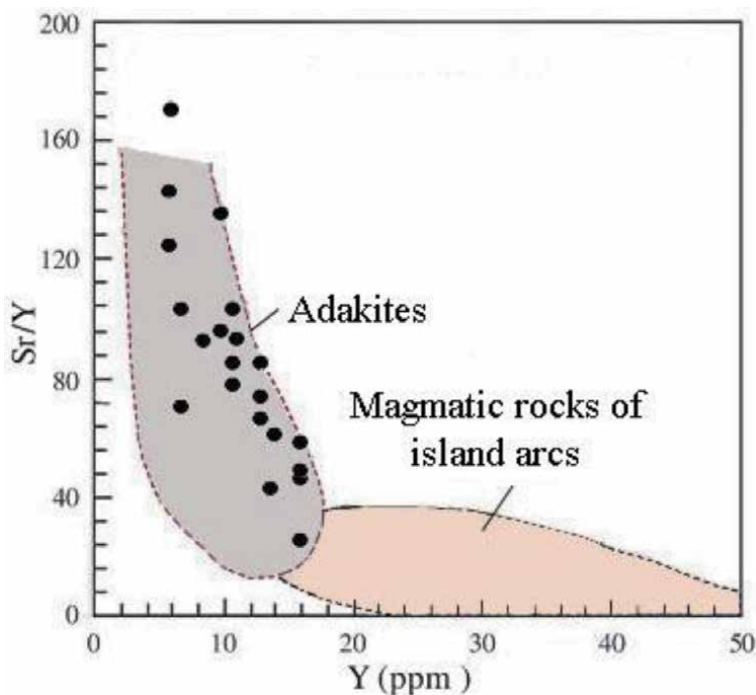


Figure 9. *Sr/Y vs. Y in the Neogene andesite-dacite-rhyolite association. The range of adakite and arc magmatic rocks is after [38].*

depth of not less than 60–80 km [8, 33]. Not be excluded on the association of andesite melting subduction oceanic crust [39]. As Upper Pliocene-Quaternary acidic volcanic rocks, as shown by the full range of studies and published isotopic data for the region, the source of rhyolite-dacite magmas could serve as a rock granite-metamorphic layer, metamorphosed to amphibolite, and granulite facies metamorphism. The high concentrations of K, Li, Rb, Cs, U, Th, Rb and low Sr, Ba, Zr, Ti and light lanthanides, the presence of a deep negative Eu – anomalies may indicate relatively low levels of fusion substrate, in which a significant portion of plagioclase and accessories remained in the restite. The eastern part of the Lesser Caucasus (Vardenis and Syunik uplands) (**Figure 1**) $^{87}\text{Sr}/^{86}\text{Sr}$ are 0,70,444–0,70,811 [18].

8.2 The role of fractional crystallization in the formation of late Cenozoic volcanic rocks

Petrochemical data show that the association of andesite-dacite-rhyolite and trachybasalt-trachyandesite association of fractional crystallization occurred. Thus, in the rocks of andesite-dacite-rhyolite association with increasing silica content decreases femic rock-forming oxides, increasing the content of incompatible elements due to fractionation of dark-colored minerals and feldspars. However, fuzzy trends show the influence of processes of assimilation and crustal contamination on the association of these rocks. Thus, an attempt to get out of andesitic dacites and from dacitic rhyolites by fractionation of clinopyroxene, amphibole, biotite, magnetite, and feldspar failed [31–33]. Therefore, as will be shown below, apparently, the formation of these rocks is dominated by a single process of AFC, that is, assimilation and fractional crystallization.

We believe that fractional crystallization played a leading role in the association of rocks trachybasalt-trachyandesite association [13, 32–33]. This is evidenced by

the behavior of a number of rock-forming trace elements. For example, a change in slope of trends MgO-SiO₂, TiO₂-SiO₂, and Ni-SiO₂ in the field trachyandesite explained by fractionation of olivine, clinopyroxene, and magnetite.

Past balance calculations on a computer showed that the evolution of the melt occurred as a result of changes in the composition and quantity of rock-forming minerals. The results of balance calculation of fractional crystallization of alkaline olivine basalt-trachybasalts showed that the latter is obtained by fractionation of 19.8% Cpx, 57.6% Pl (An₆₅), 15.0% Ol (Fo₈₄) and 7.6% Mt. As seen from **Table 4**, the absolute and calculated values for major and trace elements in the whole match ($\Delta R^2 = 0.507$). The degree of fractionation at the same time is about 61%.

Fractionation of the above minerals and amphibole leads to further differentiates associations and the result is a continuous differential series – trachybasalt-basaltic trachyandesite-trachyandesite. Possible further differentiation of the melt to the trachytes, trachyriodasites, that is, for example, in a large polygenic volcano Ishygly.

Although, FC simulation of least squares using the basic rock-forming oxides and some trace elements gives good results, the majority of trace elements do not conform to this model. Thus, the content of LREE and HREE for different types of rocks vary in narrow limits. At Harker diagrams micronutrients – SiO₂, where not all elements give a clear linear dependence. This suggests their association by other mechanisms, too.

8.3 The role of crust contamination in the formation of late Cenozoic volcanic rocks

By Imamverdiyev previously shown that the role of crustal contamination in the genesis of Late Cenozoic volcanic rocks of the Lesser Caucasus is negligible [13]. In other works [12, 18, 39] speculation is about a significant transassociation of the primary magmas of crustal processes. We obtained the last petrogeochemical data suggest involvement in petrogenesis Late Cenozoic volcanic enriched mantle source (lithospheric mantle) and a significant contribution to processes of crustal contamination. The calculations show AFC – a model of crustal material required for the appropriate changes to the source mantle composition of rocks trachybasalt-trachyandesite association can be achieved during the fractionation of basalts (degree of fractionation of $F = 0.5-0.6$) with the absorption of a large number of acid melt (the ratio of assimilation rock and cumulates $r = 0.3-0.5$) (**Table 5**). A similar pattern is observed for rocks of andesite-dacite-rhyolite association, but this shift is achieved with a high degree of fractionation ($F = 0.7-0.9$) and with a large

		SiO ₂	TiO ₂	Al ₂ O ₃	FeO*	MgO	CaO	Na ₂ O	K ₂ O	P ₂ O ₅					
Parental magma	1	51.36	1.05	16.77	7.76	6.29	10.48	3.14	2.10	1.05					
Calculated parental magma	2	51.76	0.84	16.68	7.80	6.31	10.46	3.36	1.61	1.14					
Daughter magma	3	54.60	1.07	17.13	6.85	4.28	8.57	4.28	2.14	1.07					
	Rb	Ba	Sr	V	Cr	Ni	Zr	Sc	Cu	La	Ce	Sm	Eu	Yb	Y
1	35	943	1871	105	315	105	240	11	73	63	130	9.8	2.5	2.4	19
2	44	953	1956	2119	575	56	151	22	73	158	112	7.5	1.5	0.8	12
3	64	1392	2821	150	182	46	214	21	101	81	161	10.7	2.1	1.1	17
D	0.01	0.01	0.04	1.99	4.02	1.53	0.08	1.12	0.16	0.03	0.05	0.08	0.09	0.11	0.11

D – Bulk partition coefficient (are taken from [13, 40]).

Table 4.
 Balance calculation for alkaline olivine basalt-trachybasalts (petrogenic elements recalculated to 100%).

Elements	1	2	3	4	5	6	7	8
SiO ₂	52.46	79.17	64.73	64.94	55.74	79.17	58.76	58.90
TiO ₂	1.09	0.00	0.00	0.10	1.09	0.00	0.00	0.61
Al ₂ O ₃	16.39	13.54	17.86	17.87	16.39	13.54	18.16	17.89
FeO*	7.10	0.00	4.02	4.04	6.01	0.00	5.98	5.99
MgO	6.56	0.00	2.23	2.24	4.37	0.00	3.21	2.96
CaO	9.84	0.00	5.58	5.55	8.74	0.00	7.48	7.51
Na ₂ O	4.37	4.17	3.35	3.34	4.37	4.17	4.27	3.95
K ₂ O	1.09	3.13	2.23	1.87	2.19	3.13	2.14	1.75
P ₂ O ₅	1.09	0.00	0.00	0.04	1.09	0.00	0.00	0.47
Rb	32	180	59	68	37	174	35	58
Sr	1700	100	1819	1918	2635	16	1543	1306
Ba	1060	100	815	524	1300	26	662	666
Zr	240	80	223	125	250	86	205	152
Ni	110	3	45	28	43	3	43	56
Cr	270	30	180	174	170	3	214	166
V	110	20	78	790	140	20	128	142
$\sum R^2 = 0.154$ $r = 0.53$ $F = 0.57$							$\sum R^2 = 0.93$ $r = 0.25$ $F = 0.68$	

1 – alkaline olivine basalts (initial melt), 2 – rhyolite (assimilation rock), 3 – trachyandesite (hybrid), 4 – calculated composition of trachyandesites, 5 – trachybasalt (initial melt), 6 – rhyolite (assimilation rock), 7 – basaltic trachyandesite (hybrid), 8 – calculated composition (all analyses have been converted to 100%).

Table 5.
Results AFC – modeling for rocks trachybasalt-trachyandesite association.

number of acidic substances ($r = 0.6$). Obviously, with such volumes of assimilation acidic substances are not stored petrochemical characteristics of the primary rocks (andesites and basalts). Therefore, Harkers figures are not observed clear trends.

Below are the results of AFC – modeling for rocks trachybasalt-trachyandesite association.

As seen from **Table 4**, the intermingling rhyolite and basic rocks (alkaline olivine basalts and trachybasalt) may be formed basaltic trachyandesite and trachyandesite.

Summarizing the above data, the association of Late Cenozoic volcanic series of the Lesser Caucasus can be represented as follows.

Within the Lesser Caucasus in the late Cenozoic volcanism expressed high-K calc-alkaline, mildly alkaline, and partly alkaline associations. In Neogene time (Upper Miocene-Lower Pliocene), with decompression occurs anatexis metasomatized mantle and lower strata of basalt layer at a sufficiently large depth, which determines the enrichment of these melts with alkali, alkaline earth, and light rare earth elements.

This process resulted in association of basaltic melts, enriched in alkalis. Perhaps such a melt was formed at low degrees of partial melting (3–10%) of garnet peridotite or eclogite. We can assume that it corresponds subduction oceanic crust. In the future, as a result of growing tension mantle melts penetrated the upper layers of the earth crust, where it mixes basic and acid magma, with the association of hybrid andesite, andesite-dacite lavas (**Figure 10**). Progressive

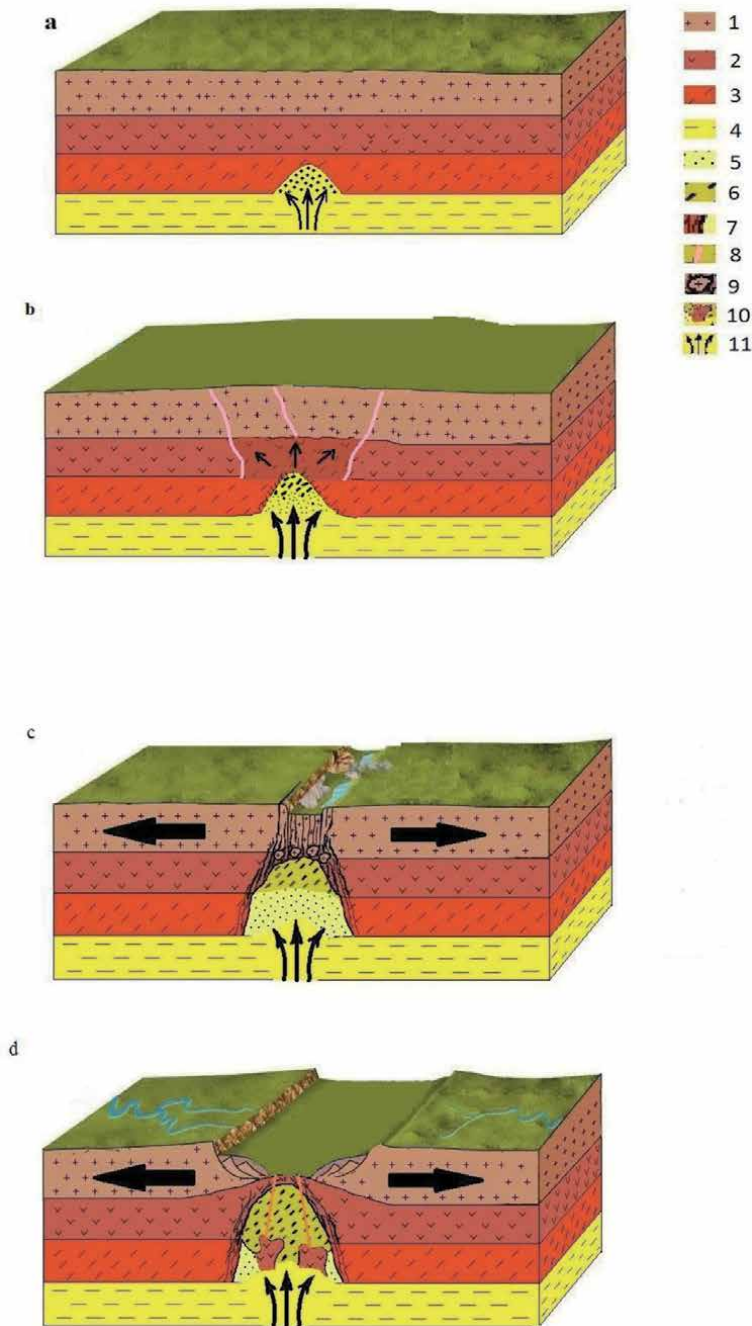


Figure 10. Scheme of tectonic development and volcanism of the areas of matium magma formation at the Late Cenozoic stage of development of the Lesser Caucasus [8]. (a) Initial stage of mantle diapir growth; (b) Upper Miocene-Lower Pliocene stage; (c) in the Upper Pliocene is a new stage; (d) Upper Pliocene-Quaternary stage – stage of general extension. 1 – granite layer; 2 – basalt layer; 3 – mantle; 4 – astonesphere; 5 – metasomatized mantle; 6 – region anatexis; 7 – partially molten basalt layer; 8 – dykes; 9 – partially molten granite-metamorphic layer; 10 – partially molten material of the upper mantle; 11 – upward mantle fluid flows.

cooling of the deep source magma origin may be the cause of education dike fields in the region studied and possibly fractured outpouring mildly alkaline volcanism observed in the other parts of the Lesser Caucasus. Due to additional heating and

the flow of volatiles formed fairly large volcanoes of calc-alkaline composition of Neogene age. Then Upper Pliocene-Quaternary formed bimodal volcanism. Thus, the temporal spatial conjugation of crustal and mantle magmatism led to the introduction of mantle melts, under conditions of tension in the lower crust, which resulted in its melting and the association of acidic volcanic rocks rich in radiogenic Sr and Nd (rhyolite association). Simultaneously, in this situation, a change of scenery compression and tensile contributed to the development rifts depressions, arching and exercise slow differentiated and undifferentiated volcanic (-trachybasalt-basaltic trachyandesite-trachyandesite and basanite-tefrite series). Thus, the evolution of the melt in the earth crust is dominated by a single process of AFC (assimilation and fractional crystallization). As the fractionation rare elements, intermediate rocks can be formed by mixing trachybasaltic and rhyolite melts.

9. Conclusions

A distinctive feature of the investigated Late Miocene-Early Pliocene rocks of the Lesser Caucasus is that they are generally medium and acid. Volcanite composition meets mainly andesites and trachyandesites, dacites and trachydacites and also rhyolites. The volcanism was very powerful in relation to the attic tectonic activity of Late Miocene-Early Pliocene. During this period, there occurs Pre-Mesozoic base uplift and volcanism is mainly manifested in the central parts of the anticlinal zones of the Lesser Caucasus. The andesites and andesidacites with acid pyroclasts dominate in the products' composition at the beginning of the volcanic phase and at its end – andesite lavas. Magmatism of the main composition of high alkalinity has locally been manifested in the extreme parts of the anticlinal zones. Subvolcanic appearances of formation invaded after volcanogenic strata (Basarkechar suite) formation and have more acid composition. After active effusive-explosive activity of Meotian-Pontian-Early Pliocene volcanoes, more acid and viscous magma, cooling at a depth, rising along fractures at shallow depths hardened in the form of dikes and other subvolcanic bodies.

On the basis of nine petrogenic elements oxides (SiO_2 , TiO_2 , Al_2O_3 , FeO^* , MgO , CaO , Na_2O , K_2O , P_2O_5) such independent groups as andesite-trachyandesite-quartz latites, dacite-trachydacites and rhyodacite-rhyolites have been defined for andesite-dacite-rhyolite formation using factorial diagram.

It has been shown that with increasing SiO_2 content in the rocks composition, the content of TiO_2 , Al_2O_3 , FeO^* , MgO , CaO , P_2O_5 decreases due to fractionation of titanomagnetite, clinopyroxene, plagioclase, amphibole, and apatite. The calc-alkaline trend of andesite-dacite-rhyolite series is controlled not only by magnetite fractionation but also by the hornblende crystallization, having a high Fe/Mg ratio and by SiO_2 under saturation. First, it has been proved that the early hornblende crystallization in the Neogene magmatism evolution is the principal factor in the calc-alkaline series formation. This regularity is especially obvious during change of SiO_2 content between 60 and 64%. The slow increase of K_2O and Na_2O content in the rocks formation is explained by potassium feldspar crystallization.

In formation's volcanites with increasing SiO_2 content from andesites to rhyolites and with decreasing MgO quantity the coherent (compatible) elements as macroelements give a linear and sometimes expressed broken dependence. The figurative points of the homogenous inclusions are at the beginning of these dependence trends. These elements distribution in the rocks of formation is controlled by fractionation of rock-forming minerals and accumulative (homogenous)

crystallization of the inclusions. The incompatible elements content (Rb, Th, Nb, Zr, Hf, LREE, etc.) is minimal in the deep-seated inclusions.

In rocks of formation the light lanthanoids prevail in relation to heavy, and therefore La/Sm, La/Yb relations are high. In medium rocks (quartz latites and andesites), it is defined approaching Eu/Eu* relation to unit ($\text{Eu}/\text{Eu}^* = 0.94\text{--}1.05$) and in more acid rocks – Eu-minimum ($\text{Eu}/\text{Eu}^* = 0.58\text{--}0.63$) that indicates on plagioclase fractionation. It has been established that the content of Ba and Ba/Y, Rb/Y, Th/Yb relations are rapidly increased in the formation's rocks. The formation's rocks enrichment with lithophilous and rare-earth elements caused by relatively high degree of fusion melting that enriched by fluids.

Based on the modeling, it was determined that as a result of high fractionation of the initial melt ($F = 0.96$) during mixing of 32.4% andesite and 63.4% rhyodacite; it is possible to obtain dacite of hybrid origin. The leading role of single process of Assimilation and Fractional Crystallization (AFC) is responsible for forming the igneous rocks of formation.

It has been shown that the enrichment of formation's rock with light rare-earth elements and many incompatible elements indicates on sufficiently important role of the enriched mantle matter in their formation. The high-alumina basalts can be considered as the parental magma for formation's rocks. Their formation is connected with fractionation in the environment of high water pressure from the initial high-magnesian melt of the olivine-clinopyroxene association.

So, the Neogene volcanic series formation of the Lesser Caucasus can be represented as follows.

At the beginning of the Late Cenozoic, the mantle metasomatism occurred as a result of regional compression in the lifting diapir. In the Late Miocene-Early Pliocene anatexis of the metasomatized mantle and lower parts of the basalt layer occurs due to decompression at sufficiently great depth that determines these melts enrichment with alkali, alkaline-earth, light rare-earth elements. As a result of this process, there is formed basalt melts enriched by alkalines. Further evolution of these melts occurs in conditions of continental Earth crust where medium-acidic rocks as steeply dipping dikes and volcanic edifices of the central, central-fractured type are formed due to melts differentiation (**Figure 10**).

The primary magma evolution was accompanied by fractionation of olivine-clinopyroxenic mineral associations and the appearance of high-alumina residual magma in the deep-seated foci. The last ones outcropping are accompanied by a stop at the intermediate foci, fractionation of plagioclase, clinopyroxene, amphibole, surrounding rock melting, crustal material contamination, and by hybrid magma formation.

The works area can be considered metallogenetically perspective in relation to new Au, Ag, Hg, As, Sb, Cu-Mo with Au, Pb-Zn, Cu-Pb-Zn fields and ore occurrences. The investigated area is also rich by non-metallic raw materials – tuffs, scorias, pumices, etc.

Therefore, for andesite-dacite-rhyolite formation, developed in the central part of Lesser Caucasus, rocks formation of high-potassium calc-alkaline series is specific unlike the rocks of calc-alkaline series of normal alkalinity. Rocks formation of andesite-dacite-rhyolite formation is caused by fractionation of the rock-forming minerals in the intermediate foci and later due to contamination of the differentiated basaltic melt by the surrounding rocks. Single process of crystallization and assimilation caused the rocks buildup of the formation.

Two volcanic formations of the Late Pliocene-Quaternary age are separated at the end of the collision stage of development of the Azerbaijan part of the Lesser Caucasus, forming a bimodal association: 1 – rhyolite; 2 – trachybasalt-trachyandesite.

In the mafic volcanics of the behavior of major elements indicate their origin by fractionation of olivine, clinopyroxene, hornblende, basic plagioclase, apatite, magnetite. Acidic volcanic rocks associated with the formation of “dry” high temperature of the melt in the intermediate chambers are not of fractional crystallization.

The distribution of rare earth elements in rocks trachybasalt-trachyandesite formation indicates that the source was the metasomatic alteration of volcanic rocks containing garnet mantle. In the studied volcanics, $(Tb/Yb)_n = 1.7-3.0$ indicates the presence of garnet in the source of the primary magma.

In the rocks of rhyolite formation contents of rare earth elements is low (REE = 66–116 ppm), there is a pronounced low ratio of europium, which indicates that early removal of the molten plagioclase and alkali feldspar.

Trace element composition of the rocks trachybasalt-trachyandesite formation and their relationships complicate the model and determine the fractional crystallization of the magma mantle interaction with the substrate of the crust. In this substrate can be rhyolites, geochemical, and isotopic composition similar to the Earth's crust and forming a spatio-temporal association with the rocks contrast trachybasalt-trachyandesite formation.

The simulation revealed that the evolution of moderately alkaline olivine basalts (considered a primary mantle melt the rocks trachybasalt-trachyandesite formation) occurs due to changes in the composition of the main rock-forming and accessory minerals. Average rock formations formed by the assimilation of poorly differentiated primary magma acidic melt. Geochemical features of moderately alkaline olivine basalts indicate that the source of magma is metasomatized, phlogopite-garnet-rutile containing lithospheric mantle. It is very possible that the melting of such a source is rutile to a restaurant, and magma is depleted Nb and Ta.

The calculations have shown that the proportion of melting rhyolitic melt separated from andesite substrate close to 15%. After removal of the remaining melt restite entirely consistent with the composition of the lower crust. The typical ratio of rare earth elements is to confirm this.

These fact sheets, model calculations indicate various sources of education salic and mafic melts. Thus, the generation of mafic melt (moderately alkaline olivine basalt composition) came from a differentiated mantle protolith formation of a salic melt occurs during lifting mafic magma by melting of crustal substrate. On the other hand, the salic is going to melt in the top of the magma reservoir and prevents lifting heavier mafic magma, and in a short time in the melt is subjected to intermediate focuses differentiated. During subsequent evolution differentiated mafic melt reacts with rhyolitic melt, which entails the formation of secondary rocks.

Thus, the formation of bimodal volcanism in contrast, the central part of the Lesser Caucasus in the Late Pliocene-Quaternary period is as follows.

Temporary space conjugate crust and mantle magmatism led to the introduction of mantle melts under tension in the lower crust, which led to its melting and the formation of acidic volcanic rocks enriched in radiogenic *Sr* and *Nd* (rhyolite formation). At the same time in this situation, a change of scenery compression tensile contributed to the manifestation of poorly differentiated volcanism. At the same time, the evolution of the melt in the earth's crust is dominated by a single process of AFC (assimilation and fractional crystallization), and intermediate chambers became necessary mixing of mafic (trachybasalt) and salic (rhyolite) melts and created the conditions for the formation of intermediate rocks. However, due to different densities and viscosities of melts, salic mafic and such mixing occurred in small quantities.

Thus, in the petrogenesis of the majority of Caucasian young volcanic rocks has played a significant role lower mantle source material which is close to the tank

“Common” with characteristic isotopic $^{87}\text{Sr}/^{86}\text{Sr} = 0.7041 \pm 0.0001$, $\epsilon_{\text{Nd}} = +4.1 \pm 0.2$; $^{147}\text{Sm}/^{144}\text{Nd} = 0.105\text{--}0.114$ and named “Caucasus” [17, 18]. The primary melt composition corresponds to K-Na moderately alkaline olivine basalts. The magma formed by the plume of the Caucasus in the atmosphere of Earth’s crust formed the ever-increasing mantle diapir; he’s at the very beginning of its process uplift served the development of large volumes of mantle fluids. Due to the hot magma mantle diapir melts the material of Earth’s crust, magma is formed, which corresponds to the isotopic composition of the Earth’s crust, and subsequently, to varying degrees due to contamination of the mantle and crustal magma formed hybrid rocks.

Author details

Nazim Imamverdiyev^{1*} and Anar Valiyev^{2*}

1 Department of Geology, Baku State University, Baku, Azerbaijan

2 Azerbaijan National Academy of Sciences, Institute of Geology, Baku, Azerbaijan

*Address all correspondence to: inazim17@yahoo.com
and velizade_anar@yahoo.com

IntechOpen

© 2020 The Author(s). Licensee IntechOpen. This chapter is distributed under the terms of the Creative Commons Attribution License (<http://creativecommons.org/licenses/by/3.0>), which permits unrestricted use, distribution, and reproduction in any medium, provided the original work is properly cited. 

References

- [1] Koronovsky NV, Demina LI. The collisional stage of development of the Caucasus sector of the Alpine fold belt: Geodynamics and magmatism. *Geotectonics*. 1999;(2):17-35
- [2] Yildirim D, Nazim I. Altun-kaynak Şafak geochemistry and tectonics of Cenozoic volcanism in the Lesser Caucasus (Azerbaijan) and the Peri-Arabian region: Collision-induced mantle dynamics and its magmatic fingerprint. *International Geology Review*. 2010;52(4–6):536-578
- [3] Ershov AV, Nikishin AM. Recent geodynamics of the Caucasus–Arabia–East Africa region. *Geotectonics*. 2004; 38(2):123-136
- [4] Keskin M. Magma generation by slab steepening and breakoff beneath a subduction-accretion complex: An alternative model of collision related volcanism in eastern Anatolia, Turkey. *Geophysical Research Letters*. 2002; 30(24):8046. DOI: 10.1029 / 2003 GL018019
- [5] Keskin MA. FC-modeler: A Microsoft excel spreadsheet program for modeling Rayleigh fractionation vectors in closed magmatic systems. *Computers & Geosciences*. 2002;28(8):919-928
- [6] Pearce JA, Bender JF, Long D, Kidd WSF, et al. Genesis of collision volcanism in Eastern Anatolia, Turkey. *Journal of Volcanology and Geothermal Research*. 1990;44:189-229
- [7] Imamverdiyev NA, Gasankuliyeva MY, Babayeva GJ. Petrogenesis of the Late Cenozoic volcanism of the central part of the Lesser Caucasus (Azerbaijan). *Russian Geology and Geophysics*. 2018;59(1): 42-55. DOI: 10.1016/j.rgg.2018.01.003
- [8] Imamverdiyev NA, Veliyev AA, Hasanguliyeva MY. Petrology and Geochemistry of the Late Cenozoic Collision Volcanism of the Lesser Caucasus. Baku. Azerbaijan; 2017. p. 317
- [9] Keskin M, Pearce J, Mitchell J. Volcano-stratigraphy and geochemistry of collision-related volcanism on the Erzurum-Kars plateau, northeastern Turkey. *Journal of Volcanology and Geothermal Research*. 1998;85(1–4): 355-404
- [10] Keskin M. Domal uplift and volcanism in a collision zone without a mantle plume: Evidence from Eastern Anatolia. 2005. Available from: www.mantleplumes.org
- [11] Rustamov MI. South Caspian Basin-Geodynamic Events and Processes. Baku: Nafta-Press; 2005. p. 245
- [12] Ismail-zadeh AD. Petrological and Geochemical Features and Geodynamics of the Late Pliocene-Quaternary Volcanism of the Lesser Caucasus. Vol. 4. Baku, Azerbaijan: News Academy of Sciences of Azerbaijan, Earth Sciences Series; 1986. pp. 53-57
- [13] Imamverdiyev NA. Geochemistry of the Late Cenozoic Volcanic Complexes of the Lesser Caucasus. Baku: Nafta-Press; 2000. p. 192
- [14] Kashkai MA, Khain VE, Shikhalibeyli ES. On the age of the Kelbajar volcanic stratum. In: Reports of National Academy of Sciences of Azerbaijan. Vol. 6. 1952. pp. 285-289
- [15] Kashkai MA, Mamedov AI. Perlites, Obsidians, Pechshteins and their Missile-Petrographic and Physicochemical Features. Baku: Publishing House of the Academy of Sciences of the Azerbaijan; 1961. p. 181
- [16] Karapetian SG, Jrbashian RT, Mnatsakanian AK. Late collision rhyolitic volcanism in the north-eastern

part of the Armenian highland. *Journal of Volcanology and Geothermal Research*. 2001;112:189-220

[17] Lebedev VA, Chernyshev IV, Bubnov SN. A new version of the geochronological scale of the Neogene-Quaternary magmatism of the Caucasus. 2006. Available from: <http://earth.jscc.ru/uu2006/avtors/Lebedev/>

[18] Lebedev VA, Bubnov SN, Chernyshev IV, et al. Geochronology and genesis features of subalkaline basalts of lava rivers of the Javakheti highlands, Lesser Caucasus: K-Ar and Sr-Nd isotopic data. *Geochemistry*. 2007;(3):243-258

[19] Imamverdiyev NA. Mineralogical features and evolution of the composition of rock-forming and accessory minerals of rocks of the late Cenozoic volcanic series of the Lesser Caucasus. *Mineralogical Journal*. 1999; 21(5/6):93-100

[20] Leake BE. A catalog of analyzed calciferous and subalciferous amphiboles together with their nomenclature and associated minerals. *Geological Society of America Special Papers*. 1968;68:38-45

[21] Le Bas MJ, Le Maitre RW, et al. A chemical classification of volcanic rocks based on the total alkali-silica (TAS) diagram. *Journal of Petrology*. 1986;27: 745-750

[22] Peccerillo A, Taylor SR. Geochemistry of Eocene calc-alkaline volcanic rocks from the Kastamonu area, northern Turkey. *Contributions to Mineralogy and Petrology*. 1976;58(1):63-81

[23] Sun SS, McDonough WF. Chemical and isotopic systematics of oceanic basalts: Implications for mantle composition and processes. In: Saunders AD, Norry MI, editors. *Magmatism in the Ocean Basin*. Vol. 42.

London: Geological Society London Special Publications; 1989. pp. 313-345

[24] Mamyrin BAIN. *Tolstikhin Helium Isotopes in Nature*. Moscow: Energoizdat; 1981. p. 222

[25] Sharkov E, Lebedev V, Chugaev A, et al. The Caucasian-Arabian segment of the Alpine-Himalayan collisional belt: Geology, volcanism, neotectonics. *Geoscience Frontiers*. 2015;6(4):513-522. DOI: 10.1016/j.gsf.2014.07.001

[26] Yarmolyuk VV, Kovalenko VI, Kuzmin MI. North-Asian superplume in Phanerozoic: Magmatism and deep geodynamics. *Geotektonika*. 2000;5: 3-29

[27] Imamverdiyev NA. Rare earth element geochemistry of late Cenozoic volcanic series in the Lesser Caucasus. *Geochemistry International*. 2003;41 (4):379-394

[28] Popov VS, Lyapunov SM, Semina VA. Rare earth elements in the Pliocene-Quaternary volcanic rocks of the Caucasus. *Geochemistry*. 1987;(8): 1159-1173

[29] Popov VS, Semina VA, Nikolaenko YS. Geochemistry of the newest volcanics of the Caucasus and their origin. In: *Geochemistry of Continental Volcanism*. Nauka: M; 1987. pp. 143-231

[30] Imamverdiyev NA. The Role of the Lithospheric Mantle in the Formation of the Late Cenozoic Post-Collisional Volcanism of the Central Part of the Lesser Caucasus (Azerbaijan). Vol. 3. Baku, Azerbaijan: News of Baku University, Series of Natural Sciences; 2010. pp. 90-98

[31] Imamverdiyev NA, Baba-zade VM, Romanko AE, et al. Formation of Late Cenozoic volcanic complexes of the Lesser Caucasus. *Geotectonics*. 2017;

51(5):489-498. DOI: 10.1134/
S0016852117050041

[32] Imamverdiyev NA, Mamedov MN. Neogene-Quaternary volcanism in the Lesser Caucasus, Azerbaijan. *Acta Vulcanologica*. 1996;**8**(1):111-113

[33] Imamverdiyev NA. Physicochemical conditions of crystallization of late Cenozoic volcanic associations in the Lesser Caucasus. *Petrology*. 2003;**11**(1): 75-93

[34] Brandshaw TK, Hawkesworth CJ, Gallagher K. Basaltic volcanism in the Southern Basin and range: No role for a mantle plume. *Earth and Planetary Science Letters*. 1993;**116**:45-62

[35] Defant ML et al. The geology, petrology, and petrogenesis of Saba Island, Lesser Antilles. *Journal of Volcanology and Geothermal Research*. 2001;**107**(1-3):87-111

[36] Kelemen PB. Genesis of high Mg \neq andesites and continental crust. *Contributions to Mineralogy and Petrology*. 2005;**120**(1):1-19

[37] Sandvol E, Turkelli N, Zor E, et al. Shear wave splitting a young continent-continent collision: An example from eastern Turkey. *Geophysical Research Letters*. 2003;**30**:24

[38] Defant MJ, Drummond MS. Derivation of some modern arc magmas by melting of young subducted lithosphere. *Nature*. 1990;**347**:662-665

[39] Popov VS. Mixing of magmas during the formation of the latest volcanics of the Caucasus. *Volcanology and Seismology*. 1981;(1):3-13

[40] Rollinson H. *Using Geochemical Data: Evaluation, Presentation, Interpretation*. London; Longman; 1993. p. 352

Seismic Geomorphology, Architecture and Stratigraphy of Volcanoes Buried in Sedimentary Basins

*Alan Bischoff, Sverre Planke, Simon Holford
and Andrew Nicol*

Abstract

Our ability to investigate both the intrusive and extrusive parts of individual volcanoes has evolved with the increasing quality of seismic reflection datasets. Today, new seismic data and methods of seismic interpretation offer a unique opportunity to observe the entire architecture and stratigraphy of volcanic systems, with resolution down to tens of meters. This chapter summarises the methods used to extract the geomorphic aspects and spatio-temporal organisation of volcanic systems buried in sedimentary basins, with emphasis on the utility of 3D seismic reflection volumes. Based on descriptions and interpretations from key localities worldwide, we propose classification of buried volcanoes into three main geomorphic categories: (1) clusters of small-volume ($<1 \text{ km}^3$) craters and cones, (2) large ($>5 \text{ km}^3$) composite, shield and caldera volcanoes, and (3) voluminous lava fields ($>10,000 \text{ km}^3$). Our classification primarily describes the morphology, size and distribution of eruptive centres of buried volcanoes, and is independent of parameters such as the magma composition, tectonic setting, or eruption environment. The close correlation between the morphology of buried and modern volcanoes provides the basis for constructing realistic models for the facies distribution of igneous systems buried in sedimentary strata, establishing the principles for a new discipline of seismic-reflection volcanology.

Keywords: seismic volcanostratigraphy, seismic geomorphology, buried volcanoes, volcanic landforms, igneous plumbing systems, seismic-reflection volcanology

1. Introduction

Subaerial and submarine volcanic landforms originate by primary constructive processes when magma erupts onto the Earth's surface. After the volcanic activity ceases, these volcanic landforms are affected by erosion and weathering, which progressively modify their original morphology. Volcanoes that erupt in environments of relatively high subsidence and low erosion rates can be buried and preserved within sedimentary strata, providing us with an opportunity to investigate the diverse types of volcanic landforms that were formed in the past [1–4].

Volcanic morphologies provide information about the primary and secondary processes that formed them [5–7], and can be used as analogues for understanding buried igneous systems [8, 9]. Our ability to identify buried volcanoes and igneous intrusions emplaced in the shallow (<10 km) layers of the crust has developed immensely over the past four decades in parallel with improvements in the quality and quantity of seismic reflection data. Today, interpretation of seismic reflection datasets indicates that buried volcanoes are characteristic elements of many sedimentary basins globally (e.g. [10–17]).

Seismic interpretation of buried volcanoes benefits from innovations made in the field of sedimentology, in which seismic datasets have been used to analyse in detail the architecture and stratigraphic signature of terrestrial and marine sedimentary systems [18–20]. As noted in [21] “since the 1960s’, attempts to make sense of the diversity of rocks, processes, stratigraphic models and deposition settings of volcanic successions have been aided by major advances in the field of sedimentology”. Now, seismic reflection data offer unique opportunities to investigate the role of intrusions, host rocks, crustal structures, and relative sea-level variations in the construction and degradation of diverse volcanic landforms [22–24].

Modern seismic reflection datasets allow us to observe the entire architecture of volcanic systems, from the intrusive to the extrusive realms, with resolutions down

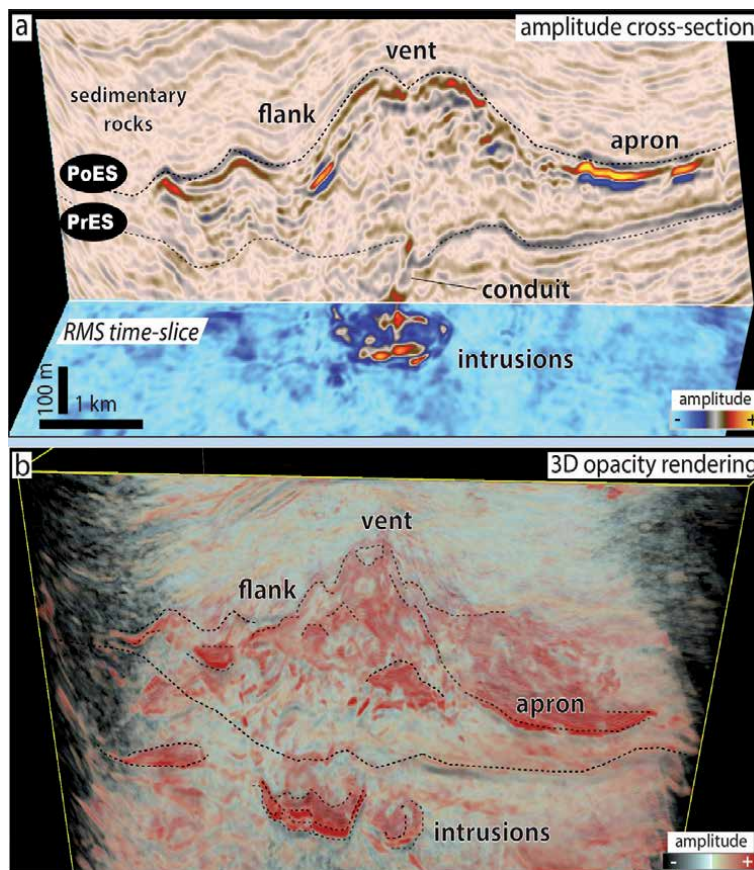


Figure 1. Seismic reflection visualisation of a small cone-shaped volcano buried in the Taranaki Basin, New Zealand. (a) Shows an amplitude display of a seismic reflection profile across the volcano, coupled with time-slice RMS amplitude display of its plumbing system. (b) 3D opacity-rendered perspective view of the volcano shown in (a) and its shallow (<200 m) plumbing system, in which the low-amplitudes are set as transparent. Note the spatial relationship between the saucer-shaped intrusion and the central vent of the volcano. PrES is the pre-eruptive surface and PoES is the post-eruptive surface.

to tens of metres [25–27]. In particular, new 3D visualisation methods of igneous seismic geomorphology and analysis of volcanic architectural elements have become valuable tools for interpreting buried volcanoes and their impact on the formation and evolution of the host sedimentary basins. The application of 3D visualisation methods leads for direct comparison of the geomorphic aspects of buried volcanoes with modern and ancient outcropping analogues, allowing us to interpret these buried igneous system in great detail [28, 29]. However, the wide variety of volcanic landforms well-documented in volcanic terrains are still not fully assessed in buried volcanic systems.

This chapter highlights the potential for using seismic geomorphology to improve the interpretation of volcanoes buried in sedimentary basins (**Figure 1**). Here, we compare the morphologies of outcropping and buried volcanoes from key localities worldwide. Examples shown in this chapter include description and interpretation of small (<1 km³) craters and cones, large (>5 km³) composite, shield and caldera volcanoes, voluminous (>10,000 km³) lava fields, and subvolcanic sheet-like intrusions. The perceived correlation between the morphology of outcropping and buried volcanoes assist the construction of realistic models from subsurface seismic data, laying the foundations for a new discipline of seismic-reflection volcanology. The information presented in this chapter may have value to geoscientists investigating the impacts of igneous activity on sedimentary basins formation and evolution, and on the processes that control the large-scale (>10² m) architecture of volcanic systems on Earth and related planets.

2. Principles of seismic interpretation of igneous rocks

The seismic reflection method is a geophysical technique designed to observe the Earth's subsurface indirectly. This method is based on the recording of artificially generated seismic waves that travel into the Earth's geological formations. At the interface of rock bodies with different physical properties, the waves reflect and refract, producing seismic events with wave amplitudes proportional to the contrast in density and velocity of the rocks that bound the interface [30, 31]. Motion- or pressure-sensitive geophones and hydrophones receivers capture the reflected wavefield from the seismic source. A systematic arrangement of the seismic sources and receivers enables the construction of cross-sections that display images of the Earth's subsurface, with better quality at depths of <10 km [32].

Igneous rocks buried in sedimentary basins are often identified by the presence of anomalously high-amplitude reflections within seismic datasets (**Figures 1 and 2**). Characteristically, dense lavas of basaltic composition and mafic intrusions have compressional (P-wave) velocities >5000 ms⁻¹, contrasting with softer sedimentary rocks which commonly have velocities <3000 ms⁻¹ [4, 33, 34]. Despite the straight-forward concept underpinning the identification of igneous rocks based on their high-amplitude reflections, seismic techniques have limitations which leads to uncertainties in the interpretations. Such interpretations are dependent on the quality and resolution of seismic data, which are controlled by geophysical parameters such as wavefield scattering due to changes in rock densities and strata geometries, increasing energy attenuation with depth, and the size of the igneous bodies relative to the wavelength of the seismic signal [35, 36].

Distinguishing buried volcanoes from sedimentary strata can be problematic when the igneous rocks have similar physical properties and geometries as the enclosing host rocks. For example, it may be challenging to differentiate volcanoes from carbonate mounds, or sequences of bedded volcanoclastic and siliciclastic rocks [37, 38]. Secondary alteration processes including mineral changes induced

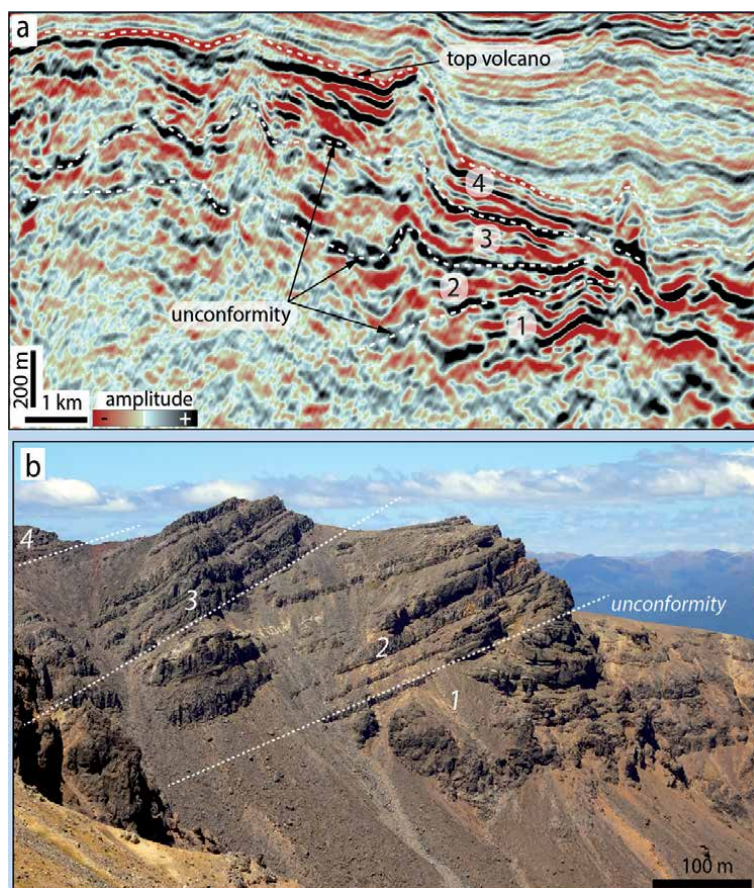


Figure 2. (a) 2D seismic section across the flank of a polygenetic volcano buried offshore Canterbury Basin, New Zealand. The highest-amplitude seismic reflector in this image marks the interface between the top of the volcanic structure and its overlying sedimentary rocks. (b) Cross-section across an outcropping sequence of lava flows of the Mangahouhounui Fm, Tongariro compound volcano, New Zealand, exposed by erosion. Note that in both seismic and outcropping examples, the relationship between the strata defines a succession of volcanic events bounded by unconformities, across which younger rocks are deposited at the top of the sequence.

by metasomatism and weathering, cementation, compaction during progressive burial, substitution of interstitial pore fluids, and fracturing can also lower the impedance contrast between igneous and sedimentary rocks [39, 40]. In addition, steeply inclined bodies such as dykes and highly heterogeneous subvolcanic zones are often poorly resolved in seismic reflection datasets. These zones can contain numerous intrusive bodies emplaced with variable geometries and spatial relationships to their host strata, leading to loss of reflection coherency [41].

In light of these limitations, seismic interpretation of buried volcanoes can benefit from a fully integrated approach that includes information from drillhole data analysis and insights from modern volcano analogues [42, 43]. In recent years, particular attention has been given to the interpretation of 3D seismic volumes from which cross-sections can be displayed in any given orientation, allowing the visualisation of complex volcanic forms in great detail [44, 45]. This new integrated seismic method, from 2D regional scale to detailed 3D analysis and correlation with drillhole data and analogues, can provide robust interpretations of volcanoes buried within sedimentary basins.

3. Methods and concepts of seismic-reflection volcanology

Interpretation of buried volcanic systems requires a multidisciplinary approach that combines insights from complementary disciplines such as sedimentology, stratigraphy, structural geology, and volcanology into a unified framework. During the last 40 years, our knowledge about the formation and evolution of sedimentary basins has improved mainly due to advances in the fields of seismic and sequence stratigraphy [46–48]. More recently, these stratigraphic approaches have been successfully applied to interpret the processes and products of igneous activity within sedimentary basins [1, 4].

Seismic-reflection volcanology is here defined as the study of buried volcanoes from seismic reflection datasets. This method is typically applied to investigate the nature and evolution of volcanic and igneous plumbing systems buried in sedimentary strata. Sedimentary basins that contain a significant amount of igneous rocks are informally referred to as “volcanic basins” [49–51]. The interpretation of volcanic basins usually begins by mapping the top and base of seismic units (sequences) that are potentially of volcanic origin using 2D regional lines. Mappable seismic facies units are then identified by their distinct aspects in, for example, reflection configuration, continuity, geometry, and interval velocity. A volcanological interpretation is then performed to determine the igneous facies and their intrusive and extrusive enclosing environments. If available, 3D datasets are subsequently interpreted to provide detailed images of the past volcanic surfaces and landforms now buried in the host basin, which is further analysed using the method of igneous seismic geomorphology [29] and volcanic architectural elements [52, 53]. Finally, a more accurate volcanological characterisation of buried igneous rocks can be achieved by correlating the seismic units with data from drillholes and outcrop analogues [26].

The methods used to characterise volcanic basins vary between interpreters and are dependent on the available dataset, scale, and purpose of the study. The following sections summarise these methods focusing on the interpretation of the spatio-temporal expression of buried volcanoes and reconstruction of the scenarios in which volcanic events occurred synchronously with basin sedimentation and erosion.

3.1 Reconstructing the geomorphic aspects, eruptive time, and environment of emplacement of buried volcanic systems

Magma that reaches the Earth’s surface can produce a variety of subaerial and subaqueous volcanic landforms. This diversity of volcanic landforms reflects a range of physical factors such as magma composition, discharge rate of effusion, degree of material fragmentation and dispersion, and tectonic and environment settings, in particular, the presence or absence of water where the eruptions occurred [54–57]. In detail, the volcanic landforms are likely the product of many competing processes such as steady versus dynamic mechanisms of fragmentation, fixed versus variable location of the eruptive centre, and single versus multiple eruption phases. Multiple variables can complicate the interpretation of the processes that shaped the geomorphic aspects of volcanoes [6], which is especially true for the characterisation of volcanoes buried in sedimentary strata. In addition to volcanic complexity and limitations of subsurface interpretation, the morphology of buried volcanoes is likely influenced by superimposed post-eruptive processes such as erosion, alteration, compaction, and faulting.

To understand the geological processes that shaped ancient volcanic landforms now buried in sedimentary strata, critical parameters such as the interval acoustic

velocity, and the amount of degradation and compaction of the buried igneous rocks have to be addressed [25]. The height of buried volcanoes is initially inferred from their present-day morphology (i.e. after erosion and compaction during burial) by multiplying the transit time of seismic waves within the volcano by an estimated acoustic velocity of the volcanic interval [58]. The degree of compaction can be estimated by seismic analysis that indicates differential compaction between the volcanic and hosts rocks [59]. Erosional features such as gullies and canyons are typically visible in seismic imagery and can help to evaluate the degree of preservation of the buried volcanic structure [27]. After determining these variables, the morphology of each buried volcanic edifice is approximated as a 3D geometric shape such as a cone, or a spherical cap to roughly estimate their volume. These estimations are “best-fit” approximations which do not affect the first-order (i.e. dimensions of $>10^2$ – 10^4 meters) interpretations of volcanic morphologies [60].

To make sense of this seismic morphological information, the interpreter of volcanic basins typically construct volcanostratigraphic frameworks that help to explain the succession of igneous and sedimentary events occurred during the evolution of the basin (**Figure 3**). The age of the volcanic rocks in the subsurface is commonly determined by correlating seismic isochron horizons with biostratigraphic markers and radiometric dating of rocks penetrated by nearby drillholes. This approach gives time resolution in the order of 0.1 to 5 Myr, assuming that the seismic reflections provide a proxy of timelines [48, 61]. Interpretation of the environment in which the buried volcanoes erupted can be determined by seismic

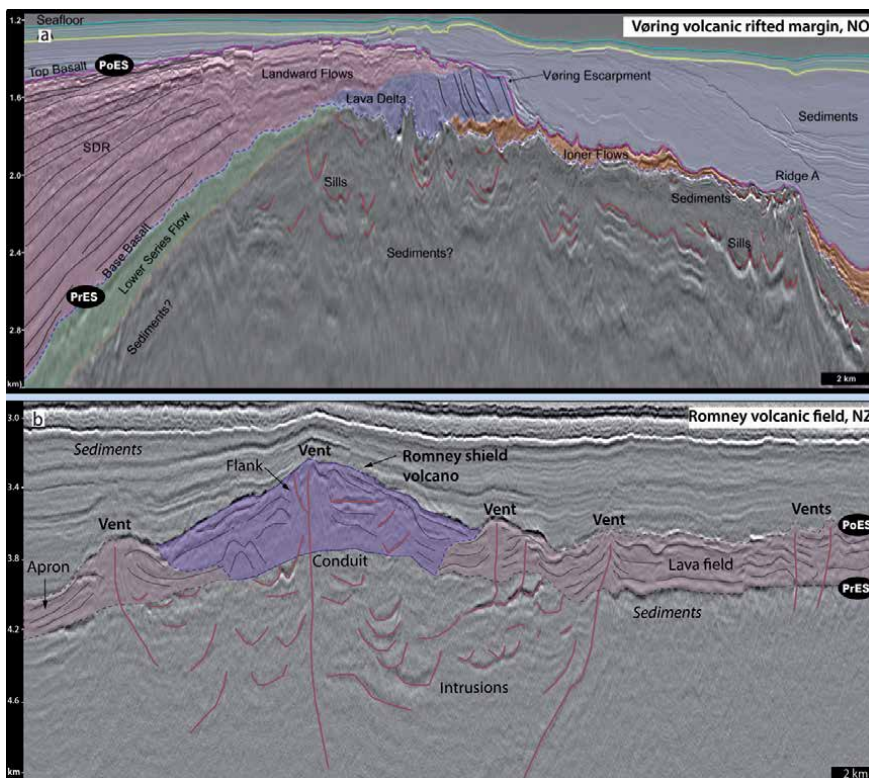


Figure 3. Amplitude display of seismic reflection profiles across the Vøring volcanic rifted margin, offshore Norway (a) and the Romney volcanic field, offshore New Zealand (b). Note that the internal and external configuration of seismic reflections determines the spatial relationship of distinctive seismic units, providing information about the succession of events that have formed these units. Data courtesy of TGS (a) and NZPAM (b).

stratigraphic analysis calibrated with paleoenvironmental data obtained from microfossils from drillholes across the studied areas or correlative outcrops [62]. As standard procedure in the analysis of seismic datasets, 2D sections and 3D perspective views are often displayed with vertical exaggeration to enhance the stratal relationship of seismic reflections, which modify the visual geometric aspect of the buried volcanic landforms.

3.2 Seismic volcanostratigraphy

Seismic volcanostratigraphy is a subset of the seismic stratigraphic method developed to analyse the geological evolution and environments of emplacement of igneous extrusive rocks using seismic reflection datasets [4]. This method consists of two main steps: (1) mapping of the top and base of volcanic sequences, and (2) seismic facies analysis, including characterisation of volcanic and enclosing sedimentary seismic facies units and their volcanological interpretation (**Figure 3**).

The application of seismic volcanostratigraphy relies on the identification of changes in basin depositional trends, placing stratigraphic boundaries at the contacts between volcanic units that are genetically related [1, 29, 63]. In non-volcanic basins, such trends represent the dispersal and accommodation of material in specific stacking patterns of progradation, retrogradation and aggradation. These depositional trends reflect oscillations of the base level that result in erosion and accumulation of sediments within the basin, which is typically controlled by the balance between variables such as tectonics, eustasy, and climate [64, 65].

Igneous activity can strongly impact the depositional trends of sedimentary basins, which requires adaption when using conventional stratigraphic concepts and nomenclature for stratigraphic interpretation of volcanic sequences (**Figure 4**). For example, the stratal trends of non-volcanic basins are typically described according to variations in the position of the shoreline through time [66]; while in volcanic

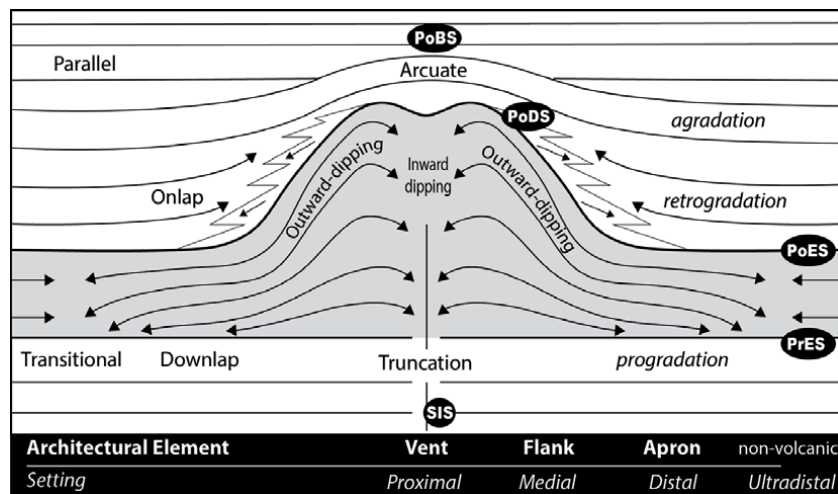


Figure 4. Simplified representation of the main stratal patterns, volcanic architecture, and depositional settings of cone-shaped volcanoes buried in sedimentary strata. The arrows indicate the patterns of material dispersal in specific stacking patterns of progradation, retrogradation and aggradation. The geometric configuration of strata reflects the interplay between volcanic and sedimentary processes experienced during the evolution of the basin. Note that the eruptive centre is the focal point that determines the spatial relationships between proximal to ultradistal depositional settings, which can be used as a model to predict how volcanic and sedimentary lithofacies may be distributed within and around the volcano. SIS: syn-intrusive surface. PrES: pre-eruptive surface. PoES: post-eruptive surface. PoDS: post-degradational surface. PoBS: post-burial surface. See [53] for detailed information of these volcano stratigraphic surfaces.

systems, the focal point for discussing stratal trends is the eruptive centre [8, 52]. This is because the addition of material sourced by eruptions and isostatic adjustments of the crust caused by magma emplaced in the subsurface can overprint normal basin processes such as sediment supply and the available accommodation space [67, 68]. As a consequence, igneous activity can have a major control on the basin stratal trends, possibly impacting the architecture and evolution of the basin over thousands of square kilometres and for millions of years (Figures 3 and 5).

Volcanic activity often causes sudden changes in basin stratal patterns, which make it relatively straight-forward to identify the large-scale unconformities that mark the boundaries of entire volcanic sequences [45]. A typical volcanic sequence initiates with a progradational or aggradational trend marked by truncations and downlaps onto the pre-eruptive surface, and it ends with a retrogradation trend visible by onlap terminations on the top of the post-eruptive surface [4, 52]. Internal unconformities and trends within the volcanic sequence are more subtle than large regional unconformities, and may only be identified in high-quality 3D datasets (Figure 2). The identification of volcanic stratal patterns can be complicated due to rapid and in some cases cyclical switches from constructional to degradational stages of polygenetic volcanoes, making it challenging to map the lateral extension of volcanic unconformities [69, 70].

In some circumstances, the reduced seismic quality below thick volcanic sequences can difficult the identification of the pre-eruptive surface [35]. Similarly, the post-eruptive surface is not always marked by onlap of overlying strata onto a volcanic structure, which depends on the interplay between the rate of material sourced by eruptions versus the rate at which the volcano has been buried by sediments sourced from other parts of the basin [52]. In other words, onlap onto an active volcanic edifice can occur if the rate of burial overcomes the rate and volume of erupted material, which may be expected during the later stages of long-lived volcanoes, especially if the eruptions do not form layers thick enough to be resolved in seismic data (Figures 4 and 5). Additional stratigraphic markers such as the syn-intrusive, post-degradational and post-burial surfaces help to constrain the impacts of igneous activity in the host basin into a spatio-temporal framework [53].

3.3 Igneous seismic facies units

Buried volcanic systems often show distinctive seismic facies units that result from the interaction of igneous activity and its surrounding sedimentary host rocks and

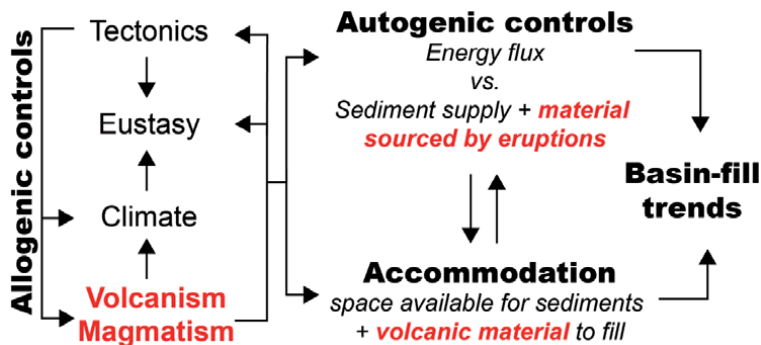


Figure 5. Processes that control the stratigraphic signature and architecture of sedimentary basins impacted by igneous activity. The interplay of competing autogenic (i.e. from within the system) and allogenic (i.e. from outside of the system) mechanisms defines the depositional trends of volcanic basins. Adapted from [66].

environments. Seismic facies analysis consists of mapping of 3D units and 2D profiles whose seismic parameters differ from those of adjacent units [71], followed by a volcanological interpretation of the mapped seismic facies units [3]. Discrete seismic reflection packages often correspond to depositional units that are genetically related and bounded by seismic discontinuities (**Figure 2**). Variations in igneous seismic facies represent changes in the volcanic processes and environments that enclose the buried volcanoes (**Figure 6**). These seismic facies units can be interpreted in terms of volcanic eruptions, magma emplacement mechanisms, and sedimentation patterns developed during the evolution of the host sedimentary basin [4, 22, 73].

Seismic attribute analysis such as coherency, amplitude, frequency, and attenuation (or a combination of these) can be used to enhance the contrasts between variations in the physical properties of the buried igneous rocks units and their

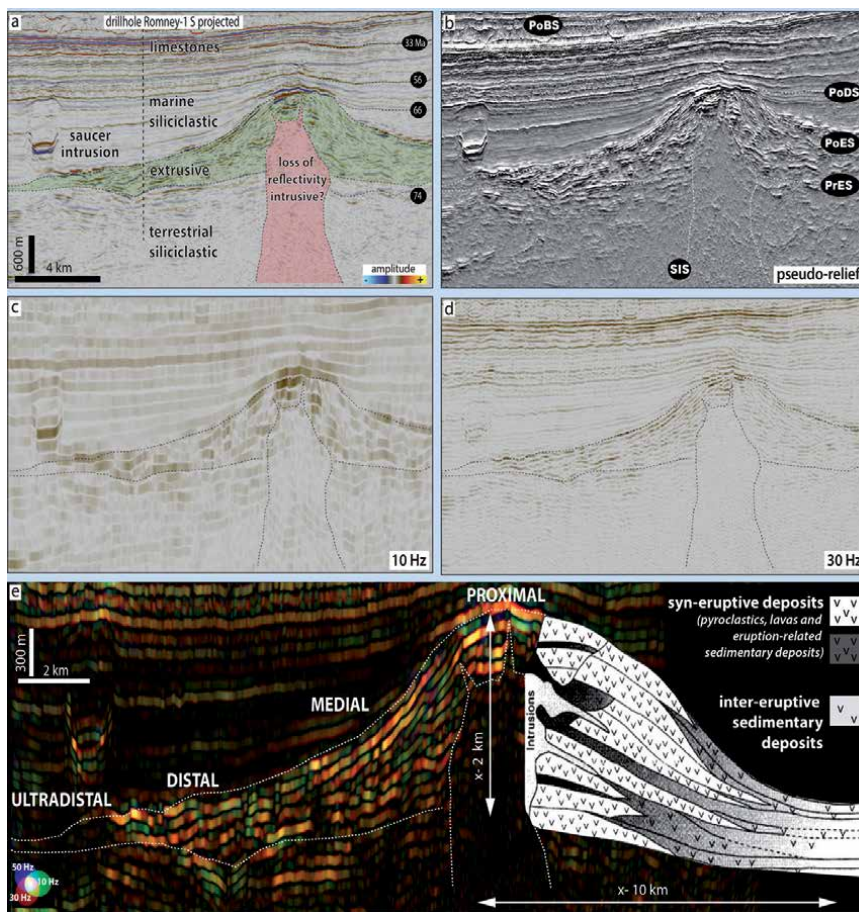


Figure 6. (a) Amplitude display of a seismic reflection profile across Vulcan composite volcano, offshore Deepwater Taranaki Basin, New Zealand, illustrating a variety of intrusive, extrusive and sedimentary seismic facies. The age and lithofacies and their correspondent seismic facies are calibrated with information from the Romney-1 petroleum exploration well, located 50 km north of Vulcan volcano. Approximate ages of the chronostratigraphic surfaces are shown in the back circles. Note how igneous and limestone rocks tend to form the highest amplitude events in this cross-section. The low reflectivity seismic facies below the volcanic edifice are often present in subvolcanic zones. (b) Pseudo-relief and amplitude displays (c and d) seismic profiles across Vulcan volcano. These seismic attributes highlight the differences between igneous and sedimentary rocks. The increase in the frequency of the seismic signal (10–30 Hz) highlights the internal structure of the volcano. (e) Spectral-decomposition display of a seismic reflection profile across Vulcan volcano illustrating the idealised facies architecture of large polygenetic volcanoes. The schematic facies diagram is adapted from [67]. X- corresponds to the average diameter and height of composite volcanoes, based on [72].

enclosing sedimentary strata (**Figure 7**) [30]. More recently, the use of machine learning techniques and artificial neural networks have been applied to delineate igneous seismic facies [74]. Description of igneous seismic units can be used to interpret volcanic landforms and different parts of volcanic systems. For example, cone-type volcanoes such as cinder cones and stratovolcanoes typically display a pair of inward- and outward-dipping reflections that mark the location of a central crater and peripheral flanks. Optimal characterisation of buried volcanoes can be obtained by analysing the igneous seismic facies as part of a genetically related network in different scales of observation, which consist in mapping intrusive and extrusive igneous seismic units into a unified interpretation framework [29, 52, 73].

3.4 Igneous seismic geomorphology

Seismic geomorphology is the application of analytical techniques to study ancient buried sedimentary systems imaged by 3D seismic data [18, 20, 75]. Similarly, igneous seismic geomorphology analyses the 3D characteristics of buried volcanoes and shallow crustal intrusions from a geomorphological perspective [29]. This technique is based on the extraction of horizons and slices from the seismic volume at scales and geometries comparable to modern volcanic morphologies (**Figures 1** and **6**). A variety of analytical techniques, such as opacity rendering, spectral decomposition, iso-proportional slicing, and mapping of geobodies can be applied to image the geometric aspects, spatio-temporal distribution and relationship of seismic units [76].

When integrated with seismic and sequence stratigraphy, seismic geomorphology provides background information to interpret the morphology and architecture of buried volcanoes (**Figure 7**). In outcrop, the morphological characteristics of volcanoes provide insights into past eruptive styles, edifice growth mechanisms, and

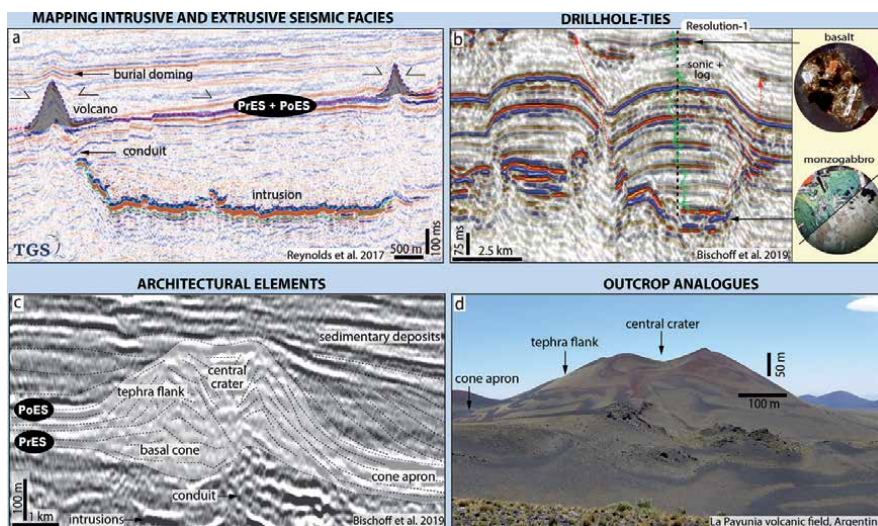


Figure 7. Examples of techniques used to recognise igneous rocks buried in sedimentary basis. (a) Amplitude seismic section displaying typical saucer-shape sill and related vents located above the termination of the sill, Bight Basin, southern Australia. From Reynolds et al. [15]. (b) 2D seismic cross-section showing a monzogabbro intrusion and associated volcanogenic deposits, tied to lithologies penetrated by the Resolution-1 exploration drillhole, Canterbury Basin, New Zealand. From Bischoff et al. [22, 37, 53]. (c) 2D amplitude seismic cross-section illustrating the main architectural elements of a small mound-shaped volcano buried in the Canterbury Basin, New Zealand. From Bischoff et al. [22, 37, 53]. (d) Photograph illustrating the main architectural elements of a Holocene cinder cone in the La Payunia volcanic field, Argentina. Note the similar morphology of volcanoes in seismic imagery and modern outcropping analogues.

cone degradation experienced during their complete history [21, 77]. Correlating the morphological aspects of buried and outcropping volcanoes can assist in developing the best possible model for the volcanic emplacement in its surrounding environments, including prediction of lithologies, stratigraphic architecture, and geological processes occurred during their evolution (**Figures 6** and 7).

3.5 Architectural elements of buried volcanoes

The concept of architectural elements was introduced to sedimentary geology during the 1980s' and 1990s' to document the fundamental building blocks of fluvial and deep-water systems [20, 78, 79]. The systematic documentation of the variety and arrangement of architectural elements such as channels, levees, and accretionary bars are critical for the interpretation of buried sedimentary environments, with particular relevance to the 3D interpretation of seismic reflection datasets [80].

An architectural element is defined as a three-dimensional genetically related rock unit characterised by its geometry, facies, composition, scale, and bounding-surfaces, and is the product of a particular process or suite of processes occurring within a depositional system [81]. The architectural elements approach investigates the internal arrangement and external bounding-surfaces that delimit co-genetic lithofacies and seismic units [47]. These elements are typically described at a scale of macroforms (i.e. bedforms with lengths of 10^2 – 10^4 meters), using [82] terminology.

Volcanic landforms including their small-scale variants such as basaltic monogenetic cinder cones and maar-diatreme volcanoes also comprise a combination of particular building blocks with scales comparable to those of sedimentary macroforms. For example, cinder cones typically display a central crater with marginal tephra flanks, while a maar volcano characteristically has a diatreme circled by a tephra ring [6, 83]. Each of these fundamental volcanic building blocks (i.e. architectural elements) are often >100 m in horizontal and vertical dimensions [72], therefore, they may be recognisable in seismic reflection datasets (**Figures 6** and 7).

Facies models of modern and ancient outcropping volcanoes show a systematic variation of macroforms and lithofacies, which are typically spatially distributed according to their distance from eruptive centres [21, 67, 84]. Comparing the variety and arrangement of buried architectural elements with volcanic facies models available in the literature helps us to predict the three-dimensional patterns of igneous and sedimentary lithofacies within buried volcanic systems (**Figures 4**, **6** and 7). This information can then be used to assist the interpretation of the geological processes that formed the volcanoes now buried in the subsurface [52, 53].

4. Morphology and architecture of buried volcanic systems

4.1 Shallow subvolcanic intrusions

The majority of melt generated by igneous activity likely fails to reach the Earth's surface [85]. Within sedimentary basins, magma often forms widespread plumbing networks that can extend laterally for tens of kilometres before it erupts [43]. The movement of magma through the shallow layers of the crust and its interaction with heterogeneous host rocks and faults are primary parameters that constrain the geometries of intrusive bodies and the location of eruptive centres [86–88].

Volcanic plumbing systems emplaced in sedimentary strata comprise numerous intrusive bodies of various shapes and sizes. These bodies are broadly classified into

sheet-like intrusions such as dykes, sills and cone sheets, and more massive equidimensional forms, including laccoliths, plugs, and plutons [24, 89, 90]. Sheet-like intrusions prevail in sedimentary basins because magma tends to propagate through and along with weakness plans of the host strata and faults. Dykes are understood to be the main vertical pathways for magma feeding eruptive centres [91], while sills mostly distribute melts laterally across the basin [92]. This is because, by definition, sills are dominantly parallel with the usual sub-horizontal basin strata (including layers of lava or sedimentary rocks), whilst dykes dominantly cross-cut layering in basin host rocks.

However, magmatic intrusions may extend for tens to hundreds of kilometres [93–95], limiting our ability to observe their complete geometry exclusively from outcrops. Seismic reflection profiles can provide large scale images (tens to hundreds of km's) of entire intrusive bodies, allowing us to describe their geometric aspects, lateral and vertical dimension, and interconnectivity in detail (**Figure 8**). Interpretation of seismic data from volcanic basins has revealed that sills can locally display geometries that are discordant with the host rocks. These discordant sills are described in terms of their geometry in relation to the orientation of the host strata, comprising morphologies such as transgressive, step-wise, and saucer- and v-shaped sills [59, 96]. This improved understanding of the migration of magma through interconnected intrusions demonstrated the critical role of sills in transferring

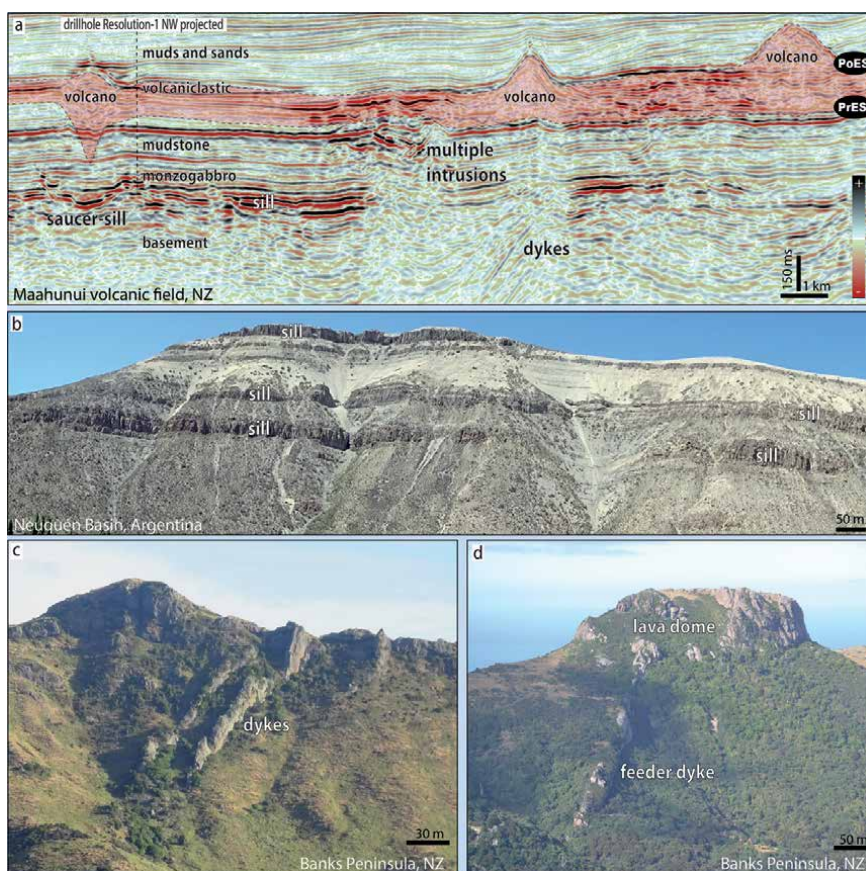


Figure 8. Seismic examples and outcrop analogues of tabular sills and dykes. (a) Amplitude seismic display across small vents and shallow correlative intrusions of the Maahunui volcanic field, offshore New Zealand [22]. (b) A series of extensive flat-lying sills emplaced parallel to marine strata of the Neuquén Basin, Argentina. (c and d) Sub-vertical dykes cross-cutting a sequence of lava and pyroclastic flows of the Banks Peninsula compound volcano, New Zealand.

magma from depths to upper layers of the crust, which has been reinforced by observations from laboratory experiments [89, 97].

Numerous sills in sedimentary basins have a saucer-shaped geometry consisting of a flat-lying inner sill connected to outer inclined sheets (**Figure 9**). Saucer-shaped sills are usually (but not always) identified in 2D seismic lines by a concave-upward high-amplitude reflection located below an anticlinal fold, suggesting that emplacement of the sill uplifted the overlying strata [98]. Reflections displaying onlap terminations on the top of these folds typically indicate the timing of intrusion emplacement [99]. The upper termination of the inclined sheets is often associated with small craters and cones that erupted at the paleosurface, suggesting a relationship between saucer-sills and vent complexes (**Figure 6a**). The vent complexes can be of both hydrothermal (phreatic) and magmatic origin [58–60].

Dykes and other thin (<50 m) sub-vertical intrusions (i.e. conduits) can be inferred using principles from fault interpretation, by the presence of narrow and sub-vertical bright discontinuities associated with disrupted enclosing reflections [52, 100]. The application of this disrupted-reflector criteria for dyke identification is more likely to be accurate if the sub-vertical discontinuities are located below a vent zone or related to flat-lying intrusions. Dike swarms have been interpreted by steeply inclined high-to-moderate amplitude reflections cross-cutting sedimentary strata in offshore Norway [101] and New Zealand (**Figure 8a**).

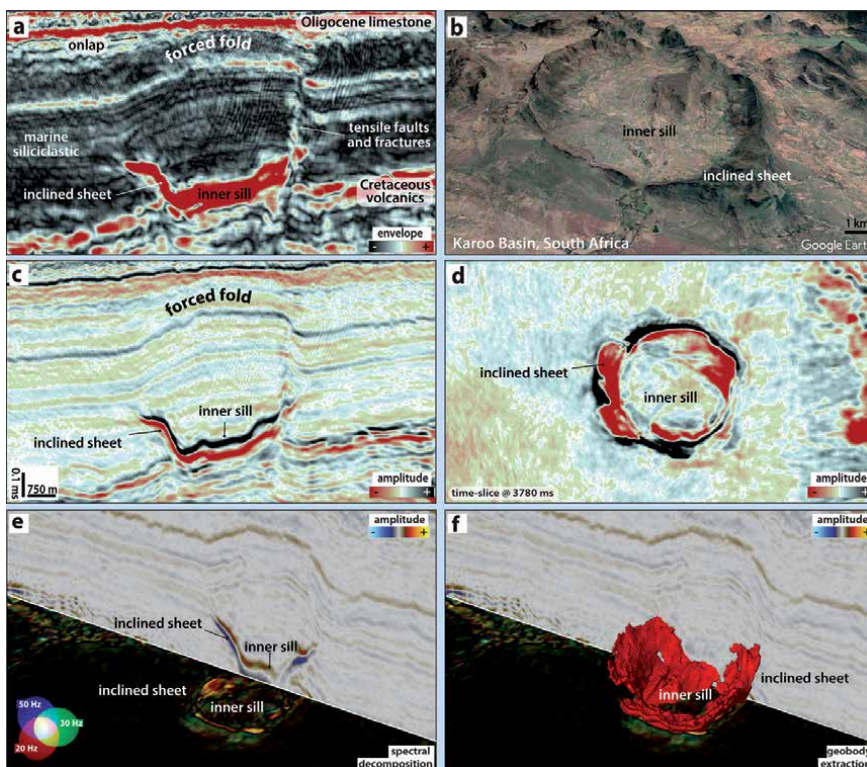


Figure 9. Seismic and outcrop examples showing the typical geometry of saucer-shaped intrusions. (a) Envelope display across a saucer-intrusion of Eocene age emplaced in Cretaceous to Paleocene strata of the Deepwater Taranaki Basin, New Zealand. (b) Saucer-intrusion emplaced in sedimentary strata of the Karoo Basin, South Africa. Cross-section (c) and in plain view (d) amplitude display of the intrusion shown in (a). (e) Composite 3D perspective display of an amplitude cross-section and a time-slice of a spectrally decomposed seismic cube across the intrusion in (a). (f) Same view as (e) extracting the seismic geobody that corresponds to the 3D geometry of the intrusion. This hybrid intrusion comprises an inner sill parallel to the sedimentary strata, and peripheral inclined sheets cross-cutting the host strata.

4.2 Clusters of small-volume craters and cones

Clusters of discrete, small-volume (i.e. $<1 \text{ km}^3$) craters and cones occur in most tectonic settings around the world. These clusters often contain tens to hundreds of volcanoes associated with rifting (e.g. Assab Volcanic Field, Ethiopia), intraplate volcanism (Newer Volcanic Province, Australia) and subduction zones (Pinacate Volcanic Field, Mexico). Typically, they comprise basaltic monogenetic volcanoes such as scoria cones, tuff rings, maars-diatremes, and hydrothermal vents, although some examples can also be of dacitic, phonolithic, trachytic, and rhyolitic composition [72, 102]. The basaltic fields are commonly derived from mantle melts with minor fractional crystallisation and little crustal assimilation, sourcing low-viscosity magmas that can feed widespread lava-flow fields adjacent to the craters and cones [103]. Clusters of dacitic to rhyolitic lava domes and explosive vents are rare and more commonly erupted as the final events of large silicic caldera-forming cycles, or from their associated fissures systems [104, 105].

The primary morphology of small craters and cones can display simple or complex geometries, which are determined by parameters such as the content of volatiles dissolved in the magma and water-melt interactions in the environment surrounding the eruption [83, 106]. Small mafic volcanoes dominated by a mound- or conical-shaped geometry (i.e. spatter, scoria, and tuff cones) are often constructed by accumulation of fragmental volcanic material (tephra) ejected by relatively low-energy pyroclastic eruptions such as fire-fountaining, Strombolian and Vulcanian eruptive styles (**Figure 10a-d**). Although each mound-shaped volcano presents characteristic morphometric forms, their simpler end-members all share a systematic distribution of macroforms in relation to the vent zone. This typical macroform distribution comprises of a proximal central crater circled by peripheral flanks that are enclosed by a distal tephra (or lava field) apron [6]. Average sizes of cone-shaped volcanoes are ca 300 m height and 1 km basal width, with spatter cones having the smallest dimensions and tuff cones the largest sizes [72]. By contrast, small volcanoes dominated by a crater-shaped geometry (i.e. tuff rings and maar-diatremes) typically result from phreatomagmatic eruptions (including Surtseyan styles) triggered by molten-fuel-coolant interactions of magma, water, CO_2 , and thermogenic gases [107, 108]. These volcanoes have craters up to 3 km in width and maximum depth up to 500 m. The distribution of macroforms in a tuff ring consists of a central crater circled by a peripheral ejecta ring and a debris apron [109], while Maar-diatremes display a root zone, a lower unbedded and upper bedded diatreme, an ejecta ring, and an associated debris apron (**Figure 10e-h**).

The seismic expression of small craters and cones are comparable to geometries observed in outcropping volcanoes [9, 27]. In seismic cross-sections, mound-shaped volcanoes are inferred from mounds that built-up above a relatively flat pre-eruptive surface. Chaotic or inward-dipping reflections at the centre of the mounds suggest the location of the vent zone, while lateral inclined, parallel, continuous or disrupted outward-dipping reflections indicate the position of the flanks (**Figure 10a-d**). The mounds may or may not contain peripheral sub-horizontal continuous to discontinuous high-amplitude reflections that represent lava-flow fields and tephra aprons. In contrast, the crater-shaped volcanoes show V-shaped excavations into the pre-eruptive surface. These craters typically contain unbedded, disrupted and chaotic reflections at the base (i.e. lower diatreme), and discontinuous to bedded reflections at the top (upper diatreme). The crater-shaped volcanoes are often circled by moderate to high-amplitude reflections that likely represent material ejected by large pyroclastic eruptions [2, 53].

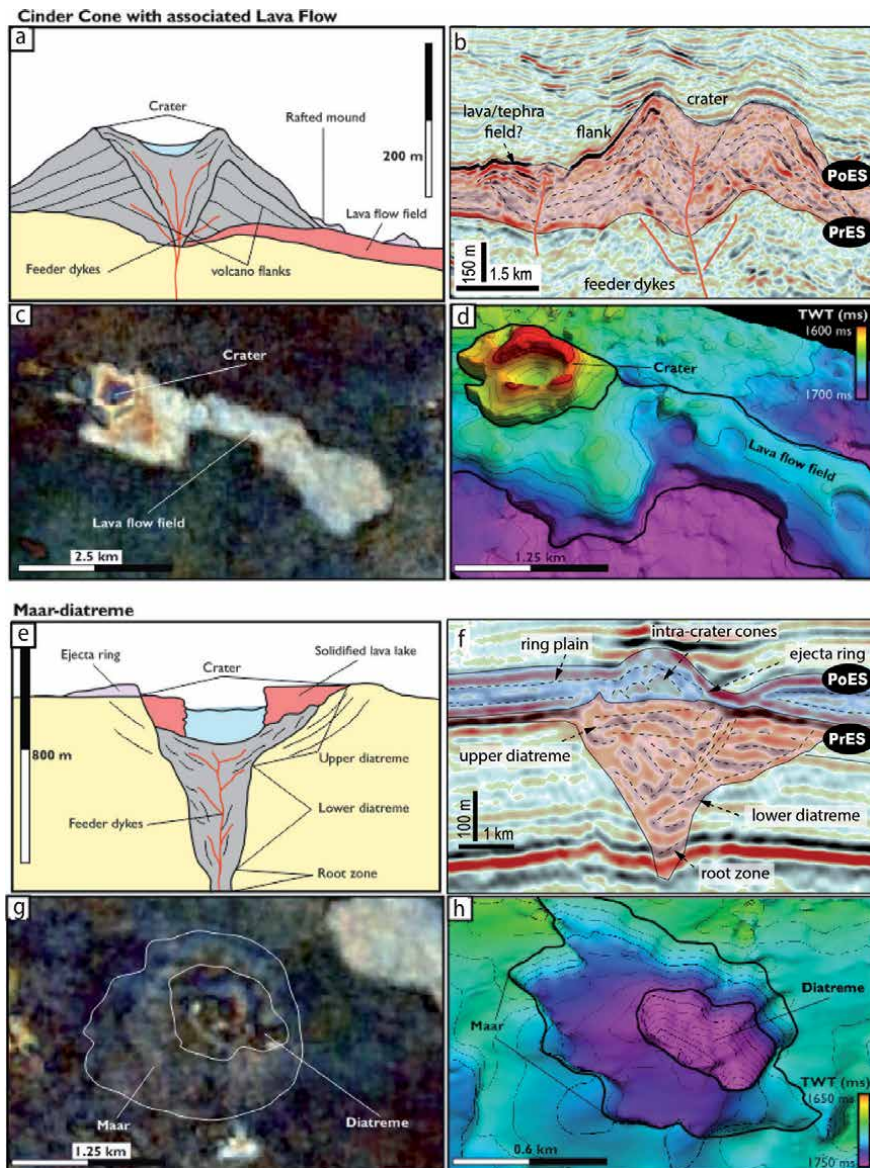


Figure 10. Illustrations of the architecture of small-volume cones and craters. (a) Schematic cross-section through a cinder cone adapted from Kereszturi and Németh [6]. (b) Seismic cross-section highlighting the general morphology and seismic response of a cinder cone and associated lava field buried offshore Taranaki Basin, New Zealand. Note the characteristic inward-dipping reflections towards the crater and the outward-dipping structure away from the vent zone. (c) Plan view spectral decomposition of the cinder cone taken from the Winnie 3D survey, Eromanga Basin, Australia, highlighting the cone-shaped morphology of the vent and associated extensive lava field [9]. (d) Horizon mapping of the top surface of the cinder cone shown in (c). (e) Cross-section through a maar-diatreme adapted from Kereszturi and Németh [6]. (f) A seismic line across a maar-diatreme volcano buried in the offshore Banks Peninsula, New Zealand [22]. The chaotic reflections indicate deep excavations of the pre-eruptive subsurface. (g) Plan view spectral decomposition of a maar-diatreme buried in the Eromanga Basin, Australia [9]. (h) Oblique, TWT view of the proposed maar-diatreme in (g).

The deduction of mounds- and crater-shaped seismic anomalies being igneous in origin can be reinforced by the presence of artefacts such as pull-up of seismic velocities (**Figure 6a**), indicating that rocks within the anomalies have a much higher acoustic velocity than the surrounding strata [25, 35]. In addition, doming of reflectors overlying mound-shaped volcanoes (**Figure 8a**) is common where

volcanic rocks are less compacted than surrounding sedimentary strata [59, 63]. Seismic interpretation shows that clusters of small craters and cones are often located above the tips of saucer-shaped intrusions or associated with high-amplitude reflections emplaced into pre-eruptive strata (**Figures 6, 8 and 10**), which suggest that magma is likely to stall in numerous interconnected batches immediately below volcanic fields [43, 89]. Multiple craters and cones have been interpreted to form hydrothermal vent complexes where shallow intrusions were emplaced within sedimentary strata [59, 110]. If the magma intrudes into organic-rich sedimentary sequences, these vent complexes could release large amounts of greenhouse gases from metamorphic aureoles, potentially triggering global warming events such as the Paleocene-Eocene Thermal Maximum; PETM [108, 111].

4.3 Large composite, shield and caldera volcanoes

Large (i.e. $>5 \text{ km}^3$) composite, shield and caldera volcanoes are discrete landforms constructed over tens to millions of years by repeated eruptions at a relatively confined vent site [7]. The most distinctive large volcanoes are cone-shaped stratovolcanoes, overlapping compound edifices, low-profile shield volcanoes, and ring-shaped caldera depressions. Typically formed by polygenetic building mechanisms, these large volcanoes represent end-member variants with a broad spectrum of intermediary elements. The range of morphologies of polygenetic volcanoes can overlap with each other through time, complicating development of empirical models for interpreting the factors controlling their edifice growth mechanisms and evolution [112]. Each of these large volcanic landforms can be constructed from magmas of any known chemical composition and in all known tectonic settings [72].

Conversely, some particular morphologies are more likely to be developed in specific tectonic conditions and under the influence of certain magmas, allowing us to recognise generalities for each volcanic type. For example, andesitic-dacitic composite volcanoes are commonly derived from partial melting of the asthenosphere at subduction zones, often erupting along volcanic arcs such as the Andes in South America and the Cascades in western USA [5]. The viscosity of andesitic-dacitic magmas favours accumulation of lava and tephra near the eruptive site, building composite morphologies such as stratovolcanoes (e.g. Mt. Fuji, Japan) and compound volcanoes (e.g. Mt. Tongariro, New Zealand). Stratovolcanoes display large (ca 2 km high and 15 km wide) steep-sided (up to 30° slopes) flanks located next to a relatively stationary central vent (**Figure 11**). Whereas, compound volcanoes are formed by several overlapping edifices that together shape a distinctive massif of volcanic rocks separated from other adjacent volcanoes (**Figure 12**). Both strato- and compound volcanoes typically comprise accumulations of interbedded lava-flows, pyroclastic material and reworked volcanic debris [113]. Primary volcanic and epiclastic accumulations follow a proximal-distal facies pattern in which thick, amalgamated and coarser-grained layers are deposited close to the vent zone, while thin, tabular and fine-grained facies accumulate distally to the vent (**Figure 7**). The overall architecture of a composite volcano comprises a central vent zone and overlapping flanks circled by a radial ring-plain deposited around an individual edifice or a group of edifices. In addition, the flanks of composite volcanoes often contain small parasitic cinder cones and lava domes [114].

Shield volcanoes are typical products of low viscosity basaltic lavas erupted at intraplate hotspots, generally associated with extensional settings such as the Hawaiian volcanoes [115]. However, shield volcanoes are also commonly found along intracontinental rifts (e. g. Dama Ali, eastern Ethiopia) and subduction-related volcanic arcs (e.g. Payun Matru, Argentina). Basaltic shield volcanoes consist of a central summit vent (which may or may not include a caldera), enclosed

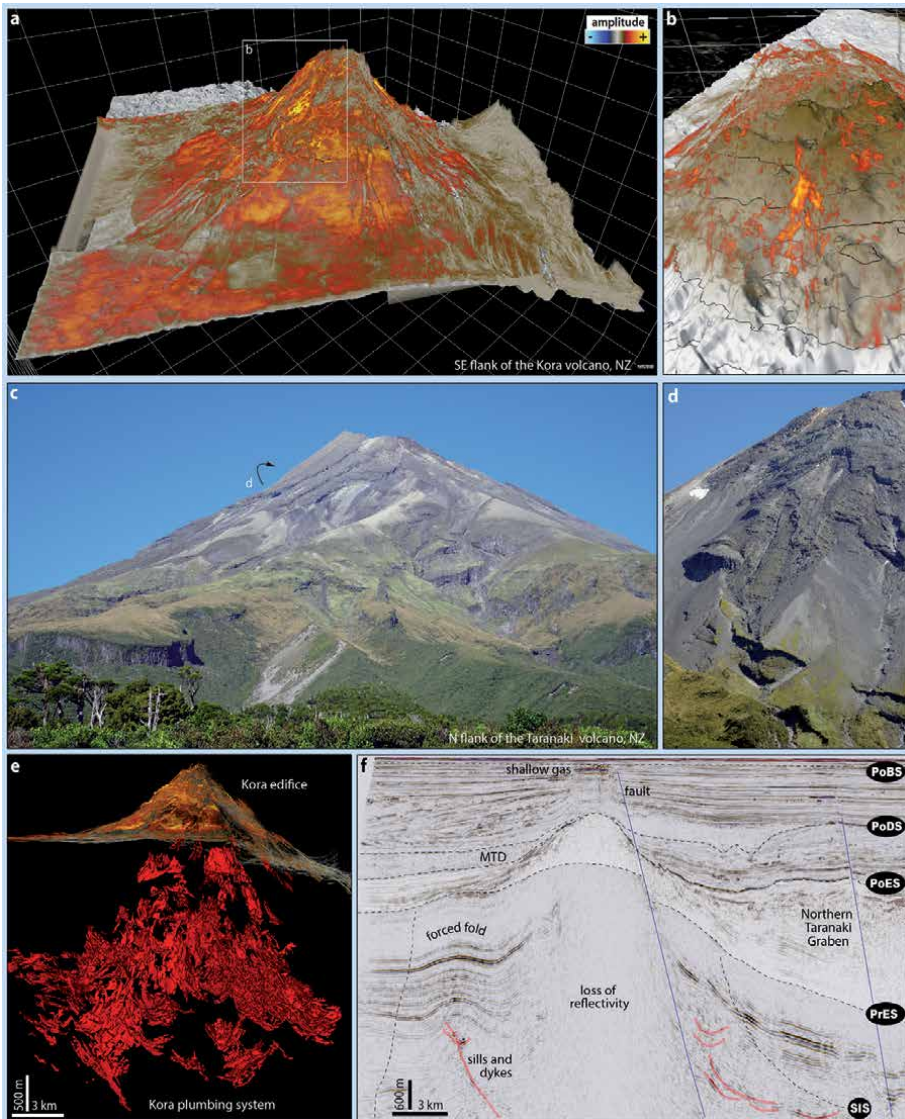


Figure 11. Seismic and outcrop examples of large (>5 km²) composite volcanoes. This type of volcanic landform typically constitutes a single cone-shaped body with a central vent located at or near the summit of the volcano. (a and b) 3D perspective of a rendered amplitude seismic cube across the Kora volcano, New Zealand. (c and d) View of the north flank of the Taranaki volcano, New Zealand. Note the disrupted and channelised geometry of proximal deposits, while distal deposits typically are lobate and more continuous. In (b), the high-amplitude reflections (red) are discontinuous and disrupted, which likely reflect multiple depositional and erosional events, such as observed to form at the flanks of Taranaki volcano (d). (e) Oblique 3D view of the intrusive and extrusive parts of the Kora volcano. The edifice is highlighted by an opacity rendered amplitude cube, while the plumbing system was mapped as numerous interconnected geobodies. (f) Amplitude display of a seismic section across the Kora volcano.

by low-angle (<10° slopes) peripheral flanks, and a flat lava apron that can extend tens of km's from the vent [116]. Parasitic vents commonly erupt on the flanks of shield volcanoes, often forming rows of spatter and scoria cones aligned with normal faults (Figure 13). In addition, oceanic and paralic shield volcanoes are likely to contain a hyaloclastite apron and associated lava-deltas, in which interaction between lava and seawater may trigger hydrovolcanic explosions that can produce large amounts of fragmented material [117].

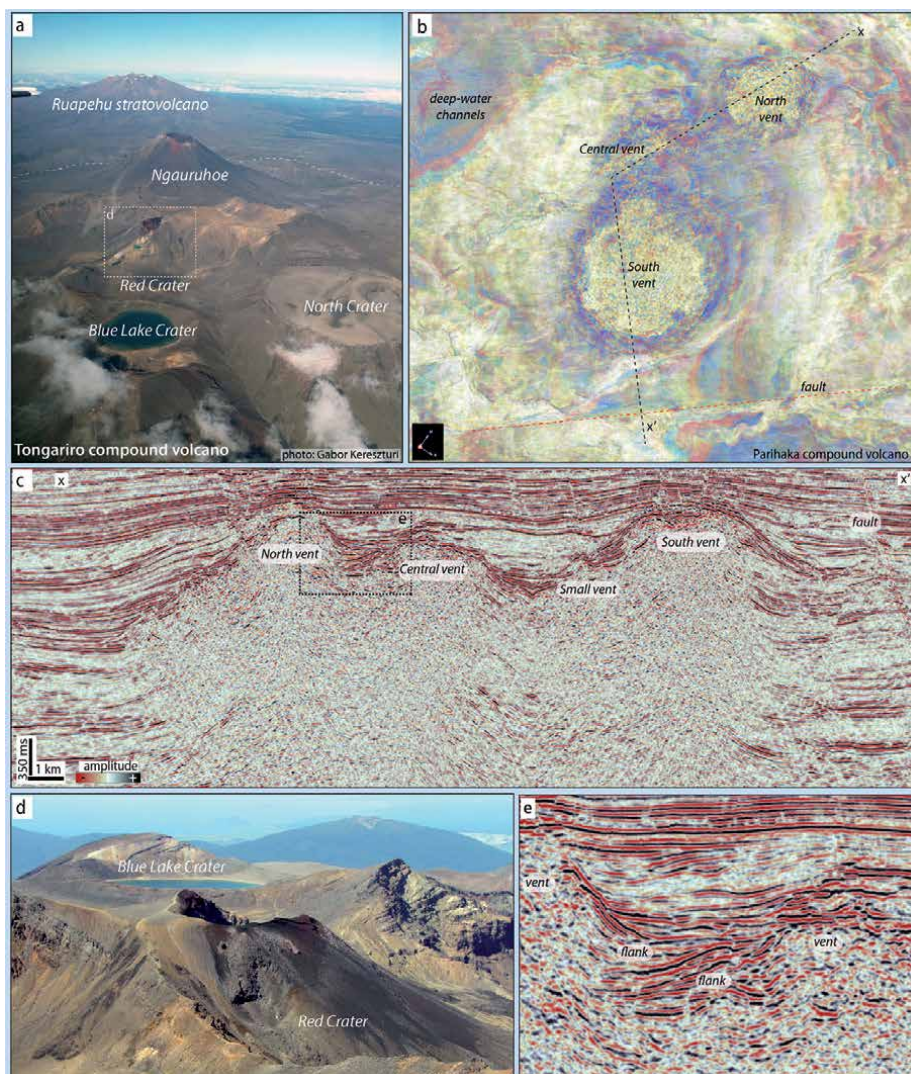


Figure 12.

Seismic and outcrop examples of large (> 5 km²) compound volcanoes. Several overlapping vents which are typically randomly distributed characterise this type of volcanic landform. (a) An aerial view of the southern sector of the Tongariro compound volcano with the Ruapehu stratovolcano in the background. (b) Plain view over a rendered amplitude seismic cube showing the location of three main vents within the Parihaka compound volcano, New Zealand. (c) Amplitude display of a seismic section across the Parihaka volcanoes. Note the overlapping flanks of the main vents. (d) Photograph from the summit of the Ngauruhoe volcano showing a detailed view of the Red Crater, Blue Lake Crater and overlapping lavas of the Mangahouhounui Fm, Tongariro compound volcano. (e) Detail of the amplitude display of a seismic section shown in (c). Note the overlapping reflections on the flanks of the vents.

Large polygenetic volcanoes have been interpreted from seismic reflection datasets since the 1980s' in many sedimentary basins globally. Similar to their smaller cone and crater equivalents (Section 4.2), the reflection configuration within and around large buried volcanoes may make it possible to interpret their broad architecture and genesis. Buried composite and shield volcanoes typically resemble small mound- and cone-shaped vents (**Figures 10–13**). Therefore, their architecture comprises chaotic and inward-dipping reflections at the vent zone, continuous to discontinuous reflections at the flanks, and a wide, almost flat ring plain evident by high-to-moderated amplitude reflections that pinch and fade with increasing

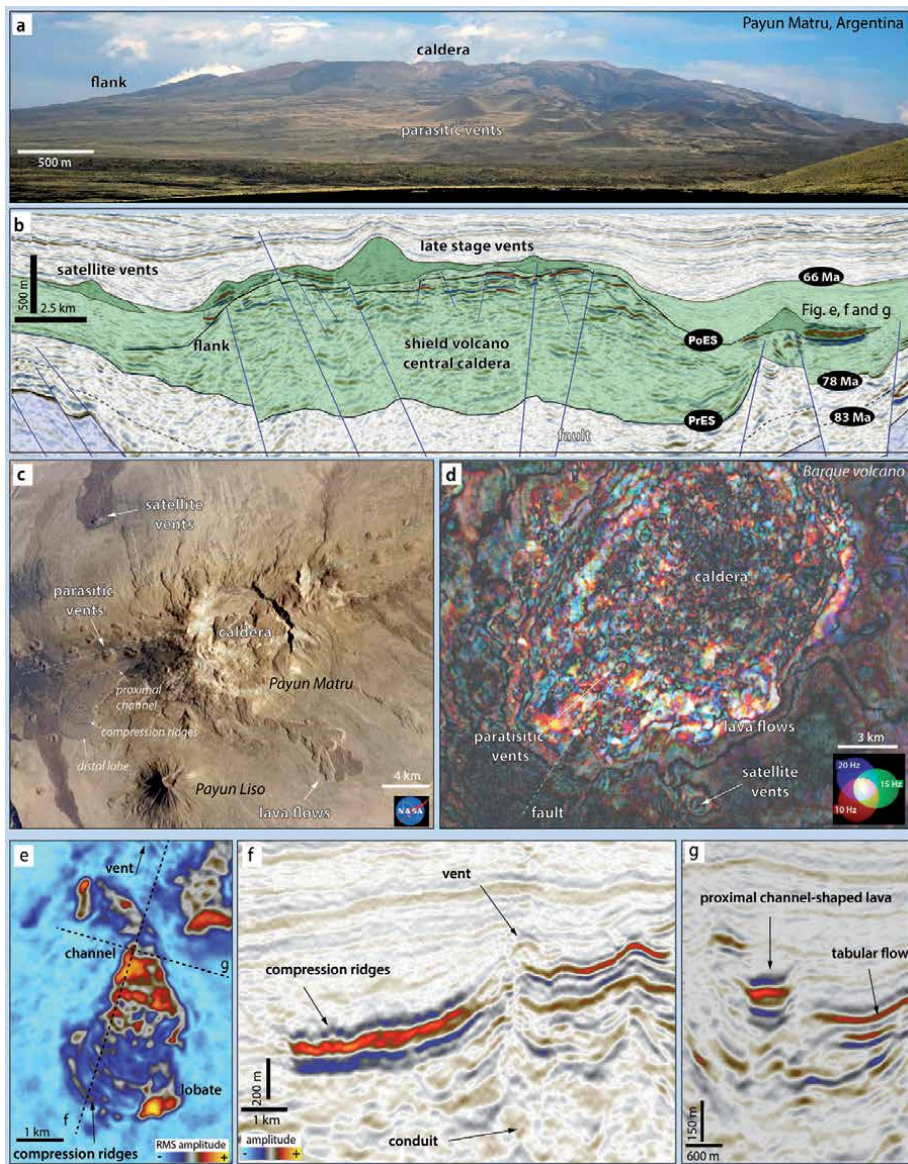


Figure 13. Seismic and outcrop examples of shield volcanoes with a central caldera. (a) Photograph of the northern flank of the Payun Matru Volcano, Argentina. (b) Amplitude display of a seismic section across the Barque volcano, offshore Canterbury Basin, New Zealand (Modified from [28]). (c) Aerial view of the region of the Payun Matru, a shield with a central caldera, and Payun Liso a stratovolcano. Note the NW alignment of cinder cones. (d) Plain view of a decomposed seismic cube showing the flanks and central depression of the Barque volcano. Parasitic and satellite vents are commonly aligned with normal faults. (e) Plain view of an RMS seismic cube across a lava flow of the Barque volcano. (f and g) Amplitude display of a seismic section across the lava flow in (e).

distance from the main volcanic body [1, 63]. Parasitic and satellite vents are often described on the flanks of these large buried volcanoes, typically located above pre-existing structures of the basement or at radial normal faults [52]. Interpretation of seismic reflection datasets suggests that the shallow (<5 km) plumbing system of large polygenetic volcanoes comprises a myriad of interconnected intrusive bodies, mainly aligned with crustal structures, markedly contrasting with the classic “balloon-and-straw” model [24, 28, 118].

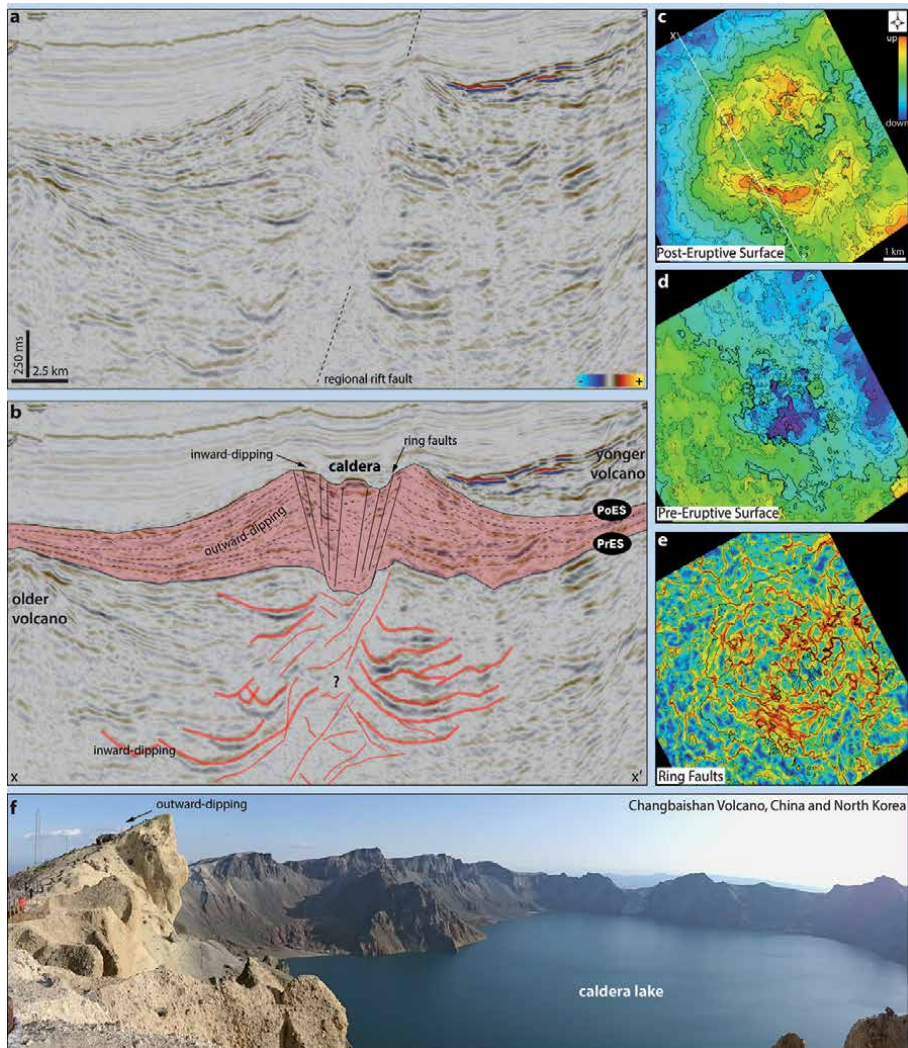


Figure 14.

Seismic and outcrop examples of shield volcanoes with a central caldera. (a) Uninterpreted and (b) interpreted amplitude display of a seismic section across the Hades caldera, offshore Deepwater Taranaki Basin, New Zealand (Modified from [28]). (c) Post-eruptive surface and (d) pre-eruptive surface isochron horizon maps of the Hades caldera. Note the wide (ca 5 km) central depression with inward-dipping reflections circled by a ring of outward-dipping layered material. (e) Pre-eruptive surface isochron horizon map applying an edge-detection attribute, which is enhancing a series of ring-shaped faults at the location of the caldera depression. (f) Photograph of the crater lake at the summit of the Changbaishan Volcano, Chinese and North Korean border. The lake marks the location of a 5 km wide caldera vent formed by a large pyroclastic eruption in 946 AD. Note the steeply inclined outward-dipping layers of white ignimbrite rocks at the left corner of the picture.

Caldera-forming volcanoes are commonly associated with subsidence and collapse of the roof of magma chambers due to partial withdrawal of magma during voluminous and short-lived eruptions [119]. Characteristic caldera volcanoes are silicic in composition and produced by ultra-Plinian eruptions, often developing in association with rifted arcs such as the Taupo Volcanic Zone in New Zealand [120, 121]. However, smaller pyroclastic and non-explosive calderas of more mafic compositions often form within the central vent zone of composite and shield volcanoes [122]. Caldera volcanoes have a variety of geometries and structures mainly defined by mechanisms of pyroclastic material dispersal, caldera collapse,

and dome resurgence [123]. The general architecture of large silicic calderas comprises a central depression of 1–2 km depth surrounded by lateral by an ignimbrite plateau or steepen flanks of pyroclastic and lava material, which can cover areas of >3000 km² [72]. The central depression is often bounded by ring faults and hosts thick sequences of intra-caldera pyroclastic deposits, late-stage andesitic-rhyolitic lava-flows and domes, lacustrine sediments and debris. Caldera volcanoes may or may not produce a post-eruptive resurgent dome, a consequence of intra-caldera uplift from a renewed rise of magma into the chamber(s), such as documented from the Toba Volcano, Indonesia, and Yellowstone, USA [124].

Interpretation of buried caldera volcanoes from seismic data is scarce, and to our knowledge, only documented in two places offshore New Zealand [28]. Barque volcano, offshore Canterbury Basin, is potentially a large (ca 20 km wide) shield volcano with a central caldera (**Figure 13**). Hades caldera, in the Deepwater Taranaki, has a semi-circular structure 10 km across with a central depression 3.5 km wide and 1 km deep bounded by ring faults, likely formed by pyroclastic mechanisms of material fragmentation and dispersion (**Figure 14**). Both examples show no evidence of a single large batch of magma sited beneath the caldera. Rather, multiple interconnected intrusions, including saucer-shaped sills and tabular bodies aligned with pre- and syn-rift faults more likely describe their magma plumbing systems (**Figures 13 and 14**).

4.4 Voluminous lava fields

Eruptions of voluminous (i.e. >10,000 km³) lava fields are commonly associated with continental break-up and upwelling of mantle plumes that form Large Igneous Provinces (LIPs). Characteristically, LIPs comprise extensive flood basalt plateaus derived from decompression melting of the mantle, but more differentiated alkalic, tholeiitic, and silicic rocks can also occur as lavas, pyroclastic, and intrusive bodies [125]. LIPs constitute the most extensive volcanic landscapes on Earth, including regional-scale igneous-dominated structures such as continental flood basalts, volcanic rifted margins, oceanic plateaus, submarine ridges, seamount chains, and ocean-basin flood basalts [126]. The voluminous lava fields often erupt at both continental (e.g. Siberian Traps, Asia) and oceanic crust (e.g. Ontong Java Plateau, Pacific Ocean), as well as at divergent plate boundaries such as the South Atlantic Margins [127].

The broad architecture of LIPs consists of stacks of sub-horizontal sheets of lava flows up to ca 10 km thick underlying by networks of subvolcanic sills and dykes [51, 128]. The extrusive part of LIPs is interpreted to be mainly fed by repeated voluminous eruptions sourced from scattered fissure vents and shield volcanoes, in which the entire volcanic pile is typically constructed in relatively short time spans (<1 Myr). Individual flows can reach volumes as much as 1000 km³ and extend for hundreds of kilometres from the vent site, such as described in the Columbia River Plateau and the Deccan Traps [72]. The Laki eruption in Iceland, for example, is one of the largest documented historical lava flows. It covered an area of near 600 km² of southern Iceland in the 1780s, with an estimated discharge of almost 15 km³ of lava from a 27 km long fissure vent system consisting of scoria, spatter, and tuff cones [129].

Most voluminous lava fields are interbedded with sedimentary basins formed by crustal extension, rifting, and continental drifting [130]. Volcanic rift margins have been the most intensively studied LIPs from seismic reflection datasets (**Figure 15**). Over the past 40 years, interpretation of enormous amounts of seismic data along the boundaries of the Atlantic, Western Australian, and Southern Indian continental crusts showed that rift margins typically comprise a set of characteristic volcanic seismic facies units [4, 11, 131]. These seismic facies units represent interactions between

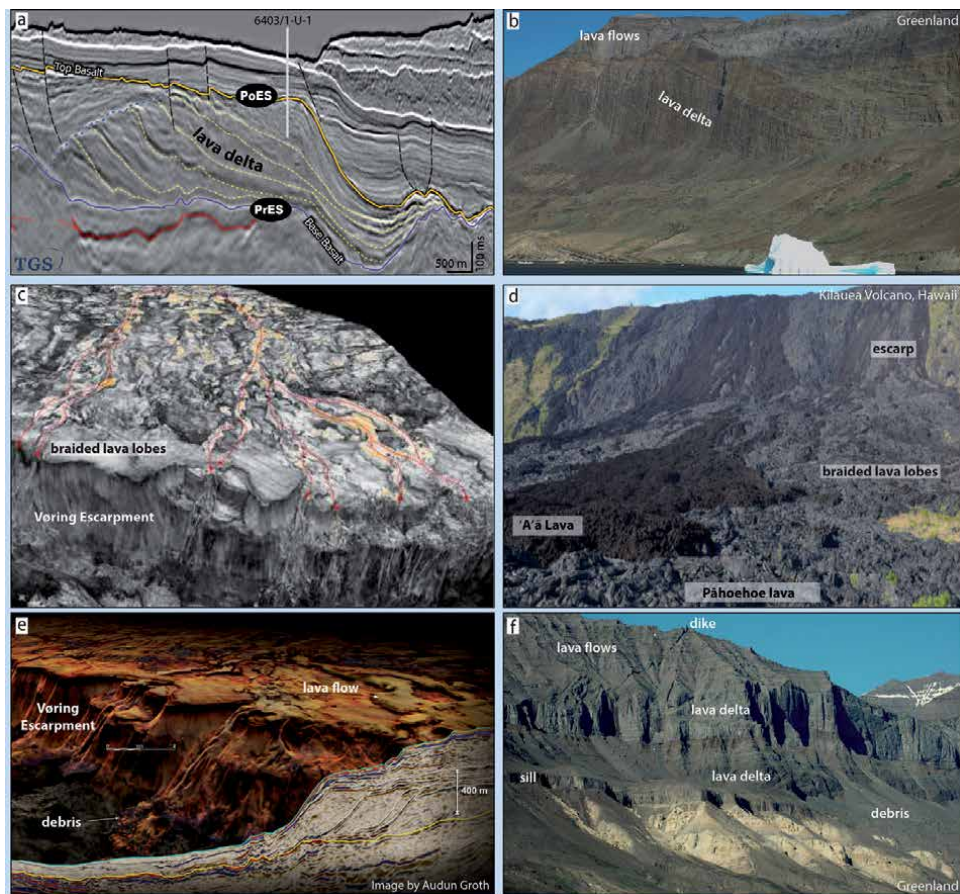


Figure 15.

Seismic and outcrop examples of volcanic rift margins and lava-fields. (a) Amplitude display of a seismic section across the Kolga Lava Delta, offshore Norway, showing the characteristic wedge of progradational deltas (From [45]). (b) Prograding foresets of a lava delta in western Greenland. (c) Perspective view of the top-basalt horizon of the Vøring Escarpment, offshore Norway (From [29]). (d) Lava field and escarpments formed during the 2018 series of eruptions of the Kilauea Volcano, Hawaii. (e) Perspective view of the Vøring Escarpment (From [29]). (f) Geometric relationship of intrusive and extrusive bodies of a voluminous lava field in western Greenland. Data courtesy of TGS (a).

volcanism and sedimentation, and their interpretation informs the construction of models for the initiation and evolution of volcanic rift margins [26]. The typical volcanic rift margin sequence initiates with aggradation of peperites, hydrobreccias, and pillow-lavas where magma interacts with water and wet sediments, while subaerial lava-flows can develop at the basin margins and on topographic highs [132]. Continued aggradation and progradation of igneous material favours more effusive and subaerial volcanism, in which eruptions tend to form extensive sheets of stacked lava-flow deposits [34]. If the lava-flows stretch an existing shoreline, a prograding lava-delta comprising of hyaloclastic and epiclastic material can be developed [133]. Subsequently, these volcanic deposits may be exposed to erosional conditions, forming escarpments surfaces, slumps, and volcanoclastic gravity flow deposits triggered by degradation of the volcanic sequence [134].

A recent seismic geomorphological study used a 2500 km² high-quality 3D seismic survey to image the top-basalt horizon of the Vøring Marginal High, offshore Norway [29]. Interpretation of this seismic horizon revealed a series of volcanic macroforms such as lava-flows with compressional ridges and braided lava-channels

with similar structure and size of morphologies described in modern subaerial lava fields (**Figure 15**). In addition, the Vøring Marginal High 3D data showed numerous pitted and irregular lava surfaces next to smooth sheet-like reflections with geometry comparable to fields of small cone and crater volcanoes and their associated peripheral lava flows. These pitted seismic features are interpreted to correspond to places where magma was emplaced into wet sediments or water [29]. Debris flows deposits along with large slumped blocks are well imaged at the top of the Vøring Escarpment, revealing a volcanic morphology influenced by erosion and degradation of pre-existing voluminous lava fields (**Figure 15**).

5. Conclusions

Interpretation of 2D and 3D seismic reflection datasets provides valuable insights into the morphology and stratigraphic signature of entire igneous systems buried in sedimentary basins. The application of 3D seismic visualisation methods offers a unique opportunity for direct comparison of the geomorphic aspects of buried and outcropping volcanoes, with resolutions down to tens of metres.

Buried volcanic systems comprise a network of intrusive, eruptive, and sedimentary architectural elements with length scales of 10^2 – 10^4 meters that are recognisable from both seismic and outcrop analyses. These architectural elements often show a spatial and temporal distribution controlled by their distance from eruptive centres. The geometry and internal arrangement of facies within these elements reflect a range of physical factors including, magma composition, effusion discharge rate, degree of material fragmentation, and the presence or absence of water at the eruption vent. Many, if not most, volcanic systems are underlain by shallow (<5 km) interconnected networks of sills, saucer-sills, laccoliths, dykes, and hybrid intrusions that often align with pre-existing crustal structures or contemporaneous faults.

Description and interpretation of seismic reflection surveys together with their outcropping volcano analogues from key localities worldwide suggest three main geomorphic categories of buried volcanoes. These categories are (1) clusters of small-volume (<1 km³) craters and cones, including maar-diatremes, tuff rings, spatter cones, scoria cones, tuff cones, and hydrothermal vent complexes, (2) large (>5 km³) composite, shield and caldera volcanoes, and (3) voluminous lava fields (>10,000 km³). This classification of buried volcanoes is based on their geometry, size, and spatio-temporal distribution of eruptive centres, and is independent of parameters such as magma composition, tectonic setting, or environment where the eruption occurred. Classifying the buried volcanoes into geomorphic categories helps us to understand the processes that link their endogenous and exogenous realms, providing insights into the architecture, edifice growth mechanisms and longevity of igneous systems buried in sedimentary basins.

The modern methods of seismic interpretation, from 2D regional scale to detailed 3D analysis, can provide an accurate understanding of the geological processes that formed the volcanoes now buried in the subsurface. Realistic models for the facies distribution and architecture of buried volcanoes can be constrained by their geomorphic similarities to outcropping volcanoes, establishing the principles for the new discipline of seismic-reflection volcanology.

Acknowledgements

We would like to thank the Ministry of Business, Innovation and Employment (MBIE) of New Zealand and TGS for access to seismic and well data, and IHS

Markit and Schlumberger for providing academic licence to use Kingdom and Petrel software. AB thanks funding from the MBIE research grant UOCX1707. SP acknowledges support from the Norwegian Research Council Centres of Excellence funding scheme (CEED; project number 223272). We appreciate the constructive reviews of Ray Cas and Jim Cole, and the contribution of Jessica Fensom in proof-reading and discussing the manuscript.

Conflict of interest

The authors declare no conflict of interest.

Author details

Alan Bischoff^{1*}, Sverre Planke², Simon Holford³ and Andrew Nicol¹


1 University of Canterbury, Christchurch, New Zealand

2 VPBR and University of Oslo, Oslo, Norway

3 University of Adelaide, Adelaide, Australia

*Address all correspondence to: alan.bischoff@canterbury.ac.nz

IntechOpen

© 2021 The Author(s). Licensee IntechOpen. This chapter is distributed under the terms of the Creative Commons Attribution License (<http://creativecommons.org/licenses/by/3.0>), which permits unrestricted use, distribution, and reproduction in any medium, provided the original work is properly cited. 

References

- [1] Herzer RH. 1995. Seismic Stratigraphy of a Buried Volcanic Arc, Northland, New Zealand and Implications for Neogene Subduction. *Marine and Petroleum Geology* 12, no. 5 511-31. [https://doi.org/10.1016/0264-8172\(95\)91506-K](https://doi.org/10.1016/0264-8172(95)91506-K).
- [2] Magee C, Hunt-Stewart E, Jackson CAL. 2013. Volcano growth mechanisms and the role of sub-volcanic intrusions: Insights from 2D seismic reflection data: *Earth and Planetary Science Letters*, doi:10.1016/j.epsl.2013.04.041.
- [3] Planke S, Alvestad E, Eldholm O. 1999. Seismic Characteristics of Basaltic Extrusive and Intrusive Rocks. *The Leading Edge* 18 (3): 342. doi:10.1190/1.1438289.
- [4] Planke S, Symonds PA, Alvestad E, Skogseid J. 2000. Seismic Volcanostratigraphy of Large-Volume Basaltic Extrusive Complexes on Rifted Margins. *J Geophys Res* 105 (B8): 19335. <https://doi.org/10.1029/1999JB900005>
- [5] Grosse P, van Wyk de Vries B, Petrinovic IA, Euillades PA, Alvarado GE. 2009. Morphometry and evolution of arc volcanoes. *Geology* 37 (7), 651e654. <http://dx.doi.org/10.1130/G25734A.1>.
- [6] Kereszturi G, Németh C. 2012. Monogenetic Basaltic Volcanoes: Genetic Classification, Growth, Geomorphology and Degradation: Updates in Volcanology - New Advances in Understanding Volcanic Systems, <https://doi.org/10.5772/51387>
- [7] Manville V, Nemeth K, Kano K. 2009. Source to sink: A review of three decades of progress in the understanding of volcanoclastic processes, deposits, and hazards. *Sedimentary Geology*. 136-161. doi:10.1016/j.sedgeo.2009.04.022.
- [8] Planke et al. 2018. Seismic Imaging and Petroleum Implication of Igneous Intrusions in Sedimentary Basins.
- [9] Hardman JPA, Holford SP, Schofield N, Bunch M, Gibbins D. 2019. The Warnie volcanic province: Jurassic intraplate volcanism in Central Australia. *Gondwana Research* 76, 322-347. <https://doi.org/10.1016/j.gr.2019.06.012>
- [10] Berndt C, Planke S, Alvestad E, Tsikalas F, Rasmussen T. 2001. Seismic volcanostratigraphy of the Norwegian Margin: Constraints on tectonomagmatic break-up processes: *Journal of the Geological Society*, 158, 413-426, doi: 10.1144/jgs.158.3.413.
- [11] Calvès G, Schwab AM, Huuse M, Clift PD, Gaina C, Jolley D, Tabrez AR, Inam A. 2011. Seismic volcanostratigraphy of the western Indian rifted margin: The pre-Deccan igneous province, *J. Geophys. Res.*, 116, B01101, doi:10.1029/2010JB000862.
- [12] Carlotto MA, Silva RCB, Yamato AA, Trindade WL, Moreira JLP, Fernandes RAR, Ribeiro OJS, et al. 2017. Libra: A Newborn Giant in the Brazilian Presalt Province. In *Giant Fields of the Decade 2000-2010*. doi:10.1306/13572006M1133685.
- [13] Field BD, Browne GH, Davy BW, Herzer RH, Hoskins RH, Raine JI, Wilson GJ, Sewell RJ, Smale D, Watters WA. 1989. Cretaceous and Cenozoic sedimentary basins and geological evolution of the Canterbury region, South Island, New Zealand. Lower Hutt: New Zealand Geological Survey. *New Zealand Geological Survey Basin Studies* 2: 94.
- [14] Paumard V, Zuckmeyer E, Boichard R, Jorry S, Bourget J, Borgomano J, Maurin T, Ferry JN, 2017, Evolution of Late Oligocene - Early Miocene attached and isolated

carbonate platforms in a volcanic ridge context (Maldives type), Yadana field, offshore Myanmar: 361-387 p., doi:10.1016/j.marpetgeo.2016.12.012.

[15] Reynolds P, Holford S, Schofield N, Ross A. 2017. Three-Dimensional Seismic Imaging of Ancient Submarine Lava Flows: An Example From the Southern Australian Margin. *Geochem. Geophys. Geosys.* doi:10.1002/2017GC007178

[16] Sacchi et al. 2019. The use and beauty of ultra-high-resolution seismic reflection imaging in Late Quaternary marine volcanoclastic settings, Napoli Bay, Italy. *Földtani Közlöny.* 149. 371. DOI: <https://doi.org/10.23928/foldt.kozl.2019.149.4.371>

[17] Sun QL, Wu SG, Cartwright J, Wang SH, Lu YT, Chen DX, Dong DD. 2014. Neogene igneous intrusions in the northern South China Sea: Evidence from high resolution three dimensional seismic data. *Marine and Petroleum Geology*, 54, 83– 95. <https://doi.org/10.1016/j.marpetgeo.2014.02.014>

[18] Davies RJ, Posamentier HW, Wood LJ, Cartwright J. 2007. Seismic Geomorphology: Applications to Hydrocarbon Exploration and Production. Geological Society Special Publications. DOI: <https://doi.org/10.1144/GSL.SP.2007.277.01.01>

[19] Hart BS. 2013. Whither seismic stratigraphy? *Interpretation* 1(1): SA3–SA20. <https://doi.org/10.1190/INT-2013-0049.1>

[20] Posamentier HW, Kolla V. 2003. Seismic Geomorphology and Stratigraphy of Depositional Elements in Deep-Water Settings. *J. Sed. Res.*, 73 (3), 367-88., doi:10.1306/111302730367

[21] Cas RAF, Wright JV. 1987. Volcanic Successions: Modern and Ancient - A Geological Approach to Processes, Products and Successions.

Chapman and Hall, UK, <https://doi.org/10.1007/978-0-412-44640-5>

[22] Bischoff AP, Rossetti M, Nicol A, Kennedy B. 2019b. Seismic Reflection and Petrographic Interpretation of a Buried Monogenetic Volcanic Field (Part 1). *Bull Volcanol* 81: 56. <https://doi.org/10.1007/s00445-019-1316-7>

[23] McLean CE, Schofield N, Brown DJ, Jolley DW, Reid A. 2017. 3D seismic imaging of the shallow plumbing system beneath the Ben Nevis Monogenetic Volcanic Field: Faroe–Shetland Basin: *J. Geol. Soc.* <https://doi.org/10.1144/jgs2016-118>

[24] Walker F, Schofield N, Millett J, Jolley D, Holford S, Planke S, Jerram DA, Myklebust R. 2020. Inside the volcano: Three-dimensional magmatic architecture of a buried shield volcano. *Geology* doi: <https://doi.org/10.1130/G47941.1>

[25] Holford SP, Schofield N, MacDonald JD, Duddy IR, Green PF. 2012, Seismic Analysis of Igneous Systems in Sedimentary Basins and Their Impacts on Hydrocarbon Prospectivity: Examples from the Southern Australian Margin. *APPEA Journal*, 52, 229-52.

[26] Planke S, Svensen H, Myklebust R, Bannister S, Manton B, Lorenz L. 2015. Geophysics and remote sensing, *Advances in Volcanology*: Springer, 1-16.

[27] Reynolds P, Schofield N, Brown RJ, Holford SP. 2016. The architecture of submarine monogenetic volcanoes - insights from 3D seismic data: *Basin Research*, v. 30, p. 437-451, doi:10.1111/bre.12230.

[28] Bischoff A, Barrier A, Beggs M, Nicol A, Cole J. 2020. Volcanoes Buried in Te Riu-a-Māui/Zealandia Sedimentary Basins. In: IAVCEI Special Issue: Cenozoic Volcanism in New Zealand. *New Zealand Journal of*

- Geology and Geophysics. 63:4, 378-401. <https://doi.org/10.1080/00288306.2020.1773510>
- [29] Planke S, Millett JM, Maharjan D, et al. 2017. Igneous seismic geomorphology of buried lava fields and coastal escarpments on the Vøring volcanic rifted margin: Interpretation, doi:10.1190/INT-2016-0164.1.
- [30] Marfurt K. 2018. Seismic Attributes as the Framework for Data Integration Throughout the Oilfield Life Cycle: Society of Exploration Geophysicists, 508 p., doi: doi:10.1190/1.9781560803522.
- [31] Sheriff RE, Geldart LP. 1995. Exploration Seismology, 2nd edn., Cambridge University Press, Cambridge, UK.
- [32] Vail PR, Mitchum RM, Todd RG, Widmier JM, Thompson S, Sangree JB, Bubb JN, Hatlelid WG. 1977. Seismic stratigraphy and global changes of sea-level. In: Payton, C.E. (Ed.), Seismic Stratigraphy – Applications to Hydrocarbon Exploration. AAPG Memoir 26, pp. 49-212
- [33] Heap MJ, Kennedy BM. 2016. Exploring the scale-dependent permeability of fractured andesite: Earth and Planetary Science Letters, doi:10.1016/j.epsl.2016.05.004.
- [34] Millett J, Hole M, Jolley D, Schofield N, Campbell E. 2015. Frontier exploration and the North Atlantic Igneous Province: New insights from a 2.6 km offshore volcanic sequence in the NE Faroe–Shetland Basin. Journal of the Geological Society. 173. 10.1144/0016-76492015-069.
- [35] Jackson CAL. 2012. Seismic reflection imaging and controls on the preservation of ancient sill-fed magmatic vents. J. Geol. Soc. <https://doi.org/10.1144/0016-76492011-147>
- [36] Rateau R, Schofield N, Smith M. 2013. The potential role of igneous intrusions on hydrocarbon migration, West of Shetland: Petroleum Geoscience, 19, 259-272, doi:10.1144/petgeo2012-035.
- [37] Bischoff AP, Nicol A, Barrier A, Wang H. 2019a. Paleogeography and Volcanic Morphology Reconstruction of a Buried Monogenetic Volcanic Field (Part 2). Bull Volcanol 81: 57. <https://doi.org/10.1007/s00445-019-1317-6>
- [38] Klarner S, Klarner O. 2012. Identification of Paleo-Volcanic Rocks on Seismic Data. In: Updates in Volcanology-A Comprehensive Approach to Volcanological Problems, IntechOpen, 181-206 pp.
- [39] Rohrman M. 2007. Prospectivity of Volcanic Basins: Trap Delineation and Acreage de-Risking. AAPG Bulletin. 91 (6), 915-39., doi:10.1306/12150606017
- [40] Mordensky S, Villeneuve M, Farquharson J, Kennedy B, Heap MJ, Gravley DM. 2018. Rock mass properties and edifice strength data from Pinnacle Ridge, Mt. Ruapehu, New Zealand: doi:10.1016/j.jvolgeores.2018.09.012.
- [41] Schofield N, Jerram DA, Holford S, Stuart A, Niall M, Hartley A, Howell J, David M, Green P, Hutton D, Stevenson C. 2016. Sills in sedimentary basin and petroleum systems: In Németh K (ed) The Series Advances in Volcanology, pp 1-22.
- [42] Jerram DA, Single RT, Hobbs RW, Nelson CE. 2009. Understanding the offshore flood basalt sequence using onshore volcanic facies analogues: An example from the Faroe-Shetland basin. Geol. Mag. <https://doi.org/10.1017/S0016756809005974>
- [43] Magee C, Stevenson CTE, Ebmeier SK, Keir D, Hammond JOS, Gottsmann JH, Whaler KA, Schofield N, Jackson CAL, et al. 2018. Magma Plumbing Systems:

A Geophysical Perspective. *Journal of Petrology*, egy064, <https://doi.org/10.1093/petrology/egy064>

[44] Infante-Paez L, Marfurt KJ. 2017. Seismic expression and geomorphology of igneous bodies: A Taranaki Basin, New Zealand, case study. *Interpretation*. 5 (3), SK121-SK140., <https://doi.org/10.1190/INT-2016-0244.1>

[45] Millett J, Manton BM, Zastrozhnov D, Planke S, Maharjan D, Bellwald B, Gernigon L, et al. 2020. Basin structure and prospectivity of the NE Atlantic volcanic rifted margin: cross-border examples from the Faroe–Shetland, Møre and Southern Vøring basins. *Geological Society, London, Special Publications*, 495, 7 January 2020, <https://doi.org/10.1144/SP495-2019-12>

[46] Catuneanu O, Abreu V, Bhattacharya JP, Blum MD, Dalrymple RW, Eriksson PG, Fielding CR, Fisher WL, Galloway WE, Gibling MR, et al. 2009. Towards the standardisation of sequence stratigraphy. *Earth-Science Reviews* 92, 1-33. Elsevier B.V.: 1-33. doi:10.1016/j.earscirev.2008.10.003.

[47] Miall AD. 2016. *Stratigraphy: A Modern Synthesis*: Cham, Springer International Publishing, doi:10.1007/978-3-319-24304-7.

[48] Vail PR, Mitchum RM. 1977. Seismic stratigraphy and global changes of sea level. I: Overview: *Memoir American Association of Petroleum Geologists*, 22, 51-52.

[49] Abdelmalak MM, Planke S, Faleide JI, Jerram DA, ZastrozhnovD, Eide S, Myklebust R. 2016. The development of volcanic sequences at rifted margins: New insights from the structure and morphology of the Vøring Escarpment, mid-Norwegian Margin: *Journal of Geophysical Research, Solid Earth*, 121, 5212-5236, doi: 10.1002/2015JB012788.

[50] Jerram DA. 2015. Hot rocks and oil: Are volcanic margins the new frontier? Elsevier R&D Solutions for Oil and Gas, Exploration & Production, https://www.elsevier.com/__data/assets/pdf_file/0008/84887/ELS_Geofacets-Volcanic-Article_Digital_r5.pdf

[51] Svensen H, Torsvik TH, Callegaro S, Augland L, Heimdal TH, Jerram DA, Planke S, Pereira E. 2017. Gondwana Large Igneous Provinces: plate reconstructions, volcanic basins and sill volumes. *Geological Society, London, Special Publications*. doi:10.1144/SP463.7

[52] Bischoff AP, Nicol A, Beggs M. 2017. Stratigraphy of architectural elements in a buried volcanic system and implications for hydrocarbon exploration: *Interpretation*. <https://doi.org/10.1190/INT-2016-0201.1>

[53] Bischoff A, Nicol A, Cole J, Gravely D. 2019c. Stratigraphy of Architectural Elements of a Buried Monogenetic Volcanic System. *Open Geosciences*, 11(1), pp. 581-616. Retrieved 23 Mar. 2020, from doi:10.1515/geo-2019-0048

[54] Bishop MA. 2009. A generic classification for the morphological and spatial complexity of volcanic (and other) landforms. *Geo-morphology* 111 (1e2), 104e109.

[55] Cas RAF, Giordano G. 2014. Submarine volcanism: A review of the constraints, processes and products, and relevance to the Cabo de Gata volcanic succession. <https://doi.org/10.3301/IJG.2014.46>

[56] Cas RAF, Simmons JM. 2018. Why Deep-Water Eruptions Are So Different From Subaerial Eruptions. *Front. Earth Sci.* 6:198. doi: 10.3389/feart.2018.00198

[57] Németh K, Palmer J. 2019. Geological mapping of volcanic terrains: Discussion on concepts, facies models, scales, and resolutions from

New Zealand perspective. *Journal of Volcanology and Geothermal Research*, <https://doi.org/10.1016/j.jvolgeores.2018.11.028>

[58] Barrier A, Bischoff AP, Nicol A, Browne GH, Bassett K. 2020. Identification and morphology of buried volcanoes from the Canterbury Basin, New Zealand. *Marine Geology*. In review. (In press)

[59] Planke S, Rasmussen T, Rey SS, Myklebust R. 2005. Seismic characteristics and distribution of volcanic intrusions and hydrothermal vent complexes in the Vøring and Møre basins, in *Petroleum Geology: North-West Europe and Global Perspectives – Proceedings of the 6th Petroleum Geology Conference*. doi:10.1144/0060833.

[60] Bischoff AP. 2019. Architectural Elements of Buried Volcanic Systems and Their Impact on Geoenery Resources. Ph.D. Thesis, Canterbury University, New Zealand. <https://ir.canterbury.ac.nz/handle/10092/16730>

[61] Tipper JC. 1993. Do seismic reflections necessarily have chronostratigraphic significance? *Geological Magazine*, doi:10.1017/S0016756800023712.

[62] Uruski C. 2019. Seismic recognition of igneous rocks of the Deepwater Taranaki Basin, New Zealand, and their distribution. *New Zealand Journal of Geology and Geophysics* 1-20.

[63] Gatliff RW, Hitchen K, Ritchie JD, Smythe DK. 1984. Internal structure of the Erlend Tertiary volcanic complex, north of Shetland, revealed by seismic reflection: *Journal of the Geological Society*, v. 141, p. 555-562, <https://doi.org/10.1144/gsjgs.141.3.0555>.

[64] Jervey MT. 1988. Quantitative geological modeling of siliciclastic rock sequences and their seismic expression. In: Wilgus, C.K., Hastings, B.S., Kendall,

C.G.St.C., Posamentier, H.W., Ross C.A. and Van Wagoner, J.C. (Eds.) *Sea Level Changes – An Integrated Approach*. Society of Economic Paleontologists and Mineralogists (SEPM), Special Publication 42, 47-69.

[65] Van Wagoner JC, Mitchum Jr RM, Campion KM, Rahmanian VD. 1990. Siliciclastic Sequence Stratigraphy in Well Logs, Core, and Outcrops: Concepts for High-Resolution Correlation of Time and Facies. In: *American Association of Petroleum Geologists, Methods in Exploration*. Series 7, 55

[66] Catuneanu O. 2006. Principles of Sequence Stratigraphy. *Changes*, 375. doi:10.5860/Choice.44-4462.

[67] Orton GJ. 1996. Volcanic Environments. Volcanic environments. In: Reading, H.G. (Ed.), *Sedimentary Environments: Processes, Facies and Stratigraphy*. Blackwell Science, Oxford, pp. 485-567.

[68] Smith GA. 1991. Facies sequences and geometries in continental volcanoclastic sequences in Fisher, R.V., and Smith, G.A., eds., *Sedimentation in volcanic settings: SEPM (Society for Sedimentary Geology) Special Publication 45*, p. 109-121.

[69] Lucchi F. 2019. On the use of unconformities in volcanic stratigraphy and mapping: Insights from the Aeolian Islands (southern Italy). *Journal of Volcanology and Geothermal Research*, <https://doi.org/10.1016/j.jvolgeores.2019.01.014>.

[70] Martí J, Gropelli G, Silveira AB. 2018. Volcanic stratigraphy: A review. *Journal of Volcanology and Geothermal Research*, 357: 68-91.

[71] Mitchum RM, Vail PR. 1977. Seismic Stratigraphy and Global Changes of Sea Level, Part 7 : Seismic Stratigraphic Interpretation Procedure. *Seismic Stratigraphy: Applications*

to Hydrocarbon Exploration. AAPG Memoir 26 Memoir 26: 135-43.

[72] de Silva S, Lindsay JM. 2015. Primary Volcanic Landforms. In: H. Sigurdsson (Ed.), *The Encyclopedia of Volcanoes* (Second Edition), Academic Press, Amsterdam: 273-297. DOI: 10.1016/B978-0-12-385938-9.00015-8.

[73] Holford S, Schofield N, Reynolds P. 2017. Subsurface fluid flow focused by buried volcanoes in sedimentary basins: Evidence from 3D seismic data, Bass Basin, offshore southeastern Australia. 39-50., doi:10.1190/INT-2016-0205.1.

[74] Kumar P, Kamaldeen O, Kalachand S. 2018. Sill Cube: An automated approach for the interpretation of magmatic sill complexes on seismic reflection data. *Marine and Petroleum Geology*. 100. 10.1016/j.marpetgeo.2018.10.054.

[75] Posamentier HW. 2000. Seismic stratigraphy into the next millennium; a focus on 3D seismic data. American Association of Petroleum Geologists Annual Conference, New Orleans, LA, 16-19

[76] Chopra S, Marfurt KJ. 2005. Seismic Attributes - A Historical Perspective. *GEOPHYSICS*. doi:10.1190/1.2098670.

[77] Fornaciai A, Favalli M, Karátson D, Tarquini S, Boschi E. 2012. Morphometry of scoria cones, and their relation to geodynamic setting: A DEM-based analysis. *J Volcanol Geotherm Res*. <https://doi.org/10.1016/j.jvolgeoes.2011.12.012>

[78] Allen JRL. 1983. *Studies in Fluvial Sedimentation: Bars, Bar-Complexes and Sandstone Sheets (Low-Sinuosity Braided Streams) in the Brownstones (L. Devonian), Welsh Borders*. *Sediment. Geol.* 33 (4), 237-93., doi:10.1016/0037-0738(83)90076-3.

[79] Miall AD. 1985. Architectural-Element Analysis: A New Method

of Facies Analysis Applied to Fluvial Deposits. *Earth Sci. Rev.* Elsevier Science Publishers. (BV 22), 261-308., doi:10.1016/0012-8252(85)90001-7

[80] Deptuck ME, Sylvester Z, Pirmez C, O'Byrne C. 2007. Migration – aggradation history and 3-D seismic geomorphology of submarine channels in the Pleistocene Benin-Major Canyon, western Niger delta slope: *Marine and Petroleum Geology* v. 24, p. 406-433.

[81] Miall AD. 2000. *Principles of Sedimentary Basin Analysis*; Springer-Verlag, New York, 616p.

[82] Jackson RG. 1975. Hierarchical attributes and a unifying model of bed forms composed of cohesionless material and produced by shearing flow. *Bull. Geol. Soc. Am.*, 86 (1975), pp. 1523-1533

[83] White JDL, Valentine GA. 2016. Magmatic versus phreatomagmatic fragmentation: Absence of evidence is not evidence of absence. *Geosphere.*, 2016, <https://doi.org/10.1130/GES01337.1>

[84] McPhie J, Doyle M, Allen R. 1993. *Volcanic textures - a guide to the interpretation of textures in volcanic rocks*. Centre for Ore Deposit and Exploration Studies, University of Tasmania

[85] White SM, Crisp JA, Spera FJ. 2006. Long-term volumetric eruption rates and magma budgets. *Geochemistry, Geophysics, Geosystems* 7(3); doi:10.1029/2005GC001002.

[86] Giba M, Walsh JJ, Nicol A, Mouslopoulou V, Seebeck H. 2013. Investigation of the Spatio-Temporal Relationship between Normal Faulting and Arc Volcanism on Million-Year Time Scales. *Journal of the Geological Society* 170 (6): 951-62. doi:10.1144/jgs2012-121.

- [87] Schofield N, Heaton L, Holford SP, Archer SG, Jackson CAL, Jolley DW. 2012. Seismic imaging of “broken bridges”: linking seismic to outcrop-scale investigations of intrusive magma lobes. *J Geol Soc.* doi:10.1144/0016-76492011-150.
- [88] Vries B, Vries M. 2018. Tectonics and Volcanic and Igneous Plumbing Systems. In: Burchardt S (eds) *Volcanic and Igneous Plumbing Systems*. Elsevier, pp. 111-136. 10.1016/B978-0-12-809749-6.00007-8.
- [89] Galland O, Bertelsen HS, Eide CH, Guldstrand F, Haug ØT, Héctor LA, Mair K, Palma O, Planke S, Rabbel O, Rogers B, Schmiedel T, Souche A, Spacapan JB. 2018. Storage and transport of magma in the layered crust-Formation of sills and related float-lying intrusions. In: Burchardt S., (Ed.), *Volcanic and Igneous Plumbing Systems*, Elsevier. 111-136
- [90] Polteau S, Ferré EC, Planke S, Neumann ER, Chevallier L. 2008. How are saucer-shaped sills emplaced? Constraints from the Golden valley sill, South Africa *J. Geophys. Res.*, 113. <https://doi.org/10.1029/2008JB005620>
- [91] Kavanagh JL. 2018. Mechanisms of magma transport in the upper crust – Dyking. In: *Volcanic and Igneous Plumbing Systems: Understanding Magma Transport, Storage, and Evolution in the Earth's Crust*, S. Burchardt (Ed.), Elsevier. <https://doi.org/10.1016/B978-0-12-809749-6.00003-0>
- [92] Burchardt S, Walter TR, Tuffen H. 2018. Growth of a Volcanic Edifice Through Plumbing System Processes - Volcanic Rift Zones, Magmatic Sheet-Intrusion Swarms and Long-Lived Conduits. In: Burchardt S., (Ed.), *Volcanic and Igneous Plumbing Systems*, Elsevier. 285-317. <https://doi.org/10.1016/B978-0-12-809749-6.00001-7>.
- [93] Galland O, Spacapan JB, Rabbel O, Mair K, Soto FG, Eiken T, Schiuma M, Leanza HA. 2019. Structure, emplacement mechanism and magma-flow significance of igneous fingers – Implications for sill emplacement in sedimentary basins. *Journal of Structural Geology*, Volume 124, Pages 120-135. <https://doi.org/10.1016/j.jsg.2019.04.013>.
- [94] Rabbel O, Galland O, Mair K, Lecomte I, Senger K, Spacapan JB, Manceda R. 2018. From field analogues to realistic seismic modelling: a case study of an oil-producing andesitic sill complex in the Neuquén Basin, Argentina. *J. Geol. Soc.* doi:10.1144/jgs2017-116
- [95] Wrona T, Magee C, Fossen H, Gawthorpe RL, Bell RE, Jackson CA-L, Faleide J. 2019. 3-D seismic images of an extensive igneous sill in the lower crust. *Geology*. 47. DOI: 10.1130/G46150.1
- [96] Hansen DM, Cartwright J. 2006. Saucer-Shaped Sill with Lobate Morphology Revealed by 3D Seismic Data: Implications for Resolving a Shallow-Level Sill Emplacement Mechanism. *J. Geol. Soc.* 163 (3), 509-23., <https://doi.org/10.1144/0016-764905-073>
- [97] Poppe S, Holohan EP, Galland O, Buls N, Gompel G, Keelson B, Tournigand PY, Brancart J, Hollis D, Nila S, Kervyn M. 2019. An inside perspective on magma intrusion: quantifying 3D displacement and strain in laboratory experiments by dynamic X-Ray computed tomography. *Front. Earth Sci.*, 7. <https://doi.org/10.3389/feart.2019.00062>
- [98] Schmiedel T, Kjøberg S, Planke S, Magee C, Galland O, Schofield N, Jackson CAL, Jerram DA. 2017. Mechanisms of overburden deformation associated with the emplacement of the Tulipan sill, mid-Norwegian margin. *Interpretation*. doi:10.1190/INT-2016-0155.1

- [99] Magee C, Murray H, Christopher JAL, Stephen JM. 2019. Burial-Related Compaction Modifies Intrusion-Induced Forced Folds: Implications for Reconciling Roof Uplift Mechanisms Using Seismic Reflection Data. *Front Earth Sci.* doi:10.3389/feart.2019.00037
- [100] Quirie AK, Schofield N, Hartley A, Hole MJ, Archer SG, Underhill JR, Watson D, Holford SP. 2019. The Rattray Volcanics: Mid-Jurassic fissure volcanism in the UK Central North Sea. *Journal of the Geological Society, London*, 176, 462-481, <https://doi.org/10.1144/jgs2018-151>
- [101] Phillips TB, Magee C, Jackson CAL, Bell RE. 2017. Determining the three-dimensional geometry of a dike swarm and its impact on later rift geometry using seismic reflection data. *Geology*; 46 (2): 119-122. doi: <https://doi.org/10.1130/G39672.1>
- [102] Valentine GA, Perry FV, Krier D, Keating GN, Kelley RE, Cogbill AH. 2006. Small-volume basaltic volcanoes: eruptive products and processes, and post-eruptive geomorphic evolution in Crater Flat (Pleistocene), southern Nevada. *Geological Society of America Bulletin* 118 (11e12), 1313e1330. <http://dx.doi.org/10.1130/B25956.1>
- [103] Németh K. 2010. Monogenetic volcanic fields; origin, sedimentary record, and relationship with polygenetic volcanism: Special Paper Geological Society of America, [https://doi.org/10.1130/2010.2470\(04\)](https://doi.org/10.1130/2010.2470(04))
- [104] Eichelberger JC, Carrigan C, Westrich HR, Price RH. 1986. Nonexplosive silicic volcanism. *Nature* 323, 598-602. <https://doi.org/10.1038/323598a0>
- [105] Kósik S, Németh K, Lexa J, Procter J. 2019. Understanding the evolution of a small-volume silicic fissure eruption: Puketerata Volcanic Complex, Taupo Volcanic Zone, New Zealand. *Journal of Volcanology and Geothermal Research.* 383. 28-46. 10.1016/j.jvolgeores.2017.12.008.
- [106] Vespermann D, Schminke H-U. 2000. Scoria cones and tuff rings. In: Sigurdsson, H., Houghton, B.F., McNutt, S.R., Rymer, H., Stix, J. (Eds.), *Encyclopedia of Volcanoes*. Academic Press, San Diego, pp. 683e694.
- [107] Lorenz V. 1985. Maars and diatremes of phreatomagmatic origin, a review. *T. Geol. Soc. South Africa.* 88, 459-470.
- [108] Svensen H, Planke S, Malthe-Sorensen A, Jamtveit B, Myklebust R, Eidem TR, Rey SS. 2004. Release of methane from a volcanic basin as a mechanism for initial Eocene global warming. *Nature.* 429, 542-545
- [109] White JDL, Ross PS. 2011. Maar-diatreme volcanoes: A review. <https://doi.org/10.1016/j.jvolgeores.2011.01.010>
- [110] Kjoberg S, Schmiedel T, Planke S, Svensen HH, Millett JM, Jerram DA, Galland O, et al. 2017. 3D structure and formation of hydrothermal vent complexes at the Paleocene-Eocene transition, the Møre Basin, mid-Norwegian margin. *Interpretation* 5: SK65-SK81. <https://doi.org/10.1190/INT-2016-0159.1>
- [111] Aarnes I, Planke S, Trulsvik M, Svensen H. 2015. Contact metamorphism and thermogenic gas generation in the Vøring and Møre basins, offshore Norway, during the Paleocene-Eocene thermal maximum. *J Geol Soc* 172: 588-598
- [112] Davidson JP, de Silva SL, 2000. Composite volcanoes. In: Sigurdsson, H., Houghton, B.F., McNutt, S.R., Rymer, H., Stix, J. (Eds.), *Encyclopedia of Volcanoes*. Academic Press, San Diego, pp. 663e680.
- [113] Hackett WR, Houghton BF. 1989. A facies model for a quaternary andesitic composite volcano: Ruapehu, New

Zealand. *Bulletin of Volcanology* 51, 51e68.

[114] Cotton CA. 1944. Volcanoes as Landscape Forms. Whitcombe and Tombs, Christchurch, New Zealand.

[115] Moore JG, Clague DA. 1992. Volcano growth and evolution of the island of Hawaii, *Geol. Soc. Am. Bull.*, 104, 1471–1484. [https://doi.org/10.1130/0016-7606\(1992\)104<1471:VGAEOT>2.3.CO;2](https://doi.org/10.1130/0016-7606(1992)104<1471:VGAEOT>2.3.CO;2)

[116] Walker GPL. 2000. Basaltic volcanoes and volcanic systems. In: Sigurdsson, H., Houghton, B.F., McNutt, S.R., Rymer, H., Stix, J. (Eds.), *Encyclopedia of Volcanoes*, first ed. Academic Press, San Diego, pp. 283e290.

[117] Skilling IP. 2002. Basaltic pahoehoe lava-fed deltas: Largescale characteristics, clast generation, emplacement processes and environmental discrimination: Geological Society, London, Special Publications 202, 91-113. <https://doi.org/10.1144/GSL.SP.2002.202.01.06>

[118] Morley C. 2018. 3D seismic imaging of the plumbing system of the Kora volcano, Taranaki Basin, New Zealand: The influences of syn-rift structure on shallow igneous intrusion architecture: *Geosphere*, 2018. doi.org/10.1130/GES01645.1.

[119] Kennedy BM, Holohan EP, Stix J, Gravley DM, Davidson JRJ, Cole JW, Burchardt S. 2018. Volcanic and Igneous Plumbing Systems of Caldera Volcanoes. In: *Volcanic and Igneous Plumbing Systems: Understanding Magma Transport, Storage, and Evolution in the Earth's Crust*, S. Burchardt (Ed.), Elsevier. <https://doi.org/10.1016/B978-0-12-809749-6.00010-8>.

[120] Cole JW, Milner DM, Spinks KD. 2005. Calderas and caldera structures: a review. *Earth-Science Reviews* 69 (1e2), 1e26.

[121] Wilson CJN, Houghton BF, McWilliams MO, Lanphere MA, Weaver SD, Briggs RM. 1995. Volcanic and structural evolution of Taupo Volcanic Zone, New Zealand: a review. *Journal of Volcanology and Geothermal Research* 68, 1e28.

[122] Martí J, Geyer A, Folch A, Gottsmann J. 2008. A review on collapse caldera modelling. In *Caldera Volcanism: Analysis, Modelling and Response*, eds J. Gottsmann and J. Martí (Amsterdam: Elsevier), 233-283.

[123] Lipman PW. 2000. Calderas. In: Sigurdsson, H., Houghton, B.F., McNutt, S.R., Rymer, H., Stix, J. (Eds.), *Encyclopedia of Volcanoes*. Academic Press, San Diego.

[124] Branney M, Acocella V. 2015. Calderas. in *The Encyclopaedia of Volcanoes*, eds H. Sigurdsson, B. Houghton, H. Rymer, and J. Stix (Cambridge: Academic Press).

[125] Coffin MF, Eldholm O. 1993. Large igneous provinces. *Scientific American*. ISSN: 0036-8733 269 (4), 42e49.

[126] Self S, Thordarson T, Keszthelyi L. 1997. Emplacement of continental flood basalt lava flows. In: *Large Igneous Provinces: Continental, Oceanic, and Planetary Flood Volcanism*, pp. 381e410.

[127] Sheth H. 2007. Large Igneous Provinces (LIPs): Definition, recommended terminology, and a hierarchical classification. *Earth-Science Reviews*. 85. 10.1016. DOI: 10.1016/j.earscirev.2007.07.005

[128] Single RT, Jerram DA. 2004. The 3D facies architecture of flood basalt provinces and their internal heterogeneity: Examples from the Palaeogene Skye Lava Field: *Journal of the Geological Society*, 161, 911-926, doi: 10.1144/0016-764903-136.

[129] Thordarson T, Self S. 1993. The Laki (Skaftár Fires) and Grímsvötn

eruptions in 1783-1785. *Bulletin of Volcanology* 55:233-263. DOI: 10.1007/BF00624353

[130] Jerram DA. Volcanology and facies architecture of flood basalts. In: Menzies MA, Klemperer SL, Ebinger CJ, Baker J, editors. *Magmatic rifted margins*: Geological society of america special paper. 2002;362:119-132.

[131] Rey SS, Planke S, Symonds PA, Faleide JI. 2008. Seismic volcano-stratigraphy of the Gascoyne margin, Western Australia, *J. Volcanol. Geotherm. Res.*, 172(1-2), 112-131, doi:10.1016/j.jvolgeores.2006.11.013.

[132] Wright KA, Davies RJ, Jerram DA, Morris J, Fletcher R. 2012. Application of seismic and sequence stratigraphic concepts to a lava-fed delta system in the Faroe-Shetland Basin, UK and Faroes: *Basin Research*, 24, 91-106, doi: 10.1111/j.1365-2117.2011.00513.x.

[133] Watton TJ, Jerram DA, Thordarson T, Davies RJ. 2013. Three-dimensional lithofacies variations in hyaloclastite deposits: *Journal of Volcanology and Geothermal Research*, 250, 19-33, doi: 10.1016/j.jvolgeores.2012.10.011.

[134] Cannon EC, Bürgmann R. Prehistoric fault offsets of the Hilina fault system, south flank of Kilauea Volcano, Hawaii: *Journal of Geophysical Research*; 2001;106:4207-4219. DOI: 10.1029/2000JB900412.

Machine Learning in Volcanology: A Review

Roberto Carniel and Silvina Raquel Guzmán

Abstract

A volcano is a complex system, and the characterization of its state at any given time is not an easy task. Monitoring data can be used to estimate the probability of an unrest and/or an eruption episode. These can include seismic, magnetic, electromagnetic, deformation, infrasonic, thermal, geochemical data or, in an ideal situation, a combination of them. Merging data of different origins is a non-trivial task, and often even extracting few relevant and information-rich parameters from a homogeneous time series is already challenging. The key to the characterization of volcanic regimes is in fact a process of data reduction that should produce a relatively small vector of features. The next step is the interpretation of the resulting features, through the recognition of similar vectors and for example, their association to a given state of the volcano. This can lead in turn to highlight possible precursors of unrests and eruptions. This final step can benefit from the application of machine learning techniques, that are able to process big data in an efficient way. Other applications of machine learning in volcanology include the analysis and classification of geological, geochemical and petrological “static” data to infer for example, the possible source and mechanism of observed deposits, the analysis of satellite imagery to quickly classify vast regions difficult to investigate on the ground or, again, to detect changes that could indicate an unrest. Moreover, the use of machine learning is gaining importance in other areas of volcanology, not only for monitoring purposes but for differentiating particular geochemical patterns, stratigraphic issues, differentiating morphological patterns of volcanic edifices, or to assess spatial distribution of volcanoes. Machine learning is helpful in the discrimination of magmatic complexes, in distinguishing tectonic settings of volcanic rocks, in the evaluation of correlations of volcanic units, being particularly helpful in tephrochronology, etc. In this chapter we will review the relevant methods and results published in the last decades using machine learning in volcanology, both with respect to the choice of the optimal feature vectors and to their subsequent classification, taking into account both the unsupervised and the supervised approaches.

Keywords: machine learning, volcano seismology, volcano geophysics, volcano geochemistry, volcano geology, data reduction, feature vectors

1. Introduction

Pyroclastic density currents, debris flow avalanches, lahars, ash falls can affect dramatically the life of people living close to volcanoes, and other volcanic products such as lava flows can severely affect properties and infrastructures. Several volcanoes

lie close to highly populated areas and the impact of their eruptions could be economically very strong. Stochastic forecasts of volcanic eruptions are difficult [1, 2], but deterministic forecasts (i.e., specifying when, where, how an eruption will occur) are even harder. Many volcanoes are monitored by observatories that try to estimate at least the probability of the different hazardous volcanic events [3]. Different time series can be monitored and hopefully used for forecasting, including seismic data [4], geomagnetic and electromagnetic data [5], geochemical data [6], deformation data [7], infrasonic data [8], gas data [9], thermal data from satellite [10] and from the ground [11]. Whenever possible, a multiparametric approach is always advisable. For instance, at Merapi volcano, seismic, satellite radar, ground geodetic and geochemical data were efficiently integrated to study the major 2010 eruption [12]; a multiparametric approach is essential to understand shallow processes such as the ones seen at geothermal systems like e.g., Dallol in Ethiopia [13]. Although many time series may be available, seismic data remain always at the heart of any monitoring system, and should always include the analysis of continuous volcanic tremor [14]; tremor has in fact a great potential [15] due to its persistence and memory [1, 2] and its sensitivity to external triggering such as regional tectonic events [16] or Earth tides [17]. Moreover, its time evolution can be indicative of variations in other parameters, such as gas flux [18]. Other information-rich time series can be built looking at the time evolution of the number of the different discrete volcano-seismic events that can be recorded on a volcano. These include volcano-tectonic (VT) earthquakes, rockfall events, long-period (LP) and very-long-period (VLP) events, explosions, etc. Counting the overall number of events is not enough: one has to detect them and classify them, because they are linked to different processes, as detailed below. For this reason it is important to generate automatically different time series for each type of volcano-seismic event.

VT can be described as “normal” earthquakes which take place in a volcanic environment and can indicate magma movement [19, 20]. LP events have a great potential for forecasting [21]. Their debated interpretation involves the repeated expansion and compression of sub-horizontal cracks filled with steam or other ash-laden gas [22], stick-slip magma motion [23], fluid-driven flow [24], eddy shedding, turbulent slug flow, soda bottle analogues [25], deformation acceleration of solidified domes [26] and slow ruptures [27]. Explosion quakes are generated by sudden magma, ash, and gas extrusion in an explosive event, often associated to VLP events [28]. In many papers also “Tremor episodes” (TRE events) are described and counted, usually associated to magma degassing [20]. However, a volcano with any activity produces a continuous “tremor” which detectability only depends on the seismic instrumentation sensitivity [29, 30]. So, the class “TRE” should be better defined as “tremor episode that exceeds the detection limits”. Of course, at volcanoes we can also record natural but non-volcanic seismic signals such as far tectonic earthquakes, far explosions, etc., and also anthropogenic signals e.g., due to industries, ground vehicles, helicopters used for monitoring, etc.

Most volcano observatories rely on manual classification and counting of such seismic events, which suffers from human subjectivity and can become unfeasible during an unrest or a seismic crisis [31, 32]. For this reason, manual classification should be substituted by an automated processing, and here is where machine learning (ML) comes into place. The same reasoning applies of course also to the automated processing of other monitoring time series, such as deformation, gas and water geochemistry, etc. Moreover, ML in volcanology is not restricted to monitoring active volcanoes but has demonstrated to be useful also when dealing with other large datasets. Examples include correlating volcanic units in general e.g., [33], of tephra e.g., [34, 35] and ignimbrites e.g., [36], a task which may become very difficult especially when many deposits of similar ages and geochemical and

Factorization (NMF) [43], Singular Value Decomposition [44], Principal Component Analysis (PCA) [45] and Auto-encoders [46]. Linear Discriminant Analysis (LDA) [47] uses the training samples to estimate the between-class and within-class scatter matrices, and then employs the Fisher criterion to obtain the projection matrix for feature extraction (or feature reduction).

In **supervised learning**, the dataset is a collection of example couples of the type (data, label) $\{(x_i, y_i)\}_{i=1..N}$. Each element x_i is called a feature vector and has a companion label y_i . In the supervised learning approach the dataset is used to derive a model that takes a feature vector as input and outputs a label that should describe it. For example, the feature vector of volcano-seismic data could contain several amplitude-based, spectral-based, shape-based or dynamical parameters and the label to be assigned could be one of those described above, i.e., VT, LP, VLP. In a volcanic geochemical example, feature vectors could contain major elements weight percentages, and labels the corresponding rock type. The reliability of the labels is often the most critical issue of the setup of a supervised ML classification scheme. Labels should therefore be assigned carefully by experts. In general, it is much better to have relatively few training events with reliable labels than to have many more, but not so reliable, labeled examples.

In **unsupervised learning**, the dataset is a collection of examples without any labeling, i.e., containing only the data $\{x_i\}_{i=1..N}$. As in the previous case, each x_i is a feature vector, and the goal is to create a model that maps a feature vector x into a value (or another vector) that can help solving a problem. Typical examples are all the clustering procedures, where the output is the cluster number to which each datum belongs. The choice of the best features to use is a difficult one, and several techniques of Unsupervised Feature Selection were proposed, with the capability of identifying and selecting relevant features in unlabeled data [48]. Unsupervised outlier detection methods [49] can also be used, where the output indicates if a given feature vector is likely to describe a “normal” or “anomalous” member of the dataset.

The **semi-supervised learning** approach stands somehow in the middle, and the dataset contains both labeled (usually a few) and unlabeled (usually many more) feature vectors. The basic idea is similar to supervised learning, but with the possibility to exploit also the presence of (many more) unlabeled examples in the training phase.

In **reinforcement learning**, the machine is “embedded” in an environment, which state is again described by a feature vector. In each state the machine can execute actions, which produce different rewards and can cause an environmental state transition. The goal in this case is to learn a policy, i.e., a function or model that takes the feature vector as input and outputs an optimal action to execute in that state. The action is optimal if it maximizes the expected average reward. We can also say that reinforcement learning is a behavioral learning model. The algorithm receives feedback from the data analysis, guiding the user to the best outcome. Here the main point is that the system is not trained with a sample dataset but learns through trial and error. Therefore, a sequence of successful decisions will result in that process being reinforced, because it best solves the problem at hand. Problems that can be tackled with this approach are the ones where decision making is sequential, and the goal is long-term, such as game playing, robotics, resource management, or logistics. Time is therefore explicitly used here, contrary to other approaches, in which in most of the cases data items are analyzed one by one without taking into account the time order in which they arrive.

In some domains (and volcanology is a good example) training data are scarce. In this case we can profit from knowledge acquired in another domain using

techniques known as **Transfer Learning** (TL) [50]. The basic idea here is to train a model in one domain with abundant data (original domain) and then use it as a pretrained model in a different domain (with less data). There is a successive fine-tuning phase using domain-specific available data (in the target domain). This approach was applied for instance at Volcán de Fuego de Colima (Mexico) [51], Mount St. Helens (USA) and Bezymianny (Russia) [52].

Among the computer languages that are most used for implementing ML techniques we can cite Python [53], R [54], Java [55], Javascript [56], Julia [57] and Scala [58]. Many dedicated, open source libraries are available for each of them, and many computer codes, also specialized for volcanic and geophysical data, can be found in open access repositories such as GitHub [59].

3. Machine learning techniques

Extracted feature vectors can become inputs to several different techniques of machine learning. We can cite among others Cluster Analysis (CA) [60], Self-Organizing Maps (SOM) [61–63], Artificial Neural Networks (ANN) and Multi Layer Perceptrons (MLP) [64–66], Support Vector Machines (SVM) [67], Convolutional Neural Networks (CNN) [51], Recurrent Neural Networks (RNN) [68], Hidden Markov Models (HMM) [3, 31, 69–71] and their Parallel System Architecture (PSA) based on Gaussian Mixture Models (GMM) [72].

CA (**Figure 2a**) is an unsupervised learning approach aimed at grouping similar data while separating different ones, where similarity is measured quantitatively using a distance function in the space of feature vectors. The clustering algorithms can be divided into hierarchical and non-hierarchical. In the former a tree-like structure is built to represent the relations between clusters, while in the latter new clusters are formed by merging or splitting existing ones without following a tree-like structure but just grouping the data in order to maximize or minimize some evaluation criteria. CA includes a vast class of algorithms, including e.g., K-means, K-medians, Mean-shift, DBSCAN, Expectation–Maximization (EM), Clustering using Gaussian Mixture Models (GMM), Agglomerative Hierarchical, Affinity Propagation, Spectral Clustering, Ward, Birch, etc. Most of these methods are described and implemented in the open-source Python package scikit-learn [73]. The use of six different unsupervised, clustering-based methods to classify volcano seismic events was explored at Cotopaxi Volcano [32]. One of the most difficult issues is the choice of the number of clusters into which the data should be divided; this number in most of the cases has in fact to be fixed a priori before running the code. Several techniques exist in order to help with this choice, such as elbow, silhouette, gap statistics, heuristics, etc. Many of them are described and included in the R package NbClust [74]. Problems arise when the estimates that each of them provides are contradictory.

Another approach to unsupervised classification is SOM (**Figure 2b**) or Kohonen maps [75, 76], a type of ANN trained to produce a low dimensional, usually 2D, discretized representation of the feature vector space. The training is based on competitive and collaboration learning, using a neighborhood function to preserve the input topological properties.

A very common type of ANN, often used for supervised classification, is MLP, which consists of at least three layers of nodes (**Figure 2c**): an input layer, (at least) one hidden layer and an output layer. Nodes use nonlinear activation functions and are trained through the backpropagation mechanism. If the number of hidden layers of an ANN becomes very high, we talk of Deep Neural Networks (DNN), which are also used mainly in a supervised fashion. Among DNN, the CNN (**Figure 2d**) contain

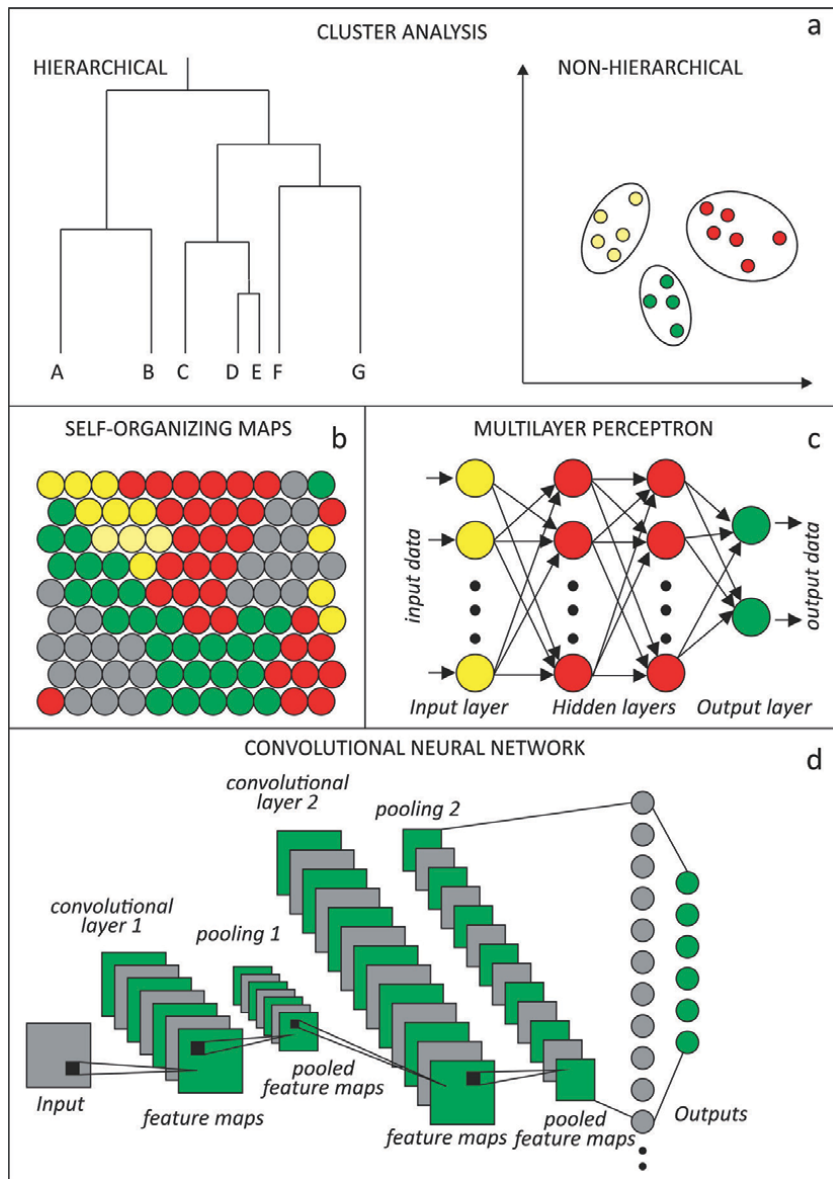


Figure 2. Schematic illustration of some of the ML techniques described in the text. (a) Cluster analysis in its hierarchical and non-hierarchical versions. (b) Self-organizing maps (c) multilayer perceptron (d) convolutional neural network.

at least some convolutional layers, that convolve their inputs with a multiplication or other dot product. The activation function in the case of CNN is commonly a rectified linear unit (ReLU), and there are also pooling layers, fully connected layers and normalization layers.

A RNN is a type of ANN with a feedback loop (**Figure 3a**), in which neuron outputs can also be used as neuron inputs in the same layer, allowing to maintain some information during the training process. Long Short Term Memory networks (LSTM) are a subset of RNN, capable of learning long-term dependencies [77] and better remember information for long periods of time. RNN can be used for both supervised and unsupervised learning.

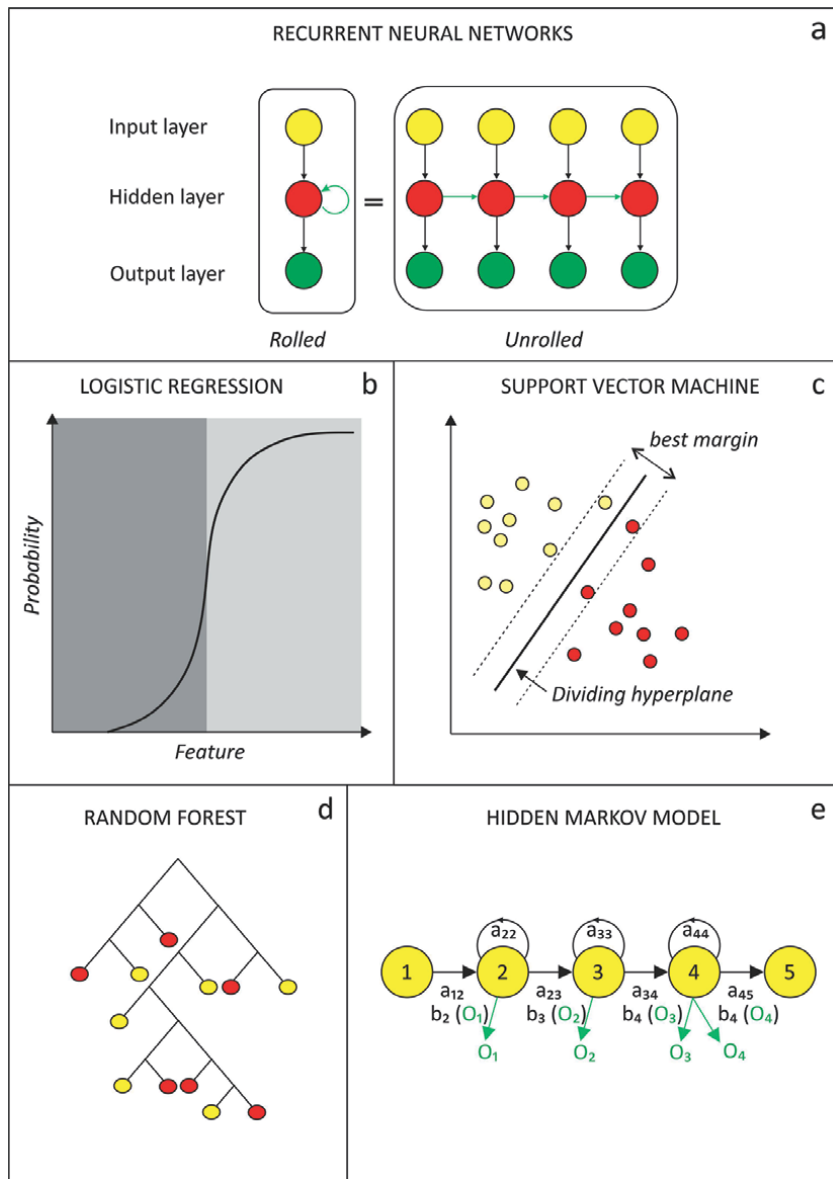


Figure 3. Schematic illustration of some of the ML techniques described in the text. (a) Recurrent neural network (b) logistic regression (c) support vector machine (d) random forest (e) hidden Markov model.

Logistic regression (LR) (**Figure 3b**) is a supervised generalized linear model, i.e., the classification (probability) dependence on the features is linear [78]. In order to avoid the problems linked to high dimensionality of the data, techniques such as the Least Absolute Shrinkage and Selection Operator (LASSO) can be applied to reduce the number of dimensions of the feature vectors which are input to LR [79].

SVM (**Figure 3c**) constitute a supervised statistical learning framework [80]. It is most commonly used as a non-probabilistic binary classifier. Examples are seen as points in space, and the aim is to separate categories by a gap that is as wide as possible. Unknown samples are then assigned to a category based on the side of the gap on which they fall. In order to perform a non-linear classification, data are mapped into high-dimensional feature spaces using suitable kernel functions.

Sparse Multinomial Logistic Regression (SMLR) is a class of supervised methods for learning sparse classifiers that incorporate weighted sums of basis functions with sparsity-promoting priors encouraging the weight estimates to be either significantly large or exactly zero [81]. The sparsity concept is similar to the one at the base of Non-negative Matrix Factorization (NMF) [82]. The sparsity-promoting priors result in an automatic feature selection, enabling to somehow avoid the so-called “curse of dimensionality”. So, sparsity in the kernel basis functions and automatic feature selection can be achieved at the same time [83]. SMLR methods control the capacity of the learned classifier by minimizing the number of basis functions used, resulting in better generalization. There are fast algorithms for SMLR that scale favorably in both the number of training samples and the feature dimensionality, making them applicable even to large data sets in high-dimensional feature spaces.

A Decision Tree (DT) is an acyclic graph. At each branching node, a specific feature x_i is examined. The left or right branch is followed depending on the value of x_i in relation to a given threshold. A class is assigned to each datum when a leaf node is reached. As usual, a DT can be learned from labeled data, using different strategies. In the DT class we can mention Best First Decision Tree (BFT), Functional Tree (FT), J48 Decision Tree (J48DT), Naïve Bayes Tree (NBT) and Reduced Error Pruning Trees (REPT). Ensemble learning techniques such as Random SubSpace (RSS) can be used to combine the results of the different trees [84].

The Boosting concept, a kind of ensemble meta-algorithm mostly (but not only) associated to supervised learning, uses original training data to create iteratively multiple models by using a weak learner. Each model would be different from the previous one as the weak learners try to “fix” the errors made by previous models. An ensemble model will then combine the results of the different weak models. On the other side, Bootstrap aggregating, also called by the contracted name Bagging, consists of creating many “almost-copies” of the training data (each copy is slightly different from the others) and then apply a weak learner to each copy and finally combine the results. A popular and effective algorithm based on bagging is Random Forest (RF). Random Forest (**Figure 3d**) is different from the standard bagging in just one way. At each learning step, a random subset of the features is chosen; this helps to minimize correlation of the trees, as correlated predictors are not efficient in improving classification accuracy. Particular attention has to be taken in order to best choose the number of trees and the size of the random feature subsets.

A Hidden Markov Model (HMM) (**Figure 2e**) is a statistical model in which the system being modeled is assumed to be a Markov process. It describes a sequence of possible events for which the probability of each event depends only on the state occupied in the previous event. The states are unobservable (“hidden”) but at each state the Model emits a “message” which depends probabilistically on the current state. Applications are wide in scope, from reinforcement learning to temporal pattern recognition, and the approach works well when time is important; speech [85], handwriting and gesture recognition are then typical fields of applications, but also volcano seismology [69, 86].

4. Applications to seismo-volcanic data

Eruptions are usually preceded by some kind of change in seismicity, making seismic data one of the key dataset in any attempt to forecast volcanic activity [4]. As we mentioned before, manual detection and classification of discrete events can be very time consuming, up to becoming unfeasible during a volcanic crisis.

An automatic classification procedure becomes therefore highly valuable, also as a first step towards forecasting techniques such as material Failure Forecast Method (FFM) [87, 88]. Feature vectors should be built in order to provide most information about the source, minimizing e.g., path and site effects. In many cases features can be independent from a specific physical model describing a phenomenon. This allows ML to work well even when there is no scientific agreement on the generation of a given seismic signal. A good example in volcano seismology is given by the LP events. Standardizing data, making them independent from unwanted variables is also in general a convenient approach [31]. Time-domain and spectral-based amplitudes, spectral phases, auto- and cross-correlations, statistical and dynamical parameters have been considered as the output of data reduction procedures that can be included into feature vectors [14]. In the literature, these have included linear predictor coding for spectrograms [66], wavelet transforms [89], spectral autocorrelation functions [90], statistical and cepstral coefficients [91]. Extracted feature vectors become then the input to one or another ML method.

CA is probably the most used class of unsupervised techniques and the applications to volcano seismology follow this general rule. Spectral clustering was applied e.g., to seismic data of Piton de la Fournaise [60]. The fact that e.g., LP seismic signals can be clustered into families indicates that the family members are very similar to each other. The existence of similar events implies similar location and similar source process, i.e., it means the presence of a source that repeats over time in an almost identical way. Clustering data after some kind of normalization forces CA algorithms to look for similar shapes, independently of size. If significant variations in amplitude are then seen within families, this can indicate that the source processes of these events are not only repeatable but also scalable in size, as observed e.g., at Soufrière Hills Volcano, Montserrat [92] or at Irazú, Costa Rica [93]. The similarity of events in the different classes can then be used to detect other events, e.g., for the purpose of stacking them and obtain more accurate phase arrivals; this was done e.g., at Kanlaon, Philippines [94]. For this purpose, an efficient open-source package is available, called Repeating Earthquake Detector in Python (REDPy) [95].

In volcano-seismology SOM were applied e.g., to Raoul Island, New Zealand [61]. A hierarchical clustering was applied to results of SOM tremor analysis at Ruapehu [62] and Tongariro [96] in New Zealand, using the Scilab environment. A similar combined approach was applied in Matlab to Etna volcanic tremor [97]. Several geometries of SOM were used, with rectangular or hexagonal nearest neighbors cells, planar, toroidal or spherical maps, etc. [61]. The classic ANN/MLP approach was applied e.g., to seismic data recorded at Vesuvius [66], Stromboli [98], Etna [99], while DNN architectures were applied e.g., to Volcán de Fuego, Colima [100]. The use of genetic algorithms for the optimization of the MLP configuration was proposed for the analysis of seismic data of Villarrica, Chile [101]. CNN were applied e.g., to Llaima Volcano (Chile) seismic data, comparing the results to other methods of classification [102]. RNNs were applied, together with other methods, to classify signals of Deception Island Volcano, Antarctica [68]. The architectures were trained with data recorded in 1995–2002 and models were tested on data recorded in 2016–2017, showing good generalization accuracy.

Supervised LR models have been applied in the estimation of landslide susceptibility [103] and to volcano seismic data to estimate the ending date of an eruption at Telica (Nicaragua) and Nevado del Ruiz (Colombia) [104]. SVM were applied many times to volcano seismology e.g., to classify volcanic signals recorded at Llaima, Chile [105] and Ubina, Peru [106]. Multinomial Logistic Regression was used, together with other methods, to evaluate the feasibility of earthquake prediction using 30 years of historical data in Indonesia, also at volcanoes [107].

RF was applied to the discrimination of rockfalls and VT recorded at Piton de la Fournaise in 2009–2011 and 2014–2015. 60 features were used, and excellent results were obtained. However, a RF trained with 2009–2011 data did not perform well on data recorded in 2014–2015, demonstrating how difficult it is to generalize models even at the same volcano [108]. RF, together with other methods, was recently used on volcano seismic data with the specific purpose to determine when an eruption has ended [104], a problem which is far from being trivial. RF was also used to derive ensemble mean decision tree predictions of sudden steam-driven eruptions at Whakaari (New Zealand) [109].

Most of the methods described so far try to classify discrete seismic events that were already extracted from the continuous stream, i.e., already characterized by a given start and end. There are therefore in general two separated phases: detection and classification [106]. Continuous HMM on the other side are able to process continuous data and can therefore extract and classify in a single, potential real-time, step. HMM are finite-state machines and model sequential patterns where time direction is an essential information. This is typical of (volcano) seismic data. For instance, P waves always arrive before S waves. HMM-based volcanic seismic data classifiers have therefore been used by many authors [87, 110–113]. HMM are also used routinely in some volcano observatories e.g., at Colima and Popocatepetl in Mexico [71]. Etna seismic data was processed by HMM applied to characters generated by the Symbolic Aggregate approXimation (SAX) which maps seismic data into symbols of a given alphabet [114]. HMM can be also combined with standardization procedures such as Empirical Mode Decomposition (EMD) when classifying volcano seismic data [31].

Another characteristic common to many of the applications published in the literature is the fact that feature vectors are extracted from data recorded at a single station. There are relatively few attempts to build multi-station classification schemes. At Piton de la Fournaise a system based on RF was implemented [115]. At the same volcano, a multi-station approach was used to classify tremor measurements and identify fundamental frequencies of the tremor associated to different eruptive behavior [60]. A scalable multi-station, multi-channel classifier, using also the empirical mode decomposition (EMD) first proposed by [31] was applied to Ubinas volcano (Peru). The principal component analysis is used to reduce the dimensionality of the feature vector and a supervised classification is carried out using various methods, with SVM obtaining the best performance [116]. Of course, with a multi-station approach particular care has to be taken in order to build a system which is robust with respect to the loss of one or more seismic stations due to volcanic activity or technical failures.

Open source software and open access papers are luckily becoming more and more common. If we consider the processing and classification of volcano seismic data, several tools are now available for free download and use, especially within the Python environment. Among the most popular, we can cite ObsPy [117] and Msnoise [118], with which researchers and observatories can easily process big quantities of continuous seismic data. Once these tools have produced suitable feature vectors, we can look for open source software to implement the different ML approaches described in this contribution. Many generic ML libraries are available e.g., on GitHub [59] but very few are dedicated specifically to the classification of volcano seismic data. Among these, we can cite the recent package Python Interface for the Classification of Seismic Signals (PICOSS) [119]. It is a graphical, modular open source software for detection, segmentation and classification of seismic data. Modules are independent and adaptable. The classification is currently based on two modules that use Frequency Index analysis [120] or a multi-volcano pre-trained neural network, in a transfer learning fashion [52]. The concept of a multi-volcano

recognizer is also at the core of the EU-funded VULCAN.ears project [31, 121]. The aim is to build an automatic Volcano Seismic Recognition (VSR) system, conceptually supervised (as it is based on HMM) but practically unsupervised, because once it is trained on a number of volcanoes with labeled sample data, it can be used on volcanoes without any previous data in an unsupervised fashion. The idea is in fact to build robust models trained on many datasets recorded by different teams on different volcanoes, and to integrate these models on the routinely used monitoring system of any volcano observatory. Also in this case, the open source software is made freely available; this includes a command interface called PyVERSO [122] based on HTK, a speech recognition HMM toolkit [123], a graphical interface called geoStudio and a script called liveVSR, able to process real-time data downloaded from any online seismic data server [124], together with some pre-trained ML models [125].

As we mentioned before, in order to train supervised models for classifying seismic events, few events with reliable labels are better than many unreliably labeled examples. Just to give a rough idea, 20 labeled events per class is a good starting point, but a minimum of 50 labeled events per class is recommended. Labelling discrete events is enough for many methods, but for approaches like HMM, where the concept is to run the classification on continuous data, it is essential to have a sufficient number of continuously labeled time periods, in order to “show” the classifier enough examples of transition from tremor to a discrete event, and then back to tremor. It is important to have many examples also of “garbage” events, i.e., events we are not interested in, so that the classifier can recognize and discard them. Finally, it is advisable to have a wide variability of events within each given class rather than having many very similar events. There is not yet an agreement on a single file format to store these labels. As speech recognition is much older and more developed than seismic recognition, it is suggested to adopt standard labelling formats of that domain, i.e., the transcription MLF files, which are normal text files that include for each event the start time, the end time and of course the label. These files can be created manually with a simple text editor, or by using a program with a GUI, such as geoStudio [124] or Seismo_volcanalysis [126]. Other graphical software packages like SWARM [127] use other formats to store the labels, such as CSV, but it is always possible to build scripts that convert the resulting label files into MLF format, which remains the recommended one.

5. Applications of machine learning to geochemical data

ML applications to geochemical data of volcanoes are increasing in the last years, although most of them are limited to the use of cluster analysis. CA has been used for example to identify and quantify mixing processes using the chemistry of minerals [128], also for the study of volcanic aquifers [129, 130] or to differentiate magmatic systems e.g., [131]. Platforms used to carry out these analyses include the Statistical Toolbox in Matlab [132], or the R platform [54]; some geochemical software made in this last platform include the CA as the GCDkit [33]. In most ML analyses on geochemical samples it is common to use whole rock major elements and selected trace elements; some applications also include isotopic ratios. Many ML applications to geochemical data use more than one technique, frequently combining both unsupervised and supervised approaches.

A combination of SVM, RF and SMLR approaches were used by [37] to account for variations of geochemical composition of rocks from eight different tectonic settings. The authors note that SVM used to discriminate tectonic settings as used by [34] is a powerful tool. The RF approach is shown to have the advantage, with

respect to SVM, of providing the importance of each feature during discrimination. The weakness of applying the RF for tectonic setting discrimination is that the evaluation based only on a majority vote of multiple decision trees often makes the obtained quantitative geochemical interpretation of these elements and isotopic ratios difficult. The authors suggest that the best quantitative discriminant is that of SMLR, as it allows to assign to each sample a probability of belonging to a given group (tectonic setting in this case), with still the possibility of identifying the importance of each feature. This tool is a notable step forward in the discrimination of the geochemical signature of the different tectonic settings, which is commonly assessed based on binary or ternary diagrams e.g., [133, 134] which are useful with many samples but are not able to differentiate a tectonic setting where a complex evolution of magmas has occurred. In the last decade multielement variation diagrams were proposed e.g., [135] and also the use of Decision Trees e.g., [136] or LDA e.g., [137] to accurately assign a tectonic setting based on rock geochemistry. Based on rock sample geochemistry, [37] show that a set of 17 elements and isotopic ratios is needed to clearly identify the tectonic setting. Two new discriminant functions were recently proposed to discriminate the tectonic settings of mid-ocean ridge (MOR) and oceanic plateau (OP). 10 datasets (original concentrations as well as isometric log-ratio transformed variables; all 10 major elements as well as all 10 major and 6 trace elements) were used to evaluate the quality of discrimination from LDA and canonical analysis [138].

The software package Compositional Data Package (CoDaPack) [139] and a combination of unsupervised (CA) and supervised (LDA) learning approaches was used by [36] to identify compositional variation of ignimbrite magmas in the Central Andes, trying to use these methods as a tool for ignimbrite correlation. They have used the Statistica software [140] for both CA and LDA.

Correlating tephra and identifying their volcanic sources is a very difficult task, especially in areas where several volcanoes had explosive eruptions in a relatively short period of time. This is particularly challenging when volcanoes have similar geochemical and petrographic compositions. Electron microprobe analysis of glass compositions and whole-rock geochemical analyses are used frequently to make these correlations. However, correlations may not be so accurate when using only geochemical tools that may mask diagnostic variability; sometimes one of the most important advantages of ML in this regard is the speed at which correlations can be made, rather than the accuracy [35]. Other contributions however demonstrate how ML techniques can make these correlations also accurate. Some highly accurate results of ML techniques applied to tephra correlation include those of LDA [141, 142] and SVM e.g., [143]; however, SVM may fail in specific cases and for the case study of tephra from Alaska volcanoes, the combination of ANN and RF are the best ML techniques to apply [35]. The authors use the R software [54] to apply these methods, and they underline the advantage of producing probabilistic outputs.

SOM was used as an unsupervised neural network approach to analyze geochemical data of Ischia, Vesuvius and Campi Flegrei [144]. The advantage of this method is that there is no need of previous knowledge of geochemical or petrological characteristics and that it allows the use of large databases with large number of variables. The SOM toolbox for Matlab [132] was used by [144] to perform two tests, the first based on major elements and selected trace elements to find similar evolution processes, the second to investigate the magmatic source, so a vector containing a selection of ratios between major and trace elements was adopted. One of the enhancements of this method is that the resulting clusters permitted to differentiate rock samples that were only comparably distinguished by 2D diagrams of isotopic ratios; in other words, similar results were obtained with the limited availability of less expensive geochemical data.

One of the applications of ML techniques that maybe extremely useful in geochemistry is the apparent possibility of predicting the concentration of unknown elements if a large number of data of other elements is known. A combination of ML techniques was used by [38] to predict Rare Earth Elements (REE) concentrations on Ocean Island Basalts (OIB) using RF. They used 1283 analyses of which 80% were used for training and the remaining 20% to validate the results. They found good estimations only in the Light Rare Earth Elements (LREE), suggesting that the results may be improved by using a larger set of input data for training. One possible solution may be the use of not only major elements for training but also of other trace elements obtained through the same analytical method of major elements.

The origin of the volcanoes in Northeast China, analyzed by RF and DNN using the full chemical compositional data, was associated to the Pacific slab, subducting at Japan, reaching ~600-km depth under eastern China, and extending horizontally up to Mongolia. The boundary between volcanoes triggered by fluids and melts from the slab and those not related to it was located at the westernmost edge of the deeply buried Pacific slab [145].

As highlighted by [143] ML methods require the integration with other techniques such as fieldwork, petrographic observations and classic geochemical studies to obtain a clearer picture of the investigated problem. While in other fields, it is relatively easy (and cheap) to acquire big amounts of data (hundreds or more), this is not the case for geochemistry. However, we underline that the application of ML techniques to the geochemistry of volcanic rocks does need a minimum dataset size. In the literature a set of 250 analyses is described as sufficiently large amount of data but, as usual, one can try using the available data (often even less than 50) but thousands of examples would definitely improve the results.

6. Applications of machine learning to other volcanological data

ML appears more and more often in volcanology literature, and specific fields of application span now also other sub-disciplines.

Mount Erebus in Antarctica has a persistent lava lake showing Strombolian activity, but its location is definitely remote. Therefore, automatic methods to detect these explosions are highly needed. A CNN was trained using infrared images captured from the crater rim and “labeled” with the help of accompanying seismic data, which was not used anymore during the subsequent automatic detection [146].

Clast morphology is a fundamental tool also for studies concerning volcanic textures. Texture analysis of clasts provides in particular information about genesis, transport and depositional processes. Here, ML has still to be developed fully but e.g., the application of preprocessing techniques such as the Radon transform can be a first step towards an efficient definition of feature vectors to be used for classification, as shown e.g., at Colima volcano [147].

The Museum of Mineralogy, Petrography and Volcanology of the University of Catania implemented a communication system based on the visitor’s personal experience to learn by playing. There is a web application called I-PETER: Interactive Platform to Experience Tours and Education on the Rocks. This platform includes a labeled dataset of images of rocks and minerals to be used also for petrological investigations based on ML [148].

Satellite remote sensing technology is increasingly used for monitoring the surface of the Earth in general, and volcanoes in particular, especially in areas where ground monitoring is scarce or completely missing. For instance, in Latin America

202 out of 319 Holocene volcanoes did not have seismic, deformation or gas monitoring in 2013 [7]. A complex-valued CNN was proposed to extract areas with land shapes similar to given samples in interferometric synthetic aperture radar (InSAR), a technique widely applied in volcano monitoring. An application was presented grouping similar small volcanoes in Japan [149]. InSAR measurements have great potential for volcano monitoring, especially where images are freely available. ML methods can be used for the initial processing of single satellite data. Processing of potential unrest areas can then fully exploit integrated multi-disciplinary, multi-satellite datasets [7]. The Copernicus Programme of the European Space Agency (ESA) and the European Union (EU) has recently contributed by producing the Sentinel-2 multispectral satellites, able to provide high resolution satellite data for disaster monitoring, as well as complementing previous satellite images like Landsat. The free access policy also promotes an increasing use of Sentinel-2 data, which is often processed by ML techniques such as SVM and RF [150]. A transfer learning strategy was applied to ground deformation in Sentinel-1 data [151] and a range of pretrained networks was tested, finding that AlexNet [152] is best suited to this task. The positive results were checked by a researcher and fed back for model updating.

The global volcano monitoring platform MOUNTS (Monitoring Unrest from Space) uses multisensor satellite-based imagery (Sentinel-1 Synthetic Aperture Radar SAR, Sentinel-2 Short-Wave InfraRed SWIR, Sentinel-5P TROPOMI), ground-based seismic data (GEOFON and USGS global earthquake catalogs), and CNN to provide support for volcanic risk assessment. Results are visualized on an open-access website. The efficiency of the system was tested on several eruptions (Erta Ale 2017, Fuego 2018, Kilauea 2018, Anak Krakatau 2018, Ambrym 2018, and Piton de la Fournaise 2018–2019) [153].

Debris flow events are one of the most widespread and dangerous natural processes not only on volcanoes but more in general in mountainous environments. A methodology was recently proposed [154] that combines the results of deterministic and heuristic/probabilistic models for susceptibility assessment. RF models are extensively used to represent the heuristic/probabilistic component of the modeling. The case study presented is given by the Changbai Shan volcano, China [154].

Mapping lava flows from satellite is another important remote sensing application. RF was applied to 20 individual flows and 8 groups of flows of similar age using a Landsat 8 image and a DEM of Nyamuragira (Congo) with 30 m resolution. Despite spectral similarity, lava flows of contrasting age can be well discriminated and mapped by means of image classification [155].

The hazard related to landslides at volcanoes is also significant. DNN models were proposed for landslide susceptibility assessment in Viet Nam, showing considerable better performance with respect to other ML methods such as MLP, SVM, DT and RF [156]. The use of DNN approach could be therefore an interesting approach for the landslide susceptibility mapping of active volcanoes.

Muon imaging has been successfully used by geophysicists to investigate the internal structure of volcanoes, for example at Etna (Italy) [157]. Muon imaging is essentially an inverse problem and it can profit from the application of ML techniques, such as ANN and CA [158].

Combinations of supervised and unsupervised ML techniques have been used to map volcanoes also on other planets. A ML paradigm was designed for the identification of volcanoes on Venus [159]. Other studies have used topographic data, such as DEM and associated derivatives obtained from orbital images, to detect and classify manually labeled Martian landforms including volcanoes [160].

7. Conclusions

ML techniques will have an increasing impact on how we study and model volcanoes in all their aspects, how we monitor them and how we evaluate their hazards, both in the short and in the long term. The increasing number of monitoring equipment installed on volcanoes on one side provides more and more data, on the other often causes their real time processing unfeasible especially when most needed i.e., during unrest and eruptions. Here ML will show its best usefulness, as it can provide the perfect tools to sift through big data to identify subtle patterns that could indicate unrest, hopefully well before eruptions. One important issue is the one of generalization. We must go towards the construction of ML models that can be applied on different volcanoes, for instance when previous data is not available for training specific models. The concepts of transfer learning can be important here.

The routine use of ML tools at the different volcano observatories should be promoted by providing easy installation procedures and easy integration into existing monitoring systems. Open source software should be always chosen whenever possible. On the other hand, observatories should provide good open training data to ML developers, researchers and data scientists in order to improve the models in a virtuous circle. An easy availability of open access data, both from the ground and from satellites should be exploited for building reliable training sets in the different fields of volcanology. This will allow “scientific competition” between research groups using different ML approaches and make a direct comparison of results easier, like it is common in other disciplines where “standard” training datasets are available for download to everybody.

Acknowledgements

RC wishes to acknowledge the invaluable help resulted from discussions with his coauthors during previous works; in particular, collaborations with Luca Barbui, Moritz Beyreuther, Corentin Caudron, Guillermo Cortés, Art Jolly, Philippe Lesage, Joachim Wassermann.

This review is partially based on the results of a previous project funded under the European Union’s Horizon 2020 research and innovation program under the Marie Skłodowska-Curie Grant Agreement No. 749249 (VULCAN.ears).

Conflict of interest

The authors declare no conflict of interest.

Author details


Roberto Carniel^{1*} and Silvina Raquel Guzmán²

1 DPIA, University of Udine, Udine, Friuli, Italy

2 IBIGEO, UNSa-CONICET, Rosario de Lerma, Salta, Argentina

*Address all correspondence to: roberto.carniel@uniud.it

IntechOpen

© 2020 The Author(s). Licensee IntechOpen. This chapter is distributed under the terms of the Creative Commons Attribution License (<http://creativecommons.org/licenses/by/3.0>), which permits unrestricted use, distribution, and reproduction in any medium, provided the original work is properly cited. 

References

- [1] O. Jaquet, R. Carniel, S. Sparks, G. Thompson, R. Namar, and M. Di Cecca, "DEVIN: A forecasting approach using stochastic methods applied to the Soufrière Hills Volcano," *J. Volcanol. Geotherm. Res.*, vol. 153, no. 1-2 SPEC. ISS., pp. 97-111, May 2006.
- [2] O. Jaquet and R. Carniel, "Multivariate stochastic modelling: Towards forecasts of paroxysmal phases at Stromboli," *J. Volcanol. Geotherm. Res.*, vol. 128, no. 1-3, pp. 261-271, Nov. 2003.
- [3] W. P. Aspinall, R. Carniel, O. Jaquet, G. Woo, and T. Hincks, "Using hidden multi-state Markov models with multi-parameter volcanic data to provide empirical evidence for alert level decision-support," *J. Volcanol. Geotherm. Res.*, vol. 153, no. 1-2 SPEC. ISS., pp. 112-124, 2006.
- [4] R. Ortiz, A. García, J. M. Marrero, S. la Cruz-Reyna, R. Carniel, and J. Vila, "Volcanic and volcano-tectonic activity forecasting: A review on seismic approaches," *Ann. Geophys.*, vol. 62, no. 1, 2019.
- [5] G. Currenti, C. del Negro, V. Lapenna, and L. Telesca, "Multifractality in local geomagnetic field at Etna volcano, Sicily (southern Italy)," *Nat. Hazards Earth Syst. Sci.*, vol. 5, no. 4, pp. 555-559, 2005.
- [6] R. M. Green, M. S. Bebbington, S. J. Cronin, and G. Jones, "Geochemical precursors for eruption repose length," *Geophys. J. Int.*, vol. 193, no. 2, pp. 855-873, 2013.
- [7] S. Ebmeier *et al.*, "Satellite geodesy for volcano monitoring in the Sentinel-1 and SAR constellation era," in *International Geoscience and Remote Sensing Symposium (IGARSS)*, 2019, pp. 5465-5467.
- [8] E. Marchetti *et al.*, "Long range infrasound monitoring of Etna volcano," *Sci. Rep.*, vol. 9, no. 1, 2019.
- [9] A. Aiuppa *et al.*, "Unusually large magmatic CO₂ gas emissions prior to a basaltic paroxysm," *Geophys. Res. Lett.*, 2010.
- [10] F. Marchese, N. Pergola, and L. Telesca, "Investigating the temporal fluctuations in satellite advanced very high resolution radiometer thermal signals measured in the volcanic area of Etna (Italy)," *Fluct. Noise Lett.*, vol. 6, no. 3, pp. L305-L316, 2006.
- [11] A. J. L. L. Harris, R. Carniel, and J. Jones, "Identification of variable convective regimes at Erta Ale Lava Lake," *J. Volcanol. Geotherm. Res.*, vol. 142, no. 3-4, pp. 207-223, Apr. 2005.
- [12] Surono *et al.*, "The 2010 explosive eruption of Java's Merapi volcano-A '100-year' event," *J. Volcanol. Geotherm. Res.*, vol. 241-242, pp. 121-135, 2012.
- [13] R. Carniel, E. M. Jolis, and J. Jones, "A geophysical multi-parametric analysis of hydrothermal activity at Dallol, Ethiopia," *J. African Earth Sci.*, vol. 58, no. 5, pp. 812-819, Dec. 2010.
- [14] R. Carniel, "Characterization of volcanic regimes and identification of significant transitions using geophysical data: A review," *Bull. Volcanol.*, vol. 76, no. 8, pp. 1-22, Jul. 2014.
- [15] M. Tárraga, J. Martí, R. Abella, R. Carniel, and C. López, "Volcanic tremors: Good indicators of change in plumbing systems during volcanic eruptions," *J. Volcanol. Geotherm. Res.*, vol. 273, pp. 33-40, 2014.
- [16] R. Carniel and M. Tárraga, "Can tectonic events change volcanic tremor at Stromboli?," *Geophys. Res. Lett.*, vol. 33, no. 20, 2006.

- [17] S. Dumont *et al.*, “The dynamics of a long-lasting effusive eruption modulated by Earth tides,” *Earth Planet. Sci. Lett.*, 2020.
- [18] G. Tamburello *et al.*, “Periodic volcanic degassing behavior: The Mount Etna example,” *Geophys. Res. Lett.*, 2013.
- [19] V. M. Zobin, *Introduction to Volcanic Seismology: Third Edition*. 2016.
- [20] S. R. McNutt, “Volcano seismology and monitoring for eruptions,” *Int. Handb. Earthq. Eng. Seismol.*, pp. 383-406, 2002.
- [21] B. Chouet, “Volcano Seismology,” *Pure Appl. Geophys.*, vol. 160, no. 3, pp. 739-788, 2003.
- [22] I. Molina, H. Kumagai, and H. Yepes, “Resonances of a volcanic conduit triggered by repetitive injections of an ash-laden gas,” *Geophys. Res. Lett.*, 2004.
- [23] R. M. Iverson, “Dynamics of seismogenic volcanic extrusion resisted by a solid surface plug, Mount St. Helens, 2004-2005,” *US Geol. Surv. Prof. Pap.*, no. 1750, pp. 425-460, 2008.
- [24] B. R. Julian, “Volcanic tremor: nonlinear excitation by fluid flow,” *J. Geophys. Res.*, vol. 99, no. B6, pp. 11, 811-859, 877, 1994.
- [25] M. Hellweg, “Physical models for the source of Lascar’s harmonic tremor,” *J. Volcanol. Geotherm. Res.*, vol. 101, no. 1-2, pp. 183-198, 2000.
- [26] J. B. Johnson, J. M. Lees, A. Gerst, D. Sahagian, and N. Varley, “Long-period earthquakes and co-eruptive dome inflation seen with particle image velocimetry,” *Nature*, vol. 456, no. 7220, pp. 377-381, 2008.
- [27] C. J. Bean, L. De Barros, I. Lokmer, J.-P. Métaixian, G. O’Brien, and S. Murphy, “Long-period seismicity in the shallow volcanic edifice formed from slow-rupture earthquakes,” *Nat. Geosci.*, vol. 7, no. 1, pp. 71-75, 2014.
- [28] E. Marchetti and M. Ripepe, “Stability of the seismic source during effusive and explosive activity at Stromboli Volcano,” *Geophys. Res. Lett.*, vol. 32, no. 3, pp. 1-5, 2005.
- [29] R. Carniel, “Comments on the paper ‘Automatic detection and discrimination of volcanic tremors and tectonic earthquakes: An application to Ambrym volcano, Vanuatu’ by Daniel Rouland, Denis Legrand, Mikhail Zhizhin and Sylvie Vergnolle [J. Volcanol. Geotherm. Res. 181,” *J. Volcanol. Geotherm. Res.*, vol. 194, no. 1-3, pp. 61-62, Jul. 2010.
- [30] A. Jolly, C. Caudron, T. Girona, B. Christenson, and R. Carniel, “‘Silent’ Dome Emplacement into a Wet Volcano: Observations from an Effusive Eruption at White Island (Whakaari), New Zealand in Late 2012,” *Geosci.*, vol. 10, no. 4, pp. 1-13, 2020.
- [31] G. Cortés, R. Carniel, M. A. Mendoza, and P. Lesage, “Standardization of Noisy Volcanoseismic Waveforms as a Key Step toward Station-Independent, Robust Automatic Recognition,” *Seismol. Res. Lett.*, vol. 90, no. 2 A, pp. 581-590, 2019.
- [32] A. Duque *et al.*, “Exploring the unsupervised classification of seismic events of Cotopaxi volcano,” *J. Volcanol. Geotherm. Res.*, p. 107009, 2020.
- [33] V. Janoušek, C. M. Farrow, and V. Erban, “Interpretation of whole-rock geochemical data in igneous geochemistry: Introducing Geochemical Data Toolkit (GCDkit),” *J. Petrol.*, vol. 47, no. 6, pp. 1255-1259, 2006.
- [34] M. Petrelli and D. Perugini, “Solving petrological problems through machine learning: the study case of tectonic discrimination using geochemical and isotopic data,” *Contrib. to Mineral. Petrol.*, 2016.

- [35] M. S. M. Bolton *et al.*, “Machine learning classifiers for attributing tephra to source volcanoes: an evaluation of methods for Alaska tephra,” *J. Quat. Sci.*, 2020.
- [36] M. Brandmeier and G. Wörner, “Compositional variations of ignimbrite magmas in the Central Andes over the past 26 Ma — A multivariate statistical perspective,” *Lithos*, 2016.
- [37] K. Ueki, H. Hino, and T. Kuwatani, “Geochemical discrimination and characteristics of magmatic tectonic settings: A machine-learning-based approach,” *Geochemistry, Geophys. Geosystems*, 2018.
- [38] J. Hong, C. Gan, and J. Liu, “Prediction of REEs in OIB by major elements based on machine learning,” *Earth Sci. Front.*, 2019.
- [39] A. Burkov, *The Hundred-Page Machine Learning Book*. Andriy Burkov (January 13, 2019), 2019.
- [40] T. M. Mitchell, “The Discipline of Machine Learning,” *Mach. Learn.*, 2006.
- [41] G. Cortés, M. Carmen Benitez, L. Garcia, I. Alvarez, and J. M. Ibanez, “A Comparative Study of Dimensionality Reduction Algorithms Applied to Volcano-Seismic Signals,” *IEEE J. Sel. Top. Appl. Earth Obs. Remote Sens.*, 2016.
- [42] G. Cabras, R. Carniel, and J. Wasserman, “Signal enhancement with generalized ICA applied to Mt. Etna Volcano, Italy,” *Boll. di Geofis. Teor. ed Appl.*, 2010.
- [43] R. Carniel, G. Cabras, M. Ichihara, and M. Takeo, “Filtering wind in infrasound data by non-negative matrix factorization,” *Seismol. Res. Lett.*, vol. 85, no. 5, pp. 1056-1062, 2014.
- [44] R. Carniel, F. Barazza, M. Tárraga, and R. Ortiz, “On the singular values decoupling in the Singular Spectrum Analysis of volcanic tremor at Stromboli,” *Nat. Hazards Earth Syst. Sci.*, vol. 6, no. 6, pp. 903-909 ST-On the singular values decoupling in, 2006.
- [45] A. Tharwat, “Principal component analysis - a tutorial,” *Int. J. Appl. Pattern Recognit.*, 2016.
- [46] J. Guo, H. Li, J. Ning, W. Han, W. Zhang, and Z. S. Zhou, “Feature dimension reduction using stacked sparse auto-encoders for crop classification with multi-temporal, quad-pol SAR Data,” *Remote Sens.*, 2020.
- [47] A. Tharwat, T. Gaber, A. Ibrahim, and A. E. Hassanien, “Linear discriminant analysis: A detailed tutorial,” *AI Commun.*, 2017.
- [48] S. Solorio-Fernández, J. A. Carrasco-Ochoa, and J. F. Martínez-Trinidad, “Ranking based unsupervised feature selection methods: An empirical comparative study in high dimensional datasets,” in *Lecture Notes in Computer Science (including subseries Lecture Notes in Artificial Intelligence and Lecture Notes in Bioinformatics)*, 2018.
- [49] P. Caroline Cynthia and S. Thomas George, “An Outlier Detection Approach on Credit Card Fraud Detection Using Machine Learning: A Comparative Analysis on Supervised and Unsupervised Learning,” in *Intelligence in Big Data Technologies---Beyond the Hype*, 2021, pp. 125-135.
- [50] S. J. Pan and Q. Yang, “A survey on transfer learning,” *IEEE Trans. Knowl. Data Eng.*, vol. 22, no. 10, pp. 1345-1359, 2010.
- [51] M. Titos, A. Bueno, L. García, C. Benítez, and J. C. Segura, “Classification of Isolated Volcano-Seismic Events Based on Inductive Transfer Learning,” *IEEE Geosci. Remote Sens. Lett.*, vol. 17, no. 5, pp. 869-873, 2020.
- [52] A. Bueno, C. Benitez, S. De Angelis, A. Diaz Moreno, and J. M. Ibanez,

- “Volcano-Seismic Transfer Learning and Uncertainty Quantification with Bayesian Neural Networks,” *IEEE Trans. Geosci. Remote Sens.*, vol. 58, no. 2, pp. 892-902, 2020.
- [53] G. Van Rossum and F. L. Drake, *Python 3 Reference Manual*. Scotts Valley, CA: CreateSpace, 2009.
- [54] R Core Team, “R: A Language and Environment for Statistical Computing.” Vienna, Austria, 2013.
- [55] K. Arnold, J. Gosling, and D. Holmes, *The Java programming language*. Addison Wesley Professional, 2005.
- [56] D. Flanagan, *JavaScript: the definitive guide*. “O’Reilly Media, Inc.,” 2006.
- [57] J. Bezanson, A. Edelman, S. Karpinski, and V. B. Shah, “Julia: A fresh approach to numerical computing,” *SIAM Rev.*, 2017.
- [58] M. Odersky, L. Spoon, and B. Venners, *Programming in scala*. Artima Inc, 2008.
- [59] github, “GitHub.” 2020.
- [60] C. X. Ren, A. Peltier, V. Ferrazzini, B. Rouet-Leduc, P. A. Johnson, and F. Brenguier, “Machine Learning Reveals the Seismic Signature of Eruptive Behavior at Piton de la Fournaise Volcano,” *Geophys. Res. Lett.*, vol. 47, no. 3, p. e2019GL085523, 2020.
- [61] R. Carniel, L. Barbui, and A. D. Jolly, “Detecting dynamical regimes by Self-Organizing Map (SOM) analysis: An example from the March 2006 phreatic eruption at Raoul Island, New Zealand Kermadec Arc,” *Boll. di Geofis. Teor. ed Appl.*, 2013.
- [62] R. Carniel, A. D. Jolly, and L. Barbui, “Analysis of phreatic events at Ruapehu volcano, New Zealand using a new SOM approach,” *J. Volcanol. Geotherm. Res.*, 2013.
- [63] A. Köhler, M. Ohrnberger, and F. Scherbaum, “Unsupervised pattern recognition in continuous seismic wavefield records using Self-Organizing Maps,” *Geophys. J. Int.*, 2010.
- [64] R. Carniel, “Neural networks and dynamical system techniques for volcanic tremor analysis,” *Ann. di Geofis.*, vol. 39, no. 2, pp. 241-252, 1996.
- [65] A. M. Esposito, L. D’Auria, F. Giudicepietro, T. Caputo, and M. martini, “Neural analysis of seismic data: Applications to the monitoring of Mt. Vesuvius,” *Ann. Geophys.*, vol. 56, no. 4, 2013.
- [66] S. Scarpetta *et al.*, “Automatic classification of seismic signals at Mt. Vesuvius volcano, Italy, using neural networks,” *Bull. Seismol. Soc. Am.*, vol. 95, no. 1, pp. 185-196, 2005.
- [67] M. Masotti, S. Falsaperla, H. Langer, S. Spampinato, and R. Campanini, “Application of Support Vector Machine to the classification of volcanic tremor at Etna, Italy,” *Geophys. Res. Lett.*, vol. 33, no. 20, 2006.
- [68] M. Titos, A. Bueno, L. García, M. C. Benítez, and J. Ibañez, “Detection and Classification of Continuous Volcano-Seismic Signals with Recurrent Neural Networks,” *IEEE Trans. Geosci. Remote Sens.*, vol. 57, no. 4, pp. 1936-1948, 2019.
- [69] M. Beyreuther, R. Carniel, and J. Wassermann, “Continuous Hidden Markov Models: Application to automatic earthquake detection and classification at Las Canãdas caldera, Tenerife,” *J. Volcanol. Geotherm. Res.*, 2008.
- [70] M. Beyreuther and J. Wassermann, “Hidden semi-Markov Model based earthquake classification system using

- Weighted Finite-State Transducers,” *Nonlinear Process. Geophys.*, vol. 18, no. 1, pp. 81-89, 2011.
- [71] G. Cortés *et al.*, “Evaluating robustness of a HMM-based classification system of volcano-seismic events at COLIMA and Popocatepetl volcanoes,” in *International Geoscience and Remote Sensing Symposium (IGARSS)*, 2009, vol. 2, pp. II1012-II1015.
- [72] G. Cortés, L. García, I. Álvarez, C. Benítez, Á. de la Torre, and J. Ibáñez, “Parallel System Architecture (PSA): An efficient approach for automatic recognition of volcano-seismic events,” *J. Volcanol. Geotherm. Res.*, 2014.
- [73] F. Pedregosa *et al.*, “Scikit-learn: Machine Learning in {P}ython,” *J. Mach. Learn. Res.*, vol. 12, pp. 2825-2830, 2011.
- [74] M. Charrad, N. Ghazzali, V. Boiteau, and A. Niknafs, “Nbclust: An R package for determining the relevant number of clusters in a data set,” *J. Stat. Softw.*, 2014.
- [75] T. Kohonen, “Self-organized formation of topologically correct feature maps,” *Biol. Cybern.*, 1982.
- [76] T. Kohonen, *Self-organizing maps*, 3rd ed. Berlin: Springer, 2001.
- [77] S. Hochreiter and J. Schmidhuber, “Long Short-Term Memory,” *Neural Comput.*, vol. 9, no. 8, pp. 1735-1780, 1997.
- [78] P. McCullagh and J. A. Nelder, *Generalized Linear Models, Second Edition (Monographs on Statistics and Applied Probability)*. 1989.
- [79] T. Hastie, R. Tibshirani, and J. Friedman, *Elements of Statistical Learning 2nd ed.* 2009.
- [80] C. Cortes and V. Vapnik, “Support-vector networks,” *Mach. Learn.*, vol. 20, no. 3, pp. 273-297, 1995.
- [81] B. Krishnapuram, L. Carin, M. A. T. Figueiredo, and A. J. Hartemink, “Sparse multinomial logistic regression: Fast algorithms and generalization bounds,” *IEEE Trans. Pattern Anal. Mach. Intell.*, 2005.
- [82] G. Cabras, R. Carniel, and J. Jones, “Non-negative Matrix Factorization: An application to Erta Ale volcano, Ethiopia,” *Boll. di Geofis. Teor. ed Appl.*, vol. 53, no. 2, pp. 231-242, 2012.
- [83] B. Krishnapuram, L. Carin, and A. J. Hartemink, “Joint classifier and feature optimization for cancer diagnosis using gene expression data,” in *Proceedings of the Annual International Conference on Computational Molecular Biology, RECOMB*, 2003.
- [84] B. T. Pham *et al.*, “Ensemble modeling of landslide susceptibility using random subspace learner and different decision tree classifiers,” *Geocarto Int.*, 2020.
- [85] L. R. Rabiner and R. W. Schafer, “Introduction to digital speech processing,” *Found. Trends Signal Process.*, 2007.
- [86] P. Alasonati, J. Wassermann, and M. Ohrnberger, “Signal classification by wavelet-based hidden Markov models: application to seismic signals of volcanic origin,” in *Statistics in Volcanology*, 2018.
- [87] A. Boué, P. Lesage, G. Cortés, B. Valette, and G. Reyes-Dávila, “Real-time eruption forecasting using the material Failure Forecast Method with a Bayesian approach,” *J. Geophys. Res. Solid Earth*, vol. 120, no. 4, pp. 2143-2161, 2015.
- [88] M. Tárraga, R. Carniel, R. Ortiz, and A. García, “Chapter 13 The Failure Forecast Method: Review and

- Application for the Real-Time Detection of Precursory Patterns at Reawakening Volcanoes,” *Dev. Volcanol.*, vol. 10, no. C, pp. 447-469, 2008.
- [89] J. P. Jones, R. Carniel, and S. D. Malone, “Subband decomposition and reconstruction of continuous volcanic tremor,” *J. Volcanol. Geotherm. Res.*, vol. 213-214, pp. 98-115, 2012.
- [90] H. Langer, S. Falsaperla, T. Powell, and G. Thompson, “Automatic classification and a-posteriori analysis of seismic event identification at Soufrière Hills volcano, Montserrat,” *J. Volcanol. Geotherm. Res.*, vol. 153, no. 1-2 SPEC. ISS., pp. 1-10, 2006.
- [91] J. M. Ibáñez, C. Benítez, L. A. Gutiérrez, G. Cortés, A. García-Yeguas, and G. Alguacil, “The classification of seismo-volcanic signals using Hidden Markov Models as applied to the Stromboli and Etna volcanoes,” *J. Volcanol. Geotherm. Res.*, 2009.
- [92] D. N. Green and J. Neuberg, “Waveform classification of volcanic low-frequency earthquake swarms and its implication at Soufrière Hills Volcano, Montserrat,” *J. Volcanol. Geotherm. Res.*, vol. 153, no. 1-2 SPEC. ISS., pp. 51-63, 2006.
- [93] R. Villegas, R. Carniel, I. Petrinovic, and C. Balbis, “Clusters of long-period (LP) seismic events at the Irazú Volcano: what are they telling us?,” *J. South Am. Earth Sci.*, no. under final revision, 2020.
- [94] W. I. Sevilla, L. A. Jumawan, C. J. Clarito, M. A. Quintia, A. A. Dominguiano, and R. U. Solidum, “Improved 1D velocity model and deep long-period earthquakes in Kanlaon Volcano, Philippines: Implications for its magmatic system,” *J. Volcanol. Geotherm. Res.*, 2020.
- [95] A. J. Hotovec-Ellis and C. Jeffries, “Near real-time detection, clustering, and analysis of repeating earthquakes Application to Mount St. Helens and Redoubt volcanoes,” in *Seismological Society of America Annual Meeting*, 2016.
- [96] A. D. Jolly *et al.*, “Seismo-acoustic evidence for an avalanche driven phreatic eruption through a beheaded hydrothermal system: An example from the 2012 Tongariro eruption,” *J. Volcanol. Geotherm. Res.*, vol. 286, pp. 331-347, 2014.
- [97] A. Messina and H. Langer, “Pattern recognition of volcanic tremor data on Mt. Etna (Italy) with KAnalysis-A software program for unsupervised classification,” *Comput. Geosci.*, vol. 37, no. 7, pp. 953-961, 2011.
- [98] S. Falsaperla, S. Graziani, G. Nunnari, and S. Spampinato, “Automatic classification of volcanic earthquakes by using multi-layered neural networks,” *Nat. Hazards*, 1996.
- [99] H. Langer, S. Falsaperla, M. Masotti, R. Campanini, S. Spampinato, and A. Messina, “Synopsis of supervised and unsupervised pattern classification techniques applied to volcanic tremor data at Mt Etna, Italy,” *Geophys. J. Int.*, 2009.
- [100] M. Titos, A. Bueno, L. Garcia, and C. Benitez, “A Deep Neural Networks Approach to Automatic Recognition Systems for Volcano-Seismic Events,” *IEEE J. Sel. Top. Appl. Earth Obs. Remote Sens.*, 2018.
- [101] G. Curilem, J. Vergara, G. Fuentealba, G. Acuña, and M. Chacón, “Classification of seismic signals at Villarrica volcano (Chile) using neural networks and genetic algorithms,” *J. Volcanol. Geotherm. Res.*, vol. 180, no. 1, pp. 1-8, 2009.
- [102] J. P. Canário *et al.*, “In-depth comparison of deep artificial neural network architectures on seismic events

classification,” *J. Volcanol. Geotherm. Res.*, vol. 401, 2020.

[103] B. Pradhan and S. Lee, “Landslide susceptibility assessment and factor effect analysis: backpropagation artificial neural networks and their comparison with frequency ratio and bivariate logistic regression modelling,” *Environ. Model. Softw.*, 2010.

[104] G. F. Manley *et al.*, “Understanding the timing of eruption end using a machine learning approach to classification of seismic time series,” *J. Volcanol. Geotherm. Res.*, 2020.

[105] M. Curilem *et al.*, “Pattern recognition applied to seismic signals of Llaima volcano (Chile): An evaluation of station-dependent classifiers,” *J. Volcanol. Geotherm. Res.*, vol. 315, pp. 15-27, 2016.

[106] M. Malfante, M. Dalla Mura, J. P. Metaxian, J. I. Mars, O. Macedo, and A. Inza, “Machine Learning for Volcano-Seismic Signals: Challenges and Perspectives,” *IEEE Signal Process. Mag.*, 2018.

[107] I. M. Murwantara, P. Yugopuspito, and R. Hermawan, “Comparison of machine learning performance for earthquake prediction in Indonesia using 30 years historical data,” *Telkomnika (Telecommunication Comput. Electron. Control.)*, 2020.

[108] C. Hibert, F. Provost, J. P. Malet, A. Maggi, A. Stumpf, and V. Ferrazzini, “Automatic identification of rockfalls and volcano-tectonic earthquakes at the Piton de la Fournaise volcano using a Random Forest algorithm,” *J. Volcanol. Geotherm. Res.*, 2017.

[109] D. E. Dempsey, S. J. Cronin, S. Mei, and A. W. Kempa-Liehr, “Automatic precursor recognition and real-time forecasting of sudden explosive volcanic eruptions at Whakaari, New Zealand,” *Nat. Commun.*, 2020.

[110] M. C. Benítez *et al.*, “Continuous HMM-based seismic-event classification at deception Island, Antarctica,” in *IEEE Transactions on Geoscience and Remote Sensing*, 2007.

[111] M. Bicego, C. Acosta-Munoz, and M. Orozco-Alzate, “Classification of seismic volcanic signals using hidden-markov-model-based generative embeddings,” *IEEE Trans. Geosci. Remote Sens.*, vol. 51, no. 6, pp. 3400-3409, 2013.

[112] P. B. Dawson, M. C. Benítez, B. A. Chouet, D. Wilson, and P. G. Okubo, “Monitoring very-long-period seismicity at Kilauea Volcano, Hawaii,” *Geophys. Res. Lett.*, 2010.

[113] N. Trujillo-Castrillón, C. M. Valdés-González, R. Arámbula-Mendoza, and C. C. Santacoloma-Salguero, “Initial processing of volcanic seismic signals using Hidden Markov Models: Nevado del Huila, Colombia,” *J. Volcanol. Geotherm. Res.*, 2018.

[114] C. cassisi, M. Prestifilippo, A. Cannata, P. Montalto, D. Patanè, and E. Privitera, “Probabilistic Reasoning Over Seismic Time Series: Volcano Monitoring by Hidden Markov Models at Mt. Etna,” *Pure Appl. Geophys.*, 2016.

[115] A. Maggi, V. Ferrazzini, C. Hibert, F. Beauducel, P. Boissier, and A. Amemoutou, “Implementation of a multistation approach for automated event classification at Piton de la Fournaise volcano,” *Seismol. Res. Lett.*, 2017.

[116] P. E. E. Lara *et al.*, “Automatic multichannel volcano-seismic classification using machine learning and EMD,” *IEEE J. Sel. Top. Appl. Earth Obs. Remote Sens.*, 2020.

[117] M. Beyreuther, R. Barsch, L. Krischer, T. Megies, Y. Behr, and J. Wassermann, “ObsPy: A python toolbox for seismology,” *Seismol. Res. Lett.*, 2010.

- [118] T. Lecocq, C. Caudron, and F. Brenguier, “Msnoise, a python package for monitoring seismic velocity changes using ambient seismic noise,” *Seismol. Res. Lett.*, 2014.
- [119] A. Bueno *et al.*, “PICOSS: Python Interface for the Classification of Seismic Signals,” *Comput. Geosci.*, 2020.
- [120] H. Buurman and M. E. West, “Seismic precursors to volcanic explosions during the 2006 eruption of Augustine Volcano,” *US Geol. Surv. Prof. Pap.*, 2010.
- [121] G. Cortés, R. Carniel, P. Lesage, and M. A. Mendoza, “VULCAN. ears: Volcano-seismic Unsupervised Labelling and ClAssificatiON Embedded in A Real-time Scenario,” 2020. [Online]. Available: <https://cordis.europa.eu/project/id/749249/it>. [Accessed: 20-Aug-2020].
- [122] G. Cortés, R. Carniel, P. Lesage, and M. A. Mendoza, “pyVERSO - software for building and evaluating Volcano-Seismic Recognition (VSR) system,” 2020. .
- [123] E. D. Cambridge University, “HTK - Hidden Markov Model Toolkit,” 2020. [Online]. Available: <http://htk.eng.cam.ac.uk/>.
- [124] G. Cortés, R. Carniel, P. Lesage, and M. A. Mendoza, “geoStudio & liveVSR software,” 2020. .
- [125] G. Cortés, R. Carniel, M. A. Mendoza, and P. Lesage, “VSR Databases used in article ‘Standardization of noisy volcano-seismic waveforms as a key step towards station-independent, robust automatic recognition.’” Zenodo, 2018.
- [126] P. Lesage, “Interactive Matlab software for the analysis of seismic volcanic signals,” *Comput. Geosci.*, vol. 35, no. 10, pp. 2137-2144, 2009.
- [127] D. Cervelli, P. Cervelli, T. Parker, and T. Murray, “SWARM Seismic Wave Analysis and Real-time Monitor: User Manual and Reference Guide,” 2020. [Online]. Available: <https://volcanoes.usgs.gov/software/swarm/index.shtml>.
- [128] J. A. Cortés, J. L. Palma, and M. Wilson, “Deciphering magma mixing: The application of cluster analysis to the mineral chemistry of crystal populations,” *J. Volcanol. Geotherm. Res.*, 2007.
- [129] U. Morgenstern, C. J. Daughney, G. Leonard, D. Gordon, F. M. Donath, and R. Reeves, “Using groundwater age and hydrochemistry to understand sources and dynamics of nutrient contamination through the catchment into Lake Rotorua, New Zealand,” *Hydrol. Earth Syst. Sci.*, 2015.
- [130] M. O. Awaleh *et al.*, “Geochemical, multi-isotopic studies and geothermal potential evaluation of the complex Djibouti volcanic aquifer (republic of Djibouti),” *Appl. Geochemistry*, 2018.
- [131] F. Barette, S. Poppe, B. Smets, M. Benbakkar, and M. Kervyn, “Spatial variation of volcanic rock geochemistry in the Virunga Volcanic Province: Statistical analysis of an integrated database,” *J. African Earth Sci.*, 2017.
- [132] The Mathworks Inc., “MATLAB - MathWorks,” www.mathworks.com/products/matlab, 2020. .
- [133] E. S. Schandl and M. P. Gorton, “Application of high field strength elements to discriminate tectonic settings in VMS environments,” *Econ. Geol.*, 2002.
- [134] J. A. Pearce and J. R. Cann, “Tectonic setting of basic volcanic rocks determined using trace element analyses,” *Earth Planet. Sci. Lett.*, 1973.
- [135] C. Li, N. T. Arndt, Q. Tang, and E. M. Ripley, “Trace element

indiscrimination diagrams,” *Lithos*. 2015.

[136] C. A. Snow, “A reevaluation of tectonic discrimination diagrams and a new probabilistic approach using large geochemical databases: Moving beyond binary and ternary plots,” *J. Geophys. Res. Solid Earth*, 2006.

[137] S. P. Verma and J. S. Armstrong-Altrin, “New multi-dimensional diagrams for tectonic discrimination of siliciclastic sediments and their application to Precambrian basins,” *Chem. Geol.*, 2013.

[138] S. P. Verma and L. Díaz-González, “New discriminant-function-based multidimensional discrimination of mid-ocean ridge and oceanic plateau,” *Geosci. Front.*, 2020.

[139] CoDaPack, “CoDaPack - Compositional Data Package,” 2020. [Online]. Available: <http://www.compositionaldata.com/codapack.php>. [Accessed: 20-Aug-2020].

[140] C. H. Weiß, “StatSoft, Inc., Tulsa, OK.: STATISTICA, Version 8,” *AStA Adv. Stat. Anal.*, 2007.

[141] A. B. Beaudoin and R. H. King, “Using discriminant function analysis to identify Holocene tephra based on magnetite composition: a case study from the Sunwapta Pass area, Jasper National Park,” *Can. J. Earth Sci.*, 1986.

[142] A. J. Bourne *et al.*, “Distal tephra record for the last ca 105,000 years from core PRAD 1-2 in the central Adriatic Sea: Implications for marine tephrostratigraphy,” *Quat. Sci. Rev.*, 2010.

[143] M. Petrelli, R. Bizzarri, D. Morgavi, A. Baldanza, and D. Perugini, “Combining machine learning techniques, microanalyses and large geochemical datasets for tephrochronological studies in complex

volcanic areas: New age constraints for the Pleistocene magmatism of central Italy,” *Quat. Geochronol.*, 2017.

[144] A. M. Esposito, G. Alaia, F. Giudicepietro, L. Pappalardo, and M. D’Antonio, “Unsupervised Geochemical Analysis of the Eruptive Products of Ischia, Vesuvius and Campi Flegrei,” in *Smart Innovation, Systems and Technologies*, 2021.

[145] Y. Zhao, Y. Zhang, M. Geng, J. Jiang, and X. Zou, “Involvement of Slab-Derived Fluid in the Generation of Cenozoic Basalts in Northeast China Inferred From Machine Learning,” *Geophys. Res. Lett.*, 2019.

[146] B. C. Dye and G. Morra, “Machine learning as a detection method of Strombolian eruptions in infrared images from Mount Erebus, Antarctica,” *Phys. Earth Planet. Inter.*, 2020.

[147] G. Moreno Chávez, J. Villa, D. Sarocchi, and E. González-Ramírez, “A method and software solution for classifying clast roundness based on the radon transform,” *Comput. Geosci.*, 2020.

[148] D. Sinitò *et al.*, “I-PETER (Interactive platform to experience tours and education on the rocks): A virtual system for the understanding and dissemination of mineralogical-petrographic science,” *Pattern Recognit. Lett.*, 2020.

[149] Y. Sunaga, R. Natsuaki, and A. Hirose, “Proposal of complex-valued convolutional neural networks for similar land-shape discovery in interferometric synthetic aperture radar,” in *Lecture Notes in Computer Science (including subseries Lecture Notes in Artificial Intelligence and Lecture Notes in Bioinformatics)*, 2018.

[150] D. Phiri, M. Simwanda, S. Salekin, V. R. Nyirenda, Y. Murayama, and M. Ranagalage, “Sentinel-2 Data for Land

Cover/Use Mapping: A Review,” *Remote Sens.*, vol. 12, no. 14, p. 2291, 2020.

[151] N. Anantrasirichai, J. Biggs, F. Albino, P. Hill, and D. Bull, “Application of Machine Learning to Classification of Volcanic Deformation in Routinely Generated InSAR Data,” *J. Geophys. Res. Solid Earth*, vol. 123, no. 8, pp. 6592-6606, 2018.

[152] A. Krizhevsky, I. Sutskever, and G. E. Hinton, “ImageNet classification with deep convolutional neural networks,” in *Advances in Neural Information Processing Systems*, 2012, vol. 2, pp. 1097-1105.

[153] S. Valade *et al.*, “Towards global volcano monitoring using multisensor sentinel missions and artificial intelligence: The MOUNTS monitoring system,” *Remote Sens.*, 2019.

[154] A. Si *et al.*, “Debris flow susceptibility assessment using the integrated random forest based steady-state infinite slope method: A case study in Changbai Mountain, China,” *Water (Switzerland)*, 2020.

[155] L. Li, C. Solana, F. Canters, and M. Kervyn, “Testing random forest classification for identifying lava flows and mapping age groups on a single Landsat 8 image,” *J. Volcanol. Geotherm. Res.*, 2017.

[156] D. T. Bui, P. Tsangaratos, V. T. Nguyen, N. Van Liem, and P. T. Trinh, “Comparing the prediction performance of a Deep Learning Neural Network model with conventional machine learning models in landslide susceptibility assessment,” *Catena*, 2020.

[157] D. Carbone, D. Gibert, J. Marteau, M. Diament, L. Zuccarello, and E. Galichet, “An experiment of muon radiography at Mt Etna (Italy),” *Geophys. J. Int.*, 2013.

[158] G. Yang, D. Ireland, R. Kaiser, and D. Mahon, “Machine Learning for Muon

Imaging,” in *Lecture Notes in Computer Science (including subseries Lecture Notes in Artificial Intelligence and Lecture Notes in Bioinformatics)*, 2018.

[159] M. C. Burl *et al.*, “Learning to recognize volcanoes on Venus,” *Mach. Learn.*, 1998.

[160] T. F. Stepinski, S. Ghosh, and R. Vilalta, “Machine learning for automatic mapping of planetary surfaces,” in *Proceedings of the National Conference on Artificial Intelligence*, 2007.

Section 3

Monogenetic Volcanism

Effusive Monogenetic Volcanism

Hugo Murcia and Károly Németh

Abstract

The study of monogenetic volcanism around Earth is rapidly growing due to the increasing recognition of monogenetic volcanic edifices in different tectonic settings. Far from the idea that this type of volcanism is both typically mafic and characteristic from intraplate environments, it occurs in a wide spectrum of composition and geological settings. This volcanism is widely known by the distinctive pyroclastic cones that represent both magmatic and phreatomagmatic explosive activity; they are known as scoria or spatter cones, tuff cones, tuff rings, maars and maar-diatremes. These cones are commonly associated with lava domes and usually accompanied by lava flows as part of their effusive eruptive phases. In spite of this, isolated effusive monogenetic emissions also appear around Earth's surface. However, these isolated emissions are not habitually considered within the classification scheme of monogenetic volcanoes. Along with this, many of these effusive volcanoes also contrast with the belief that this volcanism is indicative of rapidly magma ascent from the asthenosphere, as many of the products are strongly evolved reflecting differentiation linked to stagnation during ascent. This has led to the understanding that the asthenosphere is not always the place that directly gives rise to the magma batches and rather, they detach from a crustal melt storage. This chapter introduces four singular effusive monogenetic volcanoes as part of the volcanic geoforms, highlights the fact that monogenetic volcanic fields can also be associated with crustal reservoirs, and outlines the processes that should occur to differentiate the magma before it is released as intermediate and acidic in composition. This chapter also provides an overview of this particular volcanism worldwide and contributes to the monogenetic comprehension for future studies.

Keywords: lava dome, coulé, small-shield, lava flow

1. Introduction

Monogenetic volcanoes (typically $\leq 1 \text{ km}^3$ and $\leq 10^2$ years) are usually distinguished as dominantly formed by either magmatic or phreatomagmatic explosive activity and accompanied effusive processes. The magmatic explosive eruptions typically build scoria or spatter cones, while explosive phreatomagmatic eruptions characteristically form tuff cones, tuff rings, maars and maar-diatremes [1]. Associated with either activity, effusive emissions forming lava domes and lava flows are also common; consequently, these products are part of the mentioned volcanic edifices [2–4]. Frequently, individual effusive monogenetic emissions are also released into the Earth's surface, thus forming exclusively, or dominantly, effusive monogenetic volcanoes (e.g. [5]). In spite of this, they are usually not part of the monogenetic classification schemes (e.g. [1, 6, 7]), although many have been widely studied (e.g. [8–16]; among many other studies).

Lava domes in general have been mostly described as part of eruptions in polygenetic, intermediate to acidic volcanoes (e.g. [17]). From there, several types have been defined. Based on the growing mechanism, they are either endogenous whether they expand by intrusion of new magma or exogenous whether they enlarge by extrusion of it [18]; they are also called cryptodomes whether the magma did not reach the surface [19]. Furthermore, based on the geoform, they have received different names such as *tortas*, *platy*, *axisymmetric*, *lobate*, *spines* or *peléean-type*, *upheaved plugs*, *viscous coulées* lava streams, among others [17, 20–22]. As minor centers (i.e. as monogenetic volcanoes), the only classification that exist for our knowledge, is that outlined by De Silva and Lindsay [23] who grouped them in: 1) lava domes or *tortas*, 2) *coulées*, 3) *peléean*, and 4) *upheaved plugs*, based on their morphology. Individual monogenetic lava flows, in addition, are not part of this or any other classification scheme with the exception of the *scutulum*, *low shields* or *small-shields* (cf. [24, 25] that are mentioned by De Silva and Lindsay [23] within the mafic monogenetic volcanoes classification).

It is worth mentioning that the concept of “monogenetic” volcanism has even been considered in association with 1) Large Igneous Provinces (LIPs) that are overwhelmingly effusive, but formed in very short period of time in single flare ups [26], or 2) effusive dominated fields that are smaller than typical Large igneous provinces but significantly bigger than a “normal” monogenetic field [25]. In this work, however, we refer to small-volume monogenetic volcanoes, understood as small magma batches reaching the surface dispersed and episodically.

We herein propose the expansion of the existing monogenetic classification scheme after including the effusive volcanoes based on the above mentioned. This classification is based on their geoform, similarly to the explosive volcanoes. Furthermore, we provide a framework of the processes that act during the magma ascent and cause differentiation to produce intermediate to evolved volcanic products. Thus, we outline magmatic plumbing system options, which include crustal magma reservoirs as zones for detaching magma batches. Finally, we provide an overview of this particular poorly known volcanism worldwide, contributing to the monogenetic comprehension for future studies.

2. Effusive monogenetic volcanoes

The way that magma is monogenetically released to the Earth surface is related to the internal magma dynamic that occurred in the last dozens of meters [27]. It also depends on the form and dimensions of the conduit with the ascending magma. Whether the magma encounters water en route, a process known as MFCI (Molten-Fuel Coolant Interaction) occurs and therefore, it drives the eruption [28, 29]. In this case, the eruptive style depends mostly on the amount of water that the magma encounters [30] and the lithology where this water (usually an aquifer) is stored (e.g. sediments vs. fractured metamorphic rocks) (e.g. [31–33]; this last also associated with the easiness for the water to be released. However, whether the magma reaches the surface without any interaction with water, the eruption may occur in two ways: 1) explosive, whether the magma is fragmented by the volatiles dynamics (i.e. exsolution, nucleation, growth and coalescence) associated with pressure decreasing, or 2) effusive, whether degassing is effective, linked to bubbles interconnection avoiding the magma fragmentation [34]. The first eruptive manner builds scoria cones (e.g. the historical Jorullo [35–37] and Parícutín volcanoes in México [38]), while the second one produces lava bodies (e.g. The Villamaría-Termal Monogenetic Volcanic Field in Colombia; [5]). As previously mentioned, these emissions are commonly part of the explosive activity forming any kind of pyroclastic cone; however, they can also

dominate and create individual effusive volcanoes (**Figure 1**). Because of this, we propose here these effusive products as part of a monogenetic volcano classification scheme and add them to those produced by magmatic activity (**Figure 2**). Accordingly, we propose to distinguish them between lava domes, coulées, small-shields and lava

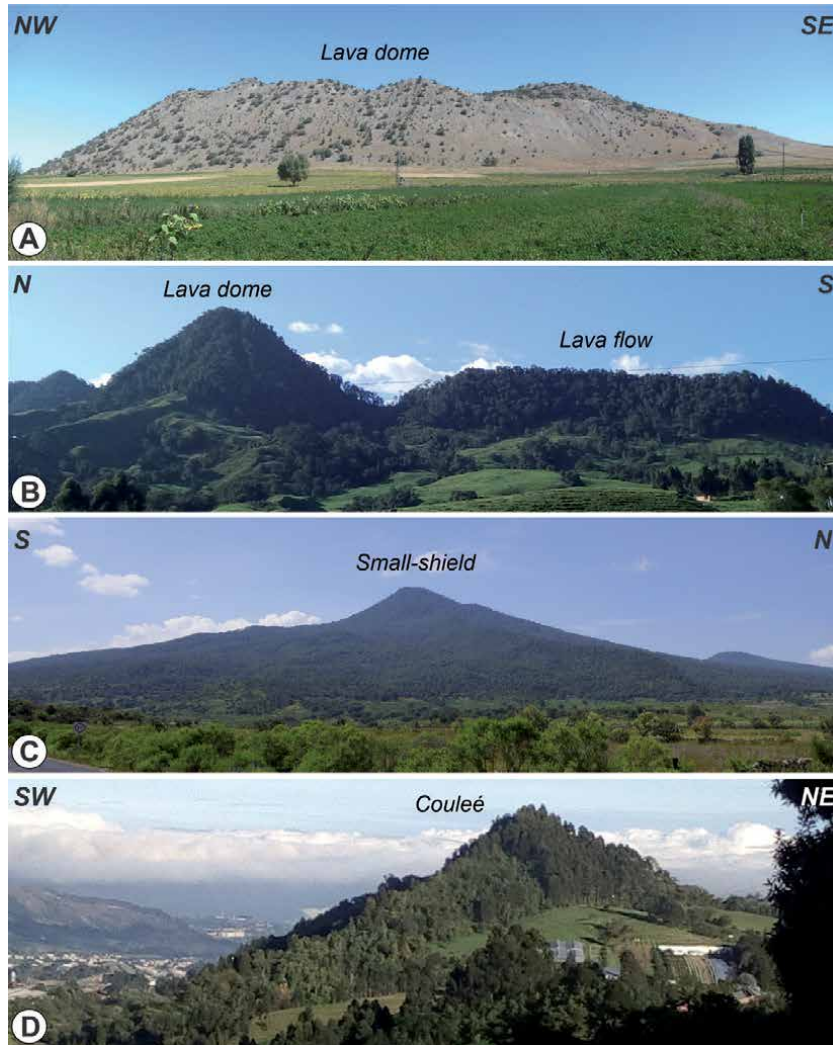


Figure 1. Effusive monogenetic volcanoes. (A) Güneydag lava dome in Anatolia, Turkey; (B) Victoria lava dome and Victoria lava flow in Manizales, Colombia; (C) El Bosque small-shield in Morelia, México. (D) Tesorito coulée in Manizales, Colombia.

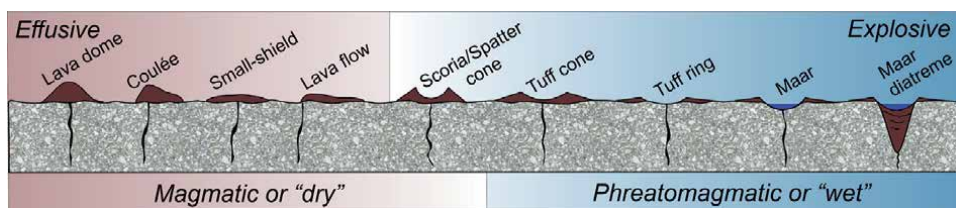


Figure 2. Classification scheme of monogenetic volcanoes and their relationship with their eruptive style.

flows based on their geoform. The construction of every volcano is linked to the internal dynamics of the magma, but also to the form and dimension of the ascending conduit, the interaction of the conduit with the surface, and the topography where the magma is released. Every factor should be in-depth investigated. An overview of these elements is the topic of the following sections.

2.1 Evidences of internal dynamics

Coherent lava bodies of effusive monogenetic volcanoes have usually a glassy groundmass, which is the evidence of the rapid cooling when magma reaches the surface (**Figure 3A**). Commonly, the magma hosts phenocrysts (i.e. crystals greater than 0.5 mm) and microphenocrysts (i.e. crystals between 0.5 and 0.05 mm), although they do not dominate in the products. Occasionally, when the magma reaches the surface, decompression triggering solubility decreasing, oversaturation and degassing, induces crystal nucleation and therefore growing of multiple small crystals [39]; if these crystals can be distinguished in type, they are called microliths (usually between 50 and 5 μm) and the groundmass can be defined as microcrystalline if they dominated (**Figure 3B**), on the contrary the crystals can be called nanoliths (<5 μm) and the groundmass denominated as cryptocrystalline (**Figure 3C**). This crystal nucleation, along with temperature, composition (mostly SiO_2 but also MgO content) and dissolved volatiles (mostly H_2O but also CO_2), are the factors controlling the magma viscosity and somehow the volcano that is built (i.e. a lava dome, couleé, small-shield or lava flow). The higher the crystals and silica content, the higher the viscosity [39]; so, these magmas tend to form lava domes or couleés. On the contrary, small-shields and lava flows are related to low amount of crystals and low silica. Magma temperature tends to indicate relative low values in lava domes and high values in lava flows, while volatiles have a special behaviour [39]: their content is higher in viscous, high-silica magmas, but at the same time they keep viscosity lower; therefore, under a similar composition, a rapid degassing yields a lava dome formation, while a slow degassing leads to a lava flow geoform. Overall, slow ascent times are related to lava domes, while fast ascent times to lava

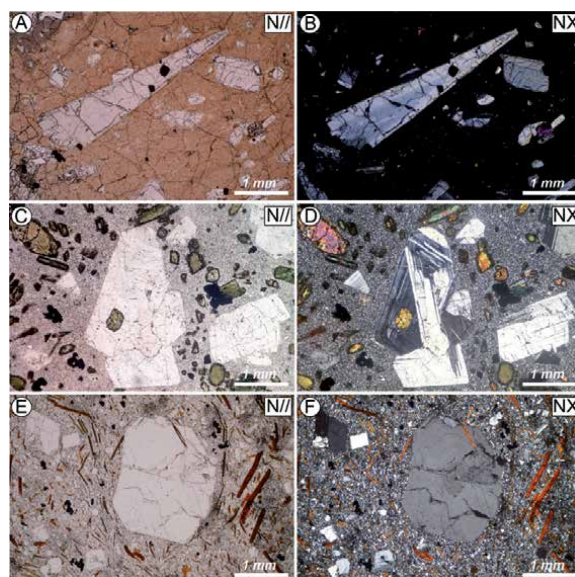


Figure 3. Groundmass in effusive monogenetic products. (A, B) Glassy groundmass. (C, D) cryptocrystalline groundmass. (E, F) microcrystalline groundmass. Parallel nichols to the left, crossed nichols to the right.

flows. The relationship between the mentioned elements, however, are somehow circular or themselves dependent, and consequently without a linear relation. Thus, although the groundmass and the major crystals are evidence for the dynamics of magma propagation during ascent, from our experience, no direct relationships can be drawn between any of the elements vs. the volcanoes, even in a thin section study of the eruptive products under the microscope. This is worth mentioning because it explains why the definition of these volcanoes is purely dependent on the geoform and do not consider, for instance, petrographic characteristics. In spite of this, we consent some approaches that can be made from a rock. For example, an increase in decompression rates results in (1) bubbles and crystals with smaller sizes, (2) a lower crystallinity and thus higher glass fraction, and (3) a higher abundance of unstable hydrous phases [17, 40]. This may help as a starting point for subsequent studies when a rock from effusive monogenetic volcanoes is analysed.

2.2 Magma conduit and topography

Monogenetic effusive volcanoes are related to physical elements such as the conduit form and dimension, and the interaction with the surface, but also to the topography where the magmas are released. Thus, the volcanoes can be formed through a cylindrical vs. a fissural conduit and in a flat vs. a hilly topography. This complex emplacement can deviate the resulting geoforms from what we normally would expect. For instance, a lava flow volcano that could be linked to a low viscosity magma, could be really the result of a high viscosity magma released and emplaced through a long fissure in a flat topography; also a dome-like geoform that could be linked to high viscosity magma, could be really the result of a lava-type, low viscosity magma, released in a valley or basin that limited its movement. A more complex circumstance could also occur when the magma solidifies forming barriers for subsequent melt to come out, although clearly this situation would not play any role in large volume of magma outpourings. Thus, the upper dozens of meters of the conduit geometry in turn related to the shape of the crater and the magma rheology will be very important in the resulting landform type. Because of the obvious complexity and due to most of the times the construction of the volcanoes is not witnessed, the proposed classification scheme is based on geoforms, thus avoiding terminology complication associated with the source. **Figure 4** details the ideal geoforms when related to conduit and topography.

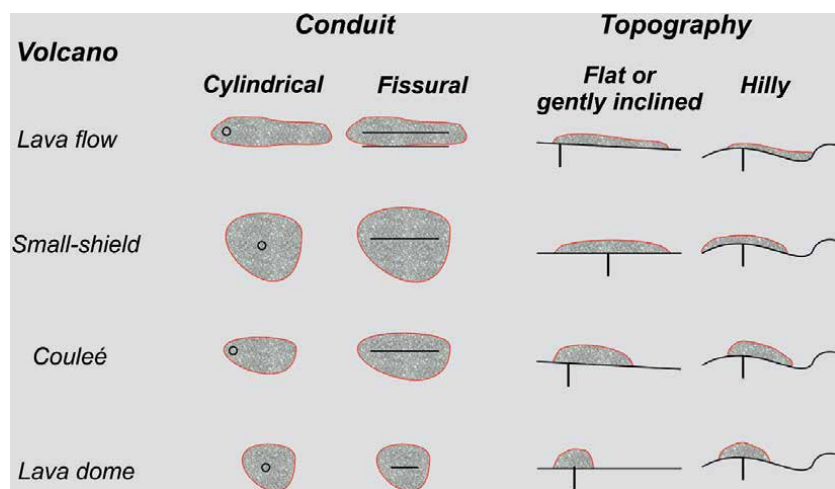


Figure 4. Volcanic geoforms vs. ascent conduit type and emplacement topography.

2.3 Magma releasing

Magma fragmentation is associated with bubble nucleation and growth. Thus, fragmentation occurs when the gas volume fraction reaches a critical value, i.e. when the magma changes from a liquid with bubbles to a medium of bubbles with liquid [40]. Bubbles, in turn, are a function of water diffusivity and melt viscosity during magma ascent and decompression; diffusivity is important for the feeding of the bubbles, while viscosity for allowing their growing [39]. Considering high efficiency of bubbles feeding and growing in a magma, it is possible to state that: a rapid decompression linked to a relative high ascent time, produces a high rate of bubbles nucleation, expansion and coalescence, and therefore a magma fragmentation to form a scoria/spatter cone. On the contrary, a slow decompression linked to a relative low ascent time, produces a low rate of bubbles nucleation; this yields to expansion, coalescence, channelling and the generation of a permeable network, which allows outgassing; the result is a magma reaching the surface without being fragmented, thus forming an effusive monogenetic volcano. In conclusion, effusive volcanoes in general are indicative of slow ascent times, at least, in the last part of their journey before reaching the Earth's surface.

3. Magma evolution

Although monogenetic volcanism is widely known as part of basaltic magmatic systems (e.g. [7, 27, 41]), it is also known as accompanying more complex mafic or even intermediate to acidic systems [42–48], thus indicating magmatic evolution during ascent. This evolution points to significant magma differentiation necessarily associated with low ascent rates or even magma crustal stagnation, and therefore evolution through processes such as fractional crystallisation and assimilation. This evolution is evidenced in the erupted magmas by trails such as: 1) the common presence of significant amount of intermediate plagioclase and mainly amphibole that requires relatively low magma temperatures to crystallise (<1000°C) (e.g. [10, 49, 50]), 2) the common presence of crustal xenoliths and xenocrysts indicating time for incorporation and partial or total dilution (e.g. [8]), 3) the almost ubiquitous wide range of liquid compositions of glass within the same products indicating microscale magma interaction/evolution while minerals are forming; this yields heterogeneous portions of magma (e.g. [51]), 4) the strong variation of trace elements at constant SiO₂ or MgO values within the same volcanic field (e.g. [10]), and 5) the diverse isotopic ratios indicating strong assimilation from the basement, also within the same volcanic field (e.g. [8, 26]). Magma mixing and self-mixing are possible additional processes linked to the magma evolution (e.g. [13, 43, 52]). Evidences of these are mineral disequilibrium textures (e.g. coronate, embayment, sieve, skeletal), reverse compositional zoning in minerals others than plagioclase (e.g. [53]), and also glass compositional differences in the same products [51]).

4. Magmatic plumbing systems

A magma plumbing system under a monogenetic volcanic field can be understood as a network of interconnected dikes and sills that reach the surface in several points via different pathways [54]. Usually, these fields are understood as originated by magma reaching the surface directly from the asthenosphere in

terms of weeks or months through simple conduits without any pattern [7]. This is evidenced in the very common primitive magmas and scattered volcanoes that characterise many volcanic fields (e.g. [55]). There is also a “common wisdom” that acidic compositions produce large monogenetic volcanoes only and that most of these volcanoes are related to magma chambers feeding polygenetic volcanoes [1] due to stagnation in the crust makes the magma batches un-eruptible [7]. However, typical (in volume) monogenetic volcanoes, which are intermediate to acidic in composition, are commonly forming monogenetic fields, thus indicating: 1) “normality” rather than “rarity”, and 2) stalling magma zones en route without cooling and crystallisation inhibiting the eruptivity. This stagnation has been evidenced as occurring within the lithosphere (e.g. [9]), particularly in the upper mantle-lower crust limit, or within the crust itself (e.g. [10, 12, 56], occasionally leaving small intrusive igneous bodies underneath the surface (e.g. [57]). This stagnation forming melt storage zones is a common geological explanation for many evolved monogenetic volcanic fields on different tectonic settings on Earth (e.g. [8, 11, 13, 14, 43, 52]). Thus, magmas coming to the planet surface directly from the asthenosphere tend to be mafic, while those coming from crustal melt storages tend to be either intermediate or felsic (**Figure 5**). Already near the surface, the eruptive style is driven by the internal magma characteristics but also by the external conditions linked to the lithology and the environment [27]. If the magmas do not reach the surface, they could form what would receive a name such as “monogenetic plutonic field.” Monogenetic volcanoes can also be associated with polygenetic volcanoes and therefore with magma chambers; in this case, the composition of the products is fully related to the processes involved in that chamber (**Figure 5**).

4.1 Examples

A well-known place on Earth where effusive monogenetic volcanoes are located is the Altiplano-Puna Volcanic Complex [58] in the Central Volcanic Zone in South America [59]. In this place, several of these volcanoes have been identified, usually

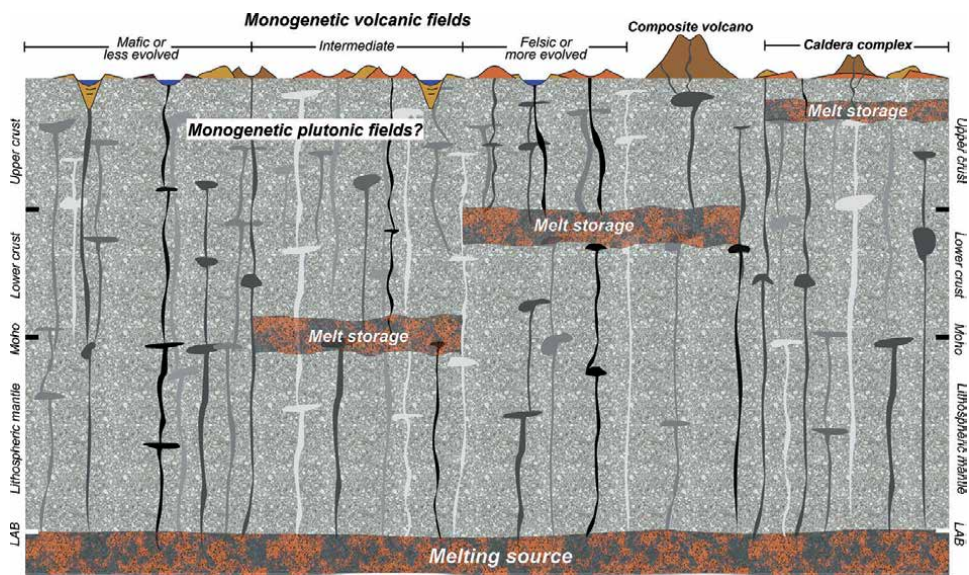


Figure 5. Schematic framework of magmatic plumbing systems for monogenetic volcanic fields. LAB: Lithosphere-Asthenosphere Boundary. Not to scale.

with intermediate compositions (e.g. SC2 shield-like volcano; [8]), and occasionally related to post-caldera activity (e.g. El Viejo Couleé, [60]). After several studies, it has been proposed partial melting zones linked to magma stagnation either around the Moho boundary or within the continental crust (e.g. [8, 10]).

The French Massif Central is another widely known example where effusive monogenetic volcanoes exist. The iconic Puy de Dôme [61] along with other effusive and explosive volcanoes (e.g. [62, 63], form the Chaîne des Puys volcanic field [64]. Volcanoes from this field have been interpreted as formed by magma detached from a melt storage or reservoir in the upper crust, where crystal fractionation plus self-mixing and minor crustal contamination occur (e.g. [13]).

In the west part of the Arabian shield [42, 52, 65], where mostly lava flows as effusive monogenetic emissions have occurred through time [66, 67], recent investigations have proposed a plumbing system composed of a melting region in the asthenosphere with magma stagnation zones in the upper part of the lower crust (e.g. [14]). Similarly, in the Colombian Andes, recently identified intermediate to acidic effusive monogenetic volcanoes forming volcanic fields have been linked to a plumbing system that include a magmatic reservoir located in the upper part of the lower crust [12]. This melt storage zone gives rise to the monogenetic volcanoes, but also to at least 10 composite volcanoes that exist in a 140 km-long volcanic chain.

Finally, it is important to mention the widely known Michoacán-Guanajuato Volcanic Field in México [68–71], where more than 1000 monogenetic volcanoes have been identified [72]. Lava domes, small-shields and lava flows are characteristic of there (e.g. [15, 16, 73]). Although most of the volcanoes seems to be mafic to intermediate (between 50 and 62 wt.% in SiO₂; [72]) some reach up to 69 wt.% (e.g. [11]), thus invoking crustal stagnation linked to evolution. Some others, however, seems to be the result of magmas detachment directly from the asthenosphere (e.g. [74]), as it also seems to occur in the Acigöl rhyolite field in Anatolia, Turkey [48], where interesting effusive volcano geofoms exist.

5. Conclusions

Small, short-lived and dispersed effusive monogenetic volcanoes are common in different tectonic settings. They can be mafic but also intermediate to silicic in composition and grouped in field arrangements with their explosive counterparts. The volcanoes are common in convergent plate margins like the Andean arc, but also in orogenic regions like Anatolia or intracontinental settings like Arabia or Sudan. Crustal stagnation is common and eventually ready to act as a “source of melt” in small volume and distinct release; this leads to magmatic plumbing systems related to sort of extensional tectonic, small-scale, regimes acting as “windows” for melt releasing, even in compressional regional settings.

In the monogenetic mafic systems, the chemical signatures most likely reflect the source processes (i.e. magma generation, source depth, melting rate, among others), however, in effusive, commonly silicic systems, these primary features are overprinted by the shallow storage and melt segregation signatures. This makes somehow more complex the understanding of the magma evolution. This adds to the fact that the recognition of such silicic effusive monogenetic volcanic systems in the geological record is not easy and requires some petrologic work and the understanding of the overall stress-field.

Finally, we emphasise that effusive monogenetic systems as a conceptual framework could work in volcanic fields overwhelmingly effusive, with a huge volume of effusive products or even classified as large igneous provinces.

Acknowledgements

Support from *Universidad de Caldas* to run a volcanology field course over four years that allowed to expand a greater collaboration between research students and researchers as well as to create an international expansion of collaborative works along the subject of this chapter is gratefully acknowledged.

Author details

Hugo Murcia^{1*} and Károly Németh²

1 Departamento de Ciencias Geológicas - Department of Geological Sciences, Instituto de Investigaciones en Estratigrafía (IIES), Universidad de Caldas, Manizales, Colombia

2 School of Agriculture and Environment, Massey University, Palmerston North, New Zealand

*Address all correspondence to: hugofmurcia@gmail.com

IntechOpen

© 2020 The Author(s). Licensee IntechOpen. This chapter is distributed under the terms of the Creative Commons Attribution License (<http://creativecommons.org/licenses/by/3.0>), which permits unrestricted use, distribution, and reproduction in any medium, provided the original work is properly cited. 

References

- [1] Németh, K. & G. Kereszturi, (2015). Monogenetic volcanism: personal views and discussion. *International Journal of Earth Sciences*. 104(8): 2131-2146.
- [2] Pioli, L., E. Erlund, E. Johnson, K. Cashman, P. Wallace, M. Rosi, & H. Delgado Granados, (2008). Explosive dynamics of violent Strombolian eruptions: The eruption of Parícutin Volcano 1943-1952 (Mexico). *Earth and Planetary Science Letters*. 271(1-4): 359-368.
- [3] Agustin-Flores, J., K. Németh, S.J. Cronin, J.M. Lindsay, G. Kereszturi, B.D. Brand, & I.E.M. Smith, (2014). Phreatomagmatic eruptions through unconsolidated coastal plain sequences, Maungataketake, Auckland Volcanic Field (New Zealand). *Journal of Volcanology and Geothermal Research*. 276: 46-63.
- [4] Murcia, H., K. Németh, N.N. El-Masry, J.M. Lindsay, M.R.H. Moufti, P. Wameyo, S.J. Cronin, I.E.M. Smith, & G. Kereszturi, (2015). The Al-Du'aythah volcanic cones, Al-Madinah City: implications for volcanic hazards in northern Harrat Rahat, Kingdom of Saudi Arabia. *Bulletin of Volcanology*. 77(6).
- [5] Botero-Gómez, L.A., P. Osorio, H. Murcia, C. Borrero, & J.A. Grajales, (2018). Campo Volcánico Monogenético Villamaría-Termale, Cordillera Central, Andes colombianos (Parte I): Características morfológicas y relaciones temporales. *Boletín de Geología*. 40(3): 85-102.
- [6] Kurszlaukis, S. & V. Lorenz, (2017). Differences and similarities between emplacement models of kimberlite and basaltic maar-diatreme volcanoes. In: K. Németh, G. Carrasco-Nuñez, J.J. Aranda-Gomez, & I.E.M. Smith, Editors, *Monogenetic Volcanism*, The Geological Society Publishing House: Bath, UK. p. 101-122.
- [7] Smith, I.E.M. & K. Németh, (2017). Source to surface model of monogenetic volcanism: a critical review. In: K. Németh, G. Carrasco-Nuñez, J.J. Aranda-Gomez, & I.E.M. Smith, Editors, *Monogenetic Volcanism*, The Geological Society Publishing House: Bath, UK. p. 1-28.
- [8] Mattioli, M., A. Renzulli, M. Menna, & P.M. Holm, (2006). Rapid ascent and contamination of magmas through the thick crust of the CVZ (Andes, Ollagüe region): Evidence from a nearly aphyric high-K andesite with skeletal olivines. *Journal of Volcanology and Geothermal Research*. 158(1-2): 87-105.
- [9] Bolos, X., J. Marti, L. Becerril, L. Planaguma, P. Grosse, & S. Barde-Cabusson, (2015). Volcano-structural analysis of La Garrotxa Volcanic Field (NE Iberia): Implications for the plumbing system. *Tectonophysics*. 642: 58-70.
- [10] Maro, G., P.J. Caffè, R.L. Romer, & R.B. Trumbull, (2017). Neogene Mafic Magmatism in the Northern Puna Plateau, Argentina: Generation and Evolution of a Back-arc Volcanic Suite. *Journal of Petrology*. 58(8): 1591-1618.
- [11] Pérez-Orozco, J.D., G. Sosa-Ceballos, V.H. Garduño-Monroy, & D.R. Avellán, (2018). Felsic-intermediate magmatism and brittle deformation in Sierra del Tzirate (Michoacán-Guanajuato Volcanic Field). *Journal of South American Earth Sciences*. 85: 81-96.
- [12] Murcia, H., C. Borrero, & K. Németh, (2019). Overview and plumbing system implications of monogenetic volcanism in the northernmost Andes' volcanic province. *Journal of Volcanology and Geothermal Research*. 383: 77-87.
- [13] Deniel, C., P. Boivin, D. Miallier, & M.C. Gerbe, (2020). Multi-stage

growth of the trachytic lava dome of the Puy de Dôme (Chaîne des Puys, France). Field, geomorphological and petro-geochemical evidence. *Journal of Volcanology and Geothermal Research*. 396: 106749.

[14] Stelten, M.E., D.T. Downs, D.E. Champion, H.R. Dietterich, A.T. Calvert, T.W. Sisson, G.A. Mahood, & H. Zahran, (2019). The timing and compositional evolution of volcanism within northern Harrat Rahat, Kingdom of Saudi Arabia. *GSA Bulletin*. 132(7-8): 1381-1403.

[15] Avellán, D.-R., G. Cisneros-Máximo, J.L. Macías, M.G. Gómez-Vasconcelos, P.W. Layer, G. Sosa-Ceballos, & J. Robles-Camacho, (2020). Eruptive chronology of monogenetic volcanoes northwestern of Morelia – Insights into volcano-tectonic interactions in the central-eastern Michoacán-Guanajuato Volcanic Field, México. *Journal of South American Earth Sciences*. 100: 102554.

[16] Gómez-Vasconcelos, M.G., J. Luis Macías, D.R. Avellán, G. Sosa-Ceballos, V.H. Garduño-Monroy, G. Cisneros-Máximo, P.W. Layer, J. Benowitz, H. López-Loera, F.M. López, & M. Pertón, (2020). The control of preexisting faults on the distribution, morphology, and volume of monogenetic volcanism in the Michoacán-Guanajuato Volcanic Field. *GSA Bulletin*. 132(11-12):2455-2474.

[17] Calder, E.S., Y. Lavallée, J.E. Kendrick, & M. Bernstein, (2015). Lava dome eruptions. In: *H. Sigurdsson, B. Houghton, S.R. McNutt, H. Rymer, & J. Stix, Editors, Encyclopedia of Volcanoes (2nd edition)*, Academic Press, Elsevier: USA. p. 343-362.

[18] Anderson, S.W. & J.H. Fink, (1990). The Development and Distribution of Surface Textures at the Mount St. Helens Dome. In: *J.H. Fink, Editor, Lava flows and Domes: Emplacement mechanisms*

and hazard implications - IAVCEI Proceedings in Volcanology 2., Springer: Berlin Heidelberg, New York. p. 25-46.

[19] Stewart, A.L. & J. McPhie, (2003). Internal structure and emplacement of an Upper Pliocene dacite cryptodome, Milos Island, Greece. *Journal of Volcanology and Geothermal Research*. 124(1-2): 129-148.

[20] Blake, S., (1990). The Development and Distribution of Surface Textures at the Mount St. Helens Dome., *J.H. Fink, Editor, Lava flows and Domes: Emplacement mechanisms and hazard implications - IAVCEI Proceedings in Volcanology 2.*, Springer: Berlin Heidelberg, New York. p. 88-126.

[21] Fink, J.H. & S.W. Anderson, (2000). Lava domes and coulees. In: *H. Sigurdsson, B. Houghton, S.R. McNutt, H. Rymer, & J. Stix, Editors, Encyclopedia of Volcanoes (first edition)*, Academic Press: San Diego. p. 307-319.

[22] Francis, P. & C. Oppenheimer, (2004). *Volcanoes*. Oxford: Oxford University Press.

[23] de Silva, S. & J.M. Lindsay, (2015). Chapter 15 - Primary volcanic landforms. In: *H. Sigurdsson, Editor, The Encyclopedia of Volcanoes (Second Edition)*, Academic Press: Amsterdam. p. 273-297.

[24] Greeley, R., (1982). The Snake River Plain, Idaho: Representative of a new category of volcanism. *Journal of Geophysical Research*. 87(B4): 2705-2712.

[25] Hare, A.G. & R.A.F. Cas, (2005). Volcanology and evolution of the Werribee Plains intraplate, basaltic lava flow-field, Newer Volcanics Province, southeast Australia. *Australian Journal Of Earth Sciences*. 52(1): 59-78.

[26] Sheth, H.C. & E. Canon-Tapia, (2015). Are flood basalt eruptions

monogenetic or polygenetic?

International Journal of Earth Sciences.
104(8): 2147-2162.

[27] Kereszturi, G. & K. Németh, (2012). Monogenetic basaltic volcanoes: genetic classification, growth, geomorphology and degradation. In: K. Németh, Editor, *Updates in Volcanology - New Advances in Understanding Volcanic Systems*, inTech Open: Rijeka, Croatia. p. 3-88.

[28] Zimanowski, B., R. Buettner, V. Lorenz, & H.-G. Haefele, (1997). Fragmentation of basaltic melt in the course of explosive volcanism. *Journal of Geophysical Research*. 102(B1): 803-814.

[29] Zimanowski, B., R. Buttner, & V. Lorenz, (1997). Premixing of magma and water in MFCI experiments. *Bulletin of Volcanology*. 58(6): 491-495.

[30] Wohletz, K.H. & M.F. Sheridan, (1983). Hydrovolcanic Explosions .2. Evolution Of Basaltic Tuff Rings And Tuff Cones. *American Journal Of Science*. 283(5): 385-413.

[31] Kereszturi, G., K. Németh, G. Csillag, K. Balogh, & J. Kovács, (2011). The role of external environmental factors in changing eruption styles of monogenetic volcanoes in a Mio/Pleistocene continental volcanic field in western Hungary. *Journal of Volcanology and Geothermal Research*. 201(1-4): 227-240.

[32] Ross, P.-S., S. Delpit, M.J. Haller, K. Nemeth, & H. Corbella, (2011). Influence of the substrate on maar-diatreme volcanoes - An example of a mixed setting from the Pali Aike volcanic field, Argentina. *Journal of Volcanology and Geothermal Research*. 201(1-4): 253-271.

[33] Borrero, C., H. Murcia, J. Agustin-Flores, M.T. Arboleda, & A.M. Giraldo, (2017). Pyroclastic deposits of San Diego maar, central Colombia: an example of a silicic magma-related

monogenetic eruption in a hard substrate. In: K. Németh, G. Carrasco-Núñez, J.J. Aranda-Gómez, & I.E.M. Smith, Editors, *Monogenetic Volcanism - Geological Society, London, Special Publications*, 446(1): London, UK. p. 361-374.

[34] Cashman, K.V. & B. Scheu, (2015). Magmatic fragmentation. In: H. H. Sigurdsson, B. Houghton, S.R. McNutt, H. Rymer, & J. Stix, Editors, *Encyclopedia of Volcanoes (2nd edition)*, Academic Press, Elsevier: USA. p. 459-471.

[35] Fries, C., (1953). Volumes and weights of pyroclastic material, lava, and water erupted by Paricutin volcano, Michoacan, Mexico. *EOS, Trans. Am. Geophys. Union*. 34(4): 603-616.

[36] Guilbaud, M.N., C. Siebe, P. Layer, S. Salinas, R. Castro-Govea, V.H. Garduno-Monroy, & N. Le Corvec, (2011). Geology, geochronology, and tectonic setting of the Jorullo Volcano region, Michoacan, Mexico. *Journal of Volcanology and Geothermal Research*. 201(1-4): 97-112.

[37] Luhr, J.F. & I.S.E. Carmichael, (1985). Jorullo volcano, Michoacan, Mexico (1759-1774): the earlier stages of fractionation in calc-alkaline magmas. *Contribution to Mineralogy and Petrology*. 90: 142-161.

[38] Luhr, J.F. & T. Simkin, (1993). *Paricutin. The volcano born in a Mexican cornfield.*, Phoenix: Geosciences Press. 427.

[39] Burgisser, A. & W. Degruyter, (2015). Chapter 11 - Magma Ascent and Degassing at Shallow Levels. In: H. Sigurdsson, Editor, *The Encyclopedia of Volcanoes (Second Edition)*, Academic Press: Amsterdam. p. 225-236.

[40] Cashman, K.V. & J. Blundy, (2000). Degassing and crystallization of ascending andesite and dacite. *Philosophical Transactions of the*

Royal Society of London. Series A: Mathematical, Physical and Engineering Sciences. 358(1770): 1487-1513.

[41] McGee, L.E., M.-A. Millet, I.E.M. Smith, K. Nemeth, & J.M. Lindsay, (2012). The inception and progression of melting in a monogenetic eruption: Motukorea Volcano, the Auckland Volcanic Field, New Zealand. *Lithos.* 155: 360-374.

[42] Camp, V.E., M.J. Roobol, & P.R. Hooper, (1991). The Arabian continental alkali basalt province; Part II, Evolution of harrats Khaybar, Ithnayn, and Kura, Kingdom of Saudi Arabia; with Suppl. Data 91-06. *Geological Society of America Bulletin.* 103(3): 363-391.

[43] Franz, G., C. Breitzkreuz, D.A. Coyle, B. El Hur, W. Heinrich, H. Paulick, D. Pudlo, R. Smith, & G. Steiner, (1997). The alkaline Meidob volcanic field (Late Cenozoic, northwest Sudan). *Journal of African Earth Sciences.* 25(2): 263-291.

[44] Franz, G., G. Steiner, F. Volker, D. Pudlo, & K. Hammerschmidt, (1999). Plume related alkaline magmatism in central Africa - the Meidob Hills (W Sudan). *Chemical Geology.* 157(1-2): 27-47.

[45] Riggs, N.R., J.C. Hurlbert, T.J. Schroeder, & S.A. Ward, (1997). The interaction of volcanism and sedimentation in the proximal areas of a mid-tertiary volcanic dome field, central Arizona, USA. *Journal of Sedimentary Research.* 67(1): 142-153.

[46] Németh, K. & M.R. Moufti, (2017). Geoheritage values of a mature monogenetic volcanic field in intra-continental settings: Harrat Khaybar, Kingdom of Saudi Arabia. *Geoheritage.* 9(3): 311-328.

[47] Kósik, S., M. Bebbington, & K. Németh, (2020). Spatio-temporal hazard estimation in the central

silicic part of Taupo Volcanic Zone, New Zealand, based on small to medium volume eruptions. *Bulletin of Volcanology.* 82(6): 50.

[48] Siebel, W., A.K. Schmitt, E. Kiemele, M. Danisik, & F. Aydin, (2011). Acigol rhyolite field, central Anatolia (part II): geochemical and isotopic (Sr-Nd-Pb, delta O-18) constraints on volcanism involving two high-silica rhyolite suites. *Contributions to Mineralogy and Petrology.* 162(6): 1233-1247.

[49] Grove, T.L., L.T. Elkins-Tanton, S.W. Parman, N. Chatterjee, O. Müntener, & G.A. Gaetani, (2003). Fractional crystallization and mantle-melting controls on calc-alkaline differentiation trends. *Contributions to Mineralogy and Petrology.* 145(5): 515-533.

[50] Putirka, K.D., (2008). Thermometers and barometers for volcanic systems. In: *K.D. Putirka & F.J. Tepley, Editors, Minerals, Inclusions and Volcanic Processes - Reviews in Mineralogy and Geochemistry* 69, Mineralogical Society of America and Geochemical Society: USA. p. 61-120.

[51] Salazar-Muñoz, N., C.A. Ríos de la Ossa, H. Murcia, D. Schonwalder-Angel, L.A. Botero-Gómez, G. Hincapie, & J.C. Da Silva, (2020). Evolved (SiO₂: ~60 wt.%) monogenetic volcanism in the northern Colombian Andes: Crystallisation history of three Quaternary lava domes. *Journal of Volcanology and Geothermal Research [in review]*.

[52] Camp, V.E. & M.J. Roobol, (1989). The Arabian continental alkali basalt province; Part I, Evolution of Harrat Rahat, Kingdom of Saudi Arabia; with Suppl. Data 89-04. *Geological Society of America Bulletin.* 101(1): 71-95.

[53] Laeger, K., R. Halama, T. Hansteen, I.P. Savov, H.F. Murcia, G.P. Cortés, & D. Garbe-Schönberg, (2013).

Crystallization conditions and petrogenesis of the lava dome from the ~900 years BP eruption of Cerro Machín Volcano, Colombia. *Journal of South American Earth Sciences*. 48: 193.

[54] Burchardt, S. & O. Galland, (2016). Studying volcanic plumbing systems; multi-disciplinary approaches to a multi-faceted problem. In: K. Nemeth, Editor, *Updates in Volcanology – From Volcano Modelling to Volcano Geology* inTech Open: Rijeka, Croatia. p. 23-53.

[55] McGee, L.E., I.E.M. Smith, M.-A. Millet, H.K. Handley, & A.M. Lindsay, (2013). Asthenospheric Control of Melting Processes in a Monogenetic Basaltic System: a Case Study of the Auckland Volcanic Field, New Zealand. *Journal of Petrology*. 54(10): 2125-2153.

[56] Londono, J.M., (2016). Evidence of recent deep magmatic activity at Cerro Bravo-Cerro Machín volcanic complex, central Colombia. Implications for future volcanic activity at Nevado del Ruiz, Cerro Machín and other volcanoes. *Journal of Volcanology and Geothermal Research*. 324: 156.

[57] Jaramillo, J.S., A. Cardona, G. Monsalve, V. Valencia, & S. León, (2019). Petrogenesis of the late Miocene Combia volcanic complex, northwestern Colombian Andes: Tectonic implication of short term and compositionally heterogeneous arc magmatism. *Lithos*. 330: 194.

[58] de Silva, S.L., (1989). Geochronology and stratigraphy of the ignimbrites from the 21°30'S to 23°30'S portion of the Central Andes of northern Chile. *Journal of Volcanology and Geothermal Research*. 37: 93-131.

[59] Stern, C.R., (2004). Active Andean volcanism: its geologic and tectonic setting. *Revista Geologica De Chile*. 31(2): 161-206.

[60] Bustos, E., W.A. Báez, L. Bardelli, J. McPhie, A. sola, A. Chiodi, V. Simón, & M. Arnosio, (2020). Genesis of megaspherulites in El Viejo Rhyolitic Coulee (Pleistocene), Southern Puna, Argentina. *Bulletin of Volcanology*. 82: 43.

[61] Miallier, D., P. Boivin, C. Deniel, A. Gourgaud, P. Lanos, M. Sforza, & T. Pilleyre, (2010). The ultimate summit eruption of Puy de Dôme volcano (Chaîne des Puys, French Massif Central) about 10,700 years ago. *Comptes Rendus Geoscience*. 342: 847.

[62] Miallier, D., T. Pilleyre, P. Boivin, P. Labazuy, L.S. Gailler, & J. Rico, (2017). Grand Sarcoui volcano (Chaîne des Puys, Massif Central, France), a case study for monogenetic trachytic lava domes. *Journal of Volcanology and Geothermal Research*. 345: 125-141.

[63] Colombier, M., L. Gurioli, T.H. Druitt, T. Shea, P. Boivin, D. Miallier, & N. Cluzel, (2017). Textural evolution of magma during the 9.4-ka trachytic explosive eruption at Kilian Volcano, Chaîne des Puys, France. *Bulletin of Volcanology*. 79(2).

[64] Boivin, P. & J.-C. Thouret, (2014). The Volcanic Chaîne des Puys: A Unique Collection of Simple and Compound Monogenetic Edifices, M. In: Fort & M.-F. André, Editors, *Landscapes and Landforms of France*, Springer Netherlands: Dordrecht. p. 81-91.

[65] Camp, V.E., P.R. Hooper, M.J. Roobol, & D.L. White, (1987). The Madinah eruption, Saudi Arabia: Magma mixing and simultaneous extrusion of three basaltic chemical types. *Bulletin of Volcanology*. 49(2): 489-508.

[66] Moufti, M.R., A.M. Moghazi, & K.A. Ali, (2013). Ar-40/Ar-39 geochronology of the Neogene-Quaternary Harrat Al-Madinah

intercontinental volcanic field, Saudi Arabia: Implications for duration and migration of volcanic activity. *Journal of Asian Earth Sciences*. 62: 253-268.

[67] Murcia, H., K. Nemeth, M.R. Moufti, J.M. Lindsay, N. El-Masry, S.J. Cronin, A. Qaddah, & I.E.M. Smith, (2014). Late Holocene lava flow morphotypes of northern Harrat Rahat, Kingdom of Saudi Arabia; implications for the description of continental lava fields. *Journal of Asian Earth Sciences*. 84: 131-145.

[68] Hasenaka, T. & I.S.E. Carmichael, (1985). A compilation of location, size, and geomorphological parameters of volcanoes of the Michoacan-Guanajuato volcanic field, central Mexico. *Geofisica Internacional*. 24(4): 577-608.

[69] Hasenaka, T. & I.S.E. Carmichael, (1985). The cinder cones of Michoacán-Guanajuato, central Mexico: their age, volume and distribution, and magma discharge rate. *Journal of Volcanology and Geothermal Research*. 25: 105-124.

[70] Hasenaka, T., (1985). Differentiation of cinder cone magmas from the Michoacan-Guanajuato volcanic field, central Mexico. *Abstracts with Programs - Geological Society of America*. 17(7): 605-605.

[71] Hasenaka, T., (1994). Size, Distribution, and Magma Output Rate for Shield Volcanos of the Michoacan-Guanajuato Volcanic Field, Central Mexico. *Journal of Volcanology and Geothermal Research*. 63(1-2): 13-31.

[72] Hasenaka, T. & I.S.E. Carmichael, (1987). The cinder cones of Michoacan-Guanajuato, central Mexico: Petrology and chemistry. *Journal of Petrology*. 28: 241-269.

[73] Osorio-Ocampo, S., J. Luis Macias, A. Pola, S. Cardona-Melchor, G. Sosa-Ceballos, V. Hugo Garduno-Monroy,

P.W. Layer, L. Garcia-Sanchez, M. Perton, & J. Benowitz, (2018). The eruptive history of the Patzcuaro Lake area in the Michoacan Guanajuato Volcanic Field, central Mexico: Field mapping, C-14 and Ar-40/Ar-39 geochronology. *Journal of Volcanology and Geothermal Research*. 358: 307-328.

[74] Losantos, E., J.M. Cebria, D.J. Moran-Zenteno, B.M. Martiny, J. Lopez-Ruiz, & G. Solis-Pichardo, (2017). Petrogenesis of the alkaline and calkalkaline monogenetic volcanism in the northern sector of the Michoacan-Guanajuato Volcanic Field (Central Mexico). *Lithos*. 288: 295-310.

Study of Monogenic Volcanism in a Karstic System: Case of the Maar of Lechmine n'Aït el Haj (Middle Atlas, Morocco)

*Sara Mountaj, Hassan Mhiyaoui, Toufik Remmal,
Samira Makhoukhi and Fouad El Kamel*

Abstract

The Lechmine n'Aït el Haj maar (LNH) is a mixed phreatomagmatic-strombolian vent located in the Causse of the Middle Atlas. The application of tephrostratigraphic, and geophysical studies to the volcanoclastic deposits allowed interpreting the volcanic dynamics of this volcano set up during the Quaternary. Pyroclastic deposits allow us to understand the chronology of the eruptions. These are organized in four eruptive phases. The basal sequences are phreatomagmatic, followed by a strombolian unit. The last activity of LNH is phreatomagmatic. The structural analysis revealed a localized distension signed by fracture geometry, the mixed nature of the volcanism, tectonic markers, and the mechanisms of syn-eruptive tectonics. This subsidence, controlled by the NW-SE to WNW-ESE directions tends towards a strike-slip regime fault NE-SW during the phreatomagmatic-strombolian transition. The latter is favored by the position of the LNH volcano on the path of faults of cryptokarstic origin. The LNH maar is one of numerous well preserved monogenic volcanoes of the Causse of the Middle Atlas. The appropriation of this geoheritage is very important for tourism and territorial development of the region.

Keywords: Lechmine n'Aït el Haj, maar, karst, monogenetic volcanoes, geoheritage, Middle Atlas

1. Introduction

Monogenetic volcanic provinces have recently attracted the interest of volcanologists especially in intracontinental settings [1, 2]. The Middle Atlas Volcanic Province (MAVP) is an example of those small volcanic systems with dispersed magmatic plumbing systems that erupt predominantly basaltic magmas [3, 4].

In the last thirty years, many studies have concerned the volcanism of the Middle Atlas. A hundred of cones and maars have been listed and mapped over an area of almost 1000 km² [5, 6]. The distribution of volcanoes is controlled by the tectonic context of the region [7, 8]. The petrological study of eruptive vents allowed distinguishing four lava types dominated by under-saturated alkali basaltic flows (68.5%). The basanites cover 22.5% of the plateau surface, the subalkaline basalts cover 7.8%, and finally the nephelinite with the smallest proportion

(1,2%). The three first types are exclusively Plio-Quaternary (3.77–0.60 Ma), the K-Ar age of the last one is Middle Miocene (16.25–5.87 Ma), and Plio-Quaternary (3.92–0.67 Ma) [9]. This magmatism results from a partial melting that occurred at around 2 GPa, i.e. near the lithosphere–asthenosphere boundary beneath the Middle Atlas (60–80 km) [10]. The analysis of the Middle Atlas aeromagnetic data allowed the characterization of the regional magnetic anomalies, their location and delimitation corresponding to the major accidents of the Middle Atlas [11, 12].

30% of MAVP volcanoes are represented by maar-diatreme-type volcanic systems [6]. They have a negative shape forming a crater that intersects the pre-eruptive surface. Lechmine n'Aït el Haj is the first maar ever studied in this region. After a previous work on the analysis of the eruptive sequence of the maar [13], the aim of this chapter is to understand the structural context of the formation of this maar and its eruptive dynamic.

2. General features of monogenic volcanism

Magma system volumes can occur in an intraplate context devoid of a mantle plume [14]. This type of volcanism is characterized by “small” volcanoes with magmatic system often basaltic [4–6], derived mostly from a mantle that stays in the crust just the time to allow a minor fractional crystallization [15]. These monogenic volcanic fields occur in any tectonic setting [2, 16–18], not only on Earth but also on other planets such as Mars [19].

Much research has been done on monogenic volcanoes, focusing on their nature from source to surface [15, 20]. The rapid ascent of magma and the short eruptive history of volcanoes allow to understand, for example, the magmatic evolution of the systems that fed several small volcanoes over long periods of time (millions of years) [21, 22].

In many cases, the eruptive style is controlled not only by the internal properties of the magma but also by the external environmental conditions to which it has been exposed. The resulting morphology is often related to the mechanism of the dominant eruptive style, making it important criteria in the study and especially in the classification. The estimated time for the formation of these volcanoes is in the order of a few days to a decade [23].

Monogenic volcanoes are referred to as the product of a single eruption [24], however, a magma ascent is not always related to a single magma influx, which usually involves several episodes producing a geochemical evolution even over a single eruption [15, 20, 25]. This magma may come directly from the mantle or from a volume of magma trapped in a zone of contrasting density, such as the upper mantle/crustal boundary [25]. The magma ascension begins with an inter-connectivity between the small volumes of magma in the mantle and their vertical migration forming dykes [26, 27]. These dykes generally follow pre-existing structures such as faults of the basement rocks as they move towards the surface [28].

The magma of monogenic volcanoes is often primitive. It rarely expresses itself individually; it tends to form several monogenic volcanoes in a volcanic field, where there may be tens or even thousands of individual volcanoes [29]. However, a monogenic volcanic field could experience repeated monogenic eruptions across a broad area over millions of years [30].

Once a batch (or batches) of magma begins its ascent to the surface, it faces continuous outgassing and interactions with the host environment. Once at the surface, this magma can produce a volcanic eruption that can be explosive or effusive. This is controlled by the characteristics of the eruption which are determined at a superficial depth ($\leq 1\text{--}2$ km) by the balance between internal and external factors [4].

3. The Middle Atlas Volcanic Province (MAVP)

The Atlas mountain chain is the result of the Oligocene compression induced by the Europe–Africa convergence and continent–continent collision. Its basement is structured during the Hercynian orogeny [$307,5 \pm 6,8$ – $364,0 \pm 8,2$] [31]. It is continental and outcrops only at a few inlier [32]. The cover consists mainly of Jurassic deposits. It is deformed in the folded Middle Atlas, whereas it is sub-tabular in the Causse of the Middle Atlas [32]. This latter zone is distinguished with a simple structural style of inclined blocks, manifesting itself in the topography by a succession of subhorizontal layers (Tabular Middle Atlas). It is the area where the Plio-Quaternary volcanism occurred with a hundred of eruptive centers aligned in a sub-meridian direction (**Figure 1**). It is crossed by the Tizi n'Tritten Fault (TTF) and a network of faults between the North Middle Atlas Fault NMAF and TTF. All these accidents, which are at least Hercynian, from direction N45 to N70, affect the recent Quaternary deposits [8].

The emission points located between Azrou and Timahdite have an NNW–SSE orientation along 50 km. The basalt flow covers the ancient Quaternary formations up to the Saïs plain in the north (**Figure 1**). They are channeled to the East by the

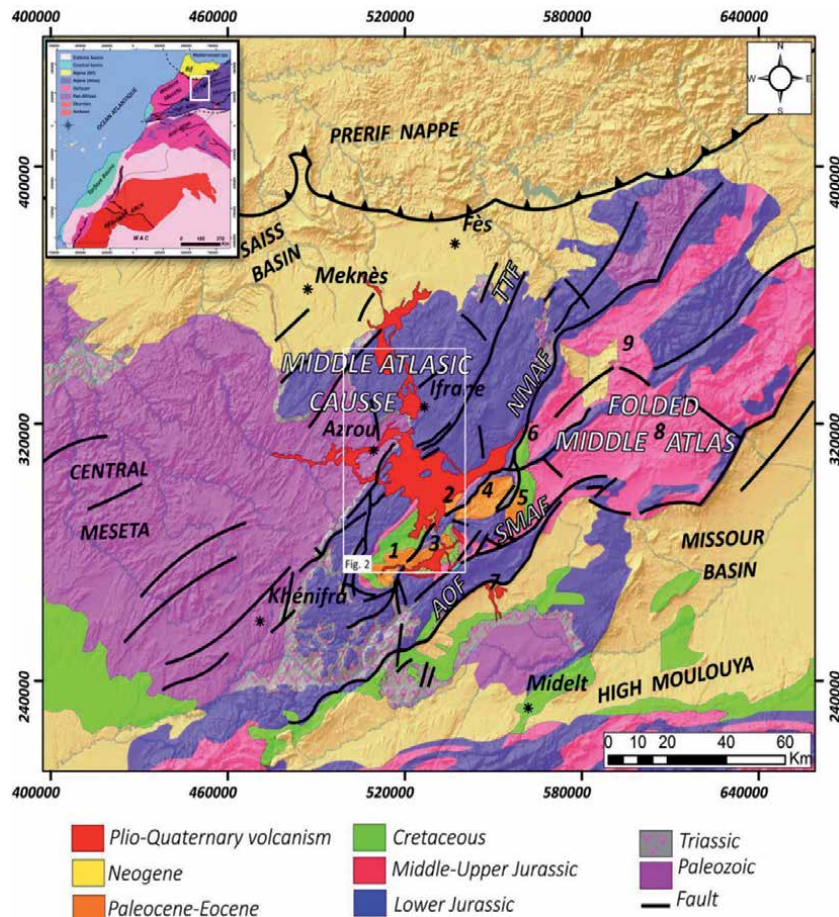


Figure 1. Structural map of the Middle Atlas with the location of the volcanic field [33]. SMAF: South Middle Atlas fault, AOF: Ait Oufella fault, NMAF: North Middle Atlas fault, TTF: Tizi n'Tretien fault. Jurassic, cretaceous, and Paleogene synclines: 1: Bekrite, 2: Timahdite, 3: Bou-Anguer, 4: Aïn-Nokra, 5: Oudiskou, 6: Tirhboula, 7: Ait Oufella, 8: El-Mers, 9: Guigou.

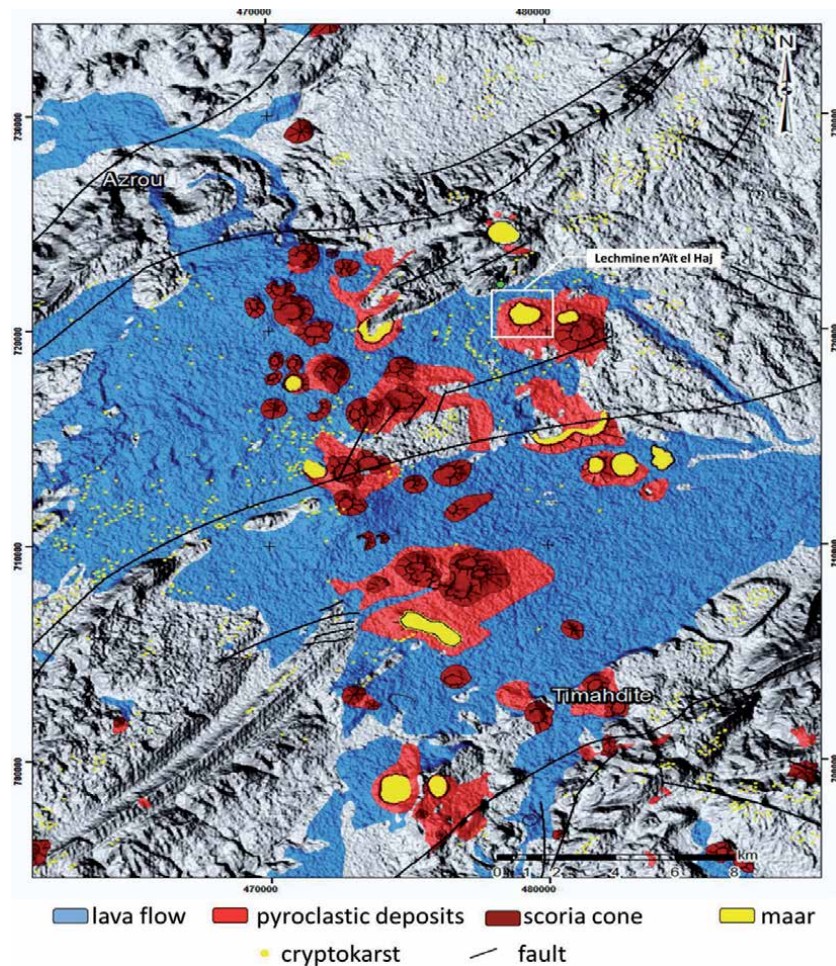


Figure 2. Geographical location of the study area. Most of the volcanoes and lava flow units are settled between Azrou and Timahdite where the cryptokarstic cavities are dominating.

depression of the Guigou Valley and to the West by the Wadis of the Beht and Oum Rbia. Most of the volcanoes are strombolian (70%) disseminated in the entire volcanic area. on the other hand, maars are focused in the eastern part of the volcanic province [5] (**Figure 2**). The karstic-carbonate nature of the region combined with the fluctuations in rainfall contributes to the formation of the water table in the epikarstic level [34, 35]. The variation of the karstic water at this level has an impact on the volcanic dynamic and the changing of the eruptive style. In The MAVP, 8% of volcanic vents have witnessed a shifting between wet and dry dynamics during the same monogenic eruption [5].

4. Case of study: the Lechmine n’Ait el Haj maar

4.1 Lithology and deposition process

The Lechmine n’Ait El Haj maar is located in the volcanic plateau near Azrou, in the eastern part of the province (**Figure 2**). The maar deposits are mainly formed of pyroclastic breccia consisting of accidental lithics extracted from the substrate

associated with juvenile fragments, and volcanic ash. Several lithological sections were established around the rim of the LNH crater, using a graphical semiology that shows the cadence of the eruptive sequences and their variability according to the nature of the activity phase (**Figure 3**). Two criteria allowed understanding the environmental condition at the time of the eruption: The outcrop of the Liasic limestone, and the lacustrine deposits in the northern flank of the maar.

The LNH maar is set on the limestone of the Middle Lias. It occupies less surface comparing to the dolomite of the Lower Lias in the Causse of Middle Atlas. The distribution of limestone follows often the structural undulations in the region [6]. With their white color, their stratification is clearly visible. Typical karstic forms (lapiez) are distinguished at the surface.

On the northern flank, between the limestone and the first phreatomagmatic unit appears a 1,5 m thick level of reddish deposits (**Figure 4a**). This facies appears also in small outcrops cleared by streams (**Figure 4b**). It is formed by a mixture of fine tuffs and clay interspersed with centimetric levels of breccia with juvenile and limestone fragments (4 mm to 4 cm) (**Figure 4d**). This aspect indicates an

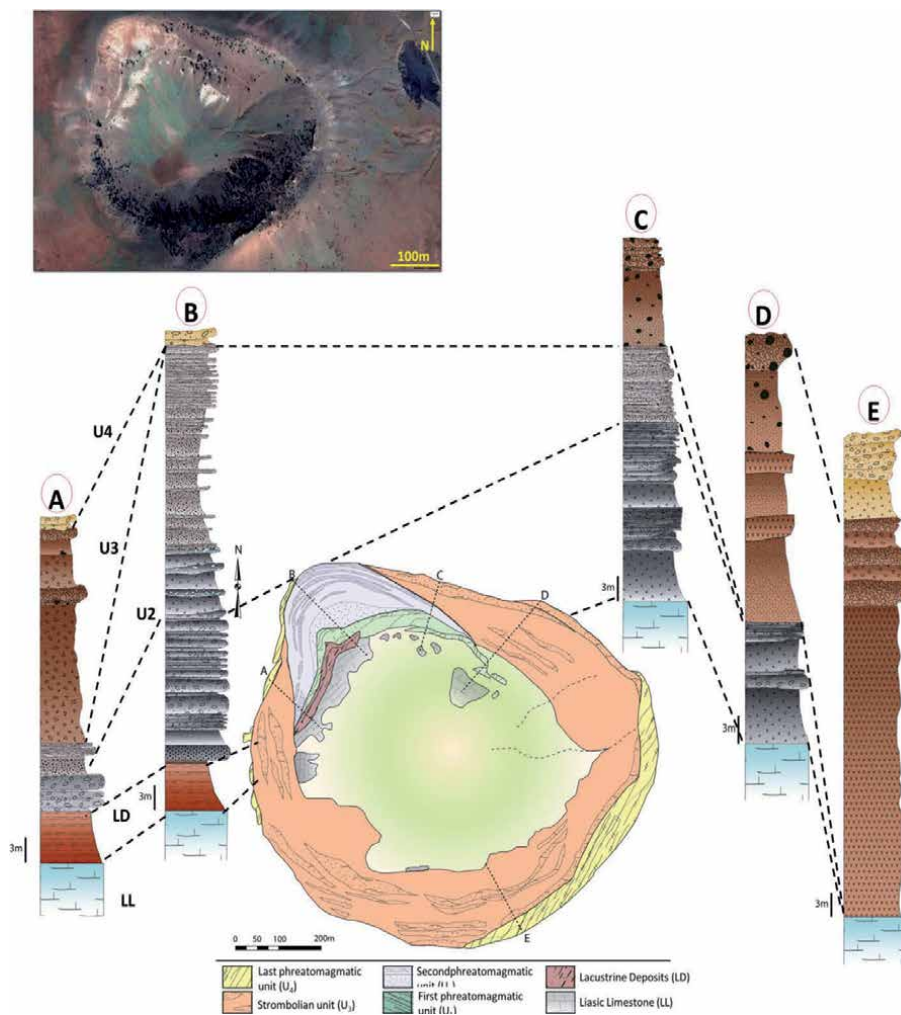


Figure 3. Volcanic map of the maar of Lechmine n'Ait el Haj in the Causse of the Middle Atlas with logs describing the evolution of the eruptive dynamics of the maar.



Figure 4. The lacustrine deposits at the base of the first phreatomagmatic unit (U_1) of the maar of Lechmine n'Ait el Haj.

explosive dynamism that occurred while the sediment was still rich in water. Towards the summit appears fine gray ash overlain by gray and reddish vacuolar and scoriaceous beds revealing the eruptions that preceded the hydromagmatic explosion (**Figure 4c**). A palynological analysis was carried out on these lacustrine deposits at the GEOBIO laboratory of the Scientific Institute of Rabat. It showed that these deposits are extremely poor in palynomorphs. The gray deposits are rich in bisaccate called “Pinus pollens” that have existed from the Paleozoic to the present day [36, 37].

The tephrostratigraphic sequence of deposits shows color and dip variation corresponding to four eruptive phases (U_1 – U_4). The first two units are describing a phreatomagmatic activity with heterogeneous lithology; U_1 is highlighted by alternating beds of variable thickness rich in limestone blocks, while U_2 shows relatively thin regular bedding compared to the first deposit, with a white basal level formed almost of blocks and fragments of accidental lithics overlain by another level of red

scoriaceous to finely pulverized fragments. The third unit (U3) results from strombolian activity. Its eruptive products are composed of massive breccia tuffs rich in volcanic bombs and mantle-derived xenoliths. The activity of the maar ends with a final phreatomagmatic activity highlighted by the deposition of pyroclastic breccia located in the north and south of the crater [13].

4.1.1 *The phreatomagmatic phase*

The first phreatomagmatic deposits show a heterogeneous lithology characterized by the association of juveniles formed by basalts and accidental lithics from the substratum of limestone. The pyroclastic projections fall around the maar in crossed strata centered on an axis that describes a semi-annular geometry. Depending on the abundance, size, and sequential organization of the constituent elements, the phreatomagmatic unit is subdivided into two units U1 and U2 [13].

Unit 1: it corresponds to the initial explosive phase, declined in two sequences of deposits with a weak external dip of 15° to 20° (**Figure 5a**). These two sequences indicate a variation in fragmentation intensity during the activity of the maar. The first phase (U1a) of vent opening is highlighted by an alternation of beds of variable thickness between 50 cm and 1.5 m, composed of breccia and fine tuffs, rich in accidental lithics (1 to 10 cm in diameter) (**Figure 5b**). In the second stage (U1b) describes thin regular bedding compared to the first deposit with a clear decrease in the accidental lithic and an increase of juveniles (**Figure 5c**). The beds at the base correspond to lapilli-tuffs with calcareous interstitial ramifications, resulting from the circulation of water.

Unit 2: It shows a succession of heterogeneous cross-bedded layers of lapilli tuffs (**Figure 6a**). It is distinguished by a white color at the bottom (U2a) because of the abundance of blocks and fragments of accidental lithics (**Figure 6d**). This level indicates the resumption of hydromagmatic activity since enclaves of breccias from the first explosion are packed into the deposit (**Figure 6b**). It is overlain by (U2b), a thick column (40 to 50 m) of parallel, locally crossbedded, strata, formed essentially of scoriaceous to finely red pulverized material interspersed with fine beds of accidental lithics (**Figure 6c**). In this unit a range of sedimentation features characterizing maar projections are observed, notably mud crack at the summit of the phreatomagmatic deposit (**Figure 6e**).

4.1.2 *The strombolian phase*

The maar is surrounded on the northern and southern sides by strombolian deposits (U3) (**Figure 7a**) which announces the transition to an activity where water participation has substantially decreased. The first deposits on the eastern and southern flanks are essentially rust-colored, centimetric scoria, well-classified, more or less vesicular (U3a) (**Figure 7b**). They correspond to pyroclastic fallout from a plume. The color variations indicate a beginning of alteration suggesting that the pyroclastics were wet at the time of their deposition. The beds become heteromeric with centimetric scoria with dense and angular bombs. Towards the top, the fallout has a relatively chaotic character (U3b). The hot fallout can weld together locally and form conical accumulations of scoria (spatter cones), piled up lava, and blocks or bombs of lava (**Figure 7c**). The summit of this unit is composed of a mixture of scoria and bombs (U3c). The whole is globally homogeneous with a reddish color due to hot oxidation. It is an eruption in a regular regime but with some slightly more powerful explosions; levels richer in bombs (**Figure 7d**). On the western flank, the U3c unit is poorly deposited. The lava flow that caps U3b is formed by agglutination

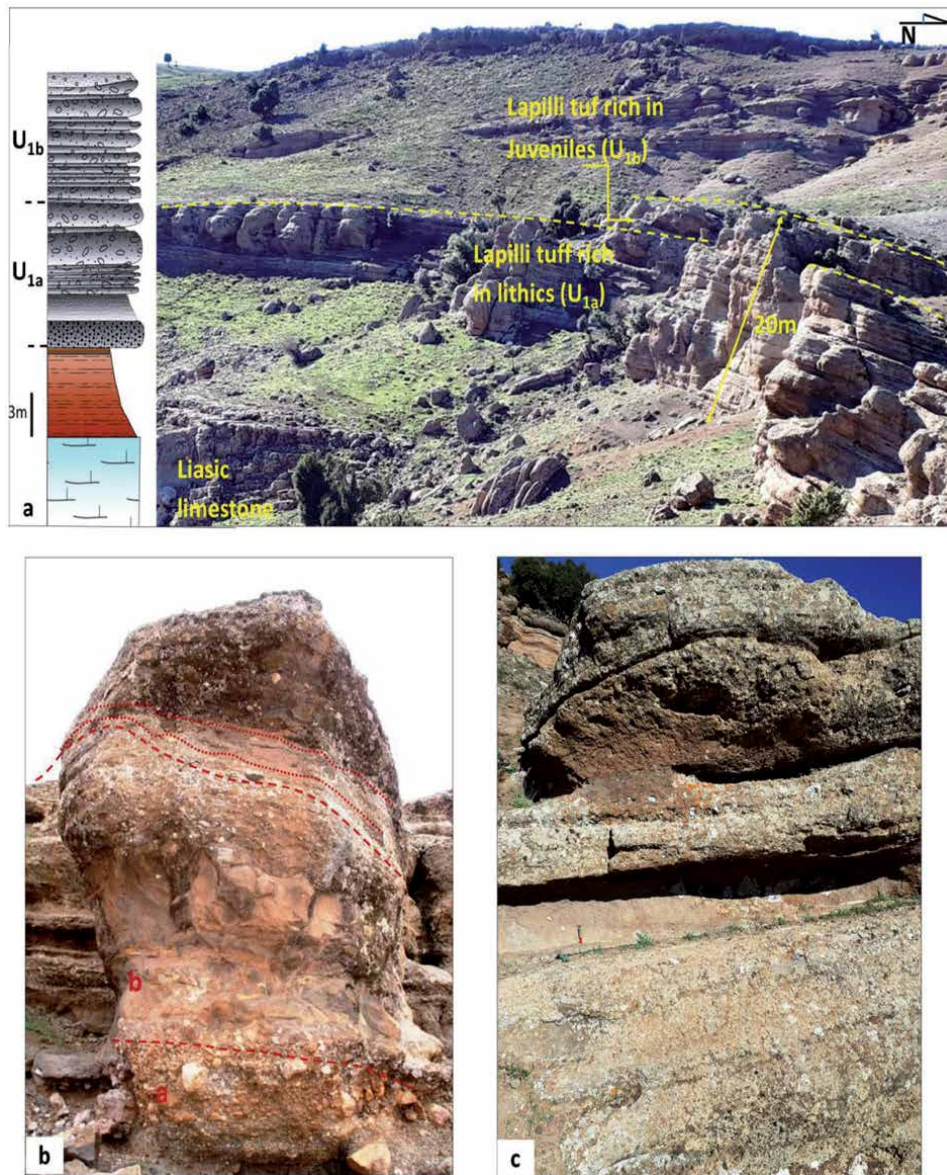


Figure 5. The northern flank of the Lechmine n'Aït el Haj crater; (a) the contact between the limestone base and the first phreatomagmatic phase (U₁); (b) the first sequence (U_{1a}) showing an opening facies with unsorted accidental lithics (level a) and beds rich in scoriaceous basalt (level b); (c) the second sequence (U_{1b}) with regular and less thick bedding, where the proportion of accidental lithics decrease.

of packages of low-viscosity lava flowing towards the center of the crater (**Figure 8**), through a path oriented ENE-WSW probably linked to a sectorial collapse.

4.1.3 Terminal phreatomagmatic deposits

The activity of LNH ended with a phreatomagmatic phase, highlighted by the deposition of pyroclastic lapilli tuff layers thicker on the northern flank of the maar (10 to 15 m) than on the southern flank (2 m to 5 m). This unit (U₄) is formed essentially of scoria and rare lava blocks mixed with accidental lithics. The whole forms a rhythmic sequence that is particularly well represented on the southern flank (**Figure 9**).

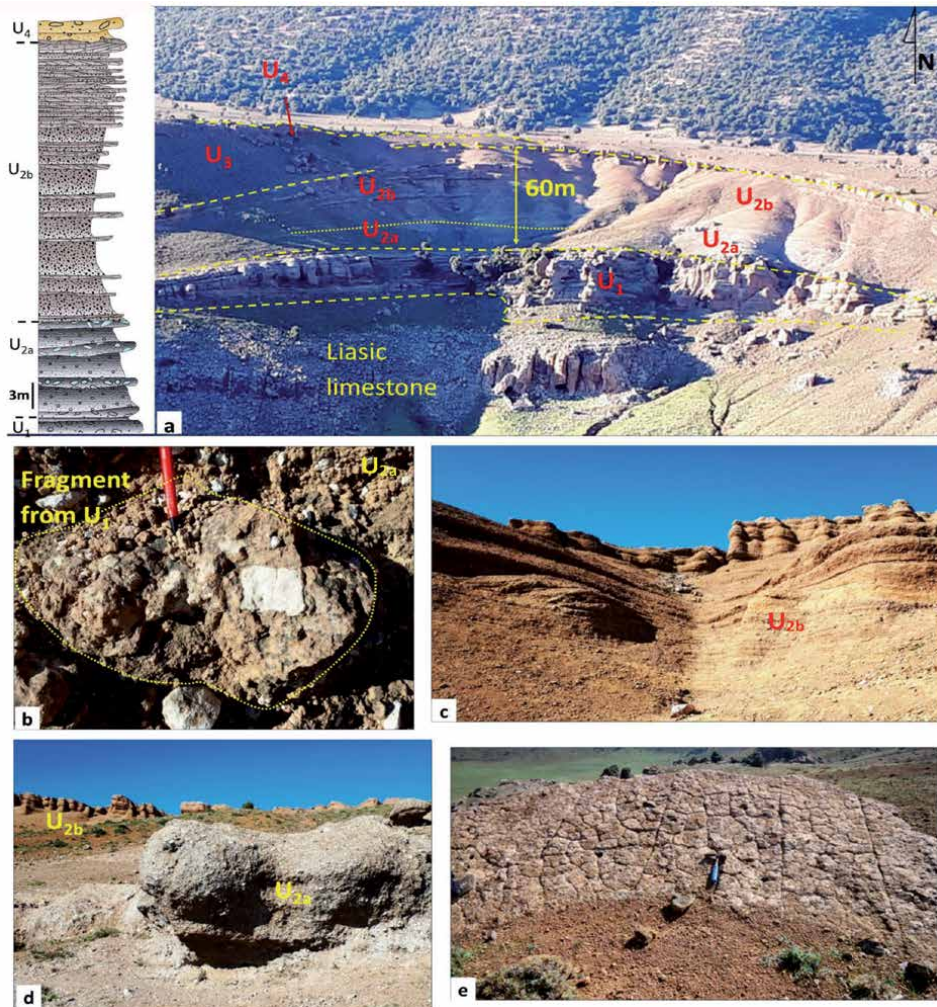


Figure 6. Volcanic lithofacies accompanying the two sequences U_{2a} and U_{2b} of the second phreatomagmatic phase (U₂); (a) the succession of the first and the second sequence of U₂ (U_{1a} and U_{2b}) with varying thicknesses and compositions; (b) enclave of the first phreatomagmatic phase (U₁) packed in the fallout of the second phreatomagmatic phase (U_{2a}); (c) the second sequence (U_{2b}) with reddish color richer in juvenile pyroclasts; (d) variation of composition and color between U_{2a} and U_{2b}. (e) Mud cracks structure at the summit of U_{2b}.

4.2 Volcanic dynamics and structural context of the formation of Lechmine n'Ait el Haj

The LNH maar is set on the path of the Lbouatène tectonic corridor (ALB) (Figure 2), between the Fault of Tizi n'Traten (TTF) and North Middle Atlas Fault (NMAF). This area is particularly distinguished with cryptokarst cavities. These are aligned according to the orientations of the major faults in the Causse of the Middle Atlas (Figures 2, 10). It has been shown [8] that the formation of the cryptokarsts in the Quaternary basaltic flow is controlled by the fracturing. Around the maar, the cryptokarstic cavities are arranged in two alignments N60 and N160 conforming to those recognized in the Causse of Middle Atlas [8, 38] highlighting the karstic context of the formation of the maar. In order to analyze the instability at the scale of LNH, fracturing measurements were made in both phreatomagmatic and strombolian deposits (Figure 11).

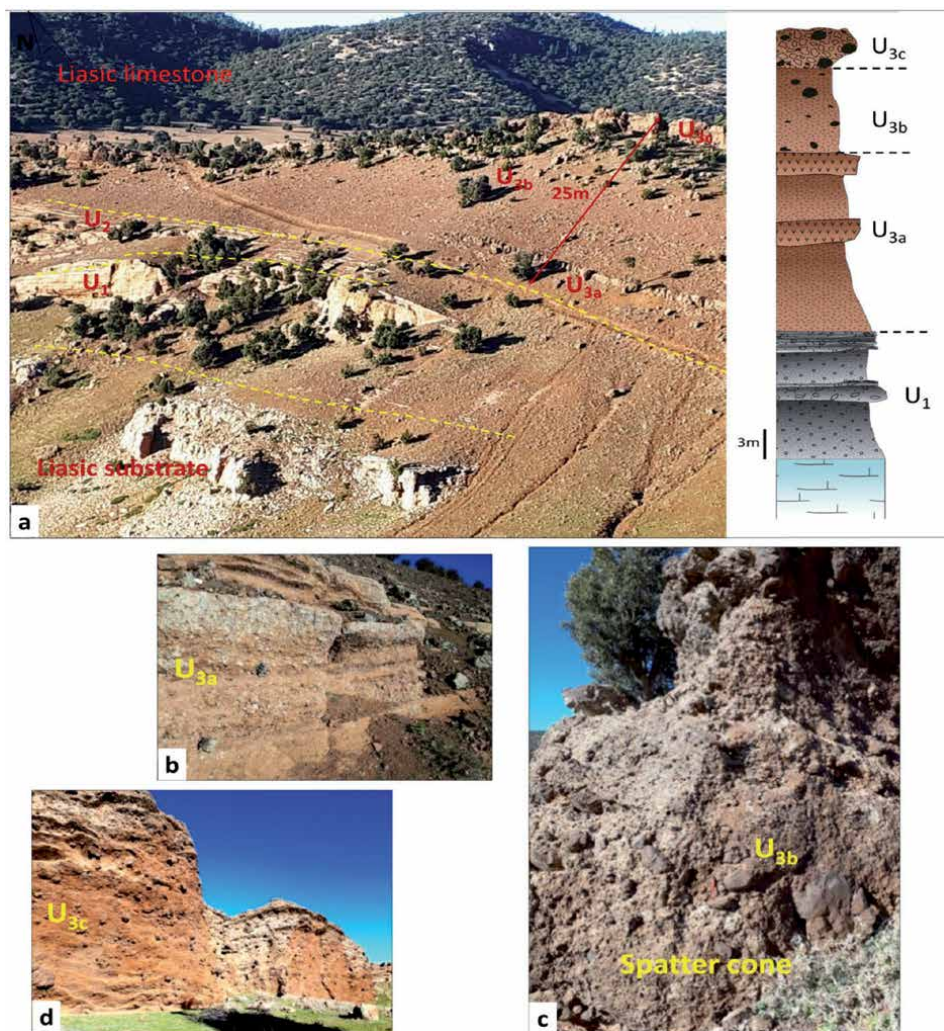


Figure 7. *Strombolian pyroclastic fallout on the eastern flank of LNH; (a) succession of phreatomagmatic deposits overlain by the strombolian unit (U₄); (b) air fallout from the first plume of the strombolian phase; (c) formation of spatter cone near the emission zone; (d) fallout of scoria with bombs far from the volcanic eruptive center.*

In the phreatomagmatic deposits (U₁, U₂) general subsidence is marked by conjugate fault-systems (**Figure 12d**) found also in the limestone basement (**Figure 11**). In the uppermost part of U₂ (**Figure 12e**), there is a shift from an extension by normal fault perpendicular to the NE–SW structural direction, to a strike-slip system by permutation of the stress axes $\sigma_1 - \sigma_2$ (**Figure 13**).

The distribution of strombolian deposits have an elliptical shape in map view with a 900 m long axis (550 m short axis) oriented N60E which corresponds to the regional structural direction. The NE and SW extremities of the major axis are distinguished by markers that reflect a general northward collapse movement. This distension controls the injection of basalt and its massive westward flow;

- On the western flank, a shear has been observed at the southern limit, cutting the blocks of the massive basalt flow with a right lateral movement of 30° dip towards the foci as shown by the striation on the fault plane (**Figure 12a**). On this flank,

basalt flows are piled up or corded. These flows form lobes that slide towards the center of the crater or that follow the gaps between the blocks of laves of the initial massive flow. The overlying scoriaceous layers attesting the strombolian explosion are affected by conjugate faults systems (**Figure 12c**) which could be an indicator of an extension oscillating swinging between WNW-ESE and NNW-SSE.

- On the eastern flank, the faults are sometimes decametric where the scarp is outlined by the bleached zone of alteration (**Figure 12b**). Subparallel cracks are associated with conjugate fault system related to this sectoral collapse NW-SE (**Figure 12d, e, f**).

4.3 Characterization of the structure of the LNH maar by applied geophysics

The treatment of the magnetic anomalies of the Middle Atlas allowed highlighting the existence of anomalies of short and long wavelengths. These last are linked to magnetized sources, notably the plio-quaternary basalts. Other anomalies

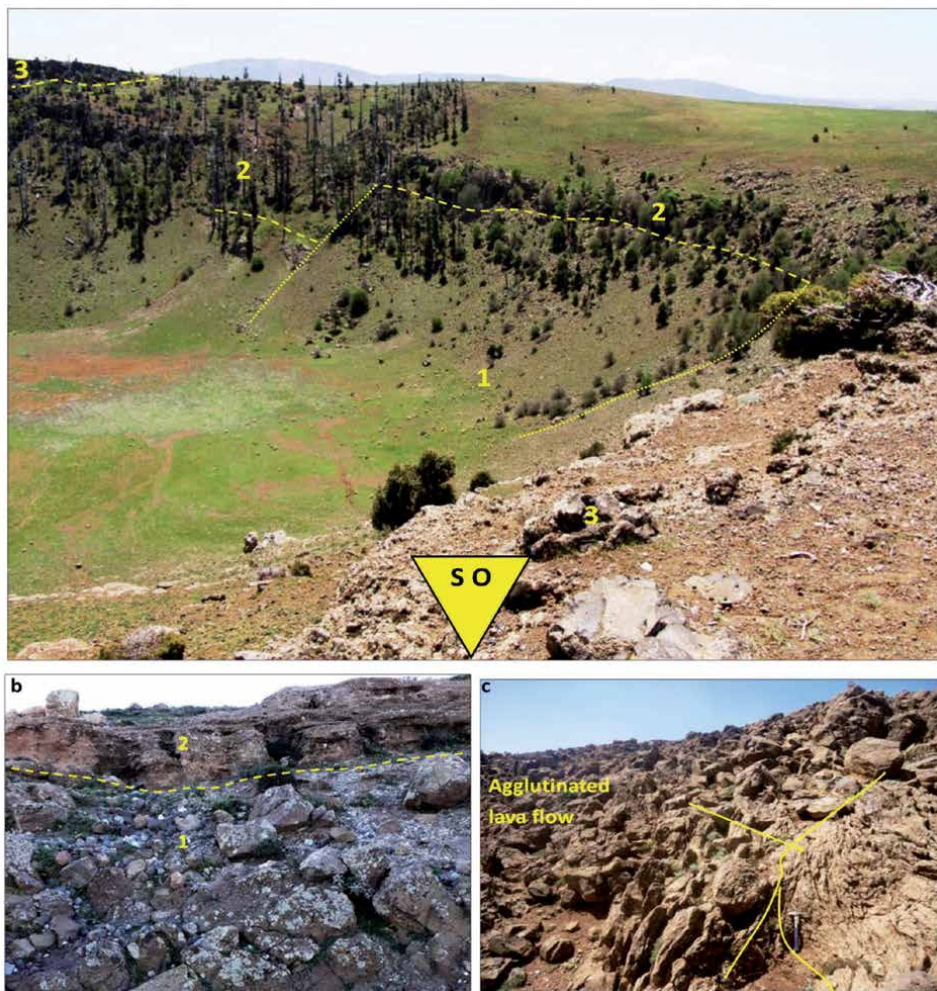


Figure 8. Modality of expression of the eruptive activity in the maar of Lechmine n'aït el Haj in the Causse of Middle Atlas; (a) flow of basalt emitted during a collapse of the western sector of the crater (1) overlain by Strombolian (2) and then phreatomagmatic fallout (3); (b) basalt prisms (1) overlain by Strombolian fallout of U3b (2); (c) corded lava flow resulting from the agglutination of lava.

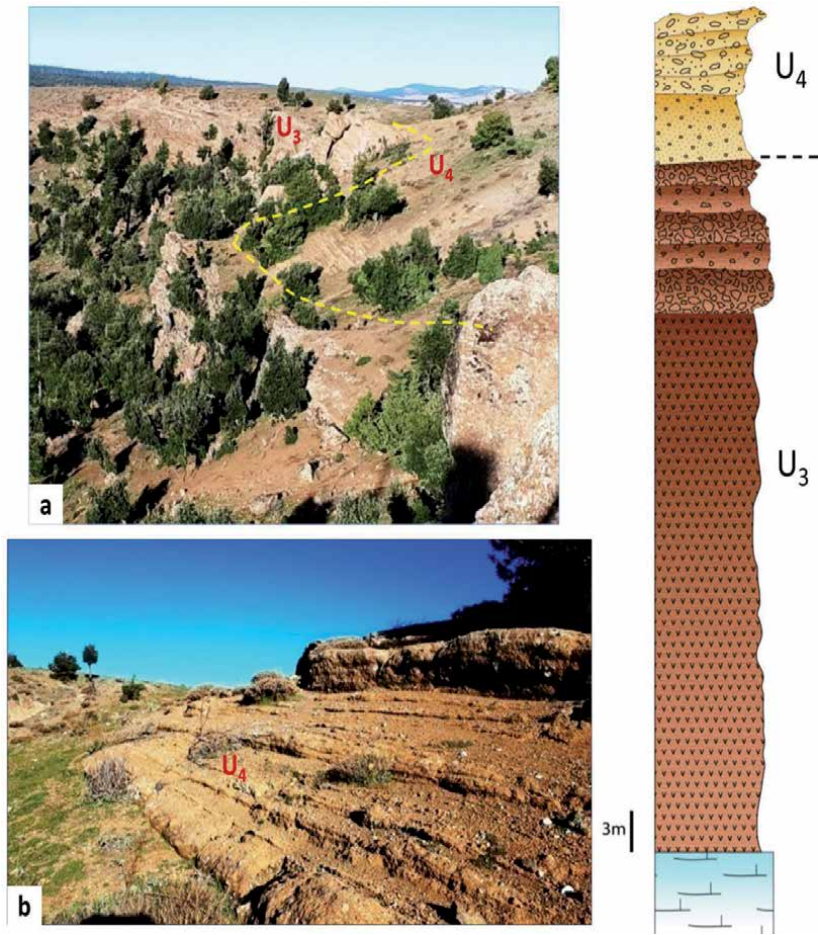


Figure 9. Volcanic lithofacies of the last phreatomagmatic unit (U_4); (a) in the northern flank; (b) in the southern flank.

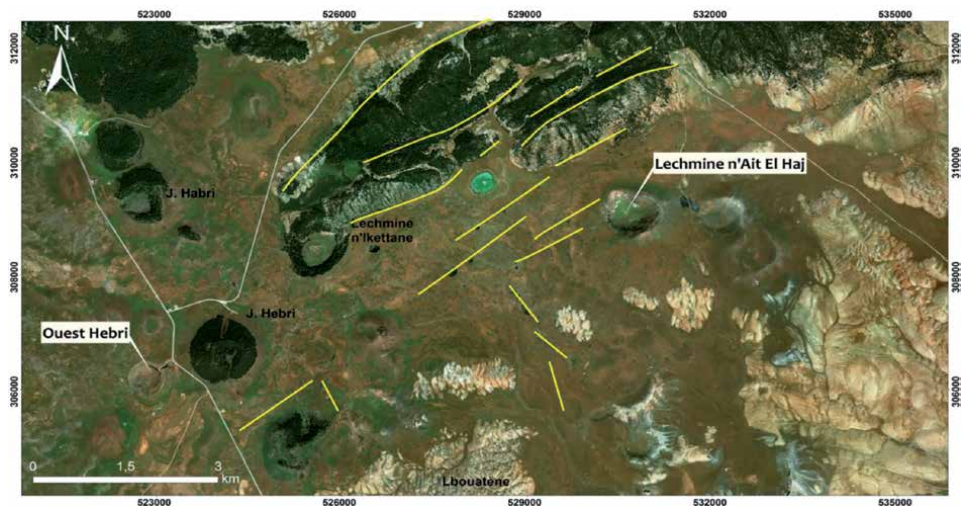


Figure 10. The outcrop of the Maar of Lechmine n'Ait el Haj in the middle of basaltic lava flows where cryptokarstic cavities are aligned according to the major directions of the Middle Atlas.

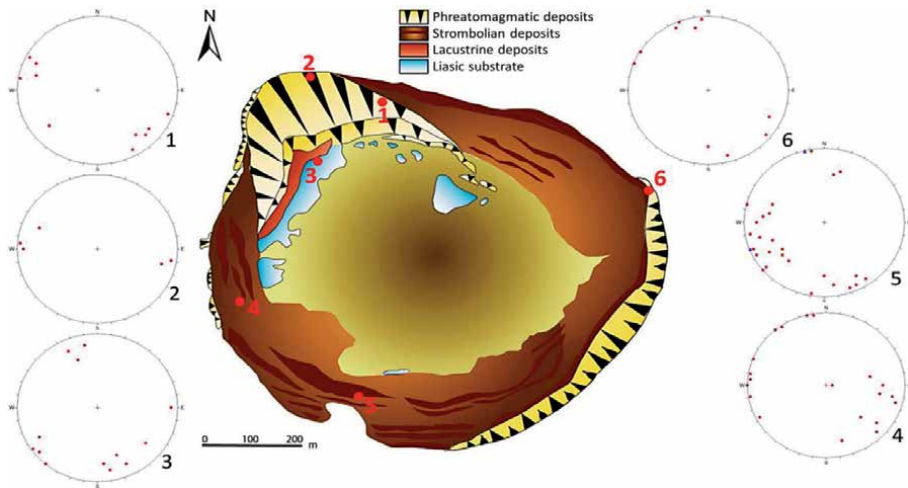


Figure 11.
 Distribution of fracturing in the Maar of Lechmine n'Ait el Haj (southern hemisphere) [38].

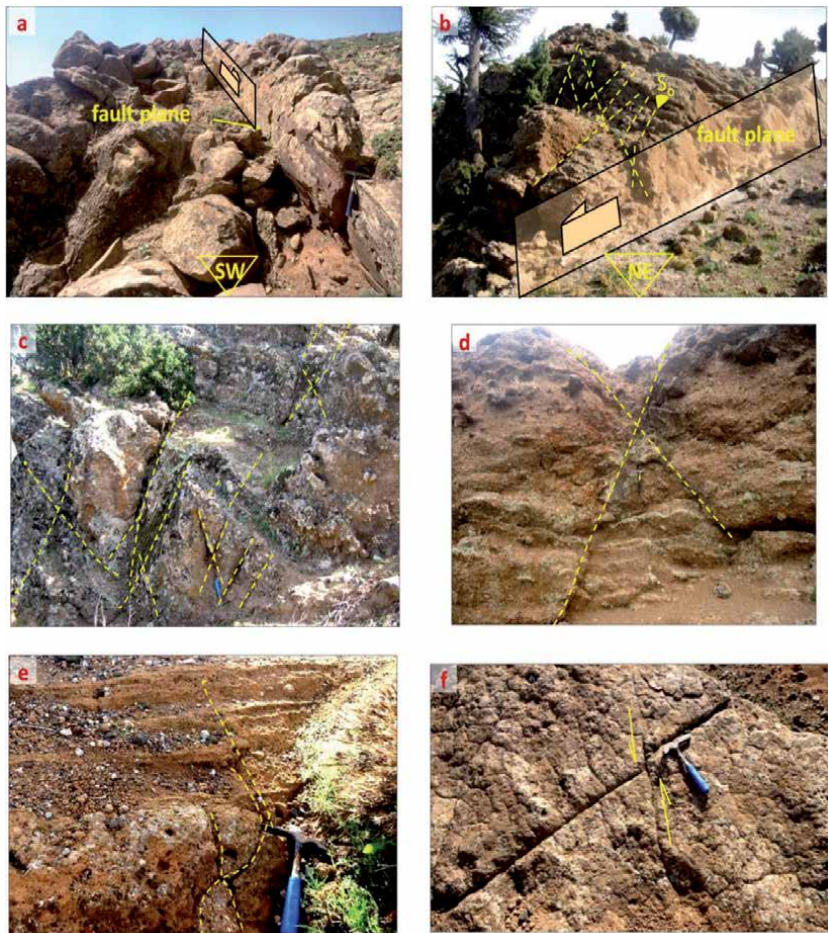


Figure 12.
 Fracturing systems in the Lechmine n'Ait el Haj maar; (a) striated fault in the basalt casting west of the maar; fracture types affecting the strombolian (b,c) and phreatomagmatic (d,e) formations of the maar; (f) geometric feature indicating a permutation of the stress parameters controlling fracturing.

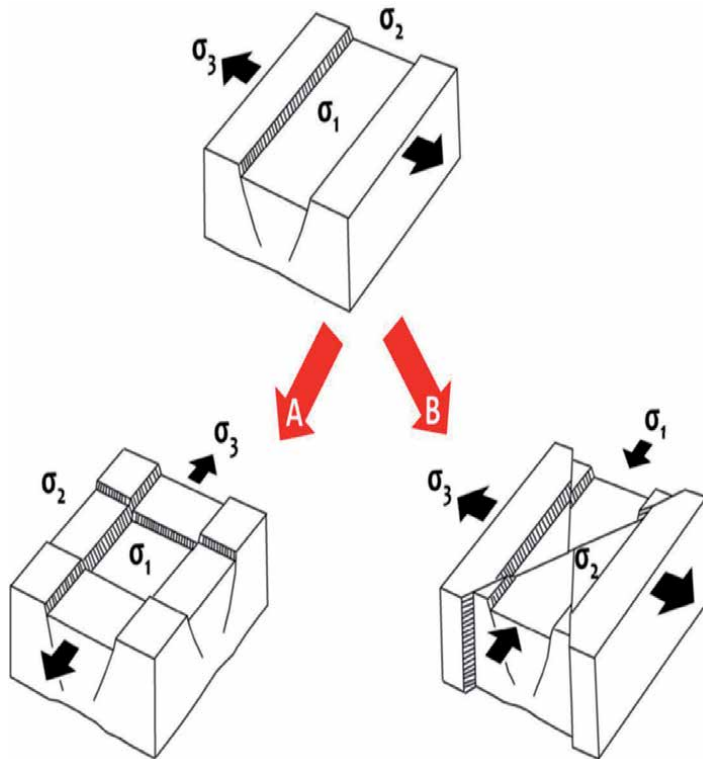


Figure 13.
Stress permutation during the volcanic activity of LNH maar.

coincide with the major accidents, such as those delimiting the Middle Atlas [39]. On the other hand, for the entire volcanic field of the Middle Causse atlas, very few studies focus on physical volcanology [40]. For example, a recent study [38] provides new information, based on geophysical prospecting combining magnetic and gravimetric methods, to the analysis of volcanoclastic deposits of LNH maar.

Gravity and magnetic data were obtained from a geophysical campaign in the LNH maar. The treatment and modelization of the collected data allowed understanding the geological features of the volcanic center and its geophysical properties [38]. Each model is limited by available geological information, including petrophysical properties, surficial geology and interpretation of geophysical data (regional and local magnetic survey data).

The 2D model was built by the GM-SYS software incorporating the geological and petrophysical properties of the study area [39] or those of comparable materials [41], and a design of the structures expected in these types of volcanoes. Approximate diatreme depths were constrained based on accessory lithic fragments observed in pyroclastic deposits. However, they represent minimum values, as phreatomagmatic explosions at deeper levels are often too small to transport material to the surface [42–44]. The gravity anomaly is modeled considering the topography. The gravity value is calculated at the surface and compared to the observed data. The reduced magnetic field to the pole (RTP) is calculated at an altitude of 2 m which corresponds to the height of the sensor. Since the magnetic susceptibility values considered represent minimum values, the susceptibility of the model has been increased to the maximum range expected for basaltic rocks [45, 46].

In the LNH model, the low gravity observed through the volcanic crater corresponds to shallow diatremes (~500 m), of lower density than their environment.

Local positive gravity anomalies, associated with magnetic anomalies of similar wavelength, are observed in the volcanic edifice (**Figure 14**). These anomalies express the presence of intrusive dykes or vents that have a higher density and magnetic susceptibility than those of the diatremes and surrounding host rocks [38]. The low magnetic signal around the diatreme fits with the pyroclastic nature of the volcanic deposits. Model adjustments suggest the involvement of a karst component to minimize the gaps between the calculated and observed anomalies. These adjustments take into consideration the density and magnetic susceptibility values of the volcanic materials.

Wide and shallow diatremes indicate abundant water supply and/or poorly lithified sediments. Deeper diatremes suggest a downward propagation of water-magma interaction due to the drying of water in the deep levels [44, 47, 48]. This suggests that explosive magma-water interactions in LNH initially occurred with shallow, poorly lithified, and water-saturated sediments, before propagating downward.

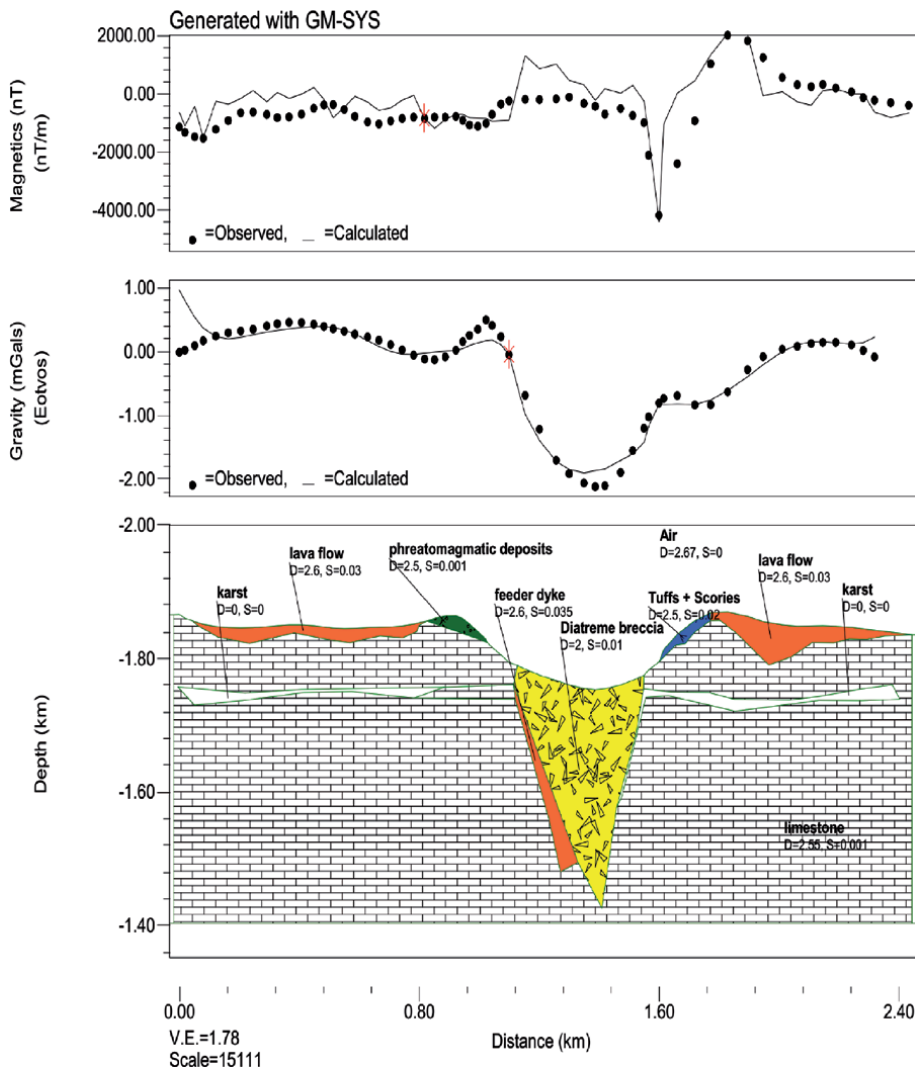


Figure 14. Simulated model of the maar Lechmine n'Ait el Haj from observed and measured values of gravity and pole-reduced magnetic response [38].

5. Discussion and interpretation

The installation of the crater of Lechmine n'Aït el Haj is the result of explosive phenomena associated with concentric collapses at the crater. These explosions imply the meeting of basaltic magma with water, here probably underground and/or superficial water. The crater is probably open on the path of lake or streams that feed the depressions that emerge near the limestone chain in the north of the limestone plateau. The involvement of groundwater of karstic origin in the phreatomagmatic activity is justified by the position of the maar on the path of faults of cryptokarstic origin (**Figure 3**). The second phreatomagmatic phase highlighted at LNH is probably due to an input of underground water that interacts with the magma and causes the deposition of the last pyroclastic breccia (**Figure 15**).

Tectonic analysis of the fractures in the quaternary pyroclastic deposits in the LNH crater allows reconstructing the stress systems. That helped to highlight vertical markers coupled with horizontal shifts. These localized distensions are confirmed by the geometry of the fractures, the presence of tectonic markers, the mixed eruption style of the maar (strombolian-phreatomagmatic), and the mechanisms of syn-eruptive tectonics.

The eruptive activity of LNH is controlled by an NW-SE to WNW-ESE subsidence, with a changing depending on the eruptive style evolution. Thus, the activity of the LNH maar, whose first phreatomagmatic then shifted to strombolian; there is a transition from an extending system to a strike-slip system. This permutation of the stress regime $\sigma_2 - \sigma_3$ can be linked to a short-term instability (at the scale of an eruption) that can be enhanced by several factors, notably: 1. the accumulation of volcanic products that vary the position of the center of gravity and deform the edifice [49], 2/a sudden change in the composition of the magmas, notably the increase in the SiO₂ content [50] or in water [51], and thus of the eruptive behavior.

During the explosions, collapse phenomena along curved fractures contribute to the widening of the crater [51]. The direction of collapse, particularly sectoral, is generally normal to the direction of active faults (normal or inverse), to alignments of parasitic cones and preferential directions of intrusion [52]. In a strike-slip context similar to that of LNH emplacement, collapse tends to have a parallel direction to the fault direction [53]. However, these relationships between tectonics and the direction of collapse are not always obvious [53]. The direction of the substrate slope, reflecting local tectonics, erosion, or volcanic activity, is generally parallel to the direction of sectoral collapse [54, 55].

The shallow diatremes suggest an eruption where the water-magma interaction remained at shallow levels. It is also an indication of a water-saturated or weakly lithified to unconsolidated host rock [47], which is consistent with the LNH volcanic structure. The multiple vents observed in this eruptive center constitute another indication of an eruption hosted in a substrate weakened by karstic corrosion or poorly consolidated sedimentation [56]. The substrate is unable to support the sloping walls of the diatreme and eventually collapses and obstructs the vent, provoking its migration and explosion in another place [56]. This explains the structure of the LNH maar, distinguished by the non-centered position of the first phreatomagmatic explosion, comparing to the center of the Strombolian explosion. The transition between magmatic and phreatomagmatic eruptive styles is explained by the variation in the groundwater supply and/or variable magma flow [57]. The preservation of the dykes in contact with the diatreme means that they took place during the later phases of the eruption, otherwise they would have been destroyed by the progressive mixing of the diatreme when deeper explosions transported material upwards [42]. This suggests that in the final stages of the eruption, the explosive fragmentation is reduced to become predominantly magmatic.

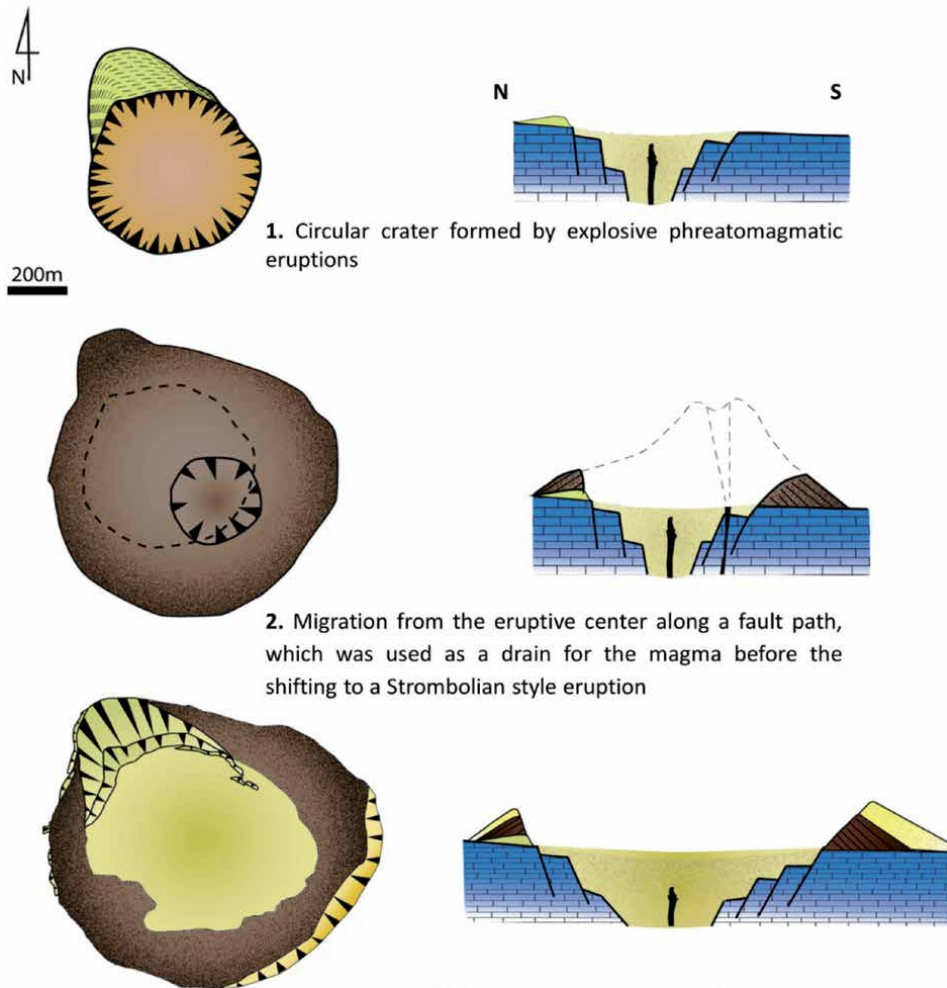


Figure 15. Reconstruction of the volcanic evolution of the maar of Lechmine n'Ait el Haj in the Causse of Middle Atlas. (in yellow: Phreatomagmatic activity; in brown: Strombolian activity).

6. Conclusion

The application of the methods of tephrostratigraphy and geophysics to the pyroclastic deposits of the volcano Lechmine n'Ait el Haj in the Causse of the Middle Atlas allowed understanding and interpretation of the volcanic dynamics of this mixed edifice set up during the quaternary.

The LNH maar is a large-diameter explosion crater, settled in the Liasic limestone substrate and the overhanging Plio-Quaternary basaltic flows that cover the plateau. The fragments of lithics from the substrate constitute an important part of the projected products (pyroclastics), associated with the juvenile magma. The data provided by the pyroclastic deposits allow us to estimate the importance, frequency, and chronology of the eruptions of the LNH volcano. It is structured by two phases of eruptive activity, phreatomagmatic and strombolian. The pyroclastic projections of the first phreatomagmatic phase offer numerous variants with a clear dominance of Liasic limestone fragments which constitutes 60 to 70% of the deposits. Their very clear stratification is due to the rhythmicity of the explosions. The juvenile fragments only present 30 to 40% of projections in the form of scoria, bombs, and blocks.

Two important eruptive sequences marked the first phreatomagmatic phase composed of stratified deposits with an abundant lithic fraction of limestone from the Liasic basement and juvenile pyroclasts. The accidental lithics decrease during the emissive process. This phreatomagmatic activity is initiated by lake water attested by lacustrine deposits.

A second explosive phase of the strombolian eruption style follows the first phreatomagmatic phase. It begins with the effusion of a thick basalt flow due to a collapse inclined slightly to the west, and then it is a pyroclastic plume that will be launched with the fallout of different sizes and shapes depending on the proximity of the eruptive center.

The last pyroclastic breccia surrounds the crater of LNH. It occurs in discontinuous pyroclastic deposits with well-sorted bedding where the fraction of lithics is less abundant than that of the early phreatomagmatic stages.

The tectonic analysis allowed the reconstruction of the stress systems and the highlighting of the mechanisms of syn-eruptive tectonics which had an important impact on the transition of the eruptive style (phreatomagmatic-strombolian).

LNH is only one example of the 105 monogenic volcanoes of the Causse of the Middle Atlas, this study represents a first step towards the discovery of this province at the scale of volcanoes, in order to build a model of volcanic dynamics in this region, starting from the approaches mentioned above. Scientific knowledge can be exploited in addition to the natural potentialities of the region to build a model of development that fits with the particularities of this territory. Finally, the richness of the Causse of the Middle Atlas in recent monogenic volcanoes with well-preserved forms in a karstic geological context, as well as the great variety of morphology, both in terms of flows and volcanic devices, make this territory a privileged area to establish a natural geopark accessible to all and easily mediated.

Acknowledgements

This work is part of the framework of the research project entitled: Multidisciplinary research on the Geomaterials and Volcanic Geosites of Morocco: the need for their valorization and exploitation in the prospects for sustainable development, supported and financed by Hassan II Academy of Sciences and Techniques and staged in partnership with a consortium of institutions composed of the Faculty of Sciences of Hassan II University— Casablanca, the Scientific Institute in Rabat and the Faculty of Sciences and Techniques of Hassan II University—Mohammadia. Special thanks to Pr. Pierre Boivin and Pr. Benjamin Van Wyke de Vries for their contribution in this project.

Author details

Sara Mountaj*, Hassan Mhiyaoui, Toufik Remmal, Samira Makhoukhi
and Fouad El Kamel
Faculty of Sciences Ain Chock, Hassan II University, Casablanca, Morocco,

*Address all correspondence to: sara.mountaj@gmail.com

IntechOpen

© 2020 The Author(s). Licensee IntechOpen. This chapter is distributed under the terms of the Creative Commons Attribution License (<http://creativecommons.org/licenses/by/3.0>), which permits unrestricted use, distribution, and reproduction in any medium, provided the original work is properly cited. 

References

- [1] Kereszturi G, Csillag G, Németh K, Sebe K, Balogh K, Jäger V. Volcanic architecture, eruption mechanism and landform evolution of a Plio/Pleistocene intracontinental basaltic polycyclic monogenetic volcano from the Bakony-Balaton Highland Volcanic Field, Hungary. *Cent Eur J Geosci.* 2010;2(3):362-384.
- [2] Németh K, Cronin S, Haller M, Brenna M, Csillag G. Modern analogues for Miocene to Pleistocene alkali basaltic phreatomagmatic fields in the Pannonian Basin: “soft-substrate” to “combined” aquifer controlled phreatomagmatism in intraplate volcanic fields Research Article. *Open Geosci.* 2010;2(3):339-361.
- [3] Keating GN, Valentine GA, Krier DJ, Perry FV. Shallow plumbing systems for small-volume basaltic volcanoes. *Bull Volcanol.* 2008;70(5):563-582.
- [4] Kereszturi G, Németh K. Monogenetic basaltic volcanoes: genetic classification, growth, geomorphology and degradation. In: *Updates in Volcanology-New Advances in Understanding Volcanic Systems.* InTech; 2012.
- [5] Amine A, El Hassani I-EEA, Remmal T, El Kamel F, De Vries BVW, Boivin P. Geomorphological classification and landforms inventory of the Middle-Atlas volcanic Province (Morocco): Scientific value and educational potential. *Quaest Geogr.* 2019;38(1):107-129.
- [6] Martin J. Le Moyen Atlas central étude géomorphologique. Vol. 258. Editions du Service géologique du Maroc; 1981.
- [7] Harmand C, Cantagrel JM. Le volcanisme alcalin tertiaire et quaternaire du moyen atlas (Maroc): chronologie K/Ar et cadre géodynamique. *J Afr Earth Sci* 1983. 1984 Jan 1;2(1):51-5.
- [8] Menjour F, Remmal T, Hakdaoui M, El Kamel F, Lakroud K, Amraoui F, et al. Role of Fracturing in the Organization of the Karst Features of Azrou Plateau (Middle Atlas, Morocco) Studied by Remote Sensing Imagery. *J Indian Soc Remote Sens.* 2017 Dec;45(6):1015-30.
- [9] El Azzouzi M, Maury RC, Bellon H, Youbi N, Cotten J, Kharbouch F. Petrology and K-Ar chronology of the Neogene-Quaternary Middle Atlas basaltic province, Morocco. *Bull Société Géologique Fr.* 2010;181(3):243-257.
- [10] Bosch D, Maury RC, Bollinger C, Bellon H, Verdoux P. Lithospheric origin for Neogene-Quaternary Middle Atlas lavas (Morocco): Clues from trace elements and Sr-Nd-Pb-Hf isotopes. *Lithos.* 2014;205:247-265.
- [11] Mhiyaoui H, Manar A, Remmal T, Boujamaoui M, El Kamel F, Amar M, et al. Structures profondes du volcanisme quaternaire du Moyen Atlas central (Maroc): Apports de la cartographie aéromagnétique. *Bull L’Institut Sci Rabat Sect Sci Terre.* 2016;(38):111-25.
- [12] Ayarza P, Carbonell R, Teixell A, Palomeras I, Martí D, Kchikach A, et al. Crustal thickness and velocity structure across the Moroccan Atlas from long offset wide-angle reflection seismic data: The SIMA experiment. *Geochem Geophys Geosystems.* 2014 May;15(5):1698-717.
- [13] Mountaj S, Remmal T, El Amrani I-EEH, Makhoukhi S, Lakroud K, de Vries BVW. Phreatomagmatic plioquaternary volcanism in the Middle Atlas: Analysis of the eruptive sequence of the Lechmine n’Aït El Haj maar. *Arab J Geosci.* 2020;13(13):1-16.

- [14] Németh K. Monogenetic volcanic fields: Origin, sedimentary record, and relationship with polygenetic volcanism. In: Geological Society of America Special Papers [Internet]. Geological Society of America; 2010 [cited 2018 Aug 3]. p. 43-66. Available from: <https://pubs.geoscienceworld.org/books/book/624/chapter/3805526/>
- [15] Smith IEM, Blake S, Wilson CJN, Houghton BF. Deep-seated fractionation during the rise of a small-volume basalt magma batch: Crater Hill, Auckland, New Zealand. *Contrib Mineral Petrol.* 2008;155(4):511-527.
- [16] Connor CB, Stamatakos JA, Ferrill DA, Hill BE, Ofoegbu GI, Conway FM, et al. Geologic factors controlling patterns of small-volume basaltic volcanism: Application to a volcanic hazards assessment at Yucca Mountain, Nevada. *J Geophys Res Solid Earth.* 2000;105(B1):417-432.
- [17] Canon-Tapia E, Szakács A. What is a Volcano? Geological Society of America; 2010. 152 p.
- [18] Márquez A, Verma SP, Anguita F, Oyarzun R, Brandle JL. Tectonics and volcanism of Sierra Chichinautzin: extension at the front of the Central Trans-Mexican Volcanic belt. *J Volcanol Geotherm Res.* 1999;93(1-2):125-150.
- [19] Baloga SM, Glaze LS, Bruno BC. Nearest-neighbor analysis of small features on Mars: Applications to tumuli and rootless cones. *J Geophys Res Planets.* 2007;112(E3).
- [20] Németh K, White JD, Reay A, Martin U. Compositional variation during monogenetic volcano growth and its implications for magma supply to continental volcanic fields. *J Geol Soc.* 2003;160(4):523-530.
- [21] Kereszturi G, Németh K, Csillag G, Balogh K, Kovács J. The role of external environmental factors in changing eruption styles of monogenetic volcanoes in a Mio/Pleistocene continental volcanic field in western Hungary. *J Volcanol Geotherm Res.* 2011;201(1-4):227-240.
- [22] Valentine GA, Perry FV. Tectonically controlled, time-predictable basaltic volcanism from a lithospheric mantle source (central Basin and Range Province, USA). *Earth Planet Sci Lett.* 2007;261(1-2):201-216.
- [23] Gutmann JT. Strombolian and effusive activity as precursors to phreatomagmatism: eruptive sequence at maars of the Pinacate volcanic field, Sonora, Mexico. *J Volcanol Geotherm Res.* 2002;113(1-2):345-356.
- [24] Walker GPL, Sigurdsson, H, Houghton B, Rymer H, Stix J, McNutt S. Basaltic volcanoes and volcanic systems. In: *Encyclopedia of Volcanoes.* Academic Press; 2000. p. 283-9.
- [25] Brenna M, Cronin SJ, Németh K, Smith IE, Sohn YK. The influence of magma plumbing complexity on monogenetic eruptions, Jeju Island, Korea. *Terra Nova.* 2011;23(2):70-75.
- [26] Kelemen PB, Hirth G, Shimizu N, Spiegelman M, Dick HJ. A review of melt migration processes in the adiabatically upwelling mantle beneath oceanic spreading ridges. *Philos Trans R Soc Lond Math Phys Eng Sci.* 1997;355(1723):283-318.
- [27] Sleep NH. Tapping of melt by veins and dikes. *J Geophys Res Solid Earth.* 1988;93(B9):10255-10272.
- [28] Valentine GA, Krogh KE. Emplacement of shallow dikes and sills beneath a small basaltic volcanic center—The role of pre-existing structure (Paiute Ridge, southern Nevada, USA). *Earth Planet Sci Lett.* 2006;246(3-4):217-230.

- [29] Connor CB. Cinder cone clustering in the TransMexican Volcanic Belt: implications for structural and petrologic models. *J Geophys Res Solid Earth*. 1990;95(B12):19395-19405.
- [30] Guilbaud M-N, Siebe C, Layer P, Salinas S, Castro-Govea R, Garduño-Monroy VH, et al. Geology, geochronology, and tectonic setting of the Jorullo Volcano region, Michoacán, México. *J Volcanol Geotherm Res*. 2011;201(1-4):97-112.
- [31] Huon S, Piqué A, Clauer N. Etude de l'orogénèse hercynienne au Maroc par la datation K-Ar de l'évolution métamorphique de schistes ardoisiers. Study of the Hercynian orogeny in Morocco by the K-Ar isotopic datation of metamorphic evolution in slates. *Sci Géologiques Bull Mém*. 1987;40(3):273-84.
- [32] de Lamotte DF, Zizi M, Missenard Y, Hafid M, El Azzouzi M, Maury RC, et al. The atlas system. In: *Continental evolution: the geology of Morocco*. Springer; 2008. p. 133-202.
- [33] Zizi M. Triassic-Jurassic extensional systems and their neogene reactivation in northern Morocco. *BRides Préifaines Guercif Basin Notes Mém Serv Géol Maroc*. 2002;416.
- [34] Charriere A. Évolution néogène de bassins continentaux et marins dans le Moyen Atlas central (Maroc). *Bull Société Géologique Fr*. 1984;7(6):1127-1136.
- [35] Williams PW. The role of the epikarst in karst and cave hydrogeology: a review. *Int J Speleol*. 2008;37(1):1.
- [36] Boulouard C. Contribution à l'étude des "saccates": essai de classification et application stratigraphique [PhD Thesis]. Université de Paris; 1963.
- [37] Chateaufeuf Jj, Reyre Y. Eléments de palynologie. Applications géologiques. Cours de 3eme cycle en science de la terre. 1974.
- [38] Mhiyaoui H. Approche géophysique du volcanisme quaternaire du Moyen Atlas : Caractérisation magnétique et gravimétrique. Thèse, Université Hassan II, Faculté des Sciences Aïn Chock de Casablanca, 2019, 139p.
- [39] El Azzab D, El Wartiti M. Mise en place de la chaîne volcanique du moyen Atlas (Maroc): Traitement des données aéromagnétiques. The Middle Atlas volcanic orogen setting (Morocco): aeromagnetic data analysis. *Pangea*. 1998;29:45-51.
- [40] Mountaj S. Dynamique éruptive du volcan mixte Lachemine n'Aït el Haj (Moyen Atlas-Maroc): Caractérisation pétro-structurale, chimico-minéralogique et valorisation du géosite volcanique. Thèse. Université Hassan II Faculté des Sciences Aïn Chock-Casablanca;p.174. 2020.
- [41] Blaikie TN, Ailleres L, Betts PG, Cas RAF. Interpreting subsurface volcanic structures using geologically constrained 3-D gravity inversions: examples of maar-diatremes, Newer Volcanics Province, southeastern Australia. *J Geophys Res Solid Earth*. 2014;119(4):3857-3878.
- [42] Valentine GA, White JD. Revised conceptual model for maar-diatremes: Subsurface processes, energetics, and eruptive products. *Geology*. 2012;40(12):1111-1114.
- [43] Lefebvre NS, White JDL, Kjarsgaard BA. Unbedded diatreme deposits reveal maar-diatreme-forming eruptive processes: Standing Rocks West, Hopi Buttes, Navajo Nation, USA. *Bull Volcanol*. 2013;75(8):739.
- [44] Ross P-S, White JDL, Valentine GA, Taddeucci J, Sonder I, Andrews RG. Experimental birth of a maar-diatreme volcano. *J Volcanol Geotherm Res*. 2013 Jun;260:1-12.

- [45] Clark DA. Comments on magnetic petrophysics. *Explor Geophys.* 1983;14(2):49-62.
- [46] Clark DA. Magnetic petrophysics and magnetic petrology: aids to geological interpretation of magnetic surveys. *AGSO J Aust Geol Geophys.* 1997;17:83-104.
- [47] Auer A, Martin U, Németh K. The Fekete-hegy (Balaton Highland Hungary) “soft-substrate” and “hard-substrate” maar volcanoes in an aligned volcanic complex—Implications for vent geometry, subsurface stratigraphy and the palaeoenvironmental setting. *J Volcanol Geotherm Res.* 2007;159(1-3):225-245.
- [48] Lorenz V. Maar-diatreme volcanoes, their formation, and their setting in hard-rock or soft-rock environments. *Geolines.* 2003;15:72-83.
- [49] Tibaldi A. Multiple sector collapses at Stromboli volcano, Italy: how they work. *Bull Volcanol.* 2001;63(2-3):112-125.
- [50] Belousov A, Belousova M, Voight B. Multiple edifice failures, debris avalanches and associated eruptions in the Holocene history of Shiveluch volcano, Kamchatka, Russia. *Bull Volcanol.* 1999;(61):324-42.
- [51] Moore JG, Nakamura K, Alcaraz A. The 1965 eruption of Taal volcano. *Science.* 1966;151(3713):955-960.
- [52] Capra L, Macias JL, Scott KM, Abrams M, Garduño-Monroy, V.M. Debris avalanches and debris flows transformed from collapses in the Trans-Mexican Volcanic Belt, Mexico - behavior, and implications for hazard assessment. *J Volcanol Geotherm Res.* 2002;(113):81-110.
- [53] Ponomareva VV, Melekestsev IV, Dirksen OV. Sector collapses and large landslides on Late Pleistocene–Holocene volcanoes in Kamchatka, Russia. *J Volcanol Geotherm Res.* 2006;158(1-2):117-138.
- [54] Belousov A, Walter TR, Troll VR. Large-scale failures on domes and stratocones situated on caldera ring faults: sand-box modeling of natural examples from Kamchatka, Russia. *Bull Volcanol.* 2005;5(67):457-68.
- [55] Carrasco-Núñez G, Díaz-Castellón R, Siebert L, Hubbard B, Sheridan MF, Rodríguez SR. Multiple edifice-collapse events in the Eastern Mexican Volcanic Belt: The role of sloping substrate and implications for hazard assessment. *J Volcanol Geophys Res.* 2006;(158):151-76.
- [56] Ort MH, Carrasco-Núñez G. Lateral vent migration during phreatomagmatic and magmatic eruptions at Tecuítlapa Maar, east-central Mexico. *J Volcanol Geotherm Res.* 2009;181(1-2):67-77.
- [57] Houghton BF, Wilson CJN, Smith IEM. Shallow-seated controls on styles of explosive basaltic volcanism: a case study from New Zealand. *J Volcanol Geotherm Res.* 1999 Jul 1;91(1):97-120.

Syn-Eruptive Lateral Collapse of Monogenetic Volcanoes: The Case of Mazo Volcano from the Timanfaya Eruption (Lanzarote, Canary Islands)

*Carmen Romero, Inés Galindo, Nieves Sánchez,
Esther Martín-González and Juana Vegas*

Abstract

The evolution of complex volcanic structures usually includes the occurrence of flank collapse events. Monogenetic cones, however, are more stable edifices with minor rafting processes that remove part of the cone slopes. We present the eruptive history of Mazo volcano (Lanzarote, Canary Islands), including the first detailed description of a syn-eruptive debris avalanche affecting a volcanic monogenetic edifice. The study and characterization, through new geological and morphological data and the analysis of a great number of documentary data, have made it possible to reinterpret this volcano and assign it to the Timanfaya eruption (1730–1736). The eruptive style evolved from Hawaiian to Strombolian until a flank collapse occurred, destroying a great part of the edifice, and forming a debris avalanche exhibiting all the features that define collapsing volcanic structures. The existence of blocks from the substrate suggests a volcano-tectonic process associated with a fracture acting simultaneously with the eruption. The sudden decompression caused a blast that produced pyroclasts that covered most of the island. This study forces to change the current low-hazard perception usually linked to monogenetic eruptions and provides a new eruptive scenario to be considered in volcanic hazards analysis and mitigation strategies development.

Keywords: monogenetic volcano, flank collapse, debris avalanche, volcanic hazard, Timanfaya, Canary Islands

1. Introduction

The origin and characteristics of flank collapses in stratovolcanoes and volcanic islands have been recognized and described around the world (eg. [1–5]). The resulting Volcanic Debris Avalanche (VDA) deposits are composed essentially of rock fragments of the affected edifice and usually show a hummocky topography around the collapsed original volcanic landform. The magnitude of these collapses and the huge volume of involved materials make these processes the most

catastrophic events in the evolution of polygenetic volcanic structures. Factors inducing or triggering volcanic flank collapses include the violence of the eruption, high eruptive rates, hydrothermal alteration, existence of relatively steep slopes, presence and reactivation of faults, magma intrusion, high saturation of volcanic rocks in water, presence of lava plugs during the active period, structural heterogeneities and geotechnical differences between volcanic edifices and their basement, seismicity, caldera collapse or even climatic fluctuations ([2] and reference therein).

In contrast, instability processes in monogenetic volcanoes have been much less documented and have often received less attention given its less volume and less potential hazard (eg. [6–11]). Nevertheless, it should be taken into account that mafic monogenetic volcanic systems are the most frequent and widespread magmatism on Earth, usually located very close to population centers [7]. The most documented instability process in monogenetic cones are those related to the partial collapse and passive transport of fragments of the edifice during the emission of lava flows, process known as rafting (eg. [6–11]). The clearest evidence of rafting processes in monogenetic edifices is the existence of huge blocks on the surface of lava flows composed of agglutinated materials coming from the cone [12]. Rafting has been related to lava flows and sill emplacement at the base of the cone, changes in eruptive style or the existence of previous cones or topographical constrains ([13] and reference therein). Although flank collapses forming VDA with liquified non-turbulent granular flows are usually linked to stratovolcanoes [14] and rafting processes are the common result of instability in monogenetic cones, in this work we demonstrate VDA also happen in small volcanic cones, such as in the historical volcanic cone of Mazo (Lanzarote, Canary Islands). Here, we present the first detailed description of a syn-eruptive volcanic flank collapse in a monogenetic volcanic cone and describe the associated debris avalanche and blast deposits; as well as the conditioning and triggering factors of the collapse, and the implications for the volcanic eruption development. The finding of this volcanic flank collapse during a mafic fissure eruption has local implications in the interpretation, timing and reconstruction of the Timanfaya eruption and global implications in the understanding of hazards in monogenetic volcanic fields.

2. Geological setting

The geology of Lanzarote is characterized by the existence of old Miocene massifs located to the North and South of the island and by a Quaternary fissure-aligned volcanic field in the central part, in which vast volcanic fields cover discordantly the underlying Mio-Pliocene materials (**Figure 1**). Most of the eruptive centers are small monogenetic edifices arranged in several alignments trending NE–SW and ENE–WSW roughly parallel to each other, and dispersed over the territory ([15] and references therein).

Two historical eruptions took place in the central volcanic field of the island: the 1730–36 Timanfaya eruption and the 1824 eruption [16]. Both were multiple-fissure type eruptions but quite different in magnitude [17]. While in 1824 the eruption lasted nearly three months and only three small fissures (less than 500 m in length) where opened, the Timanfaya eruption lasted nearly 6 years and formed hundreds of vents aligned along a 13 km eruptive fissure, from where lava flows that covered one-third of the island were issued [9, 11, 17–21]. Thus, Timanfaya constitutes the highest magnitude eruptive process occurred in historical times in Lanzarote and the Canary Islands.

Mazo volcano is located in the central volcanic field, to the North of the eastern end of the main eruptive fissure of Timanfaya (**Figure 1**). It is a basanitic elongated

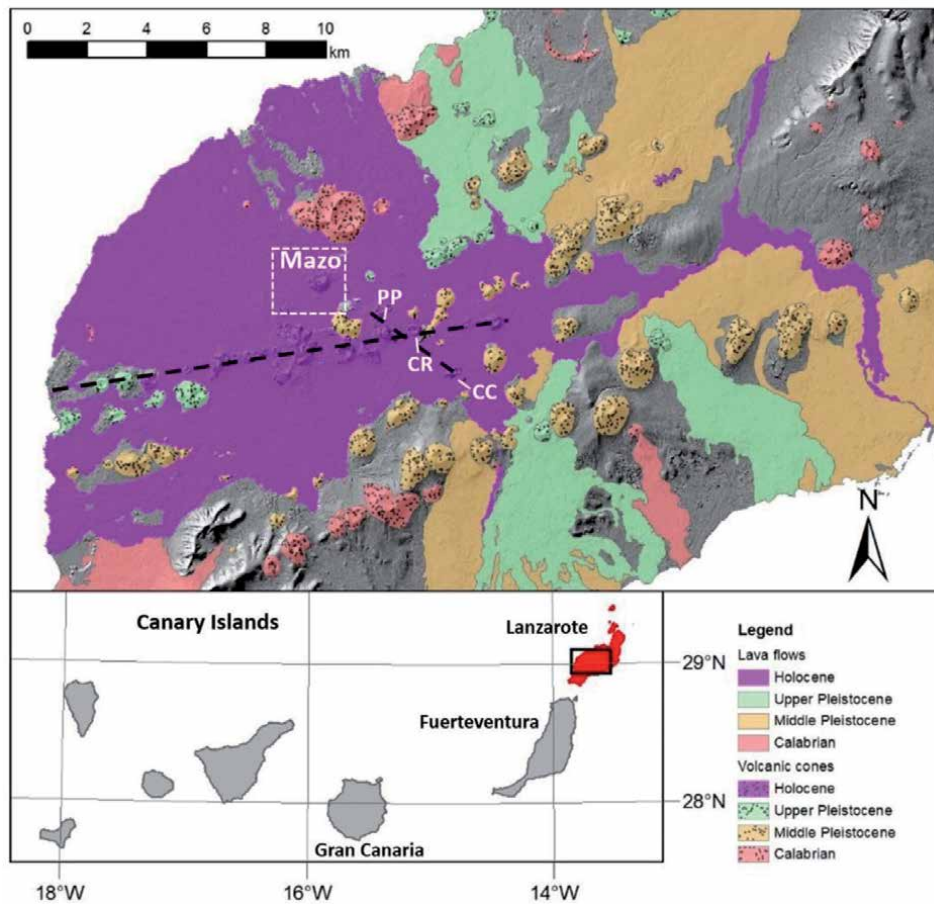


Figure 1. Location of Lanzarote Island and map of quaternary volcanic deposits of the central volcanic field of Lanzarote showing the location of Mazo volcano and the eruptive fissures of Timanfaya (dash black lines). White dashed square shows the location of **Figure 2**. CC: Caldera de los Cuervos; CR: Caldera de La Rilla; PP: Pico Partido.

scoria cone trending ENE-WSW [18]. This scoria cone and the related deposits are partially overlaid by historical lava flows.

3. Geological analysis of Mazo volcano and deposits

Mazo is a monogenetic volcano with a relative height of 179 m, resting on a leaning volcanic substrate with a difference in height of 30 m between the highest and the lowest point of its external base. The cone and deposits are partially covered by lavas from historical eruptions, leaving exposed only the highest parts of Mazo deposits. The cone has an irregular shape and a crater with two open depressions aligned in the ENE-WSW direction, with a maximum diameter of 493 m. The main crater, located to the SW, has a funnel shape, 178 m deep inside, with an internal platform on its northern slope elevated 18 m over the bottom (**Figure 2**). The other depression is of bowl type, with an interior depth of 120 m. The rim of this double depression is higher in its southern part (429 m asl), just at the contact between both depressions. From this point, the rim appears lobed towards the NE and SW, gradually decreasing in altitude until reaching a minimum height of 280 m in its NW sector.

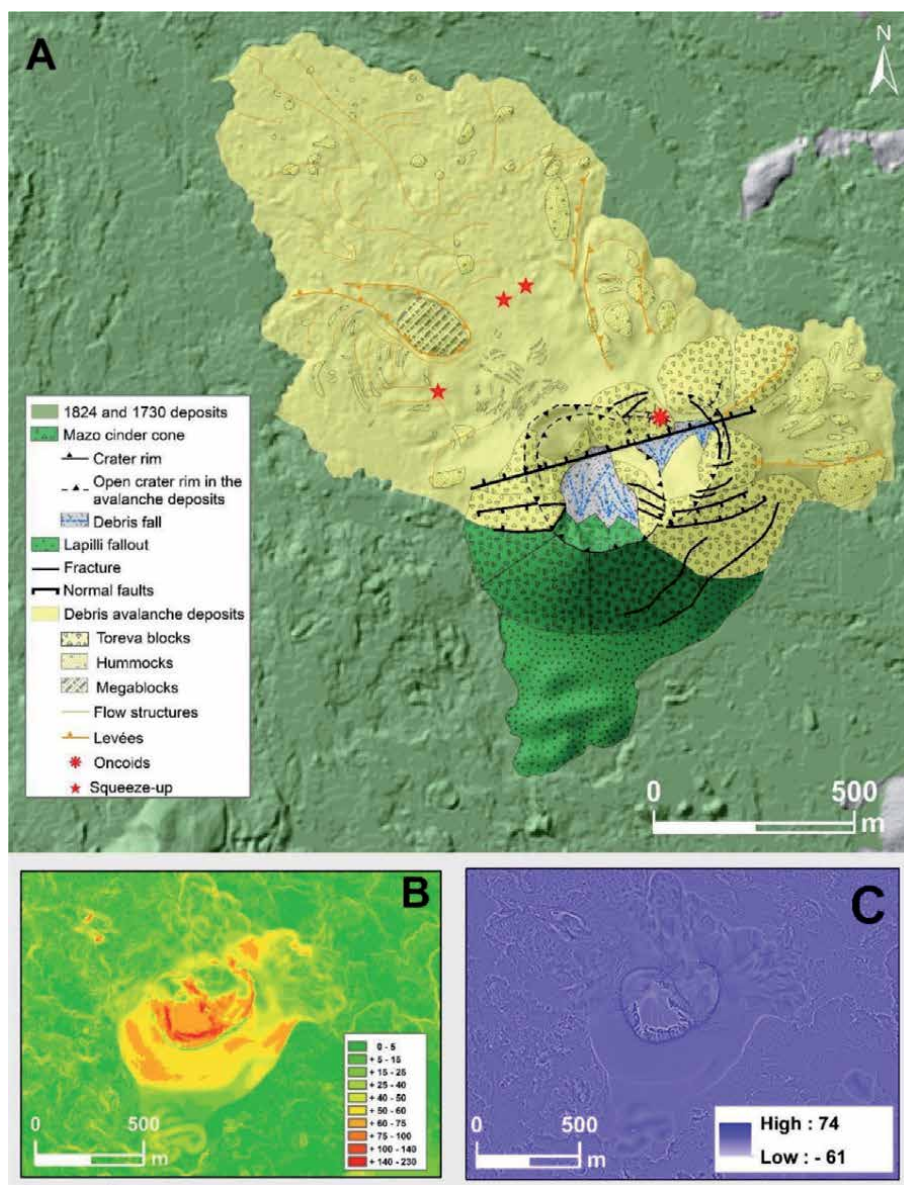


Figure 2. Geomorphological (A); slope (B); and roughness maps (C) of Mazo.

The original cone consisted of welded pyroclastics, lapilli and bombs and some interbedded clastogenic lavas that can be identified in the SSW flank, affected by small fractures. However, most of the cone is formed by a debris avalanche deposit (DAD) that extends towards the NNW and ENE covering an area of 1218 km² and reaching a maximum distance from the vent of 1.6 km (Figures 2 and 3). The thickness of the deposit is difficult to estimate but minimum values of 35 m and 5 m can be assumed for the proximal and the distal area, respectively. The DAD is made of an unconsolidated breccia without stratification. Two main facies are identified: block and mixed facies.

Most of the cone, as well as proximal areas, are composed of block facies characterized by the presence of toreva blocks (Figures 2 and 3A–C), that are fractured and backtilting blocks that slumped in an almost completely coherent manner [22, 23].

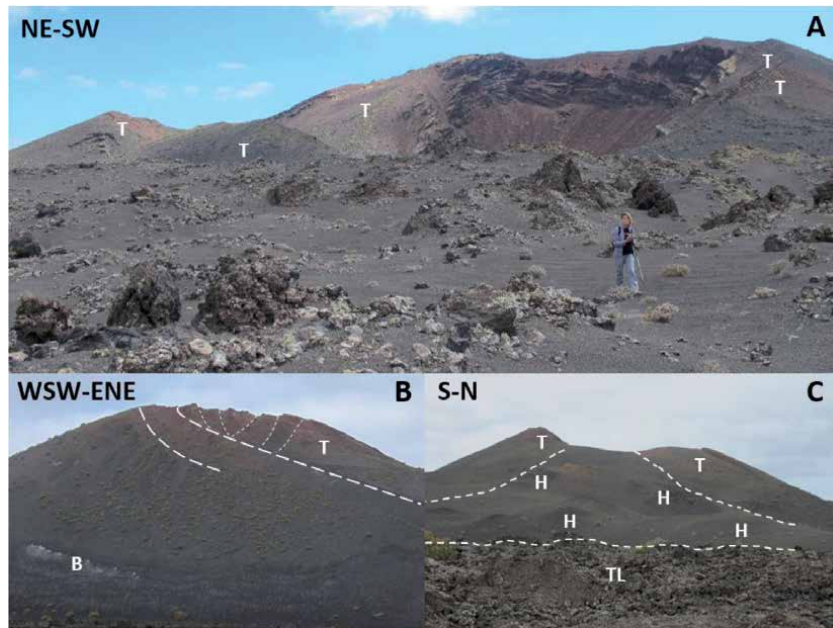


Figure 3. (A) General view of Mazo volcano showing the block facies of the proximal area with torea blocks in the background, and the distal mixed facies in the foreground. (B) Listric faults and horst-graben structure on the flank. (C) Mixed facies with hummocky topography in between torea blocks. B: Blast deposit; H: Hummocks; T: Torea blocks.

This facies consists of broken, slightly unstructured and staggered pieces of the cone (pyroclastics and clastogenic lavas), attached to the remnant cone, separated by inter-torea depressions, normal faults and small graben structures (**Figure 2**). At the southeastern flank a set of conjugated faults, which are inserted in a listric fault plane, individualize several torea blocks (**Figure 3B**). The eastern and northern flanks are also formed by several big blocks made of lapilli and scoria, as well as pyroclastic deposits.

The mixed facies is composed of a poorly sorted deposit, with milimetric to hectometric clasts and megablocks (**Figures 3A, C** and **4**). Most outcrops show a grain supported deposit, but matrix supported is also found (**Figure 4A** and **B**). Clast are mostly polyhedral and polymictic with abundant dense lavas and minor clast of vesicular lavas, welded scoria, weathered hydrovolcanic deposits, calcrete and paleosoils. Blocks and clasts are usually fractured, with frequent jigsaw cracks and slickensides (**Figure 4C–E**) or linked to deformation structures in the deposit (**Figure 4G**). Some of them show evidences of thermal alteration displaying a banded sequence of wine, reddish and yellowish colors suggesting decreasing of temperature towards the surface (**Figure 4F**).

From inter-torea depressions towards the base of the cone, flows characterized by a hummocky surface topography were emplaced (**Figures 2** and **3C**). These flows were formed as torea blocks break into smaller blocks. To the N and E of the volcanic edifice, lying on a steep slope area, these avalanche deposits consist of several flows with well-defined lobes and steep fronts. They have the highest concentration of hummocks, mostly elongated trending parallel to the flow direction. To the south of the cone there is also a hummocky surface completely covered by Mazo fallout deposits so it cannot be clearly assigned to this eruption (**Figure 2**).

To the NNW of the volcanic edifice the DAD spreads gently dipping with a roughly surface characterized by small and dispersed hummocks (**Figures 2** and **3A**).



Figure 4. *Mixed facies. (A) Grain supported; (B) matrix supported; (C) jig-saw fit cracks; (D) fractured block; (E) slickensides; (F) alteration bands and (G) deformation structures under a block.*

Here the mixed facies are not related to a hummocky terrain being in turn dominated by ridges and a blocky surface. Lateral and frontal levees are also common, being the best defined those surrounding a single isolated mega-block, 120 m in diameter and 43 m high, located 472 m far from the vent (**Figures 2 and 5**). Decametric blocks ($< 90 \text{ m}^3$) outcrop mainly on the distal area.

The single isolated mega-block (**Figure 5**) outcropping in this area consists of a stratigraphic sequence of several piled lava flows, hydromagmatic deposits with a paleosoil and a calcrete at the top with terrestrial gastropods, and finally a volcanic spatter deposit. The block is fractured and broken in the distal area and shows an injection of deformed hydromagmatic deposits into the overlying spatter. All these features lead us to interpret it as a substratum block. Part of the block was covered by molten lava during the debris avalanche emplacement.

Several squeeze-up structures (**Figures 2A and 6**) have also been identified in the distal mixed facies indicating the presence of molten lava during the debris avalanche emplacement. They are made up of massive lava sheets tens of centimeters thick that make thinner and curve towards the top, constituting authentic spines with fluted and wavy surfaces. Squeeze-up are arranged in bands more or less parallel to each other with a curved longitudinal layout, and the convex side arranged in the direction of flow. Trapped between the fingerings of the intrusions there are clasts of the deposit; slickensides are common in the margins of these lava intrusions; and lava fingers have also been injected in between clasts. These structures are located along a zone of slope break suggesting they were formed due to compression processes in the avalanche when adapting to the slope during the emplacement.

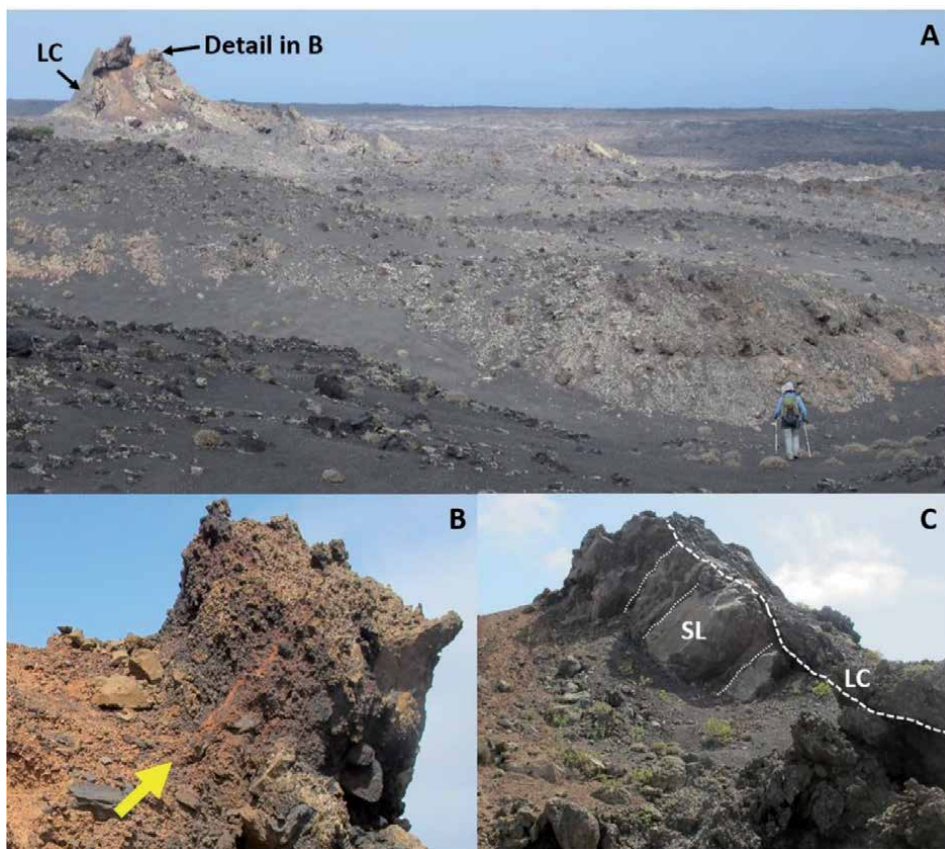


Figure 5. Isolated substrate megablock to the NNW of Mazo: (A) general view of the megablock inserted in a hummocky topography, indicating the location of the lava cover and B; (B) unstructured part of the megablock with clay injections into a scoria deposit; (C) layered deposits forming the megablock (for scale, the scar is around 10 m high). LC: Lava cover; SL: Substrate lava.

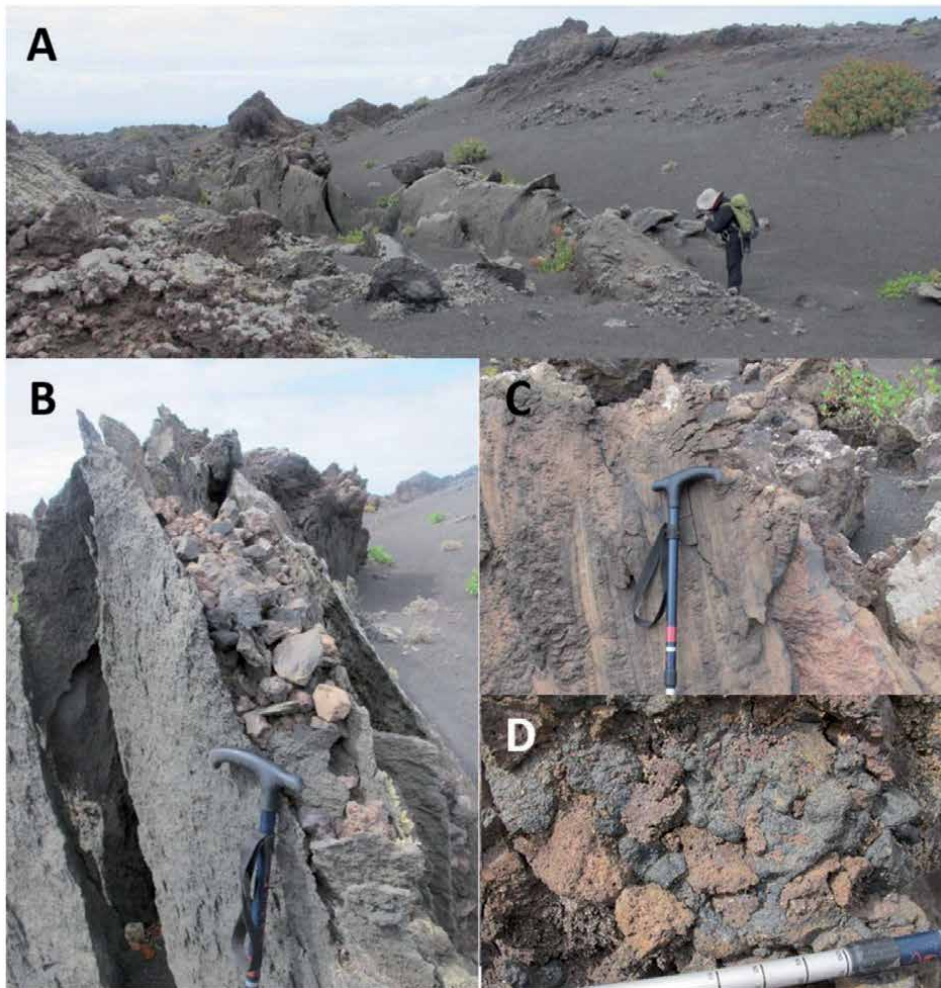


Figure 6. Squeeze-up structures in the DAD of Mazo: (A) curving pressure ridge; (B) DAD between the fingers of the squeeze-ups; (C) slickensides in a squeeze-up margin; and (D) injection of lava between DAD lithics.

The DAD is overlaid with a blast deposit in which three main layers have been identified (**Figure 3B** and 7). The first layer consists of big bombs and blocks up to 40 m³, composed of fragments of DAD or mafic dense blocks that appear scattered in proximal areas up to a distance of 500 m from the vent. Some of them are broken, split and wrapped in a fine layer of lava. Juvenile breadcrust bombs are also present. The second layer consist of a gray, clast-supported, well sorted and normal grading deposit (gravel to fine sand size) of clasts with parallel lamination up to 84 cm. Content of juvenile fragments is low. Finally, covering all previous deposits and adapting to the topography, a gray to yellow sand, matrix-supported and wavy laminated deposit is observed, being formed by hydromagmatic surges. It is better exposed in proximal areas with a thickness of around 40 cm decreasing to few centimeters in distal areas.

A blast deposit can be easily identified by a light gray layer below the strombolian fallout deposit. This layer can be observed over several cinder cones, at a distance larger than 7 km away from Mazo volcano. Although the blast deposit is distributed in patches, it should have covered the entire area, being better preserved in areas with thermal alteration like those close to the crater and in most of the



Figure 7. Blast deposit. (A) Broken bomb 500 m far from the vent; (B) core of bomb in A consisting of DAD; (C) layer two; (D) layer three overlaying an oncoids mound; (E) hydrothermal fluids escape pipes in layer 3; (F) Oncolite structure made up of a lithic nuclei covered by hematite (black in color) and several layers composed of native sulfur, gypsum, jarosite, and minor anhydrite (yellow in color).

megablocks and hummocks. The alteration affects both the DAD and the blast deposit that cover them, giving place to yellowish-colored crusts which are broken into sheets in the steepest sectors. Degassing structures are also observed affecting these deposits. At the top of the sequence there is a strombolian fallout deposit, thicker in proximal areas (**Figure 3B**). A simplified stratigraphic column has been included in **Figure 8A**.

In the northern sector of the cone and along the graben fractures near to the crater, there are clear evidences of hydrothermal alteration and fumaroles activity. At this site a mound-type deposit with an external structure similar to a cauliflower covered by hydromagmatic surges is found. This mound is formed by soldered centimetric to decimetric oncoids (**Figure 7F** and **H**), yellow to cream in color; all of them have concentric build-ups around a lithic nucleus. Mineralogy of different laminae are determined by X-ray diffraction method and major chemical analyses were made on the IGME laboratories being their general structure and composition as follows: 1) single or composed subrounded lithic nuclei that have a thin black Fe-hydroxides coating; 2) several (three to six) concentric yellow laminae of native

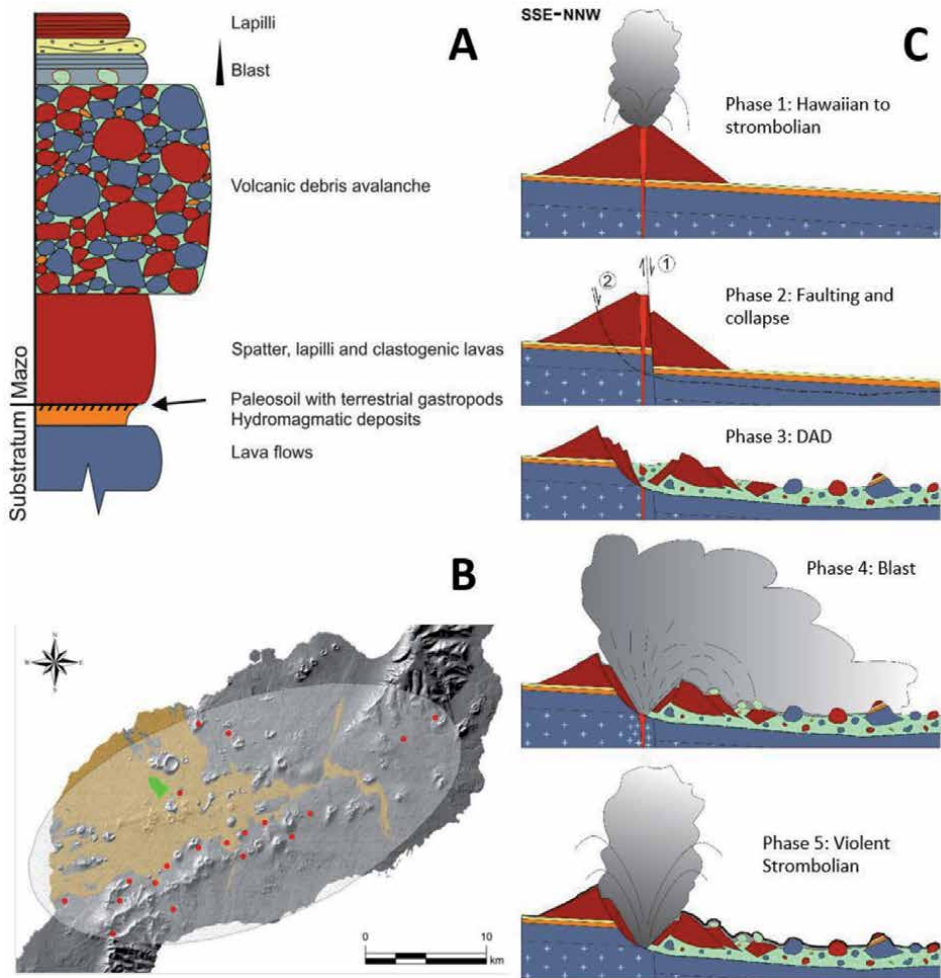


Figure 8. (A) Schematic stratigraphic column of Mazo. (B) Minimum area affected by ash dispersion (oval in gray) from Mazo volcano (in green) based on the location of affected villages (red dots). (C) Cartoons showing the main phases of Mazo eruption (see text for explanation).

sulfur, jarosite, gypsum and anhydrite; 3) a white laminae made of amorphous silica and opal-A. Occasionally, oncoids are composed of Fe-hydroxide coatings, opal-A white laminae and yellow laminae.

4. Age of Mazo eruption

Within the eruptive system of Timanfaya (1730–1736) there are very few volcanic episodes sufficiently documented in historical chronicles to establish their precise spatial and temporal location in order to reconstruct Timanfaya’s complete eruptive history. This fact has made it difficult to establish the complex formation sequences of the entire eruptive system. Although some authors have proposed evolutionary sequences that interpret the Timanfaya individual eruptions by analyzing historical information combined with chronostratigraphical studies and geological and geomorphological mapping (eg. [9, 11, 18–21]), there are still uncertainties about when, where and what volcanic processes occurred in each of the multiple eruptive vents and fissures developed during those

6 years of the 18th century [11]. This is the case of Mazo volcano whose age and eruptive style are quite controversial.

Most authors suggest that Mazo volcano was one of the multiple eruptive fissures of Timanfaya eruption [9, 11, 17, 24–26], while others assume that it was formed during a pre-Timanfaya eruption. Published geological maps include it as a Middle Pleistocene volcano but pointing out the possible existence of an historical emission center in the area due to the very recent aspect of several bombs and scoria [27, 28]. Other authors consider Mazo as an eruption prior to Timanfaya based on the following considerations [19]: 1) a visual recognition of this volcano suggest an old cone due to its color and eroded aspect; 2) paleomagnetic data of Mazo volcano show differences in magnetic parameters (declination and inclination) compared to other Timanfaya's well studied volcanoes; and 3) this volcano is surrounded by lava flows issued by vents from the Timanfaya initial eruptions, previous to Mazo.

All these criteria can be discarded if we consider that: 1) the eroded aspect of Mazo is due to the hydrothermal alteration caused by fumarolic activity and remnant heating and gas escape through the DAD; 2) the previously considered as Mazo lava flows are in fact a DAD so paleomagnetic orientations can be nearly uniform in every single block but the declination changes between blocks and from the source [14]; and 3) the origin of lava flows surrounding Mazo is not clear. It is evident that the lava flows emitted by the first vent of Timanfaya (Caldera de Los Cuervos), destroyed the village of Mazo on September 11th [9, 11, 17, 19, 24–26]; however, there is a disagreement on the source of the lava flows that overlie the eastern sector of Mazo, that have been assigned both to Caldera de Los Cuervos [19] and Pico Partido [21].

Our detailed map of lavas around Mazo (**Figure 9**) indicates that its deposits are surrounded, on the west, by lava flows from 1824 eruption and, on the east, by lava flows without direct connection to any emission center but probably coming from later eruptive phases of Pico Partido. Pre-Mazo lava flow, probably coming from Caldera de los Cuervos outcrop to the north of Mazo, partially covered by lapilli.

For more information on the possible assignment of Mazo to Timanfaya eruption we have reviewed historical chronicles. The information comes from several

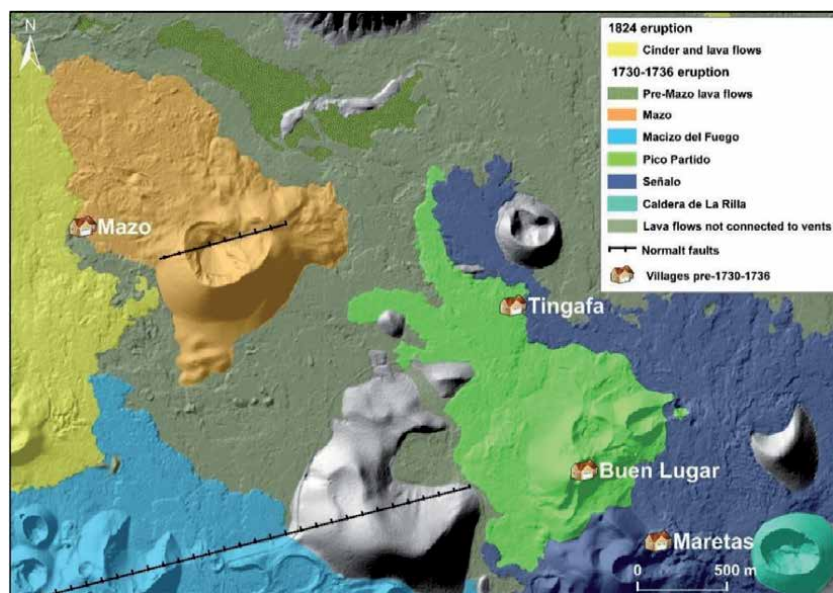


Figure 9. Lava flows and historical volcanic cones around Mazo volcano. Main normal faults trending parallel to Timanfaya main fissure are also shown.

sources: 1) the description of the eruption made in 1744 by the priest of Yaiza in his diary (hereinafter CY) (referred in [29]); 2) the data contained in a manuscript with the dossier promoted by the Royal Court of the Canary Islands, which is currently preserved in the General Archive of Simancas (hereinafter MsS) [9, 16]; and 3) notarial and religious data contemporary with the eruptions [25, 30].

It is generally accepted that Timanfaya multiple eruption began at Caldera de Los Cuervos volcano on September 1th, 1730 and lasted until mid-September [9, 11, 19, 21]. After a short rest, on October 10th, 1730 two new eruptive fissures were opened at Caldera de la Rilla and Pico Partido volcanoes forming a NW-SE alignment with Caldera de Los Cuervos (**Figure 1**). Activity in these fissures ended on November 1730 and January 16th, 1731, respectively [30]. On 20th January 1731 a new volcano erupted. Although, some authors assume that this new volcano was Caldera de la Rilla [19], the chronicles say it was located half a quarter of a league (2.4 km) from the previous eruption of Pico Partido [30] and at the destroyed village of Mazo (MsS, letter of February 19th 1731), which was burned and covered by lava flows from Caldera de Los Cuervos volcano on September 11th 1730 (MsS, letter of 17th October 1731 [29], previously to Mazo eruption. There is only one eruptive complex that meets all the conditions, namely: location in the place where the burned village of Mazo was located and distance from the Pico Partido complex of about 2.4 km. That volcano is undoubtedly Mazo. In addition, it is in the continuation of the first volcanic alignment of Timanfaya (**Figure 1**) and have a similar composition (basanitic) of those volcanoes on the NW-SE alignment [18].

Assuming Mazo is the fourth eruptive fissure of Timanfaya some information about the eruption can be extracted from the chronicles. However, it is interesting that there is no reference to this volcanic episode of January 20th in the CY manuscript, which is one of the main sources of information on the eruption. In turn, there is a mention to an eruption starting the 10th of the same month that does not appear in the rest of the consulted documentary sources. Some errors regarding the start dates of some volcanic episodes of the eruption are relatively common in this chronicle [11, 26], probably due to the great spatio-temporal extension of the eruption, to the lack of a continuous monitoring of the eruptive vents, and also to the fact that this manuscript was written 8 years after the ending of the eruption [11], or even to transcription and translation errors of the original document [26].

Even so, if the specific dates are ignored, the sequence of events is similar in all the chronicles consulted. In fact, eruptive activity developed in January 1731, whatever the source consulted or the specific dates, is characterized by the cessation of activity of the volcano opened in the sector of Pico Partido on October 10th, followed by the occurrence of a seismic crisis of considerable intensity whose effects were felt in Gran Canaria Island [9], more than 190 km away, and by the beginning of a new eruption [16, 25, 30].

The narration realized by the Priest of Yaiza for the eruption of January 20th also says: “On the 10th [in place of 20th] of January a mountain raised that the same day crumbled with and incredible crash inside its own crater, and covered the island with stones and ashes. Incandescent currents of lava collapsed onto the malpais up to the sea” [29]. Evidently, CY is describing the sudden collapse of Mazo volcanic cone and the formation of incandescent currents that reached the sea, with a total length of 6 km. The concatenation of later phenomena described in the documentary sources put in evidence that this process gave place to the formation of a high eruptive column that dispersed the pyroclasts over the whole island of Lanzarote (CY, MsS) and part of Fuerteventura (MsS). In mid-February the documentary sources (letter from Ambrosio Cayetano de Ayala; MsS) cite a score of villages in the central part of Lanzarote affected by ash fall [16, 30] (**Figure 8B**). The eruptive event of Mazo volcano lasted only seven days, as CY mentions that this eruption ended on January 27th, 1731.

5. Evolution of Mazo eruption and causes of the flank collapse

On January 20th 1731, after an intense seismic crisis, Mazo eruption started being the fourth eruptive fissure of Timanfaya. The initial activity was of hawaiian type, documented in the outcrops of agglutinates of scoria and clastogenic lavas in the flank of the preserved edifice, and also by the presence of the same type of material integrated in torea blocks and in some hummocks of the DAD. Later the style of the eruption shifted to strombolian type with emission of scoria (**Figure 8C**).

The rapid growth of the volcanic cone and a high emission rate may have been determining factors of the flank collapse that took place the same day as the eruption began. In this way, part of the collapse could be favored by accumulation processes in the cone that made it grow extremely quickly, exceeding its stability limit. Thus, once this limit is exceeded, small mass additions can generate debris avalanches [31, 32]. Also, the presence of a huge amount of lava in the crater or at the base of the cone could have favored the collapse [14, 33–35].

Doming process does not seem to be the trigger for the collapse, as the faults and fractures affecting the cone are practically parallel and do not follow the fracturing patterns associated with the intrusion and inflation processes [36, 37]. Even so, the geometry of the fractures can vary substantially depending on whether the intrusion is located within, below, or outside a volcanic edifice, and may vary according to the local geology and cause very different consequences [38]. The doming process cannot be ruled out because the original fracture pattern has been obliterated during displacement.

The existence of fractures that generate a graben structure arranged perpendicular to the direction of collapse, together with the presence of a higher and proximal torea domain and a hummock domain at the bottom of the collapsed flank, could be related to the existence of basal layers with low viscosity and ductile behavior on the substrate of the volcanic cone, located during movement under the hummock domain [39]. The presence of a basal layer with these characteristics is evidenced in the lava injection processes and squeeze-ups formations in the avalanche sectors subject to compression. In stratovolcanoes, this hypothetical low-viscosity layer belongs to the initial stratigraphic sequence of the stratovolcano and may originally be composed of weak material such as poorly consolidated proximal pyroclasts, coarse-grained tephra sequences, pyroclastic flows, or even blocky lava flows [39].

In monogenetic mafic volcanoes, the existence of basal spatter layers emitted during the initial stages of the eruption and subject to charging processes by accumulation of pyroclasts, has been used to explain rafting processes of volcanic cones. In the case of the flank collapse of a monogenetic edifice like Mazo, this layer may correspond to the spatter emitted during the initial phases, configuring the base of the stratigraphic sequence so that as the height of the volcano increases its weight and so their plasticity increases, thus causing the collapse. Any case, analogue models realized by [2], shows that the deformation of the base is needed for the formation of deep collapses that affect the central area of the cone, as well processes linked to the fracturing of the basement, both through horizontal, oblique or vertical motions.

In Mazo, the existence of a well-defined fault in the cone, parallel to a normal fault affecting recent deposits of Timanfaya [40] (**Figure 9**) with a fault displacement of at least 45 m, suggests a structural control. These faults are also parallel to the main eruptive fissure of Timanfaya. A change in the stress field during Mazo eruption is evident if we consider that Mazo is located at the end of the Timanfaya first NW-SE alignment and that Mazo fault is trending parallel to the second ESE-WSW Timanfaya fissure where the volcanic activity was concentrated after Mazo eruption. The intense seismicity previous to Mazo eruption could also be connected

with the modification of the stress regime that conditioned latter magma intrusion. The regional extension that facilitates the ascent of magma is accommodated by the formation of normal faults [41]. This orientation of extensional stress field in Timanfaya area is also confirmed by studies of fault population analysis [42]. Tectovolcanic processes affecting the basement are also supported by the large distal megablock included in the DAD. The generation of the collapse in the northern sector of the building reveals the influence of the stress regime within the volcano motivated by regional tectonic stresses in the first phase of Timanfaya or by the geometry of contact with the substrate, as it has been observed in central volcanic building collapses [43–45].

The flank collapse produced a volcanic debris avalanche that affected most of the volcanic edifice, including the summit area and part of the basement. The characteristics of the Mazo DAD are equivalent to those observed in stratovolcanoes, with a proximal area characterized by the presence of block facies through which more fractured material was emplaced forming flows at high slope and relatively short paths, while the most disaggregated material due to friction between blocks and fluidized by the presence of molten lava reached a longer distance producing more dispersed hummocks. The collapse formed a 500 m long amphitheater on the southern flank of the cone, and a DAD that, according to chronicles, reached the sea on the coast more than 6 km away. The volume of slipped cone and DAD is impossible to calculate as they are partially covered by lavas from subsequent eruptions.

The decompression caused immediately after the debris avalanche generated a blast cloud and ballistic projectiles composed of heavy blocks and bombs that were deposited in proximal areas and as far as 500 m from the vent. The blast cloud was a driven-gravity flow, probably divided in two parts [46]: 1) a coarse-grained basal flow of rock fragments; and (2) a fine-grained turbulent upper flow that originated the blast surge covering all the previous deposits. The blast deposit has been found at distances up to 6 km from the vent, and based on the historical chronicles, the fine-grained fragments affected the whole central area of Lanzarote. This deposit covered the DAD but now is only preserved in the areas where they either 1) suffered hydrothermal alteration due to its location onto hot torea blocks or hummocks, or 2) overlaid by pyroclasts from the last phase. Hydrothermal alteration in hummocks and squeeze-ups in the DAD also support this was a syn-eruptive collapse.

The presence of oncoids in an inter-torea depression located in the proximal area indicates that hydrothermal activity related to degassing along fractures was generated after the collapse. Mazo oncoids were then formed under boiling water in a degassing-phase related to a fracture close to the crater vent. Oncoids, travertine and sulfur laminated mound-type deposits have been described in other volcanic environments related to hydrothermal activity, warm and hot springs and geyser deposits [47–49].

After the blast, the eruption went on with a last strombolian phase finishing six days later. The lapilli emitted in this stage completely covered the topography burying smaller irregularities of the surface and homogenizing the geological landscape of the whole area of Mazo volcano.

6. Implications for volcanic risk assessment

Recent studies point out that monogenetic eruptions, usually characterized by hawaian-strombolian eruptive episodes, can also include sudden and more violent episodes that imply a higher risk for the population [6, 12, 14]. The identification of a syn-eruptive flank collapse and the associated blast of Mazo during the 1730–36

Timanfaya eruption provide evidence of a new hazard to be considered. It is also important to emphasize that this is not an isolated phenomenon since the historical chronicles refer to other collapse phases during the month of April 1731 that affected more than one volcanic edifice at a time [29]. However, there is no detailed description of the features of these processes except for some mentions to fractures, probably associated to semicircular collapses [9, 19, 50].

A flank collapse like that occurred during the eruption of Mazo volcano, besides the DAD and the associated blast, may originate hydromagmatic and violent strombolian episodes due to the post-collapse depressurization that significantly increases the eruption energy and form eruptive columns of great height and wide dispersion. Nevertheless, the studies on volcanic hazards in monogenetic volcanic fields are mainly concerned with the analysis of volcanic susceptibility and with the development of scenarios of lava flows, pyroclastic density currents (PDC), and pyroclastic ballistics and fallout [51–53]. Volcanic hazard assessment is rarely multi-hazard and is normally focused on lava flows invasion. In this context, it has not been considered eruptive scenarios including instability processes of volcanic edifices, ranging from less violent processes like rafting to flank collapses like this described for Mazo volcano.

The probability of flank collapses development during future mafic eruptions rises the potential risk for the population, even more when it is considered that the population has increased from 5000 inhabitants in Lanzarote in 1730 (as stated in MsS) to 205,910 nowadays plus 3,065,575 visitors [54]. An eruption with similar characteristics to that of Mazo at present times, not only would cover with ashes the whole island of Lanzarote and part of Fuerteventura but would also cause the closure of the two islands airports and ports. This would in turn cause serious damage to air and maritime transport of the islands, which are key aspects of the current economic system of both islands based on tourism and totally dependent on the outside.

In fact, the intensity of Mazo eruption and the syn-eruptive flank collapse show a high impact at a regional scale which exceeded the capacity of the insular and regional authorities. It was this fourth eruption that prompted the Royal Court of Canary Islands to carry out a dossier file to request the intervention of the King of Spain. This file is presently archived in the General Archive of Simancas in Valladolid province (Spain) and constitutes one of most complete documentary sources of the eruption. Fortunately, the fact that the eruption occurred in an area already devastated by the first episodes of Timanfaya eruption reduced its risk in 1730.

The development of debris avalanches and the generation of eruptive columns with high altitude associated to a collapse during a mafic monogenetic eruption oblige us to change the perception of hazards linked to the growth of such volcanic cones. All this indicates that we should pay more attention to this kind of processes and shows the need for detailed studies to identify and characterize them, more when the studied DAD had been previously described as lava flows [26, 27]. This will allow to obtain a deeper knowledge of the triggering factors and causes of this type of processes in order to carry out effective volcanic hazard assessment policies.

7. Conclusions

Based on detailed field work on Mazo volcano and the exhaustive review of historical documents we have been able to propose a new eruptive sequence for the first months of 1730–36 Timanfaya eruption. The inclusion of Mazo volcano as the fourth eruptive fissure of Timanfaya and the formation of a tectonic controlled

collapse previous to an important change in the eruptive dynamics is quite significant since it occurred at a time of important stress changes that notably affected the Timanfaya eruption and led to the formation of a large (>13 km) eruptive fissure along which the eruption developed from that moment on. The existence of faults affecting Timanfaya volcanic products demonstrate that there was an important structural control during the eruption. Thus, the eruptive processes produced during the first six months of this eruption, which is the best recorded in contemporary documentation, show that the previously established geological history constitutes a simplification of the events that took place in this area and that a reinterpretation of the historical chronicles and new field work should be carried out to clarify the evolution of the whole Timanfaya eruption, the largest historical eruption of the Canary Islands, and one of the most important in recent times in the world.

The example of Mazo illustrates that flank collapses are not processes uniquely linked to stratovolcanoes. Mazo is an example that during the construction of a scoria cone volcano-tectonic process might trigger a flank collapse as well, although the size of the amphitheater and the avalanche deposits are significantly smaller than those developed in stratovolcanoes. Mazo deposits display features and morphologies similar to those described to characterize volcanic instability processes generated in large volcanic structures, being the main difference the scale. This research emphasizes that mafic monogenetic volcanic eruptions can result in rafting or flank collapse. In both processes, morphology and structures in the cone can be similar, being the main difference the impact of the phenomena: while rafting is a relatively quiet emission of lavas with rafts, during a flank collapse occurs a sudden dramatic formation of an avalanche debris and a blast.

Understanding the causes of syn-eruptive collapses in monogenetic mafic eruptions is essential to correctly interpret the signs of active volcanoes during risk management for land planning and risk reduction in this type of eruptions. In addition to its implications for the Timanfaya eruption comprehension, the morphology of Mazo volcano, and its well exposed DAD deposits make it an ideal case study to characterize flank collapses and formation of DAD in monogenetic edifice, reason why it has been proposed as a geosite in the Canary Islands geoheritage inventory, being suitable to be proposed as a Global Geosite of international relevance for Spain.

Acknowledgements

This research is part of LIGCANARIAS Project (ProID2017010159) that has been partially funded by the Canary Islands Agency for Research, Innovation and Information Society (ACIISI) of the Government of the Canary Islands, co-financed by the Operational Programs FEDER and FSE of Canarias 2014-2020. The initial study was carried out within the framework of a Specific Agreement between Lanzarote Council and the Spanish Geological Survey (IGME). We would also like to highlight the collaboration of the Environmental Agents staffs from Timanfaya National Park, the National Parks Autonomous Organism, and the UNESCO Global Geopark of Lanzarote and Chinijo Islands. We appreciate the work done by Alberto Acosta thanks to a stay as a fellow of the University of Las Palmas de Gran Canaria (ULPGC) in the Unit of Canary Islands of the Spanish Geological Survey. We appreciate the review and comments made by the editor and reviewers of the manuscript.

Conflict of interest

There are no conflicts of interest.

Author details

Carmen Romero¹, Inés Galindo^{2*}, Nieves Sánchez², Esther Martín-González³
and Juana Vegas⁴

1 University of La Laguna, S/C de Tenerife, Spain

2 Spanish Geological Survey (IGME), Las Palmas, Spain

3 Natural Science Museum, S/C de Tenerife, Spain

4 Spanish Geological Survey (IGME), Madrid, Spain

*Address all correspondence to: i.galindo@igme.es

IntechOpen

© 2020 The Author(s). Licensee IntechOpen. This chapter is distributed under the terms of the Creative Commons Attribution License (<http://creativecommons.org/licenses/by/3.0>), which permits unrestricted use, distribution, and reproduction in any medium, provided the original work is properly cited. 

References

- [1] McGuire WJ. Volcano instability and lateral collapse. *Revista*. 2003; 1: 33-45
- [2] Acocella V. Modes of sector collapse of volcanic cones: Insights from analogue experiments. *Journal of Geophysical Research*. 2005; 110: B02205. DOI: 10.1029/2004JB003166
- [3] van Wyk de Vries B, Delcamp A. Volcanic Debris Avalanches. In: Shroder JF, Davies T, editors. *Landslide Hazards, Risks and Disasters*. Elsevier; 2015. p. 131-157. ISBN 9780123964526
- [4] Bernard B, van Wyk de Vries B, Barba D, Leyrit H, Robin C, Alcaraz S, Samaniego P. The Chimborazo sector collapse and debris avalanche: deposit characteristics as evidence of emplacement mechanisms. *Journal of Volcanology and Geothermal Research*. 2008; 176(1): 36-43. DOI: 10.1016/j.jvolgeores.2008.03.012
- [5] León R, Somoza L, Urgeles R, Medialdea T, Ferrer M, Biain A, García-Crespo J, Mediato JF, Galindo I, Yepes J, González FJ, Giménez-Moreno J. Multi-event oceanic island landslides: new onshore-offshore insights from El Hierro islands, Canary Archipelago. *Marine Geology*. 2017; 363: 156-175. DOI: 10.1016/j.margeo.2016.07.001
- [6] Riggs NR, Duffield WA. Record of complex scoria cone eruptive activity at Red Mountain, Arizona, USA, and implications for monogenetic mafic volcanoes. *Journal of Volcanology and Geothermal Research*. 2008; 178: 763-776 DOI: 10.1016/j.jvolgeores.2008.09.004
- [7] Smith IEM, Németh K. Source to surface model of monogenetic volcanism: a critical review. *Geological Society, London, Special Publications*. 2017; 446(1): 1-28. DOI: 10.1144/SP446.14
- [8] Harwood RD. Cinder cone breaching events at Strawberry and O'Neill craters, San Francisco volcanic field, Arizona [Master's thesis]. Flagstaff: Northern Arizona University; 1989
- [9] Romero C. La erupción de Timanfaya (Lanzarote, 1730-1736). Análisis documental y estudio geomorfológico. Ed. La Laguna: Universidad de La Laguna, Secretariado de Publicaciones; 1991. 136 p. ISBN 84-7756-272-5
- [10] Romero C. Estudio geomorfológico de los volcanes históricos de Tenerife. Ed. Santa Cruz de Tenerife: Aula de Cultura de Tenerife, Cabildo Insular de Tenerife; 1992. 265 p. ISBN 84-87340-17-2
- [11] Romero C. El relieve de Lanzarote. Ed. Cabildo de Lanzarote, Servicio de Publicaciones; 2003. 225 p. ISBN: 95938-18-9
- [12] Valentine GA, Gregg TKP. Continental basaltic volcanoes— processes and problems. *Journal of Volcanology and Geothermal Research*. 2008; 177(4): 857-873. DOI: 10.1016/j.jvolgeores.2008.01.050
- [13] Valentine GA, Perry FV, Krier D, Keating GN, Kelley RE, Cogbill AH. Small-volume basaltic volcanoes: Eruptive products and processes, and post-eruptive geomorphic evolution in Crater Flat (Pleistocene), southern Nevada. *Geological Society of America Bulletin*. 2006; 118(11-12): 1313-1330. DOI: 10.1130/B25956.1
- [14] Ui T, Takarada S, Yoshimoto M. Debris Avalanches. In: Sigurdsson H, editor. *Encyclopedia of Volcanoes*. San Diego, California: Academic Press; 2000. p. 617-626. DOI: 10.1007/978-1-4020-4399-4
- [15] Galindo I, Romero MC, Sánchez N, Morales JM. Quantitative volcanic susceptibility analysis of Lanzarote and Chinijo Islands based on kernel density

- estimation via a linear diffusion process. *Scientific reports*. 2016; 6: 27381. DOI: 10.1038/srep27381
- [16] Romero C. Crónicas documentales sobre las erupciones de Lanzarote. Ed. Torcusa, Fundación César Manrique; 1997. 237 p. ISBN: 84-88550-20-0
- [17] Romero C. Las Manifestaciones Históricas Volcánicas del Archipiélago Canario. Tenerife: Gobierno de Canarias, Consejería de Política Territorial; 1991. 695 p (vol. 1) and 768 p (vol.2)
- [18] Carracedo JC, Rodríguez-Badiola E, Soler V. Aspectos volcanológicos y estructurales, evolución petrológica e implicaciones en riesgo volcánico de la erupción de 1730 en Lanzarote, Islas Canarias. *Estudios Geológicos*. 1990; 46: 25-55. DOI: 10.3989/egol.90461-2436
- [19] Carracedo JC, Rodríguez-Badiola E. Lanzarote: la erupción volcánica de 1730. Ed. Servicio de Publicaciones, Cabildo de Lanzarote; 1991. 183 p. ISBN: 84-87021-15-8
- [20] Carracedo JC, Rodríguez-Badiola E, Soler V. The 1730-1736 eruption of Lanzarote, Canary Islands: a long, high-magnitude basaltic fissure eruption. *Journal of Volcanology and Geothermal Research*. 1992; 53: 239-250. DOI: 10.1016/0377-0273(92)90084-Q
- [21] Carracedo JC. The 1730-1736 Eruption of Lanzarote, Canary Islands. In: Gutiérrez F., Gutiérrez M, editors. *Landscapes and Landforms of Spain*. Verlag: Springer-Netherlands. 2014. p. 273-288. ISBN 978-017-8628-7
- [22] Reiche P. The torevá block—A distinctive landslide type: *Journal of Geology*; 1937: 45-538-548
- [23] Francis PW, Gardeweg M, Ramirez CF, Rothery DA. Catastrophic debris avalanche deposit of Socompa volcano, northern Chile. *Geology*; 1985. 13:600-603
- [24] Bravo T. *Geografía general de las Islas Canarias*. Tomo II. Ed. Santa Cruz de Tenerife: Goya; 1964. 594 p
- [25] De León J. Lanzarote bajo el volcán: los pueblos y el patrimonio edificado sepultados por las erupciones del s. XVIII. Ed. Arrecife: Casa de los Volcanes; 2008. 504 p. ISBN 978-84-95938-62-6
- [26] Pallarés A. Consideraciones en torno al manuscrito del cura de Yaiza, Andrés Lorenzo Curbelo, sobre las erupciones volcánicas del siglo XVIII en Lanzarote. XII Jornadas de Estudios sobre Lanzarote y Fuerteventura. 2008; vol. 1- tomo I: 187-201. ISBN: 978-84-95938-98-5
- [27] Gómez Sainz de Aja JA, Barrera Morate JL. Mapa geológico de la Hoja nº 1081I (Tinajo). In: *Mapa Geológico de España E. 1:25.000. Segunda Serie (MAGNA), 1º ed.* Madrid: Instituto Geológico y Minero de España (IGME). 2004
- [28] Balcells Herrera R, Barrera Morate JL, Gómez Sainz de Aja JA, Ruiz García MT. Memoria del Mapa Geológico de España. Escala 1:25.000. Tinajo. Madrid, Instituto Geológico y Minero de España, 2004
- [29] Buch von H. Über einen vulcanischen Ausbruch auf der Insel Lanzarote: gelesen in der Akademie der Wissenschaften d. 4. Febr. *Abhandlungen der Königlichen Akademie der Wissenschaften in Berlin*; 1819.p. 69-82.
- [30] Cazorla León S. Los volcanes de Chimanfaya. Ed. Ayuntamiento de Yaiza, Lanzarote, 2003. 127 p.
- [31] McGetchin TR, Settle M, Chouet BA. Cinder cone growth modelled after northeast crater, Mount Etna., Sicily. *Journal of Geophysical Research*. 1974; 79: 3257-3272. DOI: 10.1029/JB079i023p03257

- [32] Riedel C, Ernst GGJ, Riley M. Control on the growth and geometry of pyroclastic constructs. *Journal of Volcanology and Geothermal Research*; 2003; 127: 121-152. DOI: 10.1016/S0377-0273(03)00196-3
- [33] Németh K, Risso C, Nullo F, Kereszturi G. The role of collapsing and cone rafting on eruption style changes and final cone morphology: Los Morados scoria cone, Mendoza, Argentina. *Open Geosciences*. 2011; 3(2): 102-118. DOI: 10.2478/s13533-011-0008-4
- [34] Moufti MR, Németh K. *Geoheritage of Volcanic Harrats in Saudi Arabia*. Berlin: Springer; 2016. 205 p. DOI: 10.1007/978-3-319-33015-0_1
- [35] Kervyn M, Ernst GGJ, Carracedo JC, Jacobs P. Geomorphometric variability of “monogenetic” volcanic cones: Evidence from Mauna Kea, Lanzarote and experimental cones. *Geomorphology*. 2012; 136(1): 59-75. DOI: 10.1016/j.geomorph.2011.04.009
- [36] Troll VR, Walter TR, Schmincke, HU. Cyclic caldera collapse: piston or piecemeal subsidence? Field and experimental evidence. *Geology*. 2002; 30(2): 135-138.
- [37] Hansen DM, Cartwright J. The three-dimensional geometry and growth of forced folds above saucer-shaped igneous sills. *Journal of Structural Geology*. 2006; 28(8): 1520-1535. DOI: 10.1016/j.jsg.2006.04.004
- [38] van Wyk de Vries B, Marquez A, Herrera R, Bruña JG, Llanes P, Delcamp A. Craters of elevation revisited: forced-folds, bulging and uplift of volcanoes. *Bulletin of Volcanology*. 2014; 76(11): 875. DOI: 10.1007/s00445-014-0875-x
- [39] Andrade SD, van Wyk de Vries B. Structural analysis of the early stages of catastrophic stratovolcano flank-collapse using analogue models. *Bulletin of Volcanology*. 2010; 72: 771-789. DOI: 10.1007/s00445-010-0363-x
- [40] Tibaldi A. Morphology of pyroclastic cones and tectonics. *Journal of Geophysical Research*. 1995; 100: 24521-24535. DOI: 10.1029/95JB02250
- [41] Paguican EMR, Bursik MI. Tectonic Geomorphology and Volcano-Tectonic Interaction in the Eastern Boundary of the Southern Cascades (Hat Creek Graben Region), California, USA. *Frontiers in Earth Science*. 2016; 4: 76. DOI: 10.3389/feart.2016.00076
- [42] Sánchez N, Rodríguez MA, Perucha MA, Pérez R, Romero C, Galindo I, et al. Caracterización Volcanotectónica de los Parques Nacionales de la Caldera de Taburiente, Teide y Timanfaya: Relaciones Volcanismo-Tectónica-Sismicidad-Magnetismo. In: Amengual P, editor. *Proyectos de Investigación en Parques Nacionales: 2013-2017*. Madrid: Naturaleza y Parques Nacionales. Serie Investigación en Red. OAPN; 2019. p. 53-77. ISBN: 978-84-8014-924-2
- [43] Vallance JW, Siebert L, Rose WI, Girón JR, Banks NG. Edifice collapse and related hazards in Guatemala. *Journal of Volcanology and Geothermal Research*. 1995; 66: 377-355. DOI:10.1016/0377-0273(94)00076-S
- [44] van Wyk de Vries B, Borgia A. the role of basement in volcano formation. *Geological Society, London, Special Publications*. 1996; 110: 95-110. DOI: 10.1144/GSL.SP.1996.110.01.07
- [45] Lagmay AMF, van Wyk de Vries B, Kerle N, Pyle DM. Volcano instability induced by strike-slip faulting. *Bulletin of Volcanology*. 2000; 62(4-5): 331-346. DOI: 10.1007/s004450000103
- [46] Belousov A. Deposits from the 30 March 1956 directed blast at Bezimianny volcano, Kamchatka, Russia. *Bulletin*

of *Volcanology*. 1996; 57: 649-662. DOI: 10.1007/s004450050118

[47] Jones B, Renaut RW. Formation of silica oncoids around geysers and hot springs at El Tatio, northern Chile. *Sedimentology*. 1997; 44: 287-304. DOI: 10.1111/j.1365-3091.1997.tb01525.x

[48] Jones B, Renaut RW. Petrography and genesis of spicular and columnar geyserite from the Whakarewarewa and Orakeikorako geothermal areas, North Island, New Zealand. *Canadian Journal of Earth Sciences*. 2003; 40:1585-1610. DOI: 10.1139/e03-062

[49] McCall J. Lake Bogoria, Kenya: hot and warm springs, geysers and Holocene stromatolites. *Earth-Science Reviews*. 2010; 103(1-2): 71-79. DOI:10.1016/j.earscirev.2010.08.001

[50] Romero C, Dóniz J, Cacho LG, Guillen C, Coello E. Los hornitos y coneletes de escorias del Echadero de los Camellos en Timanfaya: rasgos morfológicos y estructurales. In: Lario J, Silva, PG, editors. *Contribuciones al Estudio del Periodo Cuaternario*. Aequa, Ávila; 2007. p. 171-172

[51] Felpeto A, Martí J, Ortiz R. Automatic GIS-based system for volcanic hazard assessment, *Journal of Volcanology and Geothermal Research*. 2007; 166: 106-116. DOI: 10.1016/j.jvolgeores.2007.07.008

[52] Laín Huerta L, Bellido Mulas F, Galindo Jiménez I, Pérez Cerdán F, Mancebo Mancebo M J, Llorente Isidro M. La cartografía de peligrosidad volcánica de Tenerife. In: Galindo Jiménez I, Laín Huerta L, Llorente Isidro M, editors. *El estudio y la gestión de los riesgos geológicos*. Madrid: Publicaciones del Instituto Geológico y Minero de España. Serie: Medio Ambiente. Riesgos Geológicos 12; 2008. p: 175-186

[53] Becerril I, Bartolini S, Sobradelo R, Martí J, Morales, JM,

Galindo I. Long-term volcanic hazard assessment on El Hierro (Canary Islands). *Natural Hazards Earth System Science*. 2014; 1853-1870. DOI: 10.5194/nhess-14-1853-2014

[54] ISTAC. 1999. Available from: <http://http://www.gobiernodecanarias.org/istac/jaxi-istac> [Accessed: 2020-08-20]

Spatial Visualization of Geochemical Data: Application to the Chichinautzin Volcanic Field, Mexico

Philippe Robidoux, Julie Roberge and César Adams

Abstract

The presence of spatial magma heterogeneities in volcanic monogenetic fields is a major observation discussed as well synthesized for worldwide volcanic fields. Magma heterogeneities still have not been visualized in the form of detailed spatial analyst tools, which could further help structuring works of geological mapping, volcanic hazard, and geoheritage evaluations. Here we synthesized 32 published datasets with a novel geochemical mapping model inspired by sub-disciplines of geomatic in one of the most documented monogenetic fields on earth: the Chichinautzin Volcanic Field (CVF) in Mexico. The volcanic units from CVF are covering the 2500 km² area, and its neighbor stratovolcanoes are bordering the limit of most volcanic centers (Popocatepetl, Iztaccihuatl, and Nevado de Toluca). The results illustrate polygons and point map symbols from geochemical markers such as Alkalis vs SiO₂, Sr/Y, and Ba/Nb. The geochemical heterogeneity of the CVF monogenetic bodies decreases as it approaches the Popocatepetl-Iztaccihuatl stratovolcanoes. This alignment is not observed in the occidental CVF portion near the flank of Nevado de Toluca, but geochemical anomalies associated to markers of continental crust interaction such as Sr/Y follow elongated patterns that are not strictly following structural lines and faults mapped on surface.

Keywords: monogenetic, spatial interpolation, trans-Mexican Volcanic Belt, geochemistry, Chichinautzin

1. Introduction

The presence of volcanic centers clustered in a monogenetic field involves possible control from the feeding plumbing system architecture. The range of chemical composition (i.e. major elements abundances such as SiO₂ contents, trace elements, etc.) from the effusive as explosive volcanic rocks also lead to various interrogations regarding origin of the magma that circulate in the lithosphere below monogenetic volcanic fields. Most of all, the presence of spatial magma heterogeneities is a major observation discussed and synthesized for volcanic fields in subduction zones [1–3]. Visualization tools are required to facilitate these observations and analyses for understanding the building of minor volcanic centers as defining the origin of the magma in monogenetic fields.

The Chichinautzin Volcanic Field (CVF) in the center of the Trans-Mexican Volcanic Belt (TMVB) represents the ideal study case to improve observations and simplify visualization of spatial heterogeneities among a volcanic field. The high sampling density of volcanic rock samples in CVF literally favor the area for such studies. Building a spatial visualization model becomes necessary regarding natural hazards because of CVF vicinity to the greater Mexico city, globally one of the most populated urban area.

A novel spatial model and geomatic tool are thus presented here to illustrate the geochemical dispersion from sampled volcanic rocks. This spatial model is simple and involves high precision for object localization on a map. Geochemical markers (geomarkers) related to classic igneous petrological analyst tools now are given quantitative symbols and projected on a digital elevation model (DEM) background. Point symbols and polygons that mark specific ranges of values from the geomarkers show clear spatial magma heterogeneities that can be interpreted and used in various disciplines of geosciences.

1.1 Chichinautzin volcanic field

The Chichinautzin Volcanic Field (CVF) in the center of the Trans-Mexican Volcanic Belt (TMVB) is a key zone to understand recent monogenetic magmatism in a subduction zone. The volcanism of CVF and seismic activity underneath is rift-related and is also affected by the subduction of the Cocos plate under North American plate [4–9]. The age of volcanism is relatively young; geochronological ^{14}C data, paleomagnetic measurements and the $^{40}\text{Ar}/^{39}\text{Ar}$ method applied on volcanic rocks give ages that goes up to 1200 ka [10–12]. The youngest eruption is the Xitle scoria cone around 1665 ± 35 years b.p., whose lavas destroyed and buried the pre-Hispanic settlement of Cuicuilco [13].

The question of where volcanism occur is particularly of interest for geologists since around the populated valley of the greater city of Mexico, the CVF includes more than 220 quaternary cinder cones and few shield volcanoes, with their associated lava flows and tephra sequences (**Figure 1a, b**). In addition, the region is still “geologically active”; the volcanic structures tend to be aligned on E-W normal faults [14] with stratovolcanoes (Popocatepetl-Iztaccihuatl and Toluca) occurring at the intersection of N-S and E-W faults [16, 18]. The source of magmatic and seismic activity is also of concern [19], beneath all CVF, the inferred depth of the slab interface is changing between 80 km and drastically to levels far deeper than 100 km [8, 20]. The crustal thickness beneath the CVF is ~40 to 50 km which is the greatest in the TMVB [8, 9].

Noteworthy in the field of geochemistry, [14] mentioned a spatial variation from the composition of volcanic rocks and schematic sections were proposed to show where are the different kind of magmas in CVF [15, 21]. Overall, there have been lots of work done in the CVF relating its heterogeneity, and with the rapid development of analytical techniques in geochemistry, a new data compilation was needed after [22].

The geochemistry of the volcanic products in the CVF is characterized by basaltic andesite to dacitic rocks with alkaline to calc-alkaline affinities [9, 23]. The majority are subalkaline, except for the most mafic samples (ex: Chichinautzin and Guespalapa) which are transitional and plot in the alkaline field [14]. Mafic melt compositions (basalt, basaltic andesites) are found in olivine phenocrysts holding glass inclusions of ~49 to <54 wt.% SiO_2 (i.e. see Xitle, [24] and Pelagatos, [25]).

Since the first proposed petrogenetic explanation from Gunn and Mooser works (1970s), the origin of magmas heterogeneities in the CVF is still debated. Two different types of mantle-derived primitive mafic magmas have been suggested for

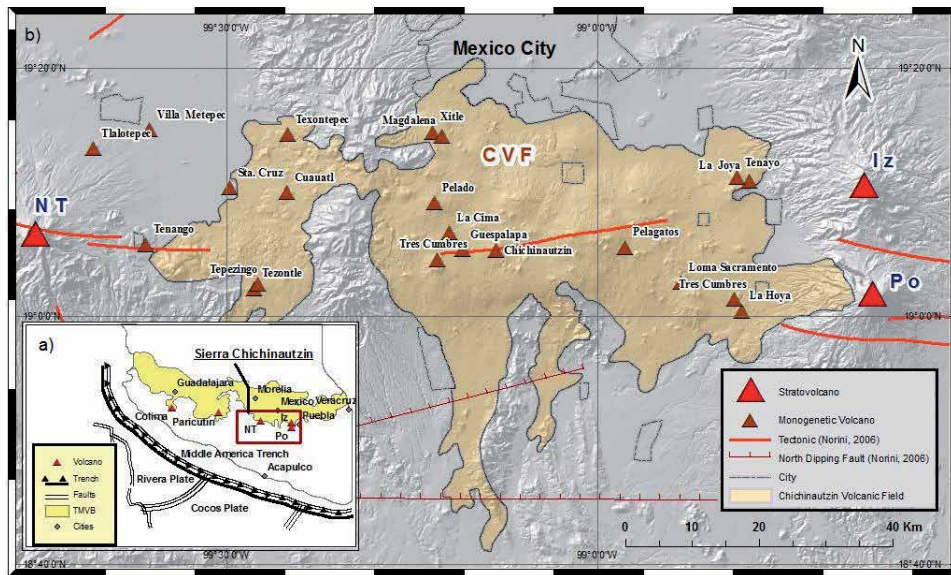


Figure 1.

Area of study (map modified from the following authors; [13–15]) including the Chichinautzin volcanic field (CVF) (shaded polygon), well known monogenetic volcanic centers (small solid triangles), stratovolcanoes (big solid triangles), the urban areas (gray limits) and tectonic features from [16] (large lines). A digital elevation model (DEM) was built to represent the topography with a 30 meter-resolution. The digital elevation model (DEM) was built in ArcGIS to represent the topography with 30 meters resolution (access from INEGI, [17]). The smaller map represents the tectonic context of the trans-Mexican volcanic fault (TMVB) and Chichinautzin volcanic field (CVF) emplacement (map modified from [14, 15]. The geological and geophysical features of the TMVB (shaded area), active volcanic centers (solid triangles), and major cities (full circles) and the CVF (shaded rectangle). Part labels “CVF” is for Chichinautzin Volcanic Field, “NT” is for Nevado de Toluca, “Po” is for Popocatepetl and “Iz” is for Iztaccihuatl.

CVF based on Sr-Nd isotopes, trace elements and mineralogical features [15, 26]. The first type is an OIB-like mafic magma, and is characterized as anhydrous [6, 9, 15, 23, 27–29]. The second type is associated to a metasomatized mantle source, with incompatible elements of a depleted mantle source, but enriched in mobile elements that are possibly coming from the subducting slab [6, 9, 23, 29].

1.2 Method

A database of whole rock composition was produced by the compilation of geochemical data from 583 samples of volcanic materials within the CVF (Appendices). A total of 32 references was used containing whole rock data (major and trace elements from (A) Scoria cones in the Chichinautzin Volcanic Field (sample of lava, bomb and scoria), (B) Iztaccihuatl, (C) Popocatepetl, (D) Nevado de Toluca. In the case of stratovolcanoes (B–C–D), only were considered juvenile samples of pyroclast, pumice or a dome fragment.

1.2.1 Geomarkers defined

Pairs of geochemical elements from whole rock analysis and representing high density sampling area were chosen based on their petrogenetic significance. All referenced data from the geochemical dataset of CVF were given latitude and longitude coordinates (Appendices I, II), then a spatial attribute is automatically associated when the tables are uploaded in a Geographic Information System (GIS). This database was projected with ArcGIS software [30] to detect any spatial trend.

The compiled data come from 32 published works between 1948 and 2011 (See Appendix II for a list of the references used). Also, for comparison, data from the neighbor polygenetic volcanoes are included: Popocatepetl, Iztaccihuatl and Nevado de Toluca.

The systematic approach described above was possible to propose with a compilation and a methodical statistical investigation of geochemical tracers of petrogenetic and tectonic processes. The statistic distribution of a single ratio is called a geochemical marker (geomarker).

In this review, 2 geomarkers were chosen based on the significance they represent in rock classification and petrogenesis. Two datasets of each geomarker were then created from the central geodatabase and plotted in the GIS map:

1. The alkali geomarker (464 datas) which represents the alkalinity of the rocks and may be indicative of assimilation from continental crust during formation of the magmas. The ratio is obtained by dividing alkalis over silica which transform the conventional bivariate graphic into a univariable value for mapping [31–33]. The Sr/Y geomarker (228 datas) is used to evaluate the significance of the alkali geomarker. The alkalinity of the rocks has high probability to be associated to the systematic of crustal thickness when high values from Sr/Y point symbols match areas with strong alkalinity. The *Updates in Volcanology – Transdisciplinary Nature of Volcano Science* equilibrium of plagioclase fractionating on Sr and both amphibole + garnet phases on Y is recognized to correlate with the variation of crust thickness in arc magmas [27].
2. The Ba/Nb geomarker (320 data) is used to geochemically characterize the tectonic environment. Ba is more soluble and mobile in subduction fluids [34]. Nb is considered immobile in subduction fluids, it is not added to the mantle asthenospheric wedge and the rising basaltic melts, because it remains in the metamorphic rocks of the subduction zone [35, 36]. High ratios of Ba/Nb are then suspected of magmas enriched in fluid coming from subduction.

1.2.2 Geostatistics to support spatial model

The method proposed in this work uses spatial interpolation models which require evaluation depending on the data dispersion of the samples and previous geostatistics made on the databases. The principle of interpolation in cartography is applied to improve visualization of regional patterns of a natural phenomenon and to generalize a numerical distribution in a certain region [37, 38]. The equations of such models can be consulted in [37, 38], and also searched in the GIS tutorials [30, 39].

Evaluations on previous interpolation approaches to CVF were resumed in [40]. Intercomparing of kriging, inverse distance weight (IDW) and Linear Decrease (LD) is necessary due to the difference of input parameters between each approach. Ordinary kriging is proposed here according to the high density of samples in several areas between Popocatepetl and Nevado de Toluca flanks, mostly between latitudes 19°00' and 19°20' (**Figure 1**). As petrologists are interested by geological factors that influence the geomarkers at different scales [27, 34–36], the semi-variogram evaluation preceding the ordinary kriging becomes necessary to determine at what distance are the geochemical changes tendencies [40]. As a matter of fact, the common analyze of nugget, sill, and range for determining the spatial dependence of geochemistry is unique to this interpolation technique [37, 38]. If the preferential orientation of data positions in the map was constrained (i.e. anisotropy), the angle (in degrees) could be manipulated by specific kriging methods in several pieces of GIS software. In CVF, as seen in **Figure 1**, the large 2500 km² area contains too many

sources of anisotropy, which lead to eliminate angles dependence along the input parameters.

1.2.3 Evaluation of the physical environment

The interpolation model is only applied for the monogenetic cones of the CVF, because the material dispersion is not the same for the eruption of stratovolcanoes. A map with punctual representation of each calculated average composition at each volcanic emission center is compared with the original dataset (**Figure 1**) and used for the interpolation model. When the raster model is obtained for the alkalis and Ba/Nb geomarkers, four categories of raster values are associated to quartiles in four categories of colors used for the geomarkers of CVF and then transformed into polygon shapefiles. The mapped results of interpolation of CVF is sliced in the GIS with the same four quartile limits (the same colors) for each range of values.

As for other interpolation techniques, the limiting distance (D_0) chosen for considering a maximum number of points is important [37, 38]. This is determined for modeling the distribution of rock geochemistry because it is setting a maximum distance of influence between different sampled sites. This limiting distance (D_0), or technically called “search radius” use a weighting exponent adjusted to the influence of the distance between sample points. First, to provide estimated values at locations of interest and second, to generate values presenting the same dispersion characteristics as the original data [38].

To determine D_0 , the physical environment must be considered. In this study, a D_0 of 6000 m was used based on the maximum length of lava flows measured from 76 cones in CVF, this is considering that effusive rocks are emitted at larger distance than ballistic projectiles from explosive eruptions. A 6000 m buffer area was thus drawn covering almost all the data on the map and tried to avoid isolated samples (sometimes outliers). The buffer separates the farthest sample on the map from this artificial boundary. The radius is especially useful for limiting the interpolation calculation. In addition, by clipping for the same distance the resulting matrix image, a better design of the geomarker dispersion model is obtained. The drawing of the four polygons color categories is recommended to fit exactly with the four quartile categories that represent the range of pixel values.

1.2.4 Evaluation of spatial model

The datasets of alkalis and Ba/Nb are analyzed with spatial geostatistical tools, specifically the Moran's Index (I) because of its simple interpretation for determining the level of spatial autocorrelation (**Table 1**). The spatial autocorrelation from such index measures dependence among nearby values in a spatial distribution [41]. It considers that variables may be correlated because they are affected by similar processes, or phenomena, that extend over a larger region [38, 41]. The index is the result of a specialized algorithm; it first takes into account the classes of distances created for point pairs that are more or less at the same distance to each other [30, 39].

For all point pairs within a distance group, the spatial autocorrelation index (I) is calculated and it can be summarized as follow [equation in ILWIS 3.7, 38]: strong positive autocorrelation ($I > 0$), strong negative autocorrelation ($I < 0$), or random distribution of values ($I = 0$).

Pattern characteristics of the data were also analyzed. The parameter Prob1Pnt was calculated using ILWIS 3.7. This calculates the probability that within a certain distance (column distance) of any point, at least one other point will be found, i.e.

Spatial autocorrelation	Alkalis	Ba/Nb
Moran's I index	0.42	0.48
Z score	2.81	3.02
Dispersion		
Prob1Pnt (m)	8250	9500

Recall the legend for Moran I: Strong positive autocorrelation ($I > 0$), Strong negative autocorrelation ($I < 0$), Random distribution of values ($I = 0$).

Table 1.
Results of parameters from spatial autocorrelation (Moran Index, Z Score) and dispersion functions (Prob1Pnt).

the probability to find the nearest neighbor of any point list within this distance. It is a direct measure of dispersion and for the case of CVF, it indicates if the sampling area is well covered for the 220 identified volcanic centers (**Table 1**).

To evaluate “how good” is the model, cross validation calculation was used where the goal is to have the smallest root-mean-squared prediction errors [30, 38]. The cross-validation method is based on percent error or PE (%) and a RMSE (root mean square error). It is the mean of the squared difference between the observed value (P_i^*) and the predicted value (P_i), where n is the number of observations.

1.3 Results

1.3.1 Alkali geomarker

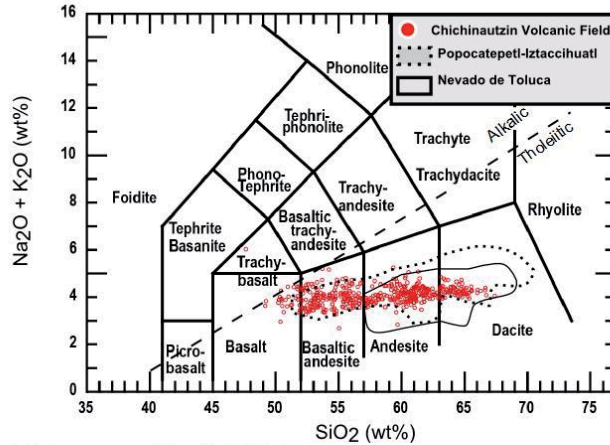
The geochemistry diagram shows alkaline enrichment in the four groups and greater dispersion for CVF (**Figure 2A**). The alkalinity is stronger for the stratovolcanoes and the rock names vary from basaltic trachy andesite to trachydacite. The CVF is classified between basaltic andesite to dacite. Iztaccihuatl have similar values from sample of East CVF or Valley of Puebla (same trend). The Nevado de Toluca has strong alkalis values (third and fourth quartiles).

As seen in **Figure 2B**, the total sample distribution is almost a Gaussian curve for all incorporated samples in the database. The Moran Index (**Table 1**) demonstrates data that are spatially clustered, but the distribution is not random. The study gives a probability pattern to find a first interpolation point for 8250 m.

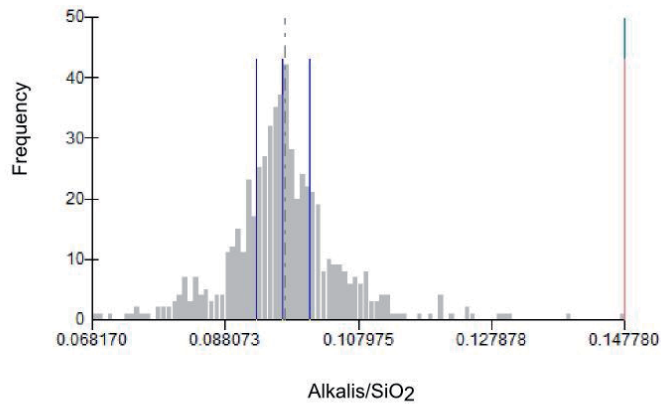
From the semi-variogram evaluation on the model (**Figure 2C**), the determined range (first plateau) is given with the spherical function model at 13,000 m which indicates a smaller scale influence compare to the other ratios. It is interesting to see a maximum over ~20,050 m and for other distances (plateau at 39,500 m) which indicates different scale influence of the alkalinity.

High values (third and fourth quartiles) from the alkali geomarker as spatial dispersion are variable at large scale in general, from east to west in CVF (**Figure 3**). Large surface of high alkalinity and high Sr/Y ratios are found near the Sierra de Las Cruces (SDLC) and Nevado de Toluca, some others south of Valley of Puebla Scoria Cones and in the center of CVF. Regionalization of low values is found for large area in the center of CVF, but some low Sr/Y ratios do not match with high alkaline contents for Guespalapa, Chichinautzin, Herradura and Suchiuc samples. The distribution of alkalinity follows elongated polygons over CVF (NE-SW and SE-NW tendencies), but small anomalies are also observed. Stratovolcanoes are represented by high values of Sr/Y among point symbols, but geostatistics show large ranges of alkalinity.

A) Alkalis vs SiO₂



B) Histogram: Alkalis/SiO₂



C) Semi-variogram: Alkalis/SiO₂

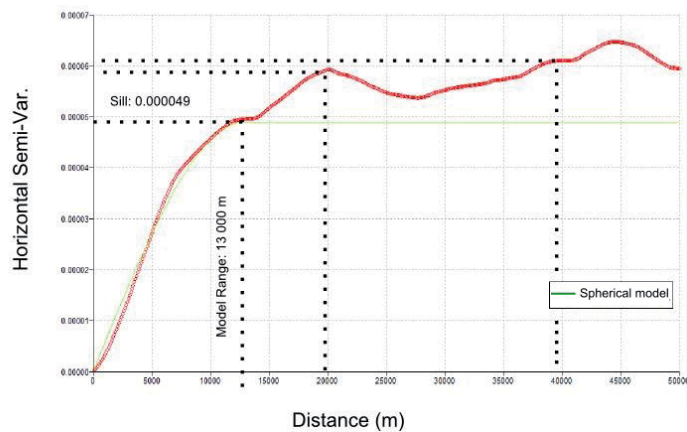


Figure 2.

(A) TAS diagram (alkali vs. silica) for all CVF data point. Data from Popocatepetl-Iztaccihuatl and Nevado de Toluca are also included for composition. (B) Distribution diagram of the alkali geomarker. The solid vertical lines are the four quartile limits (0.093, 0.097, 0.101, 0.148) with the second and fourth representing the median and the maximum and the dashed vertical line represents the average ($\bar{x}=0.097$). (C) Semi-variogram for the alkali geomarker for all CVF data points.

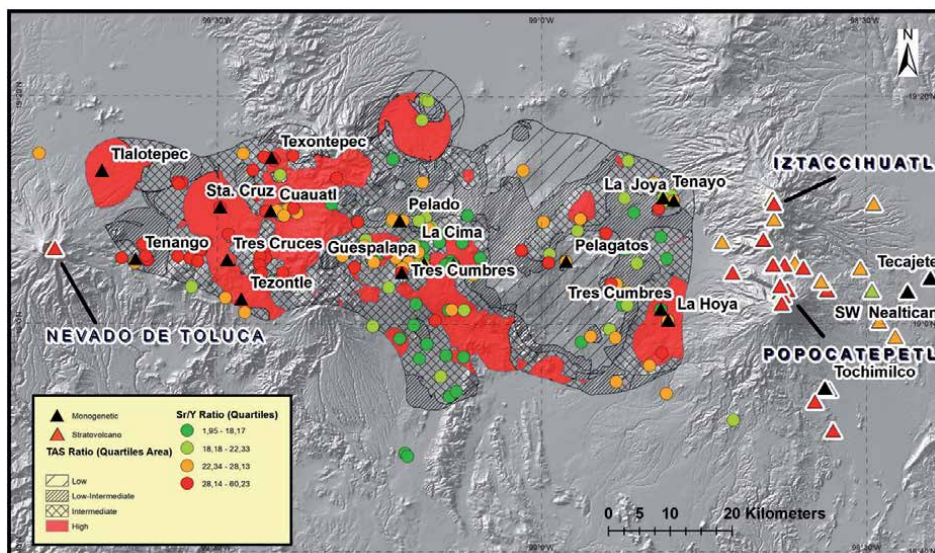


Figure 3. Symbol map and spatial overlay results of ordinary kriging for alkalinity ratio. The point map symbol overlays represent center of emission and volcanic deposits with their respective average alkalinity. The color legend is from Sr/Y ratio separated with quartiles. The circle point symbols represent monogenetic cones, and the triangle point symbols represent important deposits emitted by the stratovolcanoes. The symbol codes in the legend attributed for the ratio alkali categories in the legend are built with quartiles.

1.3.2 Ba/Nb geomarker

The geochemistry diagram, while in most cases there is no correlation with the large variation of Nb datas, Ba values generally are higher for CVF, but there are no positive-negative relationships with Nb (**Figure 4A**). CVF have widely scattered values, the Nb values of Popocatepetl and Iztaccihuatl are generally lowers, but Nevado de Toluca's values are higher.

The total sample distribution appears as two Gaussian curves. Those curves represent two populations of data with distinct patterns and two central tendencies (**Figure 4B**). Since Ba is not variable inside each group, the distribution of the Ba/Nb ratio is controlled by Nb. From Moran Index, the data form clustered pattern without a random distribution. The study gives a probability pattern to find an interpolation point for 9500 m so the influence between each sample is less important than for alkalis. From the semi-variogram, the determined range is given at 14,500 m which indicates a larger scale influence compare to the other ratios. A maximum is present at ~38,000 m (**Figure 4C**).

On the map, there are important first order tendencies. The entire CVF is exceptionally low, but regionalized and high values are found around the stratovolcanoes where the Nb is the lowest (La Hoya, Loma Sacramento, Tenayo), but also through SDLC or near Nevado de Toluca. The geochemistry changes from east to west starting from the Popocatepetl area (**Figure 5**). The polygons from the Ba/Nb spatial model are clearly elongated in a N-S direction.

1.4 Discussion

1.4.1 The visualization technique

The analysis of pattern (**Table 1**) showed that samples were grouped in disordered cluster without random dispersion, reflecting the different field strategies

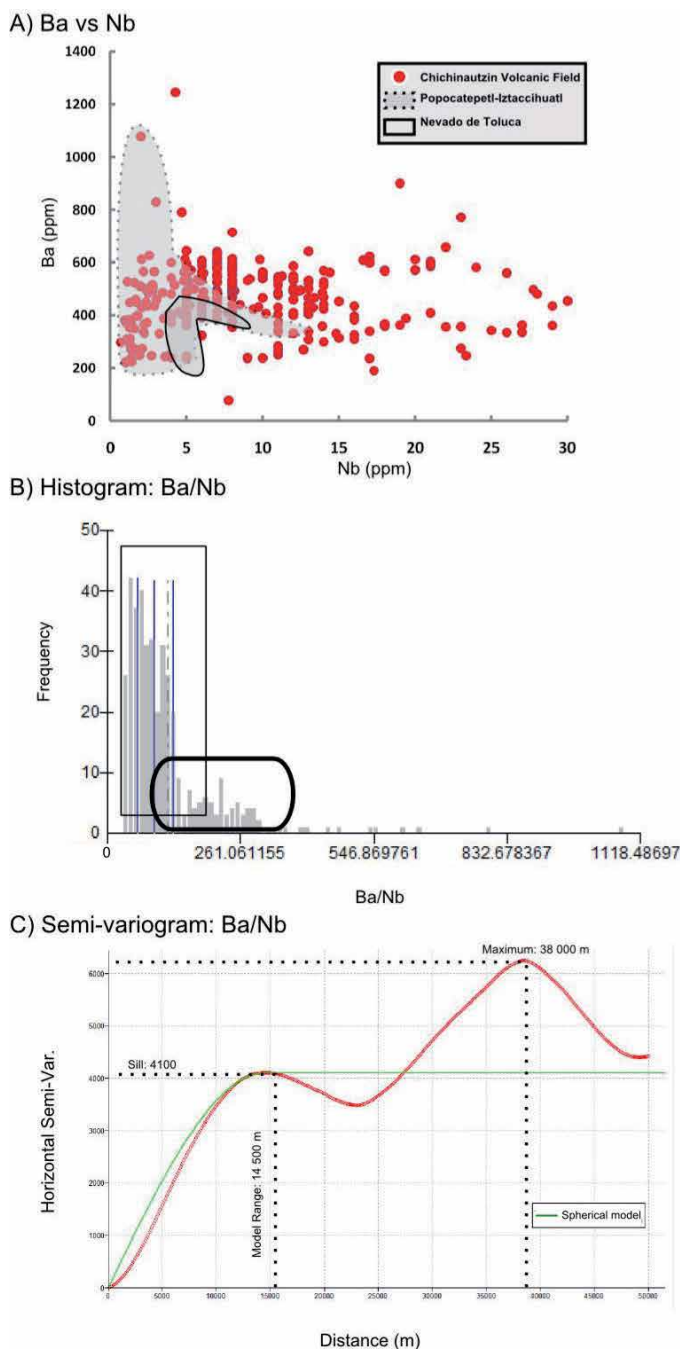


Figure 4. (A) Ba vs. Nb diagram for all CVF data point. Data from Popocatepetl-Iztaccihuatl and Nevado de Toluca are also included for composition. (B) Distribution diagram of the Ba/Nb geomarker. The solid vertical lines are the four quartile limits (41.1, 74.0, 114.0, 1081.0) with the second representing the median, and the fourth quartile represents the maximum. The dashed vertical line represents the average ($\bar{x}=104.9$). Circular box represents where are the monogenetic cones in the population, and the thin border rectangular box represents the stratovolcanoes. (C) Semi-variogram for the Ba/Nb geomarker for all CVF data points.

that influence the targeted investigated area of CVF. This dispersion diverges from systematic grids performed for small scales mineral exploration tactics or soil surveys [38].

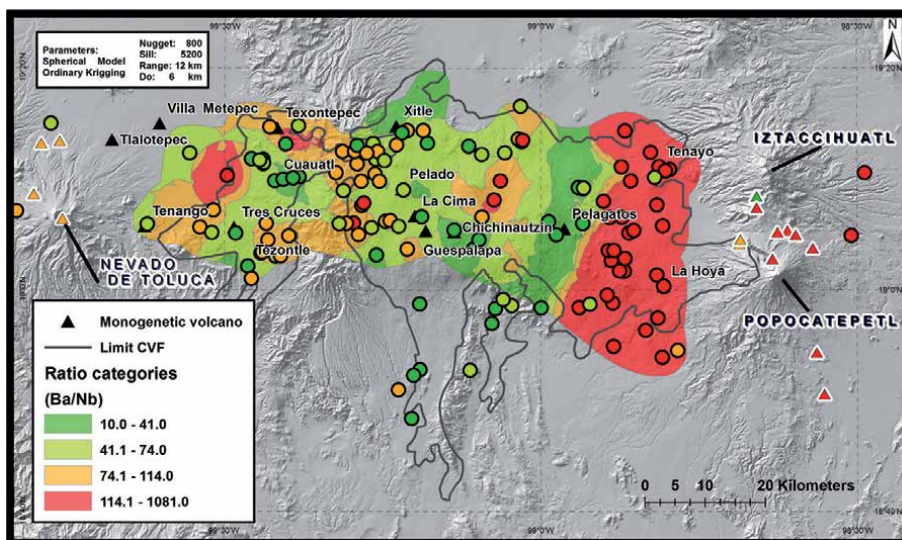


Figure 5. Symbol map and spatial overlay results of ordinary kriging for Ba/Nb ratio. The point map symbol overlays represent center of emission and volcanic deposits with their respective average Ba/Nb ratio. The circle point symbols represent monogenetic cones ($n = 134$), and the triangle point symbols represent important deposits emitted by the stratovolcanoes ($n = 16$). The color codes attributed for the ratio categories in the legend are the same for the point map symbol and surface layers.

The measure of dispersion gives values between 8250 and 12,900 meters and it is inversely proportional to the quantity of samples in each dataset. Despite those distances, the spatial dependence of the models varies between 13,000 and 18,000 meters (Figure 2C, 4C; see semi-variogram evaluation). The changes of geochemistry are interpreted to occur for small distances between eruptive centers, but also for ranges over larger distances as it is shown for alkali, Sr/Y and Ba/Nb datasets. Finally, from observation of the point value symbol maps (Appendix I), despite of the rich geological knowledge and sampling works in CVF, the measure of dispersion allows to interpret an insufficient density of certain sampling area, particularly for monogenetic cones N-E of Xitle in urban sector, in the valley around Sta. Cruz volcano, and south of the CVF (forest).

The evaluation of rock chemistry affinity can be used to evaluate target for petrological investigation and resume spatial patterns as a clear idea of geochemical distribution of a monogenetic field. On the other hand, the presented methodology finds limitations for different reasons (we proposed four factors):

1. Detailed toponymic descriptions are furnished without coordinates of samples by some authors which complicate assigning geographical coordinates (Appendix II; the number of references being $n = 15/32$). This is in addition to the quantity of elements analyzed for geochemistry in certain sectors (different analytical instrument, necessity or not to use rare earth and trace elements) as the targeted material from the publication which involve for some authors to study different kinds of external and internal petrological processes.
2. Control of arbitrary parameters such as the search radius and weighting exponent in the interpolation approach can be affecting the error and precision of the model [40]. The IDW and LD techniques are ideal in areas without anisotropy and where the quantity of point neighbors is not critical (i.e. constant in a structured sample grid [30, 37–39]).

3. Sampling density and dispersion as determined with (1) find limitations from the physical environment (topography, vent locations reported in literature, nonpreferential flow orientation, etc.).
4. Strategical sampling affects the distribution of sampling site positions (i.e. various objectives of petrological sampling, sample distance to road of access, uncertainties of rock sample association to emitting vent, etc.).

1.4.2 Surface variation of the geochemistry

Trace element ratios Ba/Nb show first-order trends and one maximum in the semi-variograms for 38 km (**Figures 2, 4**). Spatial variations of trace element ratios are correlated for limits that correspond to larger distances. These changes of geochemistry are visible in a larger area and may be related to large-scale tectonic effects which may be associated to new input material from the subduction zone [3].

Alkalis shown on the maps has tendency of second order (for 13,000 m) and have different changes of spatial dependence for larger distances interpreted in the semi-variogram (**Figures 2,4**). These second plateau and maximum can also be interpreted as secondary large-scale tendencies. At local scale, it perfectly marks the regional heterogeneity known in the CVF, but larger scale effects also occur (i.e. For example Pelagatos and the center of the monogenetic field is clearly less evolved and less alkaline; see [25, 42, 43]).

The geochemistry of monogenetic cones satellites/boundaries of Popocatepetl, Iztaccihuatl: like the neighbor stratovolcanoes have volcanic arc affinity (high Ba/Nb), influence of crustal thickness (high Sr/Y) and constitute predominantly felsic rocks. Despite of this, alkalinity anomalies are observed, in some cases, few minor eruptive centers constitute low Sr/Y ratios, but high alkalinity (ex. Nealtica, Tetela), or even the contrary, high Sr/Y ratios, but low alkalinity (Cerro Xoyaca, Loma Tepenasco, La Joya next to Iztaccihuatl; [44]). Overall, the heterogeneity of the CVF monogenetic bodies decreases as it approaches the Popocatepetl-Iztaccihuatl stratovolcanoes. This distribution suggests the possibility that the CVF and the stratovolcanoes share the same mantle source which is a petrological evidence in literature [14, 44]. The contrast of Ba/Nb values between the stratovolcanoes and the center of CVF can be explained by different degrees of sediment contribution from the mantle [45], crustal assimilation (i.e. on Sr and Y; [39]), but also fractional crystallization, all having effects on the content of Ba and Nb [36].

1.4.3 Spatial heterogeneities of magma source

The most remarkable observation in the spatial model is the similarity with the geomarkers to the east CVF and the Popocatepetl-Iztaccihuatl complex. This could imply that since Quaternary, the magma source of many monogenetic conduits east of CVF and minor eruptive vents find similar magmatic source/a common root in the mantle in the vicinity of the polygenetic edifices (ex. La Hoya, [44]).

At the eastern limit of the mapped faults in [10], a similar N-S trending corridor is observed with high Ba/Nb anomalies. This includes the Pelagatos volcano mafic rocks despite the intermediate alkalinity and Sr/Y ratios (**Figures 3, 5**). Such signatures are associated to enriched mantle in incompatible elements. No regional faults are reported, and neither are lacustrine sediment covers east of Pelagatos [11]. A clear lineation of scoria cones is observed as shown by the point map overlays (**Figure 1**; Appendices). A E-W large scale change of crustal thickness can explain the variation, but Sr/Y do not show this N-S systematic association nor gradual changes along the direction of the Cocos plate subduction under the continent [8, 20].

A different dispersion pattern of the magma conduits could occur in this area due to complexity of cortical pathways for magma, but as the interpolation model and semi-variogram indicate (**Figure 4C**), individual plumbing systems of the monogenetic field must share a deep mantle source. Large-scale geochemical changes from all geomarkers do not correlate with the subducting slab geometry [8, 20, 34, 46], which point out that spatial heterogeneities of magma source rather increase where mantle interact with continental crust.

Monogenetic cones north and south of CVF are more mafic, less alkaline and many aligned scoria cones share the same rock composition (**Figures 3, 5**). Overall, monogenetic cones are spatially associated to E-W normal faults reported in the works of [16, 18] and recent mapping advances resumed in [10, 11]. Even though, no clear geochemistry (ex. Sr/Y) vs structural orientations associations are observed (**Figure 1**) contrary to some volcanic fields (minor eruptive centers along the Liquiñe-Ofqui Fault Zone, Southern Andes; [47, 48]). The normal fault systems in CVF also affect the crust below stratovolcanoes in addition to NE faults. This could imply to redirect orientations for magmas pathways and plumbing system depths. Thus, the extend of magma differentiation is variable and therefore the geochemistry of satellite monogenetic cones is modified to the polygenic edifices (i.e. Huililco monogenetic cones versus Llaima stratovolcano in Chile; [2]).

As for Nevado de Toluca, only Sta. Cruz and Tenango have remarkably similar trace element ratios (**Figures 4, 5**); Sr/Y as for Ba/Nb are associated to the high topography from SDLC. Overall, the western part of CVF constitutes spatial changes of geochemistry that vary over small areas. For example, near the flanks of the SDLC, rocks are more diverse in SiO₂ contents, have higher alkalinity and local interpolations show high Ba/Nb ratios [subduction signature). Then, further west, the same high Ba/Nb tendency follows a N-S corridor (Texontepec to Tezontle).

Local anomalies are various west of CVF and Tenango lateral fault system. Many E-W structures [11] do not correlate with the orientation of elongated polygons of high alkalinity and neither do they follow regional tendencies of spatial Sr/Y distribution (**Figure 3**). A more complex structural system can explain this difference according to the maps published in [1, 10, 49], which may imply contrasting basement lithologies (i.e. see [11, 50, 51]), crustal thickness or lithospheric fractures distinct in depth origin, movement and geometry in comparison to the Popocatepetl-Iztaccihuatl complex.

1.5 Conclusion

The geostatistic and geographical mapping model of volcanic bulk rock chemistry in the Chichinautzion Volcanic Field (CVF) served as a methodological approach. Improve the comprehension of the spatial distribution of the magma heterogeneities inside a typical monogenetic volcanic field. The major methodological outcomes and geological explanations for such geochemical variations are resumed as follows:

1. The method presented here showed incertitude particularly for interpreting alkalis and Sr/Y lineation on the final models (**Figures 2, 3**). Limitations were encountered for assigning geographical coordinates, to control arbitrary parameters for spatial interpolation, to integrate physical environment parameters and to consider all strategical sampling objectives that may influence sample rock positions cumulated since 1948. The Moran Index (I) and the parameter Prob1Pnt helped to determine sample dispersion, which become mandatory to determine if some sectors inside a monogenetic field as CVF should be pre-

ferred for kriging, IDW or LD. It is consequently recommended to segment the area of study from monogenetic field and use the kriging method where a preferential sample orientation for high sample density cover is observed (satellite cones on the same flank from a polygenetic system, unidirectional topographic gradient, sampling along a lava flow or a structural lineation). Sectors where sample orientation is random and distribution is homogeneous should consider the Inverse Distance Weight (IDW) and Linear Decrease (LD).

2. The tectonic significance of high Ba/Nb geomarker is particularly of interest to indicate contribution of fluids derived from the subducted plate. This occurs in addition to the highly depleted mantle signature in the region of stratovolcanoes [21, 28, 29, 44]. One consideration is the presence of such anomalies related to amphibole fractioning [7] and even garnet from a deep source (~400 km; [27]). Another consideration is that such magmas are deeply sourced where hydrated fluids are produced by a metasomatized mantle source (from the slab, for example supported by [23, 29]). Despite of this association, such anomalies are geographically restricted to polygenetic systems. In addition, the Sr/Y ratio or alkalis geomarkers as Ba/Nb itself do not correlate with literature observations of the continental thickness [10, 11, 16, 18] nor the contact geometry of the subducted slab vs. lower continental crust [8, 20, 46]. Consequently, below CVF, rather than the slab influence [45], it is suggested that the role of lithospheric mantle–crust interaction is crucial to modify geochemical signature on the magmas feeding minor eruptive vents.
3. Shallow depth rigid continental crust (thickness and fractures) does not allow sufficient time and space for magmas to record subduction signature, therefore, the fast magma ascent feeding typical monogenetic systems do not easily record high Ba/Nb ratios [1]. In some cases, those magma could rather come from a fertile mantle, some with OIB signature, some hybrid depleted mantles [7, 9, 15, 21]. If this inference is correct, obstacles in the continental crust could be slowing down the frequent injection of new batches of magma feeding new minor eruptive vents around Iztaccihuatl-Popocatepetl, and Nevado de Toluca volcanic complexes. The plumbing system architecture of those stratovolcanoes already channel volumetric magmas derived from a contrasting mantle–crust source.

Acknowledgements

The persons especially thanked for the technical support are Isaac Abimelec Farraz Montes (technician), Osvaldo Franco Ramos (student at Instituto de geografía, UNAM), and Laura Luna (technical secretary at Instituto de Geología, UNAM). Dolores Ferres and Marie-Noël Guilbaud from Instituto de Geofísica (UNAM) reviewed datasets and gave important opinions about the methodology and the volcanological aspects of the work.

This work was supported by the Fonds de Recherche du Québec Nature et technologies (FRQNT) (Concours B1, Comité B4 (Maîtrise) who helped to support the Master program between 2010 and 2013 at Instituto de Geología, Universidad Nacional Autónoma de México (UNAM). The submission work process is supported by Conicyt Fondecyt Fondo Nacional de Desarrollo Científico y Tecnológico, with Project Code 11190846 attributed to Dr. Philippe Robidoux from Centro de Excelencia en Geotermia de los Andes (CEGA) and Departamento de Geología, Facultad de Ciencias Físicas y Matemáticas, Universidad de Chile.

Appendices and nomenclature

Appendice I Building the Geodatabase

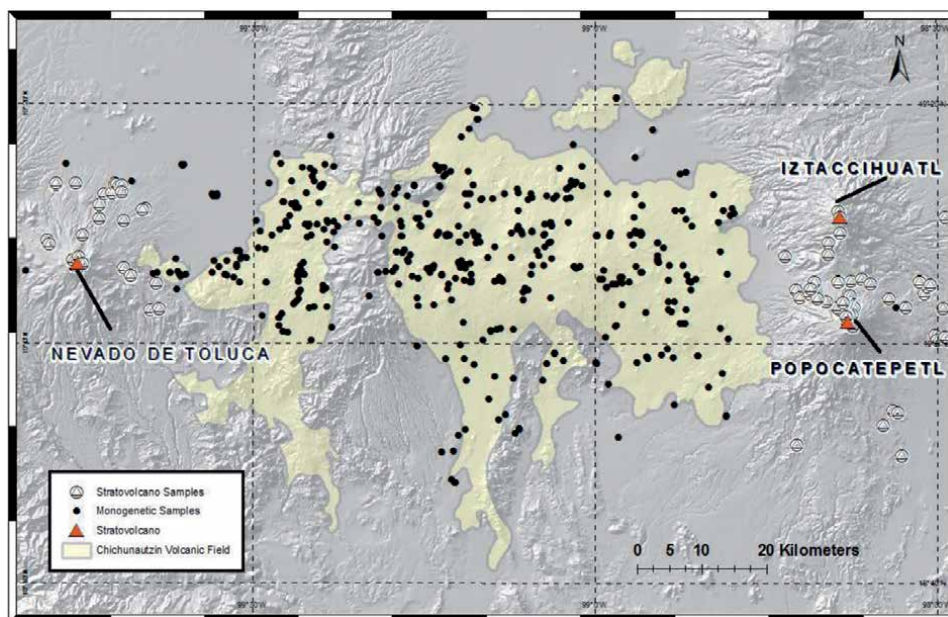


Figure A1. Dispersion of the 583 samples in study (map modified from: Siebe et al., 2005; Siebe et al., 2004). The Chichinautzin Volcanic Field (CVF) is shown (shaded polygon) over the digital elevation model (DEM) from INEGI (2011). The big pale solid triangles represent the three well known stratovolcanoes and their associated samples (small solid black triangle). The small solid black circles represent the samples from the monogenetic cones of CVF.

Appendice II Table of reference for samples used in the Geographic Information System (GIS)

Years	Complete reference	ME	RETE	Coord.
1948	Arellano, A.R.V., 1948. La composicion de las rocas volcanicas en la parte sur de la Cuenca de Mejico, Boletin de la Sociedad Geologica Mexicana, Tomo XIII, p.81-82, Cuadro 18	Yes	No	Description
1975	Whitford, D. J., Bloomfield K., 1975. Geochemistry of late Cenozoic volcanic rocks from the Nevado de Toluca area, Mexico, Year Book Carnegie Inst. Washington 75 [1975], p. 207-213, #4571 in GERMS database	Yes	Yes	Description
1975	Bloomfield, K. 1975, A late-Quaternary monogenetic volcano field in central Mexico, Aufsätze,Geologische Rundschau, 64: p.476-499	Yes	No	Maps
1985	Carrasco-Núñez, G., 1985. Estudio geológico del Volcán Popocatepetl, BS thesis, México DF, Facultad de Ingeniería, Universidad Nacional Autónoma de México, 134p.	Yes	No	Description

1987	Nixon, Graham T., 1987. Petrology of the Younger Andesites and Dacites of Iztaccihuatl Volcano, Mexico: I. Disequilibrium Phenocryst Assemblages as Indicators of Magma Chamber Process, <i>Journal of Petrology</i> , Vol. 29, Part 2, p. 213-368	Yes	No	Maps
1989	Pozzo, C. Ana Lillian Martin del Pozzo, 1989. Geoquímica y paleomagnetismo de la sierra Chichinautzin, Tesis que presenta la autor en cumplimiento parcial de los requisitos del grado Doctor en Ciencias (Geología), Mexico -D.F., 148 p.	Yes	Yes	Maps
1989	Swinamer, Ralph Terrance, 1989. The Geomorphology, Petrography, Geochemistry and Petrogenesis of the Volcanic Rocks in the Sierra Del Chichinautzin, Mexico, tesis submitted to the Department of Geological Sciences, in conformity with the requirements for the degree of Master Science, p.212	Yes	Yes	Table
1995	Cervantes, P., 1995. Eventos volcanicos al sur de la Ciudad de Mexico, BS Thesis, México DF, Facultad de Ingeniería, Universidad Nacional Autónoma de México, 74p.	Yes	Yes	Description
1998	Arana Salinas, L., 1998. Geología del volcan Pelado, BS thesis, México DF, Facultad de Ingeniería, Universidad Nacional Autónoma de México, 57 p.	Yes	Yes	Maps, description
1998	Delgado et al. 1998, Geology of Xitle Volcano in southern Mexico City - A 2000 Year-Old monogenetic volcano in an urban area, <i>Revista Mexicana e Ciencias Geologicas</i> , volumen 15, #2, 1998, p.115-131	Yes	No	Maps, description
1998	Romero Teran, Esther, 1998. Geología del Volcan Ajusco, BS thesis, Facultad de Ingeniería, Universidad Nacional Autónoma de Mexico (Instituto de Geofísica), 50 p.	Yes	Yes	Maps
1999	Verma S. P., 1999. Geochemistry of evolved magmas and their relationship to subduction-unrelated mafic volcanism at the volcanic front of the Central Mexican Volcanic Belt, <i>Journal of Volcanology and Geothermal Research</i> , Volume 93 [1999], p. 151-171, #3623 in GERMS database	Yes	Yes	Table, maps
1999	Arce S., Jose Luis, 1999. Reinterpretacion de la erupcion pliniana que dio origen a la Pomez Superior, Volcan Nevado de Toluca, Master thesis: Maestro en Sismología y Física del interior de la Tierra, Postgrado en ciencias de la tierra, Universidad Autonoma Nacional de Mexico (Instituto de Geofísica), 92 p.	Yes	Yes	Maps, description
1999	Wallace, P., and I. Carmichael (1999), Quaternary volcanism near the valley of Mexico: Implications for the subduction zone magmatism and the effects of crustal thickness variations on primitive magma compositions, <i>Contribution to Mineralogy and Petrology</i> , vol. 135, p.291-314	Yes	Yes	Table, maps

2000	Verma, P. Surendra, 2000. Geochemistry of the subducting Cocos plate and the origin of subduction-unrelated mafic volcanism at the volcanic front of the central Mexican Volcanic Belt, Geological Society of America, Special Paper 534, p.195-222	Yes	Yes	Table, maps, description
2000	Gonzalez Huesca, Alberto, 2000. Estudios de detalle estratigrafico y sedimentologico del Lahar de San Nicolas en el flanco noreste del volcan Popocatepetl, BS thesis, Facultad de Ingenieria, Universidad Nacional Autonoma de Mexico, 110 p.	Yes	No	Maps
2001	Straub, S. M., Martin-Del Pozzo, A. L., 2001. The significance of phenocryst diversity in tephra from recent eruptions at Popocatepetl volcano (Mexico), Contrib. Mineral. Petrol. 140 [2001], p. 487-510, #3506 in GERMS database	Yes	Yes	Description
2001	Cervantes de la Cruz., Karina Elizabeth, 2001. La pomez blanca intermedia: deposito producido por una erupcion plinana-subpliniana del volcan Nevado de Toluca hace 12,100 anos, Master's thesis, Postgrado en Ciencias de la Tierra, Universidad Nacional Autonoma de Mexico, 84 p.	Yes	Yes	Description, maps
2001	Velasco Tapia, Fernando, 2001. Aspectos geoestadisticos en geoquimica analitica: Aplicacion en el modelado geoquimico e isotopico de la sierra de Chichinautzin, Cinturon Volcanico Mexicano, Phd thesis: Doctor en ciencias (geoquimica), Postgrado en ciencias de la tierra, Universidad Nacional Autonoma de Mexico (Instituto de Geofisica), 273 p.	Yes	Yes	Table, maps
2004	Siebe, Claus, Rodriguez-Lara, V., Schaaf, P., Abrams M., 2004. Geochemistry, Sr-Nd isotope composition and tectonic setting of Holocene Pelado, Guespalapa and Chichinautzin scoria cones, south of Mexico City, Journal of Volcanology and Geothermal Research, Volume 130 [2004], p. 197-226, #6862 in GERMS database	Yes	Yes	Table, maps
2004	Arana Salinas, L., 2004. Geologia de los volcanes monogeneticos Teuhtli, Tlaloc, Tlacotenco, Ocusacayo y Cuauhtzin en la Sierra Chichinautzin, al Sur de la Ciudad de Mexico, Master's thesis (Vulcanologia), Postgrado en Ciencias de la Tierra, Universidad Nacional Autonoma de Mexico, 117 p.	Yes	Yes	Maps, description
2004	Raymundo G. Martinez-Serrano et al., 2004. Sr, Nd and Pb isotope and geochemical data from the Quaternary Nevado de Toluca volcano, a source of recent adakitic magmatism, and the Tenango Volcanic Field, Mexico, Journal of Volcanology and Geothermal Research, Volume 138, Issues 1-2, 15 November 2004, p.77-110	Yes	Yes	Table, maps

2005	Witter J. B., Kress V. C., Newhall C. G., 2005. Volcan Popocatepetl, Mexico. Petrology, Magma Mixing, And Immediate Sources Of Volatiles For The 1994-Present Eruption, J. Petrol. 46 [2005], p. 2337-2366, #8497 in Germs database	Yes	Yes	Description
2005	Schaaf, Peter, Jim Stimac, Claus Siebes and Jose Luis Macias, 2005. Geochemical Evidence for Mantle Origin and Crustal Processes in Volcanic Rocks from Popocatépetl and Surrounding Monogenetic Volcanoe; Central Mexico, Journal of Petrology, Volume 46, #6, p. 1243-1282	Yes	Yes	Table
2006	Ceballos, Giovanni Sosa, 2006. El Paleo-Popocatepetl: petrologia, geoquímica e isotopia de secuencias pre 23, 000 años, Master's thesis, Postgrado en Ciencias de la Tierra, Universidad Nacional Autonoma de Mexico (Colegio de Geografia), 120 p.	Yes	Yes	Description, maps
2008	Antonio, Marco, 2008. Reconstrucción del evento eruptivo asociado al emplazamiento del flujo piroclástico El Refugio hace 13 ka, volcán Nevado de Toluca (México), Revista Mexicana de Ciencias Geológicas, V.25, # 1, 2008, p.115-147	Yes	Yes	Description, maps
2008	Meriggi, Lorenzo, José Luis Macías, Simone Tommasini, 2008. Heterogeneous magmas of the Quaternary Sierra Chichinautzin volcanic field (central Mexico): the role of an amphibole-bearing mantle and magmatic evolution processes, HeterRevista Mexicana de Ciencias Geológicas, v. 25, #.2, p. 197-216	Yes	Yes	Table
2008	Straub, S. M., Martin-Del Pozzo, A. L., Langmuir, C.H., 2008. Evidence from High-Ni Olivines for a Hybridized peridotite/pyroxenite source for orogenic andesites from the central Mexican volcanic belt; Geochemistry Geophysics Geosystems 9, 33 p.	Yes	Yes	Table
2009	Guilbaud, M.-N., Siebe, C., Agustín-Flores, J., 2009. Eruptive style of the young high-Mg basaltic-andesite Pelagatos scoria cone southeast of México City. Bull. Volcanol. 71, 859–880.	Yes	Yes	Table, maps
2009	Augustin Flores, Javier, 2009. Geología y petrogenesis de los volcanes monogeneticos Pelagatos, Cerro del Agua y Dos Cerros en la Sierra Chichinautzin, al sur de la Ciudad de Mexico, Master thesis: Maestria en Ciencias (Vulcanologia), Postgrado en Ciencias de la Tierra, Universidad Nacional Autonoma de Mexico (Instituto de Geofisica), 97 p.	Yes	Yes	Table
2010	Arana-Salinas, L., Claus Siebe and José Luis Macias 2010. Dynamics of the ca. 4965 yr 14C BP "Ochre Pumice" Plinian eruption of Popocatepetl volcano, Mexico, Journal of Volcanology and Geothermal Research, Volume 192, Issues 3-4, 10 May 2010, p. 212-228	Yes	Yes	Description

2011	Augustin-Flores, Javier, Claus Siebe and Marie-Noëlle Guilbaud, 2011. Geology and geochemistry of Pelagatos, Cerro del Agua, and Dos Cerros monogenetic volcanoes in the Sierra Chichinautzin Volcanic Field, south of Mexico City, Journal of Volcanology and Geothermal Research, Volume 201, Issues 1-4, 15 April 2011, p.143-162	Yes	Yes	Table
------	--------------------------------------------------------------------------------------------------------------------------------------------------------------------------------------------------------------------------------------------------------------------------------------------------------------------------------------	-----	-----	-------

Table A1.

It is specified if major elements (ME) or Rare Earth and Trace Elements (RETE) are available from the references. Coordinates (Coord.) are taken from tables, maps or interpreted from description in the text.

Author details

Philippe Robidou^{1*}, Julie Roberge² and César Adams³


1 Departamento de Geología, Facultad de Ciencias Físicas y Matemáticas, Centro de Excelencia en Geotermia de los Andes (CEGA), Universidad de Chile, Santiago, Chile

2 ESIA-Ticomán, Instituto Politécnico Nacional, México City, México

3 México City, México

*Address all correspondence to: robidouphilippe@gmail.com

IntechOpen

© 2020 The Author(s). Licensee IntechOpen. This chapter is distributed under the terms of the Creative Commons Attribution License (<http://creativecommons.org/licenses/by/3.0>), which permits unrestricted use, distribution, and reproduction in any medium, provided the original work is properly cited. 

References

- [1] Németh K. Monogenetic volcanic fields: Origin, sedimentary record, and relationship with polygenetic volcanism. *What is a Volcano?* 2010; **470**:43. DOI: 10.1130/2010.2470(04)
- [2] McGee LE, Brahm R, Rowe MC, Handley HK, Morgado E, Lara LE, et al. A geochemical approach to distinguishing competing tectono-magmatic processes preserved in small eruptive centres. *Contributions to Mineralogy and Petrology.* 2017; **172**(6):44. DOI: 10.1007/s00410-017-1360-2
- [3] Smith IE, Németh K. Source to surface model of monogenetic volcanism: A critical review. *Geological Society of London, Special Publication.* 2017; **446**(1):1-28. DOI: 10.1144/SP446.14
- [4] Gómez-Tuena A, Orozco-Esquivel M, Ferrari L. Petrogénesis ígnea de la faja volcánica transmexicana. *Boletín de la Sociedad Geológica Mexicana.* 2005; **57**(3):227-283. DOI: 10.18268/bsgm2005v57n3a2
- [5] Gómez-Tuena A, Orozco-Esquivel MT, Ferrari L. Igneous petrogenesis of the trans-Mexican volcanic belt. *Geological Society of America Special Papers.* 2007; **422**:129-181. DOI: 10.1130/2007.2422(05)
- [6] Luhr JF, Kimberly P, Siebert L, Aranda-Gómez JJ, Housh TB, Mattiotti GK. México's quaternary volcanic rocks: Insights from the MEXPET petrological and geochemical database. *Geological Society of America Special Papers.* 2006; **402**:1-44. DOI: 10.1130/2006.2402(01)
- [7] Márquez A, Verma SP, Anguita F, Oyarzun R, Brandle JL. Tectonics and volcanism of sierra Chichinautzin: Extension at the front of the central trans-Mexican volcanic belt. *Journal of Volcanology and Geothermal Research.* 1999; **93**(1-2):125-150. DOI: 10.1016/S0377-0273(99)00085-2
- [8] Pérez-Campos X, Kim Y, Husker A, Davis PM, Clayton RW, Iglesias A, et al. Horizontal subduction and truncation of the Cocos plate beneath Central Mexico. *Geophysical Research Letters.* 2008; **35**(18). DOI: 10.1029/2008GL035127
- [9] Wallace PJ, Carmichael IS. Quaternary volcanism near the valley of Mexico: Implications for subduction zone magmatism and the effects of crustal thickness variations on primitive magma compositions. *Contributions to Mineralogy and Petrology.* 1999; **135**(4):291-314. DOI: 10.1007/s004100050513
- [10] Arce JL, Layer PW, Lassiter JC, Benowitz JA, Macías JL, Ramírez-Espinosa J. 40 Ar/39 Ar dating, geochemistry, and isotopic analyses of the quaternary Chichinautzin volcanic field, south of Mexico City: Implications for timing, eruption rate, and distribution of volcanism. *Bulletin of Volcanology.* 2013; **75**(12):774. DOI: 10.1007/s00445-013-0774-6
- [11] Arce JL, Layer PW, Macías JL, Morales-Casique E, García-Palomo A, Jiménez-Domínguez FJ, et al. Geology and stratigraphy of the Mexico basin (Mexico city), central trans-Mexican volcanic belt. *Journal of Maps.* 2019; **15**(2):320-332. DOI: 10.1080/17445647.2019.1593251
- [12] Urrutia-Fucugauchi J, Martín del Pozzo AL. Implicaciones de los datos paleomagnéticos sobre la edad de la Sierra de Chichinautzin, cuenca de México. *Geofísica Internacional.* 1993; **32**(3): 523-533. [Internet]. 2020. Available from: <http://www.revistas.unam.mx/front/> [Accessed: 04 August 2020]

- [13] Siebe C. Age and archaeological implications of Xitle volcano, southwestern basin of Mexico-City. *Journal of Volcanology and Geothermal Research*. 2000;**104**(1-4):45-64. DOI: 10.1016/S0377-0273(00)00199-2
- [14] Siebe C, Rodriguez-Lara V, Schaaf P, Abrams M. Geochemistry, Sr-Nd isotope composition, and tectonic setting of Holocene Pelado, Guespalapa and Chichinautzin scoria cones, south of Mexico City. *Journal of Volcanology and Geothermal Research*. 2004 Feb 29;**130**(3-4):197-226. DOI: 10.1016/S0377-0273(03)00289-0
- [15] Márquez A, De Ignacio C. Mineralogical and geochemical constraints for the origin and evolution of magmas in sierra Chichinautzin, central Mexican Volcanic Belt. *Lithos*. 2002;**62**(1-2):35-62. DOI: 10.1016/S0024-4937(02)00069-5
- [16] Norini G, Groppelli G, Lagmay AM, Capra L. Recent left-oblique slip faulting in the central eastern trans-Mexican Volcanic Belt: Seismic hazard and geodynamic implications. *Tectonics*. 2006;**25**(4):1-21. DOI: 10.1029/2005TC001877
- [17] National Institute of Statistics and Geography (INEGI) [Internet]. 2011. Available from: <https://www.inegi.org.mx/temas/topografia/> [Accessed: 25 November 2010]
- [18] Johnson CA, Harrison CG. Neotectonics in Central Mexico. *Physics of the Earth and Planetary Interiors*. 1990;**64**(2-4):187-210. DOI: 10.1016/0031-9201(90)90037-X
- [19] UNAM and CENAPRED Seismology Group. The Milpa Alta earthquake of January 21, 1995. *Geofisica International*. 1995;**34**:355-362. [Internet]. 2020. Available from: <http://www.revistas.unam.mx/front/> [Accessed: 04 August 2020]
- [20] Kim Y, Clayton RW, Jackson JM. Geometry and seismic properties of the subducting Cocos plate in central Mexico. *Journal of Geophysical Research - Solid Earth*. 2010 Jun;**115**(B6):1-22. DOI: 10.1029/2009JB006942
- [21] Straub SM, LaGatta AB, Martin-Del Pozzo AL, Langmuir CH. Evidence from high-Ni olivines for a hybridized peridotite/pyroxenite source for orogenic andesites from the central Mexican Volcanic Belt. *Geochemistry, Geophysics, Geosystems*. 2008;**9**(3):235-238. DOI: 10.1029/2007GC001583.
- [22] Verma SP, Tapia FV. Estado actual de la investigación geoquímica en el campo monogenético de la Sierra de Chichinautzin: análisis de información y perspectivas. *Revista Mexicana de Ciencias Geológicas*. 2001;**18**(1):1-36 [Internet]. 2020. Available from: <http://www.rmccg.unam.mx/index.php/rmccg> [Accessed: 16 August 2020]
- [23] Cervantes P, Wallace PJ. Role of H₂O in subduction-zone magmatism: New insights from melt inclusions in high-Mg basalts from Central Mexico. *Geology*. 2003;**31**(3):235-238. DOI: 10.1130/0091-7613(2003)031<0235:ROHOIS>2.0.CO;2
- [24] Cervantes P, Wallace P. Magma degassing and basaltic eruption styles: A case study of ~ 2000 year BP Xitle volcano in Central Mexico. *Journal of Volcanology and Geothermal Research*. 2003;**120**(3-4):249-270. DOI: 10.1016/S0377-0273(02)00401-8
- [25] Roberge J, Guilbaud MN, Mercer CN, Reyes-Luna PC. Insight into monogenetic eruption processes at Pelagatos volcano, sierra Chichinautzin, Mexico: A combined melt inclusion and physical volcanology study. *Geological Society of London, Special Publication*. 2015;**410**(1):179-198. DOI: 10.1144/SP410.12
- [26] Orozco-Esquivel T, Petrone CM, Ferrari L, Tagami T, Manetti P.

Geochemical and isotopic variability in lavas from the eastern trans-Mexican Volcanic Belt: Slab detachment in a subduction zone with varying dip. *Lithos*. 2007;**93**(1-2):149-174. DOI: 10.1016/j.lithos.2006.06.006

[27] Chiaradia M. Crustal thickness control on Sr/Y signatures of recent arc magmas: An earth scale perspective. *Scientific Reports*. 2015;**5**:8115. DOI: 10.1038/srep08115

[28] Verma SP. Geochemistry of evolved magmas and their relationship to subduction-unrelated mafic volcanism at the volcanic front of the central Mexican Volcanic Belt. *Journal of Volcanology and Geothermal Research*. 1999;**93**(1-2):151-171. DOI: 10.1016/S0377-0273(99)00086-4

[29] Verma SP. Geochemistry of the subducting Cocos plate and the origin of subduction-unrelated mafic volcanism at the volcanic front of the central Mexican Volcanic Belt. In: *Cenozoic Tectonics and Volcanism of Mexico*. Vol. 334. 2000. p. 195. DOI: 10.1130/0-8137-2334-5.195

[30] ESRI: Understanding Our World [Internet]. 1999. Available from: <http://www.esri.com/> [Accessed: 05 September 2011]

[31] Isaaks EH, Srivastava RM. *An Introduction to Applied Geostatistics*. Oxford University Press. p. 561. DOI: 10.1016/0012-8252(92)90044-T

[32] Pearce JAA. user's guide to basalt discrimination diagrams. Trace element geochemistry of volcanic rocks: Applications for massive sulphide exploration. Geological Association of Canada, Short Course Notes. 1996;**12**(79):113

[33] Winchester JA, Floyd PA. Geochemical discrimination of different magma series and their differentiation products using immobile elements.

Chemical Geology. 1977;**20**:325-343. DOI: 10.1016/0009-2541(77)90057-2

[34] Brenan JM, Shaw HF, Ryerson FJ, Phinney DL. Mineral-aqueous fluid partitioning of trace elements at 900 C and 2.0 GPa: Constraints on the trace element chemistry of mantle and deep crustal fluids. *Geochimica et Cosmochimica Acta*. 1995;**59**(16):3331-3350. DOI: 10.1016/0016-7037(95)00215-L

[35] Frisch W, Meschede M, Blakey RC. *Plate tectonics: continental drift and mountain building*. Springer Science & Business Media. 2010:212. DOI: 10.1007/978-3-540-76504-2

[36] Rollinson HR. *Using Geochemical Data: Evaluation, Presentation, Interpretation*. New York, USA: Routledge; 2014. DOI: 10.1180/minmag.1994.058.392.25

[37] Burrough PAGIS. *Geostatistics: Essential partners for spatial analysis*. *Environmental and Ecological Statistics*. 2001;**8**(4):361-377. DOI: 10.1023/A:1012734519752

[38] Cuador-Gil JQ, Quintero-Silverio A. Análisis estructural: punto de partida de todo estudio geoestadístico. *Minería y Geología*. 2018;**16**(3):16-22 [Internet]. 2018. Available from: <http://revista.ismm.edu.cu/index.php/revistang/article/view/17> [Accessed: 23 July 2018]

[39] ILWIS Open 3.7; Nature Worldwide, Birds, World Institute for Conservation and Environment, Wice [Internet]. 2011. Available from: <http://www.ilwis.org/index.htm>, [Accessed: 08 November 2011]

[40] Robidoux P, Roberge J, Urbina Oviedo CA. A geostatistical method applied to the geochemical study of the Chichinautzin Volcanic Field in Mexico. *AGUFM*. 2011;**2011**:V13C-V2624C [Internet]. 2020. Available from: <https://>

- ui.adsabs.harvard.edu/abs/2011AGUFM.V13C2624R/abstract [Accessed: 23 July 2020]
- [41] Thrall GI. Statistical and theoretical issues in verifying the population density function. *Urban Geography*. 1988;**9**(5):518-537. DOI: 10.2747/0272-3638.9.5.518
- [42] Guilbaud MN, Siebe C, Agustín-Flores J. Eruptive style of the young high-Mg basaltic-andesite Pelagatos scoria cone, southeast of México City. *Bulletin of Volcanology*. 2009;**71**(8):859. DOI: 10.1007/s00445-009-0271-0
- [43] Weber RM, Wallace PJ, Johnston AD. Experimental insights into the formation of high-Mg basaltic andesites in the trans-Mexican volcanic belt. *Contributions to Mineralogy and Petrology*. 2012;**163**(5):825-840. DOI: 10.1007/s00410-11-0701-9
- [44] Schaaf P, Stimac JI, Siebe C, Macías JL. Geochemical evidence for mantle origin and crustal processes in volcanic rocks from Popocatepetl and surrounding monogenetic volcanoes, Central Mexico. *Journal of Petrology*. 2005;**46**(6):1243-1282. DOI: 10.1093/petrology/egi015
- [45] Johnson MC, Plank T. Dehydration and melting experiments constrain the fate of subducted sediments. *Geochemistry, Geophysics, Geosystems*. 2000;**1**(12):1-26. DOI: 10.1029/1999GC000014
- [46] Pardo M, Suárez G. Shape of the subducted Rivera and Cocos plates in southern Mexico: Seismic and tectonic implications. *Journal of Geophysical Research - Solid Earth*. 1995;**100**(B7):12357-12373. DOI: 10.1029/95JB00919
- [47] Cembrano J, Lara L. The link between volcanism and tectonics in the southern volcanic zone of the Chilean Andes: A review. *Tectonophysics*. 2009;**471**(1-2):96-113. DOI: 10.1016/j.tecto.2009.02.038
- [48] Hickey-Vargas R, Sun M, López-Escobar L, Moreno-Roa H, Reagan MK, Morris JD, et al. Multiple subduction components in the mantle wedge: Evidence from eruptive centers in the central southern volcanic zone. Chile. *Geology*. 2002;**30**(3):199-202. DOI: 10.1130/0091-7613(2002)030<0199:MSCITM>2.0.CO;2
- [49] Garcia-Palomo A, Macias JL, Garduño VH. Miocene to recent structural evolution of the Nevado de Toluca volcano region, Central Mexico. *Tectonophysics*. 2000;**318**(1-4):281-302. DOI: 10.1016/S0040-1951(99)00316-9
- [50] Siebe C, Arana-Salinas L, Abrams M. Geology and radiocarbon ages of Tláloc, Tlacotenco, Cuauhtzin, Hijo del Cuauhtzin, Teuhtli, and Ocusacayo monogenetic volcanoes in the central part of the sierra Chichinautzin, México. *Journal of Volcanology and Geothermal Research*. 2005;**141**(3-4):225-243. DOI: 10.1016/j.jvolgeores.2004.10.009
- [51] Siebe C, Rodríguez-Lara V, Schaaf P, Abrams M. Radiocarbon ages of Holocene Pelado, Guespalapa, and Chichinautzin scoria cones, south of Mexico City: Implications for archaeology and future hazards. *Bulletin of Volcanology*. 2004;**66**(3):203-225. DOI: 10.1007/s00445-003-0304-z

Basic Volcanic Elements of the Arxan-Chaihe Volcanic Field, Inner Mongolia, NE China

Boxin Li, Károly Németh, Julie Palmer, Alan Palmer, Jing Wu, Jonathan Procter and Jiaqi Liu

Abstract

The Arxan-Chaihe Volcanic Field, Inner Mongolia, NE China is a Pleistocene to Recent volcanic field still considered to be active. In this chapter we provide an update of current volcanological research conducted in the last four years to describe the volcanic architecture of the identified vents, their eruptive history and potential volcanic hazards. Here we provide an evidence-based summary of the most common volcanic eruption styles and types the field experienced in its evolution. The volcanic field is strongly controlled by older structural elements of the region. Hence most of the volcanoes of the field are fissure-controlled, fissure-aligned and erupted in Hawaiian to Strombolian-style creating lava spatter and scoria cone chains. One of the largest and most complex volcano of the field (Tongxin) experienced a violent phreatomagmatic explosive phase creating a maar in an intra-mountain basin, while the youngest known eruptions formed a triple vent set (Yanshan) that reached violent Strombolian phases and created an extensive ash and lapilli plains in the surrounding areas. This complex vent system also emitted voluminous lava flows that change the landscape by damming fluvial networks, providing a volcanological paradise for the recently established Arxan UNESCO Global Geopark.

Keywords: scoria, spatter, fissure, maar, tuff ring, pyroclastic density current, ash, tumuli, lava flow

1. Introduction

The Arxan-Chaihe Volcanic Field (ACVF) is a young intracontinental volcanic field located in the northeast of China (**Figure 1**). The volcanic field is best defined as a monogenetic volcanic field on the basis of the presence of small-volume volcanic edifices, eruptive products and typical landforms such as tuff rings, scoria (cinder) cones, fissure controlled vents, and complex, but small volcanic cones being the key elements of the volcano types preserved. Early research in the region focused on characterizing the volcanology of the area, however, in recent years research on the active volcanism in Northeast (NE) China has shed some light on magma genesis, volcanic edifice growth and volcanic hazards at some iconic locations such as the Changbaishan volcano, Longgang or Wudalianchi Volcanic Fields (**Figure 1**) [1]. This research has defined the basic characteristics of some of these

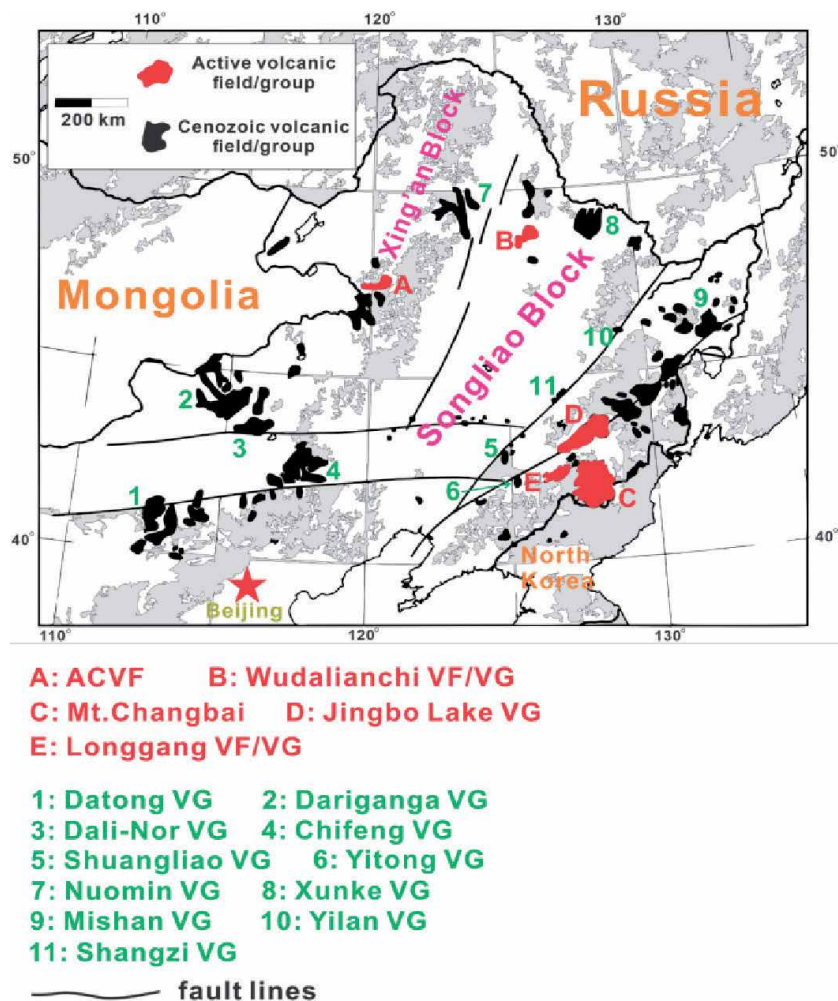


Figure 1. The general geological map of NE China: The red areas mark the active volcanic fields; the black areas indicate the ceased Cenozoic volcanic fields; also the solid lines in the territory of NE China are the markers of regional fault systems [1]. VF- volcanic field, VG – Volcanic group.

volcanic regions, outlining the geochemical characteristics of the volcanic rocks and linking magma genesis to lithospheric processes. Volcanological research from NE. China are increasingly appearing in the international literature [2–8], however, there volcanic regions are largely unstudied. Among these is the Arxan-Chaihe Volcanic Field (ACVF). Several research outputs have made basic observations of the volcanic history of the region, but a systematic study has only recently been undertaken. Here we report a summary of volcanological observations made in the last six years of research on the ACVF. The aim of the study is to understand the eruptive history, volcanic stratigraphy, eruption styles and associated volcanic hazards that may be associated with the ACVF.

In this book chapter, we summarize the field-based observations of two major field campaigns to provide some basic descriptions of the recognized volcanic products including the most accessible and iconic volcanoes that form the core of the newly established Arxhan UNESCO Global Geopark [9]. We included Tongxin Lake on the northeast corner of ACVF, the Heaven Lake, Tuofengling Lake, Dichi Lake and Yanshan volcanic group (informally identified as the “Triple Vent”) (Figure 2) to

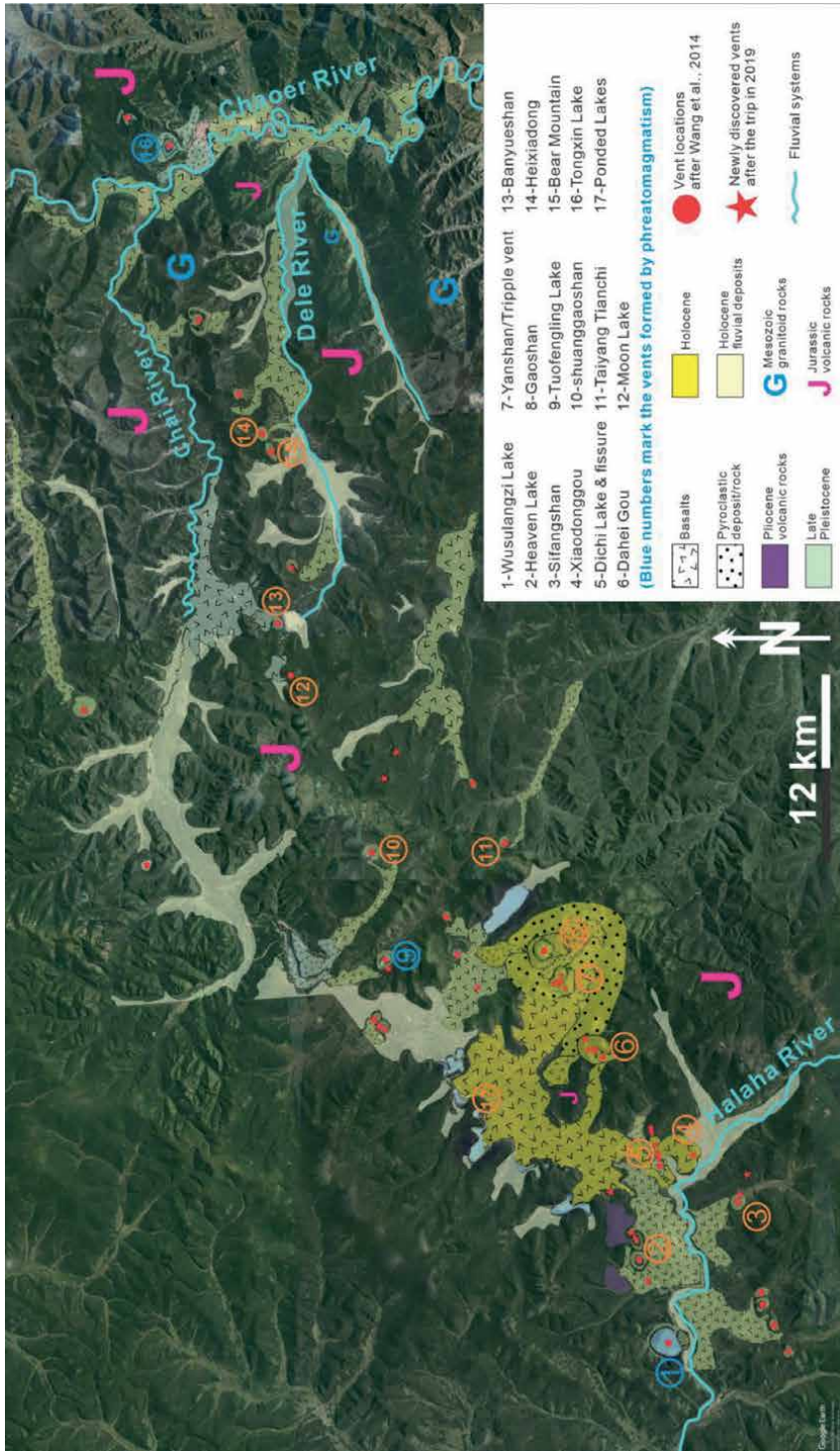


Figure 2. The map of vent distributions of ACVF (red dots) in relationship with the patterns indicating the distributions of volcanic eruptive products from previous research [10]. Numbers refer to locations mentioned in the text.

provide evidence of the important role of explosive hydrovolcanism, fissure-fed eruptions, Strombolian-style eruptions and various large-volume lava outpouring to the volcanic architecture of the field. We demonstrate that the Tongxin Lake near Chaihe township (**Figure 2**) is a tuff ring of explosive phreatomagmatic origin that covered an area of at least 13 km² (**Figure 2**). Eruptions from Tongxin Volcano were probably the most violent in the ACVF indicating the importance of externally-driven explosive hydrovolcanism during the eruptive history of ACVF. In contrast, the youngest known eruption site at Yanshan (C14–2040 +/-75; 1960 +/-70; 1990 +/-100; 1900 +/-70, BP) [11] is a nested scoria and spatter cone with three distinct vents forming a volcanic complex producing scoria-fall, agglutinated and clastogenic lavas. This location demonstrates probably the most common type of volcanic eruption in the ACVF. They are also the most voluminous and the youngest.

The region at and nearby Dichi Lake vent produced the smallest eruptive volumes in ACVF (**Figure 2**). The crater wall of Dichi Lake is composed of lava flows. These were disrupted by an explosive event that left produced angular breccias as a pyroclast ring around the now water-filled crater, best defined as a maar volcano. From Dichi Lake, however, a NE–SW trending fissure exposing a chain of vents gradually builds spatter cones and small scoria cones (**Figure 2**).

The majority of the volcanoes in the western side of the ACVF, closer to Arxan are clearly volcanoes that erupted through magmatic explosion and effusive processes and formed lava spatter cones, spatter ramparts, scoria cones and associated lava flows. Large, elongate craters in this region is filled by water, for example Tuofengling (**Figure 2**). Tuofengling was first interpreted as a scoria cone, but recent field mapping has revealed it is a complex volcanic cone with a basal tuff ring capped by a scoria cone complex. The field-based data presented here provide evidence of one of the largest Pleistocene phreatomagmatic explosive eruptions in the ACVF that formed a maar within a closed intramountain basin (**Figure 2**).

2. Geological setting

ACVF is located about 2000 km away from the Japan subduction zone (**Figure 1**). Thus, the background settings are generally under controls by intra-continental settings influenced by a distant convergent plate margin.

From the satellite map, ACVF is located toward the southeast end of Great Xing'an Range (also known as Da Hinggan Mountains; both names are legitimate, but this paper utilizes the name as Great Xing'an Range). The highest ridges in ACVF are nearly 1500 m above sea level. The ACVF is located near the current political boundaries between China, Russia and Mongolia (**Figure 1**). The regional fault systems align NE–SW with the vents of ACVF, suggesting that the volcanic field is associated with major supracrustal weakness zones or even be linked to rifting and/or reactivation of Mesozoic structural zones separating major tectonic terrains (**Figures 1 and 2**). The rifting history of the region occurred in two major phases [12] around the Songliao Graben (**Figure 1**). It is believed that Songliao Graben subsidence is related delamination of the lithosphere and thinning of the upper crust of NE. China [12–15]. One of the conventional concepts is that the ascending asthenosphere caused by subduction of the down-going slab into the upper mantle initiated and sustained the delamination processes that were manifest as rifting in NE. China [1]. ACVF is located on the west flank of Songliao Graben (**Figure 1**). Hence the regional tectonic setting, characterized by the fault-controlled features, resulted fissures and NE-SW orientation and alignment of vents of (**Figure 2**). These are correlated with macro scale the tectonics of NE

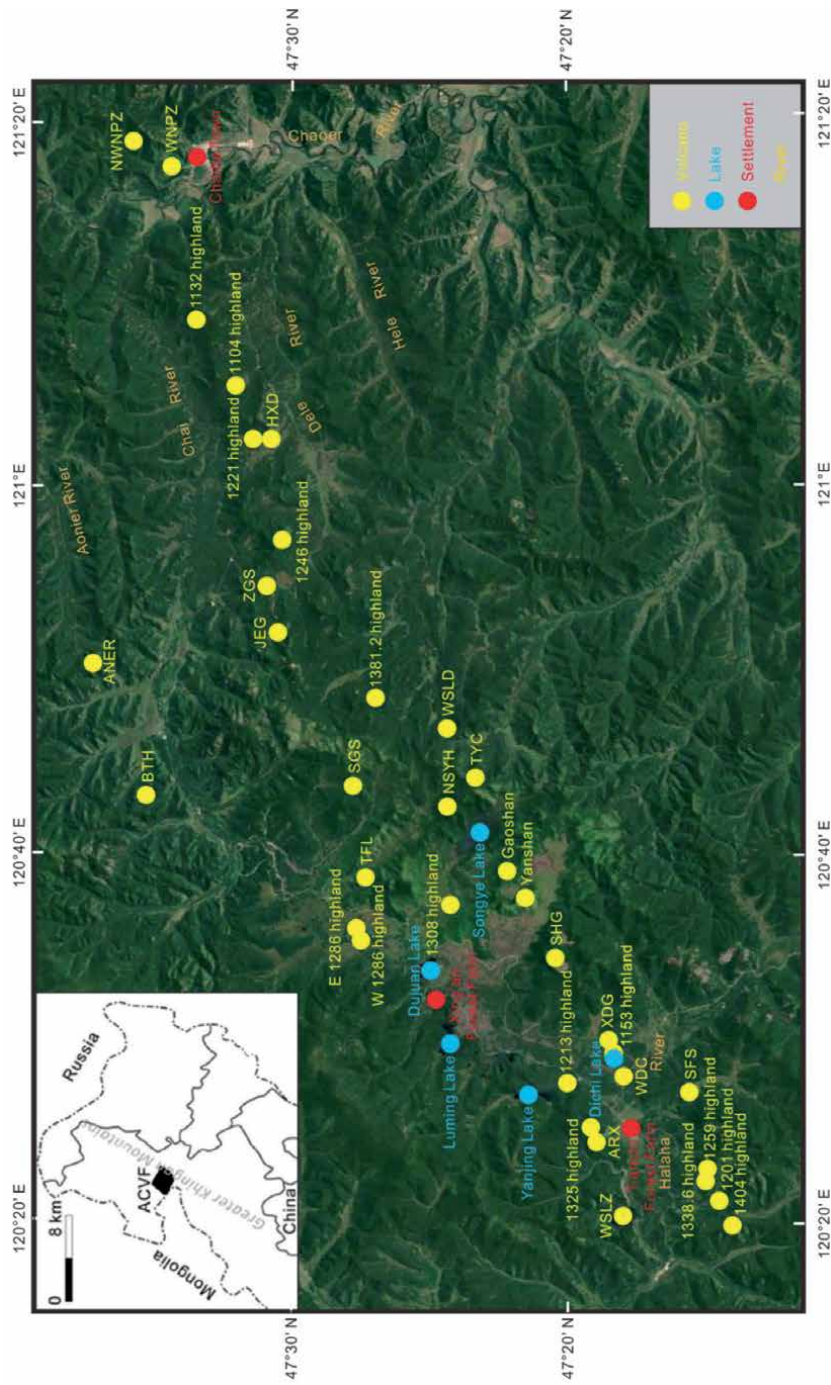


Figure 3. A GoogleEarth map showing the volcanic locations from where basic volcanological information is available. The names and abbreviations also correspond to the common name the locations entered to various publications.

China. Volcanoes of ACVF overlie from Mesozoic basement rocks, such as granites and metamorphosed sediments [16–20]. The eruptive products are interfingering with various Quaternary sediments that accumulated in intra-mountain basins and along fault-controlled valley networks (**Figure 2**). The granitoid basement is strongly fractured, intruded by younger mafic to intermediate dyke swarms and usually covered by thick surface material derived from erosion and in situ weathering. Basement rocks are abundant in pyroclastic rocks as accidental lithics, especially those formed during explosive magma and water interaction. These lithics are preserved as xenoliths in individual or cored bombs in pyroclastic breccias or as accidental lithics of ash and lapilli in pyroclastic density current (PDC) deposits and within lava flows. Among the country-rock debris, there are low-grade metamorphic rocks or meta-sediments (commonly referred informally as “mudrocks”) in minor amounts within the pyroclastic beds. These rocks are also part of the Late Mesozoic basement assemblages.

The region around ACVF includes two main fluvial systems (Halaha River and Chaer River) and several lacustrine systems (**Figures 2 and 3**). The lacustrine systems likely been formed after major lava flows diverted the fluvial channels. For example, a lake formed when a lava flow from the Yanshan – Gaoshan volcanic systems blocked the Halaha River approximately 2000 years ago (**Figures 2 and 3**) [11]. Major structural zones facilitated the storage of groundwater that was driven downward to the lowlands where springs and/or channels developed between major lava flow units [1, 21].

Annual precipitation is about 450 mm; the average temperature is around -2.7°C in the range of -25.1°C in January to 16.8°C in July with about six months of the year below 0°C . These data indicate that ACVF lies within typical subarctic conditions with a strong monsoonal influence [22]. Data relating to paleo-monsoon conditions in NE China are rarely found. However, research based on the lacustrine sediments found in the bottom of crater lakes in ACVF show that around the Last Glacial Maximum (LGM), about 18,000 BP, there was a significant enlargement of the northern grassland areas and warm periods are recorded during mid-Holocene (10000–6000 BP) [21]. These stages were influenced by the East Asian Monsoon. More recently the areas in forest are enlarging; this might indicate influence from the warm periods of mid-Holocene [21]. The present region is covered by typical subarctic forest (*Betula*), grass and shrubland. Volcanic landforms are heavily vegetated, and large and continuous exposures are rare, making geological mapping challenging. Soil formation is intense and even a seemingly young volcanic landforms are covered by thick Holocene sediments or typical sub-arctic mass-movement generated cover beds. The sub-arctic environments and high latitude lead to frozen ground for half the year (Oct to Apr) and only five months when the ground is not frozen (mid-Apr to Sep). A major wildfire in 1987, the Black Dragon fire event, caused widespread destruction of the vegetation around Yanshan-Triple Vent and Gaoshan. Nowadays, that area of forest and vegetation are regenerating and nearly cover the volcanic sites. This means that during field trips some of the areas cannot be assessed and observed.

3. Arxan-Chaihe volcanic field

The Arxan-Chaihe Volcanic Field (ACVF) is recognized as a monogenetic volcanic field covering an area nearly 2000 km^2 [9, 10, 23]. Within this area, at least 47 vents have been identified so far; however, this is likely a minimum number [9]. ACVF has been experiencing high erosion triggered by dramatic temperature changes and fluctuating surface water runoff. Two major fluvial systems within ACVF, the Halaha

River and Chaoer River, facilitate surface erosions (**Figures 2 and 3**). They rework the volcanic materials and modify the general topography. Within ACVF volcanic landforms typical of a monogenetic volcanic field, such as tuff rings, scoria/cinder cones, fissures, lava flows, as well as ponded lava flows, have been recognized [9, 10]. This great diversity of monogenetic volcanic landforms gives the region its high geoheritage value and was the basis for protecting of volcanic landforms by the establishment of a geopark network in the region through intensive work since 2004. The western side of the ACVF became part of the UNESCO Global Geopark Network in 2017 (<http://www.unesco.org/new/en/natural-sciences/environment/earth-sciences/unesco-global-geoparks/list-of-unesco-global-geoparks/china/arxan/>). The recognition of the region's volcanic geoheritage in the highest level shows the importance of the ACVF as an intraplate volcanic field that is far from active plate margin processes and still recognized as an active volcanic region [9]. The ACVF is one of the lesser known volcanic regions of the world, and its physical volcanology and the implications to potential volcanic hazard have not yet been studied extensively.

4. Vent locations and volcano morphology

So far, ACVF preserves at least 47 (known) vents in a 2000 km² area (**Figure 2**). From these 47 vents, only 35 were investigated in more detail and assigned to some volcanic geoforms (**Figure 3**, and **Table 1**). The age of the volcanoes were mostly assigned by their relative stratigraphy (**Table 1**) as sporadic and random absolute age dates are available [10, 24–26] only from a handful of identified volcanoes (**Table 2**). As absolute age dating using radiometric tools such as K-Ar or Ar-Ar methods are problematic in young mafic volcanics, most of the data derived from lava flows and coherent lava as pyroclasts from volcanic edifices. Lava flows however shows that volcanism was spread through time in the wider ACVF region (**Table 2**). This means that the available age data should be viewed with care and many data may not representative for an eruption age of the volcano located in the vicinity of the sampling point but shows ages of earlier lava flows. The volcanic landforms identified in ACVF include tuff rings, scoria/spatter cones, complex volcanic cones and tumuli structures, respectively (**Figure 4**). Tongxin Volcano (**Figure 4A**), is the largest tuff ring preserved in the ACVF with a rim to rim diameter of 1.4–1.1 km. The volcanic edifice is sandwiched between cliffs of basement rock (granite and metavolcanics) forming a typical intramountain basin that has been gradually filled from the north by an alluvial fan (**Figure 4A**). Bedrock is exposed about 306 m above the present-day crater lake surface that is commonly flanked with debris. The average elevation of the ring boundary is approximately 800 m above sea level. The central bottom of the lake is nearly flat with the present-day water depth of no more than 13 m.

The volcanic edifice itself is partially stripped off due to surficial erosion and the thickest tephra succession preserved in its western side is about 22 m thick. Due to thick soil cover (commonly over 2 meters thick, and impenetrable by manual trenching) and grass cover, the pyroclastic deposits associated with the former volcano commonly form only a thin drape of ash and lapilli. In well-protected areas in foothills, however, deposits have been identified over 10-meter thickness about 2–3 km away from the volcano. As preliminary field mapping showed, most of the deposits derived from Tongxin Volcano accumulated in a broad braided river system of the Chaoer River and post-eruptive fluvial processes are likely responsible for the removal of the erodible ash and lapilli.

There are no similar, large preserved tuff rings known from the ACVF, however, small phreatomagmatic volcanoes are suspected or been associated with the basal

Name on Figure 3	Formation Age	Location	Map view shape	Type of volcano or main eruptive product	Area of lava flow [km ²]	Main type of eruption	Relative height of edifice (m)
1 Gaoshan	Holocene	47°22'N, 120°39'E	Circular Horseshoe	Composite Cone	5	Violent Strombolian	362
2 Yanshan	Holocene	47°21'28"N, 120°37'30"E	Circular Horseshoe	Scoria Cone	50	Violent Strombolian	233
3 SHG	Holocene	47°20'28"N, 120°34'14"E	Circular Horseshoe	Scoria Cone	25	Strombolian	224
4 XDG	Holocene	47°18'28"N, 120°29'40"E	Circular Horseshoe	Spatter Cone	5	Hawaiian	110
5 WNPZ	Late Pleistocene	47°34'13"N, 121°17'22"E	Circular	Maar With Tuff Ring, Base-Surge	7	Phreatomagmatic	198
6 WSLZ	Late Pleistocene	47°17'54"N, 120°20'10"E	Circular	Maar With Tuff Ring, Base-Surge	2	Phreatomagmatic	150
7 BTH	Late Pleistocene	47°35'18"N, 120°43'08"E	Ellipse	Tuff Ring, Base-Surge		Phreatomagmatic?	
8 ZGS	Late Pleistocene	47°30'52"N, 120°54'44"E	Long Horseshoe	Collapsed or Breached Scoria Cone	23	Strombolian	136
9 JEG	Middle Pleistocene	47°30'25"N, 120°52'00"E	Circular Horseshoe	Composite Cone	3	Strombolian	178
10 TFL	Middle Pleistocene	47°27'19"N, 120°38'36"E	Long Horseshoe	Composite Cone	12	Strombolian and Phreatomagmatic	170
11 SGS	Middle Pleistocene	47°27'51"N, 120°43'34"E	Long Horseshoe	Collapsed or Breached Scoria Cone	12	Strombolian	168
12 TYC	Middle Pleistocene	47°23'23"N, 120°44'00"E	Circular Horseshoe	Composite Cone	11	Strombolian	122
13 1104 highland	Middle Pleistocene	47°32'2"N, 121°5'00"E	Circular Horseshoe	Composite Cone	20	Strombolian	154

Name on Figure 3	Formation Age	Location	Map view shape	Type of volcano or main eruptive product	Area of lava flow [km ²]	Main type of eruption	Relative height of edifice (m)
14 1132 highland	Middle Pleistocene	47°33'00"N, 121°9'20"E	Circular Horseshoe	Composite Cone	10	Strombolian	182
15 ANER	Middle Pleistocene	47°37'17"N, 120°50'30"E	Circular Horseshoe	Composite Cone	25	Strombolian	172
16 NWNPNZ	Middle Pleistocene	47°35'35"N, 121°19'00"E	Circular Horseshoe	Spatter Cone	1	Hawaiian	205
17 1404 highland	Middle Pleistocene	47°14'8"N, 120°19'47"E	Circular Horseshoe	Collapsed or Breached Scoria Cone		Strombolian	254
18 1201 highland	Middle Pleistocene	47°14'31"N, 120°21'3"E	Long Horseshoe	Fissure Oriented Breached Scoria Cone		Hawaiian, Strombolian	50
19 WSLD	Middle Pleistocene	47°24'25"N, 120°46'49"E	Horseshoe	Collapsed or Breached Scoria Cone		Strombolian	50
20 SFS	Middle Pleistocene	47°15'45"N, 120°26'54"E	Horseshoe	Composite Cone	8	Strombolian	126
21 1153 highland	Middle Pleistocene	47°18'21"N, 120°29'4"E	Long Horseshoe	Fissure Oriented Breached Scoria Cone		Hawaiian, Strombolian	35
22 WDC	Middle Pleistocene	47°18'00"N, 120°27'50"E	Circular Horseshoe	Collapsed or Breached Scoria Cone		Strombolian	20
23 1213 highland	Middle Pleistocene	47°20'2"N, 120°27'27"E	Circular Horseshoe	Collapsed or Breached Scoria Cone		Strombolian	73
24 1308 highland	Middle Pleistocene	47°24'17"N, 120°37'8"E	Long Horseshoe	Collapsed or Breached Scoria Cone		Strombolian	38
25 1381.2 highland	Middle Pleistocene	47°26'53"N, 120°48'32"E	Circular Horseshoe	Collapsed or Breached Scoria Cone		Strombolian	131
26 1246 highland	Middle Pleistocene	47°30'18"N, 120°57'06"E	Circular Horseshoe	Collapsed or Breached Scoria Cone		Strombolian	196

Name on Figure 3	Formation Age	Location	Map view shape	Type of volcano or main eruptive product	Area of lava flow [km ²]	Main type of eruption	Relative height of edifice (m)
27 NSYH	Middle Pleistocene	47°24'23"N, 120°42'28"E	Circular Horseshoe	Collapsed or Breached Scoria Cone		Strombolian	66
28 1259 highland	Middle Pleistocene	47°14'56"N, 120°22'13"E	Circular Horseshoe	Collapsed or Breached Scoria Cone		Strombolian	60
29 1338.6 highland	Middle Pleistocene	47°14'56"N, 120°22'40"E	Circular Horseshoe	Collapsed or Breached Scoria Cone		Strombolian	138
30 W 1286 highland	Middle Pleistocene	47°27'30"N, 120°35'18"E	Horseshoe	Collapsed or Breached Scoria Cone		Strombolian	76
31 E 1286 highland	Middle Pleistocene	47°27'39"N, 120°35'49"E	Horseshoe	Collapsed or Breached Scoria Cone		Strombolian	45
32 1325 highland	Middle Pleistocene	47°19'09"N, 120°25'00"E	Horseshoe	Collapsed or Breached Scoria Cone		Strombolian	175
33 ARX	Middle Pleistocene	47°19'00"N, 120°24'16"E	Semi-Round	Scoria Cone	25	Strombolian	130
34 HXD	Middle Pleistocene	47°30'44"N, 121°2'35"E	Horseshoe	Composite Breached Scoria Cone	6	Strombolian	204
35 1221 highland	Middle Pleistocene	47°31'18"N, 121°3'32"E	Cone	Spatter Cone	8	Hawaiian, Strombolian	117

Table 1. Parameters for previously studied volcanoes in the ACVF.

Sample No.	Location, Code (on Table 2) or Type	Dating method	Age	Reference
08AES02	WNPZ - 5	K-Ar	0.162 ± 0.02 Ma	Fan et al. [24]
07AES02	TFL - 10	K-Ar	0.246 ± 0.05 Ma	Fan et al. [24]
07CH04	Chaoer River – lava flow	K-Ar	0.269 ± 0.03 Ma	Fan et al. [24]
08AES09	WSLZ - 6	K-Ar	0.45 ± 0.03 Ma	Fan et al. [24]
08AES12	Budong River – lava flow	K-Ar	0.587 ± 0.06 Ma	Fan et al. [24]
07CH11	JEG - 9	K-Ar	0.743 ± 0.07 Ma	Fan et al. [24]
07CH09	Dele River – lava flow	K-Ar	1.365 ± 0.16 Ma	Fan et al. [24]
08AES04	TFL - 10	K-Ar	2.3 ± 0.06 Ma	Fan et al. [24]
08AES10	Budong River – lava flow	K-Ar	6.7 ± 0.18 Ma	Fan et al. [24]
Nt202	Tianchi forest farm – lava flow	K-Ar	0.34 ± 0.203 Ma	Liu et al. [25]
NW223	Wuchagou – lava flow	K-Ar	8.93 ± 0.64 Ma	Liu et al. [25]
NW214	Wuchagou – lava flow	K-Ar	9.94 ± 0.63 Ma	Liu et al. [25]
ARS002	TFL - 10	K-Ar	0.34 ± 0.03 Ma	Meng et al. [27]
ARS003	Dujuan Lake – lava flow	K-Ar	0.42 ± 0.10 Ma	Meng et al. [27]
ARS004	ARX - 33	K-Ar	0.53 ± 0.03 Ma	Meng et al. [27]
YL708	JEG - 9	tephra	14.2 ka	Sun et al. [26]
	Yanshan – 2 - under scoria fall	¹⁴ C	1990 cal a BP	Bai et al. [11]
	Yanshan – 2 - under scoria fall	¹⁴ C	1900 cal a BP	Bai et al. [11]

Table 2. Absolute dating results for the volcanic rocks of the ACFV [11, 24–26]. Samples marked as “lava flow” derived from extensive flow fields without exact information from their source vent.

sections of large scoria cones. Tuofengling Lake (Camel Humps Lake in Chinese) is a good example for such volcano edifice architecture (**Figure 4B**). This volcano hosts an elongated lake suggesting that this volcano might be a complex volcano with multiple vents along the lake axis. This volcano appears different in its edifice architecture from Tongxin Volcano. In Tongxin Volcano, the country rocks are exposed in the inner basement hosting the crater lake while in Tuofengling, no basement is exposed. The volcanic edifice surrounding the crater lake is entirely volcanic in origin and part of a larger volcanic edifice. The preserved and accessible sites exposing typical lava spatter, agglomerate, scoriaceous deposits and various clastogenic lava flows suggest a largely magmatic explosive eruption style being responsible for the formation of them. However, from observations of the crater rim, at least two different volcanic deposits were found. The majority is typical of a scoria and spatter cone complex, while in the basal sections thick pyroclastic successions indicate explosive hydrovolcanism occurred as recorded by chilled pyroclast-dominated units predating the formation of the main central cones that were later disrupted giving space to form a broad and elongated crater within them (**Figure 4B**).

The youngest volcanic sites of the ACFV, i.e. approximately 2000 years ago [11], demonstrate a typical volcanic landform considered to be a common form of volcano types across the ACFV. Yanshan Hill marked as a single volcanic edifice, in

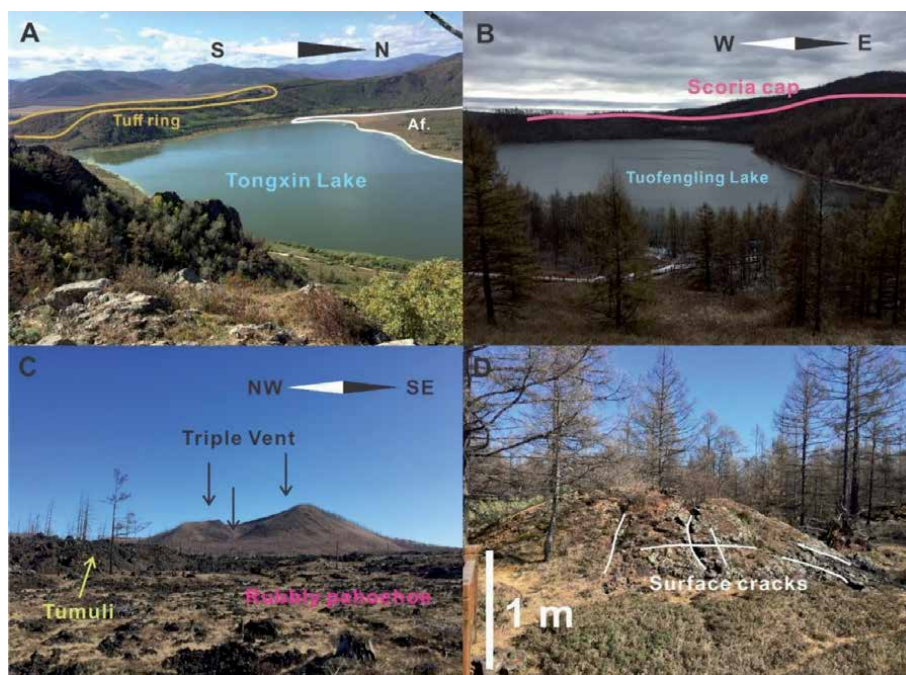


Figure 4. Four types of volcanic geomorphs identified in ACVF, such as (A) tuff ring; (B) complex cone; (C) scoria/cinder cone; (D) tumuli.

fact, consists of at least three preserved volcanoes, informally named as the Triple Vent forming a volcanic complex. This volcano is a nested and closely spaced scoria cone edifice (**Figure 4C**). The main edifice is a steep-sided scoria cone with slope angles about 45° . The elevation of this volcano is about 1590 m above sea level. The volcanic complex was the source of extensive lava flows that reached 4 km to the west and captured the Halaha River causing major landscape modification and damming of the fluvial system. The lava flows show inflation and deflation features, development of pressure ridges, tumuli and outbreaks leading to the formation of a complex laterally changing surface flow morphologies ranging from rubble pahoehoe to aa lava morphotypes. Such large and complex volcanoes are the main volcanic landforms along with the main structurally controlled vents and with NE-SW trending structural elements. The complexity and estimated edifice volumes, as well as the large volume of associated lava flows of these volcanoes, suggest these eruptions changed the actual erupting points within km-ranges, were likely long-lasting events and were capable for sustained eruptions such as sub-Plinian or violent Strombolian style eruptions. This is supported by the extensive ash plain mapped around Yanshan.

Across the field, there is evidence of ponded lava flows, leaving behind a range of ponded lakes, clastogenic lava flows or agglomerates (**Figure 4D**). Based on the previous studies and evidence from 2019 fieldwork, the vents in ACVF are mostly fissure-controlled.

5. Evidence of explosive hydrovolcanism

Explosive hydrovolcanism is the result of magma and water explosive interactions [28]. Phreatomagmatism is a term reserved for magma and groundwater interaction commonly involving molten-coolant interaction [28]. In the ACVF,

pyroclast textures and deposit characteristics indicate that in low-lying areas, along fluvial valleys, phreatomagmatic explosive eruptions took place (**Figure 2**). While shreds of evidence of sustained phreatomagmatic explosive eruptions that formed maar or tuff ring volcanoes alone are not common, evidence of intermittent phreatomagmatic phases during eruptions are compelling. Evidence for phreatomagmatism can be seen in the form of quenched pyroclasts, glassy and angular texture of juvenile particles and relative abundance of country-rock fragments as accidental lithics in the pyroclastic successions. Indirectly, volcanic landforms may also be linked to the occurrence of phreatomagmatism in the course of volcanic eruptions; however, typical “wet”, phreatomagmatic landforms are rarely preserved at ACVF.

The most typical and complete site where evidence for explosive hydrovolcanism, phreatomagmatism has been identified in the ACVF is Tongxin Lake (**Figures 2 and 3**). Tongxin Lake has been recognized as a large tuff ring, partially draping over the rugged mountainous region (**Figure 2**). Two significant outcrops on the west flank of the ring margin have revealed deposits primarily formed by sustained phreatomagmatic eruptions. Dune-bedded, cross-stratified and wavy, accidental lithic-rich pyroclastic successions were observed and inferred to be the product of a combination of pyroclastic density currents and fallout. The succession of interbedded coarse-grained and fine-grained units suggest rapid changes in particle concentration, transportation style and interaction with microtopography. The majority of the pyroclasts are dense (i.e. low vesicularity), angular to subangular with delicate chilled margins. Accretionary lapilli are common in the fine ash beds.

Features indicative for phreatomagmatism can be found at other sites, such as Tuofengling/Camel Humps Lake, southwestern side of Tianchi/Heaven Lake, and in sporadic outcrops south of Wusulanzhi Lake (**Figure 2**). The deposits at Tuofengling Lake form a basal unit beneath the dominant scoria/cinder deposits. This unit is composed of a range of indurated parallel bedded, pyroclastic beds abundant in angular and dense lapilli within fine ash matrix. The average grain sizes from the deposits of Tuofengling is greater than the majority of the deposits recorded at Tongxin Lake (**Figure 5A**), and they are also more indurated than those from Tongxin Volcano.

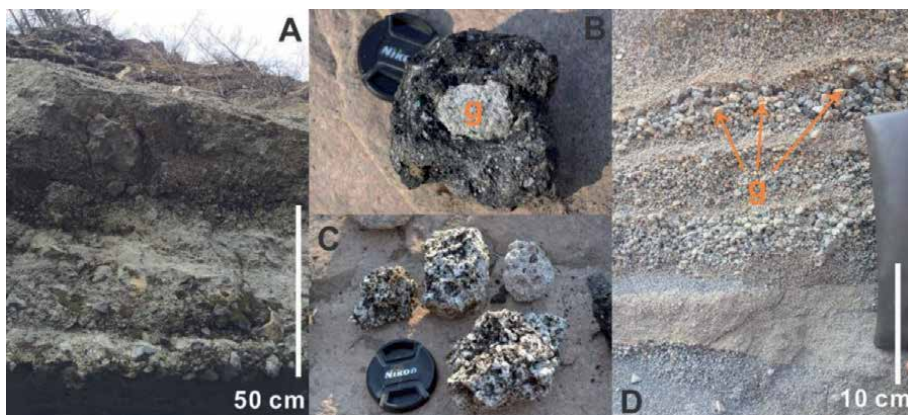


Figure 5. Typical pyroclastic deposit characteristics associated with explosive phreatomagmatic eruptions at the ACVF are linked to accidental lithic-rich pyroclastic breccias, inferred to be phreatomagmatic shower curtain deposits (A), the abundance of cored/loded (B) and partially melted accidental lithics in chilled lavas (C), and typical angular and low vesicularity juvenile pyroclasts forming typically graded beds in a combination of shower and pyroclastic density current-derived beds (D, captured on the south of Tongxin Lake, about 12 km away from the lake). Brown letter “g” indicates “granite”.

Bombs and accidental lithics in the eruptive products from Tongxin Volcano are commonly cored/loaded and/or granitoid lithics are fused or partially melted (**Figure 5B and C**). Cauliflower-shaped bombs with xenoliths are strong evidence for country-rock entrapment prior to the explosive disruption of the clasts during an eruption. Among the shell of the juvenile materials, large amounts of lithic debris are intercalated within. All these lithics are irregular-shaped, and, the juvenile materials are pasted onto the surface, chilled and form into the cauliflower-shaped bombs or juvenile pyroclasts. The general shape of those juvenile pyroclasts is sub-angular to angular. They probably came into contact with external water and became chilled, fragmented in brittle fashion to form angular, low vesicular pyroclasts. Pyroclastic successions, which are rich in accidental lithics and contain large volumes of chilled, angular juvenile pyroclasts commonly form unsorted, and graded beds intercalated with fine tuff that also contains accretionary lapilli (**Figure 5D**). These textural features and outcrop scale sedimentological characteristics are common among phreatomagmatic pyroclastic successions. Commonly, the fine-sized grains indicate the explosive phreatomagmatic fragmentation was accompanied by blasts; on the contrary, the coarse-grained and moderately sorted beds imply fallout origin.

6. Evidence of fissure-controlled volcanism

ACVF preserves a range of fissure-controlled vents (**Figure 2**). Those vents are always aligned NE-SW with the regional tectonic trend (**Figure 6**). Along with those fissures, several small craters with exposed fissures can be observed, for example Tianchi/Heaven Lake (**Figures 6 and 7**) and Dichi Lake (**Figure 8**). These two vent systems are not only the scenic spots of ACVF, but also, they preserve the typical topography and landforms of fissure-fed volcanoes.

Fissure eruption are common in monogenetic volcanic fields [29]. In ACVF, at least five distinct fissures can be identified from satellite images. They appear as linear ridge crests associated with closely spaced crater rows (**Figure 2**). In general ACVF eruptions occur along fissures formed by regional faulting systems [1];



Figure 6. Within Tianchi Lake, a shallow and elongated lake sitting well above the surrounding background topography suggesting the lake itself is a crater lake in a constructional volcanic landform such as a scoria cone. In both side (E and W) the elongated water-filled crater continuing into an elongated zone of depression surrounded by a spatter rampart (brown arrows). The overall orientation of the fissures is the same as the main structural setting of the ACVF (green arrow).

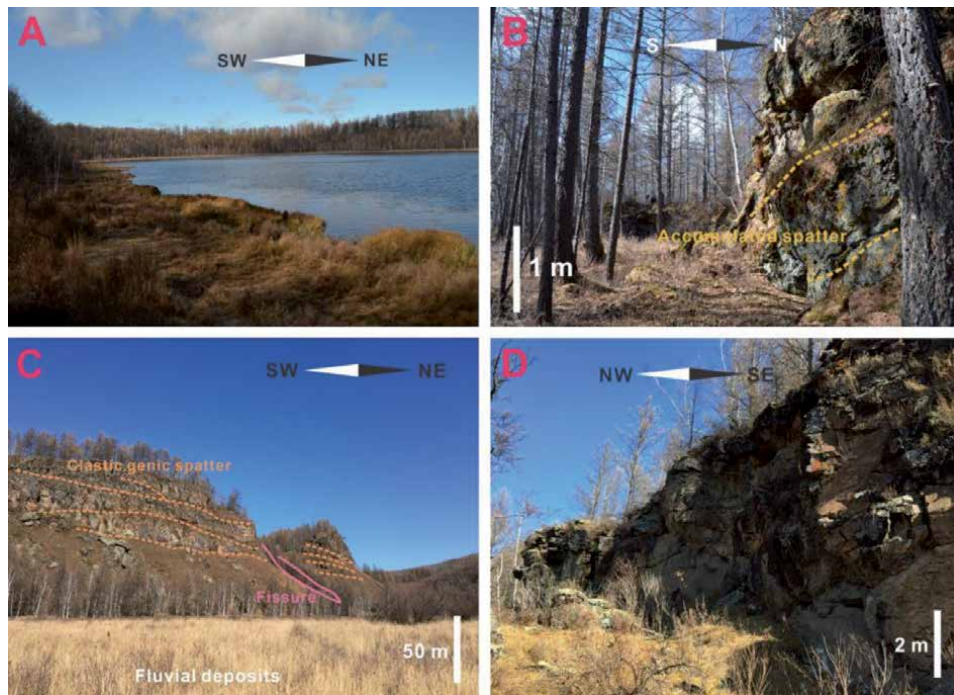


Figure 7. The field observations of Tianchi Lake (A) area showing spatter ramparts, clastogenic lava flows in the eastern (B) and western (C) regions of the Tianchi Lake. Platy lava flows also crop out more or less in the same elevation as the lake floor itself (D).

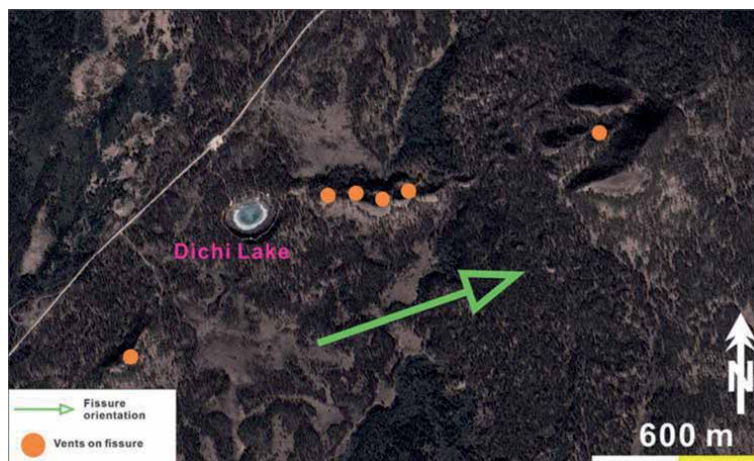


Figure 8. The GoogleEarth satellite image of the vicinity of Dichi Lake showing a chain of craters (brown dots) preserved oriented to the main structural zones of ACVF (green arrow).

however, the volcanoes have yet to be documented in detail. An elongated vent structure is apparent on a satellite view of Tianchi/Heaven Lake (Figure 6). The central part of the lake is bumped out through the surrounding topography, which indicates the presence of steep-sided and agglutinated scoria/cinder cone as the main volcano architecture in that area (Figure 6). A series of the lava flows with large amounts of scattered spatter deposits can be seen on the western side of the lake (Figure 6). The shape of the lake suggests an outpouring may have occurred on the southeast section

of the present-day water-filled, lacustrine basin (**Figure 7A**). Two other locations marking fissure structures on both sides of the lake, are shown by the large green arrow on **Figure 6**. The orientation of the fissures implies Tianchi Lake too follows the orientation of the regional structures (NE-SW). The brown dots on **Figure 6** indicator two rows of spatter and lava ramparts surrounding the margins of an eruptive fissure. This morphological setting and the presence of proximal spatter deposits, and clastogenic lava flows are interpreted to be the result of fissure eruptions that formed the Tianchi Lake Volcano. Also, the angle of repose of the main cone of Tianchi Lake Volcano is nearly 37–41 degrees suggesting a relatively young age of the volcano as Tianchi Lake Volcano is a scoria cone similar to other scoria cones in the world, i.e. the one in AVF (Auckland Volcanic Field) [30]. The total surface area of Tianchi Lake is approximately 0.1 km², with about 1.2 km in its perimeter. The well-established forests and vegetation around the lake field observations and sampling difficult (**Figure 7A**). However, on the outer rim of the lake and the surrounding areas, volcanic materials are well-exposed and easily sampled.

Preliminary observations on the Tianchi Lake Volcano so far have been interpreted as it is a complex, elongated scoria cone. No phreatomagmatic deposits have been identified yet in the area suggesting that the volcano, despite it hosting a shallow lake, formed purely by magmatic explosive and effusive processes. During the dry season (August to October, annually), the height of the water level of the crater lake drops a few metres (**Figure 7A**). Along the eastern and western side of the preserved scoria cone, the fissure is marked by a 10 meters high wall of lava consisting of flows and spatter ramparts. Evidence of agglutinated interbeds within lava flows as well as some of clastogenic origin flows attests to fissure lava fountaining and shifting of active vent locations occurring. The surface structures of the fissure are similar to the lava flow, but are considerably harder, thereby preserving the original volcano architecture well. Occasionally, some lithic xenoliths (granite) can be observed within the spatter and lava flows. The rarity of vesicles in the lava flows and the agglutinated texture suggest the lava was degassed during the eruption, indicating that some sort of lava pool must have occupied the main axis of vents. On the western side of the main cone (**Figure 7C**), an approximately 50 m high wall of weakly stratified agglomerate and interbedded clastogenic lava flows formed due to explosive magmatic eruptions from a sustained lava fountaining stage forming a wall-like topography. In the middle part of the “wall”, a small gap between them might be the fissure structures aligning with the orientation. Field observations could only be taken from one side of the branch of the Halaha River. On the other side the bedded and agglutinated nature of the rocks are clearly visible suggesting the proximal location of the region. The horizontally stratified structures of the “wall” might indicate various stages of the cone building as well as the longevity of the eruptive phase. The thickness of the lava flows in the western side of the Tianchi/Heaven Lake is about 4–6 m (**Figure 7D**). The lava displays textures consistent with fluid transportation; there are also a moderate amount of bubbles. Within the bulk rock, some mafic minerals, including olivines and pyroxenes, can be seen. The top of these lava flow structures is eroded by the vegetation, but in some places the typical structures of aa type are still preserved.

Along with Tianchi/Heaven Lake, Dichi Lake is another small vent sitting on a fissure estimated to be about 3 km long. This lake might be the smallest one in ACVF (**Figure 8**). The green arrow on **Figure 8** marks the regional trend of the fissure orientation, which is also NE–SW, same orientation as Tianchi Lake. In comparison to Tianchi Lake, this fissure system is narrower but longer. The surrounding topography is flat without the tiny bumps due to local tumuli (**Figure 8**). Observations from the proximal areas of the Dichi Lake confirms the presence of pyroclastic breccias composed of dm-to-m sized angular blocks of lava commonly

forming well-defined zones several metres across. This deposit is estimated to be a few metres thick and sitting on a lava platform exposed in the crater wall of the Dichi Lake. There is no sign of deposits that may indicate PDC-generating eruptions or accumulation of typical base surge deposits. On the basis of this observation, Dichi Lake is likely a product of a short-lived, single explosive blast triggered by magma-water interaction along a fissure when the fissure hit the lowermost point of the region (**Figure 8**).

In the densely vegetated area of the Dichi Lake a volcanic cone chain (**Figure 9A**) with small preserved craters is still recognizable (**Figure 9B**). On the top of the small volcanic cones along the fissure, large blocks of scoria can be found hosting dm-sized spindle-shaped bombs (**Figure 9D**). The reddish color of most of the recovered bombs indicates high-temperature emplacement.



Figure 9. The field observations of Dichi Lake show small (tens of metres across) crater chains (a) with shallow but recognizable craters (B). In the crater wall of Dichi Lake lava flows exposed that are covered by pyroclastic breccia deposits (C). In the flank of the crater chains, fluidly shaped lava bombs suggest proximal portions of those areas (D). Dichi Lake best to interpret as a result of a single, short-lived phreatomagmatic blast (explosion crater) in the fissure edge.

7. Evidence of spatter-dominated volcanism

Spatter deposits are the typical dry eruption phase during the building of volcanic cones. In ACVF, spatter deposits are shown on the vents, which are scoria cones or fissure-related vents, such as Dichi Lake. However, one location preserves intact spatter deposits in the basal section of Tongxin Volcano (**Figure 10A**). The rest of the vents in ACVF only preserve scoria deposits from non-welded (black) to welded (red) varieties.

At Tongxin Volcano, the basal pyroclastic deposits along the western rim of the phreatomagmatic volcano preserve an about 2 m thick undulating, laterally discontinuous spatter unit (**Figure 10A**). On the top of the spatter unit, 30–50 cm of unsorted and laterally continuous PDC deposits were found suggesting dramatic eruption style change from a lava fountain stage to a phreatomagmatic blast eruption prior to the eruption becoming more sustained phreatomagmatic in style. Here the spatter deposits are in contact with the country-rock. Based on the contact relationships, Tongxin Volcano might have experienced an initial dry-eruptive phase followed by explosive phreatomagmatism. The distribution of the spatter deposits on Tongxin Volcano are elongated and expanded about 30 m long. On both ends of the spatter deposit, the thickness is thinner than the thickness on the middle part, and the shape is lens-like. Large accidental lithic bombs and blocks are commonly

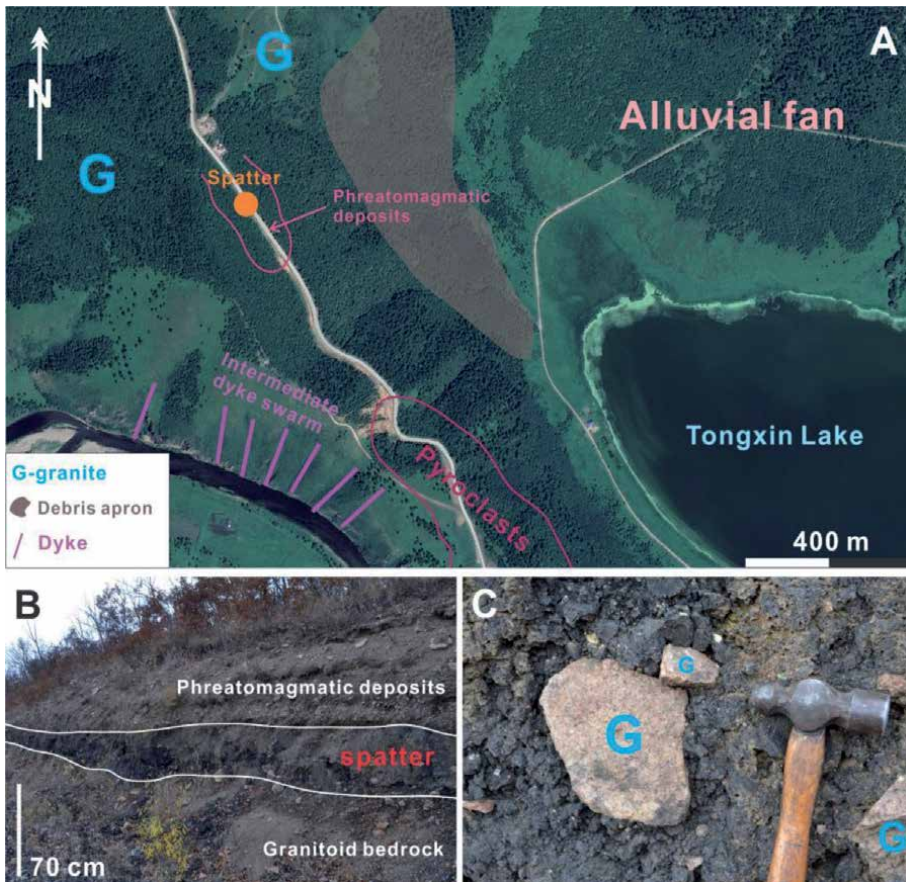


Figure 10. The spatters deposits on the northwestern side of Tongxin Lake (A). The blue letter “G” means “granite” for country-rocks. Spatter deposits lay on the bedrocks (B), and granitoid lithics commonly captured within the spatter deposit (C).

intercalated into the spatters suggesting some sort of excavation of the country-rock through the initial magmatic explosive phase of the Tongxin eruption. The weight of debris of the spatter is low due to the high vesicularity of the spatters. The spatter deposits are hardly found on other areas surrounding Tongxin Lake. However, at least two outcrops preserving the deposits in contact with bedrock indicate the dry-eruption phases, which are correlated with this spatter deposit.

Spatter beds are common elsewhere in the ACVF, especially along the previously described fissure aligned vents. Spatter deposits have also been recovered within exposed scoria cone sections indicating a switching on and off nature of the cone growing phases of those eruptions between Hawaiian and Strombolian style eruptions.

8. Evidence of lava-ponding in craters and topography lows

Lava ponding in ACVF is another feature characteristic of the volcanism in the region. The topography of the lava flows indicates an overwhelming dominance of various types of aa and rubbly pahoehoe lava flow morpho-types for the ACVF.

In ACVF, not only are small vents formed, but also, large craters formed that acted as traps for lava flows. In addition, lava commonly ponded in local basins or valley networks. A large crater (about 1.1 km across) from where one of the youngest and most extensive lava flows initiated to forms a significant volcanic landform with a typical volcanic morphology (**Figure 11**). The local name for this location as Dahei Gou, where it means “the big melanocratic valley”. Actually, there are two territories with the same name, but in considerations to the descriptions of volcanism of ACVF, the name “Dahei Gou” can only be a marker to define this unique location of ponded lava in a large crater. Dahei Gou Crater is located about 4.9 km northeastern of the three young volcanic cones of Yanshan (**Figure 11**). The satellite image (**Figures 2 and 11**) indicates that these two groups of vents (cones) have the same orientation as the Tianchi and Dichi fissures. Thus, it is believed there are at least two major regional structures controlling the vent distributions of ACVF.

The Dahei Gou crater is heavily vegetated, and only small tracks lead to the remote interior of a complex crater system. From the entrance of the valley,

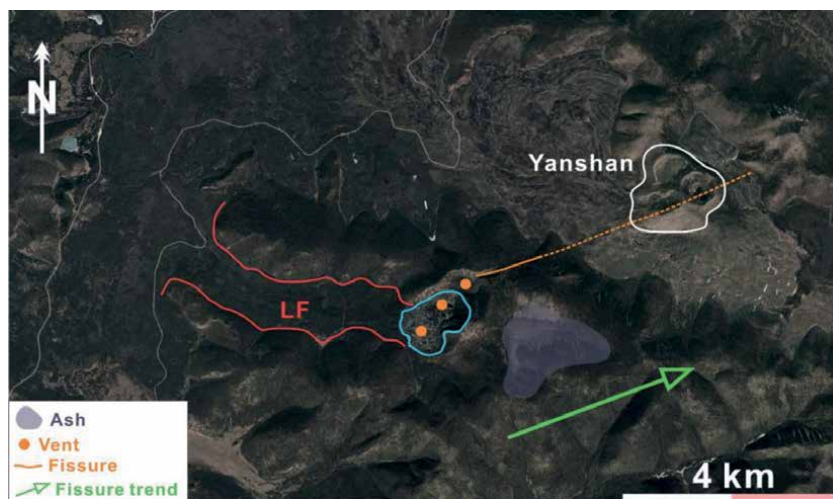


Figure 11. The satellite view of Dahei Gou (big Black Valley), also this photo depicts the relationship with Yanshan-triple vent. The dashed line indicates the extrapolation of the major fissure trend. The blue curve marks the caldera rim of Dahei Gou.

where the main lava flows spread along the Halaha River valley to the crater is about 4 km (**Figure 11**). The valley from the crater is filled with about 1 km wide lava flow along 4 km length, exposing typical flow margin features such as small to medium-sized tumuli and pressure ridges (**Figure 12A and B**).

Within the crater, a breakout zone can be identified along which the lava flow outpoured. In that area, rafted spatter sections and large slabs of lava in a randomly packed chaotic nature is evident. Inside the crater, individual tumuli, ramped up lava rubble and large piles of aa blocks form a rugged topography. Along the crater margin, lava flows preserve several meter-long cracks parallel with the crater margin (**Figure 12D**). These zones are interpreted as fractures along the inflated and ponded intra-crater where ponded lava collapsed upon the partial emptying of the large crater. The major body of the intra-crater lava flow is shown in **Figure 12C**. Along the crater margin, on the inner crater wall, drain back features can be seen that are partially collapsed back to the crater suggesting a dramatic outpouring event tapped the lava toward the valley. Dahe Gou is composed of at least three major nested crater systems, indicating vent migration, crater infill and sudden lava release forming a pit-like crater system. The total area of this crater is approximately 1 km². The perimeter is about 4 km (**Figure 11**). Observations from the field indicate the presence of scoriaceous pyroclastic beds and agglomerate layers that formed due to explosive magmatic eruptions. On the eastern flank of the Dahe Gou, thick, black scoria ash drapes the landscape that has been partially down-cut by erosion (**Figure 11**). The textural similarities and the proximity of these ash plains to Yanshan deposits suggests that it might be part of the youngest eruptions of the Yanshan – Gaoshan volcanic system; however, this needs to be confirmed in future research.

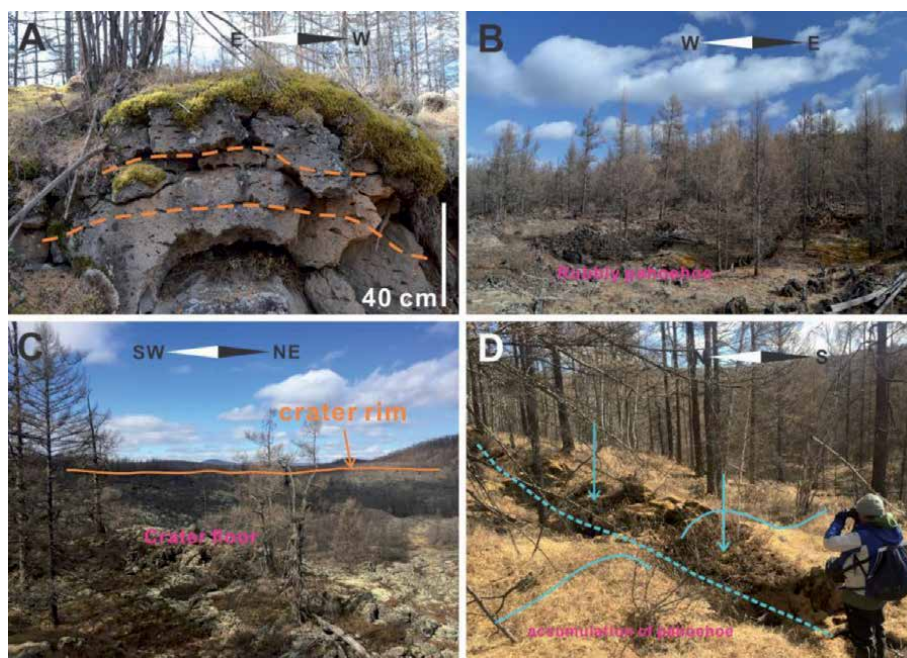


Figure 12.

The major characteristics of Dahe Gou. Lava flows from the Dahe Gou shows pahoehoe surface textures in the lava fan regions with vesicles aligned following inflationary features (A), while deflationary features leaving behind collapsed lava tube roofs (B). The crater is filled with remaining parts of collapsed ponded lava zones, and along with the crater margins lava drawback features are prominent (C). Along the crater margins, margin-parallel cracks indicate collapse events (D).

In the Arxan region, where lava flows are captured in the river valley, they form tumuli and lava tube networks that are partially collapsed, e.g. the fluvial areas of Halaha River. Such areas are prominent around the Wusulanzhi Lake and Tianchi Lake (**Figure 13**). Eventually, in these areas, the lava flows are ponded around and form a range of significant landforms, some of them have already become the scenic spots for the volcanological educational purposes.

Along Halaha River large lava caves are partially open reaching a width of about 4 metres (**Figure 13A**). The lava flows formed successive layers with unambiguous and parallel boundaries. This suggests the flows ponded during several influx stages contemporaneously. The lava dripped from the ceiling (**Figure 13B**) but had no time on the ground consolidating while the processes were ongoing giving them a typical shape that is well preserved. Due to the roughness of the lava flow surface, the ponded lakes developed as the Halaha River became blocked (**Figure 13C**). The lake is no more than 6 m deep. Some of the ponded lakes have been misinterpreted as the sites of small cones; however, they are tumuli that formed along the flow margin. Cone and star shape tumuli displaying the cone shape form a group of dozens of tumuli in this region (**Figure 13D**). The cracks on the top of the tumuli indicate the upwelling and shape-forming processes were accompanied by tremendous volumes of steam. During the slow movement of lava flows, the gas and vaporized steam would occasionally gather and form large bubbles. Some of them were emitted through the surface of the flow. Thus, the inner parts of the tumuli are empty voids with a cone shape. In the Halaha River area, some tumuli are linear in shape (about 4 m in length and about 3 m in height) and align with each other. Most are similar size and volume.

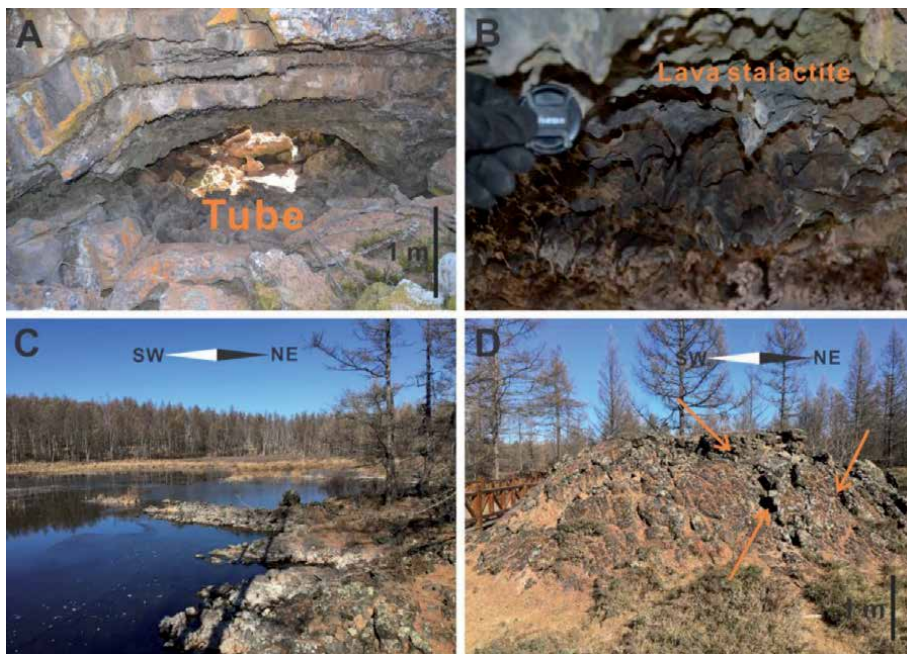


Figure 13. The ponded lava flow topography around fluvial areas of Halaha River exposes partially open lava tubes (A) that are draped by lava stalagmites (B). The blocked Halaha River forms a network of lakes and swamps (C). Tumuli are typically formed in the flat Halaha River valley where the cooling effect slowed down and eventually ponded the lava flows derived from the Dahei Goe volcano and Yanshan- Gaoshan volcanic system about 500 m above the valley floor (D).

9. Evidence of violent Strombolian style eruptions

Dry-eruption types of volcanism are the most common type of explosive volcanism in the ACVF. Large cones along the NE-SW trending ridge tops form a chain of cones that are vegetated and difficult to access. Most of these cones preserved edifice-building sections where ash, lapilli and bomb beds suggest normal Strombolian style volcanism. In the youngest known vent complex, the Gaoshan (High Hill) and Yanshan (Hill of Fire)-Triple vent large amounts of scoriaceous deposits form the cones and also spread across the landscape to form an extensive “ash plain” (Figure 14). The location of Gaoshan and Yanshan on the southeastern boundary of ACVF, is the location of several scoria cones representing the eruptive products of Strombolian style volcanism. In this section, Yanshan-Triple Vent form a more closely spaced vent system than those at Gaoshan inferred on the basis of the special distribution pattern of the volcanic products and the presence of multiple vents within one volcanic massif. The origins of Gaoshan are still being investigated.

Yanshan - Triple Vent, is located in the central part of ACVF (Figure 2). The highest peak in Yanshan is 1597 m above sea level. The total area of this “dry” hill is approximately 2 km², with a perimeter of nearly 5.3 km. On every side of the hill, the burnt forests cover the slopes of the hill; this was a fire hazard at the end of 1987, i.e. Black Dragon fire.

As Figure 14 shows, the lava flows cover most of the area surrounding Yanshan. The slope on the right side of the cone complex reaches 44° due to the welded nature of the proximal scoria beds. Slope angles are lower in the eastern side of the cone complex where a breached section of the cone formed the lava outpouring point from where a lava flow at least 3.77 km long flowed into the Halaha River valley. Some 5 km from the source, scoriaceous ash and lapilli formed at least 1 m thick units suggesting the youngest eruption products were dispersed widely. This dispersal pattern is suggestive of a violent Strombolian, or sub-Plinian stage of eruption during growth of the edifice complex.

Outlines of the ridge crests of the three vents can be pointed out from various observation points. Vent 1 is a flattened, shallow scoria ring structure (Figure 14A and B). In the crater rim crest, a scoria deposit can be reached beneath



Figure 14. The satellite view of Yanshan-triple vent. White lines mark the outlines of the three vents; red lines mark the outlines of the lava flow (LF). Yellow arrowheads show viewpoints from where Figure 15A–C was taken.

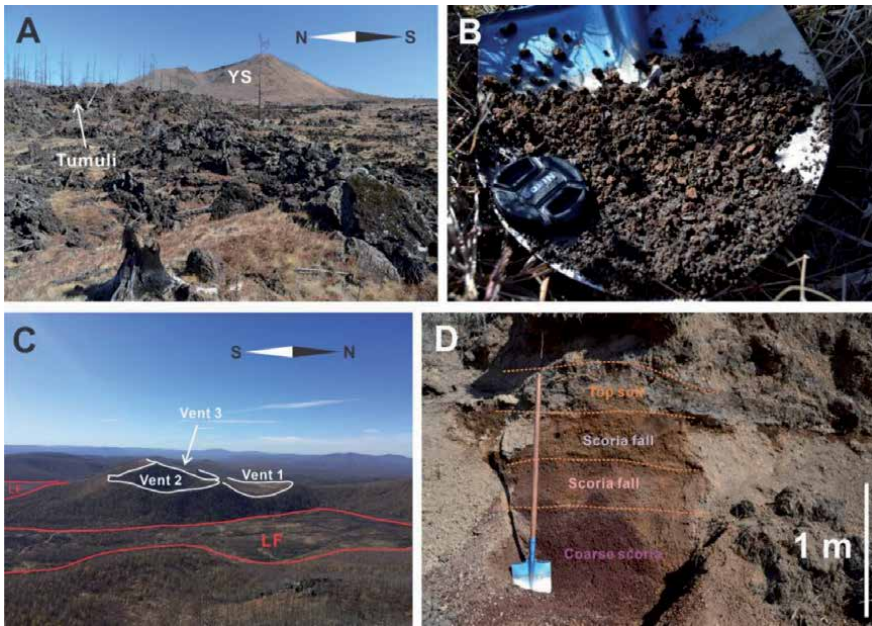


Figure 15. The detailed field observations of Yanshan-triple vent. A view from the south shows a complex cone and an open crater toward the west. Rubby pahoehoe and tumuli around the cone form a rugged surface morphology (A). The surrounding area is covered by thick ash and lapilli blanket of black, and reddish scoria (B). At least three vents can be identified forming the Yanshan-triple vent as it can be seen from Gaoshan peak (C). The ash plain trench just about 2 km east of the vents shows multiple tephra layers indicating repeated and sustained eruptions (D).



Figure 16. Yanshan - triple vent field details. A photo that was taken from the western rim of the vent 1 showing the overgrow of the vent 2 and 3 (A). The crater floor of vent 1 is filled with lava flow creating a rugged grass-covered morphology (B). Vent 3 is the source of the main lava flows outpoured from a breached section of the elongated (fissure-aligned) crater (C). The inner crater wall of the vent 3 exposes a set of agglomerates, welded scoria, spatter and localized clastogenic lava flows, all indicative for lava fountain dominated eruptions and intermittent more violent Strombolian phases (D).

a c. 50 cm thick soil. On vent 3, a clear crater wall collapse, and rafting from where the main lava flow escaped the crater are recorded (**Figure 16C**). The lava ponded in the crater and flowed out of the ring structures forming an outlet. The width of the breakage is narrow (**Figure 16C**), not more than about 250 m, which means the flux of the lava flows may reach a threshold value triggering the collapse of the edifice sector. The crater rim of the main crater composed of agglutinate, clastogenic lava and densely welded scoria beds (**Figure 16D**).

10. Discussion and comparison of ACVF to other similar volcanic fields elsewhere

The volcanism and volcanoes of ACVF were the subject of field work during 2018 and 2019. The observations made play a critical role in understanding the genesis, evolutionary history, types of landforms, and classification of topography. The observations made at ACVF are compared to several volcanic fields elsewhere in the world in terms of type and topography (**Table 3**).

1. The Crater of Moon, Idaho, USA, is an extensive volcanic field alongside the eastern bank of Snake River in the NE USA. It has about 25 cinder cones and large areas covered with the lava flows over an area of about 1600 km² [31–33]. In early research, this volcanic field was interpreted as a continental rift system, with c. 45 km long segment of the Great Rift. The lava flow morphotypes, the dominance of explosive magmatic eruptions over phreatomagmatic volcanism, and the type of monogenetic volcanoes made this field a good analogy with ACVF; however, the volcanoes of the Crater of Moon are smaller, less complex and closer spaced than those at ACVF.
2. The Laki fissure in Iceland is a fissure-driven volcanic cluster. Within it, there are two major vents, volcano Grímsvötn and volcano Thordarhyrna, which represent the genesis of polygenetic volcanism. Significantly, the eruptions in 1783–1785 led to huge mortalities, famine, as well as the global temperature drop [34–36]. The Iceland volcanic fields belong to the Mid-Atlantic Ridge and the Greenland–Iceland–Faeroe Ridge, which are triggered by mantle plumes and formed North Atlantic Igneous Province. The fissure-controlled nature of the Laki eruption can be adopted as an analogy for the fissure-controlled volcano distribution in small and large scale at ACVF. The lava flow morphotypes, however, are more pahoehoe types, e.g. low viscosity melt, and make the lava flow fields of Laki appear different from those at ACVF.
3. Harrats of Saudi Arabia are clusters of the basaltic volcanic fields on the western coastal territories and part of the Red Sea Rift between the African and Arabian continental slabs. Harrat Rahat is one of the large Harrats among them. It is about 20,000 km², and within it, there are approximately 500 individual vents radiating in every direction. The lava flows extend about 100 km to the west along the axis of the field [37, 38]. Harrat Rahat is a good analogy for ACVF in respect of the common large size of the volcanoes, complex volcano architecture, common features of ponding, inflation, deflation and occurrences of ponded lava within large craters and outside in flat-lying areas. Phreatomagmatism in Harrat Rahat has been recognized associated with the smallest volcanoes of the field [37]. The size of the field and the number of vents are also significantly larger to those recorded at ACVF [38].

Volcanic fields Ages	Rock Types	Tectonic Settings	Vent numbers Surface area	Volcano types
Arxan-Chaihe Volcanic Field (ACVF) Late-Pleistocene to Holocene	Majority: Basalt/Trachybasalt Minority: Basaltic Andesite	Intra- continental, rifting system	47+ 2000+ km ²	Tuff rings, Scoria cones, Fissures vents, Caldera, Complex cones
Craters of Moon Idaho, USA Holocene	Basalt/Picro-Basalt, Trachybasalt/Tephrite Basanite, Trachyandesite/ Basaltic Trachyandesite	Rift zone, Continental crust (> 25 km)	25 1600 km ²	Cinder cones, Fissure vents, Tuff rings
Laki Fissure, Iceland Holocene	Basalt / Picro-Basalt	Rift zone, Oceanic crust (< 15 km)	130 600 km ²	Calderas, Craters, Fissure vents
Harrat Rahat Saudi Arabia Pliocene to Holocene	Majority: Basalt/Picro-Basalt, Trachybasalt/Tephrite Basanite, Trachyandesite/ Basaltic Trachyandesite Minority: Trachyte/ Trachydacite	Intraplate, Continental crust (> 25 km)	500 20,000 km ²	Tuff cones, Tuff rings, Scoria cones, Lava domes
Chichinautzin Mexico Pleistocene to Holocene	Majority: Andesite/Basaltic Andesite, Trachyandesite/ Basaltic Trachyandesite, Dacite, Basalt/Picro-Basalt Minority: Trachybasalt/ Tephrite Basanite	Subduction zone, Continental crust (> 25 km)	220 6000 km ²	Tuff cones, Scoria cones, Lava shields, tuff rings
Auckland Volcanic Field (AVF) New Zealand Late-Pleistocene to Holocene	Trachybasalt/Tephrite Basanite, Basalt	Subduction zone, Continental crust (> 25 km)	53 360 km ²	Maars, Tuff rings, Lava shields, Scoria cones

Table 3.
 Comparisons of ACVF to other volcanic fields [data from <https://volcano.si.edu>].

4. The Chichinautzin Monogenetic Volcanic Field is located on the central part of Mexico and belonged to Trans Mexican Volcanic Belt. There are more than 220 vents located within c. 6000 km² area. Most volcanoes in this field are basaltic andesite or basaltic trachyandesite [39–41]. Chichinautzin shares similarities to ACVF in respect to the similar individual volcano sizes, geochemistry, surface area and some aspects of forming nested vents and complex vent systems. However, Chichinautzin is a far more evolved complex and it is likely volcanoes were longer lived compared to those in ACVF where other than nested vent complex formation, the majority of its volcanoes are more typical of monogenetic volcanism.

11. Conclusion and volcanic eruption scenarios

Volcanism always cause a range of significant hazards to human societies. Not only to the life expectancy but they can also harm the foundations of infrastructures, exposed communities, disrupt the business, and put additional risks on the surrounding environments [42]. The hazards and threats from volcanic eruptions

and its related tectonic disasters are increasing annually to vulnerable societies. This is caused by the specific natural features of a volcanic field. The volcanic products, especially the mapped PDC deposits at Tongxin Volcano, can generate a range of very fertile soils and lands, which are utilized intensively for agriculture. However, the presence of thick and extensive PDC deposits indicate the threat of violent phreatomagmatic explosive events that can devastate large regions are ever present. On the other hand, the lava flows common at ACVF, which constitute the bulk of the volcanic products, are the very good construction materials. In general, the major effective regions under the shadows of volcanic eruptions are the proximal and intermediate areas, which can be impacted by the significant and severe threats from lava flows as well as deadly PDC flows.

In ACVF, several volcano types have been identified, but all of them show features of typical monogenetic volcanoes with small eruptive volume, small edifice size, typical deep sourced magma systems and suspected short eruption duration. The majority of the volcanoes identified formed through dry magmatic explosive eruptions forming lava spatter cones (**Figure 17A**), scoria cones (**Figure 17B**) or complex fissure aligned volcano chains (**Figure 17C**). These volcanoes pose hazards to their immediate surroundings; however, because we do not know where the next eruption will take place, they pose prediction uncertainty. The strong fissure alignments of the vents in hundreds of metres to tens of kilometers length, however, suggests that new vents likely will open along those main regional structure-controlled zones. The identification of fissure-fed, dominantly Hawaiian and Strombolian style eruptions suggests that once a new vent opens, the active vents likely will migrate along the fissure axis within the hundreds of metres to several kilometers length, making it difficult to mitigate the volcanic hazard. Due to the propagation of fissure through periods, volcanoes can be classified not only by type but also by eruption types. Generally, Strombolian eruptions, phreatomagmatic eruptions are the two major eruption types. Otherwise, the transition type or switching of the eruption types between two major eruptive behaviors is another major hazard event. It seems that phreatomagmatism occurred at ACVF (**Figure 17D**), but it is not the most significant type of volcanism. Phreatomagmatism seems to have occurred in low lying areas and/or along major fluvial networks. This style of volcanism formed a very violent event at Tongxin (**Figure 17D**). Similar eruptions in the fluvial valleys, where most of the human population lives today, could be catastrophic. It is also evident that the Tongxin eruption started just like any other volcanic eruption at ACVF, as lava fountaining along a migrating fissure (**Figure 17D1**). Once the rising magma along the fissure hit an active hydrogeological zone, violent phreatomagmatic explosions took place (**Figure 17D2**). Similar situations were suggested at Dichi Lake only on a significantly smaller scale. (**Figure 17E**) The nature of this eruption style transition accompanied by the fissure-fed nature of the volcanism needs further study to develop realistic eruptions scenario-based volcanic hazard study of the region.

Effects to the local topography are represented as the lava pouring into the fluvial systems changes the river flow patterns (**Figure 17F**). By damming rivers, temporary lakes can form changing the local hydrogeology that may promote explosive phreatomagmatism in the course of the ongoing eruption.

The lava ponding has also been recognized as an important process in the development of the lava fields. The complex high altitude volcanoes with multiple vents, shifting active vent locations and lava ponding in large craters are features that need to be considered in volcanic hazard eruption scenarios, as sudden collapse of scoria cone sectors and outpour of ponded lava could initiate large lava flows to areas that normally would not be considered as regions susceptible to lava flow hazards (**Figure 17G**).

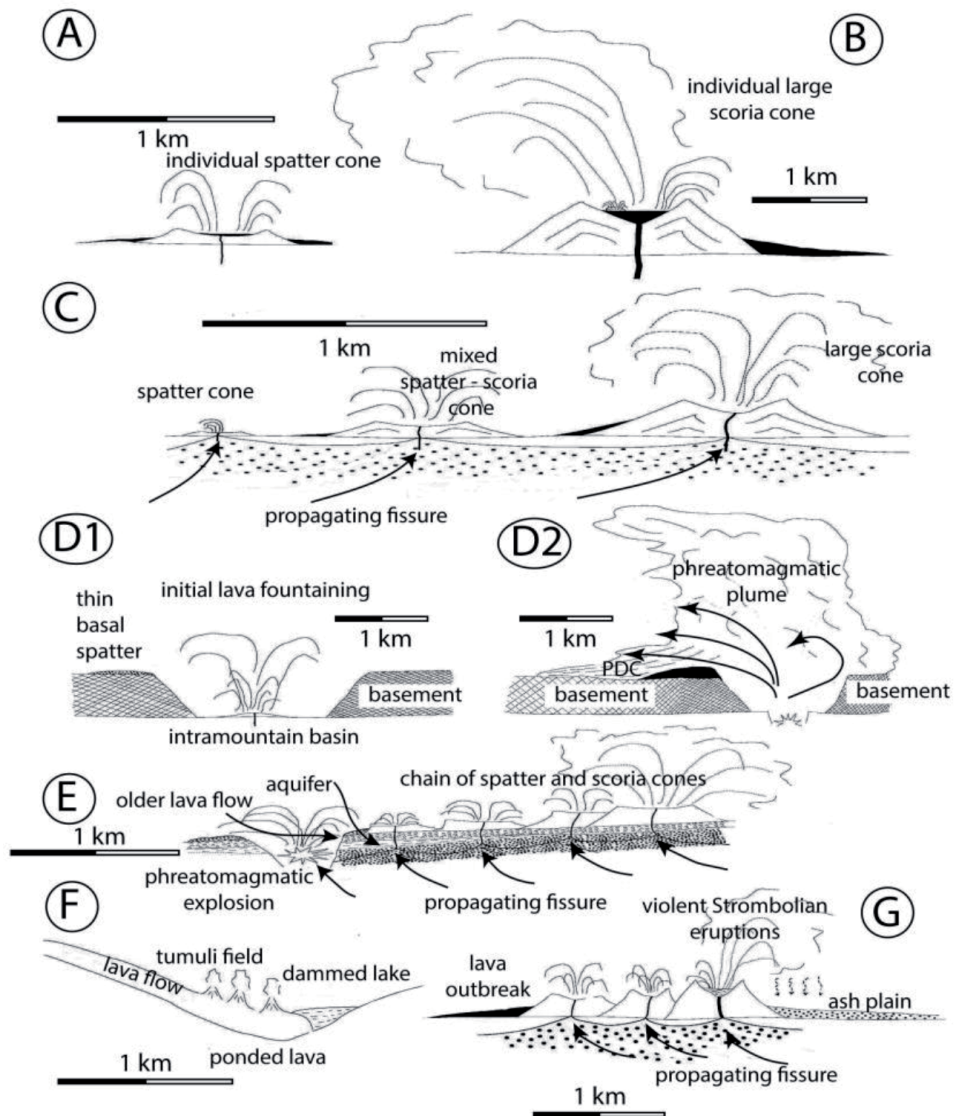


Figure 17. Typical volcano types identified at ACVF and their inferred schematic volcanic eruption scenarios. The ACVF has abundant individual lava spatter cones (A) and individual scoria cones (B) separated from other volcanoes by large (few kilometres) distances. More common volcano types of the ACVF are closely spaced spatter-and-scoria cone chains inferred to be formed due to fissure-fed magmatic explosive eruptions (C). Phreatomagmatic volcanoes are rare at ACVF and their eruptive sequence commonly starts with a succession indicating initial magmatic explosive phases (D1) and thick laterally extensive pyroclastic density current (e.g. base surge) deposited pyroclastic successions (D2). Occasionally, fissure-fed spatter-and-scoria cones terminate to a maar-forming eruption in low-land such as the Dichi Lake (E). Large-volume and long lava flows tend to dam syn-eruptive river network forming lakes where lava blisters such as tumuli field can form (F). Large and complex scoria cones in elevated ridges form multiple cone complexes, where outbreak of lava lakes can cause cone rafting and trigger sustained ash plumes to create ash and lapilli plains through violent-Strombolian style eruptions (G). Horizontal scales are approximate only.

Acknowledgements

The authors wish to thank the support of the School of Agriculture and Environment, Massey University PhD Fellowship, the China – New Zealand Academic Exchange Program as part of the Royal Society of New Zealand Catalyst

Programme and the support from the Institute of the Geology and Geophysics of the Chinese academy of Sciences, Beijing. An earlier version of the manuscript was kindly reviewed by Dr. Gaby Gomez (U Morelia, Mexico) what for we are really thankful. Formal Anonymous reviewers' comments helped to elevate the quality of the chapter we thank for.

Funding

This research was funded by the Massey University's Volcanic Risk Solution and School of Agriculture and Environment PhD-research fellowship. Fieldwork and logistics were supported by the Chinese Academy of Sciences and the Catalyst: Leaders New Zealand-China Scientist Exchange Programme.

Author details


Boxin Li¹, Károly Németh^{1*}, Julie Palmer¹, Alan Palmer¹, Jing Wu², Jonathan Procter¹ and Jiaqi Liu²

¹ Volcanic Risk Solutions, School of Agriculture and Environment, Massey University, Palmerston North, New Zealand

² Institute of Geology and Geophysics, Chinese Academy of Sciences, Beijing, China

*Address all correspondence to: k.nemeth@massey.ac.nz

IntechOpen

© 2020 The Author(s). Licensee IntechOpen. This chapter is distributed under the terms of the Creative Commons Attribution License (<http://creativecommons.org/licenses/by/3.0>), which permits unrestricted use, distribution, and reproduction in any medium, provided the original work is properly cited. 

References

- [1] Liu, J.Q., J.T. Han, & W.S. Fyfe, (2001). Cenozoic episodic volcanism and continental rifting in northeast China and possible link to Japan Sea development as revealed from K-Ar geochronology. *Tectonophysics*. 339(3-4): 385-401.
- [2] Wu, J., Z. Zhu, C. Sun, P. Rioual, G. Chu, & J. Liu, (2019). The significance of maar volcanoes for palaeoclimatic studies in China. *Journal of Volcanology and Geothermal Research*. 383: 2-15.
- [3] Sun, C., K. Nemeth, T. Zhan, H. You, G. Chu, & J. Liu, (2019). Tephra evidence for the most recent eruption of Laoheishan volcano, Wudalianchi volcanic field, northeast China. *Journal of Volcanology and Geothermal Research*. 383: 103-111.
- [4] Ramos, F.C., J.A. Wolff, J.E. Buettner, H.Q. Wei, & J. Xu, (2019). Ra/Th ages of sanidine in young trachytes erupted at Changbaishan Volcano, China. *Journal of Volcanology and Geothermal Research*. 374: 226-241.
- [5] Pan, B., S.L. de Silva, J. Xu, Z. Chen, D.P. Miggins, & H. Wei, (2017). The VEI-7 Millennium eruption, Changbaishan-Tianchi volcano, China/DPRK: New field, petrological, and chemical constraints on stratigraphy, volcanology, and magma dynamics. *Journal of Volcanology and Geothermal Research*. 343: 45-59.
- [6] Wei, H., G. Liu, & J. Gill, (2013). Review of eruptive activity at Tianchi volcano, Changbaishan, northeast China: implications for possible future eruptions. *Bulletin of Volcanology*. 75(4).
- [7] Xiao, L. & C.Z. Wang, (2009). Geologic features of Wudalianchi volcanic field, northeastern China: Implications for Martian volcanology. *Planetary And Space Science*. 57(5-6): 685-698.
- [8] Feng, M. & J.L. Whitford-Stark, (1986). The 1719-1721 eruptions of potassium-rich lavas at Wudalianchi, China. *Journal of Volcanology and Geothermal Research*. 30: 131-148.
- [9] Németh, K., J. Wu, C. Sun, & J. Liu, (2017). Update on the Volcanic Geoheritage Values of the Pliocene to Quaternary Arxan-Chaihe Volcanic Field, Inner Mongolia, China. *Geoheritage*. 9(3): 279-297.
- [10] Wang, L., M. Tian, X. Wen, L. Zhao, J. Song, M. Sun, H. Wang, Y. Lan, & M. Sun, (2014). Geoconservation and geotourism in Arxan-Chaihe Volcano Area, Inner Mongolia, China. *Quaternary International*. 349: 384-391.
- [11] Bai, Z., M. Tian, F. Wu, D. Xu, & T. Li, (2005). Yanshan, Gaoshan - Two active volcanoes of the volcanic cluster in Arshan, Inner Mongolia. *Earthquake Research in China*. 21(1): 113-117.
- [12] Liu, J., (1989). On the origin and evolution of continental rift system in Northeast China. *Chinese Journal of Geology*. 3: 209-319.
- [13] Jia, H., H. Ji, L. Wang, D. Yang, P. Meng, & C. Shi, (2016). Tectono-sedimentary and hydrocarbon potential analysis of rift-related successions in the Dehui Depression, Songliao Basin, Northeastern China. *Marine and Petroleum Geology*. 76: 262-278.
- [14] Gao, Y.-G. & Y.-H. Li, (2014). Crustal thickness and V-p/V-s in the Northeast China-North China region and its geological implication. *Chinese Journal of Geophysics-Chinese Edition*. 57(3): 847-857.
- [15] Zheng, Y., W. Shen, L. Zhou, Y. Yang, Z. Xie, & M.H. Ritzwoller, (2011). Crust and uppermost mantle beneath the North China Craton, northeastern China, and the Sea of Japan from

ambient noise tomography. *Journal of Geophysical Research-Solid Earth*. 116.

[16] Zhang, C., J.-Y. Quan, Y.-J. Zhang, Z.-H. Liu, W. Li, Y. Wang, C. Qian, L. Zhang, & J.-T. Ge, (2020). Late Mesozoic tectonic evolution of the southern Great Xing'an Range, NE China: Evidence from whole-rock geochemistry, and zircon U-Pb ages and Hf isotopes from volcanic rocks. *Lithos*. 362.

[17] Liu, Y., S.-H. Jiang, L. Bagas, C.-L. Chen, N. Han, & Y.-Y. Wan, (2020). Petrogenesis and metallogenic potential of the Wulanba granite, southern Great Xing'an Range, NE China: constraints from whole-rock and apatite geochemistry. *Geological Magazine*. 157(3): 411-434.

[18] Wan, L., C. Lu, Z. Zeng, A.S. Mohammed, Z. Liu, Q. Dai, & K. Chen, (2019). Nature and significance of the late Mesozoic granitoids in the southern Great Xing'an range, eastern Central Asian Orogenic Belt. *International Geology Review*. 61(5): 584-606.

[19] Ji, Z., W.-C. Ge, H. Yang, Q.-h. Wang, Y.-l. Zhang, Z.-h. Wang, & J.-H. Bi, (2018). Late Jurassic rhyolites from the Wuchagou region in the central Great Xing'an Range, NE China: Petrogenesis and tectonic implications. *Journal of Asian Earth Sciences*. 158: 381-397.

[20] Wang, T., L. Guo, L. Zhang, Q. Yang, J. Zhang, Y. Tong, & K. Ye, (2015). Timing and evolution of Jurassic-Cretaceous granitoid magmatism in the Mongol-Okhotsk belt and adjacent areas, NE Asia: Implications for transition from contractional crustal thickening to extensional thinning and geodynamic settings. *Journal of Asian Earth Sciences*. 97: 365-392.

[21] Zhao, C., X. Li, X. Zhou, K. Zhao, & Q. Yang, (2016). Holocene vegetation succession and responses to climate

change in the northern sector of Northeast China. *Science China Earth Sciences*. 46(1674-7240): 870.

[22] Liu, T. & Z. Ding, (1998). Chinese Loess and the Paleomonsoon. *Annual Review of Earth and Planetary Sciences*. 26: 111.

[23] Zhao, Y., Q. Fan, Z. Bai, Q. Sun, N. Li, J. Sui, & X. Du, (2008). Preliminary study on Quaternary volcanoes in the Halaha River and Chaoer River area in Da Hinggan Ling. *Yanshi Xuebao = Acta Petrologica Sinica*. 24(11): 2569-2575.

[24] Fan, Q., Y. Zhao, D. Li, Y. Wu, & D. Zheng, (2011). Studies on Quaternary volcanism stages of Halaha river and Chaoer river area in the Great Xing'an Range: Evidence from K-Ar dating and volcanic geology features. *Acta Petrologica Sinica*. 27(10): 2827-2832.

[25] Liu, J., (1987). Study on geochronology of the Cenozoic volcanic rocks in northeast China. *Acta Petrologica Sinica*. 6(2): 49-51.

[26] Sun, C., Q. Liu, J. Wu, K. Németh, L. Wang, Y. Zhao, G. Chu, & J. Liu, (2017). The first tephra evidence for a Late Glacial explosive volcanic eruption in the Arxan-Chaihe volcanic field (ACVF), northeast China. *Quaternary Geochronology*. 40: 109-119. S1871101416301558 [http://dx.doi.org/10.1016/j.quageo.2016.10.003].

[27] Meng F-c, Safonova I, Chen S-s, Rioual P (2018) Late Cenozoic intra-plate basalts of the Greater Khingan Range in NE China and Khangai Province in Central Mongolia. *Gondwana Research* 63:65-84

[28] Németh, K. & S. Kósik, (2020). Review of Explosive Hydrovolcanism. *Geosciences*. 10(2): 44.

[29] Kereszturi, G. & K. Németh, (2012). Monogenetic basaltic volcanoes: genetic classification, growth, geomorphology and degradation, K. Németh, Editor,

Updates in Volcanology - New Advances in Understanding Volcanic Systems, inTech Open: Rijeka, Croatia. p. 3-88 [<http://dx.doi.org/10.5772/51387>].

[30] Kereszturi, G. & K. Nemeth, (2016). Sedimentology, eruptive mechanism and facies architecture of basaltic scoria cones from the Auckland Volcanic Field (New Zealand). *Journal of Volcanology and Geothermal Research*. 324: 41-56.

[31] Leeman, W.P., C.J. Vitaliano, & M. Prinz, (1976). Evolved lavas from Snake-River Plain - Craters of Moon National Monument, Idaho. *Contributions to Mineralogy and Petrology*. 56(1): 35-60.

[32] Green, J. & N.M. Short, (2012). *Volcanic landforms and surface features: a photographic atlas and glossary*. Springer Science & Business Media.

[33] Greeley, R. & J.S. King, (1977). *Volcanism of the Eastern Snake River Plain, Idaho: A comparative planetary geology-guidebook*. National Aeronautics and Space Administration; 1st Edition (January 1, 1977) [ASIN : B000L7Z6NS]

[34] Thordarson, T., D.J. Miller, G. Larsen, S. Self, & H. Sigurdsson, (2001). New estimates of sulfur degassing and atmospheric mass-loading by the 934 AD Eldgja eruption, Iceland. *Journal Of Volcanology And Geothermal Research*. 108(1-4): 33-54.

[35] Thordarson, T. & S. Self, (1993). The Laki (Skaftár Fires) and Grímsvötn eruptions in 1783-1785. *Bulletin of Volcanology*. 55(4): 233-263.

[36] Thordarson, T. & S. Self, (2003). Atmospheric and environmental effects of the 1783-1784 Laki eruption: A review and reassessment. *Journal of Geophysical Research: Atmospheres*. 108(D1): AAC 7-1-AAC 7-29.

[37] Murcia, H., K. Németh, N.N. El-Masry, J.M. Lindsay, M.R.H. Moufti,

P. Wameyo, S.J. Cronin, I.E.M. Smith, & G. Kereszturi, (2015). The Al-Du'aythah volcanic cones, Al-Madinah City: implications for volcanic hazards in northern Harrat Rahat, Kingdom of Saudi Arabia. *Bulletin of Volcanology*. 77(6): 54.

[38] Murcia, H., K. Nemeth, M.R. Moufti, J.M. Lindsay, N. El-Masry, S.J. Cronin, A. Qaddah, & I.E.M. Smith, (2014). Late Holocene lava flow morphotypes of northern Harrat Rahat, Kingdom of Saudi Arabia; implications for the description of continental lava fields. *Journal of Asian Earth Sciences*. 84: 131-145.

[39] Nieto-Torres, A. & A.L. Martin Del Pozzo, (2019). Spatio-temporal hazard assessment of a monogenetic volcanic field, near México City. *Journal of Volcanology and Geothermal Research*. 371: 46-58.

[40] Nieto-Torres, A. & A.L. Martin Del Pozzo, (2019). Spatio-temporal hazard assessment of a monogenetic volcanic field, near Mexico City. *Journal of Volcanology and Geothermal Research*. 371: 46-58.

[41] Lorenzo-Merino, A., M.N. Guilbaud, & J. Roberge, (2018). The violent Strombolian eruption of 10 ka Pelado shield volcano, Sierra Chichinautzin, Central Mexico. *Bulletin of Volcanology*. 80(3).

[42] Blong, R.J., (1984). *Volcanic hazards. A sourcebook on the effects of eruptions*. Academic Press, Inc., Orlando, FL. Medium: X; Size: Pages: 427.

An Overview of the Mafic and Felsic Monogenetic Neogene to Quaternary Volcanism in the Central Andes, Northern Chile (18-28°Lat.S)

Gabriel Ureta, Károly Németh, Felipe Aguilera, Matias Vilches, Mauricio Aguilera, Ivana Torres, José Pablo Sepúlveda, Alexander Scheinost and Rodrigo González

Abstract

Monogenetic volcanism produces small eruptive volumes with short eruption history, different chemical compositions, and relatively simple conduit. The Central Volcanic Zone of the Andes is internationally known as a natural laboratory to study volcanism, where mafic and felsic products are present. In this contribution, the spectrum of architectures, range of eruptive styles, lithological features, and different magmatic processes of the mafic and felsic monogenetic Neogene to Quaternary volcanoes from the Central Volcanic Zone of the Andes in northern Chile (18°S-28°S) are described. The major volcanic activity occurred during the Pleistocene, where the most abundant activity corresponds to effusive and Strombolian eruptions. This volcanism is characterized by external (e.g., magma reservoirs or groundwater availability) and internal (e.g., magma ascent rate or interaction en-route to the surface) conditions, which determine the changes in eruptive style, lithofacies, and magmatic processes involved in the formation of monogenetic volcanoes.

Keywords: monogenetic volcanoes, small-volume volcanoes, magmatic and hydromagmatic eruptions, Central Volcanic Zone, Altiplano-Puna

1. Introduction

Monogenetic volcanoes are the most common type of subaerial volcanoes on the Earth [1] that occur in any tectonic setting as intraplate, extensional, and subduction [2]. They can be distributed as isolated centers, monogenetic volcanic fields [3], or associated with large volcanic systems as polygenetic volcanoes or calderas [4], displaying a plumbing system relatively simple or of a dispersed nature [5]. Monogenetic volcanoes are associated with small eruptions fed from one or multiple magma batches, with volumes typically $\leq 1 \text{ km}^3$ of basic to silicic composition and form over

a short period from hours to decades. Monogenetic centers can build several volcanic landforms in response to their relationship with different environmental settings [6]. They can be produced by different eruptive styles (e.g., Hawaiian, Strombolian, violent Strombolian, phreatomagmatic, Surtseyan, and effusive activity) that are determined by internal- and external- factors [7], and evidencing several magmatic processes (e.g., fractionation, mixing, contamination) [5]. Therefore, each monogenetic volcanic system is different depending on many factors (mentioned above). For this reason, current efforts around the world focus on understanding monogenetic volcanism in different scenarios, in order to provide a better understanding of this variability and to provide tools to estimate possible scenarios of future eruption [8].

The Central Volcanic Zone (CVZ) of the Andes and particularly northern Chile (18–28°S) (**Figure 1**), is an excellent natural laboratory to study monogenetic systems of changing magma compositions in time and space related to the evolution of an active continental margin, and a ~ 70 km thick orogenic crust [12]. Despite this,

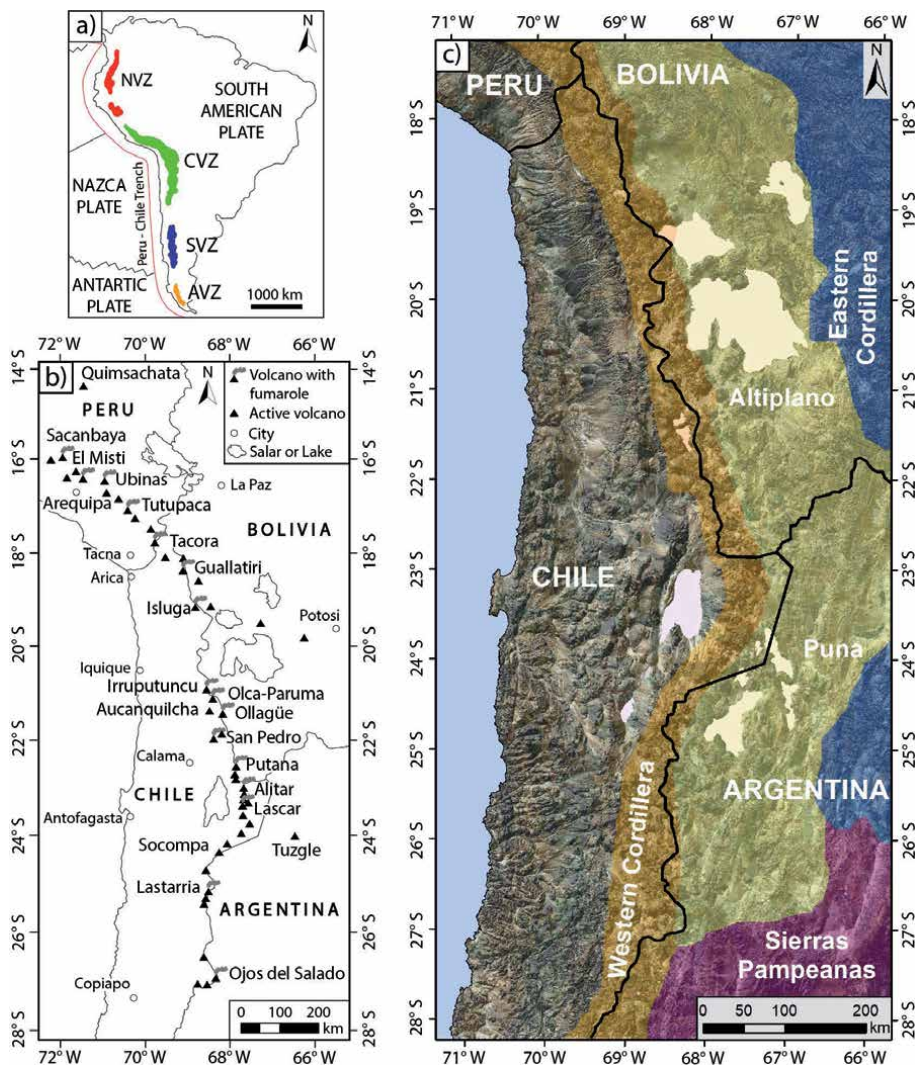


Figure 1. a) Map showing the location of the Northern, Central, Southern, and Austral Volcanic Zones (NVZ, CVZ, SVZ, and AVZ, respectively) of the Andes defined by Thorpe and Francis [9] (modified from [10]). b) Location map of the CVZ (modified from [10]) showing the central active polygenetic volcanoes [11]. c) Map of northern Chile showing the major morpho-tectonic units of the Central Andes (modified from [12]).

prominent active polygenetic volcanoes in Chile such as Parinacota [13], Guallatiri [14], Aucanquilcha [15], Ollagüe [16], Lascar [17], Socompa [18], Lastarria [19], and Ojos del Salado [20] have received priority of research over monogenetic volcanoes (**Figure 1**). Monogenetic volcanism studies in northern Chile have rarely been mentioned, such as Chao dome [21], Tilocálar volcanoes [22], Juan de la Vega maar [23], Corral de Coquena maar [24], SC2 scoria cone [25], or Tinto dome [26]. Monogenetic volcanoes usually have been studied indirectly through i) regional geologic mapping from the Chilean Geological Service (Sernageomin); ii) only previously reported as disaggregated or preliminary data (conference papers and undergraduate thesis); iii) or by researches of a large magmatic system (such as polygenetic volcanoes or calderas) mainly associated to petrological knowledge, leaving aside the mechanisms that control eruptive styles (volcanological sense) [27, 28]. Nevertheless, recently, several monogenetic volcanoes have been studied such as Cerro Chascón dome [29], Cerro Overo maar [30], La Poruña scoria cone [31], Chanka, Chac-Inca, and Pabellón domes [32], El País lava flow field [33], Tilocálar monogenetic field [34], Cerro Tujle maar [35], and many others preliminary data reports, which have increased our understanding of the monogenetic volcanism in this part of the Central Andes and provided tools to estimate possible scenarios of future eruptions that could affect the communities of the Altiplano.

In this contribution, an overview of the monogenetic volcanism that overlaps spatially and temporally the spectrum of architectures, range of eruptive styles, lithological features, and different magmatic processes of mafic and felsic monogenetic volcanoes of northern Chile (18°S–28°S) is reported. Previous studies, such as research publications and preliminary data reports, were used to assemble the volcanological, petrological, and geochronological information in the framework of this overview. A total of 907 Miocene-Quaternary monogenetic volcanoes (individual and parasite) have been identified, carefully evaluating their distribution in time and space. New stratigraphic and sedimentology data of all monogenetic volcanic center types are presented, which added to compositional and geochronological data, are used to illustrate a plumbing system model. In addition, a general eruptive model for monogenetic volcanoes in northern Chile is proposed, where external (e.g., magma reservoirs or groundwater available) and internal (e.g., magma ascent rate or interaction en-route to the surface) conditions determine the changes in eruptive style, lithofacies, and magmatic processes involved in the formation of monogenetic volcanoes. The methods used and databases generated in this contribution are available in the supplementary material.

2. Geological background

The CVZ is located between 14°S (Quimsachata, Peru) and 28°S (Ojos del Salado, Chile) of the Andean Cordillera, including southern Peru, northern Chile, southwestern Bolivia, and northwestern Argentina (**Figure 1a** and **b**). This volcanic zone is a highly elevated region, reaching a width of 350–400 km at much of it over 4000 m a.s.l., constituting the Western Cordillera and Altiplano-Puna physiographic provinces (**Figure 1c**). It is the second-highest altitude plateau in the world in size (after Tibetan Plateau of Central Asia) [36] built on a thickened continental crust that attains a maximum thickness of ~70 km [37]. The crustal thickening and high elevation of the CVZ are related to the crustal shortening [38], sub-crustal magmatism [39], delamination of eclogitic lower crust and lithosphere [40], and climatically controlled low erosion rates with limited sedimentation on the subduction trench [41]. In addition, this crustal thickness is the reason for the magma composition features that characterize the rocks that make up the CVZ as residual garnet during differentiation, crustal contamination,

melting-assimilation-storage-homogenization (MASH), and assimilation by depletion of heavy rare earth elements (HREE) in volcanic rocks [28].

The magmatic activity of the CVZ has been continuous from the Upper Oligocene to the present day [42]. The basement is mainly comprised by i) Paleozoic, Mesozoic, and Miocene-Oligocene continental volcanic and sedimentary rocks; ii) Paleozoic and Mesozoic marine sedimentary rocks; iii) Precambrian and Paleozoic metamorphic rocks; and iv) Paleozoic, Mesozoic, and Paleocene intrusive rocks ([43] and references therein).

The Central Andes is known as the home of “andesitic” magmatism [36]; nevertheless, lava and pyroclastic rocks of dacitic, rhyolitic, and occasionally basaltic andesite and basaltic composition volcanic rocks also occur in the CVZ, building calderas, extensive ignimbrite sequences, stratovolcanoes and monogenetic volcanoes [44].

3. Volcano-tectonic implications: the relationship between vent locations and the structural elements

In this study, 907 monogenetic volcanic centers were identified in northern Chile (Figure 2). Among which, 306 centers correspond to parasitic monogenetic volcanoes associated with polygenetic volcanoes (Figure 2a), which are at the flank of stratovolcanoes linked to crustal/edifice magma storage [45], and 601 centers correspond to individual monogenetic volcanoes (Figure 2a). The monogenetic centers

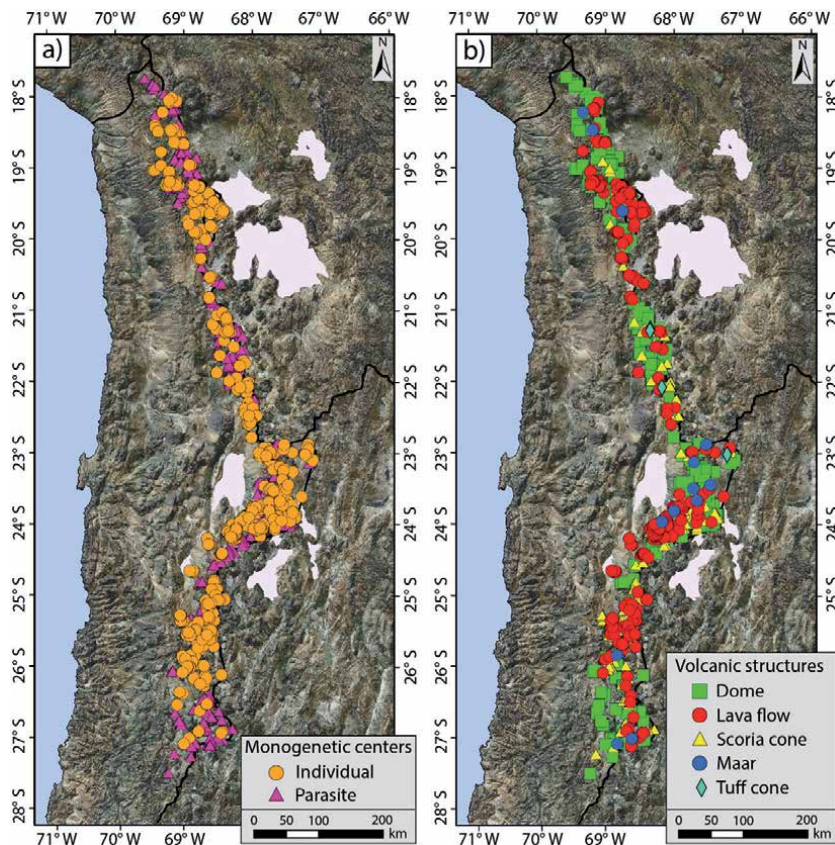


Figure 2. Distribution of monogenetic volcanoes across northern Chile based on a) their relationship with polygenetic volcanoes and b) their volcanic landform.

show a variety of volcanic structures such as domes (35.1%), lava flows (33.4%), scoria cones (29.6%), maars (1.5%), and tuff cones (0.4%) (**Figure 2b**). These centers can be found as isolated centers (e.g., Cerro Punta Negra), clusters (e.g., Purico-Chaskón complex), or forming small volcanic fields (e.g., Negros de Aras).

Using the location of the total number of the monogenetic volcanoes (i.e. 905), the average nearest neighbor analysis can be used to differentiate the distribution of each kind of monogenetic landforms (e.g., [3, 46]). The average nearest neighbor analysis shows R-statistic values of 0.71 for all monogenetic volcanoes of northern Chile, 0.74 for domes, 0.69 for scoria cones, and 0.62 for lava flows (**Table 1**). These value ranges are identified as a clustered distribution of volcanic centers [46]. For maars and tuff cones, the average nearest neighbor analysis was not obtained due to the small number of centers identified (18 monogenetic centers that are 1.9% of the total) to generate a statistically significant result.

On the other hand, using the total number of monogenetic volcanoes (i.e. 907) and the area in which the monogenetic volcanoes are distributed in northern Chile (46,610 km²), the area that envelopes all the monogenetic volcanic centers identified is of 1.95×10^{-2} centers/km². The temporal distribution is characterized by a decrease in eruptive centers from Miocene (268 monogenetic centers) to Pliocene (258 monogenetic centers), and a later increase in the Pleistocene (363 monogenetic centers) (**Figure 3**). Domes and scoria cones abundance show the same trend mentioned before, whereas lava flows, maars, and tuff cones display a trend to increase from Miocene to Pleistocene (**Figure 3**). The activity during the Holocene (18 monogenetic centers) is mainly dominated by dome eruptions (**Figure 3**).

The temporal evolution of the monogenetic volcanoes from older to younger shows a migration from south to north with a concentration in the central part of northern Chile (cluster 3: Antofagasta Central). Based on the kernel density map, the monogenetic volcanoes of northern Chile may be mainly grouped into five regional clusters (**Figure 4a**). These distributions of volcanic centers display a high density of features and a preferred elongation trending. Monogenetic centers are alienated NW-SE preferentially for clusters 1 and 2, N-S, NW-SE, and NE-SW for cluster 3, NE-SW for cluster 4, and WNW-ESE and NW-SE for cluster 5 (**Figure 4a**). The volcanic structures distribution across the northern Chile map (**Figure 4b**) exhibits that scoria cones and domes are mainly associated with NNW-SSE, NW-SE, and WSW-ENE tectonic structures and lineaments, in decreasing order of frequency. Lava flows are mainly aligned N-S and NW-SE, while maars and tuff cones occur mainly along N-S, NW-SE, and WSW-ENE trending tectonic structures and lineaments, in decreasing order of frequency. The distribution of magma paths suggests that for Miocene, the main direction of the shortening of structures at the upper crust should have been about E-W, WNW-ESE, and NNW-SSE [47]. This is consistent with the development of N-S and NNE-SSW reverse faults and folds reported for cluster 2 (Antofagasta Norte; **Figure 4a**), cluster 3 (Antofagasta Central; **Figure 4a**) and cluster 4 (Antofagasta Sur; **Figure 4a**), and WSW-ENE structures for cluster 5

Feature	Ro (km)	Re (km)	R-statistic	ZR	Pattern
All monogenetic structures	2.56	3.61	0.71	-16.63	Clustered
Domes	4.51	6.05	0.74	-8.71	Clustered
Lava flows	3.85	6.2	0.62	-12.62	Clustered
Scoria cones	4.57	6.45	0.69	-9.48	Clustered

Ro: Observed Mean Distance; Re: Expected Mean Distance; R-statistic: Nearest Neighbor Ratio; ZR: Z-score.

Table 1.
 Results for the average nearest neighbor in northern Chile.

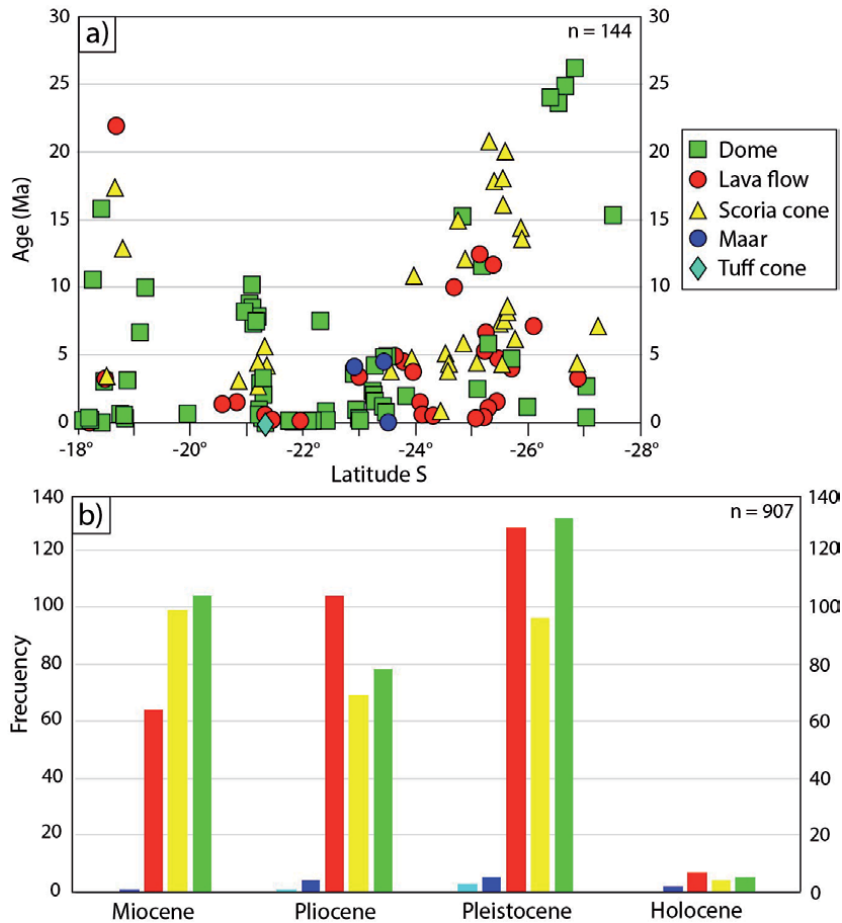


Figure 3. a) Temporal distribution of monogenetic volcanic landforms across northern Chile. b) Histogram of the temporal distribution of monogenetic volcanic landforms during Miocene, Pliocene, Pleistocene, and Holocene.

(Atacama; **Figure 4a**) in previous studies [48]. During the Pliocene to Holocene, the main direction of shortening inferred to have been E-W, NE–SW, WNW–ESE, and NNW–SSE direction of contraction, in decreasing order of frequency. This is consistent with the N-S and NW-striking normal faults, NE-striking reverse faulting, NW-SE, and WSW–ENE strike-slip faults reported in previous studies [20, 48].

The spatial–temporal correlation of monogenetic centers, combined with the tectonic structures within northern Chile, allows the identification of three different structural styles of monogenetic volcanoes (Figure A.1), as has been suggested by Le Corvec et al. [2] for monogenetic volcanism and by Tibaldi et al. [49] for the CVZ. The first case (Figure A.1a) corresponds to a compressional environment mainly characterized by N-S and NNE–SSW reverse faults and folds over the monogenetic feeding conduits. Nevertheless, in this case, the magmatic plumbing system has been associated with the development of normal or strike-slip faults allowing the ascent of magmas to the surface such as the Tilocálar complex [22] at the south of the Salar de Atacama basin into the cluster 3 (Antofagasta Central; **Figure 4**). The second scenario (Figure A.1b) is mainly characterized by N-S and NW-SE, striking normal faults into an extensional environment. This case has been reported to scoria cones, lava flows, and mainly domes into the Ollagüe region and San Pedro-Linzor volcanic chain area [16, 50], which correspond to cluster 2 (Antofagasta Norte; **Figure 4**). The last scenario (Figure A.1c) corresponds to a strike-slip environment mainly

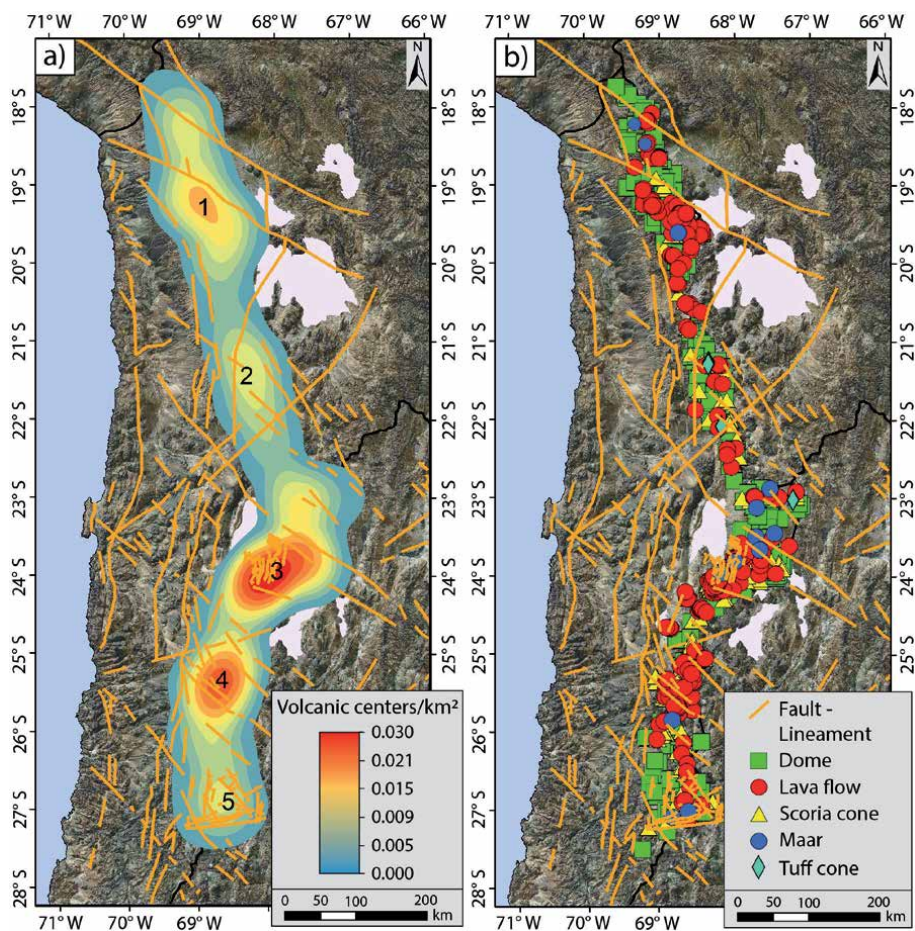


Figure 4.
 a) Kernel density map for monogenetic volcanoes and the main clusters identified. The numbers represent the main regions: 1. Arica-Iquique, 2. Antofagasta Norte, 3. Antofagasta Central, 4. Antofagasta Sur, and 5. Atacama. b) Map of the major fault systems and lineaments across northern Chile.

characterized by NW-SE left lateral and WSW-ENE strike-slip faults. Monogenetic volcanism associated with this scenario has been mainly reported by Tibaldi et al. [49] for cluster 3 (Antofagasta Central; **Figure 4**), Baker et al. [20], and González-Ferrán et al. [51] for cluster 5 (Atacama; **Figure 4**). These scenarios have also been reported in others areas of monogenetic volcanism in the CVZ of the Andes such as the Uyuni region by Tibaldi et al. [50], Antofagasta de la Sierra Basin by Báez et al. [52], or in the southern Puna Plateau by Haag et al. [3]. These interpretations were developed based on the distribution and alignment of the monogenetic centers. Therefore, it is essential to consider that the tectonic structures have been formed before of the magma intrusion that originated monogenetic centers. In this context, the emplacement of these volcanic centers was favored by these tectonic structures.

4. The spectrum of architecture and lithofacies of volcanic structures: internal versus external-factor implications

In this study, 318 domes, 303 lava flows, 268 scoria cones, 14 maars, and 4 tuff cones have been identified. This identification is primarily based on the morphological aspects of the volcanic edifices, which is characterized by the dominant

eruption style and number or combination of eruption phases following Bishop [53] and Walker [54] (Figures 1 and 2).

Scoria cones (Figure 5a) are mainly characterized by circular to elliptical shape in plan-view, showing different landforms as ideal (e.g., La Poruña), gully, horseshoe, tilted, amorphous or crater row that in some cases display lava flows associated (e.g., Negros de Aras volcanic field). These lava flows (Figure 5b) are mainly characterized by ‘a‘ā flow structures associated with early (e.g., Del Inca) or late-stage (e.g., Ajata) eruptions with channel, ogive, levee, lobe, and breakout lobe structures.

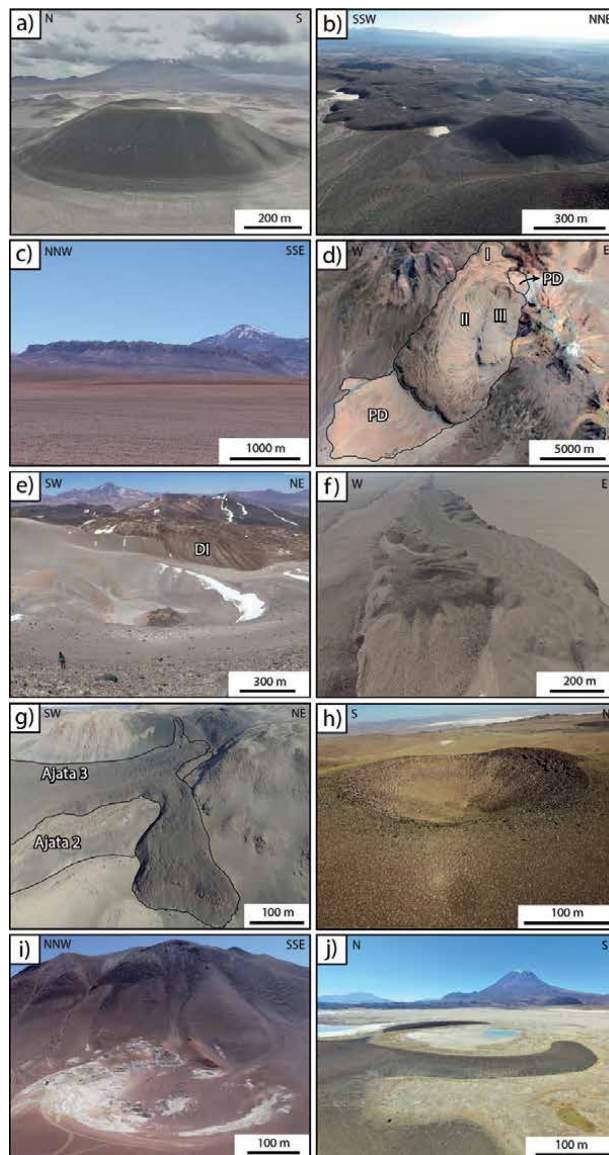


Figure 5. Volcano types from northern Chile. a) Poruñita scoria cone (Ollagüe stratovolcano in the background). b) Scoria cone and lava flows from Negros de Aras monogenetic volcanic field. c) La Torta de Tócorpuri dome. d) Chao dome with its pyroclastic deposit (PD) and lava dome stages (I, II, and III) (Google earth™ image). e) La Espinilla maar-dome and Del Indio dome (DI). f) Tilocálar Norte lava flow. g) Ajata lava flows. h) Cerro Tujle maar. i) Alitar maar; fumaroles occur in white areas (Alitar stratovolcano in the background). j) Luna de Tierra tuff cone (Ollagüe stratovolcano in the background).

Domes (Figure 5c) of northern Chile are characterized by a pile up of lava in large thicknesses over their vents. They are often referred to as *tortas* (pies or pancakes) (e.g., La Torta de Tocorpuri), controlled by the slope angle of the pre-eruptive surface, viscosity, effusion rate, phenocryst contents, and in some cases, related to early pyroclastic density currents (e.g., Chao). Overall, domes (**Figure 5d**) show coulee (e.g., Chao), lobate (e.g., Chascón), platy (e.g., Pabellón-Apacheta), and axisymmetric (e.g., Chillahuita) landform structures. Few domes (**Figure 5e**) in northern Chile occur within craters (e.g., La Espinilla).

Lava flows (Figure 5f) are mainly characterized by a jumble of irregular and coherent block of lava (up to meters), across with smooth, planar, and angular surfaces. They can be classified as ‘a’ā (e.g., El Negrillar) and blocky (e.g., Tilocálar Norte) lavas, and may display a simple (e.g., Ajata) or compound (e.g., Tilocálar Sur) landform with several features as a channel, ogive, levee, lobe, and breakout lobe structures (**Figure 5g**).

Maars (Figure 5h) show a characteristic landform characterized by a preserved crater that cut into the pre-eruptive landscape (e.g., Tujle). The crater cavities reach from 30 m to 200 m deep; they are partially sediment filled with a crater diameter from 300 m to 3 km. Sulfur deposits (e.g., Juan de la Vega maar), fumaroles (e.g., Alitar maar), and domes (e.g., La Espinilla) are present in maar volcanoes associated with events that appear late of the maar eruptions (**Figure 5e–i**).

Tuff cones (Figure 5j) in northern Chile display a horseshoe landform, a wider crater relative to basal diameter than the scoria cones, exhibiting a crater rim from a flat surface up to 10 m dominated by salt deposits. They are mainly associated with salt plains or *salares* (e.g. Luna de Tierra).

The monogenetic volcanic centers (mafic and felsic volcanism) are characterized by the heterogeneity of volcanic products, which can be mainly classified into eight lithofacies based on field observation, componentry and sedimentological characteristics such as:

1. **Bombs and lapilli beds (BL)**: This lithofacies is mainly found both at the base and the summit of scoria cones. It is poorly sorted, reversed graded to massive and mostly clast-supported, and consists of poorly to non-agglutinated juvenile clasts (**Figure 6a and b**). BL lithofacies is interpreted as the result of Strombolian eruptions.
2. **Lapilli and ash beds (LA)**: This lithofacies is mainly located at the base of scoria cones. It is well sorted, normal or reversed graded to massive, with parallel or cross-lamination, and mostly clast-supported with non-agglutinated juvenile clasts (**Figure 6c**). This lithofacies is interpreted as the result of hydromagmatic eruptions.
3. **Agglutinated to spatter bomb and lapilli beds (AS)**: This lithofacies is mainly found at the summit of scoria cones or pyroclastic deposits. It comprises a brittle core and fluid rim to completely fluid clasts (spatter) that agglutinate moderately forming beds (up to 5 m thick) (**Figure 6d**). LA lithofacies is interpreted as the result of Hawaiian to transitional eruptions.
4. **Welded scoria to clastogenic lavas (CL)**: This lithofacies is mainly located at the summit of scoria cones and pyroclastic deposits. It is formed by scoria of lapilli and bombs size fragments highly welded (coalesced), forming dense agglutinate layers (clastogenic lava) (**Figure 6e**). CL lithofacies is interpreted as the result of Hawaiian to transitional eruptions.

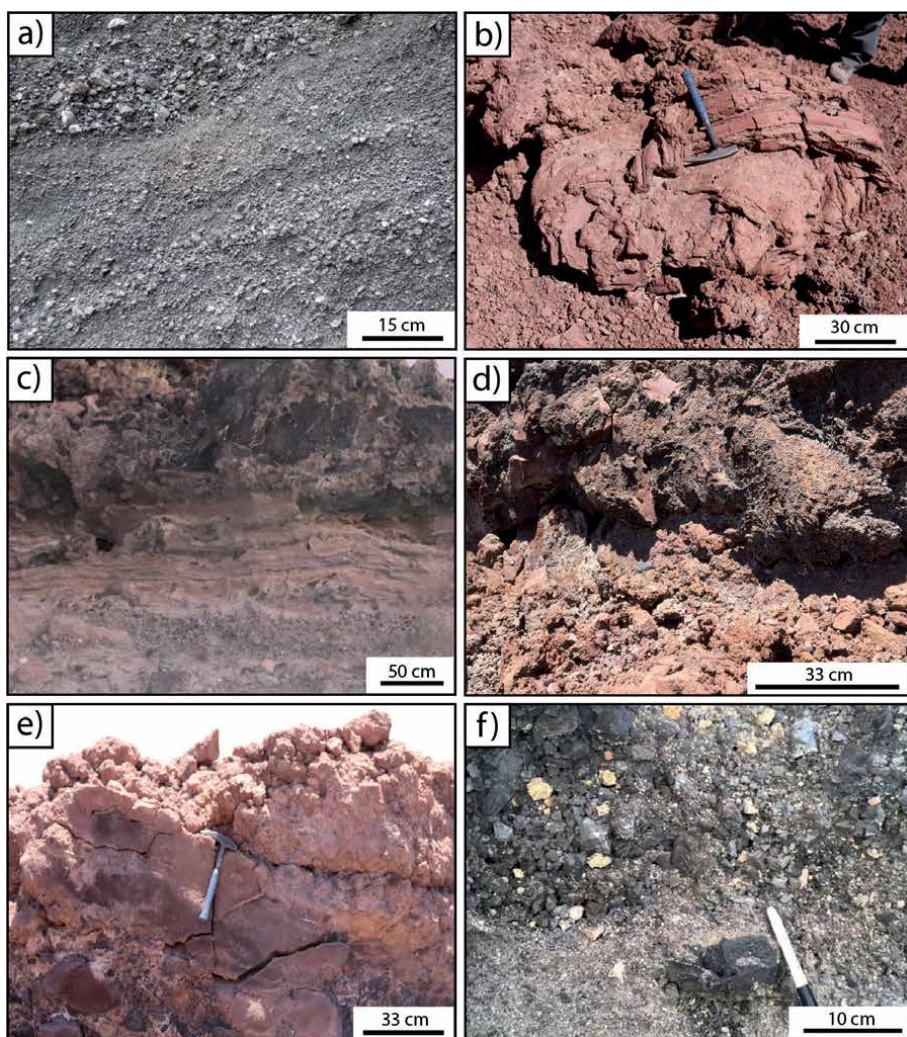


Figure 6. Field photographs of lithofacies of the monogenetic volcanoes in northern Chile. a) Lithofacies BL from Poruñita scoria cone. b) Lithofacies BL from La Poruñia scoria cone. c) Lithofacies LA from Negros de Aras scoria cones. d) Lithofacies AS from Ajata scoria cone. e) Lithofacies CL from Tilocálar Sur pyroclastic deposit. f) Lithofacies LAL from Cerro Overo maar.

5. *Lapilli and ash beds with lithic fragments (LAL)*: This lithofacies is mainly found both at the base and the summit of scoria cones and pyroclastic deposits. It is moderately sorted, normal or reversed graded to massive and mostly clast-supported deposits with abundant lithic fragments (>20%) locally moderate to no agglutination/welding (**Figures 6f** and **7a**). LAL lithofacies is interpreted as the result of hydromagmatic eruptions.
6. *Peperite (P)*: This lithofacies is located at the base of scoria cones and pyroclastic deposits, overlying the pre-eruptive surface. It is mainly a mingling of juvenile material and unconsolidated host sediment (**Figure 7b**). P lithofacies is interpreted as the result of magma-wet sediment/shallow water eruptions.
7. *Lava flow (LF)*: This lithofacies is found at the flank and ring plain of strato-volcanoes, both at the base and at the summit of scoria cones (from *boccas*) (**Figure 7c** and **d**), at the crater of other volcanic edifices (polygenetic or

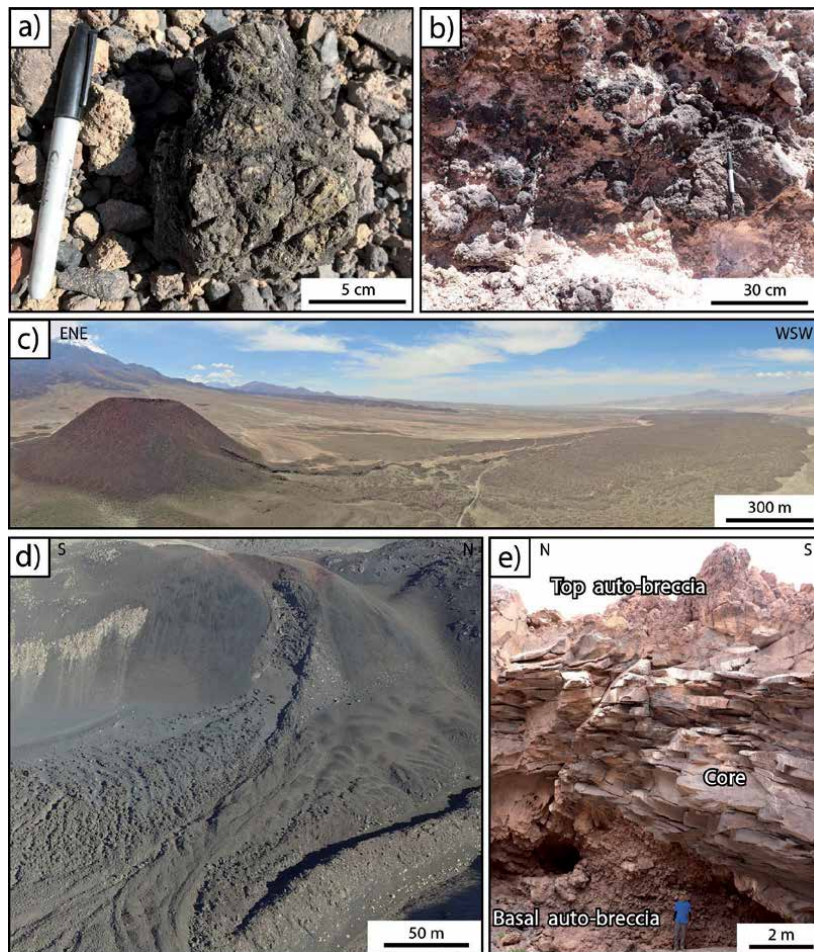


Figure 7. Field photographs of lithofacies of the monogenetic volcanoes in northern Chile. *a)* Lithofacies LAL showing a juvenile fragment with cauliflower-shaped from Cerro Overo maar. *b)* Lithofacies P showing a mingling of juvenile material and unconsolidated host sediment from Tilocálar Sur pyroclastic deposit. *c)* La Poruña lava flow and scoria cone. *d)* Lithofacies LD showing the boccas of the Ajata scoria cone with levee structures of the Ajata 3 lava flow. *e)* Lithofacies LD showing the primary three principal levels of this lithofacies (top auto-breccia, core, and basal auto-breccia) from El País lava flow field.

monogenetic), and as an isolated vent. Lava flow lithofacies is characterized by three primary vertical levels (**Figures 7e** and **8a–e**). This lithofacies flowed, reaching length up to 11 km and piling up from low to large thicknesses (< 1 m – 400 m), and based on their morphology, it can be classified as lava flows or domes. LF lithofacies is mainly interpreted as the result of Strombolian eruptions.

8. *Raft blocks* (RB): This lithofacies corresponds to mounds or blocks of agglutinate to welded pyroclasts located on top of lava flows and associated with scoria cones (**Figure 8f** and **g**). The individual blocks are the result of the cone rafting (RB lithofacie), which initially were the product of Strombolian style eruptions.

The spectrum of architecture and lithofacies of volcanic structures involve several interactions between internal and external processes. It is affected by the continuous degassing and interactions of the magma with the environment at different levels en-route during its ascent from the source to the surface, resulting in a volcanic eruption that can be explosive or effusive [55]. In many cases,

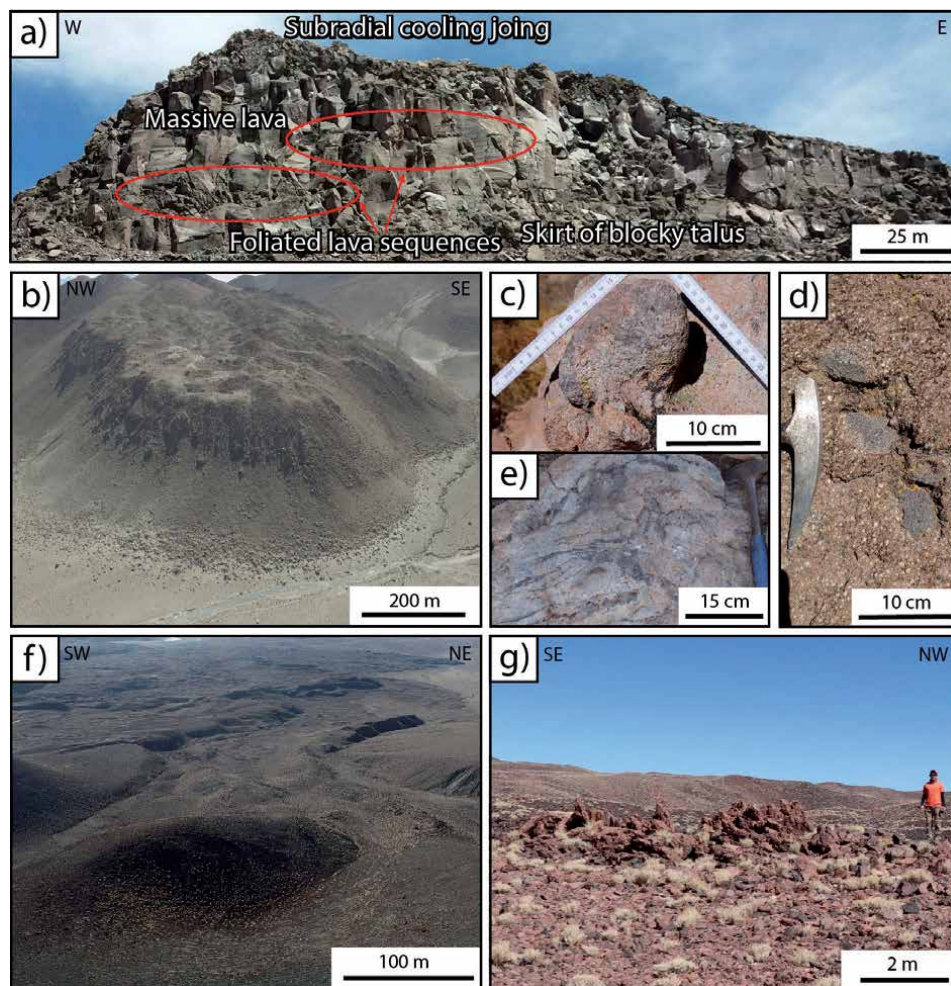


Figure 8.

Field photographs of lithofacies of the monogenetic volcanoes in northern Chile. a) South dome (Guallatiri volcano area) showing the three primary levels of this lithofacies. Red areas indicate foliated lava sequences that are described in Watts et al. [26] in refs therein. b) El Ingenio (also called La Celosa) felsic dome (Ollagüe volcano area) exhibiting a torta type morphology. c-d) mafic enclaves from El Ingenio dome and south dome, respectively. e) Flow structures of El Mani dome. f) Scoria cone from Negros de Aras showing a horseshoe morphology associated with lava flow and with agglutinated material deposited on the summit crater. g) Lithofacies RB of unconsolidated and agglutinated pyroclastic material located at the distal part of the lava flow of Figure 8f from Negros de Aras.

the outcrops of monogenetic volcanic centers are covered by some debris flank due to desert physical weathering and mass movements or covered by eolian deposits. Nevertheless, integrating the different lithofacies identified and the cross-sections from different edifices are possible to build the history of the eruptive style involved in the formation of the monogenetic volcanoes of northern Chile.

In general, scoria cones are composed of the lithofacies that indicate a rapid and continuous evolution from the Strombolian eruption style (lithofacies BL) to Hawaiian and Transitional styles (lithofacies AS and CL). This transition is characterized from the base to the upper levels by poorly sorted, reversed graded to massive and mostly clast-supported deposits, which consist of poorly to non-agglutinated juvenile clasts, to the summit by clastogenic lavas and welded agglutinated bomb (e.g., Ajata, La Poruña, Del Inca, Negros de Aras scoria cones). In addition, magmatic effusive stages are associated with the lithofacies LF (lava flow)

and RB (raft blocks). They are represented by lava flows at the base or the summit of the scoria cones (e.g., Ajata, La Poruña, Del Inca, Negros de Aras scoria cones), and mounts from the volcanic edifice of scoria cones at the lava flows (e.g., Negros de Aras), respectively. That means scoria cones show a range of magmatic activity from explosive to effusive styles (**Figure 9**).

Nevertheless, in some cases (e.g., Negros de Aras scoria cones), hydrovolcanic records may be identified either at the summit or at the bases of the scoria cones (**Figure 9**). This corresponds to the lithofacies LAL (lapilli and ash beds with lithic fragments) and LA (Lapilli and ash beds), which suggest magma-water interactions during the initial (e.g., Poruña scoria cone) or later phases (e.g., Negros de Aras scoria cones), where shallow water levels are available. This characteristic is also recognized at the base in some pyroclastic deposits (e.g., Tilocálar Sur), where fluidal and jigsaw-fit textures are locally preserved (lithofacies P) (**Figure 7b**).

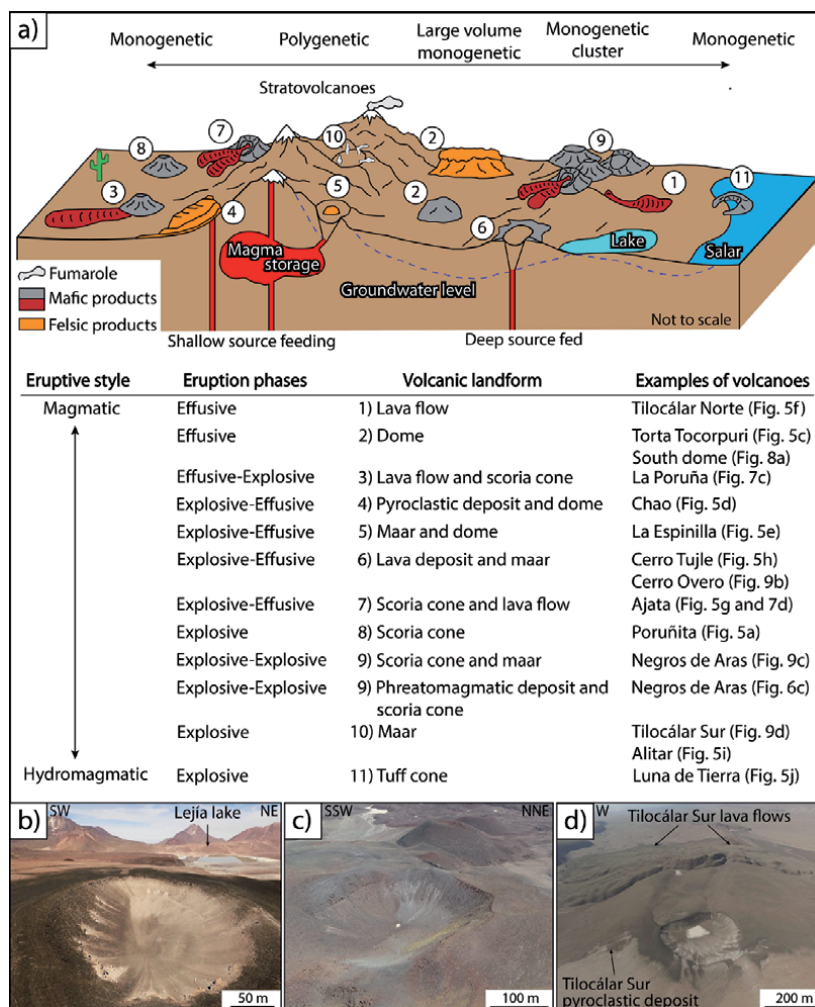


Figure 9. a) Schematic drawing of monogenetic volcanic landforms of northern Chile, showing the conceptual link between monogenetic and polygenetic volcanoes and their relationship with their environmental setting. The numbers indicate the volcanic landforms detailed in the diagram of the theoretical link/transition between eruptive styles, eruption phases, and volcanic landforms for monogenetic volcanoes of northern Chile. Examples of Chilean volcanoes in each case. b) Cerro Overo maar. c) Scoria cone from Negros de Aras with a crater associated with a phreatomagmatic eruptive phase. d) Tilocálar Sur maar.

On the other hand, lava flows and lava domes are characterized by the lithofacies LF (lava flow), suggesting a magmatic effusive nature with different morphological features (**Figure 9**). The main differences between lava flows (e.g., El País lava flow field; **Figure 7e**) and lava domes (e.g., Tinto dome; **Figure 8a**) are the changes in the viscosity, volatile content, and magma ascent rate [55]. These features control the magma degassing during their ascent from the source to the surface, and therefore, the fragmentation processes [56]. Despite these differences, deposits that are inferred to represent explosive phases have been found at the base of the lava domes (e.g., Chao dome), which corresponds to the initial stages of pyroclastic deposits characterized by bombs and lapilli beds (lithofacies BL).

Maars (e.g., Cerro Overo) and tuff cones (e.g., Luna de Tierra) are characterized by LAL (lapilli and ash beds with lithic fragments) and LA (Lapilli and ash beds) lithofacies, which are associated with hydromagmatic eruptions, suggesting magma-water interactions. These phreatomagmatic and Surtseyan eruptions may be associated with external factors that trigger the magma-water interaction at different degrees of ratio and different depths of magma-water interaction [57]. The maars are mainly associated with areas characterized by i) folded ignimbrite basement (e.g., Tilomonte ridge for Tilocálar Sur maar, Cerro Tujle ridge for Cerro Tujle maar or Altos del Toro Blanco ridge for Cerro Overo maar), ii) groundwater aquifers (e.g., Monturaqui-Tilopozo-Negrillar aquifer for Tilocálar Sur maar), and iii) salt flats or lagoons as discharge zones (e.g., Salar de Atacama for Cerro Tujle maar or Laguna Lejía for Cerro Overo maar) (**Figure 9**). In contrast, tuff cones are located at low topographic positions filled with poorly consolidated sediments as salt flats (e.g., Salar de Carcote for Luna de Tierra) or caldera basins (e.g., La Pacana caldera for Corral de Coquena), where the resulting tephra came from phreatomagmatic eruptions through shallow surface water [58] (**Figure 9**).

Overall, the architecture spectrum and the volcanic lithofacies of the monogenetic centers of northern Chile (**Figure 9**) are similar to those reported for the northern Puna region (Argentina) by Maro and Caffè [59] and Maro et al. [60]. This suggests a wide range of eruptive styles involved in the eruption history of this small-volume volcanism, and in some cases, large volume as well. Nevertheless, in northern Chile, this range of eruptive styles is characterized by effusive (e.g., Ajata lava flows or Tinto dome) and/or explosive magmatic (e.g., Tilocálar Sur or Chao dome) activities dominated by Strombolian to Hawaiian/Transitional styles (e.g., La Poruña scoria cone), and hydromagmatic activities, as phreatomagmatic (e.g., Cerro Overo maar) or Surtseyan (e.g., Luna de Tierra tuff cone) styles, which were often simultaneous or alternating during the growth of the monogenetic volcanoes in northern Chile (**Figure 9**).

5. Magmatic processes: textural and petrological evidence

Petrographically, products from scoria cones, lava flows, maars, and tuff cones comprise mainly aphyric rocks (e.g., SC2). On the other hand, domes can be variable from aphyric (e.g., La Albondiga) to porphyritic rocks, which in some cases show mafic enclaves (e.g., Tinto dome). Overall, samples are characterized by hypocrySTALLINE, hypidiomorphic, and hyalopilitic textures, where aphyric rocks show 40–50% vol. microphenocryst and microlite content, whereas porphyritic rocks exhibit 20–50% vol. phenocryst. The main mineral assemblage corresponds to euhedral to subhedral clinopyroxene (15% vol.; max 1.15 mm) and plagioclase (25–40% vol.; max 7 mm) with subordinated olivine (5% vol.; max 0.9 mm) and Fe–Ti oxide phases (1% vol.; max 0.2 mm). Nevertheless, in some cases, orthopyroxene (3% vol.; max 0.4 mm) and hydrous minerals, such as amphibole (**Figure 10a**),

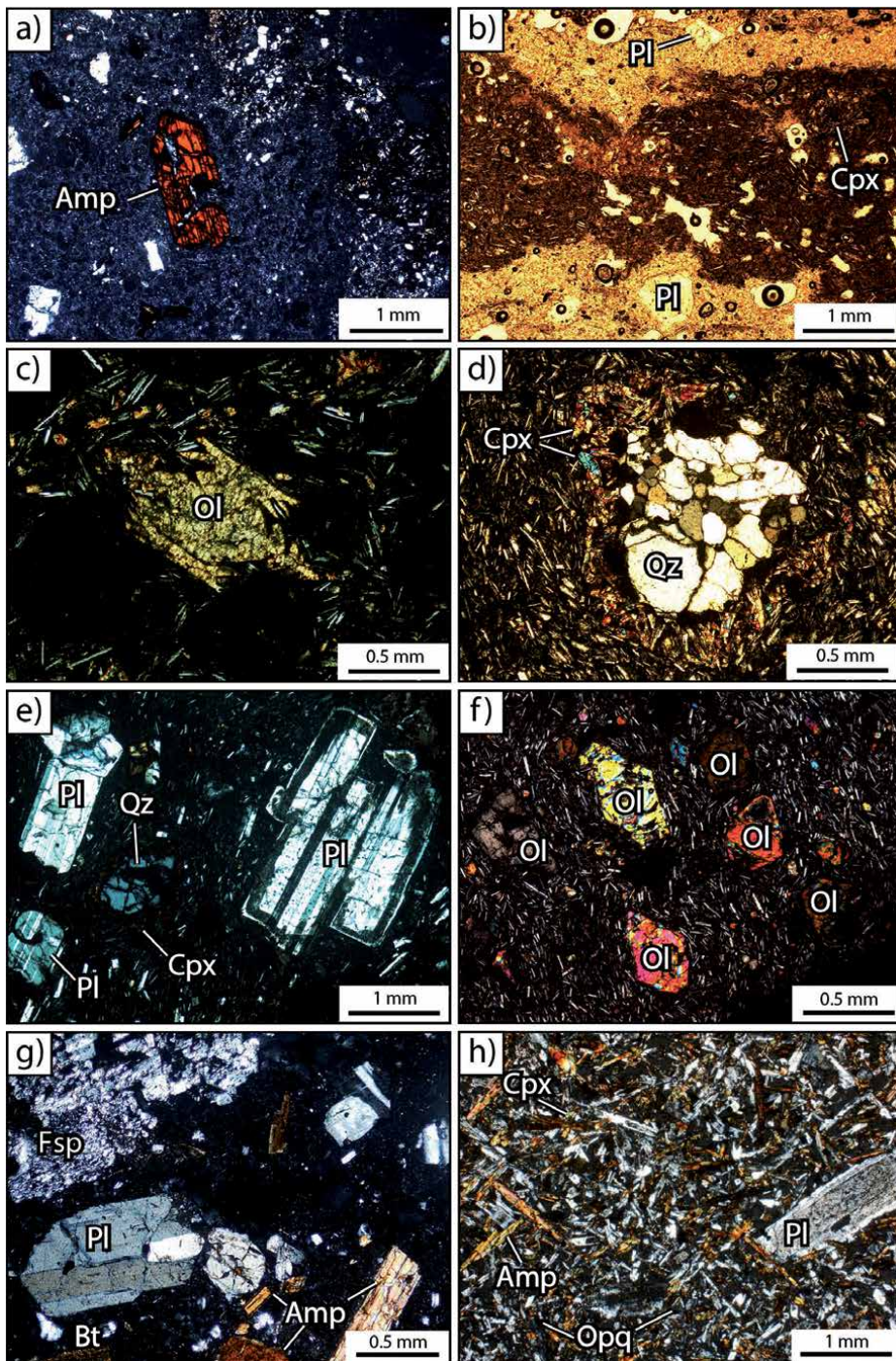


Figure 10. Photomicrographs and micro-vesiculated photos are showing typical petrographic textures of monogenetic volcanoes products from northern Chile. Thin sections under cross-polarized- (a, c-h) and plane-parallel- (b) light. a) Amphibole breakdown/reaction rim with skeletal and sieve textures from Cerro Tujle maar. b) Mafic and felsic bands are showing mingling texture from El Maní dome. c) Olivine phenocryst showing skeletal growth from SC2 scoria cone. d) Quartz xenocryst resorbed and rimmed mainly by clinopyroxenes from Tilocálar Sur lava flow. e) Plagioclase with sieve and reabsorption textures and showing zoned rim from Luna de Tierra tuff cone. f) Fluidal texture showing olivines with absorption and skeletal growth textures from Cerro Overo maar. g) Silicic product from El Ingenio dome. h) the diktytaxitic-like texture of the groundmass of the enclave from El Ingenio dome. Mineral abbreviations are amphibole (amp), plagioclase (Pl), Clinopyroxene (Cpx), olivine (Ol), quartz (Qz), K-feldspar (Fsp), Biotite (Bt), opaque mineral (Opq).

biotite, or sideromelane (10% vol; max 5 mm) can also be found. The main textures correspond to fluidal, reabsorption, and disequilibrium textures, such as mingling (**Figure 10b**), skeletal (**Figure 10c**), and resorbed edges rimmed by a network of clinopyroxenes (**Figure 10d**), sieve texture, and zoned rims (**Figure 10e**). The groundmass (50–80% vol.) is glassy with a microlites of plagioclase > clinopyroxene > olivine > amphibole/biotite > orthopyroxene, and opaque phases, where tabular-shaped microlites display flow structures (**Figure 10f**). In general, the mafic inclusions commonly are fine-grained and microvesiculated and range from 2 to 20 cm in size (**Figure 10g**). They exhibit crystal assemblages of plagioclase, pyroxene, amphibole, biotite, olivine, and quartz. The groundmass shows mainly plagioclase > pyroxene > amphibole and rare biotite and Fe-Ti oxides, with acicular phases and diktytaxitic texture (vesicles with plagioclase around cavity; **Figure 10h**).

In general, products of monogenetic centers in northern Chile contain two or three plagioclase populations. The first one is characterized by defined edges and no resorption features (**Figure 10e**). The second population of plagioclase show inner zones with sieve texture overgrown by euhedral rims of plagioclase, and plagioclase that is thoroughly sieved (**Figure 10e**). The last population of plagioclase exhibits oscillatory zoning and, in some cases, coarse-sieve texture and smooth edges. The mineral assemblage consists of plagioclase, olivine, orthopyroxene, and clinopyroxene, in order of decreasing abundances, with amphibole and opaque mineral (e.g., magnetite and ilmenite) as minor phases for mafic products, and plagioclase, amphibole, biotite, quartz, K-feldspar, pyroxene, titanite and opaque mineral (e.g., magnetite and ilmenite), in order of decreasing abundances, with apatite and zircon as accessory phases for felsic products. For mafic products, olivines are present in samples showing reabsorption features characterized by different types of skeletal crystal morphologies (**Figure 10f**). Pyroxene is commonly recognized as individual crystal, and as reaction rims on olivine crystals or glomerocrystals. Quartz xenocrysts are also identified and are resorbed and rimmed by a network of mafic microlites (e.g., clinopyroxene) (**Figure 10d**). For felsic products, quartz crystals have rounded edges; amphibole and biotite show euhedral to subhedral habits affected by the intense breakdown (**Figure 10g**). Overall, the groundmass is very finely crystalline, with microlites of plagioclase, ortho- and clinopyroxene, olivine, amphibole, and opaque minerals with interstitial glass (**Figure 10**).

These characteristics correspond to disequilibrium textures, giving evidence of magma mixing, heating of the reservoirs where the crystals are located or assimilation of crustal rocks, fast ascent, cooling, and decompression (e.g. [61]). The mixing processes correspond to mechanical mixing processes or mingling [62], which occur when mafic magma had insufficient interaction time with the felsic magma to generate a chemical mixing [62]. This process occurs at around 0.1–10 km depth [63], developed in different degrees, being evidenced by mafic enclaves (e.g., Tinto dome) and alternating mafic and felsic bands (e.g., El Maní dome) with flow structures [64]. Assimilation and fractional crystallization can be interpreted by the role of amphibole fractionation and plagioclase crystallization, respectively [32]. Whereas, all rims on amphibole and biotite phenocrysts suggest a fast magma ascent as a consequence of decompression [65].

Geochemically, based on the total alkali-silica diagram (after [66]), mafic monogenetic volcanism in northern Chile range mainly from basaltic andesite to dacitic in composition, which corresponds to scoria cones, lava flows, domes, maars, and tuff cones (**Figure 11a**). On the other hand, felsic products range from dacitic to rhyolitic composition, which corresponds to domes (**Figure 11a**). All the samples have calc-alkaline composition (not shown; after [72]), whilst mafic and felsic samples are mainly in the medium-K and high-K fields, respectively (not shown; after [73]). Based on geochemical compositional variations (Sr/Y, Sm/Yb,

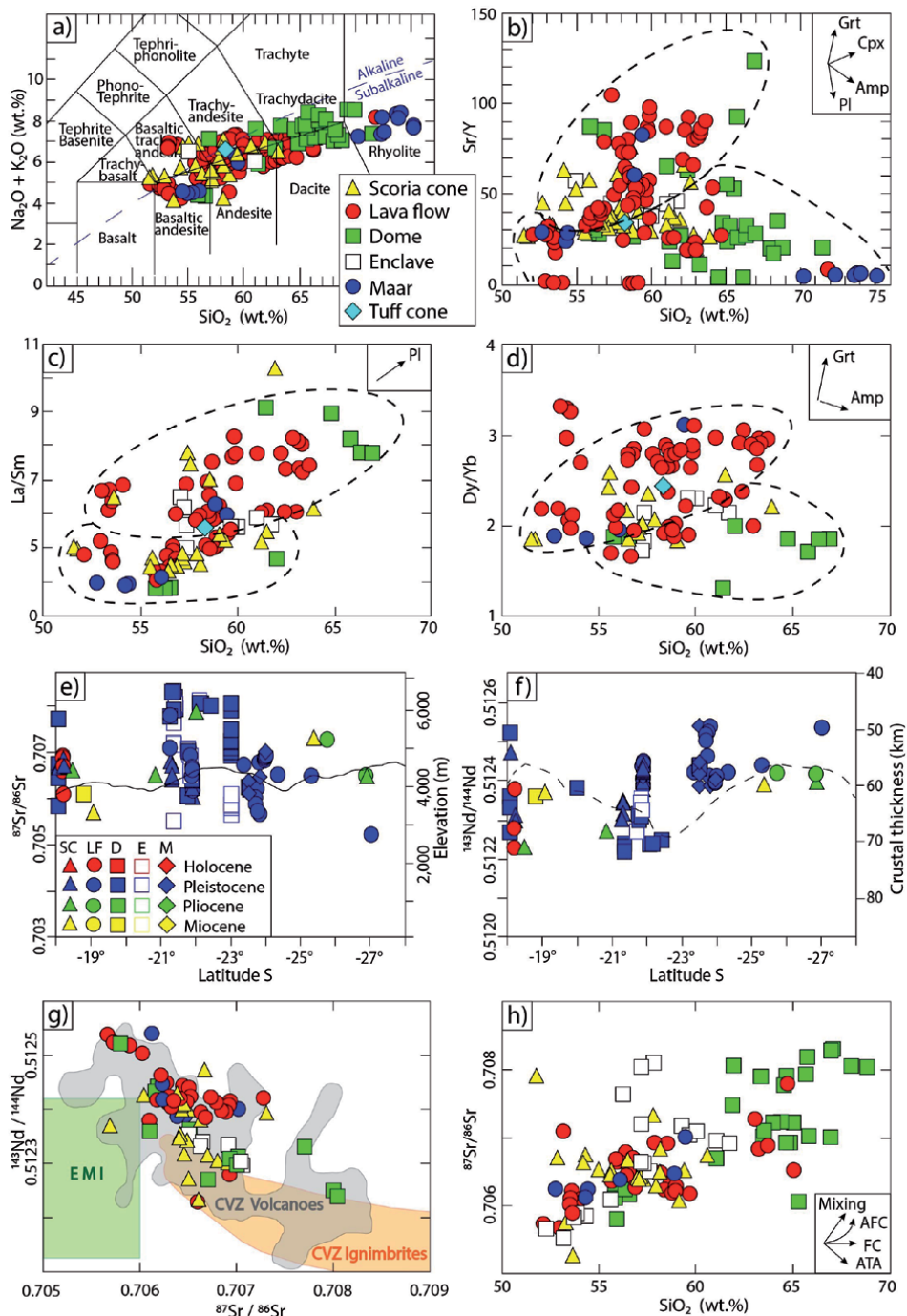


Figure 11.
 a) Total alkalis-silica diagram (after [66]). b) SiO_2 vs. Sr/Y diagram. c) SiO_2 vs. La/Sm diagram. d) SiO_2 vs. Dy/Yb diagram. The segmented lines correspond to the two group areas described in the text. e-f) comparison of whole-rock $^{87}\text{Sr}/^{86}\text{Sr}$ and $^{143}\text{Nd}/^{144}\text{Nd}$ ratios of monogenetic volcanoes with elevation (continuous line) and crustal thickness (dashed line), respectively. Arc front means elevation and crustal thickness profiles taken from Scott et al. [67]. SC: Scoria cone; LF: Lava flow; D: Dome; E: Enclave; M: Maar. g) $^{87}\text{Sr}/^{86}\text{Sr}$ vs. $^{143}\text{Nd}/^{144}\text{Nd}$ diagram; EMI (enriched mantle I) green area from Lucassen et al. [68] and references therein; the gray area from Scott et al. [67] and orange area from Franz et al. [69]. h) $^{87}\text{Sr}/^{86}\text{Sr}$ vs. SiO_2 diagram. Arrows of differentiation trends (with relative mineral contribution) after Mamani et al. [70] and Delacour et al. [71]. Grt: Garnet; Cpx: Clinopyroxene; amp: Amphibole; Pl: Plagioclase; AFC: Assimilation fractional crystallization; FC: Fractional crystallization; ATA: Assimilation during turbulent magma ascent.

Dy/Yb, and La/Sm ratio contents), monogenetic products can be divided into two types (**Figure 11b-d**). A group with high contents of Sr/Y, Sm/Yb, Dy/Yb, and La/Sm ratio shows deep assimilation under high pressures and thick crust assimilation garnet signature [70]. The second group has low Sr/Y, Sm/Yb, Dy/Yb, and La/Sm ratios, and displays shallow assimilation with amphibole and clinopyroxene fractionation [74].

Eruptive products of monogenetic volcanoes of northern Chile show values between 0.705–0.708 for $^{87}\text{Sr}/^{86}\text{Sr}$, and 0.5122–0.5126 for $^{143}\text{Nd}/^{144}\text{Nd}$ (**Figure 11e-g**). These values are higher than expected for magmas derived from the asthenospheric mantle, and relatively restricted compared to isotopic data of stratovolcanoes from the CVZ (**Figure 11e**). Overall, less differentiated products show $^{87}\text{Sr}/^{86}\text{Sr}$ values lower (< 0.707) than more differentiated products (> 0.707) (**Figure 11e,f**). The $^{87}\text{Sr}/^{86}\text{Sr}$ vs. SiO_2 diagram shows that assimilation and fractional crystallization (AFC) occur at different degrees and levels during the magmatic ascent from the source to the surface (**Figure 11h**). Fractional crystallization processes characterize these products, with a low degree of contamination and increasing HREE depletion (e.g., Dy, Yb, or Y), which suggest residual garnet of mantle melting enhanced by lithospheric delamination [75]. Nevertheless, a group of samples of mafic lava flows and scoria cones displays a reverse isotopic behavior of decreasing $^{87}\text{Sr}/^{86}\text{Sr}$ ratio values with the increasing of the SiO_2 (**Figure 11h**). This trend cannot be explicated by mixing processes where is an increase of LILE content compared with HFSE or by AFC processes that expect an enrichment of $^{87}\text{Sr}/^{86}\text{Sr}$ ratio values during the differentiation [76]. In this context, assimilation during turbulent ascent process has been proposed (ATA; [77, 78]). This ATA process generates a selective fusion and assimilation of felsic crust, enriching of LILE (e.g., Sr or Rb; **Figure 11b**) compared with HFSE (e.g., Y or La; **Figure 11b,c**), and an enrichment of radiogenic strontium (**Figure 11e, f, and h**) like the more evolved silicic products over a relatively short time [77, 79].

On the other hand, the felsic products can be explained by the presence of a magma reservoir located in the middle-shallow crust (e.g., polybaric crystallization using the amphibole thermobarometer; [80, 81]). Two feeding reservoir systems have been identified for silicic magmas at ~4–8 km depth (~740–840°C) and at ~15–20 km (~940–1000°C) depth, respectively [80, 81]. In addition, melting-assimilation-storage-homogenization (MASH; [76]) zones have been interpreted and identified by petrological and seismic tomographic studies at ~15–40 km depth such as Altiplano-Puna Magma Body (APMB), Lazufre Magma Body (LMB) or Incahuasi Magma Body (IMB) [82–84]. These magmatic reservoirs are associated with a magmatic flare-up and magmatic steady-stage during the formation of the large ignimbrite deposits and growth of stratovolcanoes in northern Chile [85, 86]. This suggests that after these magmatic phases (flare-up and steady stage), the formation of shallow magmatic reservoirs (at 4–8 km depth) could have been formed as remnants of these eruptions. These would have been fed by a magmatic system of super-eruption scale (e.g., APMB, LMB, or IMB) of dacitic magmas and by new magma batches of less-evolved magmas [32, 87], triggering silicic eruptions of large volume with mafic inclusions as enclaves.

Therefore, based on the geochemical and isotopic compositional variations, the monogenetic volcanic products of northern Chile are characterized by two groups of magmas. One of them presents a magma evolution dominated by a high-pressure garnet source at deepest crust levels [71, 88] (**Figure 12**) characterized by different magmatic processes as FC, AFC, and ATA (**Figure 12**). The second group of magmas presents a magma evolution dominated by low-pressure garnet-free source middle-upper crust level to shallow crustal levels. This group of magmas is characterized by crystallizing of amphibole during the magma ascent (e.g. [32, 87]), and by AFC magmatic processes with different mixing degree (**Figure 12**).

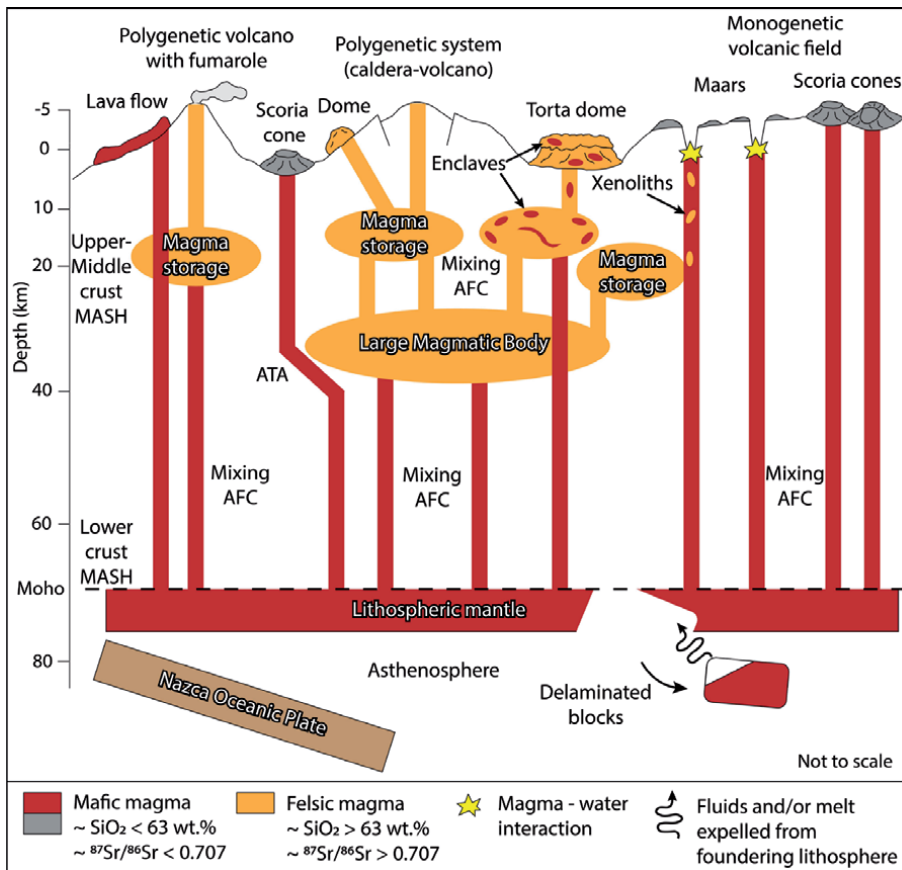


Figure 12. Conceptual model diagram of the magmatic system for monogenetic volcanoes in northern Chile. This model relates mantle-derived magmas with felsic upper crustal partially melted levels of magma storages such as shallow pre-eruptive reservoirs and large magmatic bodies (e.g., Altiplano-Puna Magma body). Processes during the magma ascent from source to the surface, such as MASH (melting-assimilation-storage-homogenization), mixing, AFC (assimilation fractional crystallization), ATA (assimilation during turbulent magma ascent) or magma-water interaction (phreatomagmatism). Distribution of these zones is constrained by stratigraphic [33–35], petrologic and thermobarometric [29, 79, 87–89], and geophysical [82–84] data. Partial melting and assimilation of lithospheric mantle by delaminated material at the base of the lithosphere model were taken from [75].

6. Concluding remarks

Monogenetic volcanism in northern Chile (18–28° Lat. S) is represented by 907 centers characterized by small (e.g., SC2 scoria cone) and large-volume (e.g., La Torta de Tocorpuri dome) volcanic structures. It exhibits a wide range of composition, from basaltic andesite (e.g., Cerro Overo) to rhyolite (e.g., Corral de Coquena) and a wide spectrum of volcanic landform, lithofacies, and hydromagmatic and magmatic eruptive styles (with the transition from explosive to effusive, and vice versa).

Among these eruptive styles, the most abundant activity corresponds to effusive and Strombolian eruptions. In contrast, the fewer frequency activities are the phreatomagmatic and Surtseyan eruptions (Figure 3), which is concordant with an arid climate in northern Chile from the Miocene [41, 90]. This could be related to the degree of glaciation because when everything is too cold and frozen, not a lot of water can infiltrate to become groundwater. At the same time, in warmer periods, meltwater can form lakes or flow toward basins from the peaks.

Although the numbers of monogenetic volcanoes represented in this contribution are limited by the exposure, and more features could be hidden by Neogene sedimentary and volcanic cover. Monogenetic volcanoes were mainly emplaced during Pleistocene and Miocene, generating scoria cones, domes, lava flows, maars, and tuff cones, in order to decrease. The relative abundance of volcanic features is, in part, limited by the amount of time for eruptions, where the spike in the Pleistocene is prominent, for being a short time period (~2 Ma). While the preservation of Miocene features is also notable in that they are still accessible favored by the arid climate in northern Chile from the Miocene.

Spatially, monogenetic volcanoes are mainly associated with NW-striking lineaments or with the intersections of NW-striking lineaments, NNW-to-NNE-striking faults, and WNW-striking lineaments, in decreasing order. Although the main tectonic setting in northern Chile corresponds to the compressional environment, tectonic phases of Quaternary crustal relaxation (neutral to extensional stresses) could have favored the rising of magmas in small batches up from the source (deep or shallow) to the surface.

A general eruptive model for monogenetic volcanoes in northern Chile is proposed in this work, where the external (e.g., magma reservoirs or groundwater availability) and internal (e.g., magma ascent rate or interaction *en-route* to the surface) conditions determine the changes in eruptive style, lithofacies, and magmatic processes involved in the formation of monogenetic volcanoes. Especially during explosive volcanic eruptions, which involve interaction with water, the resulting volcanic lithofacies and architecture will be diverse, reflecting the potential hazards that future eruptions could generate. The understanding of the tectonic and hydrologic setting of the region using traditional geophysics and volcanology surveys should play an essential role in volcanic monitoring, particularly in localities of the Altiplano (e.g., Ollagüe and Talabre village) located nearby active stratovolcanoes presenting permanent fumarolic activity (e.g., Guallatiri, Ollagüe or Lascar stratovolcanoes). This is especially important if such monogenetic volcanoes are surrounded by water-saturated high altitude sedimentary basins, such as salt flats (e.g., Salar de Carcote, Lejía, or Chungara lakes), where even a small-volume of any type of magma ascent could erupt in complex volcanic eruptions in northern Chile.

7. Supplementary data

Methods and databases (Table A.1. Monogenetic volcanoes location database; Table A.2. Geochronological database; Table A.3. Geochemical database; Figure A.1. Structural styles of monogenetic volcanoes in northern Chile; Figure A.2. Tectonic structures and lineaments database). <https://drive.google.com/drive/u/1/folders/1dwmvUiYTMF-XOoDXTwPhRYyHy88wNehJ>.

Acknowledgements

The authors wish to thank the Collaborative Research Center 1211–Earth Evolution at the Dry Limit and Dr. Eduardo Campos for providing the vehicle used during fieldwork. The authors would also like to thank all members of the Núcleo de Investigación en Riesgo Volcánico - Ckelar Volcanes team for fruitful discussions and support during fieldwork. The authors highly appreciate the time and effort of Dr. Alison Graettinger for her comments to improve this contribution.

Funding

This research is part of G.U. Ph.D. thesis, which is funded by CONICYT-PCHA Doctorado Nacional 2016–21161286 fellowship and supported by the Universidad Católica del Norte. This study is emerged and funded by CONICYT-PAI MEC 2017–80170048 (titled “Fortalecimiento del área de volcanismo en el Departamento de Ciencias Geológicas”), and the Antofagasta Regional Government, FIC-R project, code BIP N°30488832-0 (titled “Mitigación del riesgo asociado a procesos volcánicos en la Región de Antofagasta”); based on the Memorandum of Understanding of Research Cooperation between Universidad Católica del Norte and Massey University.

Conflict of interest

There are no conflicts of interest.

Author details

Gabriel Ureta^{1,2,3*}, Károly Németh⁴, Felipe Aguilera^{1,3,5}, Matias Vilches^{1,5}, Mauricio Aguilera^{1,5}, Ivana Torres¹, José Pablo Sepúlveda^{1,6}, Alexander Scheinost^{1,2} and Rodrigo González^{1,5}

1 Núcleo de Investigación en Riesgo Volcánico - Ckelar Volcanes, Universidad Católica del Norte, Antofagasta, Chile

2 Universidad Católica del Norte, Programa de Doctorado en Ciencias Mención Geología, Antofagasta, Chile

3 Centro Nacional de Investigación para la Gestión Integrada del Riesgo de Desastres (CIGIDEN), Santiago, Chile


4 Volcanic Risk Solutions, School of Agriculture and Environment, Massey University, Palmerston North, New Zealand

5 Universidad Católica del Norte, Departamento de Ciencias Geológicas, Antofagasta, Chile

6 Dipartimento di Scienze della Terra, Università degli Studi di Firenze, Florence, Italy

*Address all correspondence to: gabriel.ureta@ucn.cl

IntechOpen

© 2020 The Author(s). Licensee IntechOpen. This chapter is distributed under the terms of the Creative Commons Attribution License (<http://creativecommons.org/licenses/by/3.0>), which permits unrestricted use, distribution, and reproduction in any medium, provided the original work is properly cited. 

References

- [1] Valentine GA, Gregg TKP. Continental basaltic volcanoes — Processes and problems. *Journal of Volcanology and Geothermal Research*. 2008; 177: 857-873. [10.1016/j.jvolgeores.2008.01.050](https://doi.org/10.1016/j.jvolgeores.2008.01.050)
- [2] Le Corvec N, Spörli KB, Rowland J, Lindsay J. Spatial distribution and alignments of volcanic centers: Clues to the formation of monogenetic volcanic fields. *Earth-Science Reviews*. 2013; 124: 96-114. [10.1016/j.earscirev.2013.05.005](https://doi.org/10.1016/j.earscirev.2013.05.005)
- [3] Haag MB, Baez WA, Sommer CA, Arnosio JM, Filipovich RE. Geomorphology and spatial distribution of monogenetic volcanoes in the southern Puna Plateau (NW Argentina). *Geomorphology*. 2019; 342: 196-209. <https://doi.org/10.1016/j.geomorph.2019.06.008>
- [4] de Silva SL. Altiplano-Puna volcanic complex of the central Andes. *Geology*. 1989; 17: 1102-1106. [10.1130/0091-7613\(1989\)017<1102:Apvcot>2.3.Co;2](https://doi.org/10.1130/0091-7613(1989)017<1102:Apvcot>2.3.Co;2)
- [5] Smith IEM, Németh K. Source to surface model of monogenetic volcanism: a critical review. In: *Monogenetic Volcanism* (eds Németh K, Carrasco-Núñez G, Aranda-Gómez JJ, Smith IEM). Geological Society (2017). 1-28. doi.org/10.1144/sp446.14
- [6] Kereszturi G, Németh K. Monogenetic Basaltic Volcanoes: Genetic Classification, Growth, Geomorphology and Degradation. In: *Updates in Volcanology - New Advances in Understanding Volcanic Systems* (ed Németh K). Intech Open (2012). 3-88 [10.5772/51387](https://doi.org/10.5772/51387)
- [7] Németh K, Kereszturi G. Monogenetic volcanism: personal views and discussion. *International Journal of Earth Sciences*. 2015; 104: 2131-2146. doi.org/10.1007/s00531-015-1243-6
- [8] Hopkins JL, Smid ER, Eccles JD, Hayes JL, Hayward BW, McGee LE, van Wijk K, Wilson TM, Cronin SJ, Leonard GS, Lindsay JM, Németh K, Smith IEM. Auckland Volcanic Field magmatism, volcanism, and hazard: a review. *New Zealand Journal of Geology and Geophysics*. 2020: 1-22. [10.1080/00288306.2020.1736102](https://doi.org/10.1080/00288306.2020.1736102)
- [9] Thorpe RS, Francis PW. Variations in andean andesite compositions and their petrogenetic significance. *Tectonophysics*. 1979; 57: 53-70. [https://doi.org/10.1016/0040-1951\(79\)90101-X](https://doi.org/10.1016/0040-1951(79)90101-X)
- [10] de Silva SL, Francis PW. *Volcanoes of the central Andes*. Springer-Verlag (1991).
- [11] Global Volcanism Program. *Volcanoes of the World*, v. 4.8.5. In: Smithsonian Institution (ed Venzke Ee) (2013).
- [12] Trumbull RB, Riller U, Oncken O, Scheuber E, Munier K, Hongn F. The Time-Space Distribution of Cenozoic Volcanism in the South-Central Andes: a New Data Compilation and Some Tectonic Implications. In: *The Andes: Active Subduction Orogeny* (eds Oncken O, *et al.*). Springer Berlin Heidelberg (2006). 29-43. [10.1007/978-3-540-48684-8_2](https://doi.org/10.1007/978-3-540-48684-8_2)
- [13] Hora JM, Singer BS, Worner G. Volcano evolution and eruptive flux on the thick crust of the Andean Central Volcanic Zone: 40Ar/39Ar constraints from Volcan Parinacota, Chile. *Geological Society of America Bulletin*. 2007; 119: 343-362. [10.1130/b25954.1](https://doi.org/10.1130/b25954.1)
- [14] Inostroza M, Aguilera F, Menzies A, Layana S, González C, Ureta G, Sepúlveda J, Scheller S, Böehm S, Barraza M, Tagle R, Patzschke M. Deposition of metals and metalloids in the fumarolic fields of Guallatiri and Lastarria volcanoes, northern Chile. *Journal of Volcanology and Geothermal Research*. 2020; 393: 106803. <https://doi.org/10.1016/j.jvolgeores.2020.106803>

- [15] Klemetti EW, Grunder AL. Volcanic evolution of Volcán Aucanquilcha: a long-lived dacite volcano in the Central Andes of northern Chile. *Bulletin of Volcanology*. 2008; 70: 633-650. 10.1007/s00445-007-0158-x
- [16] Vezzoli L, Tibaldi A, Renzulli A, Menna M, Flude S. Faulting-assisted lateral collapses and influence on shallow magma feeding system at Ollagüe volcano (Central Volcanic Zone, Chile-Bolivia Andes). *Journal of Volcanology and Geothermal Research*. 2008; 171: 137-159. 10.1016/j.jvolgeores.2007.11.015
- [17] Calder ES, Sparks RSJ, Gardeweg MC. Erosion, transport and segregation of pumice and lithic clasts in pyroclastic flows inferred from ignimbrite at Lascar Volcano, Chile. *Journal of Volcanology and Geothermal Research*. 2000; 104: 201-235. [https://doi.org/10.1016/S0377-0273\(00\)00207-9](https://doi.org/10.1016/S0377-0273(00)00207-9)
- [18] Francis PW, Gardeweg M, Ramirez CF, Rothery DA. Catastrophic debris avalanche deposit of Socompa volcano, northern Chile. *Geology*. 1985; 13: 600-603. 10.1130/0091-7613(1985)13<600:cdados>2.0.co;2
- [19] Aguilera F, Layana S, Rodríguez-Díaz A, González C, Cortés J, Inostroza M. Hydrothermal alteration, fumarolic deposits and fluids from Lastarria Volcanic Complex: A multidisciplinary study. *Andean Geology*. 2016; 43: 166-196.
- [20] Baker PE, Gonzalez-Ferran O, Rex DC. Geology and geochemistry of the Ojos del Salado volcanic region, Chile. *Journal of the Geological Society*. 1987; 144: 85-96. 10.1144/gsjgs.144.1.0085
- [21] de Silva SL, Self S, Francis PW, Drake RE, Carlos RR. Effusive silicic volcanism in the Central Andes: The Chao dacite and other young lavas of the Altiplano-Puna Volcanic Complex. *Journal of Geophysical Research: Solid Earth*. 1994; 99: 17805-17825. 10.1029/94jb00652
- [22] González G, Cembrano J, Aron F, Veloso EE, Shyu JBH. Coeval compressional deformation and volcanism in the central Andes, case studies from northern Chile (23°S–24°S). *Tectonics*. 2009; 28: TC6003. <https://doi.org/10.1029/2009TC002538>
- [23] Cornejo PN, J.A. Azufrera Juan de la Vega: un maar de origen freatomagmático, Andes del norte de Chile (25°52'S). . In: ^V Congreso Geológico de Chile; Santiago, Chile); 209-227
- [24] Self S, de Silva SL, Cortés JA. Enigmatic clastogenic rhyolitic volcanism: The Corral de Coquena spatter ring, North Chile. *Journal of Volcanology and Geothermal Research*. 2008; 177: 812-821. 10.1016/j.jvolgeores.2008.01.047
- [25] Mattioli M, Renzulli A, Menna M, Holm PM. Rapid ascent and contamination of magmas through the thick crust of the CVZ (Andes, Ollagüe region): Evidence from a nearly aphyric high-K andesite with skeletal olivines. *Journal of Volcanology and Geothermal Research*. 2006; 158: 87-105. 10.1016/j.jvolgeores.2006.04.019
- [26] Watts RB, Clavero Ribes J, Sparks RSJ. The origin and emplacement of Domo Tinto, Guallatiri volcano, Northern Chile. *Andean Geology*. 2014; 41. 10.5027/andgeoV41n3-a04
- [27] Godoy B, Taussi M, González-Maurel O, Renzulli A, Hernández-Prat L, le Roux P, Morata D, Menzies A. Linking the mafic volcanism with the magmatic stages during the last 1 Ma in the main volcanic arc of the Altiplano-Puna Volcanic Complex (Central Andes). *Journal of South American Earth Sciences*. 2019; 95: 102295. <https://doi.org/10.1016/j.jsames.2019.102295>

- [28] Davidson JP, Harmon RS, Wörner G. The source of central Andean magmas; Some considerations. In: Andean magmatism and its tectonic setting). Geological Society of America (1991). 233. 10.1130/SPE265-p233
- [29] Burns DH, de Silva SL, Tepley F, Schmitt AK, Loewen MW. Recording the transition from flare-up to steady-state arc magmatism at the Purico–Chascon volcanic complex, northern Chile. *Earth and Planetary Science Letters*. 2015; 422: 75-86. <https://doi.org/10.1016/j.epsl.2015.04.002>
- [30] van Alderwerelt BMEdR. Diverse monogenetic volcanism across the main arc of the central Andes, northern Chile. [PhD Thesis]. Iowa: University of Iowa; 2017.
- [31] González-Maurel O, Godoy B, le Roux P, Rodríguez I, Marín C, sMenzies A, Bertin D, Morata D, Vargas M. Magmatic differentiation at La Poruña scoria cone, Central Andes, northern Chile: Evidence for assimilation during turbulent ascent processes, and genetic links with mafic eruptions at adjacent San Pedro volcano. *Lithos*. 2019; 338-339: 128-140. <https://doi.org/10.1016/j.lithos.2019.03.033>
- [32] Taussi M, Godoy B, Piscaglia F, Morata D, Agostini S, Le Roux P, Gonzalez-Maurel O, Gallmeyer G, Menzies A, Renzulli A. The upper crustal magma plumbing system of the Pleistocene Apacheta-Aguilucho Volcanic Complex area (Altiplano-Puna, northern Chile) as inferred from the erupted lavas and their enclaves. *Journal of Volcanology and Geothermal Research*. 2019; 373: 179-198. <https://doi.org/10.1016/j.jvolgeores.2019.01.021>
- [33] Torres I, Németh K, Ureta G, Aguilera F. Characterization, origin, and evolution of one of the most eroded mafic monogenetic fields within the central Andes: The case of El País lava flow field, northern Chile. *Journal of South American Earth Sciences*. 2020:102942. <https://doi.org/10.1016/j.jsames.2020.102942>
- [34] Ureta G, Németh K, Aguilera F, Kósik S, González R, Menzies A, González C, James D. Evolution of a magmatic explosive/effusive to phreatomagmatic volcanic system: birth of a monogenetic volcanic field, Tilocálar volcanoes, northern Chile. *Journal of Volcanology and Geothermal Research*. Unpublished.
- [35] Ureta G, Aguilera F, Németh K, Inostroza M, González C, Zimmer M, Menzies A. Transition from small-volume ephemeral lava emission to explosive hydrovolcanism: The case of Cerro Tujle maar, northern Chile. *Journal of South American Earth Sciences*. 2020; 104: 102885. <https://doi.org/10.1016/j.jsames.2020.102885>
- [36] Wörner G, Schildgen TF, Reich M. The Central Andes: Elements of an Extreme Land. *Elements*. 2018; 14: 225-230. 10.2138/gselements.14.4.225
- [37] Yuan X, Sobolev SV, Kind R. Moho topography in the central Andes and its geodynamic implications. *Earth and Planetary Science Letters*. 2002; 199: 389-402. [https://doi.org/10.1016/S0012-821X\(02\)00589-7](https://doi.org/10.1016/S0012-821X(02)00589-7)
- [38] Beck SL, Zandt G, Myers SC, Wallace TC, Silver PG, Drake L. Crustal-thickness variations in the central Andes. *Geology*. 1996; 24: 407-410. 10.1130/0091-7613(1996)024<0407:ctvittc>2.3.co;2
- [39] Schmitz M, Heinsohn WD, Schilling FR. Seismic, gravity and petrological evidence for partial melt beneath the thickened Central Andean crust (21-23°S). *Tectonophysics*. 1997; 270: 313-326. [https://doi.org/10.1016/S0040-1951\(96\)00217-X](https://doi.org/10.1016/S0040-1951(96)00217-X)
- [40] Kay SM, Coira B, Viramonte J. Young mafic back arc volcanic rocks as

- indicators of continental lithospheric delamination beneath the Argentine Puna Plateau, central Andes. *Journal of Geophysical Research: Solid Earth*. 1994; 99: 24323-24339. doi:10.1029/94JB00896
- [41] Lamb S, Davis P. Cenozoic climate change as a possible cause for the rise of the Andes. *Nature*. 2003; 425: 792-797. 10.1038/nature02049
- [42] Wörner G, Hammerschmidt K, Henjes-Kunst F, Lezaun J, Wilke H. Geochronology ($^{40}\text{Ar}/^{39}\text{Ar}$, K-Ar and He-exposure ages) of Cenozoic magmatic rocks from Northern Chile (18-22°S): implications for magmatism and tectonic evolution of the central Andes. *Revista geológica de Chile*. 2000; 27: 205-240.
- [43] Stern CR. Active Andean volcanism: its geologic and tectonic setting. *Revista geológica de Chile*. 2004; 31: 161-206.
- [44] González-Ferrán O. Volcanes de Chile. Instituto Geográfico Militar (1995).
- [45] De la Cruz-Reyna S, Yokoyama I. A geophysical characterization of monogenetic volcanism. *Geofísica internacional*. 2011; 50: 465-484.
- [46] Bishop MA. Point pattern analysis of eruption points for the Mount Gambier volcanic sub-province: a quantitative geographical approach to the understanding of volcano distribution. *Area*. 2007; 39: 230-241. 10.1111/j.1475-4762.2007.00729.x
- [47] Pardo-Casas F, Molnar P. Relative motion of the Nazca (Farallon) and South American Plates since Late Cretaceous time. *Tectonics*. 1987; 6: 233-248. 10.1029/TC006i003p00233
- [48] Tibaldi A, Bonali FL. Contemporary recent extension and compression in the central Andes. *Journal of Structural Geology*. 2018; 107: 73-92. 10.1016/j.jsg.2017.12.004
- [49] Tibaldi A, Bonali FL, Corazzato C. Structural control on volcanoes and magma paths from local- to orogen-scale: The central Andes case. *Tectonophysics*. 2017; 699: 16-41. 10.1016/j.tecto.2017.01.005
- [50] Tibaldi A, Corazzato C, Rovida A. Miocene–Quaternary structural evolution of the Uyuni–Atacama region, Andes of Chile and Bolivia. *Tectonophysics*. 2009; 471: 114-135. 10.1016/j.tecto.2008.09.011
- [51] González-Ferrán O, Baker PE, Rex DC. Tectonic-volcanic discontinuity at latitude 27° south Andean Range, associated with Nazca Plate Subduction. *Tectonophysics*. 1985; 112: 423-441. doi.org/10.1016/0040-1951(85)90189-1
- [52] Báez W, Carrasco Nuñez G, Giordano G, Viramonte JG, Chiodi A. Polycyclic scoria cones of the Antofagasta de la Sierra basin, Southern Puna plateau, Argentina. In: *Monogenetic Volcanism* (eds Németh K, Carrasco-Núñez G, Aranda-Gómez JJ, Smith IEM). Geological Society (2017). 311-336. 10.1144/sp446.3
- [53] Bishop MA. A generic classification for the morphological and spatial complexity of volcanic (and other) landforms. *Geomorphology*. 2009; 111: 104-109. <https://doi.org/10.1016/j.geomorph.2008.10.020>
- [54] Walker GPL. Compound and simple lava flows and flood basalts. *Bulletin Volcanologique*. 1971; 35: 579-590. 10.1007/bf02596829
- [55] Burgisser A, Degruyter W. Magma Ascent and Degassing at Shallow Levels. In: *The Encyclopedia of Volcanoes (Second Edition)* (eds Sigurdsson H, Houghton B, McNutt SR, Rymer H, Stix J). Academic Press (2015). 225-236. 10.1016/b978-0-12-385938-9.00011-0
- [56] Cassidy M, Manga M, Cashman K, Bachmann O. Controls on explosive-effusive volcanic eruption styles.

Nature Communications. 2018; 9: 2839. 10.1038/s41467-018-05293-3

[57] Németh K, Kósik S. Review of Explosive Hydrovolcanism. *Geosciences*. 2020; 10: 44.

[58] de Silva S, Lindsay JM. Primary Volcanic Landforms. In: *The Encyclopedia of Volcanoes (Second Edition)* (eds Sigurdsson H, Houghton B, McNutt SR, Rymer H, Stix J). Academic Press (2015). 273-297. 10.1016/b978-0-12-385938-9.00015-8

[59] Maro G, Caffè PJ. Neogene monogenetic volcanism from the Northern Puna region: products and eruptive styles. In: *Monogenetic Volcanism* (eds Németh K, Carrasco-Núñez G, Aranda-Gómez JJ, Smith IEM). Geological Society (2016). 337-359. 10.1144/sp446.6

[60] Maro G, Caffè PJ, Báez W. Volcanismo monogenético máfico cenozoico de la Puna. In: *Ciencias de la Tierra y Recursos Naturales del NOA. Relatorio del XX Congreso Geológico Argentino San Miguel de Tucumán, Argentina*; 548-577

[61] Sosa-Ceballos G, Macías JL, García-Tenorio F, Layer P, Schaaf P, Solís-Pichardo G, Arce JL. El Ventorrillo, a paleostructure of Popocatepetl volcano: insights from geochronology and geochemistry. *Bulletin of Volcanology*. 2015; 77: 91. 10.1007/s00445-015-0975-2

[62] Barbarin B, Didier J. Genesis and evolution of mafic microgranular enclaves through various types of interaction between coexisting felsic and mafic magmas. *Earth and Environmental Science Transactions of the Royal Society of Edinburgh*. 1992; 83: 145-153. 10.1017/S0263593300007835

[63] De Campos CP, Perugini D, Ertel-Ingrisch W, Dingwell DB, Poli G. Enhancement of magma mixing

efficiency by chaotic dynamics: an experimental study. *Contributions to Mineralogy and Petrology*. 2011; 161: 863-881. 10.1007/s00410-010-0569-0

[64] Perugini D, Poli G. The mixing of magmas in plutonic and volcanic environments: Analogies and differences. *Lithos*. 2012; 153: 261-277. <https://doi.org/10.1016/j.lithos.2012.02.002>

[65] Rutherford MJ. Magma Ascent Rates. *Reviews in Mineralogy and Geochemistry*. 2008; 69: 241-271. 10.2138/rmg.2008.69.7

[66] Le Maitre RW, Bateman P, Dudek A, Keller J, Lameyre J, Le Bas MJ, Sabine PA, Schmid R, Sorensen H, Strekeisen A, Woolley AR, Zanettin B. A classification of igneous rocks and glossary of terms: recommendations of the International Union of Geological Sciences, Subcommittee on the Systematics of Igneous Rocks. *International Union of Geological Sciences* (1989).

[67] Scott EM, Allen MB, Macpherson CG, McCaffrey KJW, Davidson JP, Saville C, Ducea MN. Andean surface uplift constrained by radiogenic isotopes of arc lavas. *Nature Communications*. 2018; 9: 969. 10.1038/s41467-018-03173-4

[68] Lucassen F, Kramer W, Bartsch V, Wilke H-G, Franz G, Romer RL, Dulski P. Nd, Pb, and Sr isotope composition of juvenile magmatism in the Mesozoic large magmatic province of northern Chile (18-27°S): indications for a uniform subarc mantle. *Contributions to Mineralogy and Petrology*. 2006; 152: 571. 10.1007/s00410-006-0119-y

[69] Franz G, Lucassen F, Kramer W, Trumbull RB, Romer RL, Wilke H-G, Viramonte JG, Becchio R, Siebel W. Crustal Evolution at the Central Andean Continental Margin: a Geochemical Record of Crustal Growth, Recycling

and Destruction. In: *The Andes: Active Subduction Orogeny* (eds Oncken O, *et al.*). Springer Berlin Heidelberg (2006). 45-64. 10.1007/978-3-540-48684-8_3

[70] Mamani M, Worner G, Sempere T. Geochemical variations in igneous rocks of the Central Andean orocline (13 S to 18 S): Tracing crustal thickening and magma generation through time and space. *Geological Society of America Bulletin*. 2010; 122: 162-182. 10.1130/b26538.1

[71] Delacour A, Gerbe M-C, Thouret J-C, Wörner G, Paquereau-Lebti P. Magma evolution of Quaternary minor volcanic centres in southern Peru, Central Andes. *Bulletin of Volcanology*. 2007; 69: 581-608. 10.1007/s00445-006-0096-z

[72] Irvine TN, Baragar WRA. A Guide to the Chemical Classification of the Common Volcanic Rocks. *Canadian Journal of Earth Sciences*. 1971; 8: 523-548. <https://doi.org/10.1139/e71-055>

[73] Peccerillo A, Taylor SR. Geochemistry of eocene calc-alkaline volcanic rocks from the Kastamonu area, Northern Turkey. *Contributions to Mineralogy and Petrology*. 1976; 58: 63-81. <https://doi.org/10.1007/bf00384745>

[74] Wörner G, Mamani M, Blum-Oeste M. Magmatism in the Central Andes. *Elements*. 2018; 14: 237-244. 10.2138/gselements.14.4.237

[75] Murray KE, Ducea MN, Schoenbohm L. Foundering-driven lithospheric melting: The source of central Andean mafic lavas on the Puna Plateau (22 S–27 S). *Geodynamics of a Cordilleran Orogenic System: The Central Andes of Argentina and Northern Chile: Geological Society of America Memoir*. 2015; 212: 139-166.

[76] Hildreth W, Moorbath S. Crustal contributions to arc magmatism in the

Andes of Central Chile. *Contributions to Mineralogy and Petrology*. 1988; 98: 455-489. 10.1007/bf00372365

[77] Huppert HE, Stephen R, Sparks J. Cooling and contamination of mafic and ultramafic magmas during ascent through continental crust. *Earth and Planetary Science Letters*. 1985; 74: 371-386. [https://doi.org/10.1016/S0012-821X\(85\)80009-1](https://doi.org/10.1016/S0012-821X(85)80009-1)

[78] Kerr AC, Kempton PD, Thompson RN. Crustal assimilation during turbulent magma ascent (ATA); new isotopic evidence from the Mull Tertiary lava succession, N. W. Scotland. *Contributions to Mineralogy and Petrology*. 1995; 119: 142-154. 10.1007/BF00307277

[79] Maro G, Caffè PJ, Romer RL, Trumbull RB. Neogene Mafic Magmatism in the Northern Puna Plateau, Argentina: Generation and Evolution of a Back-arc Volcanic Suite. *Journal of Petrology*. 2017; 58: 1591-1617. 10.1093/petrology/egx066

[80] Gorini A, Ridolfi F, Piscaglia F, Taussi M, Renzulli A. Application and reliability of calcic amphibole thermobarometry as inferred from calc-alkaline products of active geothermal areas in the Andes. *Journal of Volcanology and Geothermal Research*. 2018; 358: 58-76. <https://doi.org/10.1016/j.jvolgeores.2018.03.018>

[81] Ridolfi F, Renzulli A, Puerini M. Stability and chemical equilibrium of amphibole in calc-alkaline magmas: an overview, new thermobarometric formulations and application to subduction-related volcanoes. *Contributions to Mineralogy and Petrology*. 2010; 160: 45-66. 10.1007/s00410-009-0465-7

[82] Zandt G, Leidig M, Chmielowski J, Baumont D, Yuan X. Seismic Detection and Characterization of the

Altiplano-Puna Magma Body, Central Andes. pure and applied geophysics. 2003; 160: 789-807. [10.1007/pl00012557](https://doi.org/10.1007/pl00012557)

[83] Kay SM, Mpodozis C, Gardeweg M. Magma sources and tectonic setting of Central Andean andesites (25.5-28°S) related to crustal thickening, forearc subduction erosion and delamination. In: *Orogenic Andesites and Crustal Growth* (eds Gómez-Tuena A, Straub SM, Zellmer GF). Geological Society (2013). 303-334. [10.1144/sp385.11](https://doi.org/10.1144/sp385.11)

[84] Ward KM, Delph JR, Zandt G, Beck SL, Ducea MN. Magmatic evolution of a Cordilleran flare-up and its role in the creation of silicic crust. *Scientific Reports*. 2017; 7: 9047. [10.1038/s41598-017-09015-5](https://doi.org/10.1038/s41598-017-09015-5)

[85] de Silva SL, Riggs NR, Barth AP. Quickening the Pulse: Fractal Tempos in Continental Arc Magmatism. *Elements*. 2015; 11: 113-118. [10.2113/gselements.11.2.113](https://doi.org/10.2113/gselements.11.2.113)

[86] Perkins JP, Ward KM, de Silva SL, Zandt G, Beck SL, Finnegan NJ. Surface uplift in the Central Andes driven by growth of the Altiplano Puna Magma Body. *Nat Commun*. 2016; 7: 13185. [10.1038/ncomms13185](https://doi.org/10.1038/ncomms13185)

[87] Godoy B, McGee L, González-Maurel O, Rodríguez I, le Roux P, Morata D, Menzies A. Upper crustal differentiation processes and their role in 238U-230Th disequilibria at the San Pedro-Linzor volcanic chain (Central Andes). *Journal of South American Earth Sciences*. 2020; 102: 102672. <https://doi.org/10.1016/j.jsames.2020.102672>

[88] González-Maurel O, le Roux P, Godoy B, Troll VR, Deegan FM, Menzies A. The great escape: Petrogenesis of low-silica volcanism of Pliocene to Quaternary age associated with the Altiplano-Puna Volcanic Complex of northern Chile (21°10'-22°50'S). *Lithos*. 2019; 346-347: 105162. <https://doi.org/10.1016/j.lithos.2019.105162>

[89] de Silva SL, Kay SM. Turning up the Heat: High-Flux Magmatism in the Central Andes. *Elements*. 2018; 14: 245-250. <https://doi.org/10.2138/gselements.14.4.245>

[90] Vandervoort DS, Jordan TE, Zeitler PK, Alonso RN. Chronology of internal drainage development and uplift, southern Puna plateau, Argentine central Andes. *Geology*. 1995; 23: 145-148. [10.1130/0091-7613\(1995\)023<0145:coida>2.3.co;2](https://doi.org/10.1130/0091-7613(1995)023<0145:coida>2.3.co;2)

Section 4

Complex and Polygenetic Volcanism

The Caldera of Mount Bambouto: Volcanological Characterization and Classification

Ghislain Zangmo Tefogoum, David Guimolaire Nkouathio, Armand Kagou Dongmo and Merlin Gountié Dedzo

Abstract

Mount Bambouto culminates at 2744 m (Meletan Mountain) where an elliptical caldera of 16×8 km is found. Although that caldera has been a subject of numerous scientific works, complementary studies were needed to bring out additional data used to classify it through the Caldera DataBase of Geyer and Marti (2008). It emerges that Bambouto Caldera codes are 2 and 203 because it is respectively located in Africa and Central Africa according to the numbering system developed in the Catalog of Active Volcanoes of the World. The collapse type of the caldera is piecemeal; this relies on the fact that the caldera floor is uneven. Several rocks crop out in the caldera; accordingly, its code is B, I, T, P, and Ig viz. basalts, intermediate rocks, trachytes, phonolites, and ignimbrites. Bambouto depression is the ignimbrite caldera because it is associated with thick ignimbrite sheer, that ruled its collapse. The chemical analysis of rocks reveals that the magmatic series of Bambouto Caldera is of alkaline type. It has been built through the continental rifting of extensional type (RC-EXT). The collapse process has been followed by post-caldera protrusion of trachytic and phonolitic domes; then, its codes are Type-S and type-MS.

Keywords: caldera, continental rifting, basalts, trachytes, phonolites, ignimbrites, Cameroon

1. Introduction and geological context

Internal geodynamics is manifested on the Earth's surface by volcanic phenomena. Most of these phenomena are controlled by volcanoes located in the tectonically and structurally weak areas of the globe, notably accretion zones, convergence zones, and intra-plate zones. Some of these volcanoes are characterized by a simple crater, while others have one or more complex craters (distinguished by the collapse events). These complex craters are defined by one or more calderas [1–4]. The term caldera derives from the depression called Taburiente (Canary Islands) and has been firstly used by [5]. The Caldera de Taburiente in fact, is the frequently quoted example of erosion caldera. Erosion calderas are volcanic depression erosionally formed on the summit or on the flanks of the volcano, which may be several kilometers in diameter [6–8]. However, geologically, calderas are volcanic depressions resulting from the collapse of the roof of the magma chamber due to the rapid

retreat of the magma during an eruption [9, 10]. They can be elliptical, sub-circular or circular in map view. These shapes are induced by the shape of the underlying magma reservoir [11, 12]. In Refs. [9, 13], five types of collapse such as *piston*, *piece-meal*, *trapdoor*, *downsag*, and *funnel* have been defined to ease the comprehension of the caldera formation processes.

Nevertheless, insufficient work on the dynamics of caldera emplacement limits the understanding of the functioning and evolution of volcanic massifs worldwide. Some calderas deserve to be characterized according to the models of [9] and [13] in order to classify them according to the Collapse Caldera DataBase established by [14]. The Collapse Caldera DataBase makes it possible to better study the caldera formation processes and to classify them. The study of calderas for decades has been of paramount importance for the development of science; it allows us to understand the functioning of volcanic apparatus around the world and the environmental impact that can result from them. Since calderas constitute a natural heritage for the economic development of several countries and a laboratory for education and research [15–17], their classification will heighten their promotion and valorization.

Mount Bambouto, which was once a very active volcano, was truncated at their summit by a caldera like some volcanoes along the Cameroon Volcanic Line (**Figure 1**). It caldera was chosen for the present study because Mount Bambouto have been the subject of numerous studies focusing mainly on petrography, geochemistry, geochronology, geo-heritage, hazards and associated risks [18–29]. With the exception of [20, 21, 29], the studies on the caldera of Mount Bambouto are generally carried out in the specific areas [22, 30, 31]. Mount Bambouto is the third largest volcano (in volume) in the Cameroon Volcanic Line after Mount Cameroon and Mount Manengouba. It is located in the NE extension of Mount Manengouba from which it is separated by the Mbô plain. It is almost continuously contiguous to the NE with Mount Bamenda and covers an area of about 800 km². It is located between longitudes 09°55' and 10°15'E and latitudes 05°25' and 05°50'N. They straddle the Departments of Bamboutos in the East, Menoua in the South, Lebialem in the West and Mezam in the NW and, culminate at 2744 m at Meletan Mountain where they dominate the West Cameroon Highlands. Mount Bambouto is a huge shield volcano with a general SW-NE orientation [18]. This massif is characterized by the asymmetry of its slopes [32]. Its summit caldera is located between longitudes 09°57' and 10°07'E and latitudes 05°37' and 05°44'N. The Caldera of the Mount Bambouto has an elliptical map view (16 × 8 km) that opens in a horse-shoe shape toward the west (**Figure 2**). Throughout the caldera, rocks (basalts, hawaiites, mugearites, phonolites, trachytes, and ignimbrites) are found in different forms: flows, domes, peaks, teeth and needles that characterize the interior, the external slopes and the floor of the caldera. Thus, the inside of the caldera is marked by a sinuous “s” line punctuated by trachytic and phonolitic peaks, necks, and domes [18, 20, 29]. Moreover, the crystalline basement made up of granite, is observed on the western side of the volcano [21, 22, 29]. The floor of the caldera has a structure of stairs decreasing from the east to the west of the massif. The caldera rims are sub-vertical to vertical. In addition, several steep valleys (in “v” shape) accidentally affect the topography of the whole caldera (about 78% of the slopes are susceptible to mass movements) [29].

Despite these previous studies, the dynamics of the establishment of the caldera of the Mount Bambouto remains poorly understood. Moreover, that caldera is not yet classified in the Caldera DataBase established by [10]. However, some data do exist on this caldera. These data need to be completed and this will allow us to characterize that caldera according to the model of [9]. This characterization will make it possible to obtain and organize the data in order to classify the caldera of the Mount Bambouto in the Caldera Database of [14]. This work is essential for

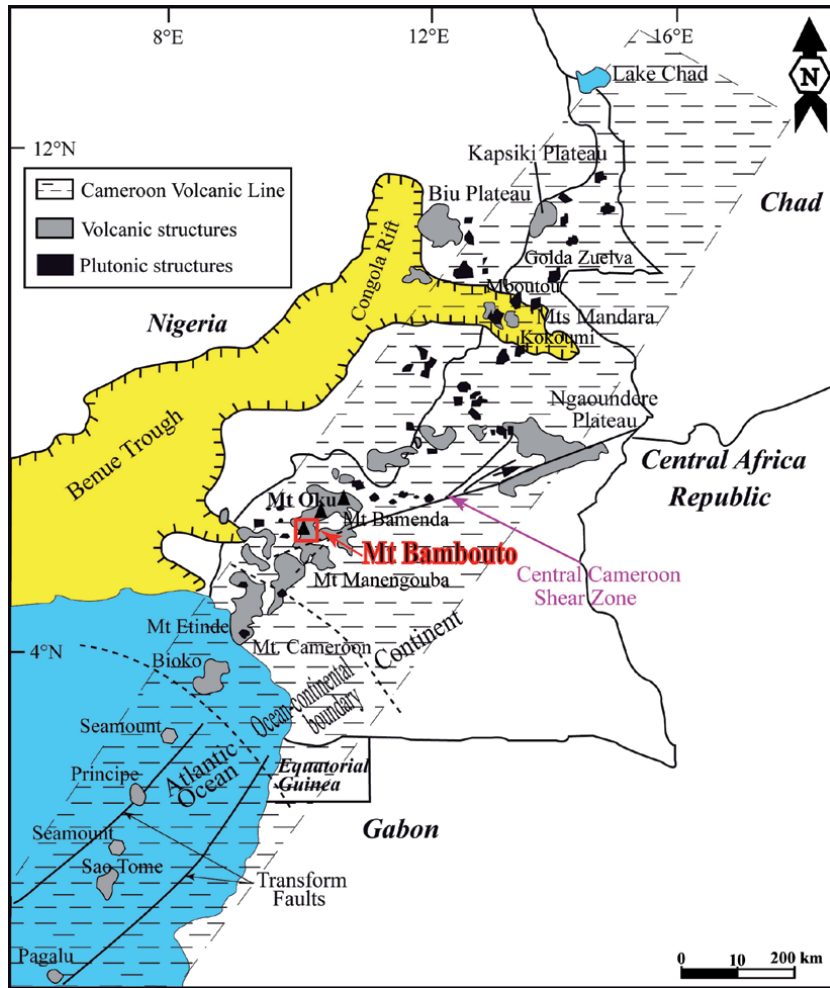


Figure 1.
The Cameroon volcanic line.

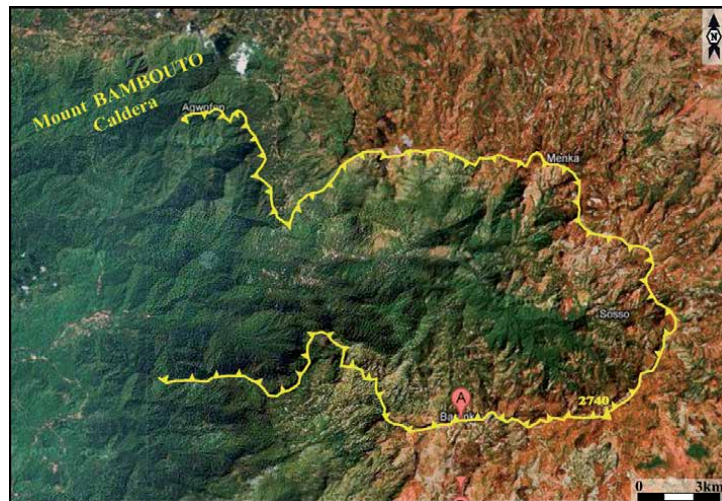


Figure 2.
Satellite image of the Mount Bambouto caldera.

understanding the functioning and evolution of the Mount Bambouto and, consequently, the dynamics of the Cameroon Volcanic Line, which remains a subject of discussion by many researchers nowadays.

2. Method of study

2.1 The volcanological study

2.1.1 The petrographic study

Several field trips were made. They made it possible to describe rock outcrops, take rock samples and take the coordinates of the various samples. These samples were then described and labeled. In the laboratory, the coordinates of the various rock sampling points were plotted on the topographic map of the study area. Through these different points and the macroscopic description of the samples, a geological map is produced [33]. In order to complete the macroscopic study of the rocks, thin sections of samples were taken at the University of Orleans and the University of Paris-Sud (Orsay Campus) in France. These thin sections were studied with the polarizing microscope of the Laboratory of Environmental Geology of the University of Dschang and at the Laboratory of Life and Earth Sciences of the University of Maroua. Some samples were analyzed with microprobe also at the University of Orleans and the University Paris-Sud (Orsay Campus) and in Nancy for the nomenclature of rock minerals and the determination of the nature of rocks. These microscopic and chemical studies have made it possible to refine the geological map of the caldera of the Mount Bambouto [33]. In addition, some complementary geochemical analyses were made to determine the chemical nature of different lavas.

2.1.2 The volcanological evolution of the caldera of the mount Bambouto

For the volcanological evolution of the caldera of the Mount Bambouto we have:

- carried out a cartographic study through the analysis of satellite images, about 70 aerial photos, digital elevation models, and topographic maps. This study allowed us to determine the exact boundaries and structure of the caldera.
- The geochronological data available in the literature made it possible to produce through DTM, the different stages of caldera formation according to the model of [9].

2.2 The classification of calderas

For the classification of the Caldera of the Mount Bambouto, we used the Caldera DataBase from [14]. To do so, we used the data obtained through volcanological studies and those existing in the literature.

3. Results

3.1 Field observations

In the Caldera of the Mount Bambouto the flows, mostly trachytic, have extensions ranging from 150 to 250 m; with an average height of between 10 and 30 m.

They are generally roughly and irregularly priced and are observable at the level of the caldera ramparts, on certain escarpments, road embankments and riverbeds. On the other hand, mafic lava flows are poorly represented in the caldera and have extensions of just a few meters. The domes are generally circular to sub-circular in shape with a base slightly above the top. They are dominated by coarse prisms and sometimes numerous diaclasses which favor the sporadic detachment of polygonal blocks generally observable at their base. Felsic and mafic flows are also observable in polygonal blocks accumulated near caldera ramparts and on stream beds (**Figure 3**). The lava texture is mostly microlitic porphyritic except for ignimbrites, which have a vitroclastic texture.



Figure 3. Some geological features of the Mount Bambouto caldera: (A–C)—post-caldera protrusions. (D)—erratic boulders; (E–G)—caldera’s floor structure; and (H)—caldera rim.

Basalts, hawaiites and trachytes all have a grayish alteration patina and are less than 3 mm thick. However, this patina has, in some places, crystals of automorphic alkaline feldspar of 4 mm or less in size. Ignimbrites have a strong patina of less than 3 mm thick and are gray to brown.

3.2 Microscopic petrography

Basalts (Figures 4 and 5) are characterized by a porphyritic microlitic texture in which pyroxene phenocrysts (10–25% of the rock), plagioclase (1–3% of the rock), olivine (2–7% of the rock) and opaque oxides (<3% of the rock) are embedded in a microlitic mesostase.

Hawaiites (Figure 4) are also characterized by a porphyritic microlitic texture in which pyroxene phenocrysts (2–5% of the rock), plagioclase (3–10% of the rock), olivine (15–35% of the rock) and opaque oxides (5–7% of the rock) are embedded in a microlitic mesostase.

Mugearites (Figure 5) are dominated by a subporphyritic microlitic texture materialized by amphibole (kaersutite), apatite and oxide phenocrysts. These phenocrysts constitute less than 10% of the rock. These rocks are kaersutite mugearites.

Generally speaking, the *trachytes* (Figure 4) of the Mount Bambouto Caldera have a subporphyritic microlitic texture rich in phenocrysts of alkaline feldspar

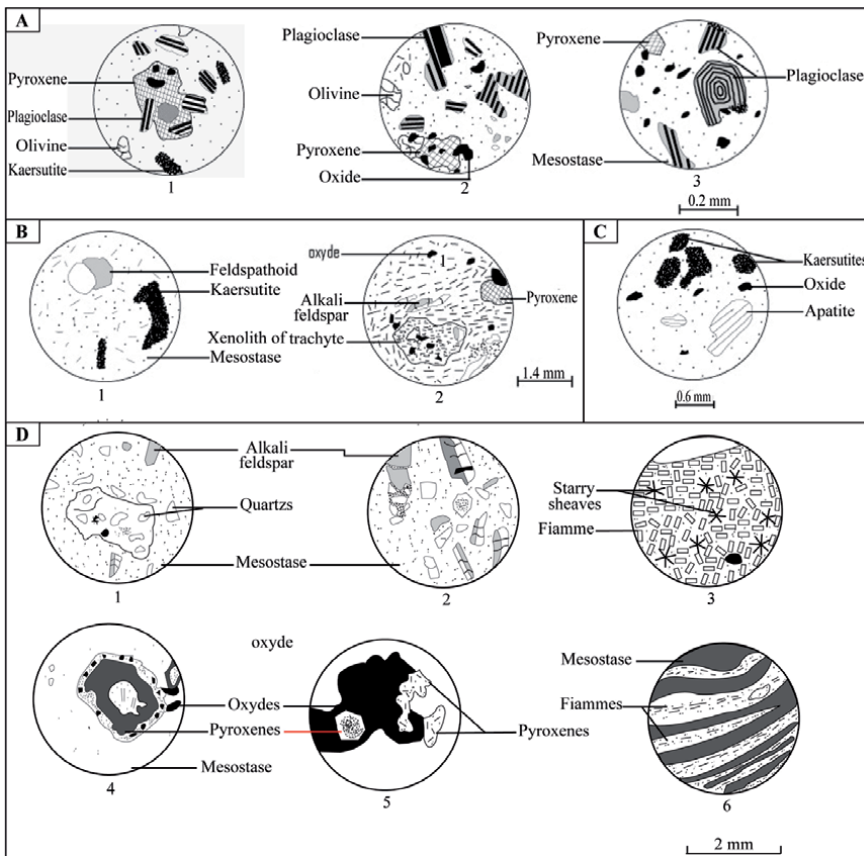


Figure 4. Drawings of some thin sections of rocks in the Mount Bambouto caldera: (A)—basalts; (B)—phonolites; (C)—kaersutite-mugearite; and (D)—ignimbrites.

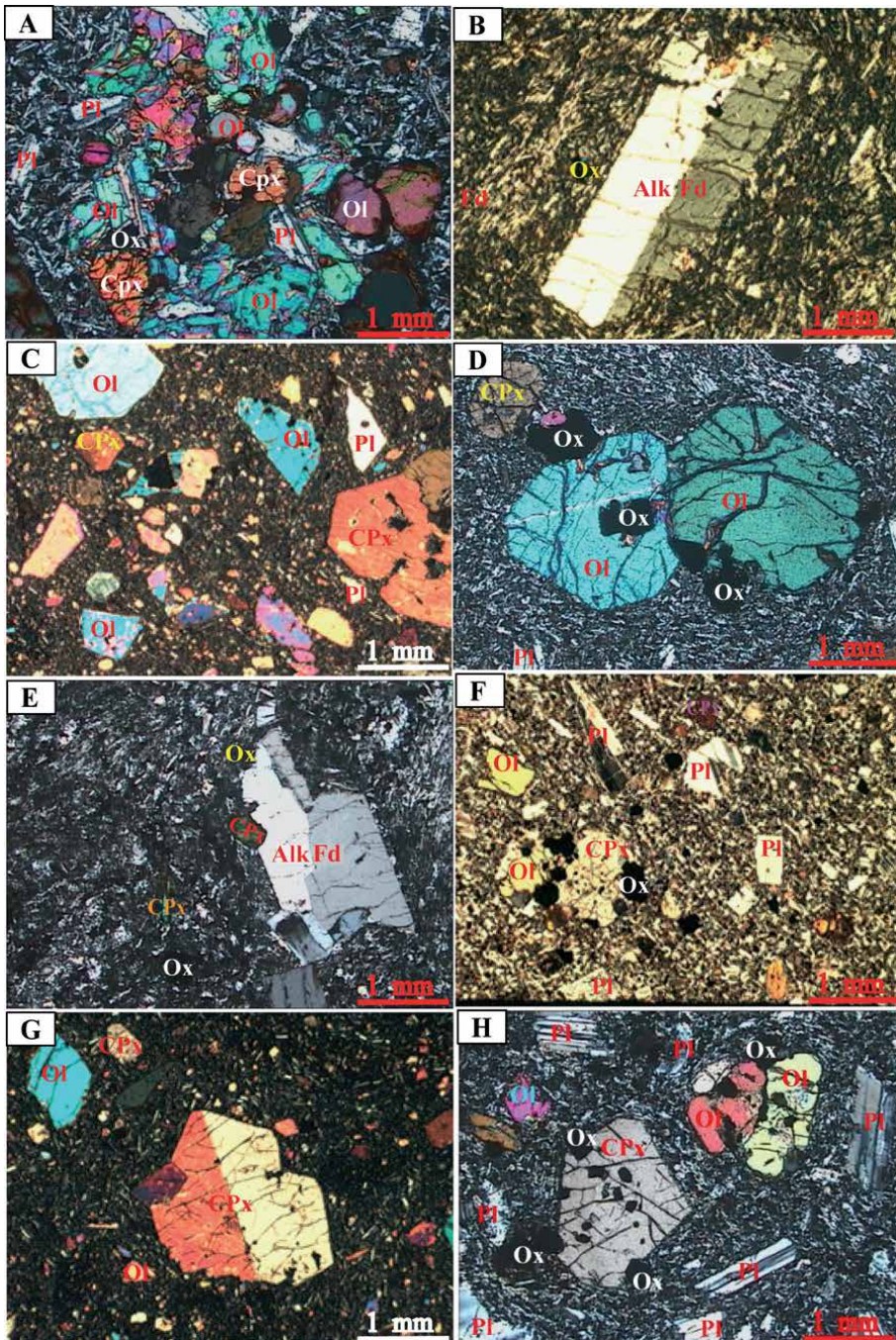


Figure 5.
 Photographs of thin sections of rocks in the Mount Bambouto caldera: (A, D, and H)—hawaiites; (B)—phonolites; (C, F, and G)—Basalts; (E)—trachytes.

(30% of the rock), plagioclase, pyroxene (<4% of the rock), amphibole (<1% of the rock), oxide (5% of the rock) and apatite.

Phonolites (Figures 4 and 5) show a light brown alteration patina of almost 3 mm thick. The fresh, greenish gray to greenish gray sample shows large crystals of alkaline feldspar (30% of the rock); 0.5 to 5 mm in size and some pyroxene granules. Microscopically, the rock has a subaphyric to porphyritic microlitic

texture containing phenocrystals and microcrystals of alkali feldspars, pyroxene, feldspathoid, amphiboles and oxides.

Ignimbrites (Figures 4 and 5) have a vitroclastic texture dominated by a facies-dominated matrix and whole or broken sections of alkali feldspar, quartz, pyroxene, and rock enclaves (trachytes and basement) in the form of rounded balls or subangular fragments.

3.3 Nomenclatures of some rock minerals

3.3.1 Olivines

In the caldera of the Mount Bambouto, olivine is present in the basalts with an average size of 0.5×3 mm. It is automorphic to subautomorphic. Their section is traversed by numerous cracks along which one notes the beginning of iddingsitization and serpentinization. Some sections have a core and borders corroded by mesostase. The olivine in the caldera of the Mount Bambouto is globally magnesian with forsterite contents between Fo57 and Fo75 (Figure 6).

3.3.2 Oxides

The lava oxides in the study area are represented by titanomagnetite and ilmenite (Figure 7). These two minerals coexist in some lava, notably dolerite mugearites. They are sometimes automorphic with various shapes (square, rectangular and rod-shaped), with sizes ranging from 0.2 to 1 mm. They occur as phenocrystals and microcrystals either embedded in minerals such as olivine, clinopyroxene and feldspars; or embedded in mesostase. Furthermore, titanomagnetite appears as the most abundant oxide in basalts, mugearites and trachytes.

3.3.3 Apatite

Apatite is observed in almost all the lavas of the caldera of the Mount Bambouto. It occurs as elongated crystals, xenomorphic to sub-automorphic and sometimes with transverse breaks in the intermediate lavas. Their size is between 0.2 and 0.8 mm and is observable as inclusions in olivine, oxides, and alkaline feldspars.

3.3.4 Clinopyroxenes

In the caldera of Mount Bambouto, clinopyroxenes in lavas are found in most sub-automorphic to automorphic crystal rocks with an average size of 0.5×1 mm. They show two directions of cleavage in some sections. They show gulfs of corrosion

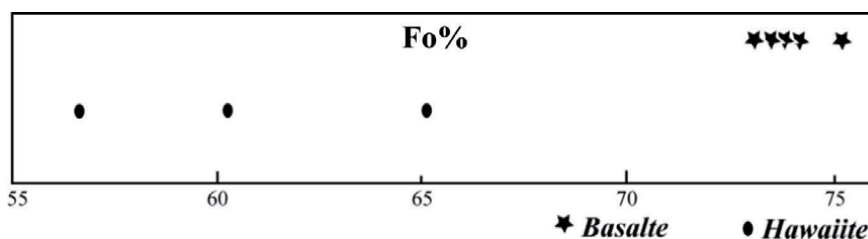


Figure 6. Evolution of the forsterite content in lavas in the Mount Bambouto caldera.

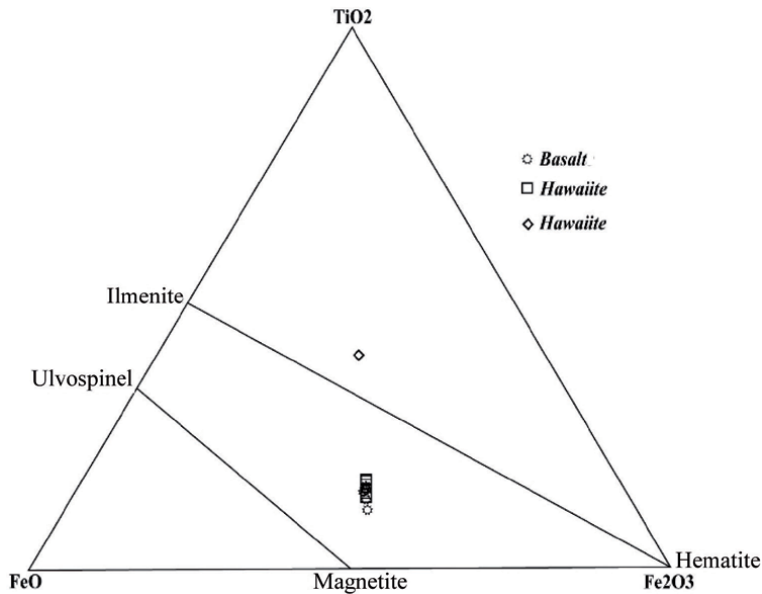


Figure 7.
 Position of oxides of lavas of the Mount Bambouto caldera in the $\text{FeO-TiO}_2\text{-Fe}_2\text{O}_3$ diagram.

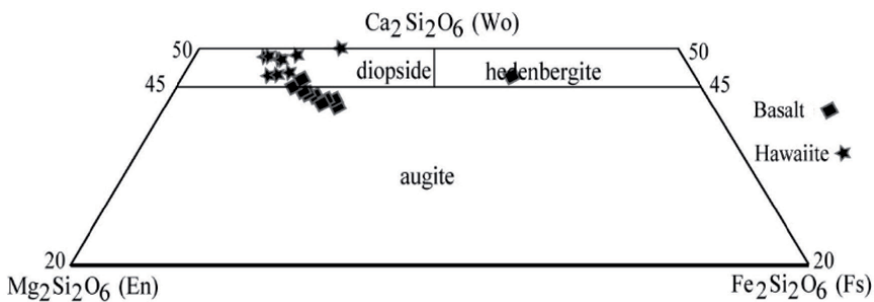


Figure 8.
 Classification of clinopyroxènes of lavas of the mount Bambouto caldera in the en-Wo-Fs diagram.

in some sections. They are cracked in the trachytes and show a macle h^1 in the basalts. The classification of [34] has made it possible to identify three types of clinopyroxene in the lavas of the caldera of Mount Bambouto (**Figure 8**); diopside, augite and hedenbergite.

3.3.5 Feldspars

Feldspars are the minerals most represented in the lava of the caldera of the Mount Bambouto. Their edges are corroded in certain sections of the phonolites. However, they are sub-automorphic to automorphic, cracked and elongated depending on the flow. They are found in microlites and phenocrystals with sizes ranging from 0.1×0.3 to 0.5×0.8 mm for plagioclases and from 0.1×0.4 to 1×2 mm for alkaline feldspars. The latter have a Carlsbad twin, unlike plagioclases with a polysynthetic twin. The most frequent plagioclases (An_{30-60}) in lava are andesine and labrador. In phonolites, the alkaline feldspars are anorthose (Or17 and Or37) and sanidine (Or37 and Or44) (**Figure 9**). However, anorthoses are in the

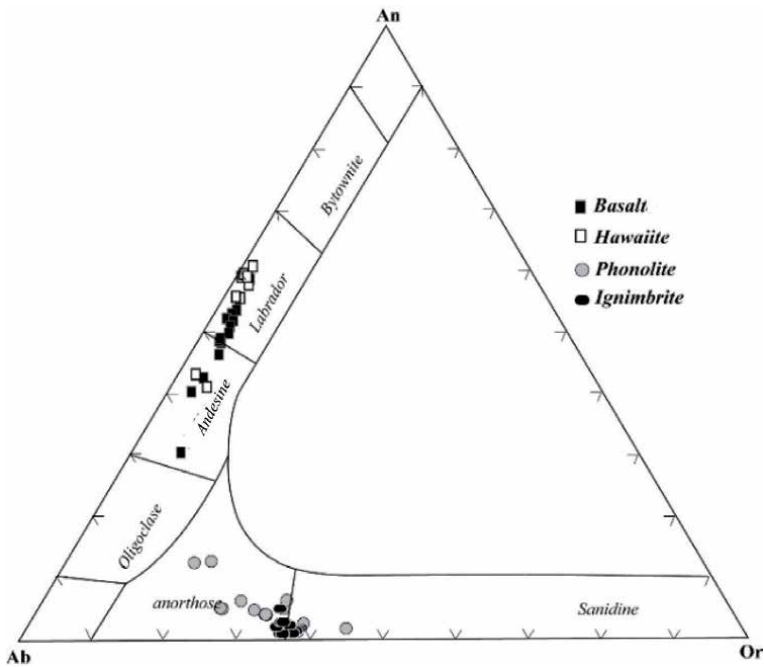


Figure 9.
Evolution of the anorthite content in lavas of the Mount Bambouto caldera.

majority. In ignimbrites, the composition of alkali feldspars is between Or33 and Or37 and are therefore exclusively anorthoses.

3.4 Classification of lava in the study areas

The lavas in the caldera of Mount Bambouto are alkaline in nature as shown in the following diagrams in **Figure 10**. The data used to make these diagrams have been supplemented by the data in [20, 22].

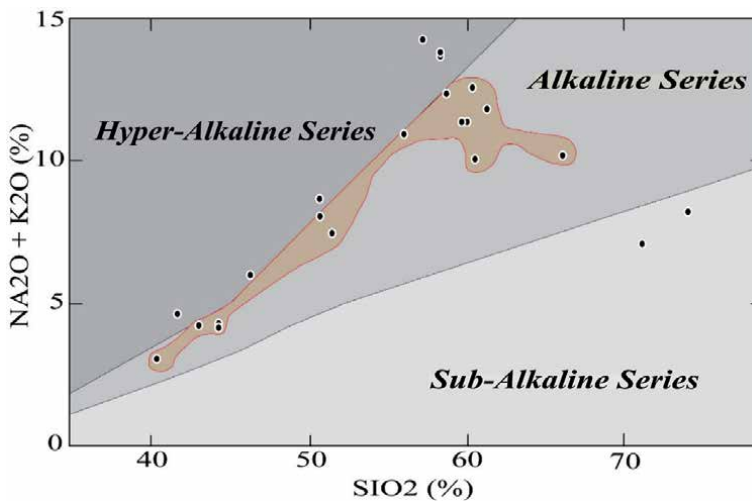


Figure 10.
Chemical nature of lavas in the Mount Bambouto caldera.

3.5 The volcanological evolution of the caldera of mount Bambouto

Mount Bambouto is a Hawaiian shield volcano [18]. Its history has been ruled by volcanic and tectonic events that led to the formation of a huge caldera on the Pan-African granitoid basement [35–37]. The Mount Bambouto Caldera formation (**Figure 11**) included three main stages [38] as follow:

The *Precaldera Stage* (Over 19 Ma) is characterized by the tumescence of the volcanic shield due to magma injection giving rise to several annular fissures observed in the whole volcano.

The *Syncaldera stage* (18–15.28 Ma) is materialized by two features: firstly, explosive eruptions are responsible for scoria, ignimbrites, trachytes and rhyolites; secondly, piecemeal intravolcanic collapse of the magmatic chamber roof is followed by the protrusion of trachytic domes and some basaltic supplies.

The *Postcaldera stage* (15–0.5 Ma) is typified by some trachytic and basaltic supplies and the protrusion of phonolitic domes. Activity ends with the explosive eruptions on the northeastern flank of the volcano where is built the multiple scoria cones.

3.6 Classification of calderas

3.6.1 Location

To assign the code of a given caldera, one must use the numbering system developed in the Catalog of Active Volcanoes of the World. In fact, the world is divided in 19 main regions that are subdivided, in turn, in several subregions. Hence, the study area is located in the African Region with the corresponding database code 2. In addition, these calderas are located in the Central African Sub-Region with the corresponding database code 203.

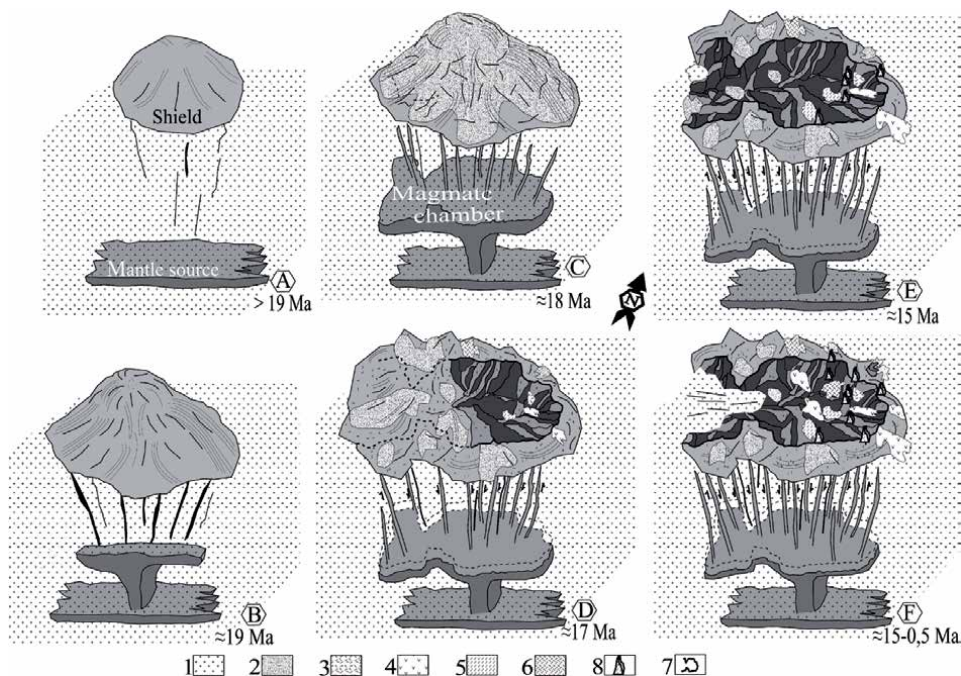


Figure 11. Sketch highlighting the stages of the formation of the Mount Bambouto caldera.

3.6.2 Ramparts and type/geometry of collapse

In the caldera ramparts are almost vertical at some levels (**Figure 3**); but on the whole these ramparts seem to merge with the floor.

At the level of the Mount Bambouto, the floor of the caldera is very dissected and presents in places a stepped structure (**Figure 3**), which indicates a piecemeal collapse.

3.6.3 Petrographic types

Several petrographic types are observed in the study area. These petrographic types are dominated by basalts, intermediate rocks, trachytes, phonolites and ignimbrites. Thus, the caldera of the Mount Bambouto is assigned the code B, I, T, P and Ig.

3.6.4 Magmatic series

The study area is characterized by an alkaline magmatic series as they are dominated by mafic, intermediate, and felsic terms. They are assigned the codes ALKAf (Alkaline felsic), ALKAi (Alkaline intermediate) and ALKA_m (Alkaline mafic).

3.6.5 Crust type and tectonic setting

Mount Bambouto rests on a granito-gneissic bedrock with a thickness (hc) of about 35.5 km [39]. According to the Database [14], these crustal thicknesses in the study areas are greater than the 30–35 km interval; hence the code is C.

From the internal geodynamic point of view, the Mount Bambouto Caldera is located in the Cameroon Volcanic Line which originates, according to some authors [40–43], from a Continental Rift; Its code is be RC. This nascent rift [44, 45], at the origin of the Cameroon Volcanic Line in general and of Mount Bambouto and its respective caldera system in particular, is of the extensional type and their code is EXT.

3.6.6 Pre-caldera volcanism

A Pre-caldera regional dome occurred through a tumescence that created numerous concentric faults. These fissures favored a pre-caldera magmatic activity that further contributed to the building of the Bambouto stratovolcano. Its code is therefore STR.

3.6.7 Caldera collapse period and post-caldera volcanic activity

The collapse of the Caldera of Mount Bambouto occurred at the beginning of the sequence of eruptions that contributed to their formation. Their code is A.

In the Mount Bambouto, this volcanic activity is dominated by the presence of several eruptive vents, notably on the ramparts, the eastern floor of the caldera and the NE slope of the volcano. Thus, the Mount Bambouto is classified as Type-S and Type-MS.

3.6.8 Preservation of the caldera

On the other hand, the ramparts of the Mount Bambouto Caldera are threatened by growing urbanization and agro-pastoral activity, particularly to the south and east of the caldera. Its boundaries are therefore slightly destroyed. Its code is PD.

The overall results have been used to fill the CCDB table (**Table 1**).

Collapse caldera database	Criteria	Data
	Latitude	05°37'–05°44' N
	Longitude	09°57'–10°07' E
	Region	2
	Subregion	203
	Age (Ma)	15
	Maximum Caldera diameter	Not Applicable
	Minimum Caldera diameter	Not Applicable
	Surface (km ²)	155.1
	Subsidence	—
	Caldera volume (km ³)	—
	Type of collapse	Piecemeal
	Name linked to the deposits	Ignimbritic
	Thickness of deposits	—
	Volume of deposits (km ³)	—
	Total volume of lavas (km ³)	—
	Petrographic types	B, I, T, P
	Magmatic series	ALKAm, ALKAi, ALKAf
	Magmatic chamber depth (km)	35.5
	Ratio depth/width of magmatic chamber	—
	Plate tectonic setting (PTS)	RC
	Crustal type (CT)	C
	Type of tectonic faulting (TF)	Ext
	Periods of pre-caldera doming (PCD)	Over 19 Ma
	Type of pre-caldera volcanism (PCV)	STR
	Timing of caldera onset (TCO)	A
	Post-caldera volcanic activity (PCVA)	S, MS
	Post-caldera resurgence (PCR)	Absence
	Caldera preservation (CPR)	PD

Table 1.
 Classification of the Mount Bambouto caldera in the CCDB of [10].

4. Discussion

Through the mode of outcropping of different rocks in the caldera of Mount Bambouto, all types of dynamism (extrusive, effusive, explosive) exist in the caldera. These are therefore polygenic volcanoes marked by long periods of activity and varied dynamisms, resting and erosion phases during different tectonic episodes [46]. In addition, the diversity of rocks is indicative of the high degree of magma differentiation induced here by the fractional crystallization process [21, 47, 48]. The presence of the trachytes in ignimbrites of the study area

is an indicator of a relative chronology of the rocks. Indeed, there was an ante-ignimbritic trachytic volcanic phase. This means that there has been in the course of the evolution of the Bambouto volcano, the eruption of trachytic rocks before that of ignimbritic materials [49, 50].

The caldera of Mount Bambouto was formed at a well-defined time. The stages of formation of these calderas correspond globally to the model of [9]: a regional tumescence, a volcanic eruption, a collapse of the caldera, volcanism on the annular fractures and sedimentation. The present structure of the caldera floor shows that the roof of the magma chamber collapsed piecemeal during its formation. The border faults generally observed on calderas in certain volcanic environments in Cameroon, which are evidence of the different phases of caldera collapse, are difficult to observe in the caldera of Mount Bambouto. These faults, when identifiable on certain ramparts, present a some stages of collapse (**Figure 3**). In this caldera, the ramparts are often confused with the floor. The latter constitutes the most dissected floor of all the caldera units studied along the Cameroon Volcanic Line and their arrangement in decreasing steps from west to east, would testify to the multiple collapses that marked its formation [51, 52]. On the other hand, in the Eboga and Lefo calderas, where the ramparts are clearly visible from the caldera floor, there are boundary faults marked by about 2–4 stages of collapse [29]. Post-caldera volcanism has manifested itself on the Mount Bambouto. This has been observed in other caldera environments on the Cameroon Volcanic Line, notably the Santa-Mbu and Lefo caldera in the Bamenda Mountains, the Eboga and Elengoum calderas in Mount Manengouba and the Bangou caldera in Mount Bangou. It is at the origin of numerous doleritic, phonolitic and trachytic protrusions and, cones and maars found on the floor and external slopes of these calderas [33, 51–54]. These post-caldera geomorphological units give the caldera of Mount Bambouto the S and MS types according to [14]. Mount Bambouto constitutes a stratovolcano [20, 33]. The shape of this caldera is comparable to the elliptical shape of the calderas of Suswa, Kenya [55] and Chã das of Fogo Island in Cape Verde [56] and the calderas of the basaltic shields described by [9, 57]. This shape results from the geometry of the magma chamber which is the main factor controlling the final morphology of the calderas [58]. The presence of ignimbrites, tuffs, trachytes and rhyolites in the caldera of the Mount Bambouto qualifies it as an ignimbrite caldera. Ignimbrite calderas are usually over 10 km in diameter and over 1 km in depth, formed after the voluminous deposition of silicic ignimbrites [9, 11, 59]. We can list the example of Batur Caldera in Bali, New Zealand [60]. However, the term ignimbrite caldera is clearly used by (2015) [61] to qualify the calderas of the Southern Rocky Mountain Volcanic Field in Colorado (USA) notably Bonanza, Bachelor, Cochetopa Park, Creede, and Platoro calderas. Their presence in Mount Bambouto is explained by the fact that, considering the ages, this massif is sufficiently old compared to the other massifs, especially Mount Manengouba, because these acid magmas, according to [62], require a significant period of time for their formation to be elaborated.

Calderas are places where several natural hazards occur, including volcanic eruptions and mass movements [63, 64]. According to [65], calderas are destructive volcanic forms because they cause pre-existing reliefs to collapse, unlike post-caldera cones and domes, which are constructive because pre-existing reliefs are put in place. Moreover, the volcanic formations that cover them favor the formation of fertile soils and the development of a plant cover of various species conducive to an agropastoral activity [16]. These are environments where hydrothermal activities and mineralization processes generally occur [57, 66, 67]. In this respect, it is clear that calderas have a strong educational value as they allow us to understand the complexity of certain craters in volcanic environments around the world. As

such, they allow us to understand the degree of fracturing of the ante-caldera substratum, the superposition of eruptive products and the slices of the flows at the ramparts and the post-eruptive geological processes. For this reason, calderas have been the subject of several studies in the field of geological heritage, notably the Mount Teide caldera in Spain, Aso caldera in Japan; Santorini caldera in Greece; Erta Alé and Fentale caldera in Ethiopia; Cha Das caldera in Cape Verde; Eboga, Santa Mbu, Lefo and Bambouto caldera in Cameroon [17, 68–72]. Thus, calderas are often the seat of later volcanic activities that leave exceptional geomorphological units with several values suitable for geotourism [33, 51, 52, 56, 73–75].

5. Conclusion

The Caldera of Mount Bambouto is a volcanic unit that formed at a period between 18.68 and 22 Ma. Its emplacement model is comparable to that of Cole et al. 2005. Its formation and evolution gave it a rather varied petography and a characteristic structure. Its classification according to the Caldeira DataBase of Geyer and Marti (2008) allows us to conclude that its type of collapse is piecemeal. Chemically, the caldera is alkaline with codes ALKAf, ALKAi, and ALKA_m. Furthermore, this caldera was formed through a continental rifting of extensional type, and their postcaldera protrusions give them Type-S and Type-MS. Moreover, it is a well-preserved caldera because its ridge lines are well observable.

The classification of the caldera of Mount Bambouto made within the framework of this work makes it possible to understand the similarities of this caldera with other calderas around the world on the one hand and to understand part of the global dynamics of the functioning of the Cameroon Volcanic Line on the other hand. Furthermore, this study contributes to elucidate the origin of the Cameroon Volcanic Line, which is still a subject of discussion among Cameroonian and foreign researchers today. Moreover, through this work, the Mount Bambouto Caldera is promoted next to the world scientific community that is still ignoring his existence.

Author details

Ghislain Zangmo Tefogoum^{1*}, David Guimolaire Nkouathio²,
Armand Kagou Dongmo² and Merlin Gountié Dedzo³

1 Department of Earth Sciences, University of Maroua, Maroua, Cameroon

2 Department of Earth Sciences, Faculty of Sciences, University of Dschang, Dschang, Cameroon

3 Department of Life and Earth Science, High Teacher Training College, University of Maroua, Maroua, Cameroon

*Address all correspondence to: zangmotefogoum@gmail.com

IntechOpen

© 2020 The Author(s). Licensee IntechOpen. This chapter is distributed under the terms of the Creative Commons Attribution License (<http://creativecommons.org/licenses/by/3.0>), which permits unrestricted use, distribution, and reproduction in any medium, provided the original work is properly cited. 

References

- [1] Newhall CG, Dzurisin D. Historical Unrest at Large Calderas of the World. Reston, USA: U.S. Geological Survey; 1988. p. 1109
- [2] Cole JW. Structural control and origin of volcanism in the Taupo volcanic zone, New Zealand. *Bulletin of Volcanology*. 1990;52:445-459
- [3] Yoshida T. The evolution of arc magmatism in the NE Honshu arc, Japan. *Tohoku Geophysical Journal*. 2001;36:131-249
- [4] Bosworth W, Burke K, Strecker M. Effect of stress fields on magma chamber stability and the formation of collapse calderas. *Tectonics*. 2003;22(4):1042. DOI: 10.1029/2002TC001369
- [5] Lyell C. A manual of elementary geology, II. In: London Macdonald GA (1972) *Volcanoes*. NJ: Prentice Hall Englewood Cliffs; 1855. 510p
- [6] Karatson D, Thouret JC, Moriya I, Lomoschitz A. Erosion calderas: Origins, processes, structural and climatic control. *Bulletin of Volcanology*. 1999;61(3):174-193. DOI: 10.1007/s004450050270
- [7] Karatson D, Thouret JC. Reply to the comment on the article “Erosion calderas: Origins, processes, structural and climatic control” by Alexandru Szakacs and Michael Ort. *Bulletin of Volcanology*. 2001;63(4):291-292. DOI: 10.1007/s004450100149
- [8] Geshi N, Acocella V, Ruch J. From structure- to erosion-controlled subsiding calderas: Evidence thresholds and mechanics. *Bulletin of Volcanology*. 2012;74(6):1553-1567. DOI: 10.1007/s00445-012-0617-x
- [9] Cole JW, Milner DM. Spinks. Calderas and caldera structures: A review. *Earth-Science Reviews*. 2005;69:1-26
- [10] Geyer A, Martí J. A Short review of our current understanding of the development of ring faults during collapse caldera formation. *Frontiers in Earth Science*. 2014; 2:1-13. doi: 10.3389/feart.2014.00022
- [11] Smith RL, Bailey RA. Resurgent cauldrons. *Memoir - Geological Society of America*. 1968;116:613-662
- [12] Geyer A, Folch A, Martí J. Relationship between caldera collapse and magma chamber withdrawal: An experimental approach. *Journal of Volcanology and Geothermal Research*. 2006;157(4):375-386
- [13] Lipman PW. Subsidence of ash-flow calderas: Relation to caldera size and magma-chamber geometry. *Bulletin of Volcanology*. 1997;59/3:198-218
- [14] Geyer A, Martí J. The new world wide collapse caldera data base (CCDB): A tool for studying and understanding caldera processes. *Journal of Volcanology and Geothermal Research*. 2008;175:334-354. DOI: 10.1016/j.jvolgeores.2008.03.017
- [15] Kagou DA, Wandji P, Pouclet A, Nkouathio DG, Tchoua FM. Le mont Manengouba (Ligne du Cameroun), Un volcan bénéfique, mais potentiellement dangereux, typologie des aléas et évaluation des risques naturels associés. *Africa Geoscience Review*. 2005;12(2):97-109
- [16] Anschuetz Kurt F, Merlan T. More than a Scenic Mountain Landscape: Valles Caldera National Preserve Land Use History. Gen. Tech. Rep. RMRS-GTR-196. U.S. Department of Agriculture, Forest Service, Rocky Mountain Research Station: Fort Collins, CO; 2007. 277p

- [17] Zangmo Tefogoum G, Kagou Dongmo A, Nkouathio DG, Wandji P, Gountié DM. Geomorphological features of the Manengouba Volcano (Cameroon line): Assets for potential geopark development. *Geohéritage*. 2014;**6**(3):225-239
- [18] Tchoua FM. Sur la formation des calderas des monts Bambouto (Cameroun). *Comptes rendus de l'Académie des Sciences*. 1972;**274**:799-801
- [19] Tchoua MF. Contribution à l'étude géologique et pétrographique de quelques volcans de la "Ligne du Cameroun" (Monts Manengouba et Bambouto) [Doctorate thesis]. France: University of Clermont-Ferrand; 1974. 337p + Biblio +75 figures
- [20] Youmen D. Evolution volcanologique, pétrologique et temporelle de la caldeira des monts Bambouto (Cameroun) [thèse]. Allemagne: Christian-Albrechts-Universität zu Kiel; 1994. 274p + 2 cartes
- [21] Youmen D, Schminke HU, Lissom J, Etame J. Données géochronologiques: mise en évidence des différentes phases volcaniques au Miocène dans les monts Bambouto (Ligne du Cameroun). *Science, Technology and Development*. 2005;**11**(1):49-57
- [22] Kagou DA. Le mont Manengouba: Evolution volcanologique, caractères magmatologiques et risques naturels; comparaison avec les monts Bambouto et Bamenda (Ligne du Cameroun). [Doctorate thesis], Yaoundé:d'Etat, Univ Yaoundé 1; 2006. 230p
- [23] Zangmo Tefogoum G, Kagou Dongmo A, Nkouathio DG, Wandji P. Typology of natural hazards and assessment of associated risks in the mounts Bambouto caldera (Cameroon line, West-Cameroon). *Acta Geologica Sinica*. 2009;**83**(5):1008-1016
- [24] Zangmo Tefogoum G, Nkouathio DG, Kagou Dongmo A, Wandji P, Gountie DM. Study of landslide hazards and assessment of associated risks in the West-Cameroon Highlands (Central Africa). In: *Proceedings of the 8th IAG International Conference on Geomorphology*; 27-31 August 2013; Paris (France). 2013. p. 654
- [25] Gountié Dedzo M, Nono A, Njonfang E, Kamgang P, Zangmo Tefogoum G, Kagou Dongmo A, et al. Le volcanisme ignimbritique des monts Bambouto et Bamenda (Ligne du Cameroun, Afrique Centrale): signification dans la genèse des caldeiras. *Bulletin de l'Institut Scientifique*, Rabat. 2011;**33**:1-15
- [26] Gountié Dedzo M, Njonfang E, Nono A, Kamgang P, Zangmo Tefogoum G, Kagou Dongmo A, et al. Dynamic and evolution of the mounts Bambouto and Bamenda calderas by study of ignimbritic deposits (West-Cameroon, Cameroon line). *Syllabus Review*. 2012a;**3**:11-23
- [27] Gountié Dedzo A, Kamgang P, Njonfang E, Zangmo Tefogoum G, Kagou Dongmo A, Nkouathio DG. Mapping and assessment of volcanic hazards related to the ignimbritic eruption by AMS in Bambouto Volcano (Cameroon volcanic line). *The Open Geology Journal*. 2012b;**6**:72-84
- [28] Gountié Dedzo M, Zangmo Tefogoum G, Chako Tchamabé B, Fozing EM, Njonfang E, Kamgang P. Mapping of pyroclastic density currents hazards and assessment of related risks by AMS technique in the West-Cameroon highlands: Case of Bambouto and Bamenda volcanoes. *Journal of Geography, Environment and Earth Science International*. 2020;**24**(2):39-60
- [29] Zangmo TG. Caractérisation volcanologique de quelques caldeiras de la Ligne Volcanique du Cameroun. Etude du géohéritage et évaluation

des risques naturels associés: Cas descaldeiras des monts Manengouba, Bambouto et Bamenda [Doctorat thèse]. Cameroun: Université de Dschang; 2016. 252p

[30] Zogning A, Ngouanet C, Tiofack O. The catastrophic geomorphological processes in humid tropical Africa: A case study of the recent landslide disasters in Cameroon. *Sedimentary Geology*. 2007;**199**:13-27

[31] Gountié DM. Cartographie, pétrographie, caractérisation géochimique et études magnétiques des ignimbrites miocènes des Monts Bambouto et Bamenda (Ouest-Cameroun): Conditions de mise en place et localisation de leurs centres d'émission. [Doctorate/PhD thesis]. Cameroun: Université Yaoundé I; 2012. 221p

[32] Morin S. Les dissymétries fondamentales des hautes terres de l'Ouest-Cameroun et leurs conséquences sur l'occupation humaine. Exemple des monts Bambouto. L'homme et la montagne tropicale. Bordeaux: Sépanrit ed; 1988. pp 49-51

[33] Zangmo Tefogoum G, Nkouathio DG, Kagou Dongmo A, Gountié DM. Typology of geotouristic assets along the south continental branch of the Cameroon volcanic line: Case of the mount Bambouto's caldera. *International Journal of Geoheritage and Parks*. 2019;**7**:111-128

[34] Morimoto N, Fabries J, Ferguson AK, Ginzburg IV, Ross M, Seifert FA, et al. Nomenclature of pyroxenes. *Mineralogical Magazine*. 1988;**52**:535-550

[35] Toteu SF, Van Schmus WR, Penaye J, Michard A. New U–Pb and Sm–Nd data from north-Central Cameroon and its bearing on the pre-Pan African history of Central Africa. *Precambrian Research*. 2001;**108**:45-73

[36] Nzolang C, Kagami H, Nzenti P, Hotz F. Geochemistry and preliminary Sr–Nd isotopic data on the Neoproterozoic granitoids from the Bantoum area, West Cameroon: Evidence for a derivation from a Paleoproterozoic to Archean crust. *Polar Geoscience*. 2003;**16**:196-226

[37] Nzolang C. Crustal evolution of the Precambrian basement in west Cameroon: Inference from geochemistry, Sr–Nd and experimental investigation of some granitoids and metamorphic rocks [PhD thesis]. Japan: Graduate School of Science and Technology, Niigata University; 2005. 207p

[38] Kagou Dongmo A, Nkouathio DG, Pouclet A, Bardintzeff J-M, Wandji P, Nono A, et al. The discovery of late Quaternary basalt on Mount Bambouto: Implications for recent widespread volcanic activity in the southern Cameroon line. *Journal of African Earth Sciences*. 2010;**57**:87-108

[39] Tokam A-PK, Tabod CT, Nyblade AA, Julia J, Wiens DA, Pasyanos ME. Structure of the crust beneath Cameroon, West Africa, from the joint inversion of Rayleigh wave group velocities and receiver functions. *Geophysical Journal International*. 2010;**183**:1061-1076

[40] Dunlop HM. Strontium isotope geochemistry and potassium-argon studies on volcanic rocks from the Cameroon line, West Africa [PhD thesis]. USA: The University of Edinburgh; 1983. 357p

[41] Fitton JG. Active versus passive continental rifting: Evidence from the west African rift system. *Tectonophysics*. 1983;**94**:473-481

[42] Fitton JG. The Cameroon line, West-Africa and its bearing on the origin of oceanic and continental alkaline volcanism. *Geological Society, Special Publication*. 1987;**30**:273-291

- [43] Halliday AN, Dickin AP, Fallick AE, Fitton JG. Mantle dynamics: A Nd, Sr, Pb and O isotopic study of the Cameroon line chain. *Journal of Petrology*. 1988;**29**(1):181-211
- [44] Wandji P. Le volcanisme récent de la plaine du Noun (Ouest- cameroun). *Volcanologie, Pétrologie, Géochimie et Pouzzolanité* [Doctorate thesis]. Yaoundé, Cameroun: d'Etat Univ. Yaoundé 1; 1995. 295p + 3 planches + 1 carte.
- [45] Nana R. Pétrologie des Péridotites en enclaves dans les basaltes alcalins récents de Nyos: Apport à la connaissance du manteau supérieur de la Ligne du Cameroun [Doctorate thesis]. Yaoundé, Cameroun: d'Etat. Univ. Yaoundé 1; 2001. 284p
- [46] Nkouathio DG. Evolution tectono-magmatique et volcanologique de la Ligne du Cameroun: comparaison d'un volcanisme de graben (plaine de Tombel) et d'un volcanisme de horst (Monts Bambouto) [Doctorate d'Etat thesis]. Yaoundé, Cameroun: Univ Yaoundé 1; 2006. p. 231
- [47] Kamgang P, Njonfang E, Nono A, Gountié Dedzo M, Tchoua FM. Petrogenesis of a silicic magma system: Geochemical evidence from Bamenda Mountains, NW Cameroon, Cameroon volcanic line. *Journal of African Earth Sciences*. 2010;**58**:285-304
- [48] Pouclet A, Kagou Dongmo A, Bardintzeff JM, Wandji P, Chakam Tagheu P, Nkouathio DG, et al. The Mount Manengouba, a complex volcano of the Cameroon line: Volcanic history, petrological and geochemical features. *Journal of African Earth Sciences*. 2014;**97**:297-321. DOI: 10.1016/j.jafrearsci.2014.04.023
- [49] Nono A, Nkouathio DG, Gountié Dedzo M, Njonfang E, Kagou Dongmo A, Tchoua FM. Zonal and vertical variations in welding rate and composition of ignimbrites in the Bambouto volcano (Cameroon line, central africa): Volcanological importance. *Geophysical Research Abstracts*. 2003;**5**:14541
- [50] Gountié Dedzo M, Kamgang P, Njonfang E, Zangmo Tefogoum G, Nkouathio DG, Kagou DA. Remnants blocks of pyroclastic surge deposits in Bambili, Cameroon volcanic line: New insights into the lithostratigraphy of Mount Bamenda. *British Journal of Applied Science & Technology*. 2015;**7**(6):585-596. DOI: 10.9734/BJAST/2015/15958
- [51] Zangmo Tefogoum G, Kagou Dongmo A, Nkouathio DG, Gountié Dedzo M, Kamgang P. The volcanic geoheritage of the Mount Bamenda calderas (Cameroon line): Assessment for geotouristic and geoeducational purposes. *Geoheritage*. 2017;**9**(3):255-278. DOI: 10.1007/s12371-016-0177-0
- [52] Zangmo Tefogoum G, Quesada-Román A, Pérez-Umaña D. Geomorphosites inventory in Eboga volcano, Cameroon: Contribution for geotourism promotion. *Géomorphologie:Relief, Processus, Environnement*. 2020;**26**(1):19-33. DOI: 10.4000/geomorphologie.14006
- [53] Nankap Ekodo Fouda V. Cartographie et caractérisation de la caldeira du mont Bangou (Ligne Volcanique du Cameroun): Impact sur les risques naturels [Mémoire de Master]. Dshang, Cameroon: University of Dschang; 2016. p. 90
- [54] Zangmo Tefogoum G. Les caldeiras du mont Manengouba et des monts Bambouto: Études comparatives et évaluation qualitative et quantitative des risques naturels associés [Master thesis]. Dshang, Cameroun: University of Dschang; 2007. p. 125
- [55] Holohan EP, Troll VR, Walter TR, Münn S, McDonnell S, Shipton ZK.

- Elliptical calderas inactive tectonic settings: An experimental approach. *Journal of Volcanology and Geothermal Research*. 2005;**144**:119-136. DOI: 10.1016/j.jvolgeores.2004.11.020
- [56] Costa FL. Volcanic geomorphosites assessment of the last eruption, on April to May 1995, within the Natural Park of Fogo Island, Cape Verde. *GeoJournal of Tourism and Geosites*. 2011;**8**:167-177. DOI: 10.1016/j.ijgeop.2019.06.003
- [57] Lipman PW. Calderas. In: Sirgurdsson H, Houghton BF, McNutt SR, Rymer H, editors. *Encyclopedia of Volcanoes*. New York: Academic Press; 2000. pp. 643-662
- [58] Roche O, Druitt TH, Merle O. Experimental study of caldera formation. *Journal of Geophysical Research*. 2000;**105**:395-416. DOI: 10.1029/1999JB900298
- [59] Vincent PM. Les caldeiras: Dans Bourdier J-L, Bovin P, Gourgaud A, Camus G, Lenat J-F, le volcanisme. *Volcanic Research Center of Clermont-Ferrand*, edition. BRGM; 1994. n°25, pp. 181-195
- [60] Sutawidjaja IS. IGnimbrite analyses of Batur caldera, Bali, based on ¹⁴C dating. *Jurnal Geologi Indonesia*; 2009;**4**:189-202
- [61] Lipman PW, Zimmerer MJ, McIntosh WC. An ignimbrite caldera from the bottom up: Exhumed floor and fill of the resurgent bonanza caldera, southern Rocky Mountain volcanic field, Colorado. *Geosphere*. 2015;**11**(6):1902-1947. DOI: 10.1130 / GES01184.1
- [62] Wood CA. Calderas: A planetary perspective. *Journal of Geophysical Research*. 1984;**89**(B10):8391-8406
- [63] Merle O, Michon L, Bachèlery P. Caldera rim collapse: A hidden volcanic hazard. *Journal of Volcanology and Geothermal Research*. 2008;**177**:525-530
- [64] Zangmo Tefogoum G, Nkouathio DG, Kagou Dongmo A, Gountié Dedzo M, Kamgang P, Nono A. Study of multi-origin hazards and assessment of associated risks in the lefo caldera (Bamenda volcano, Cameroon line). *International Journal of Geosciences*. 2014b;**5**:1300-1314
- [65] Joyce E. Australia's Geoheritage: History of study, a new inventory of geosites and applications to geotourism and geoparks. *Geoheritage*. 2010;**2**(1-2):39-56
- [66] Stix J, Kennedy B, Hannington M, Gibson H, Fiske R, Mueller W, et al. Caldera-forming processes and the origin of submarine volcanogenic massive sulfide deposits. *Geology*. 2003;**31**:375-378
- [67] Mueller WU, Stix J, Corcoran PL, Daigneault R. Subaqueous calderas in the Archean Abitibi greenstone belt: An overview and new ideas. *Ore Geology Reviews*. 2009;**35**:4-46
- [68] Gaudru H. Reunion Island, France: Piton de la Fournaise Volcano. In: Erfurt-Cooper P, Cooper M, editors. *Volcano & Geothermal Tourism: Sustainable Geo-Resources for Leisure and Recreation*. Washington, DC, USA: Earthscan Publishing; 2010. pp. 54-56
- [69] Erfurt-Cooper P. The importance of natural geothermal resources in tourism. In: *Proceedings World Geothermal Congress*; 25-29 April 2010; Bali, Indonesia. 2010. p. 10
- [70] Newsome D, Dowling R. Geoheritage and Geotourism. In: Reynard E, Briha J, editors. *Geoheritage: Assessment, Protection, and Management*. Amsterdam, Netherlands: Elsevier; 2018. pp. 305-321. DOI: 10.1016/B978-0-12-809531-7.00017-4

[71] Williams F. Safeguarding geoheritage in Ethiopia: Challenges faced and the role of Geotourism. *Geoheritage*. 2020;**12**:31. DOI: 10.1007/s12371-020-00436-9

[72] Zangmo Tefogoum G, Kagou Dongmo A, Nkouathio DG, Wandji P. Geomorphological features of the manengouba volcano (Cameroon line): Assets for geotourism and other anthropogenic activities. In: Errami E, Brocx M, Semeniuk V, editors. *From Geoheritage to Geoparks. Geoheritage, Geoparks and Geotourism*. Switzerland: Springer International Publishing; 2015. pp. 183-198. DOI: 10.1007/978-3-319-10708-0_13

[73] Dóniz-Páez J, Guillén-Martín C, Romero-Ruiz C, Coello-De La Plaza E. Geomorphosites, volcanism and geotourism: The example of cinder cones of Canary Islands (Spain). In: *Proceedings of the International Conference on Geoheritage and Geotourism*, Lisbon. 2010. pp. 23-24

[74] Nomikou P, Carey S, Papanikolaou D, Pyle D, Parks M, Bell K, et al. The volcanic morphology of the intra-caldera Kameni islands, Santorini, based on high resolution bathymetry and LiDAR data. In: *Proceeding Abstracts of the 8th International Conference on Geomorphology*, Paris, France. 2013. p. 235

[75] Pratomo I, Permanadewi S. Batur caldera complex, the first land-form volcanic laboratory in Indonesia. In: *Proceeding Abstracts of the 8th International Conference on Geomorphology*; 27-31 August 2013: Paris, France. 2013. p. 570

Submarine Stratovolcano Peperite Syn-Formational Alteration - A Case Study of the Oligocene Smrekovec Volcanic Complex, Slovenia

Polona Kralj

Abstract

The Oligocene Smrekovec Volcanic Complex is a remnant of a submarine composite stratovolcano with a complex succession of lavas, autoclastic, pyroclastic, syn-eruptive resedimented volcanoclastic and siliciclastic deposits was a favourable environment for the development of peperites. Despite very complex alteration related to the stratovolcano-hosted hydrothermal system with a deep igneous source, locally elevated geothermal gradients and superimposed hydrothermal/geothermal regimes controlled by the emplacement of a shallow intrusive body, authigenic minerals in peperites - particularly pumpellyite and actinolite - show higher temperature stability ranges than those in the underlying and overlying volcanic deposits irrespectively of their lithofacies, porosity and permeability. The formation of authigenic minerals in peperites, such as laumontite, pumpellyite, epidote, prehnite or actinolite, was apparently controlled by ephemeral and localised high-temperature regimes originating from the parent lava flow. Heated pore waters in the host sediment that could have undergone local mixing with deuteritic fluids circulated in peperites until thermal gradients persisted, and were the cause of alteration of juvenile clasts and the mingling sediment. The development of pumpellyite required a suitable precursor - fine-grained volcanic ash.

Keywords: peperites, autoclastic deposits, hydrothermal alteration, submarine composite stratovolcano, Oligocene volcanism

1. Introduction

Peperite is a volcanoclastic rock related to *in situ* disintegration of magma intruding and mingling with the host sediment that is unconsolidated or poorly consolidated, and typically wet [1]. Peperite commonly occurs along the contacts between intrusions and wet sediments and at the base of lava flows overriding or indenting wet sediments [2–4]. The composition and texture of magmas involved in the formation of peperites may range from basaltic to rhyolitic and aphanitic to porphyritic, respectively, and the mingling sediments may have rather diverse texture, grain size and composition. As the availability of wet unconsolidated sediments is

a prerequisite for the development of peperites they have been commonly encountered in submarine environments with contemporaneous volcanic activity and sedimentation, such as volcanic arcs and back-arc basins [5–9].

The formation of peperite is a complex process and depends, in general, on the magma and host sediment properties, their mass ratio and total volume of pore water heated during their contact and mingling. For magma, the most relevant properties are composition, the content of volatiles and rheology, and for the host sediment that is texture and water-saturation. An important stage in the process of peperite formation is magma disintegration that can be brittle or ductile and attained by quenching, hydromagmatic explosions, surface tension effects, mechanical stress related to the movement of magma and density contrast to the sediment, and magma-sediment shearing. The contact of magma and wet sediment causes heating and expansion of pore waters, and the resulting disruption of coherence and sometimes fluidisation and shear liquefaction of the host sediment facilitate dispersion of clasts derived from magma away from the site of formation. The intricate processes of intermixing finally result in the formation of peperite [4, 10–14].

Two textural types of peperite have been recognised on the basis of shape of clasts derived from magma. Blocky peperite consists of sharply angular, blocky or platy clasts while in globular or fluidal peperite lensoidal, lobate, ameoboid or bulbous clasts occur [5]. The term peperitic hyaloclastite refers to a peperitic rock in which magma fragmentation is largely the result of quenching, mechanical stress, or pore-water steam explosions [4, 12].

Several detailed studies of peperite occurrence and formation have been carried out in the system of Pannonian basins, in particular, in the Tokaj Mountains [15] and Western Hungary at Hajagos-hegy, Kissomlyó and Ság-hegy [9, 16, 17]. Subaqueous Mioocene rhyolitic dome-cryptodome complex outcropping at Pálháza, the Tokaj Mountains, is surrounded by a carapace of hyaloclastites, hyaloclastite breccia, and globular and blocky peperite. Closely packed peperite zone with jigsaw-fit juvenile clasts formed next to a rhyodacitic body, and toward the boundary with the host sediment, a transition into the clast-rotated and clast dispersed zones of peperite has been recognised [17]. In the volcanic conduits, vents and crater lakes of phreatomagmatic volcanoes in Mio/Pliocene volcanic fields of Western Hungary globular and blocky peperite occur together regardless of the grain-size and texture of host sediment [15]. The study supports conclusions that the formation of different peperite textures depends on several factors, e.g., break-down of vapour films at the magma/wet-sediment interface, viscosity of magma and/or magma flux rate, a change in temperature, microlite crystallinity and gas content of magma, thermal properties of the host sediment and steam explosions [18–22].

The alteration of peperite is common and may begin contemporaneously to its formation owing to the release of deuteric magmatic fluids and volatiles, transfer of heat from magma or lava to the host sediment and heating of pore-waters therein. Large magma intrusions can cause contact metamorphism along the margins and initiate or modify fluid circulation on a several-kilometre-scale that may last a long period of time after the peperite formed [23]. Lavas undergo more rapid cooling, and effective circulation of heated pore-waters can be attained only locally along the contacts with the wet sediment until thermal gradients exist. Most often, the formation of secondary minerals such as carbonates, Fe-oxides and silica along the contacts of juvenile clasts has been reported [23–27].

The Oligocene Smrekovec Volcanic Complex (**Figures 1 and 2**) located in the south-westernmost extending of the Tertiary system of Pannonian basins, is a remnant of a submarine stratovolcano. Prior to erosion, and tectonic dissection and displacement along the Periadriatic Line, the stratovolcano extended in an area

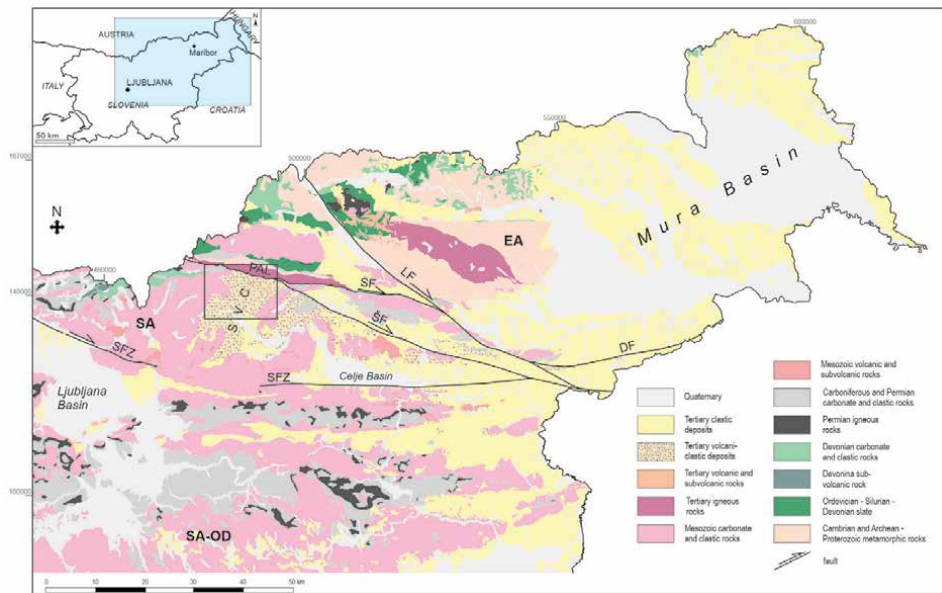


Figure 1. Simplified geological map of northern Slovenia after [28, 29] with the study area (framed) in the Smrekovec volcanic complex (SVC). PAL - Periadriatic Line; LF - Lavanttal (Labot) fault; SF - Smrekovec fault; SF̂ - Soštanj fault; DF - Donat fault; SFZ - Sava fault zone; SA - Southern Alps; EA - Eastern Alps; OD - Outer Dinarides.

of over 1000 km². Similar large submarine volcanoes have been encountered in modern and ancient environments worldwide (e.g., [30–32]), and also, within the Carpathian-Pannonian region [33–35].

The stratovolcano is composed of a succession of lavas and shallow intrusive bodies, and autoclastic, pyroclastic, resedimented volcanoclastic and mixed siliciclastic-volcanoclastic deposits. Lithofacies associations change from proximal, medial and distal zones over a distance of 0-2 km, 2-5 km and 5-20 km, respectively. The proximal zone is dominated by lavas and autoclastic deposits, and in the medial-zone pyroclastic and syn-eruptive resedimented volcanoclastic deposits become abundant. The distal zone is dominated by fine-grained pyroclastic, syn-eruptive resedimented volcanoclastic and siliciclastic deposits.

Peperites are the most abundant in medial-zone lithofacies associations. The mingling lavas range in composition from andesitic to rhyodacitic and the host sediments are mixed siliciclastic-volcanoclastic silts and calcareous muds or volcanoclastic deposits of various texture and grain size, i.e., fine- and coarse-grained tuffs, lapilli tuffs, volcanoclastic breccias [36]. Blocky and fluidal peperite and peperitic hyaloclastite are common in occurrence although their formation has not been related to the texture, grain size or porosity of the host sediment.

The stratovolcano-hosted hydrothermal system with convective-advective flow regime developed, and as a result, alteration minerals formed, the most widespread assemblage being laumontite, chlorite, ordered mixed layer chlorite-smectite, quartz and albite. Despite of complex alteration that affected lithofacies associations, peperites very often contain authigenic minerals with typically higher temperature stability ranges than those in the adjacent underlying or overlying volcanoclastic deposits [37, 38]. Their formation must have occurred contemporaneously to the development of the host rock itself owing to thermal gradients originating from the parent lava or shallow intrusive body and geochemical gradients related local circulation of heated pore waters and deuteric fluids.

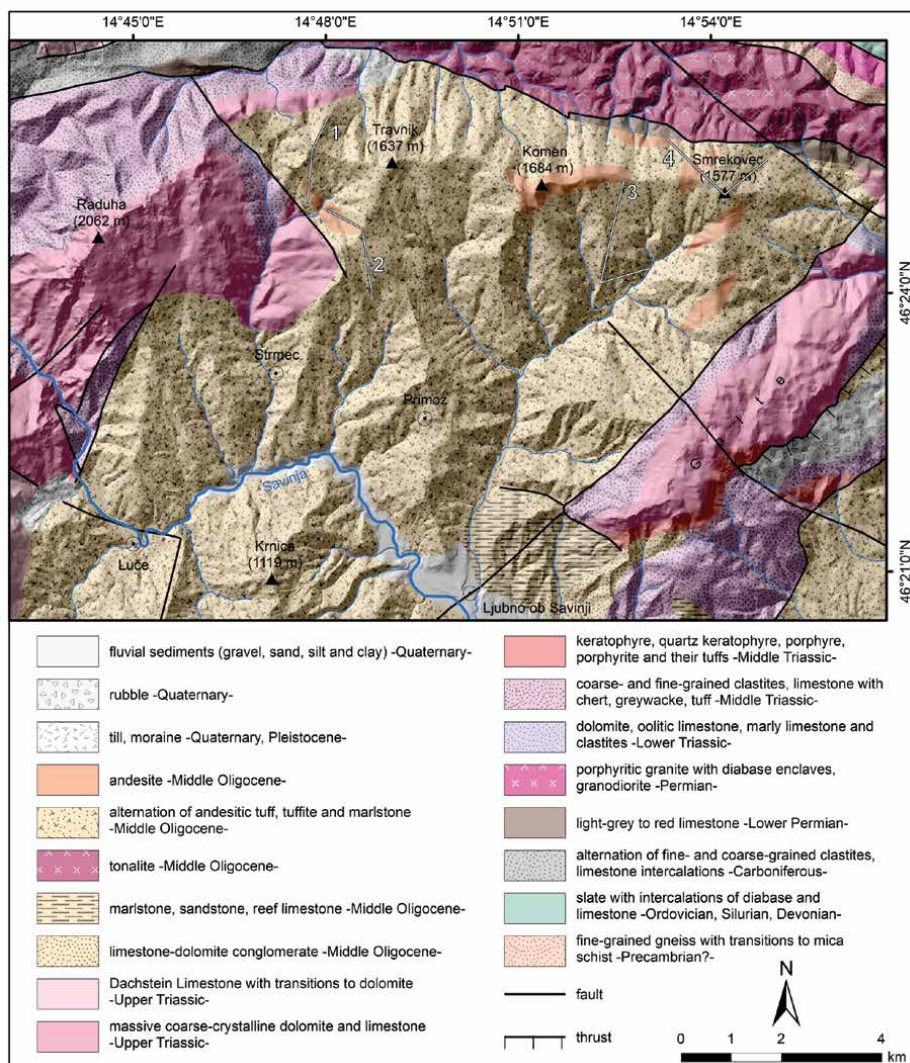


Figure 2. The study area (northern Smrekovec Volcanic Complex) after [28, 29] and the sections 1 (Presečnik), 2 (Javorec), 3 (Krnas) and 4 (Smrekovec G34). The Kramarica Sill is about 200 m thick and located at the base of the section 4 along the outcrops of lower Permian limestone.

As the Smrekovec Volcanic Complex is a remnant of an ancient submarine composite stratovolcano the processes of alteration of peperites described herein could be recognised in, and applied to, similar environments worldwide.

2. Sampling and analytical techniques

The sampling was performed in the entire area of the Smrekovec Volcanic Complex, although particularly detailed study has been carried out in two sections Krnas, and Smrekovec G34 (**Figure 2**). Lithofacies was determined by field observation, and chemical, mineralogical and petrographic analysis. Over 900 thin sections have been inspected in detail.

Alteration minerals were analysed by X-ray diffraction (XRD) techniques in altogether 260 samples. Zeolites and related calcium aluminosilicate minerals

were determined in whole-rock powdered samples. Clay minerals were analysed in oriented samples using slurries ($<2\ \mu\text{m}$) dispersed on glass slides and undergoing standard procedures including air-drying and solvation in ethylene glycol. The XRD analysis was performed using a Philips diffractometer PW 3719 and a goniometer PW 1820, owned by the Department of Geology, Faculty of Natural Sciences and Technology, University of Ljubljana. Machine settings for all analysed samples were as follows: generator operated at 40 kV and 30 mA using $\text{CuK}\alpha$ radiation (wavelengths $K_{\alpha 1} = 1.54056\ \text{\AA}$ and $K_{\alpha 2} = 1.54439\ \text{\AA}$), Ni filter, with automatic divergence slit and monochromator on. Scanning rate was $2^\circ 2\theta/\text{min}$; scanning range amounted to $2^\circ 2\theta - 70^\circ 2\theta$ for powdered samples and $2^\circ 2\theta - 45^\circ 2\theta$ for oriented samples. Digital data were processed using peak-fitting program X'Pert HighScore Plus 4.0. Semi-quantitative analysis was performed by the program using the data base, internal standard rock samples and bulk chemical composition of powdered samples.

Detailed mineral studies were performed on 9 polished thin sections using a scanning electron microscope (SEM) Jeol JSM-6490 equipped with an energy dispersive spectrometer (EDS) INCA Oxford 250, and located at Geological Survey of Slovenia. Elemental analyses were performed in thin sections having a thickness of $40\ \mu\text{m}$ and uncovered polished upper surface, at accelerating voltage of 15 kV using a defocused electron beam of $20\ \mu\text{m}$ in diameter, with a current of 10 nA and a counting time of 20 s. Synthetic and natural standards were used for calibration.

Chemical analysis of 150 bulk-rock samples of lavas and shallow intrusive bodies was performed in AcmeLabs, Vancouver, Canada, and Actlabs Activation Laboratories Ltd. Ontario, Canada. Major and trace elements were determined by a combination of X-ray fluorescence (XRF), inductively coupled plasma source (ICP) and mass spectroscopy (MS) analytical techniques.

3. Geological setting and the studied sections

In northern Slovenia, there are four large tectonic units: the Eastern Alps, the Southern Alps, the Outer Dinarides and the south-westernmost extending of the Tertiary system of Pannonian basins [28, 29] with the Smrekovec Volcanic Complex (**Figure 1**). The most outstanding geological structure is the Periadriatic Line (PAL), a complex regional fault system which represents in palinspastic reconstructions a shear zone developed by Late Cretaceous to Paleogene subduction of the European plate below the African plate [39, 40]. In the Eocene ($\sim 45\ \text{Ma}$) the subduction transformed into collision although the convergence continued during the Oligocene and resulted in break off of the southeast-dipping European slab beneath the Alps that generated magmatism along the PAL [41, 42].

The related Oligocene (28-22 Ma) volcanic activity occurred in the Smrekovec Basin (**Figure 3**) that had been subsided within the Permian and Triassic clastic and carbonate successions [43]. Tertiary sedimentation began in Late Eocene in fluvial, limnic and shallow-marine depositional environment and changed to outer neritic and bathyal during the Oligocene time [29, 43]. In a middle bathyal environment characterised by sedimentation of organic-rich clayey silts [43], simultaneous volcanic activity created a composite stratovolcano. Magmas had calc-alkaline and medium-K affinity and formed a suite ranging in composition from basaltic andesite to dacite [44–46]. Volcanic activity had entirely submarine character and after its cessation, the Upper Oligocene to Early Miocene (Egerian) sedimentation continued with fossiliferous marine clayey silt [29]. The stratovolcano hosted hydrothermal system with a deep igneous source and convective-advective flow of hydrothermal fluids (**Figure 3**).

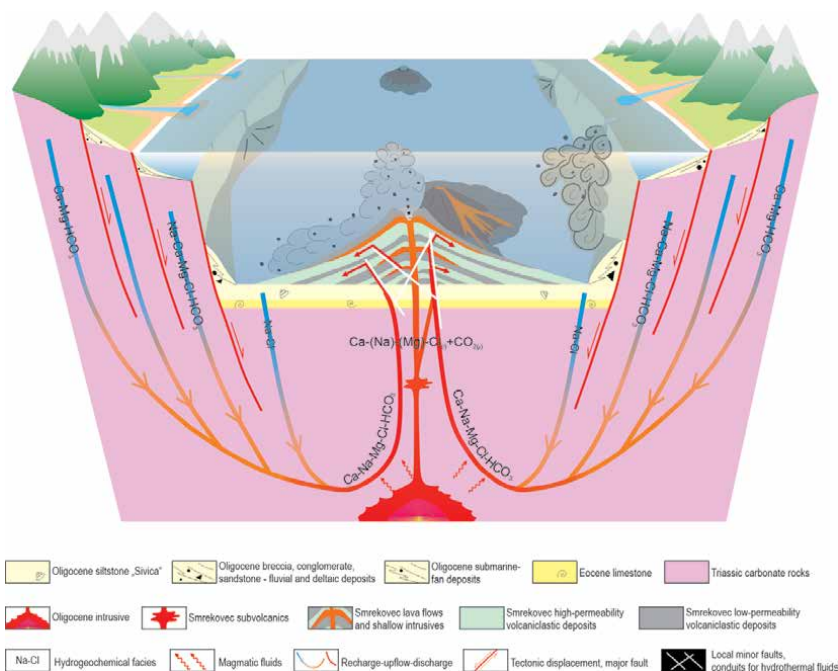


Figure 3.

A conceptual model of the Smrekovec Basin with the stratovolcano and volcanic-hydrothermal system with a deep igneous source of heat and convective-advective flow regime. Hydrothermal fluids originating from heated and chemically modified surface and marine waters ascended through fracture systems and when reached the stratovolcano edifice they outflowed laterally and downward, preferentially through high-permeability layers. High-permeability layers underwent more extensive alteration and the authigenic minerals (e.g., laumontite, prehnite) have higher temperature stability ranges than those in the adjacent underlying or overlying low-permeability layers (e.g., clinoptilolite, heulandite, analcime).

Late Miocene tectonic activity along the Periadriatic Line dissected the stratovolcano edifice and displaced its northern sector in the south-eastern direction on a 100 km scale [29]. The remaining Smrekovec Volcanic Complex probably encompasses about one quarter of the original stratovolcano edifice [36], and scarce outcroppings of volcanic rocks occurring north of the Šoštanj fault (**Figure 1**) are the assumed displaced remnants [47]. South of the Šoštanj fault Tertiary volcanic deposits occur in the Celje Basin, and together with the Smrekovec Volcanic Complex they are united in a lithostratigraphic unit termed the Smrekovec Series [29].

The succession of lavas, shallow intrusive bodies, and autoclastic, pyroclastic, syn-eruptive resedimented volcanoclastic and mixed siliciclastic-volcanoclastic rocks is over 2500 m thick, and at least 1000 m of the overlying deposits have been eroded already. In the northwest of the complex, the oldest proximal zone lithofacies associations overlie basal fossiliferous siltstone, limestone and calcarenite. As the strata, in general, verge toward the southeast, the oldest lavas can be traced over a distance of about 2 km to the east and south although their thickness changes (**Figure 4**). Younger, medial-zone lithofacies associations occur in the east and south and their development is typically complex (**Figures 5 and 6**). The Kramarica Sill is the largest shallow intrusive body in the Smrekovec Volcanic Complex. Its emplacement was related to the formation of a new vent along the Periadriatic Line, some 6 km east of the older one located northwest of Travnik (**Figure 2**).

A detailed study of lithofacies and alteration has been carried out in two sections composed of medial-zone lithofacies associations, namely Krnes and Smrekovec

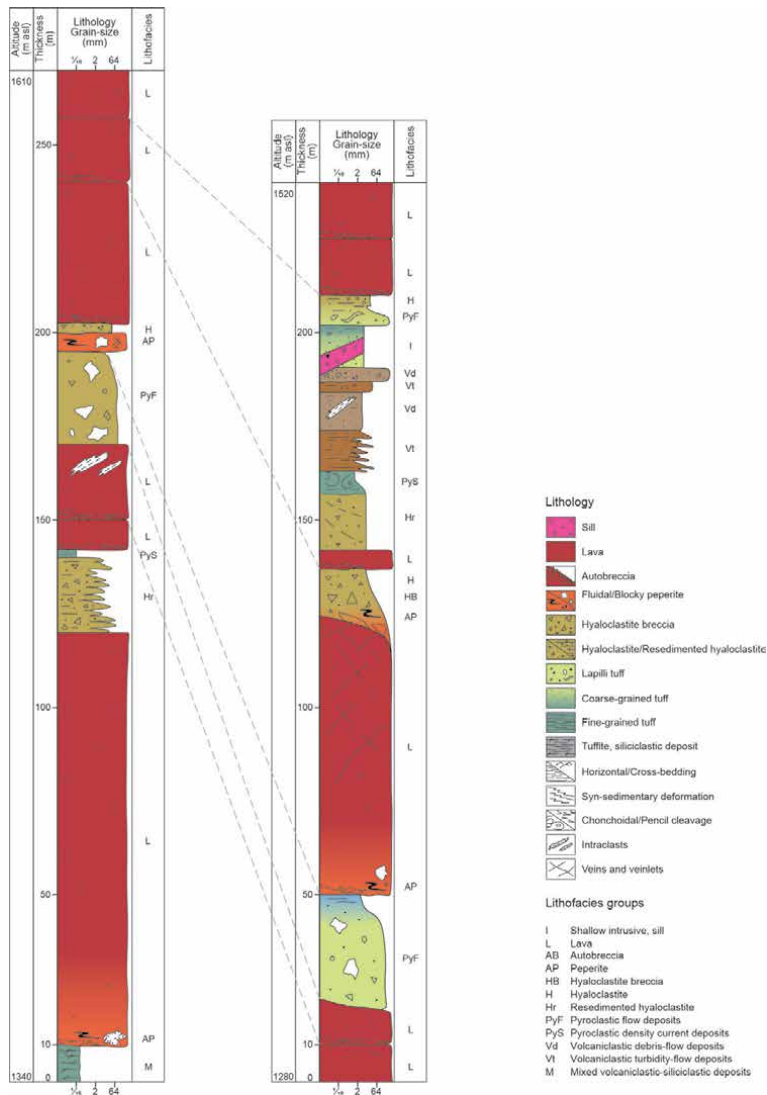


Figure 4. The sections Presečník (left) and Javorec (right) situated in the proximal zone show the change in thickness of lithofacies within a distance of 1.5–2 km toward the southeast.

G34, attaining 400 m and 470 m, respectively (Figures 5 and 6). The section Krnes consists of complexly alternating pyroclastic, autoclastic and syn-eruptive resedimented volcaniclastic deposits with only two thicker lava flows attaining some 25 m and 70 m. Pyroclastic deposits are dominated by fine-grained cross-bedded and horizontally bedded tuffs related to pyroclastic density currents [36], similar to the occurrences described by [48–51]. Pyroclastic flow deposits [36] are less abundant and commonly consist of basal massive lapilli tuff and the overlying stratified coarse- and fine-grained tuff. Syn-eruptive resedimented deposits are abundant and comprise volcaniclastic debris-flow deposits and volcaniclastic turbidity flow deposits. Hyaloclastites and resedimented hyaloclastites are subordinate in occurrence but still relatively abundant. Siliciclastic silts are very rare and occur in thin, up to some dm thick stratified units. There are nine peperite deposits occurring at the base and along terminal parts of smaller lava flows.

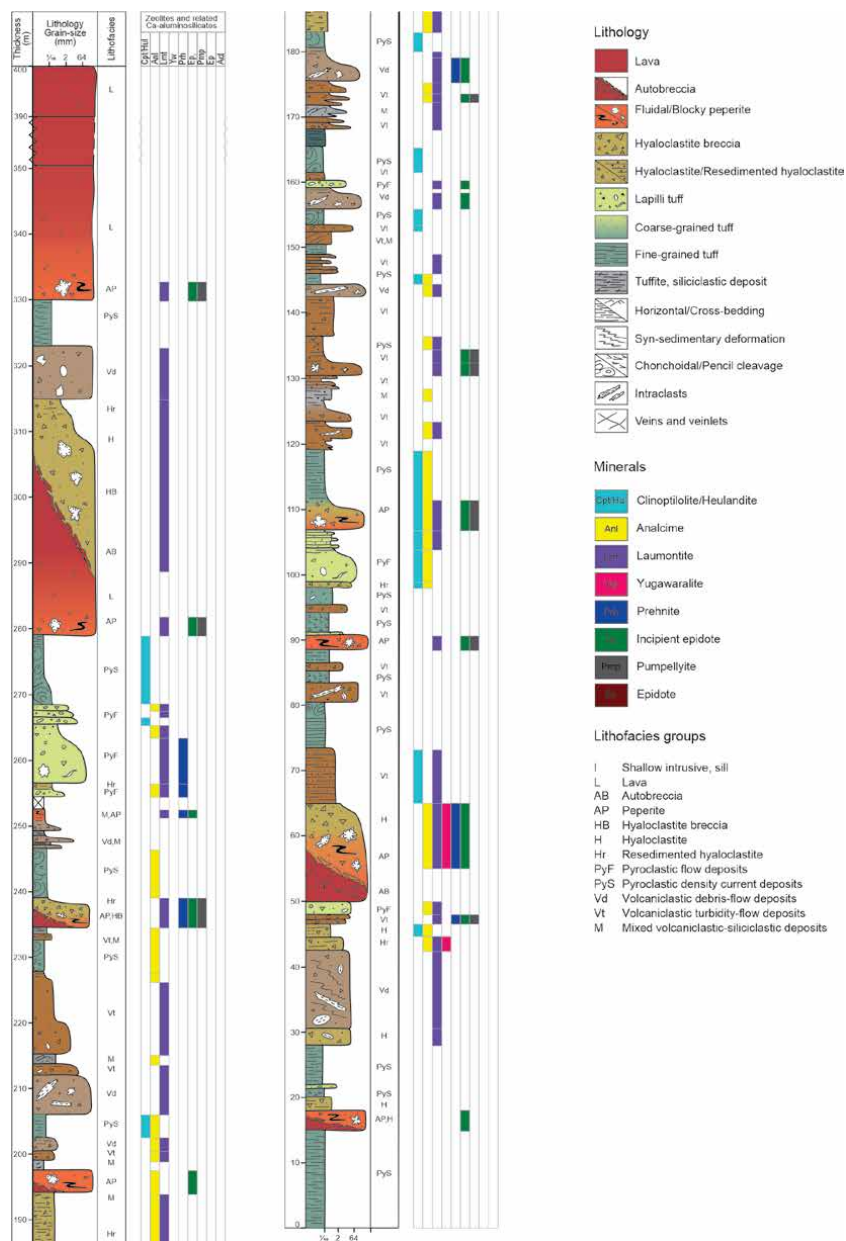


Figure 5. Lithofacies and the principal alteration minerals in the medial-zone section Krnes.

The section Smrekovec G34 begins in the Kramarica Sill (**Figure 6**) and comprises three thicker lava flows attaining some 35 m, 90 m and over 50 m, respectively. Based on the occurrence of yugawaralite [37, 52] and with respect to the middle bathyal water depths, the Kramarica Sill was emplaced about 600-800 m below the then surface of stratovolcano. Pyroclastic density current deposits are far less abundant than in the section Krnes and pyroclastic flow deposits are relatively abundant only in the upper half of the section. Syn-eruptive resedimented volcaniclastic deposits are dominated by volcaniclastic debris-flow deposits. Hyaloclastites and resedimented hyaloclastites are less abundant than in the section Krnes. Altogether fifteen peperites have been recognised and most of them are related to terminal parts of lava flows.

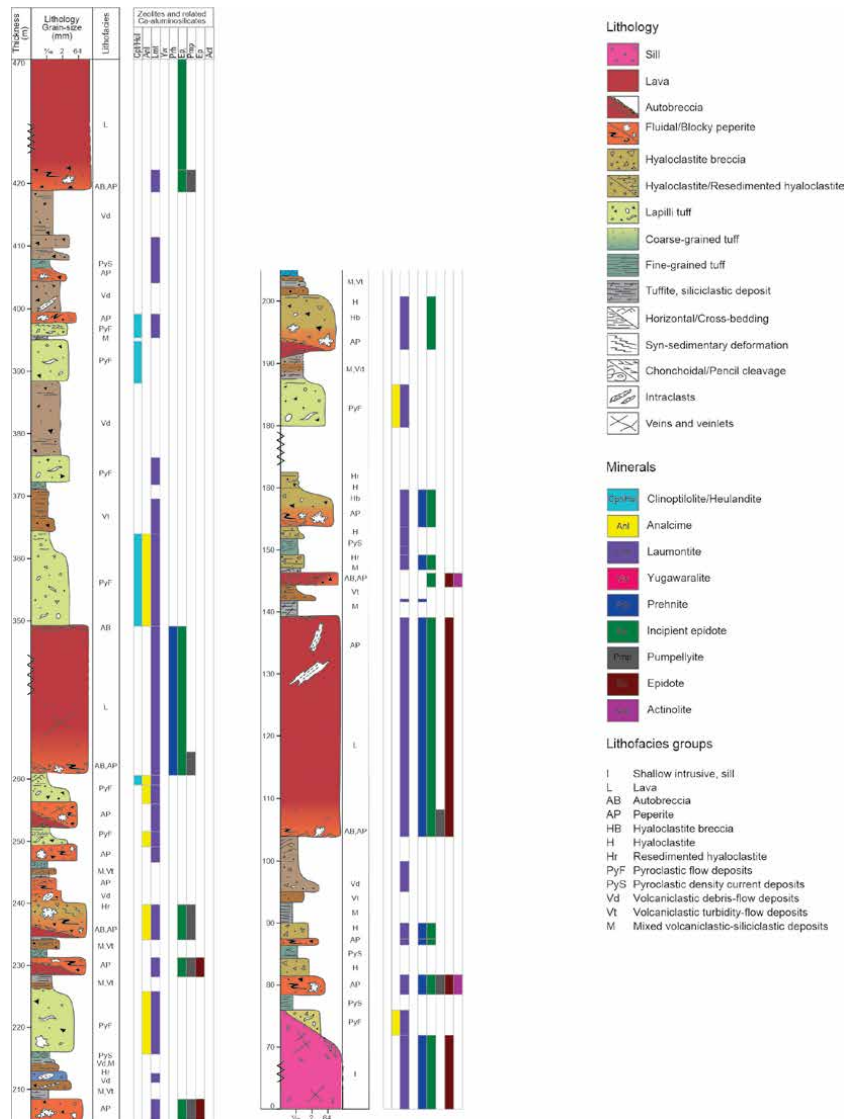


Figure 6. Lithofacies and the principal alteration minerals in the medial-zone section Smrekovec G34.

4. Occurrence, texture and composition of peperites

In the study area peperites often occur as sheet-like bodies along basal contacts of lava flows and the underlying wet sediments (Figure 7A, B). Sometimes they are encountered on the top of thin lava flows burrowing into a several m thick sequence of fine-grained sediments or along terminal parts of lava flows where they form irregularly shaped or lobate bodies. Peperite domains range in volume from less than a few m³ to several 10s m³ and sometimes they can only be some cm thick. The mingling wet sediment was commonly fine-grained volcanic ash or siliciclastic and carbonaceous silt. More rarely peperites have been recognised in association with coarser-grained volcaniclastic deposits, and most often they occur at the base of lava flows.

The most widespread type is blocky peperite whilst globular peperite and peperitic hyaloclastite are rarer in occurrence. Along the pathway of a single lava

flow overriding the same layer of wet sediment the volume and texture of peperite have commonly changed. On a macroscopic scale, an initiation of peperite development along the contact of lava and fine-grained wet sediment was deformation of the underlying strata and laminae, their disintegration into clasts (**Figure 7A**) and subsequent incorporation into the lava flow where the clasts have undergone further deformation (**Figure 7B**). Terminal parts of lava flows commonly consist of blocky peperite. A clear zonation of closely packed blocky peperite next to lava and dispersed blocky peperite closer the host sediment has not been identified. Most often irregularly distributed domains of the mentioned textural types have been encountered. Some juvenile clasts may be jigsaw-fit and in some peperite domains, a part of the mingling sediment may occur in the form of clasts (**Figure 8A, B**).

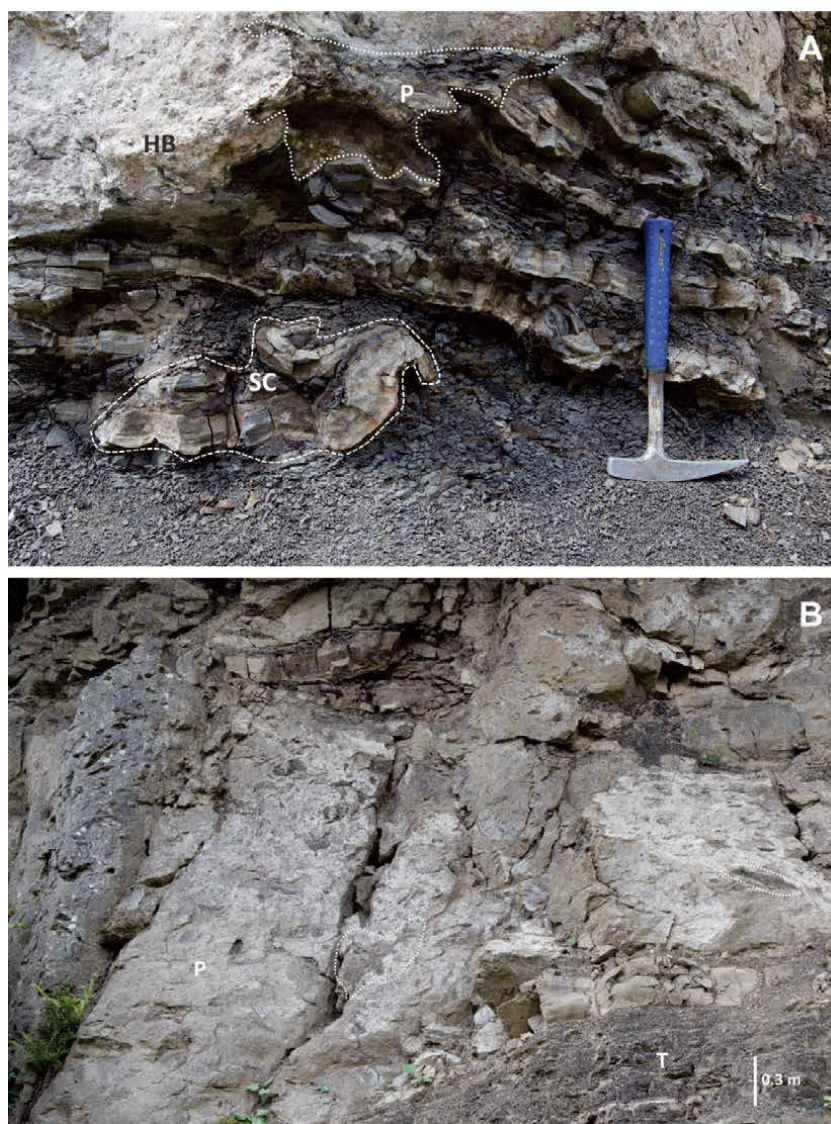


Figure 7. A, disrupted stratified fine-grained tuff underlying hyaloclastite breccia and peperite. The dotted and dashed lines mark a peperite domain (P) and a separated clast composed of disrupted and convoluted stratified tuff (SC), respectively. Hammer (33 cm) is for scale; B, peperite (P) with abundant clasts of dark-grey fine-grained tuff. The dotted lines mark two larger deformed clasts originating from the underlying deposit (T).

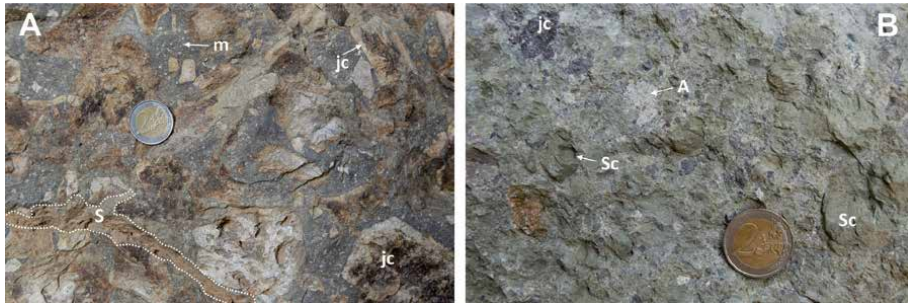


Figure 8. Blocky peperite. A, larger angular juvenile clasts (jc) and fluidised sediment (S, dotted area) in matrix (m) composed of smaller juvenile clasts and fine-grained siliciclastic sediment. Coin (2.5 cm) is for scale; B, juvenile clasts (jc) and the clasts of fine-grained tuff (Sc) in matrix composed of an intimate mixture of the host sediment and juvenile clasts. The matrix is locally extensively altered (A) to laumontite. Coin (2.5 cm) is for scale.

On a macroscopic scale, blocky, sharply angular juvenile clasts are the most common (**Figure 9A**) although other forms of juvenile clasts have been recognised as well (**Figure 9B-F**). Globular juvenile clasts can be irregularly shaped or amoeboid (**Figure 9B, C**), elongated, tapered, and a single clast can have partially fluidal and sub-planar margins. Mixed morphologies of juvenile clasts, particularly sharply angular and elongate globular have been encountered in some rhyodacitic glassy lava flows (**Figure 9E**). Glassy lavas sometimes undergo ductile fragmentation into irregularly shaped elongated and convoluted globular clasts that resemble welded glass-shards (**Figure 9F**). Intergranular space is relatively limited and poorly interconnected, and can be infilled with very fine-grained, possibly suspended sediment. Further disintegration and mingling with wet sediment produced peperites developed as intimate mixtures of both components.

The host sediment can penetrate magma in the form of curvilinear and vermicular indentations or enter lava flow through laminar boundary layers. The indentations (**Figure 10A**) reaching deeper into the juvenile clasts are commonly disconnected (**Figure 10B, C**) and initially, irregularly shaped droplets formed (**Figure 10D**). The droplets commonly advanced deeper into juvenile clasts changing their shapes into spherical and oval (**Figure 10E, F**). They may be very abundant, and the rock can be termed microglobular peperite, similar to that described by [5]. In an advanced stage peperites of this type may evolve into intimate mixtures of extremely irregularly shaped elongated clasts and tongues of sediment and tapered juvenile clasts having tendrils and wispy forms (**Figure 11A**). The host sediment that penetrates lava through laminar boundary layers at least initially follows the laminae adopting their shape (**Figure 11B**), but then the flow with the admixed sediment seems to have changed into turbulent (**Figure 11C**). Sometimes the amount of sediment that mingled with magma in that manner is very low and only isolated patches of the entrained sediment can be encountered in the predominant magma, but there are cases where peperites locally developed as intimate mixtures of nearly equal proportions of tapered juvenile clasts and deformed, elongated clasts of sediment (**Figure 11D**).

Magma can penetrate the adjacent sediments forming platy or tapered juvenile clasts (**Figure 11E**). Magma can also penetrate the host sediment along the strata boundaries or other disconformities related to syn-sedimentary tectonic activity or erosion. The emplacement of the Kramarica Sill also disrupted partially consolidated and unconsolidated sediments and made pathways for magma penetration (**Figure 11F**).

When the unconsolidated mingling sediment is composed of coarse-grained volcanoclastic deposit such as volcanoclastic turbidite or debris flow deposit,

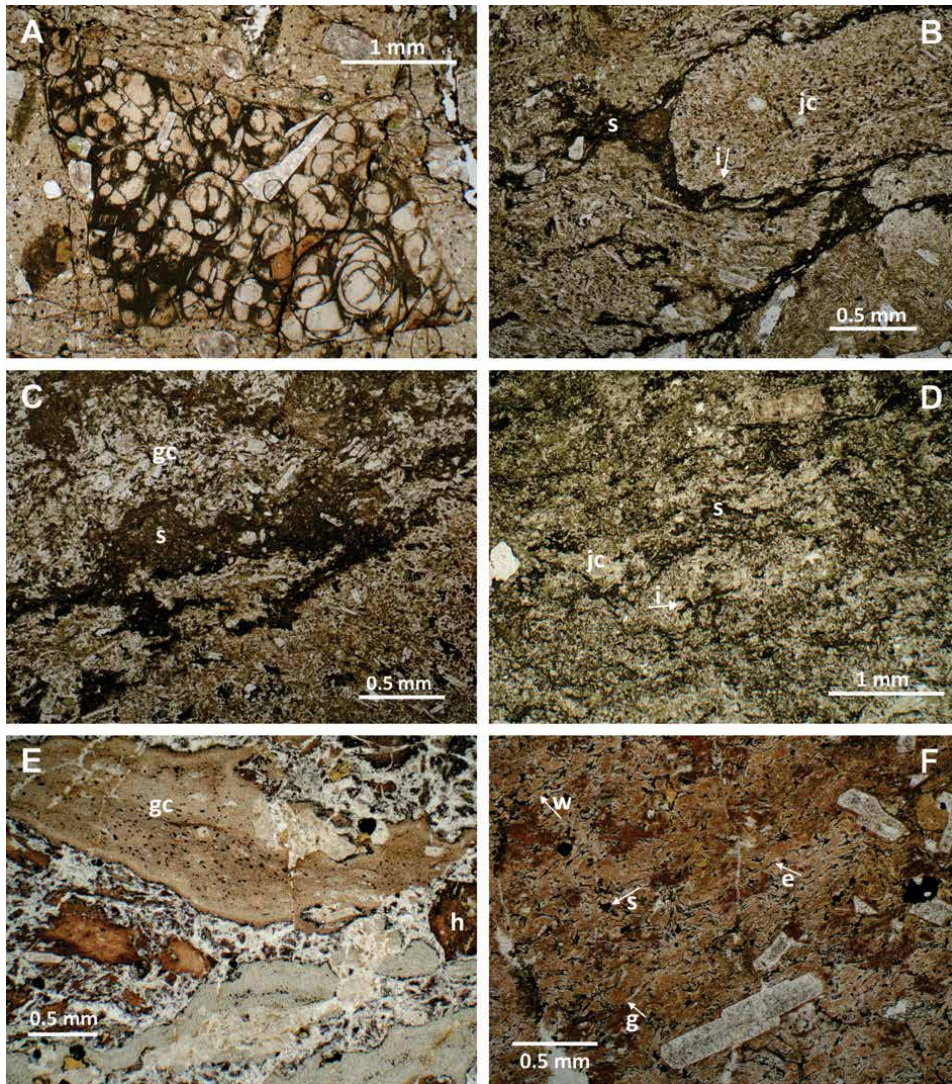


Figure 9.

(A) angular juvenile clast with perlitic cracks in siliciclastic host sediment. Volcanic glass in perlitic domains is altered to laumontite (white) and Fe-oxides (black); (B) various shapes of juvenile clasts (jc) with indentations (i) of the host sediment (s); (C) amoeboid juvenile clasts (gc) in the host sediment (s); (D) an intimate mixture of juvenile clasts (jc) with the sediment (s) indentations (i), (E) globular (gc) and angular (h) juvenile clasts; (F) a glassy lava fragmented into globular (g), elongated (e) and convoluted (w) juvenile clasts with altered sediment (s) filling interstitial space.

peperites can form by erosion and incorporation of sediment into the lava flow. A small-scale penetration of magma into interstitial space has been observed along the basal contacts of lava flows and the underlying sediments (**Figure 12A**). Sometimes magma penetrated deeper into the sediment while pushing aside and redistributing its constituents such as mineral grains and volcanic rock fragments (**Figure 12B**), although the advance seems very limited as the penetrating tongues soon became thinner (**Figure 12C**) or have been stopped by an impenetrable obstacle. Magma itself possibly underwent a sort of separation of its constituents during the process of penetration. Phenocrysts are often stacked close to the magma-sediment boundary while glassy groundmass could have penetrated deeper into the sediment (**Figure 12D**).

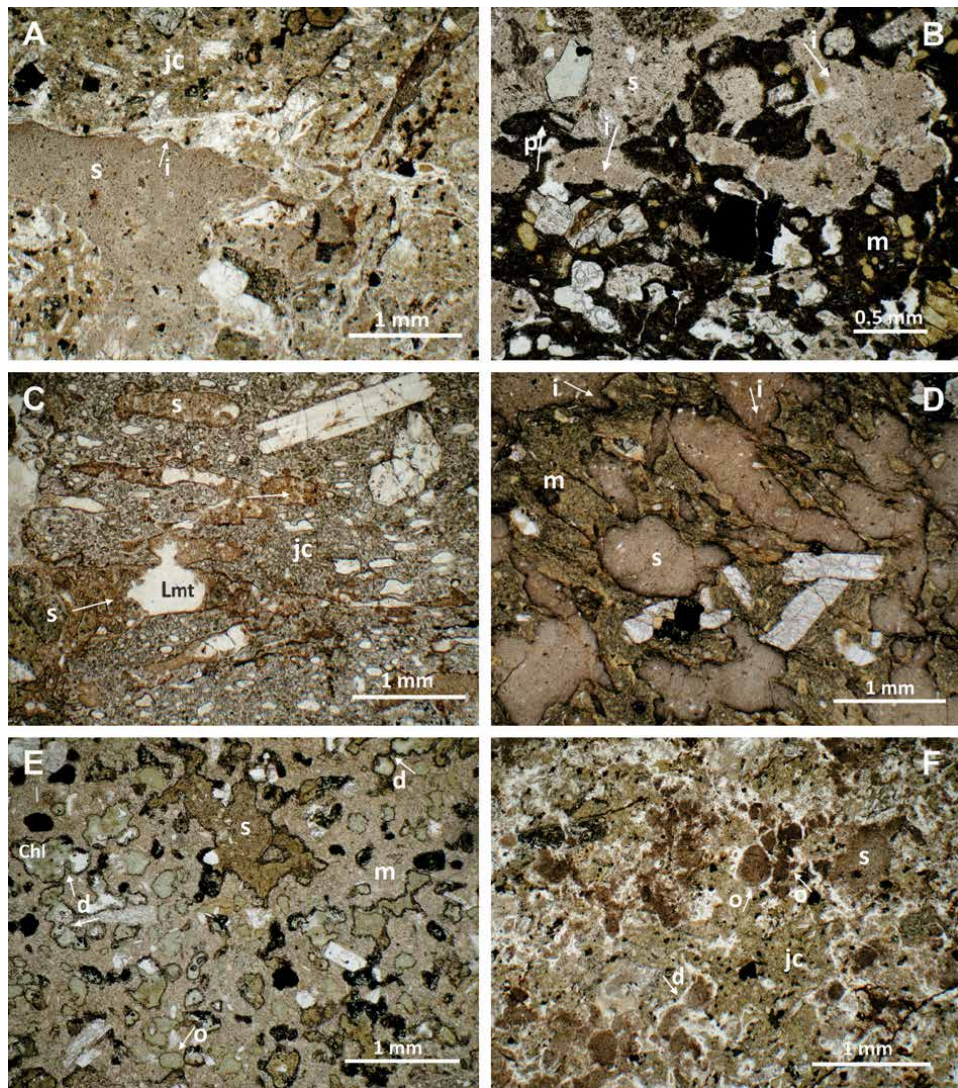


Figure 10.

(A) curvilinear indentations (*i*) of sediment (*s*) into juvenile clasts (*jc*); (B) interpenetrating sediment (*s*) and magma (*m*). The arrows *i* and *p* indicate the penetration directions of sediment and magma, respectively; (C) sediment (*s*) penetrating juvenile clast (*jc*). The arrows show the sediment penetration directions. Sediment (brownish) is partially unaltered and partially replaced by laumontite (*Lmt*). Larger detached droplets of sediment have irregular shapes whilst smaller ones tend to develop more oval or spherical shapes; (D) irregularly shaped droplets of sediment (*s*) penetrating a juvenile clast (*m*). The arrows (*i*) show the sediment penetration directions; (E) larger clast of sediment (*s*) penetrating a juvenile clast (*m*) is still unaltered, and smaller ones have already undergone alteration into chlorite (*Chl*). Some droplets of sediment show the tendency of splitting into several smaller droplets (*d*) and some smaller droplets already attained oval shapes (*o*); (F) droplets of siliciclastic sediment (*s*) in a juvenile clast (*jc*). Some droplets have oval shape (*o*) and some droplets indicate their shapes evolved by splitting of larger clasts (*d*).

5. Alteration of peperites

Microfacies of peperites has been an essential tool in recognition of alteration of peperites as it encompasses the change in mineral and chemical composition of juvenile clasts and the mingling sediment, and more rarely, the formation of interstitial cement. Juvenile blocky clasts dispersed in abundant siliciclastic silt commonly underwent only devitrification, the alteration of glassy juvenile clasts with perlitic

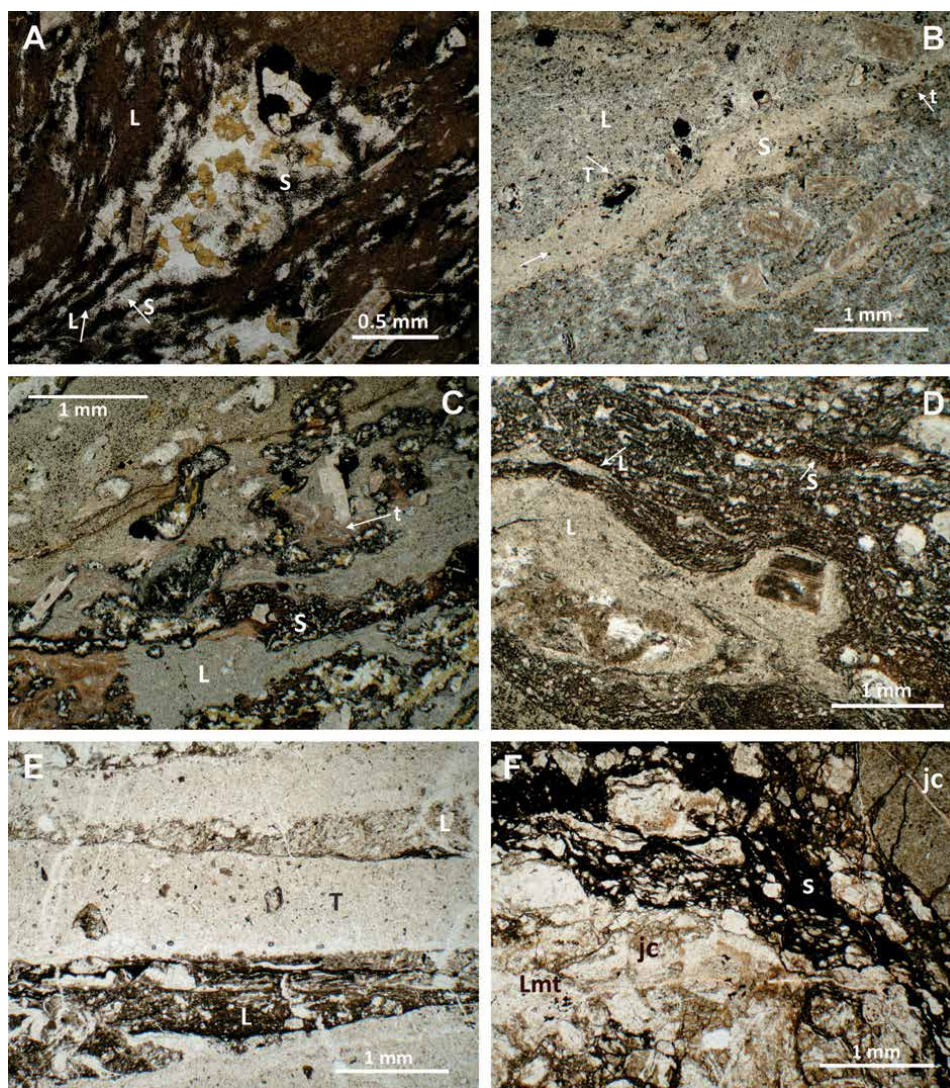


Figure 11.

(A) an intimate mixture of elongate altered clasts of sediment (S) and juvenile clasts (L); (B) sediment (S) entrained into lava flow (L) through a laminar boundary layer. The arrow shows the entrainment direction. The elongated sediment clast soon becomes thinner (t). Along the first obstacle it becomes thicker (T) by enclosing the phenocryst, and then becomes thinner by avoiding the second phenocryst; (C) microstructure of peperite indicating turbulent flow (t) by disrupted and convoluted sediment layers (S) in lava (L); (D) an intimate mixture of elongated clasts of sediment (S) and juvenile clasts (L); (E) platy juvenile clasts (L) formed by penetration of magma into fine-grained volcanic ash (T); (F) juvenile clasts (jc) and fluidised sediment (S) developed owing to the intrusion of the Kramarica Sill. The sediment is altered to iron oxides and the larger juvenile clast to laumontite (Lmt).

cracks may involve the formation of laumontite and Fe-oxides (**Figure 9A**). The mingling sediment is, in general, unaltered except for locally developed iron oxides.

Peperites with denser population of juvenile clasts, and particularly juvenile clasts having irregular fluidal or amoeboid shape, that mingled with siliciclastic silt are commonly altered to laumontite or laumontite and iron oxides. The host sediment commonly remained unaltered (**Figure 13A**).

Some juvenile clasts are replaced by the assemblage of laumontite, albite, quartz, actinolite and epidote (**Figure 13B**), or laumontite, albite, quartz, pumpellyite, incipient epidote and chlorite, or laumontite, prehnite, quartz, chlorite and

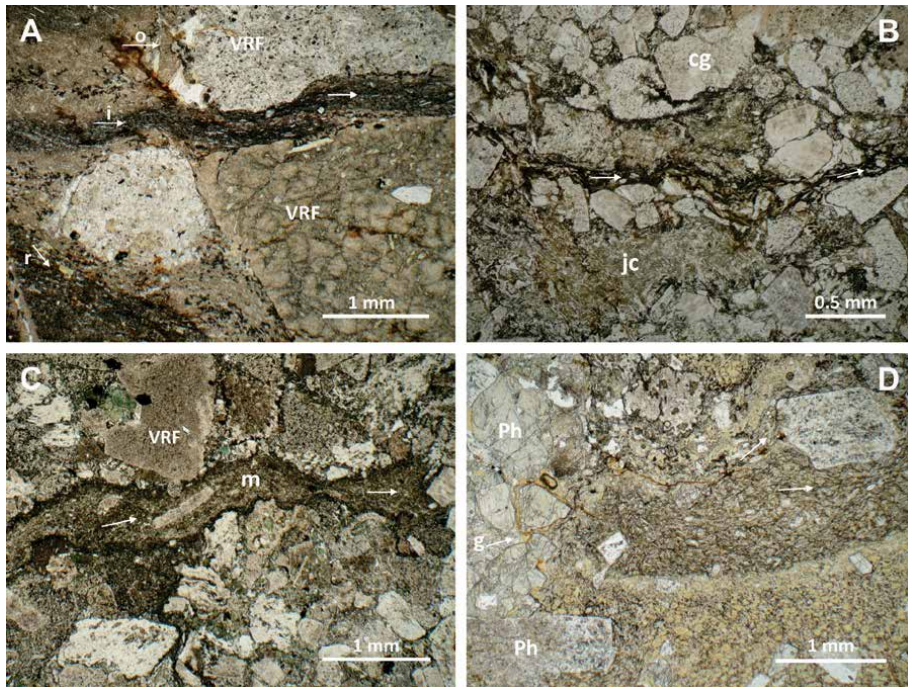


Figure 12.

(A) the arrows (i) and (r) show the directions of magma penetration in intergranular space of volcaniclastic turbidite deposit. The arrow (o) indicates the cessation of penetration along a volcanic rock fragment (VRF); (B) penetration of magma (arrows) into volcaniclastic turbidite deposit by pushing aside crystal grains (cg). The cessation of penetration resulted in the formation of a juvenile clast (jc); (C) penetration of magma (m) stopped by crystal grains, the direction is marked by arrows, VRF – volcanic rock fragments; (D) stacked phenocrysts (Ph) of augite and a glassy constituent of magma (g) that penetrated somewhat further into volcaniclastic turbidite deposit, the arrows mark the directions of magma penetration.

incipient epidote, or laumontite, analcime and interlayered chlorite-smectite. Incipient epidote [53] refers to some μm to a few $10\ \mu\text{m}$ sized, oval and highly birefringent grains. If the mingling sediment was siliciclastic silt it is often altered to microcrystalline quartz, incipient epidote and iron oxides.

If the mingling sediment was fine-grained pyroclastic deposit the alteration minerals commonly resemble those in the juvenile clasts. The most extensive alteration underwent the clasts composed of fine-grained pyroclastic deposit that were incorporated into lava flow, or fine-grained pyroclastic sediment that was entrained into lava flow through lamination boundary layers (**Figure 13C**). A common alteration assemblage is albite, prehnite, quartz, iron oxides and chlorite or interlayered chlorite-smectite with more than 80% of chlorite layers [54]. In the advanced stage of mingling (**Figure 11A**) the alteration of sediment commonly remained the same while the juvenile clasts can be altered to iron oxides and chlorite.

Penetration of the host sediment into juvenile clasts had immediate impact to its alteration. Before the sediment penetrated juvenile clasts and also in the initial stage of formation of droplets it commonly remained unaltered (**Figure 10B,C**), but with advanced penetration and subsequent dispersion into the juvenile clasts, and the transformation of shape from irregular to spherical and oval, the alteration advanced as well (**Figure 10E, 13D**). Such inclusions of the host sediment closely resemble vesicle fillings and could be easily misinterpreted. Common alteration minerals are laumontite (**Figure 13D**), and the assemblages of or prehnite, laumontite and quartz (**Figure 13E**), or pumpellyite, albite, quartz and chlorite (**Figure 13F**), or laumontite, prehnite, quartz, epidote and chlorite.

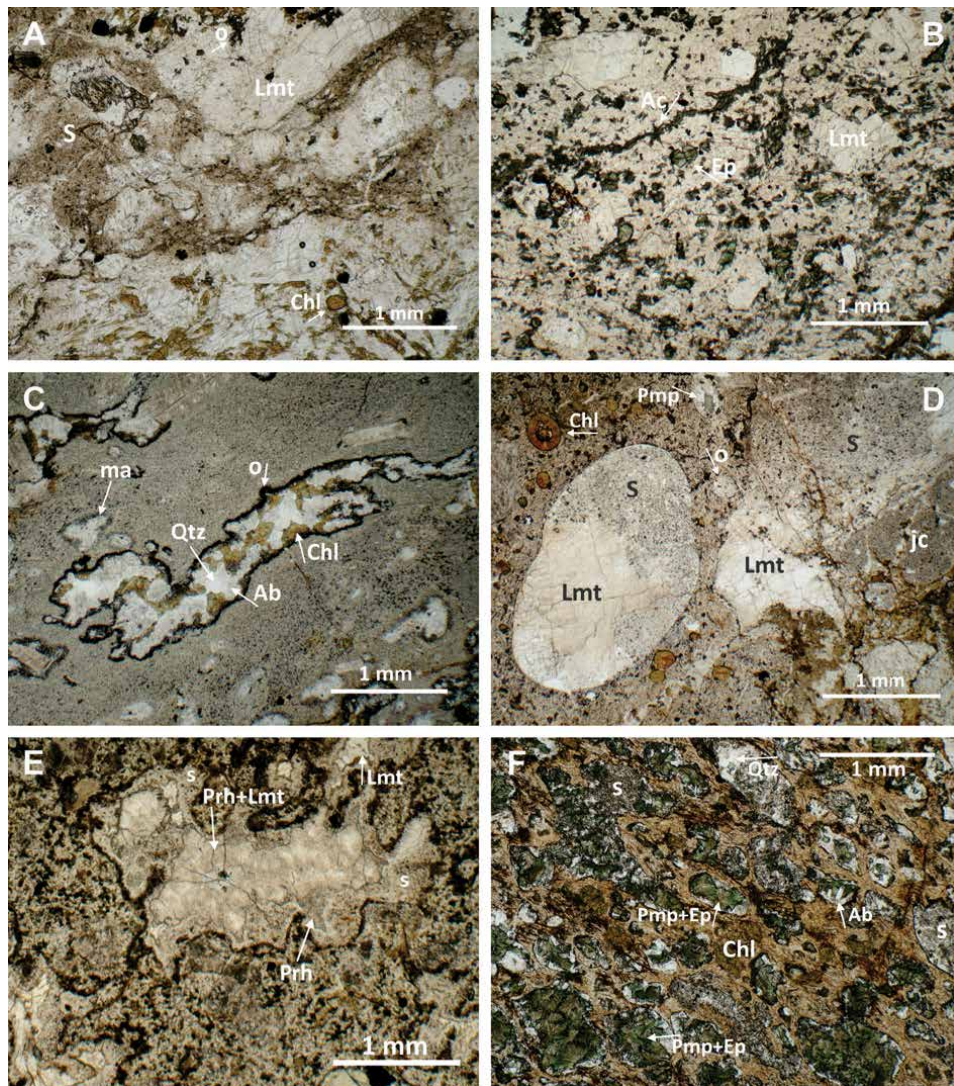


Figure 13.

(A) juvenile clasts (white) altered to laumontite (Lmt), iron oxides (o) and chlorite (Chl). The composition of the mingling siliciclastic sediment (S) remained largely unaltered; (B) a juvenile clast altered to laumontite (Lmt), epidote (Ep) and actinolite (Ac); (C) a clast of fine-grained pyroclastic deposit incorporated in a lava flow has been altered to albite (Ab), quartz (Qtz), chlorite (Chl) and Fe-oxides (o). Some clasts underwent magma assimilation (ma); (D) the mingling fine-grained pyroclastic deposit (S) formed a large oval inclusion in a juvenile clast that has been partially altered into laumontite (Lmt). Smaller inclusions are altered to pumpellyite (Pmp) and quartz, some small spherical inclusions are unaltered (o) and the other replaced by chlorite (Chl). juvenile clasts (jc); (E) an inclusion of fine-grained pyroclastic deposit (s) in a juvenile clast altered to prehnite (Prh) and laumontite (Lmt); (F) inclusions of fine-grained pyroclastic deposit in a juvenile fragment (brownish) altered to pumpellyite (Pmp), epidote (Ep), quartz (Qtz) and albite (Ab). Volcanic glass in the juvenile clast is locally replaced by chlorite (Chl).

Platy juvenile clasts related to penetration of magma into the host sediment are commonly extensively altered into laumontite and iron oxides (**Figure 11E**). The same assemblage typically replaces irregularly shaped juvenile clasts in peperites formed during the emplacement of the Krmarica Sill (**Figure 11F**).

The alteration of peperites related to coarse-grained host sediment is characterised by chlorite, interlayered chlorite-smectite with more than 90% of chlorite layers, quartz, and sometimes incipient epidote. Laumontite and other zeolites, and pumpellyite, prehnite and epidote are uncommon (**Figure 12A-D**).

6. Peperite alteration in the succession of volcanic deposits and the stratovolcano-hosted hydrothermal system in the Smrekovec Volcanic Complex

The stratovolcano-hosted hydrothermal system with convective-advective flow regime of hydrothermal fluids (**Figure 3**), and another important event in the evolution of hydrothermal alteration of volcanic deposits was the emplacement of the Kramarica Sill. Consequently, volcanic deposits underwent alteration related to diverse processes and different superimposed stages of hydrothermal activity [37].

The largest source of geothermal energy and hydrothermal fluids in the time span of volcanic activity some 28-23 mya [43] was a deep igneous body. The alteration resulting from an elevated geothermal gradient is characterised by clinoptilolite, heulandite, analcime, smectite and interstratified smectite-chlorite. The convective flow of hydrothermal fluids occurred primarily through fracture systems and the most typical mineral formed owing to hydrothermal activity is laumontite. Where the fractures were densely distributed, the adjacent rock was altered as well. Laumontite occurs as interstitial cement and replaces volcanic glass and intermediate plagioclases in assemblage with albite, and the principal phyllosilicate mineral is chlorite or interstratified chlorite-smectite with over 80% of chlorite layers. Advective outflow of hydrothermal fluids preferentially occurred through high-permeability layers of the stratovolcano edifice, and laumontite, chlorite, albite and more rarely prehnite are typical minerals encountered in coarse-grained rocks such as volcanoclastic breccias. The adjacent, lower-permeability layers contain authigenic minerals with lower temperature stability ranges, namely clinoptilolite, heulandite, analcime and interlayered chlorite-smectite (**Figures 5 and 6**) [37, 38]. Stilbite locally occurs as vein mineral and was developed during late-stage of hydrothermal activity.

The emplacement of the Kramarica Sill (**Figure 2**) was related to the formation of new vent along the Periadriatic Line. Thermal effects of the emplacement promoted a number of progressive alteration reactions such as from laumontite to prehnite, laumontite to yugawaralite, or interlayered chlorite-smectite to chlorite. During the cooling of the sill, local hydrothermal conditions persisted and controlled retrograde reactions such as from prehnite to yugawaralite, from prehnite to laumontite, from laumontite to heulandite or analcime and from chlorite to interlayered corrensite-chlorite [37, 38, 54].

7. Discussion

The formation of alteration minerals in volcanic-hydrothermal systems is a complex process affected by temperature, pressure, composition of reacting fluids, porosity, permeability and initial composition of the host-rock, duration of hydrothermal activity and superimposed thermal (or hydrothermal) regimes [55, 56]. Nevertheless, there is a general relationship between temperature and the formation of alteration minerals, and some mineral assemblages can be used to interpret temperatures within a geothermal system (**Figure 14**). For heulandite and stilbite, laumontite, yugawaralite, pumpellyite and actinolite widely accepted temperature stability ranges are 100-120°C, 120-220°C, 172-234°C, 200-310°C, 220-310°C and 280-460°C [52, 55-65]. Incipient, fine-grained and poorly crystallised epidote has been encountered in hydrothermal systems of the Philippines [53, 55] and the Nisyros Island [63], respectively, in the temperature range of 180-220°C although epidote generally forms at temperatures higher than 240°C [64, 65]. The temperature stability range of 245-265°C has been reported for mixed-layer R0 and R1 chlorite-smectite from Nesjavellir geothermal field, Iceland [66].

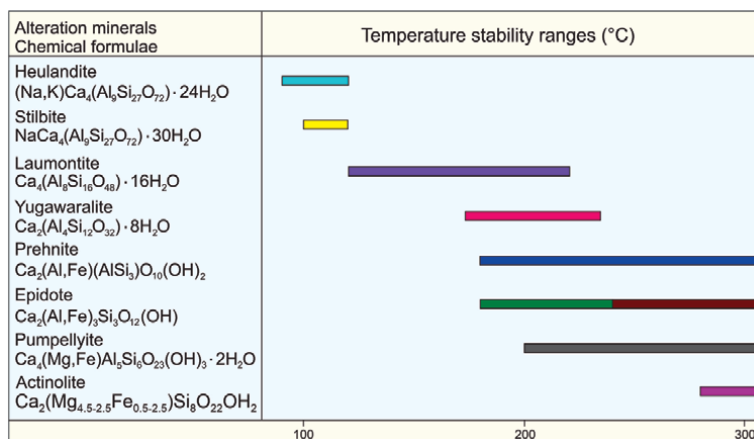


Figure 14. Authigenic calcium-aluminosilicate minerals that commonly serve as geothermometers in volcanic-hydrothermal systems, their chemical formulae and temperature stability ranges, compiled from [52, 55–65].

The alteration of peperites from the Smrekovec Volcanic Complex indicates close relationship to the rock composition and texture, and therefore, the style of peperite formation. Porosity and permeability of peperites is, in general, lower than that of the host sediment. The types involving fine-grained host sediments have low permeability and low porosity, and in the stratovolcano-hosted hydrothermal system with convective-advective flow regime (**Figure 3**) they must have functioned as aquicludes unable to drain effectively the advective flow of hydrothermal fluids that largely controlled hydrothermal alteration of volcanic deposits [37]. In such hydrothermal system, peperites involving coarse-grained host sediments should be more extensively altered and contained authigenic minerals with higher temperature stability ranges than the types involving fine-grained host-sediments, but that is not the case. On contrary, in this type of peperites significant authigenic calcium-aluminosilicate minerals are often lacking and the most common alteration mineral is chlorite or interlayered chlorite-smectite.

In dispersed blocky peperite, matrix composed of siliciclastic host sediment is usually unaltered. The alteration of juvenile clasts often indicates only the reactions of devitrification of volcanic glass, and only juvenile clasts with perlitic cracks can be altered to laumontite and Fe-oxides (**Figure 9A**). The activity of hot fluids originating from heated pore waters can be assumed, but chemical gradients favourable for the formation of laumontite were attained only inside the juvenile clasts with perlitic cracks. Perlitic cracks apparently served as conduits for hot fluids that leached volcanic glass during the flow, and in this manner underwent the changes in chemical composition (e.g. [67]) that finally resulted in crystallisation of laumontite. Far more extensive alteration of blocky peperites involving fine-grained pyroclastic host sediment supports the forementioned explanation. The interaction of heated pore fluids and highly reactive host sediment apparently controlled geochemical evolution of so-formed hydrothermal solutions and the related extensive alteration of all constituents of peperite. Laumontite or mineral assemblages of laumontite, albite, quartz, pumpellyite, incipient epidote and chlorite, or laumontite, prehnite, quartz, chlorite and incipient epidote, or laumontite, analcime and interlayered chlorite-smectite indicate that temperature gradients were prerequisite but not sufficient for alteration to occur and that the main controlling factor were geochemical gradients.

Microglobular peperite has been interpreted as a frozen example of a fuel-coolant interaction (FCI) between magma and fluidised host sediment [5], and the

temperatures of alteration reactions in direct contact with magma must have been higher than in blocky peperite. Microglobules of fine-grained pyroclastic sediment underwent alteration, and typically, smaller microglobules are commonly completely altered to authigenic mineral assemblages with higher temperature stability ranges (e.g. pumpellyite, epidote) than the larger ones that remained incompletely altered or altered to authigenic minerals with lower temperature stability ranges (e.g. laumontite) (**Figure 13D**). The relationship indicates that high-temperature conditions could not persist for a long period of time.

Despite of the complexity of alteration of volcanic deposits in lithofacies associations of the sections Krnes and Smrekovec G34 the assemblages of authigenic minerals in peperites are different than those in the adjacent underlying and overlying autoclastic, pyroclastic or resedimented volcanoclastic deposits irrespectively of their texture and grain-size (**Figures 4 and 5**). Particularly outstanding is the occurrence of pumpellyite, actinolite and epidote. In lavas pumpellyite and actinolite very rarely occur as the replacement of volcanic glass and other primary constituents although the temperatures in cooling lavas could be favourable for their formation.

If compared to the section Krnes, the alteration of volcanic deposits in the section Smrekovec G34 has been far more complex owing to the emplacement of the Kramarica Sill. Progressive reactions related to an elevated temperature regime are characterised by the occurrence of prehnite and indicate, at least in the lower half of the section, that the temperatures could have reached over 300°C. Yet, even in such elevated temperature regime the exclusive occurrence of pumpellyite and particularly actinolite in peperites indicates that higher temperatures and specific geochemical conditions related to the formation of peperites must have controlled the crystallisation of pumpellyite and actinolite. The occurrence of the same assemblage in peperites in the section Krnes is particularly important. Here, hydrothermal activity and temperature regime were mainly related to a deep igneous source and the associated convective-advective flow of hydrothermal fluids and elevated geothermal gradients in the area of stratovolcano, and they were not affected, at least significantly, by the emplacement and cooling of the Kramarica Sill. Maximum temperatures have been determined by the temperature stability of laumontite, namely, 234°C which is insufficient for the crystallisation of pumpellyite or actinolite. The alteration of juvenile clasts to laumontite in peperites indicates the presence of hydrothermal conditions although they cannot be conclusively ascribed to specific hydrothermal conditions and geochemical gradients related to the formation of peperites.

The alteration of peperites can be regarded as syn-formational hydrothermal, although it is local, specific and ephemeral lasting until thermal gradients persisted. Authigenic mineral assemblages developed in peperites from the Smrekovec Volcanic Complex are rare on a worldwide scale and have not been identified in such context yet. Geochemical evolution of heated pore fluids circulating in the vicinity of the source of heat controlled the formation of authigenic mineral assemblages and the presence of unstable, reactive volcanic material was crucial for their formation and diversity.

8. Conclusion

Peperites are commonly developed in submarine environments with contemporaneous volcanic activity and sedimentation. And although the occurrence and complex processes of formation have been studied and explained in many modern and ancient geological settings worldwide [4, 10–14], and particularly in the

Carpathian-Pannonian region [9, 15–17] where the Smrekovec Volcanic Complex belongs to [29], the studies related to their alteration have been relatively scarce [15–20]. The present study gives evidence of the existence of localised and ephemeral hydrothermal conditions related to and persisting during the formation of peperites and resulting in their distinct alteration.

The Smrekovec Volcanic Complex is a remnant of an Oligocene submarine stratovolcano characterised by a complex development of an over 2500 m thick succession of volcanic rocks. Submarine environment, the style of eruptions, morphology and the abundance of pyroclastic and syn-eruptively resedimented volcanoclastic deposits were favourable for the formation of peperites that are particularly abundant in medial-zone lithofacies associations. In a succession of volcanic deposits studied in detail in two sections Krnes and Smrekovec G34 attaining 400 m and 470 m, respectively, the alteration of peperites indicates that authigenic minerals have higher temperature stability ranges than those in the adjacent underlying and overlying deposits irrespectively of their lithofacies.

The alteration of peperites indicates close relationship to the rock composition and texture, and therefore, the style of peperite formation. Dispersed blocky peperite involving siliciclastic host sediment is commonly poorly altered. Volcanic glass in juvenile clasts is usually devitrified or hydrated, and only some clasts with perlitic texture can be altered to laumontite. In the textural types with fine-grained pyroclastic host sediment laumontite, or the assemblages of laumontite, albite, quartz, pumpellyite, incipient epidote and chlorite, or laumontite, prehnite, quartz, chlorite and incipient epidote, or laumontite, analcime and interlayered chlorite-smectite may occur. The alteration minerals indicate that thermal gradients were prerequisite but not sufficient for alteration to occur and that the main controlling factor were geochemical gradients in reacting fluids.

Microglobular peperite developed by interaction between magma and fluidised sediment [5], and the temperatures of alteration must have been higher than in blocky peperite. Smaller microglobules are often completely altered to authigenic mineral assemblages with higher temperature stability ranges (e.g. pumpellyite, epidote) while the larger microglobules remained incompletely altered or altered to authigenic minerals with lower temperature stability ranges (e.g. laumontite). The relationship indicates that high-temperature conditions could not persist for a long period of time and had ephemeral character.

Authigenic mineral assemblages developed in peperites indicate that their formation is specific and related to the formation of parent rock itself. Thermal stability ranges of actinolite and pumpellyite indicate the highest temperatures possibly exceeded 280°C and decreased when the parent lava flow and the associated peperite underwent cooling. Hydrothermal fluids mainly originated from heated pore fluids although deuteric fluids could have been locally admixed. The evolution of fluids circulating in peperite was essential for extensive alteration to occur and that was possibly attained by interaction with unstable and highly reactive host sediment. Many peperites have been developed as low-porosity and low-permeability layers, and therefore contemporaneous and later hydrothermal activity related to the stratovolcano-hosted hydrothermal system with convective-advective flow could not have exerted any critical thermal or geochemical impact.

The alteration of peperites in the Smrekovec Volcanic Complex can be regarded as syn-formational, hydrothermal, ephemeral, localised and depending on many factors such as the extent and time span of thermal regime, the process of formation of parent rock and thermal and geochemical evolution of circulating hydrothermal fluids. And although peperite deposits are not rare in similar volcanic-sedimentary settings worldwide, the alteration as recognised in the present study has not been

reported yet and indicates the formation and alteration of peperites are complex and distinctive and interrelated processes.

Acknowledgements


Slovenian Research Agency (ARRS) is acknowledged for granting the research (Programme Mineral Resources P-0025). The editorial work of Academic Editor Dr. Károly Németh and helpful comments of anonymous reviewers are greatly appreciated. Many thanks to Mrs. Mia Vulovic, Author Service Manager for her kind assistance. I thank Ms. Staška Čertalič and Mr. Mladen Štumergar from Geological Survey of Slovenia for technical support.

Author details

Polona Kralj
Geological Survey of Slovenia, Dimičeva ulica 14, 1000, Ljubljana, Slovenia

*Address all correspondence to: polona.kralj@geo-zs.si

IntechOpen

© 2021 The Author(s). Licensee IntechOpen. This chapter is distributed under the terms of the Creative Commons Attribution License (<http://creativecommons.org/licenses/by/3.0>), which permits unrestricted use, distribution, and reproduction in any medium, provided the original work is properly cited. 

References

- [1] White JDL, McPhie J, Skilling IP. Peperite: a useful genetic term. *Bulletin of Volcanology* 2000;62 65-66.
- [2] Fisher RV, Schmincke H-U. *Pyroclastic Rocks*. Berlin, New York: Springer-Verlag; 1984.
- [3] Cas RAF, Wright JV. *Volcanic Successions Modern and Ancient*. Berlin, New York: Springer-Verlag; 1988.
- [4] McPhie J, Doyle M, Allen R. *Volcanic Textures*. Hobart: Centre for Ore Deposit and Exploration Studies, University of Tasmania; 1993.
- [5] Busby-Spera CJ, White JDL. Variation in peperite textures associated with differing host-sediment properties. *Bulletin of Volcanology* 1987;49 765-775.
- [6] Kano K. Interactions between andesitic magma and poorly consolidated sediments: examples in the Neogene Shirahama Group, South Izu, Japan. *Journal of Volcanology and Geothermal Research* 1989;37 59-75.
- [7] Hanson RE. Quenching and hydroclastic disruption of andesitic to rhyolitic intrusions in a submarine island-arc sequence, northern Sierra Nevada, California. *Geological Society of America Bulletin* 1991;103 804-816.
- [8] Hanson RE, Hargrove US. Processes of magma/wet sediment interaction in a large-scale Jurassic andesitic peperite complex, northern Sierra Nevada, California. *Bulletin of Volcanology* 1999;60 610-626.
- [9] Martin U, Németh K. Blocky versus fluidal peperite textures developed in volcanic conduits, vents and crater lakes of phreatomagmatic volcanoes in Mio/Pliocene volcanic fields of Western Hungary. *Journal of Volcanology and Geothermal Research* 2007;159 163-178.
- [10] Kokelaar BP. Fluidization of wet sediments during the emplacement and cooling of various igneous bodies. *Journal of Geological Society of London* 1982;139 21-33.
- [11] Krynauw JR, Hunter DR, Wilson AH. Emplacement of sills into wet sediments at Grunehogna, western Dronning Maud Land, Antarctica. *Journal of Geological Society of London* 1988;145 1019-1032.
- [12] Skilling IP, White JDL, McPhie J. Peperite: a review of magma-sediment mingling. *Journal of Volcanology and Geothermal Research* 2002;114 1-17.
- [13] Wohletz KH. Water/magma interaction: some theory and experiments on peperite formation. *Journal of Volcanology and Geothermal Research* 2002;114 19-35.
- [14] Zimanowski B, Büttner R. Dynamic mingling of magma and liquified sediments. *Journal of Volcanology and Geothermal Research* 2002;114 37-44.
- [15] Németh K, Pécskay Z, Martin U, Gméling K, Molnár F, Cronin SJ. Hyaloclastites, peperites and soft-sediment deformation textures of a shallow subaqueous Miocene rhyolitic dome-cryptodome complex, Pálháza, Hungary. In: Thomson K, Petford, N (eds.), *Structure and Emplacement of High-Level Magmatic Systems: Geological Society Special Publications* 2008, London; 302 63-86.
- [16] Martin U, Németh K. Magma-wet sediment interaction in a crater lake of a tuff ring, developed in a pyroclastic mound valley: Kissomlyó volcano (Western Hungary). *American Geophysical Union, Charpman Conference Subaqueous explosive volcanism, 2002, Dunedin, New Zealand*, 1-37.

- [17] Martin U, Németh K. Peperitic lava lake-fed intravent sills at Ság-hegy, Western Hungary: a complex interaction of a wet tephra ring and lava. In: Petford N, Breitung C (eds) *Physical Geology of Subvolcanic Systems – Laccoliths, Sills, and Dykes*: Geological Society Special Publications, 2004, London, 234 33-50.
- [18] Brooks ER, Woods MM, Garbutt PL. Origin and metamorphism of peperite and associated rocks in the Devonian Elwell Formation, northern Sierra Nevada, California. *Geological Society of America Bulletin* 1982;93 1208-1231.
- [19] Doyle MG. Clast shape and textural associations in peperite as a guide to hydromagmatic interactions: Upper Permian basaltic and basaltic andesite examples from Kaima, Australia. *Journal of Earth Sciences* 2000;47(1) 167-177.
- [20] Polacci M, Cashman KV. Textural characterization of the pahoehoe-'a'a transition in Hawaiian basalt. *Bulletin of Volcanology* 1999;60 595-609.
- [21] Kokelaar BP. Magma-water interactions in subaqueous and emergent basaltic volcanism. *Bulletin of Volcanology* 1986;48 275-289.
- [22] Martin U, White JDL. Melting and mingling of phonolitic pumice deposits with intruding dykes: an example from the Otago Peninsula, New Zealand. *Journal of Volcanology and Geothermal Research* 2002;114 129-146.
- [23] McPhie J, Orth, K. Peperite, pumice and perlite in submarine volcanic successions: implications for VHMS mineralisation: Proceedings of Pacrim '99, Bali, Indonesia;1999.
- [24] Rawlings DJ. Mafic peperite from Gold Creek Volcanics in the Middle Proterozoic McArthur Basin, Northern Territory. *Australian Journal of Earth Science* 1993;40 109-113.
- [25] McPhie J, Hunns SR. Secondary welding of submarine pumice-lithic breccia at Mount Chalmers, Queensland, Australia. *Bulletin of Volcanology* 1995;57 170-178.
- [26] WoldeGabriel G, Keating GN, Valentine G. Effects of shallow basaltic intrusion into pyroclastic deposits, Grants Ridge, New Mexico, USA. *Journal of Volcanology and Geothermal Research* 1999;92 389-411.
- [27] Squire RJ, McPhie J. Characteristics and origin of peperite involving coarse-grained host sediment. *Journal of Volcanology and Geothermal Research* 2002; 114 45-61.
- [28] Buser S. Geological map of Slovenia 1:250.000. Ljubljana: Geological Survey of Slovenia; 2009.
- [29] Mioč P. Tolmač za list Ravne na Koroškem (in Slovenian with English abstract: Explanation to the geological map of Slovenia, scale 1:100,000 – Sheet Ravne na Koroškem). Belgrade: Zvezni geološki zavod (Federal Geological Survey); 1983.
- [30] Bischoff A, Barrier A, Beggs M, Nicol A, Cole J, Sahoo T. Magmatic and tectonic interactions revealed by buried volcanoes in Te Riu-a-Maui/Zealandia sedimentary basins. *New Zealand Journal of Geology and Geophysics* 2020.
- [31] Bischoff A, Nicol A, Beggs M. Stratigraphy of architectural elements in a buried volcanic system and implications for hydrocarbon exploration. *Interpretation - a Journal of Subsurface Characterization* 2017;5(3):SK141-SK159.
- [32] Planke S, Symonds PA, Alvestad E, Skogseid J. Seismic volcanostratigraphy of large-volume basaltic extrusive complexes on rifted margins. *Journal of Geophysical Research-Solid Earth* 2000;105(B8) 19335-19351.

- [33] Zelenka T, Balász E, Balogh K, Kiss J, Kozák M, Nemesi L, Pécskay Z, Püspöki Z, Ravasz C, Széky-Fux V, Újfalussy A. Buried Neogene volcanic structures in Hungary. *Acta Geologica Hungarica* 2004; 47 (2-3) 177-219.
- [34] Lexa J, Seghedi I, Németh K, Szakács A, Konečný V, Pécskay Z, Fülöp A, Kovacs M. Neogene-Quaternary Volcanic forms in the Carpathian–Pannonian Region: a review. *Central European Journal of Geosciences* 2010; 2 (3), 207-270.
- [35] Pánisová J, Bálasz A, Zalai Z, Bielik M, Horváth F, Harangi S, Schmidt S, Götz H-J. Intraplate volcanism in the Danube Basin of NW Hungary: 3D geophysical modelling of the Late Miocene Pásztori volcano. *International Journal of Earth Sciences* 2018;107 1713-1730.
- [36] Kralj P. Facies architecture of the Upper Oligocene submarine Smrekovec stratovolcano, Northern Slovenia. *Journal of Volcanology and Geothermal Research* 2012;247-248 122-138.
- [37] Kralj P. Hydrothermal zeolitisation controlled by host-rock lithofacies in the Periadriatic (Oligocene) Smrekovec submarine composite stratovolcano, Slovenia. *Journal of Volcanology and Geothermal Research* 2016;317 53-65.
- [38] Kralj P, Rychagov S, Kralj P. Zeolites in volcanic-igneous hydrothermal systems: a case study of Pauzhetka geothermal field (Kamchatka) and Oligocene Smrekovec Volcanic Complex (Slovenia). *Environmental Earth Sciences* 2010;59 951-956.
- [39] Dercourt J, Zonenshain LP, Ricou LE, Kazmin VG, LePichon X, Knipper AL, Grandjacquet C, Sbertshikov IM, Geyssant J, Lévrier C, Pechersky DH, Boulin G, Sibuet JC, Savostin LA, Sorokhtin O, Wesphal M, Bazhenov ML, Lauer JP, Bijou-Duval B. Geological evolution of the Tethys belt from the Atlantic to Pamir since Lias. *Tectonophysics* 1986;123 241-315.
- [40] Kázmér M, Dunkl I, Frisch W, Kuhlemann J, Oszvárt P. The Paleogene forearc basin of the Eastern Alps and Western Carpathians: subduction erosion and basin evolution". *Journal of the Geological Society* 2003;160 431-428.
- [41] von Blanckenburg FJ, Davies JH. Slab breakoff: a model for syncollisional magmatism and tectonics in the Alps. *Tectonics* 1995;14 120-131.
- [42] Handy MR, Ustaszewski K, Kissling E. Reconstructing the Alps-Carpathians-Dinarides as a key to understanding switches in subducting polarity, slab gaps and surface motion. *International Journal of Earth Sciences (Geologische Rundschau)* 2015;104 1-26.
- [43] Hanfland C, Läufer AL, Nebelsick JH, Mosbrugger V. The Paleogene Smrekovec Basin and related volcanism (Slovenia): sedimentology, geochemistry and tectonic evolution. *Neues Jahrbuch für Geologie und Paläontologie Abhandlungen* 2004;232(1) 77-125.
- [44] Altherr R, Lugović B, Meyer H-P, Majer V. Early Miocene post-collisional calc-alkaline magmatism along the easternmost segment of the Periadriatic fault system (Slovenia and Croatia). *Mineralogy and Petrology* 1995;54 225-247.
- [45] Kralj P. Lithofacies characteristics of the Smrekovec volcanoclastics, Northern Slovenia. *Geologija* 1996;39 159-191.
- [46] Kralj P, Celarc B. Shallow intrusive volcanic rocks on Mt. Raduha, Savinja-Kamnik Alps, Northern Slovenia. *Geologija* 2002;45(1) 247-253.
- [47] Hinterlechner-Ravnik A, Pleničar M. Smrekovski andezit in

njegov tuf (in Slovenian with English abstract: The Smrekovec andesite and its tuff). *Geologija* 1967;10 219-237.

[48] White JDL. Subaqueous eruption-fed density currents and their deposits. *Precambrian Research* 2000;101 87-109.

[49] Moorhouse BL, White JDL. Interpreting ambiguous bedforms to distinguish subaerial base surge from subaqueous density current deposits. *Depositional Record* 2016;2(2) 173-195.

[50] Verolino A, White JDL, Brenna M. Eruption dynamics at Pahvant Butte volcano, Utah, western USA: insights from ash-sheet dispersal, grain size, and geochemical data. *Bulletin of Volcanology* 2018; 80(11).

[51] Doronzo DM, Dellino P. Hydraulics of subaqueous ash flows as deduced from their deposits: 2. water entrainment, sedimentation, and deposition, with implications on pyroclastic density current deposit emplacement. *Journal of Volcanology and Geothermal Research* 2013; 285 176-186.

[52] Zeng Y, Liou JG. Experimental investigation of yugawaralite-wairakite equilibrium. *American Mineralogist* 1982;67 937-943.

[53] Reyes AG. Petrology of Philippine geothermal systems and the application of alteration mineralogy to their assessment. *Journal of Volcanology and Geothermal Research* 1990;43 279-309.

[54] Kralj P. Hydrothermal alteration of chlorite to randomly interstratified corrensite-chlorite: Geological evidence from the Oligocene Smrekovec Volcanic Complex, Slovenia. *Applied Clay Science* 2016;134 235-245.

[55] Reyes AG. Petrology and mineral alteration in hydrothermal systems: from diagenesis to volcanic catastrophes. Reykjavik: Geothermal

Training Programme, Report 18 for the year 1998, United Nations University, 2000.

[56] Rigault C, Patrier P, Beaufoord D. Clay minerals related to circulation of near-neutral to weakly acidic fluids in active high energy hydrothermal systems. *Bulletin de la Société Géologique de France* 2010;181(4) 337-347.

[57] Bird DK, Schiffman P, Elders WA, Williams AE, McDowell SD. Calc-silicate mineralization in active geothermal systems. *Economic Geology* 1984;79 671-693.

[58] Browne PRL, Courtney SF, Wood CP. Formation rates of calc-silicate minerals deposited inside drill hole casing, Ngatamariki geothermal field, New Zealand. *American Mineralogist* 1989;74 759-763.

[59] Savage D, Cave MR, Haigh D, Milodowski AE, Young ME. The reaction kinetics of laumontite under hydrothermal conditions. *European Journal of Mineralogy* 1993;5 523-535.

[60] Eberlein GD, Erd RC, Weber F, Beatty LB. New occurrence of yugawaralite from the Chena Hot Springs area, Alaska. *American Mineralogist* 1971;56 1699-1717.

[61] Ernst WG. Synthesis and stability relations of ferroactinolite. *American Journal of Science* 1966;264 36-65.

[62] Jenkins DM, Bozhilov KN. Stability and thermodynamic properties of ferroactinolite: a re-investigation. *American Journal of Science* 2003;303 723-752.

[63] Ambrosio M, Doveri M, Fagioli MT, Marini L, Principe C, Raco B. Water-rock interaction in the magmatic-hydrothermal system of Nisyros Island (Greece). *Journal of Volcanology and Geothermal Research* 2010;192 57-68.

[64] Kristmannsdóttir H. Alteration in the IRDP drillhole compared with other drillholes in Iceland. *Journal of Geophysical Research* 1982;87 6525-6531.

[65] Bird DK, Spieler AR. Epidote in geothermal systems. *Reviews in Mineralogy and Geochemistry* 2004;56 235-300.

[66] Schiffman P, Friedleifsson GO. The smectite to chlorite transition in drillhole Nj-15, Nesjavellir geothermal field, Iceland: XRD, BSE and electron microprobe investigations. *Journal of Metamorphic Geology* 1991;9 679-696.

[67] Utada M. Zeolites in hydrothermally altered rocks. In: Bish DL, Ming DW (eds.) *Natural zeolites: occurrence, properties, applications*. *Reviews in Mineralogy and Geochemistry* 2001; 45 305-322.

Section 5

Volcanic Geoheritage
and Geotourism

Volcanoes: Identifying and Evaluating Their Significant Geoheritage Features from the Large to Small Scale

*Margaret Brocx, Vic Semeniuk, Tom J. Casadevall
and Dan Tormey*

Abstract

Across the globe, volcanoes and volcanic terrains present one of the most complex geological systems on Earth that, depending on magma type, viscosity, and water and gas content, form a diverse range of products in terms of geomorphology, lithologic suites, structures, and stratigraphy. In broad terms, magmas, with their diagnostic composition, derive from specific tectonic settings, *e.g.*, basalt-dominated oceanic crusts, acidic magma from continental plates, and andesitic convergent-plate margins. In addition to magma composition and volcanic rock types, there is a wide range of volcanic products, manifest at all scales, dependent on how magma interacts with the Earth's surface, varying, for instance, from lava flows such as vesicular lava beds and flow-banded to flow-laminated lava beds, to breccias, tephra (ejecta) deposits, and bombs, amongst others, each commonly with their diagnostic small-scale lithological/structural features. This wealth of rock types, stratigraphy, and structures linked to geologic setting, potentially has geoheritage significance, and we provide here methods tailored for volcanoes and volcanic rocks of identifying, classifying and evaluating the complex and heterogeneous nature of volcanoes so that the full complement of their geology for a given region can be appreciated and incorporated into thematic geoparks, Nature Reserves and protected areas. For sites of geoheritage significance, we present (1) a globally-applicable Geoheritage Tool-kit to systematically identify volcanic geoheritage sites, (2) a technique to classify/categorise geoheritage sites, and (3) a semi-quantitative method to evaluate the geoheritage significance of volcanic sites.

Keywords: volcanoes, volcanic geology, geoheritage, geoconservation, geoparks

1. Introduction

Volcanoes and volcanic terrains are one of the most complex geological systems on Earth forming a range of products from the megascale and large scale to small scale that have varying geological significance. Of necessity, the ensuing text is a brief summary of a very complex and diverse subject matter, presented to a level sufficient to convey their comparative diversity and scale of expression for purposes

of geoheritage and geoconservation. More detailed and comprehensive treatment of volcanoes can be found in various encyclopaedia and text books [1–13].

Magma composition is highly variable across volcanic terrains and at a single volcano, with attendant variation also in viscosity, gas content, water content, and behaviour of the erupted material. Magma can range in composition from basic (*e.g.*, basalt) to intermediate (*e.g.*, andesite) to acidic (*e.g.*, rhyolite, rhyodacite, dacite). Volcanoes extrude magmas in any of the Earth's surface environments though most are located at plate boundaries (terrestrial and submarine rift zones, subduction and collision zones, and transform zones); they can also extrude in intra-plate and cratonic settings. Commonly, magma composition is linked to global geological setting or to regional geological setting, with basaltic magmas (basic magmas) deriving from oceanic crusts, andesitic and associated magmas (intermediate magmas) deriving from collision between oceanic crust and continental crust, and a range of acidic magmas deriving from continental crusts. Continental crusts, with their lithological variability reflecting craton heterogeneity, metamorphic history, and sedimentary basin-filling, hold scope through melting, diffusion, and mixing to create a wider range of magma compositional types than ocean-crust-derived basic magmas. Thus, in continental situations, depending on geological setting, vertically-ascending magma plumbing or conduits that feed/supply volcanic eruptions can traverse variable crust types from cratons and Precambrian stratigraphic sequences to polyolithic, stratified Phanerozoic sedimentary basins, to submarine seafloors. As such, in the process, this magma plumbing or conduits incorporate material from the host rocks they traverse via such processes as partial melting of host rocks, chemical diffusion from host rocks, and plucking and melting of solid fragments to form enclaves, xenoliths, and xenocrysts.

Volcanoes can erupt in a wide variety of environments, including relatively dry terrestrial environments, water-saturated terrestrial environments, continental edge, submarine environments, and from under ice (glaciers) and, thus, at the large scale, they can have a variety of lithologic/structural expression and a variety of geological structural and stratigraphic relationships to the host rocks that they intrude into or erupt from. Depending on a number of factors including gas content and contact with water, eruptions at one extreme can be extremely explosive (*e.g.*, phreatomagmatic eruptions where magma interfaces with groundwater; *cf.* Németh & Kósik [11]), sending tephra (various-sized pyroclastic material or ejecta such as lapilli and ash composed of rock fragments and glass), gas, and magma high up into the atmosphere (with some of the more explosive eruptions dispersing ash as plumes hundreds of kilometres from their eruptive source) or, at the other extreme, involve more quiescent effusive lava flows (for review see Németh & Kósik [11, 13]). The ejecta can be fine-grained ranging to fine-grained with or without included bombs, or can be dominated by coarse-grained to boulder-sized material and (depending on magma type, gas content, water, and geological setting) volcanic ash can be dominantly lithoclastic, or crystal-rich, or (volcanic glass) shard-rich, or mixtures of these [5].

Water and gas are important components of volcanism and play major roles in magma viscosity, development of vesicles, development of pumice, syn-eruption rain, post-eruption rain-storms, and moisture condensation effects. With an eruptive plume passing through a cloud, or volcano-associated rain-storms, or condensation of moisture within an expanding plume, there can be development of accretionary lapilli [14–16] and, with post-eruption rain and erosion, the potential for slurries of pyroclastic material, rocky debris and water (*e.g.*, lahars) which can

be erosive into the layered tephra, or can become interlayered with the volcanic deposits all producing complex stratigraphy.

At the Earth's surface, at the large scale, volcanoes are expressed in a variety of geometric and stratigraphic arrays, *viz.*, stratovolcanoes, shield volcanoes, and volcanic fissures leading to sheet flows, amongst others, with the geometry dependent on whether extrusive material, at one extreme, is tephra-dominated (mainly ash and lapilli) and built to relatively high relief (*e.g.*, cinder cones and stratovolcanoes) or, at the other extreme, lava-dominated and built to relatively low relief (*e.g.*, shield volcanoes and dome volcanoes), or intermediate with alternating tephra and lava layers and built to high relief (*e.g.*, stratovolcanoes).

At the medium scale, there is an abundance of features expressed in volcanic extrusions, *e.g.*, layered lithologically-similar ash beds, layered lithologically-heterogeneous ash beds, structureless lava beds, vesicular lava beds, flow-banded to flow-laminated lava beds, lava beds with spherulitic structures, pillows and their associated structures and mineralogy, deuteric minerals formed within lava pillows, layered ejecta deposits (ash beds), volcanic bombs, volcanic blocks, post-solidification polygonal jointing, mega-breccias and meso-breccias, micro-breccias, lava tunnels, mixing of magma types, formation of obsidian by the rapid cooling of magma to form glass, formation of pumice by super-heated, highly pressurized magma being violently erupted, diatremes and maars, secondary dykes, amongst many others [6, 9, 10].

At the small scale, there is deformation of ash-bed layering/lamination by bombs, flow-breccia structures, xenoliths and xenocrysts, surge structures, stalactitic and stalagmitic structures, lamination in obsidian, deformation (stretching) of vesicles of lava and pumice by flow, lapilli and accretionary

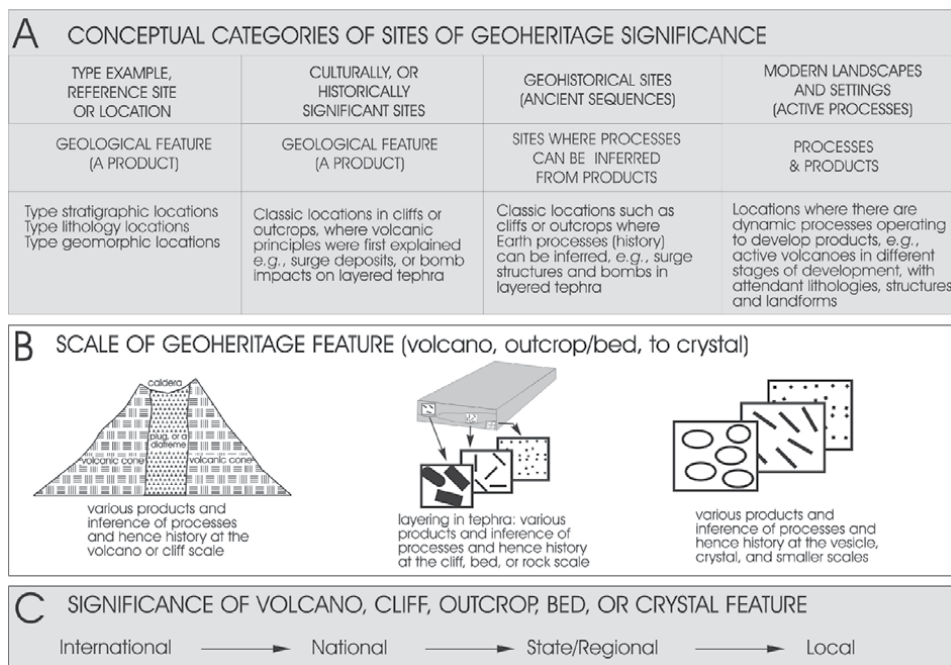


Figure 1. The categories of sites of geoheritage significance (modified from Brocx & Semeniuk [1] and tailored for volcanoes).

lapilli, a wide range of vesicle-lining or vesicle-filling minerals, crystal types and forms (e.g., zeolites, calcite, quartz, chalcedony, epidote), mineral-filled fractures, small-scale fumarolic fissures or vents (empty, or filled with crystals, filled with massive lava, or filled with vesicular lava), alteration of the

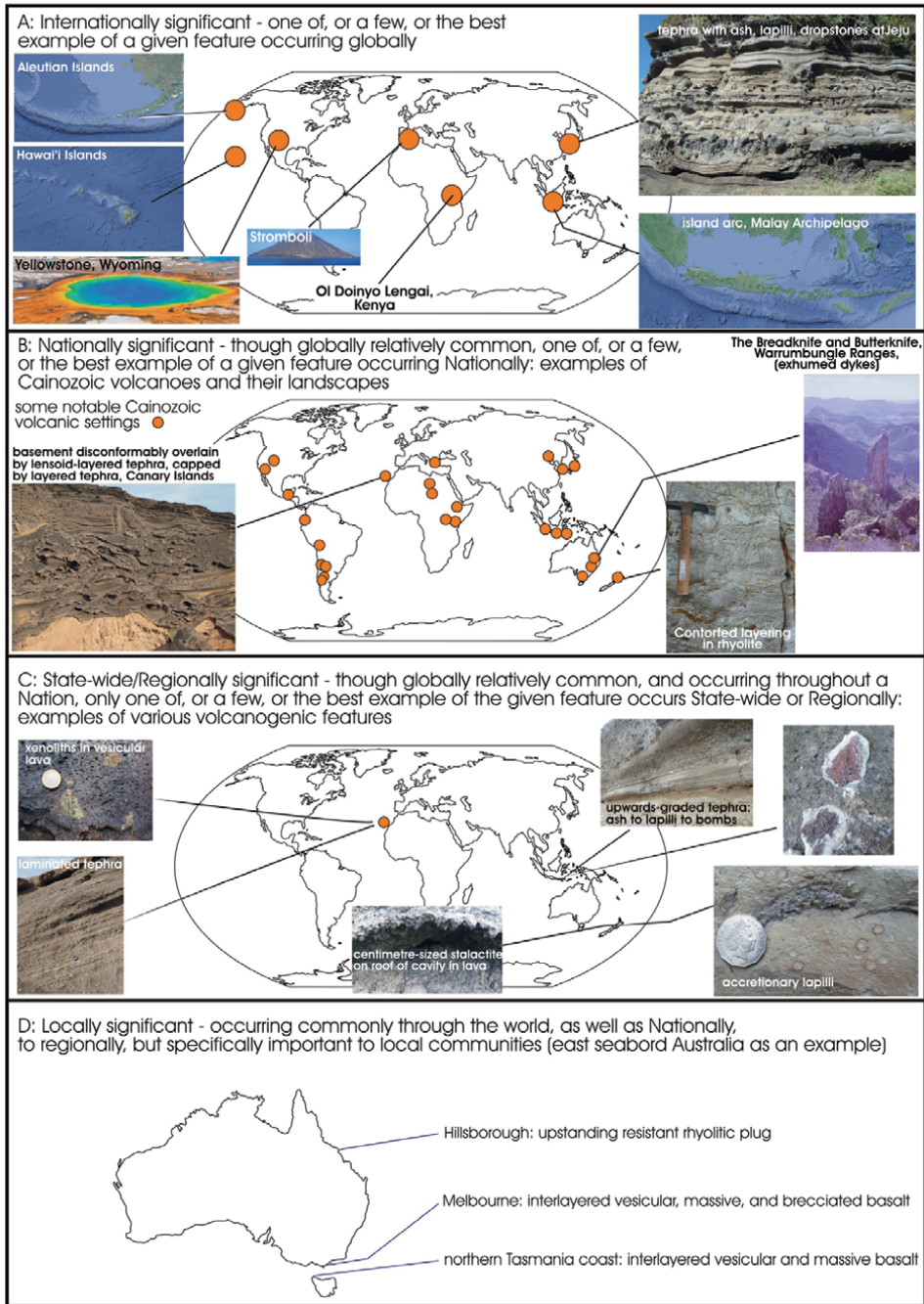


Figure 2. Following Brocx & Semeniuk [17], the four levels of significance recognised in this Chapter (modified from Brocx & Semeniuk [17, 18] and tailored for volcanoes): International, National, State-wide to Regional, and Local. Examples of many volcanoes and their deposits are included in this diagram.

primary texture and mineralogy by interactions with either fluids within the magma (deuterism [or autometasomatism]) or by fluids in the near-surface environment.

A selection of diagrams to illustrate the principles of Geoheritage and how to categorise volcanic sites and evaluate their significance are presented in **Figures 1–3**, and a series of photographic plates illustrating the variety of geometric, stratigraphic arrays, and lithology and mineralogy of volcanoes and volcanic geology are presented in **Figures 4–8**.

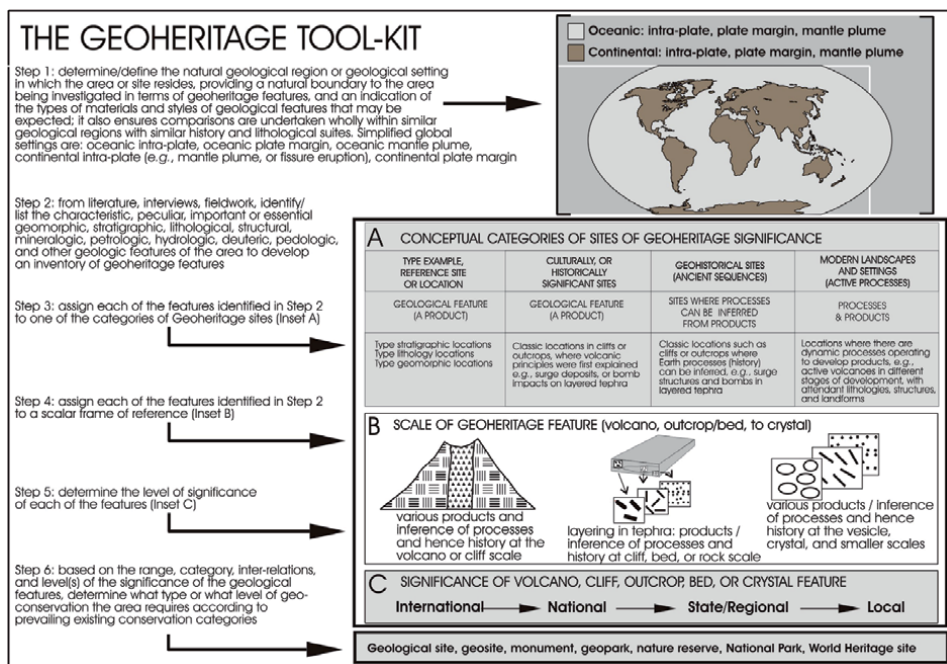


Figure 3. The Geoheritage Tool-kit used to systematically identify and assess sites of geoheritage significance (modified from Brocx & Semeniuk [17] and tailored for volcanoes).

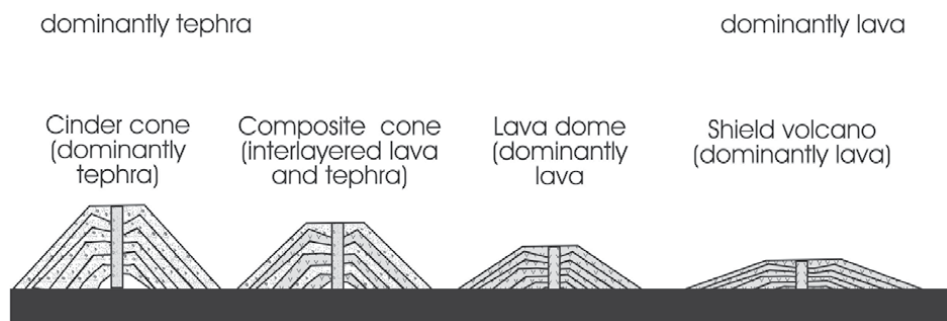


Figure 4. The variety of geometric and stratigraphic arrays of volcanoes, viz., cinder cones, composite (stratovolcanoes), lava cones, and shield volcanoes. This diagram emphasises the gradation from tephra-dominated to lava-dominated eruptions and the corresponding changes in stratigraphy and form of the volcanoes. Fissure vents, and sheet flows are not included.

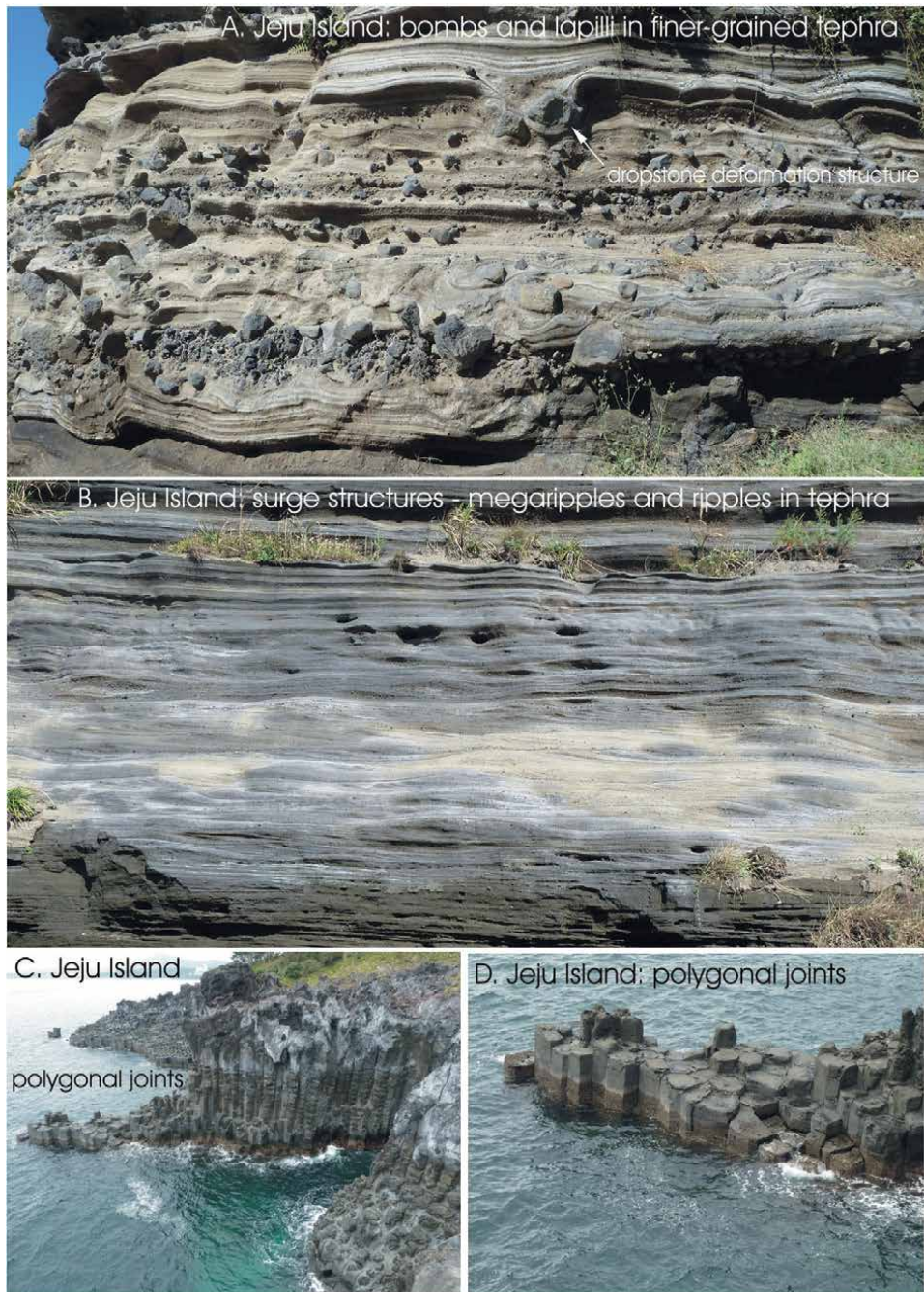


Figure 5. Illustration of a selection of volcanic features at Jeju Island that are of geoheritage significance (photographs also are annotated). A. Bombs and dropstone structures in finer-grained tephra. B. Surge structures of megaripples and ripples in tephra. C & D. Polygonal (hexagonal) columnar jointing in basalt.

2. What is Geoheritage and how does it relate to volcanoes?

Geoheritage, and its sister endeavour, geoconservation, are concerned with the identification, categorisation, and preservation of significant Earth geological features, and are recognised globally as important, as reflected in



Figure 6.

Illustration of a selection of volcanic features at Jeju Island that are of geoheritage significance (photographs also are annotated). A & B. Various interlayered vesicular and massive basalt (coins for scale). C. Vesicular lava filling a small-scale fissure. D. Carbonate stalactites and stalagmites formed by dripping groundwater in a lava tube. E. A complex arrangement of vesicle types (large, medium and small) in basalt. F. Layered tephra with various brown and black lithoclasts in laminated tephra (walking stick is 1 m long). G. Tree trunk (30 cm diameter) that was buried by vesicular lava (north island New Zealand).

various international and intra-national bodies set up for conservation, with agreements, conventions, and inter-governmental initiatives [17, 19–24]. Both endeavours are integral components of the preservation of geological features, geo-education, geotourism, planning and environmental management globally



Figure 7.

Illustration of a selection of volcanic features in the Canary Islands (A, B, C) and at Bali (D, E, F, G) that are of geoheritage significance (photographs also are annotated). A. Complex tephra layering overlying basement rocks. B. Exotic xenoliths in vesicular lava (coin for scale). C. Simple laminated ash with lapilli laminae (lens cap for scale). D. The fan-shaped volcanic deposit emanating from Mt Batur is the 1974 eruption. E. The edge of the 1974 eruption, and the breccia nature of the eruption. E & F. Breccia and mega breccia comprising the rocks of the 1974 eruption (stick in foreground of E is 0.5 m long).

under the World Heritage Convention (and especially in the United Kingdom and in Pan-Europe, *i.e.*, Continental Europe), and across the Globe under various national instrumentalities [19]. Of the large range of geological phenomena that can be assigned to sites of geoheritage significance listed in Table 1 of



Figure 8.

Illustration of a selection of volcanic features at Rotorua, New Zealand. The Rotorua volcanic area presents a complex of rhyolitic lavas and ignimbrites (including dacitic and andesitic lavas), with development of a large caldera and a series of smaller geothermal springs; these images focus on the active geothermal springs and their associated laminated siliceous sinters and sulphurous deposits. Annotated images show geothermal lakes, layered siliceous sinter lining edges of lakes, microbreccia of fragmenting sinter, sulphurous deposit precipitating from a geothermal spring, and closeup of three laminated siliceous sinters.

Brocx & Semeniuk [17], three of the most complex are coastal zones, volcanoes, and caves in that they encompass a plethora of large-scale to small-scale features. Volcanoes are particularly important in that various types of magma erupting at the Earth's surface interact with water, atmosphere, and (pre-existing) rocks, and result in a large variety of volcanic products - this Chapter is focused on the geoheritage significance of volcanoes and their associated diverse geological products.

In an overview, Geoheritage encompasses the legacy of global, national, state-wide, and local features of geology, at all scales from mountain ranges and island arcs to crystals, that are important intrinsically, scientifically, historically, or culturally, offering information or insights into the evolution of the Earth, or into the history of Science, or that can be used for research, education/teaching of geological science, or used for reference [17]. As geoheritage focuses on features that are geological, the scope and scale of what constitutes Geology will determine what is included under the umbrella term 'geoheritage'. The discipline of Geology includes igneous, metamorphic, and sedimentary rocks, stratigraphy, structural geology, geochemistry, fossils and other aspects of palaeontology, geomorphology, soils and pedology, and hydrogeology/hydrology (as listed in Table 1 of Brocx & Semeniuk [17]). From there, all that is encompassed by the discipline of Geology can be included under the umbrella of geoheritage.

The many-and-diverse large- to small-scale features of volcanoes hold potential to be of geoheritage significance particularly as they present diverse magmas,

occur in a vast range of Earth-surface settings and, depending on what materials they interact with, present a large variety of lithologies, structures, and geological relationships between volcanic materials and country rock. Further, volcanoes and volcanic sequences, depending on setting, often present an ensemble of inter-related geological features. For instance, while there may be a degree of structural and volcanic-stratigraphic overlap, the volcanic rock associations, lithologies, and structures of basaltic volcanoes in a submarine and emergent-volcanic-island settings are different to those of andesitic settings to those of rhyolitic settings.

Volcanoes and volcanic geology have existed from Precambrian times to the present, but the emphasis in this Chapter, for purposes of addressing geoheritage values, is on modern and sub-recent examples (*i.e.*, the latter Cainozoic to the latter Quaternary - older volcanic deposits carry with them the complication of imprints and overprints of geomorphic modification, sedimentary reworking, epigenesis, pedogenesis, metamorphism, and structural modifications [18, 25], and thus are outside the scope of this Chapter. However, the principles developed in this Chapter can be applied to these older deposits.

While many sites and features of geoheritage significance can be an isolated geological phenomenon or a stand-alone isolated feature (*e.g.*, Mato Tipila [The Devils Tower] in Wyoming [26–28], a volcanic feature appearing to be related to monogenetic volcanism [28]; or Pamukkale [the Cotton Castle in Turkey] [29]), the same perspective also applies to some aspects of volcanic geology. However, more typically, the majority of volcanic features occur as ensembles of geological phenomena. Thus, a volcano can carry with it several or many of the following that can be (in isolation or collectively) of geoheritage significance: 1. geomorphic form; 2. lithology-specific volcanic form; 3. internal layering of a volcanic cone; 4. complex stratigraphic layering and relationships internal to the volcano; 5. layering of distally-dispersed tephra (*e.g.*, fine-grained ejecta); 6. tephra that is lithologically and granulometrically diverse; 7. tephra with diverse structures (*e.g.*, surge structures, drop-stones structures); 8. tephra interlayered with lahar (water-saturated mudflow or debris flow composed of pyroclastic material and rocky debris); 9. rocks of diverse lithology, such as lavas, plugs, dykes, sills, and diatremes associated with volcanoes; 10. breccia and mega-breccia; 11. lapilli and accretionary lapilli; 12. lava-filled, or empty fumarolic vents (mostly small-scale fissures that are venting gases); 13. dykes (concordant to discordant to volcano layering); 14. lava tubes; 15. lenses/wedges of slumps/avalanches deriving from and inter-layered with fine-grained tephra; and 16. rain-induced mobilisation of tephra forming lenses/wedges of reworked material.

For sites of geoheritage significance, Brocx & Semeniuk designed a globally-applicable Geoheritage Tool-kit to identify geoheritage sites [17, 30, 31] (that is currently recommended by the IUCN [20] and, using Brocx & Semeniuk, the Geological Society of Australia [31]), presented this Tool-kit to categorise geoheritage sites [17]), and a semi-quantitative method to evaluate them [17]. Modified versions of these procedures, tailored for volcanoes and volcanic rocks, are illustrated here in **Figures 1** and **2**. The techniques for classifying/categorising sites of geoheritage significance are applied (following Brocx & Semeniuk [17]) in **Table 1** to four relatively geologically simple localities: 1. bomb-rich tephra, Jeju Island, 2. grainsize-graded tephra, Bali, 3. basement disconformity influencing tephra layering, Canary Islands, and 4. rhyolitic geothermal springs and sinters, Rotorua, New Zealand. Further examples of systematically evaluating levels of significance of geoheritage sites are provided in Tables 1-3 in Brocx & Semeniuk [30].

Geological feature	Type of site, and its scale (category of site from Figure 1)	Significance (based on criteria of Figure 2)	Rationale for assigning the level of significance
<p>Jeju Island (Figures 5 and 6): a regional framework of mainly Pleistocene to Holocene basaltic to trachyandesite to andesite (lavas, tephra, ignimbrites), with lapilli-rich layers alternating with lapilli-depauperate layers, alternating with bomb-rich layers; bomb-rich sequence with local deformation structures of dropped bombs; surge structures (megaripple and ripple lamination) [32]</p>	<p>Geohistorical site; medium scale to small scale; also can be reference site for (1) the variety of tephra deposits, (2) the dropstone effects of bombs, and (3) the stratigraphic/structural record of surges</p>	<p>International</p>	<p>Well-exposed cliff site of multi-lithologic sequence of tephra types and, in particular, the deformation effects of bombs as drop stones and the evidence of surge deposits as ripple lamination and megaripple lamination; useful for research, education and geotours</p>
<p>Bali (Figure 7): a regional framework of basaltic to dacitic volcanism (lavas, tephra, ignimbrites), a layered deposit of relatively fine-grained tephra (ash), overlain by coarse grained ejecta (lapilli), in turn overlain by bomb-sized and block-size ejecta [33, 34]</p>	<p>Though the volcanoes of Bali represent active geological sites, the cliff illustrated in Figure 7B is a geohistorical site; medium scale to small scale; also can be reference site for the graded upward coarsening of tephra deposits</p>	<p>State-wide to Regional</p>	<p>Well-exposed cliff site of grain-size-graded ejects grading from relatively fine-grained to block-sized showing a history of increasing intensity of volcanic activity; useful for research, education and geotours</p>
<p>Canary Islands (Figure 7): within a framework of diverse volcanic rocks ranging from basalt and basanite to trachyte to trachyandesite in which are recognised five developmental stages, there are local occurrences of basement topographic highs which influenced layering in deposition of tephra [35–38]</p>	<p>Ancient geohistorical site; medium scale to small scale; can be reference site for the effect of basement rock topography on tephra layering</p>	<p>National</p>	<p>Well-exposed site of Cainozoic tephra with complex lensoid layering above a basement topographic high followed by horizontal tephra layering; useful for research, education and geotourism</p>
<p>Rotorua (Figure 8): a framework of rhyolitic lavas and ignimbrites (including dacitic and andesitic lavas) forming a large caldera and a series of smaller geothermal springs; active geothermal springs are forming laminated siliceous sinters and sulphurous deposits [39, 40]</p>	<p>Active volcanic site; medium scale to small scale; plethora of surface features and derivative products from siliceous sinter (e.g., microbreccia of fragmenting sinter)</p>	<p>International</p>	<p>Well-exposed site of rhyolitic rocks and ignimbrites, geothermally-derived siliceous sinters, active geothermal springs; useful for research, education and geotourism</p>

Table 1.
Features of geoheritage significance Jeju Island, Bali, Canary Islands, and Rotorua, and the rationale for the assessment.

3. Application of geoheritage and geoconservation principles.

Unlike significant single geological features, such as the Siccar Point unconformity in Scotland [41] or the K/T contact at Gubbio in Italy [42], volcanoes commonly present a multitude of interrelated geological features from the large scale to the small scale each of which frequently carry geoheritage significance. Given this wide range of volcanic features on Earth in terms of their diversity, magma type, the interactions with pre-existing rocks, magma, and water, and scale of features, volcanoes and their multitude of products, in practice, present complex systems to classify and assess as sites of geoheritage significance. Leaving aside the older volcanic deposits, the modern and sub-recent examples on their own are diverse and significant enough and provide important stories about the Earth and important insights into the functioning and geochemistry of the Earth crust. For instance, at a global level, geochemically, volcanoes illustrate the chemical variability of the Earth's crust latitudinally, longitudinally, as well as in terms of geological settings (*viz.*, in broad terms, oceanic *versus* continental). At smaller scales, volcanoes and their products, in interacting with rocks, water, and atmosphere, provide a wealth of geological features that are great stories of the Earth and hence of great heritage (geoheritage) significance. In this context, the geoheritage significance of volcano types, volcanic deposits, volcanic landscapes, and secondary volcanic landscapes (such as landslides and rockfalls) was recently addressed in the Journal *Geoheritage* [43–47] and in [48].

The best way to comparatively assess and deal with the geoheritage significance of volcanoes and volcanic products is to address their diversity (often *incomparable* from site to site) and commence with an approach of geological setting, magma types, and scale. This is because volcanoes, volcanic activity, and volcanic products, though branded together under the ‘umbrella’ term of volcanoes, can be markedly different in the various geological settings, expressed as a diversity of magma types, and will express various and different geological phenomena at various scales - from these perspectives, volcanoes in these different environments are not comparable. There are proposed four spatial scales with which to systematically deal with volcanoes and their products (**Table 2**).

Examples of global to sub-global scale volcanic features
<i>Geological setting</i> : oceanic crust; sites of mantle plumes; island arcs; continental margin volcanoes; intra-continental plate volcanoes
<i>Magma type(s)</i> : basaltic suite; andesitic suite; acidic volcanic suite
Examples of regional scale volcanic features
Types of volcanoes geomorphologically; types of volcanoes behaviourally; chains of volcanoes; fissures; lava tubes
Examples of local scale volcanic features
Massive lava; layered/laminated lava; brecciated lava; bombs; pillow lava; disconformities; complex stratigraphy; types of tephra; layering in tephra; structures in surge deposits; lava tube; diatremes and their complex stratigraphy; dykes; geothermal springs; sinters
Examples of small scale volcanic features
Vesicles; stretched vesicles; lapilli; accretionary lapilli; crystal fill of vesicles; crystal fill of fractures; deuteric precipitates; stalactitic and stalagmitic deposits in lava tube; bombs and their deformation (dropstone) structures in tephra; fissures and crystal or lava filled fissures; lithoclasts/xenoliths; xenocryst; shards

Table 2.
Examples of large to small scale volcanic features occurring at the four spatial scales.

Given the scope of volcanic geology, the list above, axiomatically, is not exhaustive, but provides an insight on how to assess and evaluate the geoheritage significance of volcanoes. Outside of the spatial scale (or size) that volcanic features can occur, there is also a significance or evaluation that can be attributed to them, as follows (**Figure 3**):

1. Internationally significant.
2. Nationally significant.
3. State-wide to regionally significant.
4. Locally significant.

For geoconservation, once a site, area, or region is assessed as being of geoheritage significance, then measures should be undertaken to protect the more significant sites, and/or utilise them for conservation in perpetuity, or for research, education, and geotours in a managed manner. Sites, areas, or regions can be allocated/inscribed for geoconservation as World Heritage Sites, National Parks, geological conservation reserves, type localities for rocks and minerals, reference sites or reference localities for volcanic features, a geological monument, a geopark, or a geotrail (as described and discussed by Brocx & Semeniuk [49, 50]). Where there is an ensemble of volcanic features illustrating the story of volcanoes on the Earth, the suite of features would be ideally integrated into a thematic geopark, such as at Jeju Volcanic Island, Yellowstone National Park, and Hawaii (Hawai'i) National Park.

The large-scale sub-global array of volcanoes forming island arcs in the Malay Archipelago and that in the Aleutian Islands, being unusual and/or unique in the World, would be viewed as globally significant World Heritage Sites [51, 52]. The smaller-scale presentation of tephra deposits, their complex stratigraphy, and bombs such as that cropping out at Jeju Island would be (and is) a smaller-scale World Heritage Site [32]. So too, the island chain system located on a hot mantle plume at Hawaii (Hawai'i) would be a World Heritage Site [53]. Other volcanic centres that exhibit unusual or extraordinary features such as the carbonatite eruption at Ol Doinyo Lengai in Kenya [54, 55], and the rhyolites, tuffs, and some basalts in the Yellowstone Caldera [56, 57] also would be World Heritage Sites. Many of these volcanic sites are already allocated to globally-significant conservation reserves but the point of this text is to highlight that they have features ranging from sub-global scale to smaller scales that qualify them as being of geoheritage significance in contrast to many other volcanic sites that have a different (but also significant) set of attributes that have yet to be rigorously allocated to geoheritage significance.

In, as a result of the complex interplay between magma in the Earth's interior, its ascent through the crust, and its eruption at the surface, there is a rich geological variability in volcanoes in terms of conclusion geometry, structure, stratigraphy, lithologies, volcano-to-country-rock relationships, contact metamorphism, and near-surface alteration often specific and relevant to a particular geological region or province. Across the globe, this results in a geological natural-history resource and geological museum of geoheritage significance that is useful for research, education and geotours, and provides a window into near-surface Earth processes, deep-Earth processes, the history of the Earth and, given crustal heterogeneity, development of specific suites of volcanic features restricted to particular tectonic settings.

Author details

Margaret Brocx^{1*}, Vic Semeniuk^{2,3}, Tom J. Casadevall⁴ and Dan Tormey⁵

1 Environmental and Conservation Sciences, Murdoch University,
Western Australia

2 V & C Semeniuk Research Group, Warwick, Western Australia


3 School of Arts and Sciences, Notre Dame University, Fremantle,
Western Australia

4 United States Geological Survey, California, USA

5 Catalyst Environmental Solutions, Santa Monica, California, USA

*Address all correspondence to: geoheritage@iinet.net.au

IntechOpen

© 2021 The Author(s). Licensee IntechOpen. This chapter is distributed under the terms of the Creative Commons Attribution License (<http://creativecommons.org/licenses/by/3.0>), which permits unrestricted use, distribution, and reproduction in any medium, provided the original work is properly cited. 

References

- [1] Gill J B (ed) 1981. *Orogenic andesite and plate tectonics*. Springer, Berlin Heidelberg New York.
- [2] Thorpe R S (ed) 1982. *Andesites: orogenic andesites and related rocks*. John Wiley & Sons, Chichester. ISBN 0 47128034 8. 724 p.
- [3] Bowes D R (ed) 1989. *The encyclopaedia of igneous and metamorphic petrology*. New York: Van Nostrand Reinhold (666 p).
- [4] Sutherland L 1995. *The volcanic Earth*. UNSW Press. 248p.
- [5] Sigurdsson H (ed) 2015. *The encyclopedia of volcanoes* (2nd ed). Academic Press, 1456 p. ISBN: 978-0-12-385938-9. doi.org/10.1016/C2015-0-00175-7.
- [6] Schmincke H-L 2004. *Volcanism*. Springer, Berlin.
- [7] Andújar J, Scaillet B, Pichavant M & Druitt T H 2016. Generation conditions of dacite and rhyodacite via the crystallization of an andesitic magma. Implications for the plumbing system at Santorini (Greece) and the origin of tholeiitic or calc-alkaline differentiation trends in arc magmas. *Journal of Petrology* 57 (10): 1887-1920, <https://doi.org/10.1093/petrology/egw061>
- [8] Paredes-Marino J, Scheu B, Montanaro C, Arciniaga-Ceballos A, Dingwell D B & Perugini D 2019. Volcanic ash generation: effects of componentry, particle size and conduit geometry on size-reduction processes. *Earth and Planetary Science Letters* 514: 13-27.
- [9] White J D L & Ross P S 2011. Maar-diatreme volcanoes: a review. *Journal of Volcanology and Geothermal Research* 201: 1-29.
- [10] Lorenz V 1985. Maars and diatremes of phreatomagmatic origin, a review. *Transactions of the Geological Society of South Africa*, 88: 459-470.
- [11] Németh K & Kósik S 2020. Review of explosive hydrovolcanism. *Geosciences* 2020, 10, 44: 27 pp. <https://doi.org/10.3390/geosciences10020044>
- [12] Martí J, Gropelli G, Brum da Silveira A 2018. Volcanic stratigraphy: a review. *Journal of Volcanology & Geothermal Research* 357:68-91
- [13] Nemeth K & Palmer J 2019. Geological mapping of volcanic terrains: discussion on concepts, facies models, scales, and resolutions from New Zealand perspective. *Journal of Volcanology & Geothermal Research* 385:27-45
- [14] Gilbert J S & Lane S J 1994. The origin of accretionary lapilli. *Bulletin of Volcanology* 56: 398-411.
- [15] Schumacher R & Schmincke H-U 1995. Models for the origin of accretionary lapilli. *Bulletin of Volcanology* 56: 626-639.
- [16] Van Eaton A R & Wilson C J N 2013. The nature, origins and distribution of ash aggregates in a large-scale wet eruption deposit: Oruanui, New Zealand. *Journal of Volcanology and Geothermal Research* 250:1 29-154.
- [17] Brocx M & Semeniuk V 2007. Geoheritage and geoconservation - history, definition, scope and scale. *Journal of the Royal Society of Western Australia* 90: 53-87.
- [18] Jovic, V 1998. Epigenesis. In: Marshall C P & Fairbridge R W (eds.). *Geochemistry*. Encyclopaedia of Earth Science. p. 115. doi:10.1007/1-4020-4496-8_115. ISBN 0-412-75500-9

- [19] Brocx M 2008. Geoheritage - from global perspectives to local principles for conservation and planning. Western Australian Museum, 175p. ISBN 978-1-920843-35-9.
- [20] Worboys G L, Lockwood M, Kothari A, Feary S & Pulsford I (eds). 2015. *Protected area governance and management*. ANU Press, Canberra (2015)
- [21] Casadevall T J, Tormey D & Roberts J 2019. World Heritage volcanoes: classification, gap analysis, and recommendations for future listings. (IUCN-2019-020)
- [22] Casadevall T J, Tormey D & van Sistine D 2019. Protecting our global volcanic estate: Review of international conservation efforts. *International Journal of Geoheritage and Parks* 7(4): 182-191.
- [23] Brocx M & Semeniuk V 2010. The geoheritage significance of crystals. *Geology Today* 26: 216-225.
- [24] Díaz-Martínez E 2011. Typology of heritage: where does geoheritage fit in? *Forum GeoReg* 23-27 Oct. 2011, Villeneuve d'Ascq — Résumés / Abstract
- [25] Cas R A F & Wright J V 1988. *Volcanic successions modern and ancient*. Chapman & Hall, London. 528 p
- [26] Darton N P 1909. *Geology and water resources of the northern portion of the Black Hills and adjoining regions in South Dakota and Wyoming U.S.* Geological Survey Professional Paper 65 (1909). doi:10.3133/pp65
- [27] Robinson C S 2015. *Geology of Devils Tower National Monument, Wyoming - a contribution to general geology*. eBook #49966. <https://www.gutenberg.org/files/49966/49966-h/49966-h.htm#c4>
- [28] Závada P, Dědeček P, Lexa J & Keller G R 2015. Devils Tower (WY, USA) – a lava coulée emplaced into a maar-diatreme volcano? *Geosphere*. 11(2): 354-375.
- [29] Dilsiz C 2002. Environmental issues concerning natural resources at Pamukkale protected site, southwest Turkey. *Environmental Geology* 41: 776-784.
- [30] Brocx M & Semeniuk V 2015. Using the Geoheritage Tool-kit to identify inter-related geological features at various scales for designating geoparks: case studies from Western Australia. *In: E Errami, M Brocx & V Semeniuk (eds), From Geoheritage to Geoparks -Case Studies from Africa and Beyond*. Springer, Amsterdam, 245-259.
- [31] Brocx M 2018. The Geoheritage Tool-kit for the Geological Society of Australia Inc. https://www.gsa.org.au/Public/Geoheritage/Geoheritage-Tool-Kit/Public/Geoheritage/Geoheritage_Tool-Kit.aspx?hkey=2f275860-e038-4bfa-8a59-f13fbe657c19.
- [32] Woo K, Sohn Y, Ahn U, Yoon S, Spate A 2013. *Geology of Jeju Island*. *In: Jeju Island Geopark - A Volcanic Wonder of Korea*. Geoparks of the World (closed) (Development and Management), vol 1. Springer, Berlin, Heidelberg. https://doi.org/10.1007/978-3-642-20564-4_5.
- [33] Wheller GE & Varne R 1986. Genesis of dacitic magmatism at Batur volcano, Bali, Indonesia: Implications for the origins of stratovolcano calderas. *Journal of Volcanology and Geothermal Research* 28: 363-378.
- [34] Sutawidjaja I S 2009. Ignimbrite analyses of Batur Caldera, Bali, based on ¹⁴C Dating. *Indonesian Journal on Geoscience* 4(3): 189-202.
- [35] Pérez Torrado, F.J., 1998. Hotspot volcanism close to a passive continental

margin: the Canary Islands. *Geol. Mag.*, 135, 591-604.

[36] Anguita F. and Hernán, F., 2000. The Canary Islands origin: a unifying model. *J. Volcanol. Geotherm. Res.*, 103, 1-26.

[37] Carracedo, J.C. and Troll, V.R. (2016) *The Geology of the Canary Islands*, Amsterdam, Elsevier, ISBN 978-0-12-809663-5

[38] Viñuela J M 2010. The Canary Islands Hot Spot. <http://www.mantleplumes.org/>

[39] Healy J 1962. Geology of the Rotorua district. In: *Vulcanicity and Vegetation in the Rotorua District*, 1962 Conference. pp 53-58

[40] Leonard, G.S.; Begg, J.G.; Wilson, C.J.N. (compilers) 2010: *Geology of the Rotorua area*. Institute of Geological & Nuclear Sciences 1:250 000 geological map 5. 1 sheet + 102 p. Lower Hutt, New Zealand. GNS Science.

[41] Barclay W J, Browne M A E, McMillan A A, Pickett E A, Stone P & Wilby P R 2005. *The Old Red Sandstone of Great Britain*. Geological Conservation Review Series, No. 31, Joint Nature Conservation Committee, Peterborough, 393 p.

[42] Alvarez W 2009. The historical record in the Scaglia limestone at Gubbio: magnetic reversals and the Cretaceous-Tertiary mass extinction. *Sedimentology* 56: 137-148. doi: 10.1111/j.1365-3091.2008.01010.x.

[43] Migon P & Pijet-Migon E 2016. Overlooked geomorphological component of volcanic geoheritage-diversity and perspectives for tourism industry, Pogrze Kaczawskie Region, SW Poland. *Geoheritage* 8(4): 333-350.

[44] Nemeth K, Casadevall T, Moufti M R & Marti J (2017.) Volcanic geoheritage. *Geoheritage* 9(3):251-254

[45] Nemeth K, Wu J, Sun C & Liu J 2017. Update on the volcanic geoheritage values of the Pliocene to Quaternary Arxan-Chaihe Volcanic Field, Inner Mongolia, China. *Geoheritage* 9(3): 279-297

[46] Sheth H, Samant H, Patel V & D'Souza J 2017. The volcanic geoheritage of the Elephanta Caves, Deccan Traps, Western India. *Geoheritage* 9(3): 359-372.

[47] Fepuleai A & Nemeth K 2019. Volcanic geoheritage of landslides and rockfalls on a tropical ocean island (Western Samoa, SW Pacific). *Geoheritage* 11(2): 577-596.

[48] Dóniz-Páez J, Beltrán-Yanes E, Becerra-Ramírez R, Pérez N M, Hernández P A & Hernández W 2020. Diversity of volcanic geoheritage in the Canary Islands, Spain. *Geosciences* 10: 390, 19 pp.

[49] Semeniuk V & Brocx M 2021. A globally significant potential megascale geopark: the eastern Australian mantle hotspot interacting with a north-migrating heterogeneous continental plate creating a variety of volcano types, magmas, xenoliths, and xenocrysts. *IntechOpen* (this Volume).

[50] Brocx M & Semeniuk V 2019. The "8Gs" - a blueprint for Geoheritage, Geoconservation, Geo-education and Geotourism. In: M. Brocx, V. Semeniuk & K. Meney (eds), *Thematic Issue on Geoheritage and Geoconservation in Australia*. *Australian Journal of Earth Sciences* 66: 803-821.

[51] Hall R 2017. Southeast Asia: new views of the geology of the Malay Archipelago. *Annual Reviews of Earth and Planetary Sciences* 45: 331-358.

[52] Holbrook W S, Lizarralde D, McGeary S, Bangs N & Diebold J 1999. Structure and composition of the Aleutian island arc and implications for

continental crustal growth. *Geology*
27(1): 31-34.

[53] Decker R W, Wright T L & Stauffer
P H 1987. *Volcanism in Hawaii*. Volume 1.
US Geological Survey Professional Paper
1350. 861p.

[54] Dawson J B 1998. Peralkaline
nephelinite- natrocarbonatite
relationships at Oldoinyo Lengai,
Tanzania. *Journal of Petrology* 39:
2077-2094.

[55] Harmer R E & Gittens J 1998. The
case for primary, mantle-derived
carbonatite magma. *Journal of
Petrology* 39: 1895-1903.

[56] James D, Fouch M, Carlson R W &
Roth J 2011. Slab fragmentation, edge
flow and the origin of the Yellowstone
Hotspot Track. *Earth and Planetary
Science Letters* 311(1-2): 124-135.

[57] Christiansen R L 2001. The
Quaternary and Pliocene Yellowstone
Plateau volcanic field of Wyoming,
Idaho, and Montana. US Geological
Survey Professional Paper 729-G. 156p.

A Globally Significant Potential Megascale Geopark: The Eastern Australian Mantle Hotspot Interacting with a North-Migrating Heterogeneous Continental Plate Creating a Variety of Volcano Types, Magmas, Xenoliths, and Xenocrysts

Vic Semeniuk and Margaret Brocx

Abstract

Australia commenced separating from Antarctica some 85 million years ago, finally separating about 33 million years ago, and has been migrating northwards towards the Eurasian plate during that time. In the process, Australia, on its eastern side, progressively passed over a mantle hotspot. A magma plume intersected a variable lithocrust with various lithologic packages such as Phanerozoic sedimentary basins, fold belts and metamorphic terranes, and Precambrian rocks. As such, there was scope for compositional evolution of magmas through melting and assimilation, as well as plucking of host rocks to include xenoliths, and xenocrysts. The volcanic chain, volcanoes, and lava fields that are spread latitudinally along 2000 km of eastern Australia present a globally-significant volcanic system that provides insights into magma and crust interactions, into the variability of xenoliths and xenocrysts, into magma evolution dependent on setting, and into the mantle story of the Earth. The Cosgrove Volcano Chain is an example of this, and stands as a globally-unique potential megascale geopark.

Keywords: Australia, mantle hotspot, volcanic chain, Cosgrove Volcano Chain, heterogeneous continental plate, potential megascale geopark

1. Introduction

Heritage is a legacy from the past. It includes architectural heritage, art heritage, cultural heritage, as well as geological heritage. Geological heritage (or geoheritage) is the legacy of the Earth that has preserved the story, at all scales, of its inception and history

in terms of rock types, major geological structures, history of Life (in fossils), and many other features. In detail, Geoheritage resolves down to the identification, categorisation, and preservation of significant Earth geological features, and is recognised as important globally, as reflected in various international and intra-national bodies set up for conservation, with agreements, conventions, and inter-governmental initiatives [1–4].

To date, however, Geoheritage has mostly focused on medium and large-scale features and cliff faces of significant geology and, in some cases, geological phenomena at the crystal scale [5]. Examples of recognised sites of geoheritage significance include columnar basalt, Isle of Staffa, Scotland [6], chevron folds, Millook Haven, England [7], the Silurian and Devonian unconformity at Siccar Point, Scotland [8], the Cretaceous/Tertiary boundary (K/T contact) at Gubbio, Italy [9], Cambrian fossils, Burgess Shale, Canada [10], the Precambrian Ediacara fauna, Rawnsley Quartzite, South Australia [11], and Uluru, a very large inselberg of geological (and cultural) importance in central Australia [12]. Generally, geological features at the sub-global scale, involving 1000s of kilometres, unless partly integrated into large-scale geoparks, are not included as geoheritage sites: examples include entire mountain chains such as The Himalayas and The Andes that formed by tectonic plate collisions, or extensive (subcontinental-scale) sand-dominated deserts (e.g., the Great Sandy Desert of Western Australia), extensive plains/plateaux formed by lava outpourings (e.g., the Deccan Traps [Deccan Plateau], India), island arcs, and extensive inland-located volcanic chains (such as the Cosgrove hotspot track [13] in eastern Australia or, in our terms, the Cosgrove Volcano Chain, the subject of this Chapter). Exceptions to this are the 2300-km-long Great Barrier Reef offshore from eastern Australia, and Shark Bay (150 km x 100 km), both World Heritage Sites and with geoheritage as a component of their nominated values [14–17].

Brocx & Semeniuk developed the Geoheritage Tool-kit [18], a classification system to categorise and assess sites of geoheritage significance (**Figure 1**), and a

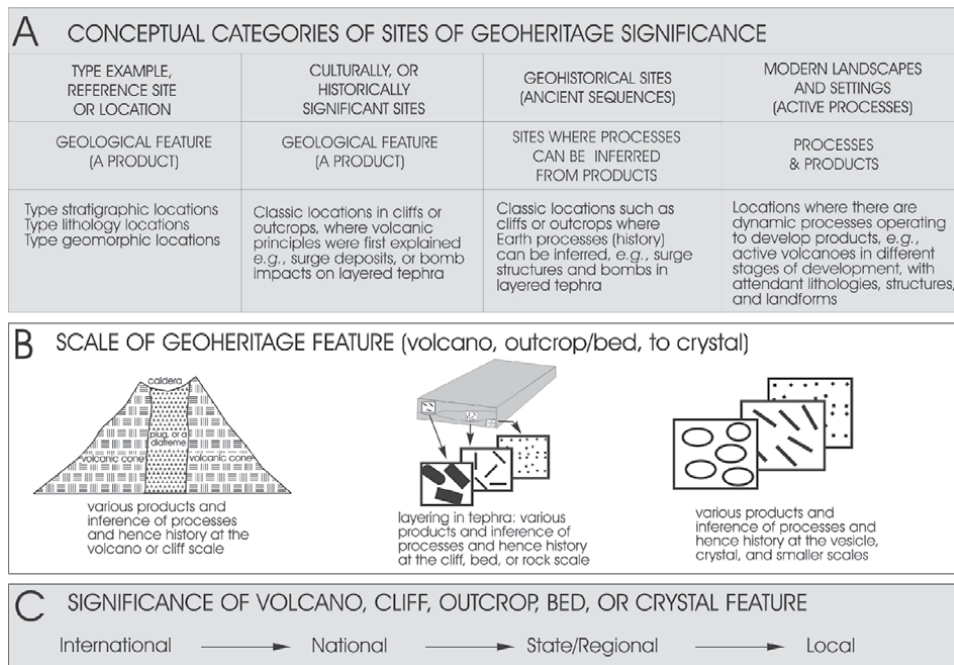


Figure 1. Diagram showing the scope of geoheritage in terms of its conceptual categories, its scales of application, and potential levels of significance (modified from Brocx & Semeniuk 2007, with an emphasis on volcanology).

semi-quantitative evaluation method to determine their International, National, State-wide to Regional, or Local significance (**Figure 2**) [1]. This system has been adopted in other countries and in different geological contexts [18–20]. Brocx & Semeniuk also addressed spatial scale in categorising sites of geoheritage value and identified/defined the small, medium, and large scales of reference

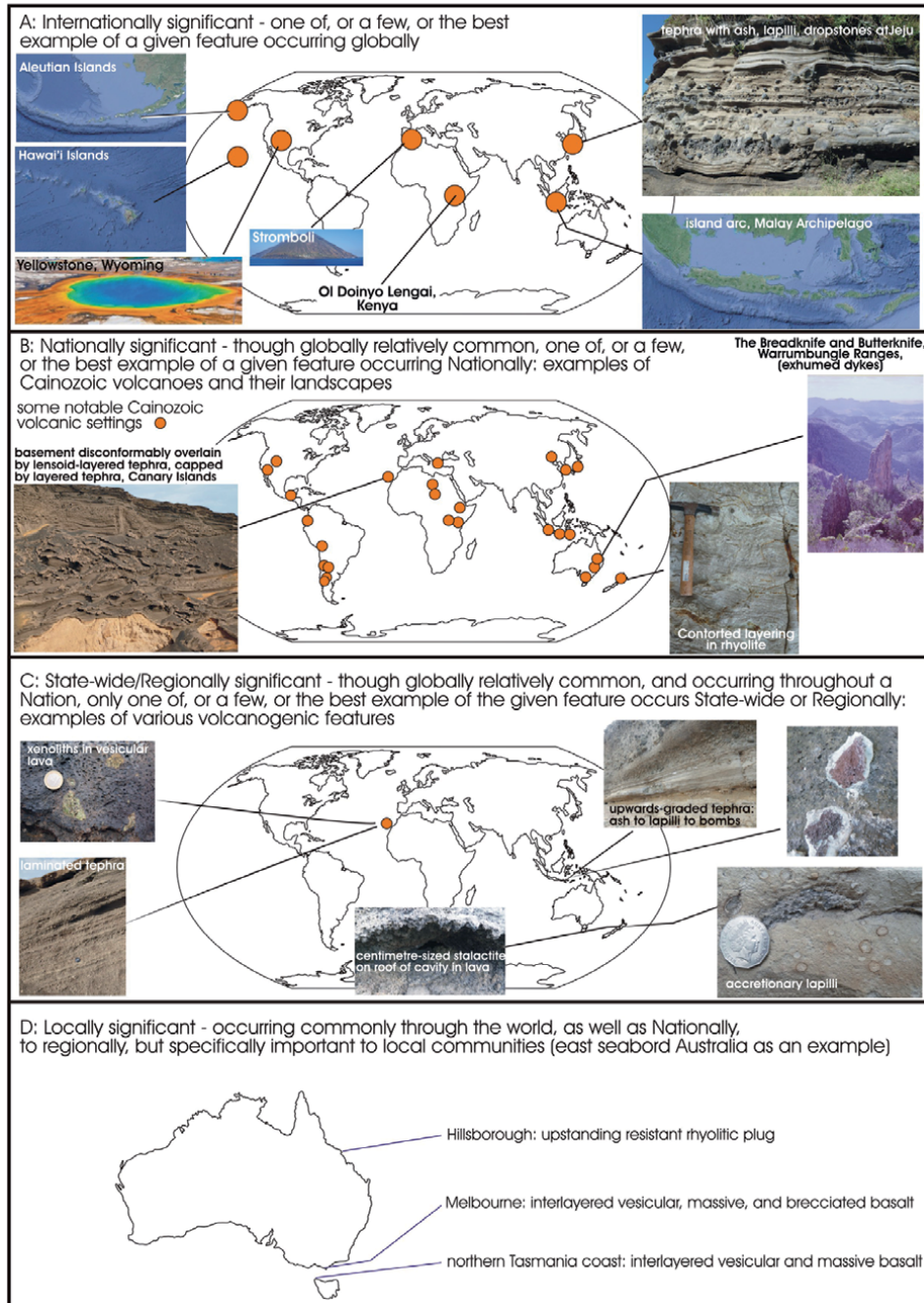


Figure 2. Diagrammatic representation of the levels of significance applicable to volcanic geoheritage features (modified from Brocx & Semeniuk 2007, with an emphasis on volcanology). A: International; B: National; C: State-wide to regional; and D: Local. Definitions (after Brocx & Semeniuk 2007) are embodied in the diagram. This method of evaluation is semi-quantitative.

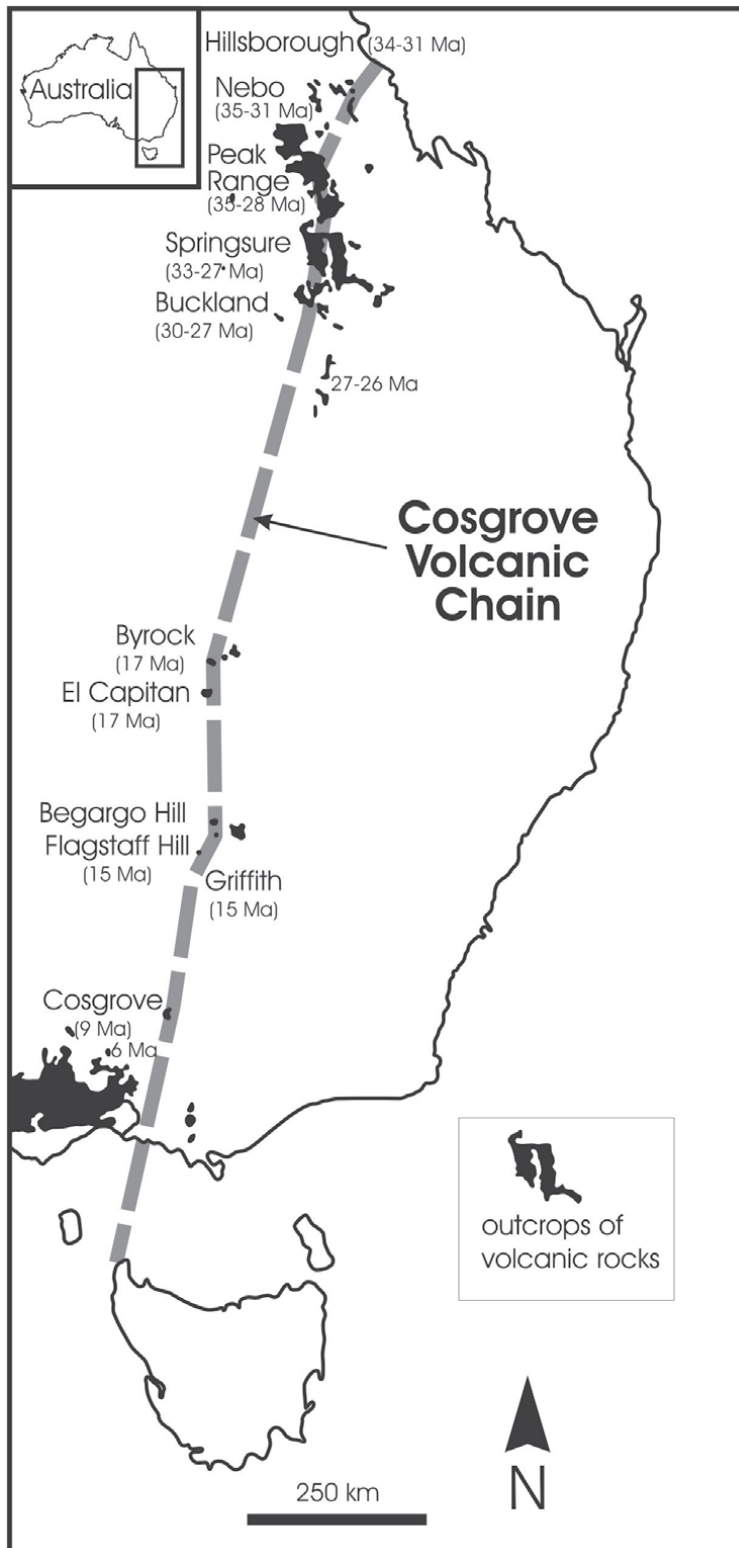


Figure 3. Map of eastern Australia showing outcrops of Cainozoic volcanism and their ages, and the general trackway of the Cosgrove volcanic chain (modified from Davies et al. [21]).

assigning numerical limits to the scale of reference [1], but did not venture to the megascala involving mountain chains and other the sub-global geological phenomena noted above.

Sites of geoheritage significance, regardless of their scale, are important to Society in that they preserve a history of the Earth, can be used for research and teaching, provide reference localities, provide a record of the history of scientific enquiry, can function as sites for geotours, and may be linked to Indigenous cultural history and values (Row A, **Figure 1**). The sites of geoheritage significance listed above [6–12] accord with these principles.

In this context, the Cosgrove Volcano Chain (some 2000 km long) in eastern Australia (**Figure 3**) is an example of an extensive suite of volcanic rocks that have global geoheritage significance and qualify to be recognised as a globally-important mega-geopark. To convey this concept, this paper is structured as follows:

1. mantle plumes, and the significance of xenoliths, xenocrysts, and magma mixing
2. the eastern Australian volcanic framework
3. the eastern Australian continent geological framework
4. geoheritage significance of the eastern Australian Cosgrove Volcano Chain
5. Discussion and Conclusions: a globally-significant mega-geopark centred on the Cosgrove Volcano Chain.

While the innumerable papers on the eastern Australian volcanic corridor have focused on petrology, geochemistry, mechanisms of emplacement and extrusion, and origin of the magma [22–26], this Chapter definitively focuses on the geoheritage significance of one volcanic chain [13].

2. Mantle plumes, and the significance of xenoliths, xenocrysts, and magma mixing

Convection of hot rock within the Earth's mantle has been proposed as the mechanism for the formation of a magmatic plume or mantle plume (acting like a diapir) that results in volcanic hotspots such as those located at Hawaii or Iceland, and for large igneous provinces such as the Deccan Traps [27–29]. Mantle plumes are thought essentially to be areas of hot, upwelling magma, with a hotspot that develops above the plume (this is the Wilson-Morgan hypothesis of hotspots, typified by high heat flow, positive gravity anomaly and alkalic volcanism, resulting in surface expressions of mantle plumes rising by thermal convection [30]). Magma generated by hotspots rises through the more rigid overlying lithosphere and produces active volcanoes and lava flows at the Earth's surface [31–34]. Accompanying, and critical to this process is the fact that, on its ascent, a plume will entrain rock fragments from deep in the Earth's crust (evident as mafic and ultramafic xenoliths) or, when traversing the lithosphere such as sedimentary basins higher in the Earth's crust, entrain Phanerozoic and Proterozoic xenoliths such as sandstone, shale, coal, low-grade metamorphic rock, and granite [21, 30, 32–36]. Where there is melting or partial melting, xenocrysts can be released [30, 37–40]. Also, where there is melting or partial melting of the lithosphere there is geochemical contamination of magma [37, 38].

To account for geochemical heterogeneity in hotspot and flood basalt lavas, Farnetani & Richards [37] suggest either inherent plume-source heterogeneity or contamination from the lithosphere through which the primary magma ascended. We accord with the latter, *i.e.*, contamination from a heterogeneous lithosphere, particularly when the magma rises through a thick lithosphere [13] or through a complex sedimentary basin.

3. The eastern Australian volcanic framework

Australia commenced separating from Antarctica some 85 million years ago, finally separating some 33 million years ago, and has been migrating northwards towards the Eurasian plate [13, 23, 33, 40, 41]. In the process, it progressively passed over a mantle hotspot on its eastern side.

Globally, volcanic activity typically is located at the edge of a tectonic plate boundary (subduction zone), or a rift, or a crustal spreading zone [35–39]. However, along the length of eastern Australia in response to the continent passing over the mantle hotspot, there is a wide ‘corridor’ or trackway of volcanoes and eruptive activity that is quite distant from the edge of the Indo-Australian Plate, and here volcanism appears related to a mantle plume, or a cluster of mantle plumes, or at least a mantle plume that, over time, found several proximally related weaknesses in the lithosphere through which to intrude and erupt. Sutherland [41] first suggested plate migration over magmatic upwellings with the oldest Australian volcanoes in north Queensland, and the eruptive centres have moved southwards as the Australian plate has drifted northwards over a mantle plume, forming a ‘corridor’ of eruptive and magmatic activity.

The volcanoes in this corridor have been active along the eastern part of Australia for at least the last 33 million years [40], showing a *series of volcanic tracks* with some starting in the north some 33 Ma ago, and others starting mid-length along the Australian eastside some 27–21 Ma ago; these various trackways have been mapped by different authors and range in age from the oldest to the north and youngest to the south [25, 40–48]. These trackways, showing a younging to the south, implicate a northward drift of the continent over a mantle hotspot as the Indo-Australian plate (a major tectonic plate that includes the continent of Australia and surrounding ocean, and extends northwest to include the Indian subcontinent and adjacent waters [43–45, 49]) migrated over a relative stable (static) mantle plume [13, 36, 42]. It has been estimated that the eastern part of the Indo-Australian Plate (Australia) is moving northward at the rate of 5.6 cm per year while the western part (India) is moving only at the rate of 3.7 cm per year due to the impediment of the Himalayas [43–46].

Within this corridor, volcanism has been expressed as eruptions determined by the thickness of the lithosphere [13]. Of interest in this Chapter, the main trackway within the corridor is what Davies *et al.* [13] termed the ‘Cosgrove hotspot track’ which we term the ‘Cosgrove Volcano Chain’ (**Figure 3**). Davies *et al.* linked the volcanoes, eruptive centres, and magmatic activity along the ‘Cosgrove hotspot track’ (or ‘Cosgrove Volcano Chain’) based on a number of criteria: *viz.*, 1. standard basaltic compositions of magma in regions where lithospheric thickness is less than 110 km, 2. volcanic gaps in regions where lithospheric thickness exceeds 150 km, and 3. low volume, leucite eruptions in regions of intermediate lithospheric thickness. Davies *et al.* found that trace-element concentrations along this track support the notion that compositional variations result from different degrees of partial melting, controlled by the thickness of overlying lithosphere, and concluded that lithospheric thickness played a dominant role in determining the volume and chemical composition of plume-derived magmas [13].

From south to north, with increasing age, the volcanoes in the Cosgrove Volcano Chain have been increasingly eroded so that with the oldest volcanoes all that often remains of the volcanic morphology is the erosion-resistant plug and the array of dykes. Clearer and more evident volcanic landscapes are present in the younger terrain to south.

The principles we intend to develop for the Cosgrove Volcano Chain in terms of magma mixing, nature of xenoliths and xenocrysts, the influence of lithospheric lithologies on both xenolith types and magma contamination, and the relationship of volcanic expression to crust thickness are applicable to other volcanic trackways in the eastern Australia volcanic corridor and, as will be discussed later, have geoheritage relevance.

4. The eastern Australian continent geological framework

Eastern Australia contains a large number of Phanerozoic and Proterozoic sedimentary basins and fold belts that, depending on geological setting, (former) palaeoclimates, and on geologic period, have quite a variable sedimentary

Basin, or fold belts	Age, thickness of the basin or fold belt and its main lithologies
Drummond Basin [50]	Late Devonian to Early Carboniferous basin filled with >5000 m quartzose, felspathic and lithic sandstones, mudstone, chert, algal limestone, volcanoclastic and volcano-quartzose sandstone, and tuff overlying folded crystalline rocks of the Cambro-Ordovician Thompson Fold Belt (siltstone, fine-grained quartzose to feldspathic sandstone, phyllite, schist, cleaved mudstone, tonalite, limestone, volcanoclastic and primary volcanic deposits, felsic volcanic detritus and primary felsic volcanics, fossiliferous sedimentary rocks, rhyolitic and basaltic lavas, ignimbrite, gabbro/diorite to syenogranite, and granite
Bowen Basin [51]	Permian to Triassic basin filled with 10,000 m of fluvial and lacustrine sediments (quartzose sandstones, mudstone), limestones, volcanic rocks, tuffs, and thick succession of coals
Surat Basin [52, 53]	Early Jurassic to Early Cretaceous basin filled with 2500 m of sandstone, coal, siltstone, shale and limestone; during the Early Jurassic, deposition was mostly fluvio-lacustrine; by the Middle Jurassic coal swamp environments predominated
Murray Darling Basin [54]	Late Silurian to Early Carboniferous basin, largely Devonian in age with up to 8000 m of mostly continental red-bed facies and marginal marine facies in the latest Silurian and Early Devonian
Lachlan Fold Belt [55–58]	Ordovician to Carboniferous folded/faulted and weakly metamorphosed rocks of turbidites, trench sedimentary complexes, volcanic arcs with andesites, oceanic crust and micro continents; individual rocks are mostly sandstone and shale interbedded with chert, limestones, and metavolcanics (andesites), and intrusive granites; because of folding, crustal shortening, thrusting/faulting, estimates of basin-filling thickness are difficult to determine though Collins <i>et al.</i> [58] provide estimates that, depending on crustal history, varied from ~20,000 m to 40,000–50,000 m
Otway Basin [59]	Early Cretaceous to Tertiary basin filled with thick continental, fluvio-lacustrine, and marine sediments, followed by volcanoclastic, fluvio-lacustrine deposition, and then Late Cretaceous coastal-plain, deltaic and marine deposition and, later, Cretaceous to Middle Eocene deposition of coastal plain, deltaic and shallow marine sediments, and Middle Eocene to Early Oligocene near-shore to offshore, mixed clastic and carbonate sediments, and Late Oligocene to Late Miocene, open-marine carbonate deposition, capped by Plio-Pleistocene deposition of mixed siliciclastic-carbonate succession

Table 1.
 Characteristics of basins/fold belts that the Cosgrove volcanic chain intersects.

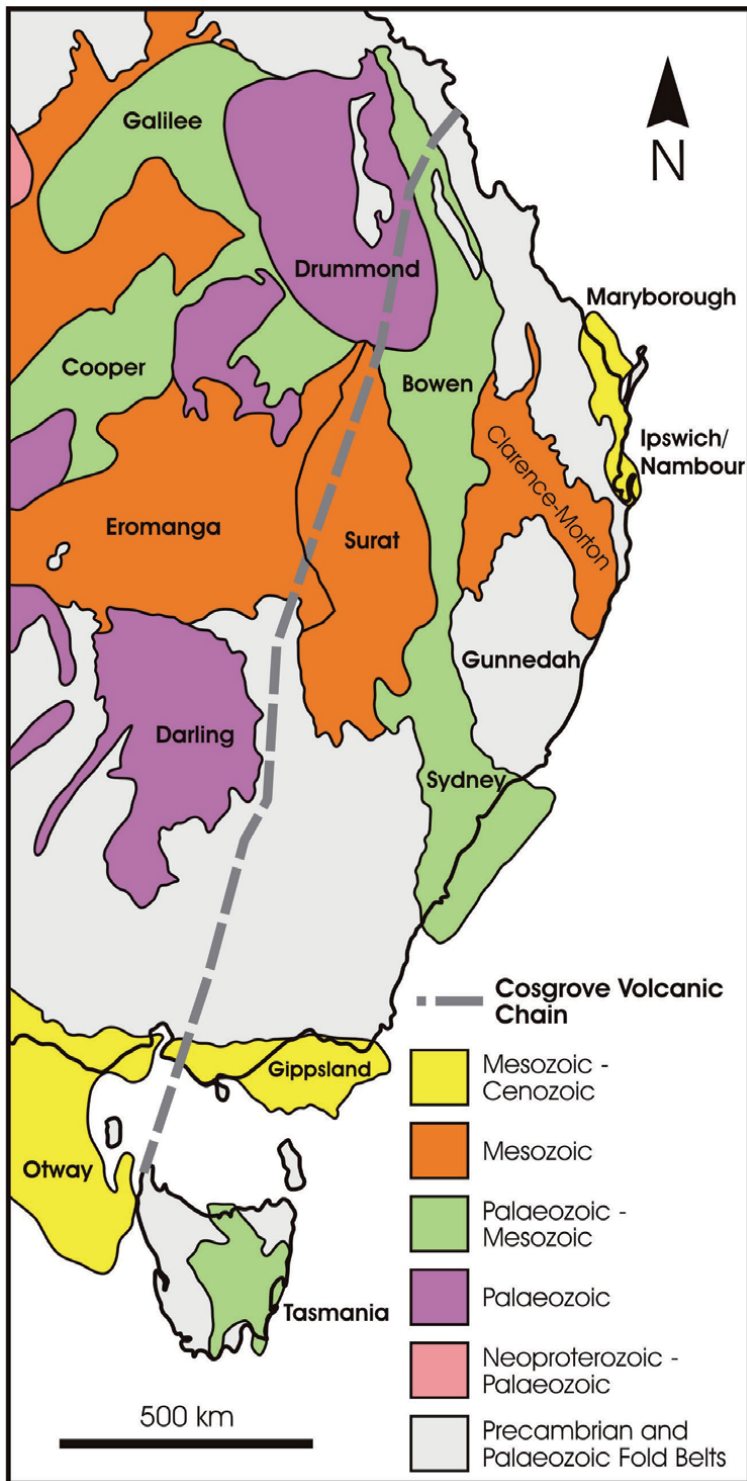


Figure 4. Map of eastern Australia showing occurrence of the sedimentary basins and fold belts (modified from geoscience Australia https://www.ga.gov.au/__data/assets/image/0020/13943/GA14654.gif) that the trackway of the Cosgrove volcanic chain will have intersected. Dominant lithologies that will yield xenoliths/xenocrysts are listed in **Table 1**.

history, metamorphic history, and structural history, *viz.*, 1. mainly siliciclastic, 2. carbonate-dominated, 3. changing mega-stratigraphically between siliciclastic and carbonate-dominated, 4. basins with sedimentary sequences as 1–3 above but with insertion of coal measures and/or volcanic events (**Table 1**). This is the geological framework that mantle plumes, in ascending towards the surface, have intersected. Thus, along eastern Australia, the range of mantle plumes (or mantle hotspots) from northernmost Australia to Tasmania (the Cosgrove Volcanic Chain trackway is shown in **Figure 3**) needed to transgress these various heterogeneous lithological systems.

As mentioned earlier, we have opted to focus only on the Cosgrove Volcanic Chain (trackway) to illustrate what this volcanic plume needed to transgress lithologically, what it needed to cross in basin thickness, and what it encountered in stratigraphic/lithologic heterogeneity. The Cosgrove Volcano Chain crosses a number of sedimentary basins and a fold belt (**Figure 4**) that are of various ages, thicknesses, and lithologies (**Table 1**) and, as such, the trackway had the potential to interface with a variety of rocks that could be involved in melting/mixing and melt contamination, and yielding of discrete xenoliths and xenocrysts. Given that the volcanic trackway may not have been strictly linear, and may have deviated from the trackway that is shown in **Figures 3 and 4**, the most probable xenolith and xenocryst contributions to the evolution of the Cosgrove mantle plume are from lithologies from the following basins and tectonic zones (from north to south): Drummond Basin, Bowen Basin, Surat Basin, Murray Darling Basin, the Lachlan Fold Belt, and the Otway Basin (**Table 1**). **Table 1** list the, thickness of the basin or fold belt, its main lithologies, and its age. The deepest part of each basin often rests on metasediments or on crystalline rocks though the bulk of the sedimentary fill of the basins tend not to be metamorphosed.

5. Geoheritage significance of the eastern Australian Cosgrove volcanic chain

The Cosgrove Volcano Chain provides a globally-unique system to explore an intra-plate migratory volcanic system and, additionally, in this context, with its globally-distinct suite of sedimentary basins that it has over time intruded through, it has global geoheritage significance. From north to south, in its younging direction, the Cosgrove Volcano Chain has a rich history and expression of volcanic activity with a range of lava types and eruptive volcanic rocks (dominantly basaltic lava [alkali olivine basalts, hawaiites, mugearites], but with occurrences of leucitite, trachyte, rhyolite, andesite, andesitic basalt, trachyandesite, and, where explosive and where expressed pyroclastically, tuff, breccia and agglomerate). Geomorphically, these volcanic eruptions are expressed as a range of primary volcanic landforms as well as eroded-residual geometry types (shield volcanoes, stratovolcanoes, domes, plugs, spires, *etc.*), and stratiform ash deposits, dykes, plugs, and sills. There are also valley fills, conic accumulations of tephra (*e.g.*, accretionary pyroclastic cones), ash sheets, and lava tubes.

In a sub-global context, the Cosgrove Volcano Chain presents a range of magma types, volcanic expressions, a history of interactions with the variable but regionally diagnostic lithosphere (*i.e.*, regionally-specific and lithologically-diagnostic sedimentary basins). It also presents a landscape-*cum*-climate response as the various volcanic and eruptive centres passed progressively through a climate gradient as Australia migrated from arctic/boreal climates through to subtropical/tropical

climates with its attendant influence on erosion and weathering styles and transformation of volcanic rock and tephra to climate-specific landforms and climate specific soils. This variability in volcanic expression, in a north-to-south gradient influences content of xenoliths and xenocrysts and magma composition, as well as volcanic landscape types, and in climate-influenced weathering styles changing progressively over 33 million years – it thus provides a globally-unique natural laboratory as a window into Earth processes, and a teaching and research resource in perpetuity.

The key elements of the Cosgrove Volcano Chain of geoheritage significance are as follows:

1. first example of a long, continent-length volcanic chain [13];
2. volcanic activity linked to lithosphere thickness;
3. volcanic magma composition linked to lithosphere heterogeneity;
4. variability of magma along the volcanic chain;
5. magma evolution at a volcano, *e.g.*, from basalt lava to rhyolitic lava;
6. magma and volcanic evolution, *e.g.*, magma flows varying to ash beds and breccias;
7. volcanic eruption style linked to magma composition;
8. volcanic xenolith/xenocryst linked to lithosphere heterogeneity and sedimentary basins;
9. volcanic expression at different scales linked to magma composition;
10. northwards volcano drift passes through different climates and weathering regimes.

To further the disciplines of geoheritage and geoconservation, Brocx & Semeniuk provided a Geoheritage Tool-kit to systematically compile an inventory of the full diversity at various scales of geological and geomorphological features in a given area, assess their levels of significance, and address whether geoheritage features are treated in isolation or as inter-related suites that should be conserved as an ensemble. Utilising the Geoheritage Tool-kit, many of the features listed 1–10 above individually would be evaluated as internationally to nationally significant, but specifically (1), (2), (3), and (8) are globally significant features of this volcanic chain. However, the cross-continent assemblage of volcanic features of the Cosgrove Volcano Chain should not be viewed as isolated separate geological phenomena spread across the north-to-south length of Australia but, from a geoheritage perspective, should be viewed as a single, integrated ensemble recording 1. a gradient of magma types, 2. the effect of a variable thickness of lithosphere, 3. the variety of volcanic landform expression, 4. the rock types intersected by the ascending plume, and 5. the changes in styles of erosion and weathering as the volcanoes passed through the various climate zones. However, while the Cosgrove Volcanic Chain is suggested as a global-significant mega-park, there is much planning, valorisation, community involvement, and government support required to achieve this (matters that are beyond the scope of this Chapter).

6. Discussion and conclusions: a globally significant mega-geopark centred on the Cosgrove volcano chain

As reiterated above, Australia, having finally split from Antarctica some 33 million years ago, has been migrating northwards towards the Eurasian plate progressively passing on its eastern side over a mantle hotspot (magma plume) which intersected various, variable lithologic packages such as Phanerozoic sedimentary basins, fold belts and metamorphic terranes, and Precambrian rocks. With xenolith plucking, enclave plucking, and xenocryst incorporation, there had been compositional evolution of the magma plume. The volcanic chain, the individual volcanoes, and the lava fields that are spread latitudinally along 2000 km of eastern Australia present a globally-significant volcanic system that provides insights into Earth magma and crust interactions, into the variability of xenoliths and xenocrysts, into magma evolution dependent on setting, and into the story of the Earth. The Cosgrove Volcano Chain stands as an example of a globally-unique example of these processes and a potential megascale geopark.

In summary, this Chapter has described the significance of a magma plume pulsing through a heterogeneous continental crust, with lithospheric heterogeneity giving rise to a mix in magma composition and a mix of xenoliths/xenocrysts. The movement of the Australian plate to northward gives clues (as a window) to sub-continental lithology via the enclosed xenoliths and xenocrysts and the influence of the thickness of crust as to whether there is volcanic expression of the magma plume at the Earth's surface [13]. And while they have been noted in previous studies and their occurrence is important, xenoliths and xenocrysts have not been a detailed focus of many studies, yet they are important as they provide clues to the sub-crustal influences and processes at the base of a magma plume. The phenomena of magma mixing, nature of xenoliths and xenocrysts, the influence of lithospheric lithologies in generating xenolith/xenocryst types and on magma contamination, and the relationship of volcanic expression to crust thickness are applicable to other volcanic trackways here in eastern Australia and elsewhere globally.

Also, it is worth pointing out that a similarly large volcanic field has been recognised for its geoheritage values in Harrat Khaybar, Kingdom of Saudi Arabia [60, 61] which has local and global implications for geo-education, research, and reference site for global volcanism.

On a final note, we emphasise that we consider the Cosgrove Volcano Chain to be a megascale geological feature of global geoheritage significance and should be considered as a potential megascale geopark. In effect, it would be the volcanic equivalent of the latitudinally extensive Great Barrier Reef which is accepted as a World Heritage Site.

Author details

Vic Semeniuk^{1,2,3} and Margaret Brocx^{3*}

1 V & C Semeniuk Research Group, Warwick, Western Australia

2 School of Arts and Sciences, Notre Dame University, Fremantle, Western Australia

3 Environmental and Conservation Sciences, Murdoch University, Western Australia

*Address all correspondence to: geoheritage@iinet.net.au

IntechOpen

© 2021 The Author(s). Licensee IntechOpen. This chapter is distributed under the terms of the Creative Commons Attribution License (<http://creativecommons.org/licenses/by/3.0>), which permits unrestricted use, distribution, and reproduction in any medium, provided the original work is properly cited. 

References

- [1] Brocx M & Semeniuk V 2007. Geoheritage and geoconservation - history, definition, scope and scale. *Journal of the Royal Society of Western Australia* 90: 53-87.
- [2] Brocx M 2008. *Geoheritage - from global perspectives to local principles for conservation and planning*. Western Australian Museum, 175p. ISBN 978-1-920843-35-9.
- [3] Worboys G L, Lockwood M, Kothari A, Feary S & Pulsford I (eds). 2015. *Protected area governance and management*. ANU Press, Canberra (2015).
- [4] Casadevall T J, Tormey D & van Sistine D 2019. Protecting our global volcanic estate: Review of international conservation efforts. *International Journal of Geoheritage and Parks* 7(4): 182-191.
- [5] Brocx M & Semeniuk V 2010. The geoheritage significance of crystals. *Geology Today* 26: 216-225.
- [6] Phillips J C, Humphreys M C S, Daniels K A, Brown R J & Witham F 2013. The formation of columnar joints produced by cooling in basalt at Staffa, Scotland. *Bulletin of Volcanology* 75: 1-17. <https://doi.org/10.1007/s00445-013-0715-4>.
- [7] Bastida F, Aller J, Toimil N C, Lisle R J & Bobillo-Ares N C 2007. Some considerations on the kinematics of chevron folds. *Journal of Structural Geology*. 29 (7): 1185-1200.
- [8] Barclay W J, Browne M A E, McMillan A A, Pickett E A, Stone P & Wilby P R 2005. *The Old Red Sandstone of Great Britain*. Geological Conservation Review Series, No. 31, Joint Nature Conservation Committee, Peterborough, 393 p.
- [9] Alvarez W 2009. The historical record in the Scaglia limestone at Gubbio: magnetic reversals and the Cretaceous-Tertiary mass extinction. *Sedimentology* 56: 137-148. doi: 10.1111/j.1365-3091.2008.01010.x.
- [10] Whittington H B 1985. *The Burgess Shale*. Yale University Press, New Haven, USA.
- [11] Drexel J F, Preiss W V & Parker A J 1993. *The geology of South Australia. Volume 1: The Precambrian*. Geological Survey of South Australia Bulletin 54.
- [12] Twidale C R & Campbell E M 2005. *Australian landforms*. Rosenberg. ISBN 1-877058-32-7.
- [13] Davies D, Rawlinson N, Iaffaldano G & Campbell I H 2015. Lithospheric controls on magma composition along Earth's longest continental hotspot track. *Nature* 525: 511-514 (2015). <https://doi.org/10.1038/nature14903>
- [14] Hopley D, Smithers S G & Parnell K E 2007. *The geomorphology of the Great Barrier Reef - development, diversity, and change*. Cambridge University Press, Cambridge.
- [15] UNESCO 1981. *Great Barrier Reef (World Heritage Site)*. <https://whc.unesco.org/en/list/154/>
- [16] Logan B W (ed) 1974. *Evolution and Diagenesis of Quaternary Carbonate Sequences, Shark Bay, Western Australia*. American Association of Petroleum Geologists Memoir 22. Tulsa, Oklahoma
- [17] UNESCO 1991. *Shark Bay, Western Australia (World Heritage Site)*. <http://whc.unesco.org/en/list/578/>.
- [18] Brocx M & Semeniuk V 2015. Using the Geoheritage Tool-Kit to identify inter-related geological features at

- various scales for designating geoparks: case studies from Western Australia. In: E Errami, M Brocx & V Semeniuk (eds), *From Geoheritage to Geoparks -Case Studies from Africa and Beyond*. Springer, Amsterdam, 245-259.
- [19] Brocx M 2018. The Geoheritage Tool-kit for the Geological Society of Australia Inc. https://www.gsa.org.au/Public/Geoheritage/Geoheritage-Tool-Kit/Public/Geoheritage/Geoheritage_Tool-Kit.aspx?hkey=2f275860-e038-4bfa-8a59-f13fbe657c19.
- [20] Worboys G L, Lockwood M, Kothari A, Feary S & Pulsford I (eds). 2015. *Protected area governance and management*. ANU Press, Canberra (2015)
- [21] Ismail M, Delpuch G, Moine B, Grégoire M, Guilbaud C & Cottin J-Y 2020. Sapphirine-bearing pyroxenite xenoliths in Cenozoic alkali basalt from Jabel El Arab (Syria): insights into the nature and composition of the lithosphere beneath the southern Syrian Rift, northern part of the Arabian Plate. *Journal of Asian Earth Sciences* 190: article 104146. doi: <https://doi.org/10.1016/j.jseas.2019.104146>.
- [22] Wilshire H G & Binns R A 1961. Basic and ultrabasic xenoliths from volcanic rocks of New South Wales. *Journal of Petrology* 2(2): 185-208.
- [23] Sutherland F L 1991. Cainozoic volcanism, Eastern Australian: a predictive model on migration over multiple 'hotspot' magma sources. In: P DeDeckker & A P Kershaw (eds), *The Cainozoic in Australia: a re-appraisal of the evidence*. Geological Society of Australia, Special Publications 18: 5-43.
- [24] Gibson D L 2007. Potassium-argon ages of late Mesozoic and Cainozoic igneous rocks of eastern Australia. CRC LEME open file report, Volume 193: Bentley, W.A., Cooperative Research Centre for Landscape Environments & Mineral Exploration and Geoscience Australia.
- [25] Whitehead P W 2010. The regional context of the McBride Basalt Province and the formation of the Undara lava flows, tubes, rises and depressions. *Proceedings 14th International Symposium on Vulcanospeleology, 2010 Undara Volcanic National Park, Queensland, Australia August 2010*.
- [26] Cohen B E 2012. The scenic rim of southeastern Queensland, Australia: A history of mid Cenozoic intraplate volcanism. *Episodes* 35(1): 103-109.
- [27] Atwater T. 1989. Plate tectonic history of the northeast Pacific and western North America. In: E L Winterer, D M Hussong & R W Decker (ed), *The Geology of North America*, Vol. N, The Eastern Pacific Ocean and Hawaii. Geological Society of America: 21-70.
- [28] Thordarson T & Höskuldsson A 2008. Postglacial volcanism in Iceland. *Jökull: The Icelandic Journal of Earth Sciences* 58: 197-228.
- [29] Dessai A G & Vaselli O 1999. Petrology and geochemistry of xenoliths in lamprophyres from the Deccan Traps: implications for the nature of the deep crust boundary in western India. *Mineralogical Magazine* 63(5): 703-722
- [30] Basu A R 1975. Hot-spots, mantle plumes and a model for the origin of ultramafic xenoliths in alkali basalts. *Earth and Planetary Science Letters* 28(2): 261-274.
- [31] Foulger G R 2010. *Plates vs. plumes: a geological controversy*. Wiley-Blackwell. ISBN 978-1-4051-6148-0
- [32] French S W & Romanowicz B 2015. Broad plumes rooted at the base of the Earth's mantle beneath major hotspots. *Nature* 525(7567): 95-99.

- [33] White W M 2010. Oceanic island basalts and mantle plumes: the geochemical perspective. *Annual Review of Earth and Planetary Sciences* 38(1): 133-160.
- [34] Wilshire H G 1961. Sedimentary xenoliths and dolerite patch pegmatites from an analcrite basalt intrusion. *American Journal of Science* April 1961, 259 (4): 260-279; DOI: <https://doi.org/10.2475/ajs.259.4.260>.
- [35] Thompson R N & Gibson S A 2000. Transient high temperatures in mantle plume heads inferred from magnesian olivines in Phanerozoic picrites. *Nature* 407: 502-506.
- [36] Krienitz M-S, Haase K, Mezger K, van den Bogaard P, Thiemann P & Shaikh-Mashail A 2009. Tectonic events, continental intraplate volcanism, and mantle plume activity in northern Arabia: Constraints from geochemistry and Ar-Ar dating of Syrian lavas. *Geochemistry Geophysics Geosystems* 10(4) 1-26. Q04008, doi: 10.1029/2008GC002254.
- [37] Farnetani C G & Richards M A 1995. Thermal entrainment and melting in mantle plumes. *Earth & Planetary Science Letters* 136: 251-267.
- [38] Cinzia G, Farnetani C G, Legras B & Tackley P J 2002. Mixing and deformations in mantle plumes. *Earth and Planetary Science Letters* 196 (2002) 1-5.
- [39] Barry T L, Saunders A D, Kempton P D, Windley B F, Pringle MS, Dorjnamjaa D & Saandar S 2003. Petrogenesis of Cenozoic basalts from Mongolia: evidence for the role of asthenospheric versus metasomatized lithospheric mantle sources, *Journal of Petrology* 44 (1): 55-91. doi.org/10.1093/ petrology/44.1.55.
- [40] Johnson R W, Knutson J & Taylor S R (eds) 1989. Intraplate volcanism in Eastern Australia and New Zealand, Cambridge, England: Cambridge University Press, 408 p.
- [41] Sutherland L 1995. The volcanic Earth. University of New South Wales Press, Sydney. 248p.
- [42] Schmincke H-U 2003. *Volcanism*. Springer, Berlin.
- [43] Knesel K M, Cohen B E, Vasconcelos P M & Thiede D S 2008. Rapid change in drift of the Australian plate records collision with Ontong Java plateau. *Nature* 454: 754-757.
- [44] Sutherland F L, Graham I T, Meffre S, Zwingmann H & Pogson R E 2012. Passive-margin prolonged volcanism, East Australian Plate: outbursts, progressions, plate controls and suggested causes. *Australian Journal of Earth Sciences* 59(7): 983-1005.
- [45] Jones I & Verdel C 2015. Basalt distribution and volume estimates of Cenozoic volcanism in the Bowen Basin region of eastern Australia: Implications for a waning mantle plume. *Australian Journal of Earth Sciences* 62(2): 255-263.
- [46] Keep M & Schellart W P 2012. Introduction to the thematic issue on the evolution and dynamics of the Indo-Australian plate. *Australian Journal of Earth Sciences* 59(6): 807-808.
- [47] Wellman P & McDougall I 1974. Potassium-argon ages on the Cainozoic volcanic rocks of New South Wales. *Journal of the Geological Society of Australia*, 21:3, 247-272, DOI: 10.1080/00167617408728849
- [48] Vasconcelos P, Knesel K, Cohen B & Heim J 2008. Geochronology of the Australian Cenozoic: a history of tectonic and igneous activity, weathering, erosion, and sedimentation. *Australian Journal of Earth Sciences* 55, 865-914

- [49] Delescluse M, Chamot-Rooke N, Cattin R, Fleitout L, Trubienko O & Vigny C 2012. April 2012 intra-oceanic seismicity off Sumatra boosted by the Banda-Aceh megathrust. *Nature* 490: 240-244.
- [50] Purdy D J, Withnall I W & Bultitude R J 2016. Geology, geochronology and geochemistry of the northeast Drummond Basin Region. Geological Survey of Queensland, Record 2016/01 134pp.
- [51] Dickins J M & Malone E J 1973. Geology of the Bowen Basin, Queensland. Bureau of Mineral Resources, Australia, Bulletin 130.
- [52] Senior B R, Harrison P L & Mond A 1978. Geology of the Eromanga Basin, Queensland. *Bureau of Mineral Resources Bulletin* 167.
- [53] Exon N F 1976. Geology of the Surat Basin in Queensland. Bureau of Mineral Resources, Australia, Bulletin 166.
- [54] Kingham R 1998. Geology of the Murray-Darling Basin — simplified lithostratigraphic groupings. AGSO Record 1998/21. Australian Geological Survey Organisation - Department of Primary Industries & Energy. 33pp.
- [55] Packham G H (ed) 1969. The Geology of New South Wales, Geological Society of Australia Inc., Sydney. 654p.
- [56] Foster R A & Gray D R 2000. Evolution and Structure of the Lachlan Fold Belt (Orogen) of Eastern Australia. *Annual Review of Earth and Planetary Science* Vol. 28:47-80.
- [57] Gray D R & Foster R A 2004. Tectonic evolution of the Lachlan Orogen, southeast Australia: historical review, data synthesis and modern perspectives. *Australian Journal of Earth Sciences* 51: 773-817.
- [58] Collins W J, Mcnwin G & Mantle G 2004. Crustal thickness variations in the Lachlan Fold Belt - implications for tectonic and metallogenic models. *In: Bierlein, F.P., Hough, M.A. (eds), Tectonics to Minerals Discovery - Deconstructing the Lachlan Orogen. Proceedings Volume and Field Guide, MORE-SGEG Conference, Orange, NSW, July 6 - 8, 2004. Geological Society of Australia Abstracts No 74: 37 - 44.*
- [59] Morton J G 1995. Otway Basin (Chapter 9). *In: J F Drexel & W V Preiss (eds), The Geology of South Australia, Volume 2, The Phanerozoic. South Australia. Geological Survey, Bulletin* 54: 142-147.
- [60] Nemeth K & Moufti R 2013. Monogenetic volcanic fields and their geoheritage values of western Saudi Arabia and their implication to holistic geoeducation projects locally and globally (Invited). *In: American Geophysical Union, Fall Meeting 2013, abstract id. ED13F-0813, pp ED13F-0813*
- [61] Nemeth K & Moufti M R (2017) Geoheritage values of a mature monogenetic volcanic field in intra-continental settings: Harrat Khaybar, Kingdom of Saudi Arabia. *Geoheritage* 9(3):311-328.

From a Bulldozer Cut to a World Heritage Site

Payson Sheets

Abstract

A Salvadoran bulldozer encountered some architecture and artifacts so well preserved that it was assumed to be recent. I examined the site in 1978 and dated the thatch roofing to 1400 BP. With collaborations of volcanologists, I have investigated the Maya village for 42 years. The eruption of Loma Caldera volcano preserved the village and its landscape extraordinarily. Food is still intact in ceramic vessels, earthen buildings are preserved, and plants are intact in gardens and fields, in spite of being in a tropical wet environment. I nominated the Cerén site to the UNESCO World Heritage list, and it was accepted, as it is the best preserved ancient village in the Americas. Every season we publish our results in English and in Spanish and make them widely available. Local high school students in the past two decades are giving reenactment public performances that are highly accurate about the precursors of phreatomagmatic eruptions, the eruptions themselves, and proper emergency behavior. The result is a widespread awareness and preparedness that is greater than I could achieve with a plethora of scientific publications. I suggest that volcanologists and archaeologists consider supporting similar performances in hazardous areas, to improve risk perception and salutary emergency behavior.

Keywords: phreatomagmatic eruptions, ancient Maya, multidisciplinary research, Cerén site, UNESCO world heritage, high school reenactments

1. Introduction

El Salvador experiences considerable volcanic activity. The catastrophic Ilopango eruption in the mid-sixth century depopulated what is now that country, and ecological recovery may have necessitated about a century [1]. A small group of Maya migrated into the area, and established a hamlet on the left bank of a major river, now called the Rio Sucio. Although they lived there only for a few generations, they had time to establish a thriving community. Their agriculture was based on many different species, with each household largely self-sufficient. Each household built their homes with wattle-and-daub walls and thatch roofs, a seismically resilient form of architecture. In addition to their household buildings, families built and maintained special-purpose religious and civic structures. Each household had a different part-time occupational specialization; thus, the system of economic exchanges built a social network integrating the community. Surplus agricultural and craft production was taken to markets in the large towns, to obtain long-distance traded commodities. Had the ancient community, which I

named Joya de Cerén, been abandoned in the usual fashion, we would never have been able to learn such details about the high quality of lives lived there. The usual abandonment of wattle-and-daub structures has people taking their most valued artifacts to their new location. Other people remaining in the area take items that are useful to them. And, when the thatch roof fails, the rains, sun, and wind reduce the buildings to low mounds. The greatly impoverished record available to archeologists limits the knowledge that can be gained from excavation and analysis.

An overview of volcanism in central El Salvador was provided by Lexa et al. [2]. What makes Joya de Cerén unique is the nature of the Loma Caldera eruption that buried it in the mid-seventh century [1]. That volcanic vent opened up less than a kilometer away, and buried the village under some 5 m of tephra [1]. An earthquake preceded the tephra emplacement, and presumably the loud noise of the eruption beginning, gave warning to the residents. They literally “headed south” as evidenced by human footprints. The alterations of phreatomagmatic and magmatic phases of the eruption preserved the buildings, foods stored, crops in gardens and fields, and the landscape to an extraordinary degree. The site provides the first clear window into the vitality of Maya commoner life.

Our publications in Spanish (e.g. [3]) were accessed by high school students and their teachers in the area, and they regularly make public presentations depicting village life before the eruption, recognizing the danger signals, and fleeing the village. These performances provide effective training to families living along this active fault, as the next eruption is coming at an unknown time.

2. From the bulldozer cut to UNESCO world heritage

As a beginning graduate student in archeology in 1969, I was intrigued by finding a white volcanic ash layer between pyramid construction phases at Chalchuapa, El Salvador [1]. After almost a decade of archeological and volcanological research it became clear that tephra was from a colossal eruption, the source was Ilopango volcano, and we named it the “Tierra Blanca Joven” tephra, meaning the young white earth [1]. During archeological survey in central and western El Salvador, I found that same tephra layer underlying and overlying cultural features, including agricultural fields, artifact-bearing soils, and various ancient constructions [1]. Project members appreciated the graciousness and generosity of Salvadorans, particularly the rural poor, and we vowed to search for something special to give back to them, and to Salvadorans in general. Surveying near the town of Joya de Cerén, in 1978, in a bulldozer cut I discovered that same Ilopango tephra underlying the floor of a house, with some five meters of tephra burying the house [1]. Radiocarbon dating the thatch proved the house was about 1400 years old [2], and finding ceramic vessels full of beans in perfect preservation in spite of the hot moist tropical environment made me think I may be seeing the rest of my professional life at the site. That is precisely what happened in the decades since that discovery. The extraordinary preservation of the village and the landscape by the Loma Caldera tephra in the mid-seventh century provides the first clear window into ancient Maya village life of commoners. The exceptional preservation even included plants, allowing the reconstruction of “plantscapes” within the community [4]. Although commoners constituted more than 90% of ancient Maya populations, not much has been known about them, when compared to Maya elites. The notable accomplishments of Maya elites has been the focus of research for the past two centuries, emphasizing their

architecture, writing, astronomy, art style, dynastic succession, history, and other domains of impressive accomplishment. Based upon our research discoveries during the 1980s and early 1990s, I nominated it for inclusion in UNESCO's World Heritage list, and it was accepted in 1993. Salvadorans are justifiably proud to have it, and many claim it is the most important cultural feature in the country.

I named the site Cerén, or Joya de Cerén, after the nearby present-day village. The villagers are justifiably proud of the association, and many are employed as guides in the park, architectural conservators, maintenance workers, and as excavators when I am conducting research at the site (**Figure 1**).

2.1 Results of integrated volcanological-archeological research

Almost all seasons of fieldwork, for surveys and excavations, have included volcanologists with archeologists and other specialists, supported by grants from the US National Science Foundation. Integrating the specialists from different disciplines within the fieldwork has resulted in much better understanding of what happened 1400 years ago, than archeologists consulting with specialists after they got home from their fieldwork.

The white tephra underlying the Cerén site is from the cataclysmic eruption of Ilopango volcano, probably in AD 539 [5], which depopulated most of El Salvador, and contributed to the mid-sixth century worldwide climatic crisis [5]. After a few decades of weathering, and floral and faunal recovery, a few Maya families immigrated and founded the village of Cerén on the left bank of the Rio Sucio. Although the village was occupied for only about three generations before the Loma Caldera eruption, they adapted to the environment with sophisticated agriculture, built earthquake-resistant household structures and intriguing special buildings, and maintained lifestyles largely separate from elite influence. A few decades after the Ilopango eruption, the village was deeply buried by tephra from nearby Loma Caldera volcano, the focus of the following section.

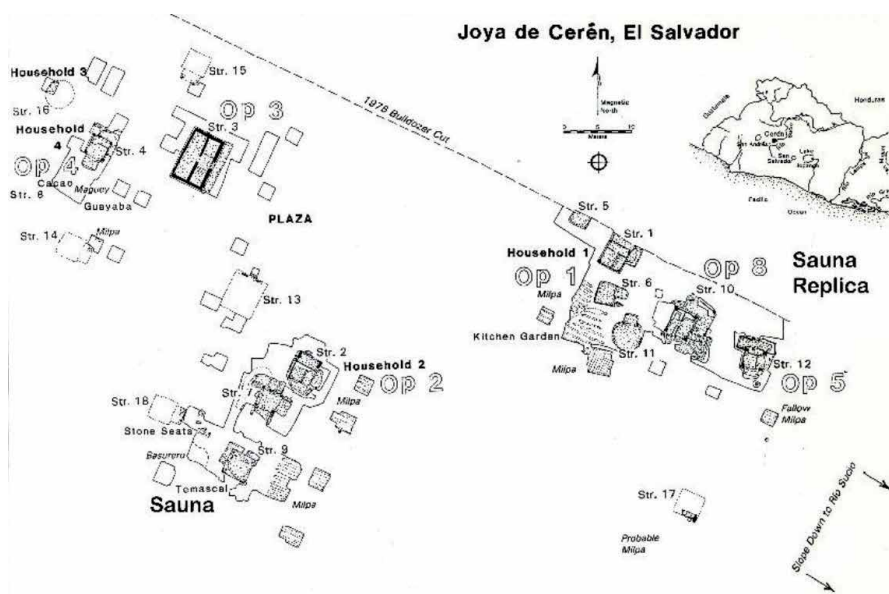


Figure 1.
Map of the ancient Maya village.

2.1.1 The Loma caldera eruption, and the burial of the Cerén village

The Loma Caldera vent is only 600 m north of the village, along the many-kilometers-long fissure that runs from north of it all the way southeast to San Salvador volcano [6]. Many hydromagmatic and explosive eruptions occurred along the fissure in centuries before Loma Caldera, and two occurred after Loma Caldera, less than 2 km distant, and one other (El Playon) in 1658, 4 km away. The social implications of these frequent eruptions are considered in a later section, below.

The eruption was preceded by seismic activity [6], including an earthquake of about 4 on the Richter scale, as we judge from a round-bottomed pot not falling off a broad flat walltop of Structure 3, and tiny fissures and subsidence in the immediate pre-eruption ground surface. The eruption began with a pyroclastic surge generated by an energetic explosive hydromagmatic eruption, followed by a drier phase of hot blocks (lava bombs) and lapilli falling. That alternation occurred at least 14 more times, taking hours, deeply burying the village of a few hundred residents. The tephra thins rapidly with distance from the source, with only about 4 square km buried deeper than a meter. Inhabited areas farther away would have received only a dusting. Because no human remains have been found to date in the village, the precursors, including the deafening sound from the north, may have been sufficient for people to evacuate (**Figure 2**).

The first tephra to arrive in the village, Unit 1 [6], was a fine-grained and moist pyroclastic surge that traveled at 100 km/hour, or faster [6]. It plastered around buildings and their roofs, and the mature corn plants and other cultigens in gardens and fields. The tephra temperature was approximately 100°C from magma in contact with water from the Rio Sucio. Unit 2 was from a dry phase, composed of blocks and lapilli fall. The larger juvenile clasts followed ballistic trajectories, landing with temperatures above 575°C. They penetrated the thatch roofs of all structures, and caught the thatch on fire on the underside, and the wooden roof-support framework. The top of the roofs did not burn because Unit 1 coated them. Because only the bottommost zone of the thatch burned, very little time elapsed between the fires starting, and Unit 3's arrival. Unit 3 is a much thicker deposit of largely pyroclastic surges, with abundant accretionary lapilli, and occasional ballistic blocks. Because it was often some 75 cm thick, its weight collapsed most roofs and snuffed the fires.

From the volcanological point of view, Units 1–3 were highly destructive to the village by collapsing all roofs, collapsing many walls, and of course creating an emergency and a natural disaster for inhabitants. Dan Miller's chapter [6] is representative of various volcanologists' considerations of the eruption's deleterious effects on the village, emphasizing the destructiveness on buildings. The emphasis is the natural disaster. The subsequent Units alternated with pyroclastic surges and dry lapilli falls until some 5 m buried the village. The archeological perspective was totally different from the volcanological, because the tephra nature and sequence were spectacularly successful in preserving the village in its cultural and natural landscape. All elements of the structures were preserved and were fully reconstructable to their condition and use right before the eruption. Units 1 and 3 preserved plants in the kitchen garden of Household 1, and the maize plants in fields. Ceramic vessels in households contained a wide variety of foods, preserved in original conditions, in spite of being in a tropical wet environment for 1400 years. A following section details what we learned about life in an ancient Maya village of commoners, that could not have been learned if the eruption did not occur and bury the site, after we consider the usual preservation of ancient households and their villages.



Figure 2.
Structure 4, the storehouse for household 4, buried under 5 m of volcanic ash from Loma caldera volcanic vent, looking north. All walls withstood the forces of the eruption, except the southern wall, that fell to the south.

2.1.2 Maya households and villages in the archeological record

In almost all cases, when people abandon their households, they take with them the most valuable and transportable artifacts. Then people still in the area scour the structures for still useful artifacts, and take structural elements away for their own purposes. When the thatch roofs disintegrate, the rains, sun, and wind reduce the wattle-and-daub walls to a small mound of dirt with some mixed broken artifacts. The cultural and natural factors immensely degrade the condition of the site, thus limiting the understanding that can be gleaned from excavations and analyses. The remains can be dated, approximately, by comparing artifacts such as ceramic sherds with other dated remains from other sites. Occasionally radiocarbon, obsidian hydration, or other quantitative dating can be done, but are done only rarely on

household remains of commoner villages. Most of Maya archeology focuses on the architecture, sculpture, art, writing and other accomplishments of the elites, especially of the royals. Thus, commoners have been largely ignored, and assumed to be the “blue collar” workers that supply elites with food and labor. Because of the nature of the eruption, the Cerén site provides the first clear window on ancient Maya commoner architecture, agriculture, life style, in their landscape.

2.1.3 Volcanic-structural impacts, and archeological discoveries

All thatch roofs caught fire on their undersides from the hot ballistic lava bombs during the emplacement of Unit 2, and most of them collapsed during the tephra loading of Unit 3 [6, 7], extinguishing the burning. The turbulent velocity of Unit 1 blew off some of the thatch of many buildings, before they collapsed. Because thatch roofs must be replaced every two to three decades, radiocarbon dating of them avoids the old wood problem, thus giving dates closer to the eruption.

Structure 3 is one of only two buildings excavated to date that had no wall damage from the eruption, because its thick walls were constructed of *terre pise*, i.e. rammed earth [7]. The downwind drifts of the Units 1 and 3 pyroclastic surges provided Dan Miller with data to estimate their velocities [6].

Structure 11, the kitchen for Household 1, anchors the other end of the spectrum of structural solidity [1, 7]. (Ref. [7] is the source of the remainder of this chapter, unless otherwise noted. The details were obtained from the unique preservation, which could not have been achieved without the volcanic burial.) The hearth, with three stones to support round-bottomed cooking vessels, could ignite flammable materials of a building, and burn it down. Therefore, it was separated from other buildings by a few meters, and it had a thinner-than-usual thatch roof, and thatch walls. Thus, it was more easily replaceable than other structures, and even had a replaceable floor in the form of the TBJ tephra. The first stage of construction of all other structures was to make a rounded low mound at or beyond the anticipated edge of the thatch roof. We even found the drip lines from the edges of the thatch roofs. Then a substantial rectangular platform was built and covered with a smooth surface of clay, dried, and then fired to make a hard floor. Holes were drilled about 10–15 cm apart and vertical poles inserted to support the roofing framework. Horizontal reinforcements of poles connected the verticals, and then were mudded on both sides up to about 1.75 m above the floor. That left a significant gap between the mudded wall and the roof, for light and air to enter. The finished walls were stabilized from below, above, and internally, so were seismically resistant. But in a big earthquake, the largest fragment to strike someone was about the size of a grapefruit, and would do little harm. Grass was used for thatching. The thatch roofs of household domiciles and storehouses extended for about 1.5 m beyond the walls, providing ample multipurpose space under the eaves that was shaded, and dry during the rainy season. The result is that the roofed area outside the walls was about double that inside the walls.

The most unusual building in the village is Structure 9, a steambath/sauna with ample seating for a dozen people. The Household 2 members looked after the functioning of it by providing firewood and water for steam and probably for rinsing off after exiting. This is the other building whose walls did not suffer from the eruption. However, it had two roofs, and both were affected by the eruption. The top roof was thatch, to shed rain, and it was coated by Unit 1, and then set afire during Unit 2. The lower roof was a marvelous dome, of wattle and daub, and is the only domed structure ever found in the ancient Maya area. It was penetrated and largely destroyed by two lava bombs. The holes in the dome were sufficiently large

and fortuitously located to allow tephra from Unit 3 and later to enter and shore up the portions of the dome that remained in-situ. Had the lava bombs not penetrated, the overburden of Units 3 and above would have completely collapsed the dome, and we would never know its original shape. This building has attracted the greatest attention from visitors and scholars, and after years of my suggesting, a 1:1 scale precise replica was constructed in the public access area of the archeological park.

Every time I entered the sauna replica, I noticed it fundamentally changed my voice. To explore this phenomenon, I made a stereo recording of my speaking voice outside, then inside, and then again outside the sauna, and took it to the Physics Department at the University of Colorado, Boulder. There, physicist Michael Thomsen analyzed the recording, and discovered that the primary resonance was at the very low tone of 64 Hertz [8]. The other frequencies decayed rapidly, while the predominant resonance continued for a long time. Mature male speaking voices, or singing, or chanting, experience this effect. However, mature female voices, or those of children, would not have this effect. It is likely this was a deliberate acoustic effect for male uses, but does not obviate female uses. Such apparent acoustic sophistication had never been imagined for the ancient Maya, especially among commoners (**Figures 3 and 4**).



Figure 3. Structure 9, the sauna, with two holes in the domed roof created by lava bombs. The stubby columns in the corners supported beams and a thatch roof that protected the earthen architecture from the elements.



Figure 4. The replica of the sauna, in the public access part of the archeological park. The architectural firm accurately reconstructed the original ancient building, so visitors can enter it and experience the acoustic phenomena.

2.1.4 Life in the Cerén Village, before the eruption

Prior to the discovery of the Cerén site, there was little data upon which to examine the quality of life of ancient Maya villagers. Thus, the assumption grew that the households must be redundant, all about the same, and just providing food, labor, some crafts, and firewood for the top class. Fortunately, Cerén has challenged that assumption since 1983 [1], and encouraged others to closely investigate commoners in various areas of the Maya world. Two recent books, with titles “Ancient Maya Commoners” [9] and “Commoner Ritual and Ideology in Ancient Mesoamerica” [10] exemplify their successes. The following material presents an overview of knowledge about life in the Cerén village [7] that would not be attainable if it were abandoned in the usual fashion, and left open to the elements of nature and to subsequent human interference. The volcanic preservation made all the difference.

The size of families was unknown; they could have been extended families with three or more generations residing together, or nuclear families of two generations. The sleeping areas of the domiciles at Cerén were sufficient for nuclear families, but not beyond. Thus, family members enjoyed abundant space in their three buildings (domiciles, kitchens, and storehouses) within the walls, and much more space under the eaves of their large thatch roofs. They stored and used valuable and important artifacts within the walls, and less valuable items outside the walls. Their work spaces for crafting items were generally under the eaves, where light and air circulation was best, yet protected from rain.

Each household crafted items for exchange, and for their internal consumption. What is notable is that each was different in their part-time occupational specialization, which resulted in economic exchanges within the village, thus providing a social network of familiarity, cooperation, and communication. Household 2 painted gourds. They maintained a set of pigments in their storehouse, of hematite, limonite, and five miniature pots with varying hues of cinnabar (HgS), a bright red pigment. The gourds grew on a nearby tree, and they cut them in half to make hemispherical bowls. They kept a few for their own use, and exchanged them within the community for the semi-specialized products of other households. Like the other households, they also took their gourds to markets in the big towns to obtain the specialty products only available there. Those items were fancy painted ceramic vessels that made up over a fifth of their household pot inventories, obsidian tools, a jade axe, and pigments.

Household 1's specialty was making groundstone tools for grinding corn and other hard substances, and making cotton thread and weaving it into garments. It appears that Household 3's specialty was preparing achiote (*Bixa orellana*) seeds into a bright red water-based organic pigment. Some spilled on the floor of their kitchen, indicating that they had recently made it and were using it. A common use of it in ancient and modern times is for body painting, and its color symbolizes blood. Because the community was celebrating the harvest the very evening the Loma Caldera eruption occurred, it appears probable that participants stopped at this household to be painted, on their way to the ceremony.

Household 4's specialty was cultivating unusual plants. They maintained a garden of some 70 mature maguey (*Agave americana*) plants, from which they obtained long fibers. They twisted them into 2-ply string, twine, and rope. We estimate their production would have been sufficient to supply the entire village of some 200–300 people with all their needs. They also grew chili plants in sufficient abundance to supply their needs and the entire village. They grew strong cane poles (*Cana americana*) for vertical reinforcements in wattle-and-daub walls of household buildings.

Service relationships are a category of social integration of a community that had not been discovered in sites prior to Cerén. A service relationship here is a household maintaining a special facility for community use. Household 1 maintained two religious buildings adjacent to them, Structures 10 and 12. Structure 10 was hosting the community harvest festival, which can be dated to the month (August when maize and manioc are harvested) and time of day (evening, as dinner had been served but the family dishes not yet washed), but ironically not to the year (radiocarbon dating range). Household 1 was providing large amounts of processed maize for the participants at the ceremony, and loaned maize husking tools and grinding stones for the event. They likely maintained the structure itself, but data are not definitive. After the earthquake, and hearing the initiation of the eruption, participants evacuated to the south, as indicated by many footprints. How far they got is unknown, as the tephra cloud of Unit 1 was moving fast.

Household 1 also evidently maintained Structure 12, just a few meters farther east than the ceremonial building. This building was highly unusual, with five different floor levels, with the highest being the largest, in the far back. By Maya canons, that denoted greater supernatural power by greater elevation. Its walls and interior partitions were more delicate than any others in the village, and had a lattice window in front, and one in the far back. A collection of minerals that was stored atop an interior partition wall provided the best clue to the function of the building. Shamans used, and still use, minerals in divination. People left artifacts in the front of the building, in reciprocity for services rendered. Many artifacts are used by both genders, but all of the gender-specific artifacts left there, food-grinding stones and spindle whorls for thread-making, are female-associated. Hence, we conclude that the shaman was a woman. She practiced in the building, but did not live in it.

Household 2 maintained the sauna, Structure 9, just a few meters south of its storehouse (Structure 7). In the storehouse they kept quite a bit of firewood along with some pine kindling, likely for the fire inside the sauna. And they had an unusual number of “ollas” to hold water, probably for pouring on top of the firebox in the middle of the building. Excess water flowed out from the firebox through the entrance of the building, leaving a tiny erosional channel, thus providing clear evidence of their producing steam inside. People likely also used the water to rinse off after exiting from the sauna. It is also likely that Household 2 maintained the structure by re-thatching its protective roof every few decades. The contemporary and historic Maya use saunas for childbirth and other feminine purposes, and both sexes use it for curing respiratory problems and other medicinal uses. Both sexes and all ages use it for personal and spiritual cleansing. The fact that it has such a profound effect on mature male voices suggests that it was also used in ways that have not been imagined before.

2.2 Anticipated and unanticipated consequences of data sharing

We present our research results regularly at our national meetings, and in journal articles and book chapters. We publish in English and Spanish for our colleagues and interested lay people. We regularly train the guides at the Cerén Archeological Park, so visitors, including hordes of schoolchildren, receive accurate information. We update the signage and displays in the on-site museum, and at the national museum in San Salvador.

Students in the modern town of Joya de Cerén, and in the nearby city of San Juan Opico, are proud of having the intriguing World Heritage site in their neighborhoods. They accessed the Spanish language literature on our website <https://www.colorado.edu/anthropology/payson-sheets> as well as took advantage of the didactic

materials and guides at the site, and on their own decided to put on performances reenacting aspects of life in the ancient village. The plays take place in August, when local farmers are engaged in the harvest of maize and manioc, just like the harvest in ancient times. The clothes made by their mothers are quite imaginative, resembling Native American costumes worn in US movies more than ancient Maya clothing, but nobody complains. The performances begin with life in the village before the eruption, with father talking about the harvest, and mother talking about processing the food in the kitchen, and the children saying they are hungry, and wanting attention. Then they go over to the community ceremonial building to unite with other families. But as the rituals were underway, giving thanks for a good harvest, and asking for a good growing season in the future, the ground started shaking. They said “is this a big one?” and waited anxiously until it attenuated. However, seconds later a horrific shrieking noise hit them, and they yelled in emergency as their oral history informed them that this is the beginning of a violent eruption. The sound came from the north, so they all ran as fast as they could to the south. The audience of the performance I witnessed was composed of many families in the town of Joya de Cerén, and they clapped exuberantly as the actors came back to the improvised stage, and took their bows.

The depictions of life in the village, the harvest ceremony, the earthquake, and the beginnings of the phreatomagmatic eruption were presented with great accuracy. The actors, and presumably their school teachers, had utilized our publications in Spanish, that were available on the internet. The presentation was strikingly reminiscent of how traditional native societies use oral history to accurately transmit detailed information about volcanic eruptions for centuries or millennia. Blong [11], for instance, discovered that the natives of Papua New Guinea retained detailed information about an eruption and tephra emplacements for about three centuries. That would be about 15 generations, and was achieved by frequent repetition in public performances. Krajick [12] notes the accuracy with which details of the Mount Mazama eruption was transmitted for about 7000 years. Therefore, it is reasonable to assume that the Cerén residents were familiar with the precursors, and the eruptions, along that active fault, and thus most if not all the participants in the ancient harvest ceremony headed south, fast. How many escaped alive is unknown, particularly because the time between the defining sound and the arrival of Unit 1 is unknown. Future excavations are likely to encounter the remains of some people who did not attend the ceremony because of illness, old age, or some other reason. More than a century of research remains to be done at the Cerén site.

Native peoples around the world, for many millennia, have been dealing with extreme events. Lacking writing, they have initiated effective ways of transmitting traditional environmental-social knowledge for many generations [11, 12], by public performances and paying close attention to variations in nature and their societies. Such indigenous knowledge provides people with time-tested resilient behavior. Oral history of extreme events has an impressive record of durability and accuracy, and oral traditions of various geological events, including volcanism, can be incorporated into cultural aspects of everyday life, including performances, dance, and even tattooing [13, 14]. However, oral history is not invulnerable to massive disruptions. The last few centuries of colonization by the world powers, depopulation by epidemic diseases, massive migrations, or other factors can cause destruction to, or elimination of, traditional ecological knowledge [15–17]. The scientific literature on hazards, disasters, and suitable responses, is not an effective substitute for most peoples around the world. However, the high school students’ reenactment of the Loma Caldera eruption, and the ancient Cerénians’ perception of the precursors, and emergency evacuation of their village, do inadvertently train local Salvadorans to the very real hazard along their volcanic vent.

This unanticipated training for disaster perception and response was “Ceréndipitously” the result of our publications in Spanish available on the internet, and high school students proud to have the only World Heritage site in the country right in their neighborhood. This need not be limited to this high-hazard zone in El Salvador. Rather, I suggest that volcanologists and archeologists explore high school or college level students and their teachers in their research areas, and encourage similar performances. In areas like this, where literacy is limited and very few residents would understand our social science and natural science literature, even when written in their native language, the reinstatement of oral history in performances could have a salutary effect of increasing hazard understanding, perception of precursors of the next extreme event, and appropriate emergency behavior.

3. Conclusions

Maya elites and royals are well known after two centuries of study, as they built their pyramids, palaces, and tombs of stone, and recorded their histories in hieroglyphics literally “written in stone.” They created one of the world’s great art styles, and their economic and political systems endured for many centuries. Commoners made up the vast majority of the population, but have been poorly known in part because they constructed their buildings of wattle-and-daub. They did not record their histories in written form, but in oral history form by repeated public performances, like so many traditional societies around the world. The frequency of eruptions along the fault indicates it is likely that people in the ancient Cerén village were well aware of the antecedents to an eruption were earthquake and a defining noise. No human remains have been found in excavations to date, and the footprints headed south, both indicate that people evacuated the village. How far they got is unknown.

The frequent reenactments of village life, eruption indicators, and the emergency evacuation by high school students both in the present-day town of Joya de Cerén, and the nearby city of San Juan Opico, are didactic means of training for families that could experience the next eruption, at any time. I encourage archeologists, volcanologists, and other scientists, to consider supporting similar performances by local students in other hazardous locations.

Acknowledgements

I gratefully acknowledge the support of the U.S. National Science Foundation, for funding the many seasons of excavation, analysis, and publication of our Cerén research project. The generosity and helpfulness of the Salvadoran rural poor people have been a testimony to their core of humanity, and all project members wish to acknowledge this. Therefore, we took pleasure in giving back to them, with a UNESCO World Heritage site in their neighborhood. Karoly Nemeth’s comments improved the text of this chapter.


Author details

Payson Sheets

Department of Anthropology, University of Colorado, Boulder, Colorado, USA

*Address all correspondence to: payson.sheets@colorado.edu

IntechOpen

© 2020 The Author(s). Licensee IntechOpen. This chapter is distributed under the terms of the Creative Commons Attribution License (<http://creativecommons.org/licenses/by/3.0>), which permits unrestricted use, distribution, and reproduction in any medium, provided the original work is properly cited. 

References

- [1] Sheets P. *Archeology and Volcanism in Central America: The Zapotitan Valley of El Salvador*. Austin: University of Texas Press; 1983
- [2] Lexa J, Sebesta J, Alexander Chavez J, Hernandez W, Pecskey Z. Geology and volcanic evolution in the southern part of the San Salvador metropolitan area. *Journal of Geosciences*. 2011;**56**(1):105-140
- [3] Sheets P, de Ceren J. San Salvador: Editorial Universitaria. 2013. https://www.colorado.edu/anthropology/sites/default/files/attached-files/joya_sheets_23_oct_2013.pdf [Accessed: 15 August 2020]
- [4] Farahani A, Chiou KL, Harkey A, Hastorf CA, Lentz DL, Sheets P. Identifying “plantscapes” at the classic Maya village of Joya de Ceren, El Salvador. *Antiquity*. 2017;**91**(358):980-997
- [5] Dull R, Southon J, Kutterolf S, Anchukaitis K, Freundt A, Wahl D, et al. Radiocarbon and geologic evidence reveal Ilopango volcano as source of the colossal ‘mystery’ eruption of 539/40 CE. *Quaternary Science Reviews*. 2019;**222**:222-239
- [6] Volcanology MD. Stratigraphy, and effects on structures. In: Sheets P Editor. *Before the Volcano Erupted: The Ancient Cerén Village in Central America*. Austin: University of Texas Press; 2002. pp. 11-23
- [7] Sheets P. *Before the Volcano Erupted: The Ancient Cerén Village in Central America*. Austin: University of Texas Press; 2002. pp. 11-23
- [8] Sheets P, Thomason M. The sounds in the dark of the Temazcal at Cerén, El Salvador. In: Gonlin N, Reed D, editors. *Night and Darkness in Ancient Mesoamerica*. Louisville CO: University Press of Colorado; 2021. pp. 203-228
- [9] Lohse J, Valdez F. *Ancient Maya Commoners*. Austin: University of Texas Press; 2004
- [10] Gonlin N, Lohse J. *Commoner Ritual and Ideology in Ancient Mesoamerica*. Boulder: University Press of Colorado; 2007
- [11] Blong R. *The Time of Darkness: Local Legends and Volcanic Reality in Papua New Guinea*. Seattle: University of Washington Press; 1982
- [12] Krajick K. Tracking myth to geological reality. *Science*. 2005;**310**:762-764
- [13] Németh K, Cronin SJ. Volcanic structures and oral traditions of volcanism of Western Samoa (SW Pacific) and their implications for hazard education. *Journal of Volcanology and Geothermal Research*. 2009;**186**(3-4):223-237
- [14] Fepuleai A, Weber E, Nemeth K, Muliaina T, Iese V. Eruption styles of Samoan volcanoes represented in tattooing, language and cultural activities of the indigenous people. *Geoheritage*. 2017;**9**(3):395-411
- [15] Pfister C. The ‘disaster gap’ of the 20th century and the loss of traditional disaster memory. *GAIA*. 2009;**18**(3):239-246
- [16] Stump D. On applied archaeology, indigenous knowledge, and the usable past. *Current Anthropology*. 2013;**54**(3):268-298
- [17] Riede F. Past-forwarding ancient calamities: Pathways for making archaeology relevant in disaster risk reduction research. *Humanities*. 2017;**6**(4):79

TFgeotourism: A Project to Quantify, Highlight, and Promote the Volcanic Geoheritage and Geotourism in Tenerife (Canary Islands, Spain)

Javier Dóniz-Páez, Pedro A. Hernández, Nemesio M. Pérez, William Hernández and Antonio Márquez

Abstract

Volcanic landscapes offer a multitude of resources to the communities that live within them. However, the main attraction that volcanoes offer is associated with volcanic heritage and geotourism. The scope of this project is to create and promote emerging geotouristic products through the empowerment of volcano tourism and thus contribute to strengthening the economic and business fabric of the volcanic island of Tenerife (Spain). In Tenerife, this great geodiversity includes the stratovolcanoes, shield volcanoes, calderas, cinder cones, maars, tuff cones and rings, and lava fields, all exposed beautifully in cliffs, ravines, beaches, deposits, etc. The main activities of the project associated with the documentation and quantification of the conservation values of the volcanic heritage are the following: production of a documentary on the volcanic geoheritage of Teide volcano, selection of the top 50 sites of geotouristic interest, creation of urban geotourism itineraries, recreation of the itinerary of Alexander von Humboldt, and creation of a web page for the project. This project will deliver an essential resource needed to diversify the leisure activities offered in Tenerife through the volcanic heritage and geotourism. It quantifies the best that Tenerife can uniquely offer and highlights it in a globally accessible and perpetual manner.

Keywords: volcanoes, volcanic geoheritage, geomorphosites, geotourism, urban geotourism, Tenerife, Spain

1. Introduction

There are some major transformations taking place in mature tourist destinations. These destinations correspond to the places with large tradition on touristic activities and situate in the mature or decline phases of the cycle of life of touristic destination [1] to refer the sun and beach tourism as Tenerife Island. These are the results of both the obsolete nature of tourism services, equipment, and infrastructures, as well as changes in the profile of demand for more sustainable products.

Both transformations have motivated tourism agents to seek innovative, creative, and imaginative solutions that prevent the decline of destinations and that represent a claim for visitors. The main examples are the changes in the touristic laws associate to the sustainability concept, the transformation of the urban spaces in the private and public places in the touristic cities, and the creation of the new touristic products such as geotourism. In this sense, within these new motivations, the diversification of the offer in the destination is being key. Therefore, the creation of new tourism products and experiences has become one of the main challenges for mature destinations to continue to occupy a significant role in the world tourism map at a time when the tourism sector is being very dynamic.

Within the diversity of new products and tourist experiences that are being developed in many parts of the world [2–3], is geotourism. Although it is true that in its landscape and esthetic conception, relief was present in the declaration of the first national parks in the world such as Yellowstone, Grand Canyon, etc., and in Spain (Picos de Europa, Teide, etc.), it is not until recent times geotourism has increased significantly [4–7], contributing to the creation of the European and global networks of geoparks in the last 20 years. Therefore, geotourism is a relatively modern term that was implemented in the modern society but welcomes multiple initiatives in different places and from different geological and geographical approaches, but they do not have to be mutually exclusive [7–8].

The island of Tenerife is an international tourist destination whose main attraction is the sun and the beach that attracts millions of visitors every year. However, Tenerife has a great variety of natural resources and tourist attractions that could diversify its offer and be the claim of other types of tourists [9]. In this sense, this chapter shows the main results of the project “Tfgeotourism: strengthening the economic and business fabric linked to the tourism sector of Tenerife by promoting volcanotourism,” whose objective is to create different geotourism products and experiences that contribute to diversifying the offer of leisure activities on the island and that can be implemented by tourism companies that already exist in Tenerife or that may be created as a result of this offer of volcano tourism products.

Therefore, the general objective and the main results of this project are in accordance with the objectives of the Global Geopark Network (GGN) to develop a leisure offer supported by geotourism that contributes to diversifying tourism and traditional economic activities in Tenerife through the creation of innovative local companies, new jobs, and highly qualified training courses for the different tourism agents [10]. But at the same time, Tfgeotourism is also in line with some of the objectives proposed by the Geoparks Commission of the International Geographical Union (IGU), which relates them to their role as a tool to communicate, recreate, and conserve nature or to understand the wide range of processes that affect the sustainable development of geoparks, including the natural environment, political, and socioeconomic processes [11].

In this sense, the choice of volcanic geotourism within the diversity of new tourism products and experiences in Tenerife responds to several reasons: 1. The island is a consolidated and well-known international destination to which several million tourists arrive annually. 2. The volcanic landscape of the island is diverse and, in it, practically all the forms and eruptive processes can be recognized, giving rise to one of the most geodiverse volcanic spaces from the point of view of the geological and geomorphological heritage [12]. 3. Tenerife already has a geotourism offer in some places such as the Teide National Park, being the most visited park in the Canary Islands and Spain, with an average of about 3 million annually [13, 14], and also in other places such as Barranco de Masca, the Macizo de Anaga, or the volcanic tube of La Cueva del Viento. 4. A large part of the insular volcanic geoheritage is not being exploited for tourism, because the principal activities associate

to the geotourism focused in the national park and some natural protected areas.
5. The practice of geotourism does not necessarily require a specialized public, which makes it very attractive and feasible for all tourists and visitors who come to Tenerife.

2. Tenerife a laboratory for the volcano tourism

Tenerife is the largest (2034 km²) and highest (3718 m a.s.l.) island of the Canary archipelago (**Figure 1**). It has been built up as a result of the accumulation of a wide variety (mafic, felsic) of fundamental volcanic materials in a relatively short period of time, which results in a world-unique variety of volcano-related tourism features in an accessible scale. In Tenerife, this great geodiversity includes the stravalcanoes, shield volcanoes, calderas, cinder cones, maars, tuff cones and rings, and lava fields, all exposed beautifully in cliffs, ravines, beaches, deposits, etc. (**Figure 2**). This volcanic geodiversity is a nonrenewable heritage [15] with various main characteristics associated with its natural and cultural heritage [16, 17]. The diversity of forms and processes of relief both directly related to volcanism as well as erosion and accumulation make up the volcanic heritage [18] and are responsible for the geodiversity of volcanic geoheritage of Tenerife Island.

Tenerife is one of the main tourist destinations in the world in relation to the number of accommodation places (>137,000 in September 2019) and the number of visitors it receives, which in 2019 exceeded 5 million [19]. We must also add the local visitors and hikers who increase this number. In turn, Tenerife has a great variety of new tourism products and experiences (geotourism, astrotourism, gastronomic, sports, health, bird watching, sailor, hiking, diving, whale watching, etc.), which are associated with diversity of attractions that the island has. Therefore, Tenerife has a diversified tourist offer capable of responding to this increasingly informed,

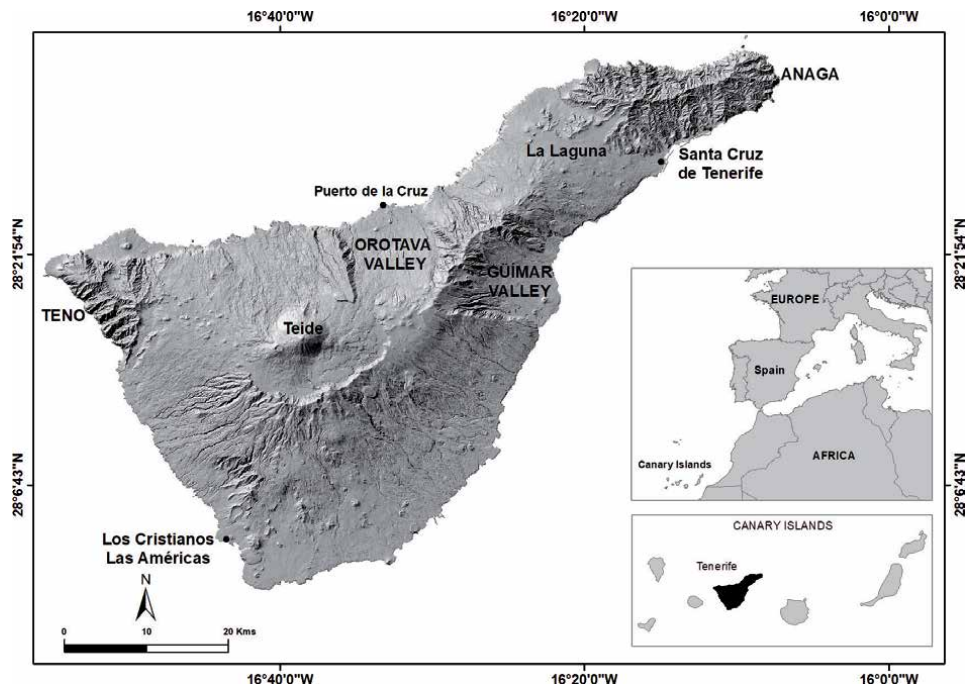


Figure 1. Location of Tenerife volcanic island. Source: Own elaboration from the DEM base of Grafcan.

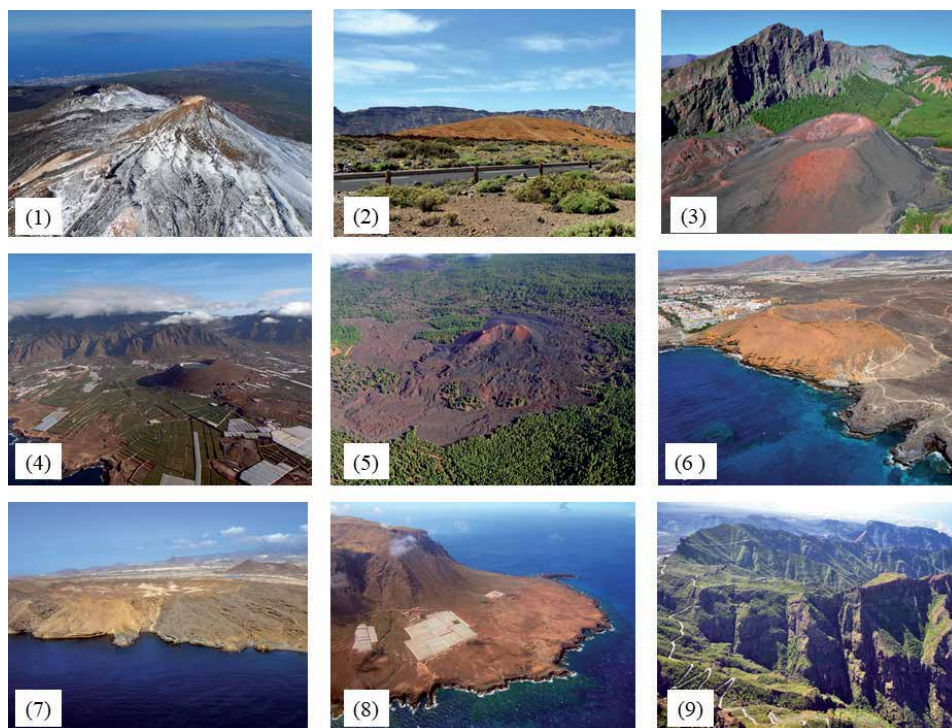


Figure 2.

Different volcanic landscapes of Tenerife. (1) Teide and Pico Viejo stratovolcanoes. (2) Las Cañadas caldera and Majua dome. (3) Arafo historical eruption. (4) cinder cone of Montaña taco. (5) last eruption of Tenerife: Chinyero cinder cones (1909). (6) Montaña Amarilla tuff cone and Bandas del Sur pumice formation. (7) Montaña Pelada tuff ring and monogenetic volcanic field. (8) Punta de Teno lava delta. (9) ravines in Teno shield volcanism.

demanding, and active demand, which makes the island an ideal destination for the introduction of new tourism products and experiences such as geotourism.

3. TFgeotourism: Tenerife's volcano tourism project

Tfgeotourism Project started in 2017, thanks to the financing of the Island Council of Tenerife. The entity responsible for executing it is the Instituto Volcanológico de Canarias (INVOLCAN). INVOLCAN, an entity unanimously demanded by the Senate (11/02/2005), the Parliament of the Canary Islands (01/11/2006), and the Congress of Deputies (12/02/2009), aims to contribute to the improvement of volcanic risk management in Spain (say the Canary Islands; the only volcanically active region of the national territory of Spain with volcanic risk) and the optimization of the management of the many benefits that come with living in a volcanic territory (geothermal resources, geotourism, etc.). Its mission and vision are intended to contribute to the sustainable development of the Canary Islands as well as other volcanic regions.

Within the TFgeotourism project and in accordance with its objectives, different products have been created associated with volcano tourism. This type of tourism in Tenerife constitutes a relatively new modality that consists of the tourist exploitation of natural and cultural aspects directly or indirectly linked to volcanoes. In this sense, the geotourism interest of volcanoes is associated with three fundamental aspects: (1) the landscapes they generate where the esthetic beauty of the processes

and forms cannot be compared to other geological territories; (2) the cultural aspect of volcanoes in relation to the societies that agree with them (archeology, history, music, folklore, gastronomy, etc.), configuring volcanic landscapes as key elements and icons in the culture of the peoples that coexist with them and its surroundings; and (3) the possibility of experiencing the power of seeing an erupting volcano as long as the safety of visitors is guaranteed.

Associated both with the objective of the project and with the geotourism interest of the volcanoes, TFgeotourism has created various products and tourist experiences that diversify both the leisure offer of Tenerife as well as geotourism. Each of the products generated within the project and whose purpose is to strengthen the economic and business fabric of the island are listed and characterized below.

3.1 Documentary on the volcanic geoheritage of Teide volcano

The need to make a documentary exclusively about the volcanic geoheritage of Teide volcano responds both to its international importance and to the fact that it had not been done until now. The global relevance of this volcano is due to the following facts: it is the National Park that receives more tourists in Spain (**Figure 3**) and is one of the most visited volcanic areas in the world [20]; it was part of the 16 volcanoes of the decade in 1990 according to the International Association of Volcanology and Chemistry of the Earth's Interior (IAVCEI) for the reduction of natural disasters; and it was one of the five European volcanoes (European Laboratory Volcanoes: Teide) of the European Commission, and since 2007, it has been a UNESCO World Heritage Site. To all these recognitions that value the volcanic heritage of the national park through its rich geoheritage, we must also add its varied and unique biodiversity and its rich cultural heritage from pre-Hispanic times to the present day [21].

Therefore, despite the relevance of its geoheritage and its tourist importance (international, national, and local), the national park did not have a specific and easily acquired tourist product for visitors who are attracted by the geotourism of Teide volcano. In this way, the documentary (**Figure 4**) that has been made is entitled "Teide, the sleeping giant"; it lasts for about 30 min, and throughout it, each and every one of the natural elements and cultural that make up the geodiversity of volcanic geoheritage of Teide volcano are displayed: stratovolcanoes, domes, cinder cones, hornitos, craters, lava flows, lava tubes, ravines, periglacial forms, and processes.

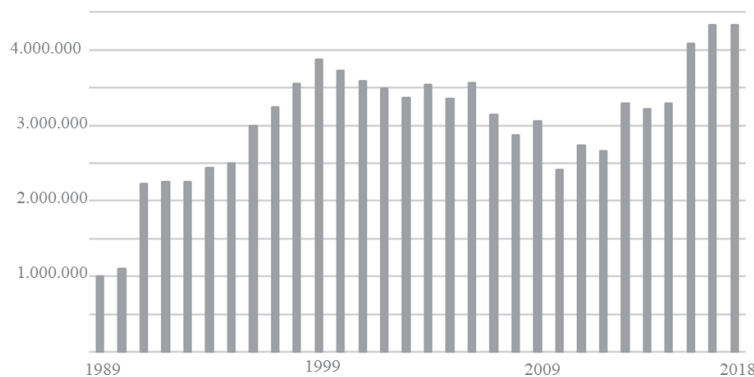


Figure 3. Visitors to Teide National Park. Source: ISTAC; Istac: <http://www.gobiernodecanarias.org/istac/>. Own elaboration.

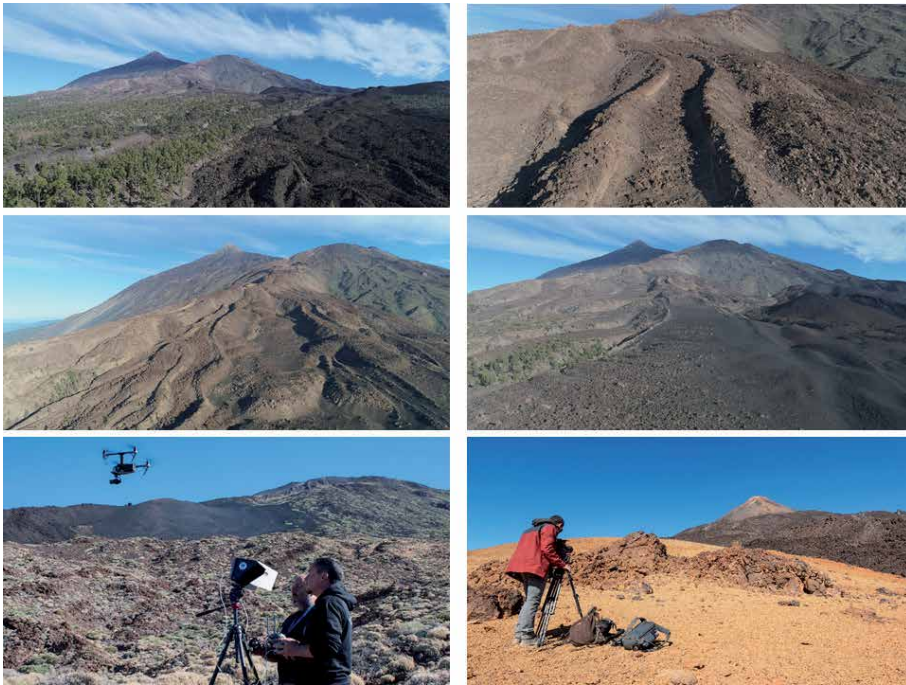


Figure 4. Some photographs about the shooting of the Teide documentary with drones. All pictures show the Teide and Pico Viejo stratovolcanoes and Roques Blancos lava dome. Source: Alas.

The documentary was presented in 2019 at the twenty-first edition of the Canary Islands International Medium-Environmental Film Festival (FIMEC) in Garachico, in the north of Tenerife, with a large influx of audiences. From there, it has been screened in various municipalities on the island (La Orotava, Guía de Isora, Los Realejos, etc.) and the objective is that it can be screened in all of them.

3.2 Tenerife's geoturistic guide

This is Tenerife's first geotourism guide (**Figure 5**). The main objective is to show the diversity of the volcanic geoh heritage of Tenerife through the selection of various places that collect aspects of its geodiversity, its geoh heritage, and its geoconservation. According with the more geographical vision of geotourism, the places listed in the guide show the values of the natural and cultural heritage associated with volcanoes. In this sense, and in addition to the geological and geomorphological heritage, aspects related to the vegetal landscape, the ornithological importance, the panoramic views or the cultural legacy that anthropic uses have left on the landscape are pointed out when using materials from the gea for the farming, the stone roads or the traditional buildings.

The guide has a selection of 50 places of geotourism interest Tenerife [22] (**Figure 6**) corresponding to the geological context of buildings and volcanic morphologies of the Canary Islands defined according to the Geological Survey of Spain (IGME). With the purpose of a greater understanding, the information of each place is presented in a file format. This has several sections in which the name of the geotourism place of interest and its UTM coordinates appear; the geological context and its main interest (tectonic, morphological, stratigraphic, and petrological); the municipality to which it belongs and its numbering; the location map; its description; the conservation and uses in it in order to establish what can and

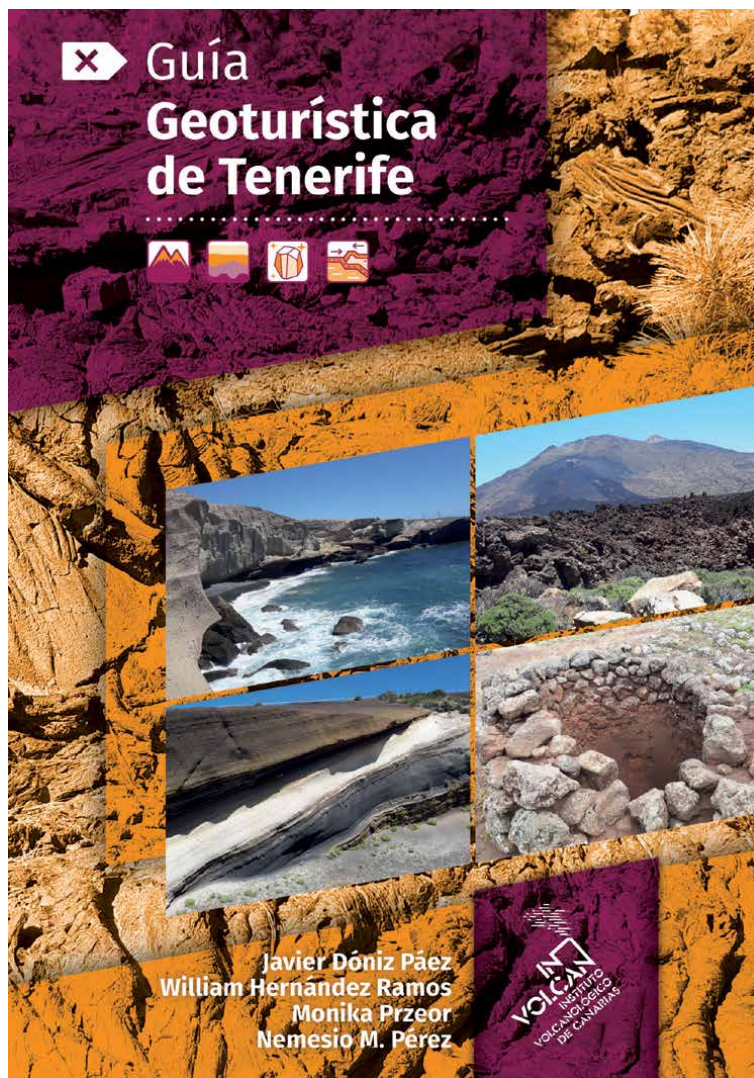


Figure 5.
Tenerife geotourism guide. Source: <http://tfgeoturismo.involcan.org/>.

cannot be done; the trails that run through each place; and the selection of the main geotourism interests of the site and the bibliographic references where you can find more information about each of the places included in the guide.

The set of 50 geotourism sites selected from the guide represent the geodiversity and volcanic geoheritage of the island of Tenerife from the topographic, volcanic, morphological, and landscape point of view [22, 23]. Topographically, the two slopes (north and south) and the different altitude levels of the island are represented. Volcanologically, the 50 places are distributed by all the volcanic buildings of Tenerife (shield volcanism-ancient volcanic massifs, rift volcanism and the central complex Cañadas-Pico Viejo-Teide), they represent both magmatic and hydromagmatic volcanism and the different dynamics and behavior eruptive (effusive, explosive and mixed). Morphologically, the places are part of both the forms and processes of direct volcanism (eruptions, volcano fields, lava fields, stratovolcanoes, etc.) and the processes of erosion and accumulation (ravines, cliffs, beaches, dunes, slopes, etc.). And, finally, from the landscape point of view, an attempt has been made that

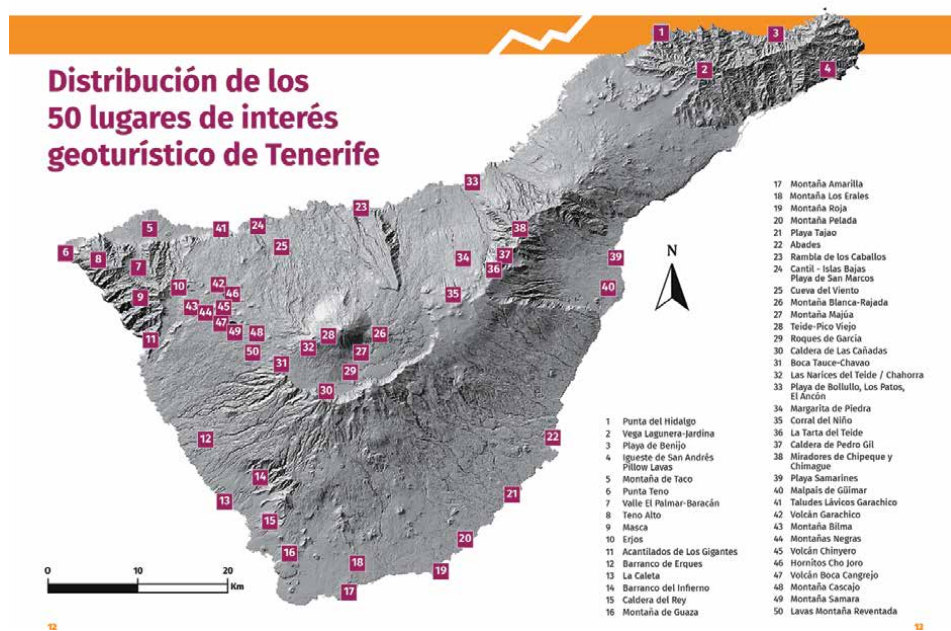


Figure 6. Spatial distribution of the 50 sites of geotourism interest. Source: <http://tfgeoturismo.involcan.org/>.

places of geotourism interest are present in all the large landscape units defined for Tenerife, which are the result of the combination of topographic, volcanic, biogeographic, and cultural criteria (landscapes of coastline with beaches and/or cliffs with xeric vegetation, embedded and open ravines with laurel and pine forests, badlands and lajiales without vegetation, volcanoes and lava with pine forests, stratovolcanoes of peaks with high mountain scrub, etc., and on which you cannot ignore all their cultural baggage) such as farming, traditional villages, churches, etc. In order to make the selected places accessible, it has also been tried that they are always within the usual itineraries (routes and circuits) of visitors to the island [23].

3.3 Urban geoturistic itineraries

In most cases, geotourism products, experiences, and activities are designed to be carried out mainly in protected natural areas. However, geotourism initiatives within cities are gaining more and more interest [24–26]. In this sense, the urban geotourism is a type of tourism which concentrates on the exploitation of the attractive parts of the relief of the cities. To do so, it is necessary to identify the places, areas, and/or elements with a geological-geomorphological interest (geosites or geomorphosites) and then design geoturistic itineraries which can be of chronological, geological, or spatial interest. The geographical relief can be found in any particular location within the city, either natural (volcanoes, lava flows, ravines, cliffs, beaches, etc.), which means those that have not been occupied by urban constructions, or those belonging to the cultural heritage (roads, buildings, etc.). The urban geotourism is recommended to a very diverse public, from local residents to visitors attracted by the geological heritage.

Within the TFgeotourism Project, 23 urban geotourism itineraries were designed in the different municipalities of Tenerife (Figure 7). In each of them, the natural geotourism sites and cultures of the cities and their environments were

"Año 1706, otra erupción lateral del Teide. Se abre la boca al sur del puerto de Garachico que por entonces era el más hermoso puerto y el más frecuentado de la isla".
 A. Humboldt

Garachico está situado en NW de Tenerife y forma parte de la comarca de Ycodem-Daute. Se extiende desde las faidas del Teide-Pico Viejo a más de 2100 metros de altitud hasta el Atlántico. La superficie del municipio es de unos 29 km². La Villa y Puerto fue fundada a finales del siglo XV por el banquero genovés Cristóbal de Ponte. La prosperidad económica del pueblo se debió a su puerto natural para el comercio con Europa y América. Los siglos XVI y XVII fueron de gran prosperidad económica para la ciudad, pero la peste, los incendios, los aluvios y la erupción de 1706 acabaron con riqueza de este pueblo y destruyeron parte del puerto y de la ciudad. Actualmente la ciudad de Garachico es un lugar con encanto de la costa norte de Tenerife que muestra un rico patrimonio natural y cultural asociado con el fenómeno volcánico.

"Year 1706, another flank eruption of Teide volcano. An eruptive vent has opened in the southern part of Garachico harbour, which at the time was the most beautiful harbour and the most visited of the island".
 A. Humboldt

Garachico is located in the NW of Tenerife and belongs to the region of Ycodem-Daute which extends from the flanks of Teide-Pico Viejo, at more than 2100 metres high, to the Atlantic Ocean. The surface of the municipality is 29 km². The city and the harbour were founded at the end of the XV century by the Italian banker Cristóbal de Ponte. The economic prosperity of the village was due to a natural harbour used in commercial transactions with Europe and America. During the XVI and XVII centuries the village was prosperous but the plague, fires, avalanches and the 1706 volcanic eruption ended the richness of this village by destroying parts of the harbour and the village itself. At present, the village of Garachico is a magical place in the northern coast of Tenerife, which has a rich natural and cultural heritage associated with the volcanic phenomenon.

El geoturismo urbano es una modalidad de turismo que se centra en la explotación de los atractivos del relieve en las ciudades. Para ello es necesario que se identifiquen los lugares, zonas y/o elementos de interés geológico-geomorfológico (lig) y a partir de los mismos diseñar itinerarios geoturísticos de tipo cronológico, geológico o espacial. El relieve en las ciudades se puede encontrar en cualquier rincón de la misma, bien de manera natural (volcanes, caladas de lava, barrancos, acantilados, playas, etc.) que no han sido ocupados por la urbanización o bien a través del patrimonio cultural tangible inmueble (trazado urbano, edificios, etc.). El geoturismo urbano está dirigido a un público muy diverso, desde los propios residentes de la ciudad hasta los visitantes que se sienten atraídos por las formas y procesos del relieve.

Urban geotourism is a type of tourism which concentrates on the attractive parts of the geographical relief of cities. To exploit this potential, it is necessary to identify the places, areas and/or elements with a geological-geomorphological interest, and then design geotouristic itineraries which can be chronological, geological or spatial. The geographical relief can be found in any particular location within the city, either natural (volcanoes, lava flows, ravines, cliffs, beaches, etc.) which means those that have not been occupied by urban constructions, or those belonging to the cultural heritage (roads, buildings, etc.). The urban geotourism is recommended to a very diverse public, from local residents to visitors attracted by the geological heritage.

Editado gracias al proyecto "FORTALECIMIENTO DEL TEJIDO ECONÓMICO Y EMPRESARIAL LIGADO AL SECTOR TURÍSTICO DE TENERIFE MEDIANTE LA POTENCIACIÓN DEL VOLCANOTURISMO" que forma el programa desarrollo 2016-2021 que coordina el Área Tenerife 2020 del Cabildo Insular de Tenerife y Fondo de Desarrollo de Canarias (FDCAN).

Geoturismo Urbano de Tenerife
 Urban Geotourism of Tenerife

Garachico

TENERIFE

IN VOLCANOTURISMO

El itinerario cuenta con 14 puntos de interés geoturístico urbano que resumen toda la geodiversidad de la ciudad de Garachico y que están directa o indirectamente relacionados con la erupción de mayo de 1706 de Arena Negra. Destacan las lenguas de lava que destruyeron parte de la villa y puerto y que cada 5 años, en las fiestas de San Roque, se conmemoran. Es muy llamativo el uso de las rocas basálticas y la toba (spatter) en la construcción y decoración de los edificios religiosos y civiles (puertas, ventanas, arcos, suelos, etc.), así como los adoquines y callaos en las calles y aceras.

The itinerary consists of 14 localities with urban geotouristic interest which synthesize the geodiversity of the village of Garachico and that, directly or indirectly, are related to the May 1706 Arenas Negras volcanic eruption. We can distinguish the lava flows which destroyed part of the village and harbour. Every 5 years, during the San Roque festivity, there is a commemoration of that event. A particular highlight is the varied use of basaltic rocks, volcanic tuffs and spatter in the construction and decoration of religious and civil buildings (doors, windows, arcs and ceilings, floors, etc) and also its use as bricks and building stones in streets and pavements.

más información:
 more information:

tfgeoturismo.involcan.org

- | | | | | |
|--------------------------------------------------------------------------------------------------------------------------------------------------------------------------------------------------------------------------------------------------------------------------------------------------------------------------------------------------------------------------------------------------------------------------------------------------------------------------------------------------------------------------------------------------------------------------------------------------------------------------------------------------------------------------------------------------------------------------------------------------------------------------|---------------------------------------------------------------------------------------------------------------------------------------------------------------------------------------------------------------------------------------------------------------------------------------------------------------------------------------------------------------------------------------------------------------------------------------------------------------------------------------------------------------------------------------------------------------------------------------------------------------------------------------------------------------------------------------------------------------------------------------------------------------------------------------|-------------------------------------------------------------------------------------------------------------------------------------------------------------------------------------------------------------------------------------------------------------------------------------------------------------------------------------------------------------------------------------------------------------------------------------------------------------------------------------------------------------------------------------------------------------------------------------------------------------------------------------------------------------------------------------------------------------------------------------------------------------------------------------|-------------------------------------------------------------------------------------------------------------------------------------------------------------------------------------------------------------------------------------------------------------------------------------------------------------------------------------------------------------------------------------------------------------------------------------------------------------------------------------------------------------------------------------------------------------------------------------------------------------------------------------------------------------------------------------|-------------------------------------------------------------------------------------------------------------------------------------------------------------------------------------------------------------------------------------------------------------------------------------------------------------------------------------------------------------------------------------------------------------------------------------------------------------------------|
| <p>1 Taludes Lávicos
 Lava talus
 Taludes lávicos.
 Lava flow and talus
 Cliffs.
 Crops.</p> <p>2 Barranco Salto de las Palomas
 Salto de los Palomas ravine
 Barrancos, cantil fósil, lavas.
 Ravines, fossil cliff, lavas.
 Canales de agua, estanques
 Water channels, ponds.</p> <p>3 Ermita de Los Reyes
 Los Reyes hermit
 Lavas, rocas basálticas, callaos.
 Lava flows, basaltic rocks, beach pebbles.
 Ermita.
 Hermitage.</p> | <p>4 Puerta de Tierra
 Earth door
 Lavas, lapilli, spatter, callaos.
 Lava flows, lapilli, spatter, beach pebbles.
 Pozo de agua.
 Water well.</p> <p>5 Iglesia de Santa Ana
 Santa Ana church
 Roca basáltica, spatter, callaos.
 Basaltic rock, spatter, pebbles.
 Iglesia.
 Church.</p> <p>6 Palacio Condes de La Gomera
 La Gomera Counts palace
 Spatter, rocas basálticas, lavas.
 Spatter, basaltic rocks, lava flows.
 Palacio.
 Palace.</p> | <p>7 Ex Convento de San Francisco
 The Mill
 San Francisco old convent
 Spatter, rocas basálticas.
 Spatter, basaltic rocks.
 Convento.
 Convent.</p> <p>8 Casa Marquesa de Quinta Roja
 House of Quinta Roja marquis
 Roca basáltica.
 Basaltic rock.
 Pelazo.
 Palace.</p> <p>9 Hacienda Lamero
 Lamero estate
 Piedra basáltica tallada.
 Carved basaltic rock.
 Hacienda, molinos, ermita.
 Hacienda, mill, hermitage.</p> | <p>10 Los Molinos
 The Mill
 Rocas basálticas.
 Basaltic rocks.
 Molinos de agua.
 Water Mill.</p> <p>11 El Roque (panorámica)
 El Roque (views)
 Lavas, roque.
 Lava flows, roque.
 Cruz cristiana.
 Christian Cross.</p> <p>12 El Calentón
 El Calentón natural pool
 Lavas az, cantil fósil
 Az lava flows, fossil cliff
 Piscinas.
 Pools.</p> | <p>13 Castillo de San Miguel
 San Miguel castle
 Rocas basálticas, lapilli, callaos.
 Basaltic rocks, lapilli, beach pebbles.
 Castillo militar.
 Military Castle.</p> <p>14 Playa del Muelle
 Pier beach
 Lavas, playa de arena negra y acantilados.
 Lava flows, black sand, cliff.</p> |
|--------------------------------------------------------------------------------------------------------------------------------------------------------------------------------------------------------------------------------------------------------------------------------------------------------------------------------------------------------------------------------------------------------------------------------------------------------------------------------------------------------------------------------------------------------------------------------------------------------------------------------------------------------------------------------------------------------------------------------------------------------------------------|---------------------------------------------------------------------------------------------------------------------------------------------------------------------------------------------------------------------------------------------------------------------------------------------------------------------------------------------------------------------------------------------------------------------------------------------------------------------------------------------------------------------------------------------------------------------------------------------------------------------------------------------------------------------------------------------------------------------------------------------------------------------------------------|-------------------------------------------------------------------------------------------------------------------------------------------------------------------------------------------------------------------------------------------------------------------------------------------------------------------------------------------------------------------------------------------------------------------------------------------------------------------------------------------------------------------------------------------------------------------------------------------------------------------------------------------------------------------------------------------------------------------------------------------------------------------------------------|-------------------------------------------------------------------------------------------------------------------------------------------------------------------------------------------------------------------------------------------------------------------------------------------------------------------------------------------------------------------------------------------------------------------------------------------------------------------------------------------------------------------------------------------------------------------------------------------------------------------------------------------------------------------------------------|-------------------------------------------------------------------------------------------------------------------------------------------------------------------------------------------------------------------------------------------------------------------------------------------------------------------------------------------------------------------------------------------------------------------------------------------------------------------------|
- Patrimonio Natural - Natural Heritage
 Patrimonio Cultural - Cultural Heritage

Figure 7.
 Example of an urban geotourism itinerary. Source: <http://tfgeoturismo.involcan.org/>.

identified, selected, inventoried, and characterized [27]. The information of each site was collected in a file whose objective is to provide more information on the places selected to make the route. The itineraries are always developed through the cities, they are easily accessible, with little unevenness, they can be developed at any time of the year given the subtropical climate of the island, the duration varies between 1.5 and 3 h and the number of places and stops is not more than 16.

3.4 Geoturistic itinerary of Alexander von Humboldt in Tenerife

On June 19, 1799, the German naturalist Alexander von Humboldt made a stop in Tenerife with the aim of ascending the Teide volcano [28]. The traveler made various observations, descriptions, and measurements of the places he visited. Among the varied information that he left us, stand out his impressions of the natural and cultural heritage associated with the volcanic landscapes through which the route ran from Puerto de la Cruz to the top of Teide stand out. In this sense, his interesting observations have allowed us to identify the 18 stops into which the journey was divided and to show the tourist interest of each one of them. In addition, given the importance of travel literature for experience tourism and the geoturistic interest

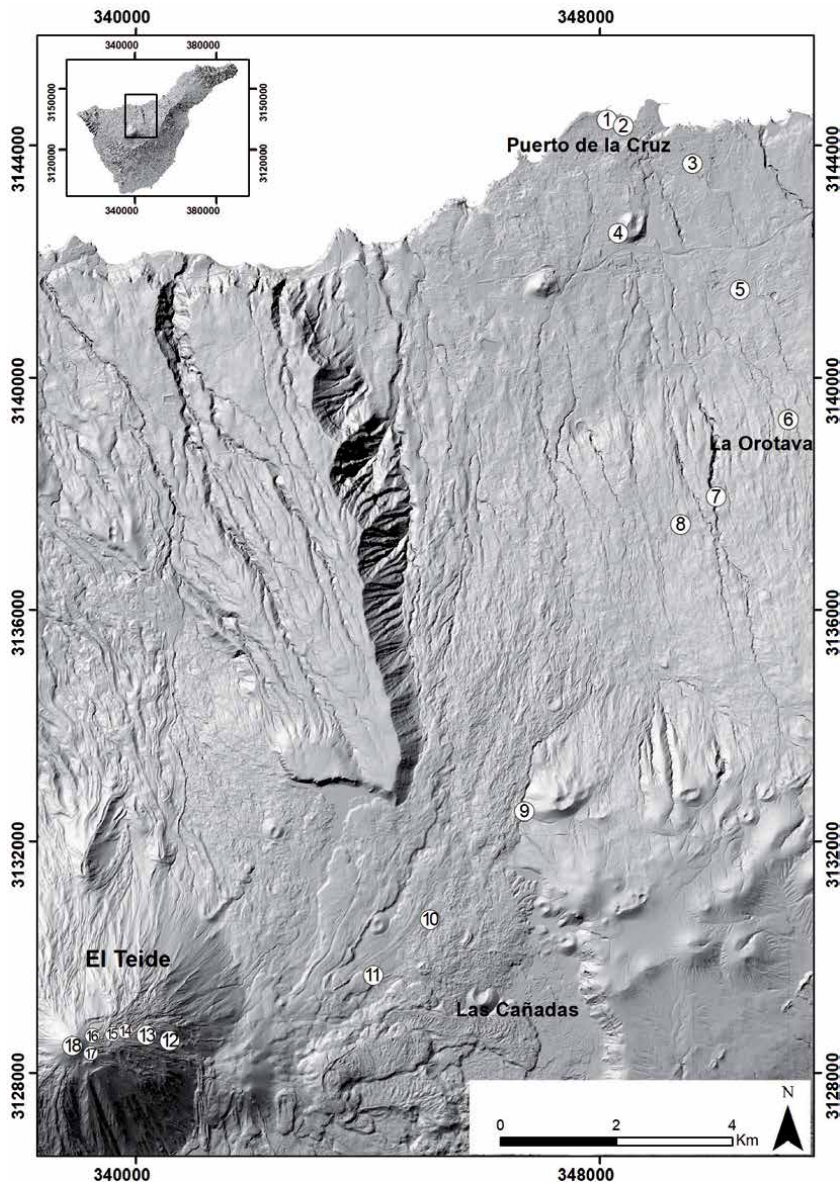


Figure 8. Special identification of Humboldt stops on his ascent to Teide. Source: Own elaboration from the DEM base of Grafcan.

of the stops on the route (**Figure 8**), it has been possible to recreate almost exactly the itinerary that Alexander von Humboldt made through the Orotava Valley and the Cañadas del Teide.

Table 1 shows the 18 stops identified and their geotourism attractiveness divided between natural and cultural heritage. The attractions refer both to the impressions taken by the German traveler in June 1799 and to those that can be observed today when the tour is made [29].

Nº	Stop	Geotouristic attractions
1	Puerto de La Orotava (Puerto de la Cruz)	Coast of La Paz, hornitos and scorias cones at Tigaiga eruption, Teide, clouds sea, taste for nature, lyrics, music, and San Juan festival in Sitio Liter
2	Casa familia Cólogan (Hotel Marquesa)	Basaltic volcanic rocks: lavas, lapilli, etc.
3	Jardín Acclimatación (Jardín Botánico)	Topographic terrace, plants, natural source, climate
4	Volcanes Fraile y Horca	Geology and geomorphology, volcanic cones, craters, lavas, volcanic ash, lapilli, pumice, basalts, eruptions, vegetation, guanches, and rural landscapes
5	Villa de La Orotava	Topography, geology, hills-watersheds, climate, mist, waters, vegetation, dragon tree, ferns, fauna, guanches, noble houses, aqueducts, mills, crops, vineyards, fruit trees, and peasants
6	Monte de los Castaños	Cobbled path, chestnut trees, laurel forest, heather, and ferns
7	Pino Dornajito	Panoramas of the north of Tenerife, rugged topography, mountainous area, volcanic mountains, volcanic cones, lava, small ravines, porous rocks, water spring, vegetation, pine trees, and footpath
8	Monteverde	Heather, fern, fern-rooted gofio, humble town, and misery
9	Portillo	Volcanoes, basalts, volcanic cones, caldera, and pine forests
10	Cañadas Occidentales-Volcán M. Corrales	Topographic plain, plateau, pumice fields, sands, Teide, lava flows, eruptions, broom thickets, summit vegetation, hunters, and straw hats
11	Roque de Gaita	Volcanoes, black streams, obsidian blocks, rocks, rabbits, and goats
12	Estancia de los Ingleses-Montón del trigo	Black streams, ravines, plateaus, lava blocks, caves, Teide, climate, gorse, horses, mules, bonfires, and pine torches
13	Altavista	Topography, slopes, escarpments, lava, snowfields, snow, mules, and indigenous
14	Malpaís (cueva del Hielo)	Malpaís, lavas, path, perpetual snow, glacier, cave, volcanic tubes, jameos, sea of clouds, and ice collection
15	Senda coladas negras	Black lava flows, aa, malpaís, python, sea of clouds, vision of other islands, sunrise, laziness of the guides, and guanches
16	Ramblata	Topographic plain, python, Narices del Teide, and fumes-gases
17	Pitón	Topography, slopes, lavas, python, lavas, cooling sidewall, ash, pumice, slag, snow, and groundwater
18	Cráter terminal	Small crater, lava flows, slags, ashes, slopes, sensation of cold, roaring fumaroles, Teide violet, climate, sky, bees, feeling of loneliness, and Malvasia wine

Table 1. Identification of the attractions with geotourism interest in the stops made by Humboldt from the port of La Orotava to Teide.

3.5 Web page of TFgeotourism project

With the aim that all the products produced within the TFgeotourism project are freely consulted and available to everyone, a web page was created (<http://tfgeoturismo.involcan.org/>). In this, in addition to the fact that you can view all the products generated and download them in digital format, you can consult additional information on the geotourism places of interest or the different urban geotourism stops.

4. Conclusions

This chapter shows the different volcano tourism products created within the TFgeotourism project for the island of Tenerife. This Spanish island is one of the main tourist destinations in the world for both the number of tourist places it offers and the millions of tourists it receives each year. The main tourist attraction on the island is the sun and the beach. However, in Tenerife, there is a great variety of tourist resources that could diversify its leisure offer, helping to avoid or minimize some of the problems that mature sun and beach tourist destinations are having. Within the variety of new tourism products and experiences that can be recognized in Tenerife, geotourism associated with volcanoes is one of them. The TFgeoturismo project aims to create different geotourism products to strengthen the economic and business fabric of the island. In this sense, this chapter indicates and characterizes the main activities of the project associated with the documentation and quantification of the conservation values of the volcanic heritage, as follows: (1) production of a documentary on the volcanic geoheritage of Teide volcano; (2) identification, inventory and selection of the top 50 sites of geotouristic interest on the island associated to geomorphosites; (3) creation of urban geotourism itineraries in the different municipalities of the island of Tenerife; (4) recreation of the itinerary of the pioneering German naturalist, Alexander von Humboldt, from Puerto de La Cruz to the top of the Teide volcano; and (5) creation of a web page for the project (<http://tfgeoturismo.involcan.org/>) that showcases all the geotouristic products generated within the framework of the project. Therefore, this project will deliver an essential resource needed to diversify the leisure activities offered in Tenerife through the volcanic heritage and geotourism. It quantifies the best that Tenerife can uniquely offer and highlights it in a globally accessible and perpetual manner.

Acknowledgements

This work is part of the research project “Strengthening the economic and business fabric linked to the tourism sector of Tenerife through the promotion of volcano tourism,” financed by the Program Tenerife Innova of the Cabildo Insular de Tenerife. We appreciate the comments and suggestions of the editor and the two anonymous reviewers. The authors thank David Calvo Fernández for his work throughout the development of the project.

Conflict of interest

The authors declare no conflict of interest.

Author details

Javier Dóniz-Páez^{1,2*}, Pedro A. Hernández^{1,3}, Nemesio M. Pérez^{1,3},
William Hernández¹ and Antonio Márquez⁴

1 Instituto Volcanológico de Canarias (INVOLCAN), La Laguna, Tenerife, Canary Islands, Spain


2 Geoturvol-Department of Geography and History, University of La Laguna, La Laguna, Tenerife, Canary Islands, Spain

3 Instituto Tecnológico y de Energías Renovables (ITER), Granadilla de Abona, Tenerife, Canary Islands, Spain

4 Unidad de Helicópteros UTF, Guardia Civil - Zona de Canarias, Tenerife, Canary Islands, Spain

*Address all correspondence to: jdoniz@ull.edu.es

IntechOpen

© 2020 The Author(s). Licensee IntechOpen. This chapter is distributed under the terms of the Creative Commons Attribution License (<http://creativecommons.org/licenses/by/3.0>), which permits unrestricted use, distribution, and reproduction in any medium, provided the original work is properly cited. 

References

- [1] Butler R. The concept of a tourist area cycle of evolution: Implications for management of resources. *Canadian Geographer*. 1980;24(1):5-12. DOI: 10.1111/j.1541-0064.1980.tb00970.x
- [2] Joyce EB. Australia's geoheritage: History of study, a new inventory of geosites and applications to geotourism and geoparks. *Geoheritage*. 2010;2: 39-56. DOI: 10.1007/s12371-010-0011-z
- [3] Alessio G, De Lucia M. Promotion and development of protected volcanic areas through field-based environmental communication activities: The "gran Cono" tour in the Vesuvius National Park (Italy). *Geoheritage*. 2017;9:435-442. DOI: 10.1007/s12371-017-0242-3
- [4] Farsani N, Coelho C, Costa C, Amrikazemi A. Geotourism and geoparks as gateways to socio-cultural sustainability in Qeshm rural areas, Iran. *Asia Pacific Journal of Tourism Research*. 2012;17(1):30-48. DOI: 10.1080/10941665.2011.610145
- [5] Ólafsdóttir R, Dowling R. Geotourism and geoparks-a tool for geoconservation and rural development in vulnerable environments: A case study from iceland. *Geoheritage*. 2014;6(1):71-87. DOI: 10.1007/s12371-013-0095-3
- [6] Ruban D. Geotourism-a geographical review of the literatura. *Tourism Management Perspectives*. 2015;15:1-15. DOI: 10.1016/j.tmp.2015.03.005
- [7] Dowling R, Newsome D. Geotourism: Definition, characteristics and international perspectives. In: Dowling R, Newsome D, editors. *Handbook of Geotourism*. Cheltenham: Edward Elgar; 2018. pp. 1-22. DOI: 10.4337/9781785368868.00009
- [8] Pásková MZ. Sustainability management of Unesco global geoparks. *Sustainable Geoscience and Geotourism*. 2018;2:44-64. <https://www.scipress.com/SGG.2.44>. DOI: 10.1016/j.pgeola.2012.07.003
- [9] Dóniz-Páez J. Aplicación De Metodologías Docentes Al Estudio De Nuevos Productos Turísticos En Destinos Maduros: El Ejemplo De Tenerife (Canarias, España). In: Ravelo A, Pérez S, Alonso J, Canino J, Travieso C, Cruz D, editors. *III Jornadas Iberoamericanas de Innovación Educativa en el ámbito de las TIC*. Las Palmas de Gran Canaria: ULPGC; 2016. pp. 381-384
- [10] Global Geoparks Networks [Internet]. 2004. Available from: <http://www.globalgeopark.org/aboutGGN/51.htm> [Accessed: 01 August 2020]
- [11] Commission on Geoparks [Internet]. 2008. Available from: <http://www.igu-cog.org/vision.htm> [Accessed: 01 August 2020]
- [12] Dóniz-Páez J, Rodríguez F, Becerra-Ramírez R, González E, Escobar E. Geodiversity, geoheritage and volcano tourism in natural protected areas of Tenerife (Canary Islands, Spain). *Geophysical Research Abstracts*. 2018;20:EGU-15572-1
- [13] Dóniz-Páez J, Becerra-Ramírez R. Geoturismo volcánico en el Parque Nacional de Las Cañadas del Teide (Tenerife, Canarias, España). *Bloc de las Islas Canarias*. 2019;9:99-109
- [14] Dóniz-Páez J, Becerra-Ramírez R, González-Cárdenas E, Rodriguez F. Volcanic geomorphosites and geotourism in Las Cañadas del Teide National Park, Tenerife, Canary Islands, Spain. *Geophysical Research Abstracts*. 2017;19:EGU-15561
- [15] Wang L, Tian M, Wen X, Zhao L, Song J, Song M, et al. Geoconservation and geotourism in Arxan-Chaihe

- volcano area, inner Mongolia, China. *Quaternary International*. 2014;**349**:384-391. DOI: 10.1016/j.quaint.2014.06.024
- [16] Gravis I, Németh K, Procter JN. The role of cultural and indigenous values in geosite evaluations on a quaternary monogenetic volcanic landscape at Ihumātāo, Auckland volcanic field, New Zealand. *Geoheritage*. 2017;**9**:373-393. DOI: 10.1007/s12371-016-0198-8
- [17] Kelley D, Page K, Quiroga D, Salazar R. In the Footsteps of Darwin: Geoheritage, Geotourism and Conservation in the Galapagos Islands. Switzerland AG: Springer Nature; 2019. p. 183. DOI: 10.1007/978-3-030-05915-6_5
- [18] Németh K, Casadevall T, Moufti MR, Martí J. Volcanic geoheritage. *Geoheritage*. 2017;**9**:251-254. DOI: 10.1007/s12371-017-0257-9
- [19] Instituto Canario de Estadística [Internet]. 1991. Available from: <http://www.gobiernodecanarias.org/istac/> [Accessed: 01 August 2020]
- [20] Erfurt-Cooper P. Volcanic tourist destinations. In: *Geoheritage*. Springer Verlag, Berlin, Heidelberg: Geoparks and Geotourism Series; 2014. p. 384. DOI: 10.1007/978-3-642-16191-9
- [21] Martínez de Pisón E, Arozema M, Beltrán E, Romero C. Los paisajes del Parque Nacional del Teide. In: Organismo Autónomo de Parques Nacionales. Madrid. vol. 9. 2009. p. 203
- [22] Dóniz-Páez J, Hernández W, Przeor M. Lugares de interés geoturístico de Tenerife (Islas Canarias, España) como estrategia para potenciar el volcanoturismo. In: Martín-González E, Coello Bravo J, Vegas J, editors. *Actas de la XIII Reunión Nacional de la Comisión de Patrimonio Geológico*. España, Madrid: IGME; 2019. pp. 93-102
- [23] Dóniz-Páez J, Hernández W, Przeor M, Pérez N. Guía geoturística de Tenerife. In: *Involcan, S/C de Tenerife*. 2019. p. 113
- [24] Pica A, Vergari F, Fredi P, Del Monte M. The Aeterna Urbs geomorphological heritage (Rome, Italy). *Geoheritage*. 2016;**8**(1):31-42. DOI: 10.1007/s12371-015-0150-3
- [25] Reynard E, Pica A, Coratza P. Urban geomorphological heritage. An overview. *Quaestiones Geographicae*. 2017;**36**(3):7-20. DOI: 10.1515/quageo-2017-0022
- [26] Aparecida Del Lama E, De La Corte Bacci D, Martins LD, Gloria Motta García M, Kazumi L. Urban geotourism and the old Centre of São Paulo City, Brazil. *Geoheritage*. 2015;**7**(2):147-164. DOI: 10.1007/s12371-014-0119-7
- [27] Dóniz-Páez J, Becerra R, Carballo M. Propuesta de itinerario geoturístico urbano en Garachico (Tenerife, Canarias, España). *Investigaciones Geográficas*. 2016;**66**:95-115. DOI: 10.14198/INGEO2016.66.06
- [28] Humboldt A. Viaje a las regiones equinociales del nuevo Mundo: Las Canarias y otros escritos. La Laguna: Fundación Canaria-Alemana Alexander Von Humboldt, Nivaria; 2005. p. 353
- [29] Dóniz-Páez, J. y Rodríguez Méndez, C. Propuesta de itinerario turístico en Tenerife a partir del viaje de Humboldt en 1799 desde Puerto de la Cruz al Teide. *Coloquios de Historia Canario Americana*. 2017;**XXII**-155:1-12

Edited by Károly Németh

Updates in Volcanology - Transdisciplinary Nature of Volcano Science is a true reflection of the recent advancement of volcano science to a geosystem science based on a strong source-to-surface or process-to-consequences nature, all centered around the transdisciplinary nature of volcanology. The book contains a balanced set of chapters dealing with traditional approaches within volcanology from petrogenetic aspects of magmatic systems to volcano models. The book also provides a comprehensive set of outputs along volcanic geoheritage.

Published in London, UK

© 2021 IntechOpen
© AZ68 / iStock

IntechOpen

